Late-life effects of earlier dietary restriction on lifespan, health span and tissue-specific phenotypes

Inaugural-Dissertation

zur

Erlangung des Doktorgrades

der Mathematisch-Naturwissenschaftlichen Fakultät

der Universität zu Köln

vorgelegt von

Lisa Franziska Drews

aus Groß-Umstadt, Deutschland

Köln, 2021

Gutachter: **Prof. Dr. Linda Partridge**

Prof. Dr. Peter Kloppenburg

Tag der mündlichen Prüfung: 07.06.2021

Dedicated to my beloved father (1953- 2017)

And my beloved grandmother (1931- 2021).

Old age is not a phase of decline and loss, but instead, if approached properly, harbours the opportunity for positive change and productive functioning.

Marcus Tullius Cicero, 44BC

Table of contents

Acknowledgements

First and foremost, I would like to express my deep gratitude to Prof. Dr. Linda Partridge, for the opportunity to conduct my PhD in her lab and her support and input on my project. I am incredibly grateful for your enthusiastic encouragements, your patient guidance and for helping me grow personally over the last years. I cannot thank Dr. Sebastian Grönke enough for entrusting this project to me, for the great supervision, critical discussion and endless support. You really helped me grow as a Scientist. I am incredibly grateful to Prof. Dr. Peter Kloppenburg, Prof. Dr. Jan Riemer and Dr. Martin Denzel for being part of my PhD thesis committee and to my previous TAC committee member Prof. Dr. Carien Niessen, who supported my project with invaluable advice and constructive feedback.

Additionally, I wish to acknowledge Carolina Monzó for her amazing work on the statistical analyses of my mouse data, for her knowledge, support and ideas. You are the best! I am particularly grateful to Dr. Oliver Hahn for the interesting discussions and of course for the effortless collaboration on the paper. A specific thanks goes to Javi for being the best colleague one can wish for and for challenging my German language teaching skills. Your friendship, support and optimism have helped me immensely through my PhD. I am particular grateful to Sina, who helped me with his expertise on intestinal organoid culture and to Christine for the great talks, the help with paper work and for sharing my passion for Yoga. In addition, I would like to acknowledge my former student Gemma Crupi for teaching me a lot about supervision and for her great help in the lab. How could I not thank the entire LP lab, current and previous members, for the vibrant working atmosphere, helping hands as well as the fun and fruitful discussions about science? It was a joy and a pleasure working with all of you over the last years. Further, I would like to extent my thanks to our wonderful technicians Oliver, Ramona Jansen, Sandra, Andre and Ramona Hoppe for their help and expertise with lab techniques, dissections, tissue sectioning and for weighing the DR food. Moreover, I cannot thank Dr. Andrea Mesaros and Martin Purrio from the phenotyping core facility enough for their assistance and help in various phenotypings. A big thank you goes to Dr. Bettina Bertalan, Dr. Sandra Buhl, Ramona Braun and all animal caretakers in the experimental barrier. In particular, I would like to thank my primary caretakers Kristina Mussmann and Doreen Briel for feeding and ensuring the wellbeing of my animals every single day. Without you and your amazing work, this project would never have run as smoothly as it did. Another big thank you goes to Jerome Henn for breeding my phenotyping cohorts and for the great discussions about cinematic novelties, politics or Science. Moreover, thank you Dr. Christian Kukat and Dr. Astrid Schauss from the MPI and CECAD imaging facilities and your amazing teams for supporting my experiments and in particular thank you Janine Klask for preparing and imaging my EM samples. I would also like to thank Dr. Daniela Morrick for all her help and support, her open

ear and her words of encouragement when I needed a lift up during challenging phases of my PhD.

Many thanks to my friends, for always having an open ear for my problems or struggles and for always lifting me up when I felt down. Fabienne, Laura and Marcel - you guys are the best. Thank you Ido, for being a central part of my life for over a year now, for sharing all of my difficulties, for your interest in my work and for cheering me up. I couldn't ask for a better partner and I am looking forward to sharing many more of life's adventures with you. Finally, I want to thank my family, Mama, Julia and Daniel for your endless support throughout my PhD, your encouragement, perseverance and for always believing in me. It has been a long journey until now and I would not have come here while staying relatively sane without you. Papa and Oma: I know both of you would have been so proud of me.

Abbreviations

Abbreviation	**Full name**
%	Percent
µl	Microliter
XM	X months
3,3′-Diaminobenzidine	DAB
95% CI	95% confidence interval
Abbreviation	Full name
Acaca	Acetyl-CoA Carboxylase Alpha
AL	ad libitum
AL_DR	Diet switch from ad libitum to dietary restriction
AL_DR12M	Diet switch from AL to DR at 12 months of age
AL_DR16M	Diet switch from AL to DR at 16 months of age
AL_DR20M	Diet switch from AL to DR at 20 months of age
AL_DR24M	Diet switch from AL to DR at 24 months of age
AT	Adipose tissue
ATSC	Adipose tissue stem cell
BAT	Brown adipose tissue
C. elegans	Caenorhabditis elegans
CLS	Crown-like structures
CPH	Cox proportional hazard
CVD	Cardiovascular disease
d	Days
DPBS	Dulbecco's phosphate-buffered saline
DR	Dietary restriction
DR_AL	Diet switch from DR back to AL feeding
Drosophila	Drosophila melanogaster
ECG	Electrocardiography
Elovl6	ELOVL Fatty Acid Elongase 6
EM	Electron microscopy

FACS	Fluorescent activated cell sorting
Fasn	Fatty acid synthase
FBS	Foetal bovine serum
FFA	Free-fatty acid
Fig.	Figure
g	Gravity
GLME	Generalized linear mixed effect models
GTT	Glucose tolerance testes
h	Hour
HR	Heart rate
Immunohistochemistry	IHC
ISC	Intestinal stem cell
ITT	Insulin tolerance test
MAT	Mesenteric adipose tissue
min	Minute
miRNA	Micro RNA
ml	Millilitre
mRNA	Messenger RNA
mtDNA	Mitochondrial DNA
NMR	Nuclear magnetic resonance
ORO	Oil Red O
OVN	Overnight
PBS	Phosphate-buffered saline
PBS-T	PBS supplemented with Triton X- 100
Pol2ri	Polymerase (RNA) II (DNA directed) polypeptide I
PQ interval	Time between atrial and intraventricular depolarization
PR interval	Time between atrial and intraventricular depolarization
QRS complex	Conduction time and depolarization of the right and left ventricles
Q-RT-PCR	Quantitative real-time polymerase chain reaction
QT dispersion	Difference between the longest and shortest QT interval

QT interval	Time between ventricular de- and repolarization
QTc dispersion	Heart rate corrected QT dispersion
QTc interval	Heart rate corrected QT interval
RER	Respiratory exchange ratio
RNA	Ribonucleic acid
RR interval	Time between two ECG peaks
RT	Room temperature
SC	Stem cell
SD	Standard deviation
Sec	Second
SEM	Standard error of the mean
Srebf1	Sterol Regulatory Element Binding Transcription Factor 1
ST segment	End of ventricular de- and the beginning of the repolarization
SVF	Stromal vascular fraction
TAC	Triacylglycerol
TBS	Tris-buffered saline
TBS-T	Tris-buffered saline with 0.1% Tween 20
TF	Transcription factor
TMA	Tissue microarray
UCP1	Uncoupling protein 1
WAT	White adipose tissue
WB	Western blot

Summary

Dietary restriction (DR), a reduction in food intake without malnutrition extends lifespan and improves health in animals ranging from yeast to rhesus monkeys. In mice, DR extends lifespan if the treatment is started early in life, however, late-onset treatment of 24 months old mice fails to extend lifespan, and it is currently not clear at which age mice become unresponsive to the DR treatment. Furthermore, the molecular mechanisms underlying late-life refractoriness to DR are currently elusive.

In my PhD work, I have conducted a systematic analysis of DR switches at different ages in female mice. Mice were switched from ad libitum (AL) to the DR diet at 3, 12, 16, 20 and 24 months of age and their lifespan and health were subsequently assessed in comparison to chronic AL controls. Mice in which DR was initiated at 3 months of age showed the longest lifespan extension. Interestingly, however, initiation of DR at 12M and 16M of age almost fully recapitulated the lifespan extension with early life DR onset. In contrast, onset of DR at 20M and 24M led to only a slight lifespan increase compared to chronic AL feeding, suggesting that mice become unresponsive to DR-mediated lifespan extension between 16 and 20 months of age. Glucose metabolism, body composition, heart function and memory were improved by DR independent of the age of DR onset, suggesting that lifespan and health span can at least partially be uncoupled by the late life dietary switches. On the other hand, reduced tumour load and frailty as well as increased fitness and insulin sensitivity were correlated with the lifespan increase upon chronic or mid-life onset of DR. Noteworthy, liver tumour incidence, a major tumour type in these mice, was only reduced when the DR treatment was started at 3M and 12M but not at 16M of age, thus uncoupling liver tumour incidence from DR- mediated lifespan extension.

Furthermore, I investigated tissue-specific, molecular effects of DR, in the white adipose tissue (WAT) and the small intestine, to identify mechanisms responsible for the lifespan differences. I observed increased macrophage infiltration in old AL WAT, suggesting that chronic DR prevents WAT inflammation during ageing. Interestingly, DR switch groups exhibited increased macrophage infiltration four months post-switch to DR, which resolved upon longer DR duration, suggesting increased clearance of apoptotic or maladaptive adipocytes during post switch WAT remodelling. Additionally, DR onset at 16 or 20 months induced transcriptional reprogramming in the WAT but the expression profiles failed to reach chronic DR levels even after long-term treatment, indicating a retained memory of prior AL feeding in the WAT. Moreover, DR and DR switch mice displayed shorter colon lengths and reduced hypodense Paneth cell granules in the small intestine at old age compared to chronic AL animals, indicating that DR improved intestinal health and plasticity irrespective of the age of onset.

However, late-onset DR did not improve the outgrowth capacity of intestinal organoids, potentially due to an inability to adapt to *in vitro* full feeding conditions after DR was initiated.

In conclusion, I discovered that DR differentially affects lifespan and health span depending on the age of DR onset in mice. Initiation of DR within the DR responsive period at 3, 12 or 16 months of age reverses the detrimental effects of previous AL feeding and improves survival and overall health at old age. In contrast, late-life initiated DR at 20 or 24 months has only limited beneficial effects as mice were mostly unresponsive towards the newly imposed dietary intervention. In the future, we aim to further characterize the underlying mechanism of DR-mediated lifespan and health span extension with the prospect of a therapeutic potential for healthy ageing in humans.

.

1. Introduction

1.1 Ageing

1.1.1 Definition of ageing and biological background

Ageing is defined as a gradual decline of various cellular and molecular phenotypes and overall tissue function, which ultimately leads to the death of the individual. An exception is the hydra, a small Hydrozoa from the *Cnidaria* phylum, which is thought to be the only organism which can escape ageing due to unlimited regenerative capacities (Martínez, 1998). The ageing rate differs greatly depending on the maximum lifespan of the species, and bigger animals, such elephants or whales are usually longer lived compared to smaller species, such as rodents (Jones et al., 2014), although with notable exception including birds and bats (Munshi-South & Wilkinson, 2010). Moreover, most species including humans, show sex-specific differences in lifespan, in which females are often longer lived compared to males (Lemaître et al., 2020). Factors which might contribute to reduced male lifespan in mammals, include the unique genetic setup with one X chromosome as well as differences in mating strategies, immune system and sex hormones (Regan & Partridge, 2013). In contrast, increased tendency towards risky behaviour such as smoking, drinking and more dangerous jobs are thought to negatively influence lifespan in human males (Regan & Partridge, 2013). However, there are some notable exceptions to the rule that males are shorter-lived than females due to their genetic sex chromosome setup.

The first exception is the naked mole rat, which despite a rodent-like size can live up to 30 years and maintains the health span almost until death (Edrey et al., 2011) irrespective of the sex chromosome setup or the reproductive state (Ruby et al., 2018). Additionally, evidence suggests that the use of other sex determination mechanism (SDM) can determine the lifespan of males or females. Birds (Austad & Fischer, 2016) or butterflies (Huylmans et al., 2017) use the ZW SDM, which is opposite from the mammalian XY setup. In the ZW determination system, females and not males are heterogametic and possess ZW sex chromosomes, whereas males possess ZZ sex chromosomes (Austad & Fischer, 2016). Following the hypothesis that heterogametic individuals are thought to be short-lived compared to homogametic (Lemaître et al., 2020), female birds or butterflies should have a shorter lifespan compared to males. Although not many lifespan studies have been conducted in birds, evidence suggests that indeed female birds are shorter lived than their male counterparts (Clutton-Brock & Isvaran, 2007). Additionally, other SDM exist in the animal kingdom, for example the temperature-dependant system which is utilized by reptile species and which relies on the outside temperature for sex hormone production independently of genetic sex determinants (Warner & Shine, 2008). In reptiles, no difference in adult mortality was observed

in species that utilized sex chromosome or temperature dependant SDM (Bókony et al., 2019), however it is possible that longevity determines the SDM, as many long-lived turtles favour the temperature over the genetic determinant system (Sabath et al., 2016). Moreover, sex does not have to be fixed throughout life, as demonstrated by distinct teleost fish species, such as *Chrysoblephus puniceus* or *Diplodus sargus*, which are changing their sex from male to female or female to male in adulthood (Benvenuto et al., 2017). While this sequential hermaphroditism improves the reproductive success of the individual fish (Benvenuto et al., 2017), it is currently unclear whether or how changing the sex in adulthood affects longevity. Studies in different round worm species yield contradicting results, attributing hermaphroditic worms a longer life in case of *Caenorhabditis elegans* (Hotzi et al., 2018) or a shorter life in case of *Pristionchus nematodes* (Weadick & Sommer, 2016) compared to male worms. Therefore, additional studies using more species with different SDM are required, to fully unravel the effect of sex chromosome or SDM and longevity.

Despite the fact that all humans age, we have just started to fully understand the changes occurring during the ageing process. Recently, nine cellular and molecular hallmarks have been proposed to impact on the ageing process, namely telomere attrition, genetic instability, altered nutrient signalling, stem cell exhaustion, epigenetic alterations, cellular senescence, loss of proteostasis, mitochondrial dysfunction and altered intracellular communication (López-Otín et al., 2013). Many of these hallmarks are tightly interconnected and continuous cellular damage ultimately leads to reduced tissue function during ageing. Nonetheless, as our current knowledge is limited, a better understanding of the ageing process itself and the underlying dysregulation of molecular parameters, which take years and even decades to manifest into age-associated diseases, is required (López-Otín et al., 2013).

1.1.2 Ageing as risk factor for age-associated diseases in humans

Over the last 150 years, advances in medicine, e.g. reduction of maternal and child mortality, vaccinations against common viral and bacterial diseases and better hygiene resulted in a steady increase in human life expectancy (World Population Ageing 2019, United Nations, 2019). However, increased life expectancy of the population cannot be equated with an increasingly healthy society (Jagger et al., 2008). On the contrary, old age is the main risk factor for various age-associated diseases, such as cardiovascular disease (CVD), diabetes, dementia (Niccoli & Partridge, 2012), cancer (Fontana et al., 2009) and increased frailty due to musculoskeletal changes (Cesari et al., 2009; Greco et al., 2019). Moreover, suffering from an age-associated disease drastically reduces the quality of life for the elderly, especially as most old people usually suffer from multiple comorbidities in the last years of their lives (Flatt

& Partridge, 2018). Additionally, an ageing population in bad health brings major challenges to the current pension and health care system as well as reducing the quality of life of the individual. Consequently, novel interventions to ameliorate the ageing process itself are required to promote healthy ageing and to expand an individual's health span with reduced risk to succumb to age-associated diseases. However, not every elderly individual is equally affected by ageing and some centenarians maintain their physical health until death (Partridge, Deelen, & Slagboom, 2018), thus highlighting the complex nature of ageing with inter-individual variation and various factors which contribute to this process (Fontana et al., 2010).

1.1.3 Factors affecting the ageing process in humans

Various genetic, dietary and environmental factors influence the human ageing process, but the individual contribution of each of these factors is not entirely clear (Partridge et al., 2018). Recent studies based on large pedigrees of long-lived families associated specific single-nucleotide polymorphisms (SNP) for example in the APOE4 gene with reduced (Deelen et al., 2019; van den Berg et al., 2019), or in the chromosome 5q33.3 gene locus with increased, lifespan (Deelen et al., 2014). However, longevity appears to be only heritable between 12-25% (Partridge, Deelen, & Slagboon, 2018), suggesting that diet and environmental factors are more important contributors to human longevity. Dietary habits and nutrition, as well as the influence of different macronutrient components in the diet have recently gained much interest in their putative role in promoting healthy ageing. In particular, the Mediterranean as well as the Okinawa diets have been associated with longevity and improved health at old age and a reduced incidence of CVD or cancer (Bonaccio et al., 2018; Miyagi et al., 2003). Both diets are rich in vegetables, poly unsaturated fatty acids from fish and nuts as well as low in meat and processed saturated fatty acids (Trichopoulou et al., 2014; Willcox et al., 2009; Yasuo Kagawa, 1978). In contrast, the Western diet is often highly processed and rich in meat, carbohydrate and saturated fatty acids and is associated with increased risk for cancer (Steck & Murphy, 2020), as well as obesity, CVD and metabolic syndrome (Drake et al., 2018). Not only dietary habits but also other environmental factors can influence the ageing process. Chronic psychological (Miller et al., 2011) and psychosocial stress (Rutters et al., 2014) as well as pollution (Burnett et al., 2018; Landrigan et al., 2018) or smoking (Pikala et al., 2020) negatively affects human health and increase mortality. Therefore, ageing and lifespan studies in humans are challenged by non-controllable factors, such as differences in lifestyle factors or intra-individual genetic variation. Moreover, the long lifespan of the individual by itself is a major limitation for ageing studies in the human population.

In contrast, model organisms, such as yeast, the invertebrate nematode *Caenorhabditis elegans* (*C. elegans*), the fruit fly *Drosophila melanogaster* (*Drosophila*) and different vertebrate species, such as rodents, the killifish or marmosets allow the study of life- and health span extending interventions under controlled laboratory conditions and have shorter lifespans than humans.

1.1.4 Utilizing model organisms to study ageing

Using model organisms has certain advantages compared to humans, such as shorter generation times which facilitate lifespan analyses, the possibility to manipulate diet, treatments or genes or the use of genetically identical individuals to reduce biological variation (Flatt & Partridge, 2018; Taormina et al., 2019). However, different model organisms have different strengths and are not always equally well suited to study all aspects of the ageing process. For instance, yeast cells, are well suited to study conserved cellular processes, such as nutrient sensing pathways, autophagy, and organelles, and the effects of genetic or pharmacological interventions, but they lack multicellular tissues and a systemic environment. In contrast, adult flies and *C. elegans* not only contain different organ systems but these organs are composed of post-mitotic cells and a stem cell compartment, similarly to some organs in adult humans (Bozcuk, 1972; Kurtz et al., 2019; Olsen, Vantipalli, & Lithgow, 2006), thus allowing systemic analysis of genes, diets or interventions in the context of the ageing organism. One of the major advantages of these invertebrate model organisms is the possibility to conduct large genetic screens in a reasonable timeframe allowing the identification of novel pathways and mechanisms involved in the regulation of the ageing process. Moreover, invertebrates show age-related deterioration similar to what is observed in humans, e.g. *Drosophila* females exhibit age-associated decline in gut barrier function as well as hyperplastic growth in the intestine (Regan et al., 2016) and reduced locomotor function measured by climbing ability (Grotewiel et al., 2005). However, there are also major differences between the invertebrate model organisms and humans that include the lack of a skeletal system, a closed cardiovascular system (Haun et al., 1998; Rotstein & Paululat, 2016) and crucial singular organs such as the liver (Gutierrez et al., 2007). Thus, the effect of ageing on these specific organ systems cannot be studied in invertebrates and therefore requires the use of vertebrate or even mammalian model organisms. In this context the killifish has recently gained interest as a vertebrate model organism in ageing research, due to its short lifespan of only a few months, fast tools for genetic manipulation and similar organs compared to humans (Harel et al., 2015). Mammalian model organisms like mouse or marmosets share an even higher similarity to humans with a high degree of genetic similarity of 83% (Taormina et al.,

2019) or 93% (Worley et al., 2014), respectively. Furthermore, these models allow the systemic analysis of ageing on multiple organs including musculoskeletal, the lymphatic, the vascular as well as the cardiovascular system. Another advantage of using rodents (Pettan-Brewer & M. Treuting, 2011) or rhesus monkeys (Mattison et al., 2017; Yamada et al., 2018) to study ageing, is the incidence of similar age-associated diseases and comorbidities, e.g. cancer or increased frailty, as elderly humans, thus enabling comparisons of different intervention outcomes between species. Although more studies are possible using mammals, genetic manipulations, lifespan studies as well as general handling require extensive training, ethical permits and are more time consuming and expensive compared to invertebrate research. Thus, it is important to evaluate which model organism is best suited to address a given research question. In summary, model organisms are crucial to gain a better understanding of the ageing process and to develop putative anti-ageing treatments**.** The next sections shed light on different genetic and pharmacological approaches that extend lifespan in model organisms and are therefore possible candidate interventions to also improve ageing in humans.

1.1.5 Genetic or pharmacological modulation of nutrient responsive pathways can extend lifespan or health span in model organisms and humans

Two evolutionarily conserved nutrient responsive pathways, are the insulin/ insulin-like signalling (IIS) and the mammalian target of rapamycin (mTOR) pathways, which are involved in various different cellular functions including cellular growth, survival, metabolism, autophagy and stress response. Interestingly, downregulation of both pathways by genetical or pharmacological interventions can ameliorate ageing in model organisms as diverse as worms, flies and mice (Fontana, Partridge, et al., 2010). Genetic manipulation of the insulin receptor (IrsKO) or it's substrate (Irs1KO), the growth hormone receptor (GHRKO) or the S6 kinase (S6K1KO) have been demonstrated to extend lifespan across species (Gems & Partridge, 2013). The first evidence that the IIS pathway is implicated in ageing, was produced in a pioneering study by Kenyon and colleagues, which studied the insulin receptor homologue *daf-2* in *C. elegans* and proved that *daf-2* mutant worms are long-lived (Kenyon et al., 1993). This ground-breaking study was soon followed by similar discoveries on lifespan extension upon genetic deletion of the insulin receptor *chico* (Clancy et al., 2001) or the *Drosophila insulin-like peptides 2-3,5* (Grönke et al., 2010) in *Drosophila*. Similarly, mice carrying loss-of function mutations in *Ghr* (Coschigano et al., 2000), *Igf-1* (Holzenberger et al., 2003), *Irs1* (Selman et

al., 2008; Selman et al., 2011) or *S6K1* (Selman et al., 2009) are significantly long-lived compared to their wild type littermates.

Furthermore, in addition to a beneficial effect on survival, downregulation of the IIS network also has beneficial effects on overall health (Bartke & Brown-Borg, 2004) or fitness (Selman et al., 2008) and reduces the tumour incidence at old age in mice (Ikeno et al., 2009). However, full body knockout of these growth pathway components results in smaller body size compared to littermate controls and it was only recently possible to uncouple the lifespan effect from the developmental defects in *Drosophila* (Yamamoto et al., 2020). Interestingly, humans with a loss of function mutation in the GHR exhibit a similar dwarfism and obesity phenotype as GHRKO mouse models and are resistant to diabetes and cancer growth, indicating an evolutionary conserved mechanism for health span extension upon reduced GHR pathway activity (Guevara-Aguirre et al., 2011). However, there is currently no evidence that GHR deficient humans also have an extended lifespan (Guevara-Aguirre et al., 2011; Shevah & Laron, 2007). Still, GWAS studies have identified SNPs in protein coding genes of the IIS or mTOR signalling pathway components in human centenarians, suggesting that modulations in these pathway components might also influence human lifespan (Deelen et al., 2013; Van Heemst et al., 2005).

In addition to genetic interventions that can increase survival, drug repurposing has gained much interest in recent years to ameliorate the ageing process. One of the most prominent examples of drug repurposing to combat ageing is rapamycin. Rapamycin was discovered in 1972 as an antifungal agent in the Easter island native bacterium *Streptomyces hygroscopicus* (Sehgal et al., 1975) and has been shown to inhibit the mTORC1 complex and thereby reduces cellular growth (Seto, 2012). High doses of rapamycin are used in the clinic as an immune suppressive agent to reduce the graft versus host rejection after transplantation (Benito et al., 2001). One drawback of rapamycin treatment, which must be carefully considered when starting the therapy, are adverse effects on metabolism (Lamming et al., 2012) and also skin disorders (Mahé et al., 2005) and immune function (Morelon et al., 2001). However, due to the growth inhibiting phenotype across species, rapamycin has also gained much interest as putative anti-ageing and anti-cancer intervention. Indeed, low doses of rapamycin significantly extend both male and female lifespan in mice when initiated early (Miller et al., 2014) or late (Harrison et al., 2010) in life and delay several ageing associated phenotypes (Wilkinson et al., 2012). The finding that administration of a low dose rapamycin analogue improved the immune response after flu vaccination and reduced infection rates in two recently published clinical studies in elderly humans (Mannick et al., 2014, 2018), indicates that rapamycin might also have beneficial effects on human ageing. This hypothesis will be further evaluated in a large-scale clinical study in the US (Participatory Evaluation (of) Aging (With) Rapamycin (for) Longevity Study (PEARL) study NCT04488601 (2020) Website

https://clinicaltrials.gov/ct2/show/NCT04488601 (last accessed January 26th 2021)). In addition, bioinformatic approaches are being used to predict new drugs or drug combinations for drug repurposing in ageing research (Dönertaş et al., 2019).

Despite many insights on the effect of specific genes or pharmacological interventions and lifespan extension in model organisms, these insights cannot be translated to humans without further studies, as we currently do not have the tools to genetically modify the IIS, mTOR or GHR in humans, nor do we have any knowledge on the long-term effects of rapamycin treatment. However, as mentioned previously, dietary habits have a major impact on the ageing process and implementing nutritional changes towards a healthier diet can positively affect human health. One of the most extensively studied dietary interventions, which extends lifespan in a variety of model organisms and has shown promising short-term results in humans, is dietary restriction (DR), which will be discussed in more detail in the following section.

1.2 Dietary restriction (DR)

1.2.1 The effect of DR on lifespan in different model organisms

Dietary restriction (DR) refers to the reduction of food intake without malnutrition and was first described in 1935 in a pioneering lifespan study in rats (McCay, Crowell, & Maynard, 1935). As to-date, DR is the most robust lifespan-extending intervention in a wide range of species including invertebrates such as yeast, nematodes and flies (Fontana & Partridge, 2015; Leonov et al., 2017) and vertebrate species such as killifish (Terzibasi et al., 2009) and rodents (Swindell, 2012). Moreover, two independent DR studies in rhesus monkeys reported improved overall health and reduced age-associated pathologies upon lifelong DR treatment (Colman et al., 2009; Mattison et al., 2012). Survival was only positively affected in one of the studies (Colman et al., 2009). The discrepancy between the studies is likely explained by different control diets (Mattison et al., 2012), whereas one study used ad libitum feeding (Colman et al., 2009), the other study used a partially restricted diet (Mattison et al., 2012), which might by itself positively affected survival (Richardson et al., 2016). In rodents, killifish or rhesus monkeys, DR is usually accomplished by a reduction of the daily food portions between 10- 40% compared to control *ad libitum* (AL) feeding, depending on the stringency of the DR regimen (Mitchell et al., 2015; Richardson et al., 2016). In contrast, *Drosophila* models of DR usually utilize a 50-75% reduction in yeast content in the food but retain AL food access. In flies, reduction in dietary protein but not calories is the main driver underlying the beneficial

effects on lifespan (Mair, Piper, & Partridge, 2005). In yeast, reduction of dietary glucose is used to mimic DR (Leonov et al., 2017). However, while the beneficial effects of DR on overall health and lifespan in model organisms are unchallenged, the underlying cellular and molecular mechanisms of DR still remain mostly elusive.

1.2.2 Effects DR on different hallmarks of ageing

Recent studies have investigated the effect of DR on the hallmarks of ageing to evaluate whether DR can ameliorate these during ageing. Deregulated nutrient-sensing is one of the hallmarks of ageing and the effect of ageing on e.g. mTOR or IIS signalling has been intensively studied due to the role of these signalling networks in cancerous growth or metabolic disease (Fontana, Partridge, et al., 2010). Interestingly, rodents exhibit decreased IGF-1 serum levels under DR (Dunn et al., 1997), which indicates a functional link between DR and the IIS pathway in DR-mediated longevity. Moreover, DR reduces mTORC1 and mTORC2 signalling in the liver in a time- dependant manner (Tulsian et a., 2018). Activation of the IIS or mTOR pathway triggers downstream signalling events, which impact on translation, proliferation or inhibition of apoptosis (Broughton & Partridge, 2009; Saltiel & Kahn, 2001). Given that both IIS and mTOR are activated by nutrients (Niccoli & Partridge, 2012), it is likely that decreased nutrient availability under DR alters activation of these fine-tuned signalling pathways, thus leading to different beneficial cellular outcomes which are yet to be identified. Indeed, genetic ablation of the nutrient sensor Sestrin or its amino acid sensing function has been recently shown to abrogate the lifespan extension upon DR (Lu et al., 2020), indicating that functional nutrient sensing is crucial to mediate the beneficial effects of DR in *Drosophila*. Interestingly, Ames dwarf and growth factor releasing hormone KO (Bartke et al., 2007; Sun et al., 2013) but not GHRKO mice (Bonkowski et al., 2006) are even longer lived upon DR, suggesting at least a partially additive effect of growth hormone signalling and DR.

Aside from deregulated nutrient sensing, epigenomic and genomic changes, such as hypermethylation of tumour suppressor genes, genomic instability, telomere attrition and cellular senescence are implicated in tumour formation or loss of tissue function. Similar to the beneficial effects on nutrient sensing, DR positively affects the epigenome as well as genomic stability, cellular senescence and telomere length. Short-or long-term DR reduces spontaneous mutations in various tissues (Garcia et al., 2008), potentially due to increased DNA repair (Cabelof et al., 2003). Furthermore, DR protects against heterochromatin loss (Jiang et al., 2013) and induces local hypermethylation associated with decreased lipid metabolism and shorter triglyceride chains in mice (Hahn et al., 2017). Moreover, telomere length is maintained under DR (Vera et al., 2013) and fewer senescent cells are present in

tissues with high or low cell turnover and could thus improve tissue function during ageing (Wang et al., 2010). In addition to accumulation of cellular damage, aged tissues exhibit stem cell depletion or exhaustion, which reduces the tissue's capacity to regenerate, thus contributing to the functional decline. Interestingly, DR attenuated loss of muscle mass in rhesus monkeys or mice (Colman et al., 2009; Jang et al., 2012) and improved stem cell function in the muscle (Cerletti et al., 2013) as well as the small intestine (Mihaylova et al., 2018; Yilmaz et al., 2012) suggesting a protective effect of DR on stem cells.

Mitochondrial dysfunction can greatly impair tissue function and can negatively contribute to ageing by increased generation of reactive oxygen species (ROS), thus inducing intracellular oxidative stress. Moreover, mitochondrial dysfunction has been associated with neurodegenerative disorders, such as Alzheimer's disease or metabolic syndrome in humans (Monzio Compagnoni et al., 2020; Peoples et al., 2019). Moreover, increased cellular oxidative stress damages the proteome, leading to misfolded and non-functional proteins, which require refolding via chaperones or proteolytic degradation using the ubiquitin proteasome system or autophagy (Hipp et al., 2019). However, proteostasis is decreased during ageing and the accumulation of misfolded proteins in cells can cause protein aggregation, cell death and subsequently contributes to disease formation (Hipp et al., 2019). Strikingly, DR leads to increased mitochondrial biogenesis (Nisoli et al., 2005; R. Zhang et al., 2019) and reduced oxidative stress (Qiu et al., 2010), thus retaining mitochondrial function in several tissues during ageing, such as the BAT and the muscle (Lanza et al., 2012; Valle et al., 2008). Furthermore, DR increased proteostasis (Matai et al., 2019) and was associated with increased lifespan in a strain-dependant manner in mice (Mitchell et al., 2016).

Lastly, DR has also been shown to protect against altered intercellular communication. The aged immune system for example exhibits skewing towards increased myeloid lineage and decreased lymphoid lineage differentiation (Rossi et al., 2005), which is improved under DR (Chen et al., 2003). Additionally, DR maintains metabolic health (Mitchell et al., 2016), decreases energy expenditure compared to AL controls (Cameron et al., 2011) and stably reduces body weight (Hahn et al., 2017). By improving different hallmarks of ageing, DR can protect against diabetes or cancer (Colman et al., 2012; Weindruch et al., 1986) and improves neurodegenerative diseases and frailty in several model organisms (Wang et al., 2005; Yamada et al., 2018), thus making it a potential therapeutic intervention for human ageing. In summary, DR affects a plethora of different cellular as well as systemic processes and it is currently unclear which of these are causal for the beneficial effects of DR on health and lifespan.

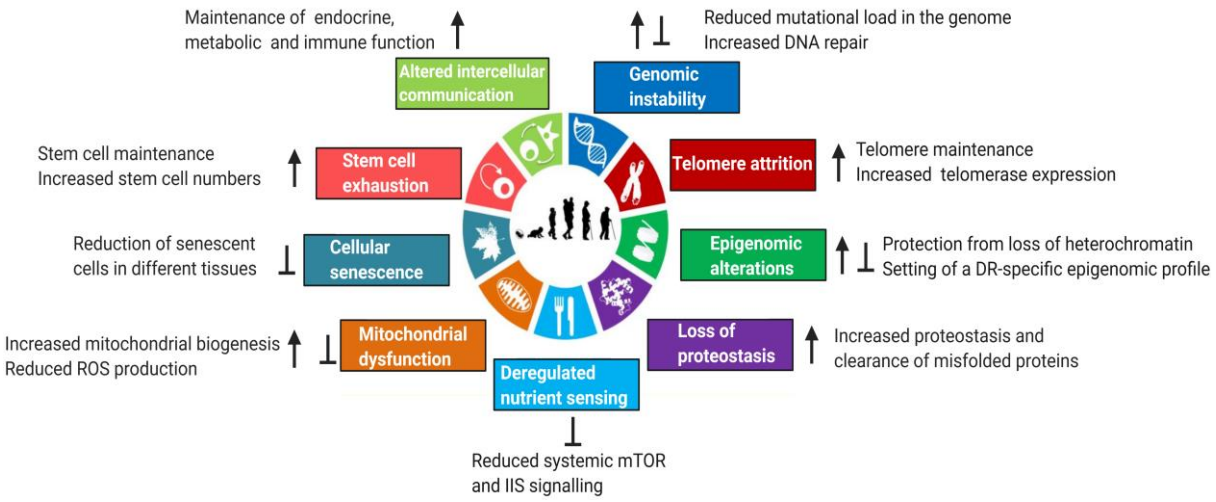

Figure 1.2. 1: The beneficial effects of DR on the nine hallmarks of ageing.

Arrows indicate improvement by DR and inhibitory marks indicate reduction upon DR. Adapted from López-Otín et al., 2013 and schematic created using BioRender.com.

1.2.3 Lessons of late-life DR in mice

In most rodent studies, DR is implemented in young animals directly after weaning or adult-onset at the age of three months and is maintained lifelong until the animals die. However, despite many beneficial effects of DR on health and survival, long-term DR has been shown to cause detrimental effects, such as reduced wound healing (Reed et al., 1996), increased susceptibility to infection as well as decreased bone density (Flatt & Partridge, 2018; Villareal et al., 2006). Therefore, identifying the latest age of onset, at which DR still exhibits beneficial effects on health and survival could limit the duration of DR and thus reduce potential side effects. Furthermore, this information would be valuable in the context of human ageing, to know at what age DR could still be used effectively as an anti-ageing intervention. Surprisingly, however, in contrast to early onset DR, much less information is available about the effects of late-onset DR on subsequent health and survival and on associated tissue specific molecular changes. A pioneering study by Weindruch and colleagues showed in 1982 that mid-life DR onset at 12M of age increased murine lifespan and was associated with reduced lymphoma incidence in male mice (Weindruch et al., 1982). Consistently, DR onset at 19M of age significantly decreased mortality, reduced tumour load and induced transcriptional reprogramming in the liver of male hybrid mice (Dhahbi et al., 2004). However, as both studies did not include chronic DR controls, it is unclear if animals upon 12M or 19M onset DR were equally long-lived compared to chronic DR or whether the late-life switches affected survival to a lesser extent. Moreover, the results on 12M or 19M DR onset contrast other findings in

male mice, which demonstrated that switching male mice from AL feeding to DR at 17M of age even increased mortality in different murine strains (Forster et al., 2003). Similarly, late-onset DR at 24M of age did not acutely decrease mortality rates of female mice after the switch, and had only mild effects on the longer term (Hahn et al., 2019). Additionally, mice, which were switched from lifelong DR back to AL feeding, showed increased mortality and reduced survival. Nonetheless, late-onset DR in rats or mice has been shown to improve cognitive as well as cardiac function, indicating that DR can still induce some, but potentially not all, beneficial effects compared to early onset treatment (Singh et al., 2012; Yan et al., 2013).

Differences in the diet composition, the stringency of the DR regimen, as well as sex- or strain-specific responses towards DR can all contribute to variable results in studies of DR. Mitchell and colleagues demonstrated in 2016 that 20% or 40% DR had differential effects on the lifespan of two commonly used strains DBA/2J or C57B6J (Mitchell et al., 2016). Interestingly, a lifelong 40% reduction of food intake shortened, whereas a 20% reduction increased the lifespan of C57B6J females, whereas DBA/2J females were long-lived with both DR stringencies. In contrast, male C57B6J showed lifespan extension in both DR groups but male DBA/2J mice showed detrimental effects early in life but are longer lived at old age upon 40% restriction. In general, female mice show greater response to DR and lifespan extension upon DR compared to their male counterparts, suggesting that the animal's sex also influences the effects of DR (Liao et al., 2010; Mitchell et al., 2016). Moreover, DR can either prolong or shorten murine lifespan depending on the genetic background of the utilized mouse strain, demonstrating that genes play an important role in the DR-mediated effects on lifespan (Liao et al., 2010). Therefore, systematic studies with additional DR onset groups are required to identify at which point in murine life, initiation of DR can still improve health and survival. Moreover, the identification of a DR responsive period in mice could help to define at which age humans should start restricting their food intake to gain beneficial effects late in life.

1.2.4 Lessons of DR in humans

Due to lifespan and health span extending effects in various model organisms, DR has also gained much interest as potential anti-ageing intervention in humans. Therefore, several clinical studies have assessed the effect of short-or-long-term DR on clinical parameters of heart function (Meyer et al., 2006), serum protein or metabolite composition (Barazzoni et al., 2020; Fontana et al., 2004) and the metabolism (Heilbronn et al., 2006). In obese but also non-obese humans DR caused health benefits including improved insulin sensitivity (Barazzoni et al., 2020; Fontana et al., 2016) and reduced levels of circulating growth factors (Fontana et al., 2009), cholesterol (Walford et al., 1992), thyroid hormones or arteriosclerosis risk factors

(Omodei & Fontana, 2011; Walford et al., 2002). Additionally DR lead to a reduction in inflammation (Meydani et al., 2016) and energy expenditure in normal or overweight humans (Heilbronn et al., 2006; Redman et al., 2018). Moreover, reduced circulating insulin and IGF-1 levels indicate, that DR in humans leads to a significant reduction in IIS signalling similar to what has been observed in model organisms (Fontana et al., 2016). Additionally, obese humans benefit from short-term DR with loss of body weight and fat mass, thus reducing detrimental effects of obesity or diabetes risk upon dietary changes (Barazzoni et al., 2020; Beekman et al., 2020). Members of the caloric restriction society, who conduct self-imposed long-term DR, show reduced thickness of the carotid artery intima- media, a known CVD risk factor (Fontana et al., 2004) and improved diastolic function (Meyer et al., 2006) and are thus potentially protected from age-associated CVD. Therefore, DR could be a strong intervention to promote healthy ageing in humans but more long-term studies are needed to elucidate the effect of DR on age-associated diseases and longevity. However, DR in humans requires a high degree of individual dedication to adhere to the strict dietary regimen and decreased compliance in clinical studies makes it difficult to evaluate long-term protective effects of DR during ageing in human subjects. As a result, it is important to narrow down, at which age switching the diet from AL to DR still extends life span and exhibits beneficial effects on the overall health and tissue level in laboratory animals to define a time point in human life when DR can achieve positive effects on health. Furthermore, additional studies are required to understand the cellular and molecular effects of DR, in order to pinpoint at which age initiation of DR is beneficial in humans or develop DR-mimicking drugs for convenient health improvement at old age and to define the starting point of these interventions in human ageing.

1.3 The White adipose tissue (WAT)

1.3.1 Motivation to study the WAT

The white adipose tissue (WAT) is a heterogenous tissue, which can respond to different energy states and nutrient availability with tissue expansion or shrinkage of the stored lipids in mature adipocytes (Choe et al., 2016). Most notably, the WAT is the tissue which is most affected by obesity (Giordano et al., 2013) or DR (Racette et al., 2006) and can thereby directly affect the metabolism. The following sections provide an overview on the types of WAT, the differentiation process for mature adipocytes as well as the role of the WAT in the systemic regulation of the metabolism and changes during the ageing process.

1.3.2 Types of adipose tissue, morphology, sexual dimorphism and function in the murine and human body

The adipose tissue (AT) is a heterogeneous tissue, which is composed of mature adipocytes and stromal vascular fraction cells, which encompass different immune cells, such as macrophages, endothelial cells, adipocyte precursor and stem cells (Church et al., 2014). The primary function of the AT is the storage of excessive energy in the form of free fatty acids (FFA), which are stored as triacylglycerides in lipid droplets inside the cytoplasm. Two types of adipose depots, namely brown adipose tissue (BAT) and white adipose tissue are present within the human and murine body and they have distinct biological functions and display characteristic morphological features. White adipose depots include the subcutaneous adipose tissue (SCAT), the mesenteric adipose tissue (MAT) as well as the perigonadal adipose tissue (WAT) (Choe et al., 2016). Mature white adipocytes of the WAT, MAT and SCAT are characterized by one unilocular lipid droplet, containing triacylglycerol and cholesteryl ester, which encompasses almost the entire cell with little cytoplasm and a small nucleus located at the cell membrane. The SCAT located below the skin is mainly responsible for insulating the body against cold but also plays a role in energy storage and in protection of underlying organs against force (Wang et al., 2003). The MAT surrounds the intestine and, aside from its function in fat storage, also contributes to the maintenance of the intestinal barrier (Wu et al., 2018). Moreover, the MAT harbours lymphatic vessels and mesenteric lymph nodes, which are responsible for lipid uptake and serve as immune checkpoint against penetrating intestinal pathogens (Bernier-Latmani et al., 2015; Macpherson & Uhr, 2004).

In contrast, the BAT is mainly involved in adaptive thermogenesis in mice and human new-borns and is located in the murine intrascapular or the human supraclavicular region (Entringer et al. 2017; Gilsanz, Hu, and Kajimura 2013; Nedergaard et al., 2007). Moreover, studies have demonstrated that the BAT plays a role in thermogenesis upon cold exposure in lean human adults (Coolbaugh et al., 2019; van Marken Lichtenbelt et al., 2009) but BAT depots are depleted upon adult or childhood-onset obesity (Leitner et al., 2017; Rockstroh et al., 2014). Aside from the differences in location and functionality, the morphological features of mature adipocytes in the BAT differ greatly from mature adipocytes in the WAT. Brown adipocytes exhibit multilocular, smaller lipid droplets in addition to multiple mitochondria in the cytoplasm. The main function of the BAT is heat production via uncoupling of the electron transfer chain via the uncoupling protein 1 (UCP1) (Ricquier & Bouillaud, 2000).

Recent studies showed that white adipocytes in the SCAT or WAT can undergo transcriptional and morphological changes that include increased expression of UCP1 and increased mitochondrial biogenesis to resemble a brown adipocyte phenotype, a process called

browning, in response to diet or cold exposure and β3 adrenergic stimulus (Bertholet et al., 2017; Fabbiano et al., 2016; Paschos et al., 2018). Since the BAT takes up FFA from the blood as fuel for heat generation (Saari et al., 2020), metabolic activation of the BAT and WAT browning have gained much interest as potential weight loss intervention in obesity in humans (Betz & Enerbäck, 2018; Li et al., 2018).

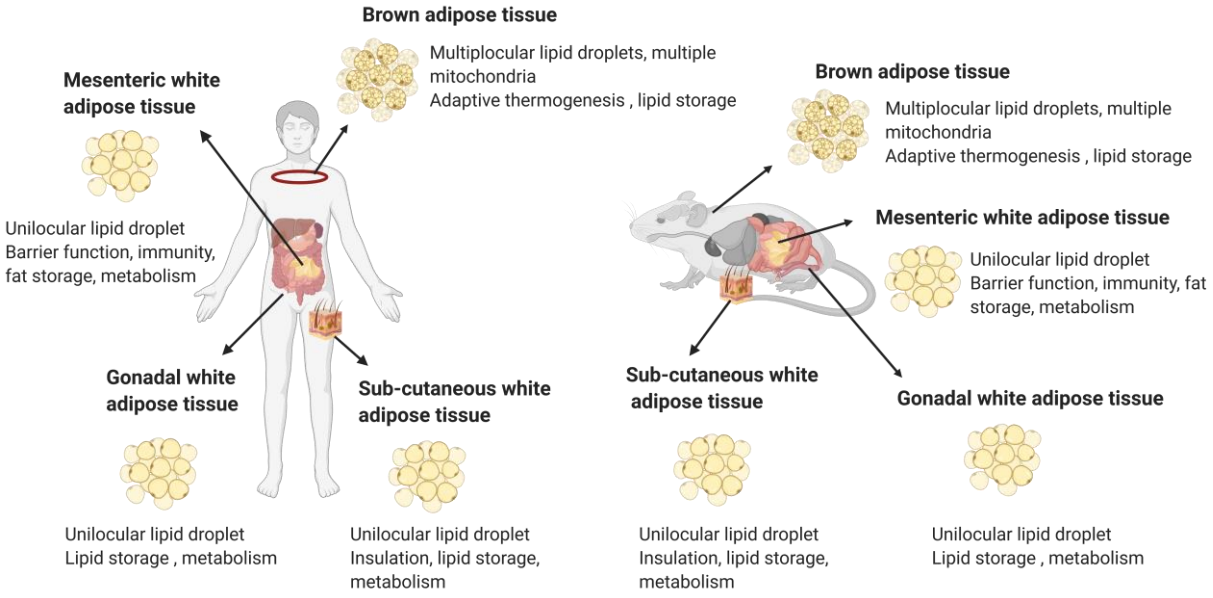

Figure 1.3. 1: The different locations, morphological features and major functions of adipose tissue in humans and mice. *The schematic was created using Biorender.com.*

Interestingly, the AT shows a sexual dimorphism in the distribution of fat at different sites in the body and total body fat steadily increases until adulthood (Fried et al., 2015; Staiano and Katzmarzyk 2012). In particular, the expression of steroid sex hormones during puberty determine the typical sex-specific male or female distribution of body fat in adolescent children (Karastergiou et al., 2012; Maynard et al., 2001). In general, women have a higher body fat content compared to men and the adipose tissue depots are mainly located subcutaneously in the lower body around the femurs and glutes (Lee & Fried, 2017). In contrast, men tend to accumulate more mesenteric and gonadal fat, which is associated with reduced testosterone levels during ageing (Allan et al., 2008) and a higher risk towards cardiometabolic events and increased mortality (Karastergiou et al., 2012; Kuk et al., 2006). Moreover, the adipose tissue is highly flexible and can reduce or increase the depot size towards different nutritional or reproductive stimuli, such as pregnancy (Pujol et al., 2006) or during obesity (Choe et al., 2016).

1.3.3 The differentiation process of mature adipocytes from precursor cells

Despite being a primarily quiescent tissue, mature adipocytes in the WAT are frequently replaced and the annual adipocyte turnover rate in the WAT is approx. 8% in humans (Spalding et al., 2008). Furthermore, it has been demonstrated that the WAT of obese mice contains more replicating cells compared to lean mice, indicating that mature adipocytes in obese mice are more often replaced (Rigamonti et al., 2011). Adipocyte precursor cells can be isolated from WAT by collagenase digestion and subsequent sorted using antibodies (Rodeheffer et al., 2008). Moreover, addition of insulin, PPARγ agonists, such as rosiglitazone, the steroid hormone dexamethasone and the thyroid hormone T3 into the culture medium can induce *in vitro* differentiation of pre-adipocytes.

Pre-adipocytes or adipose tissue stem cells (ATSC) in the WAT undergo mitosis and without adipogenic stimuli remain in the replicative state and continue cell division (Altiok et al., 1997). Upon receiving adipogenic stimuli, the pre-adipocytes exit the cell cycle and induce differentiation into mature adipocytes (Rosen & MacDougald, 2006). Several signalling pathways have been identified, which activate or inhibit adipogenesis via activation or repression of adipogenic effector proteins. For example, signalling via IRS or the bone morphonenetic protein (BMP) promote adipogenesis, whereas the Wnt and the sonic hedgehog (SHH) signalling pathways block adipogenesis (de Sá et al., 2017; Rosen & MacDougald, 2006). Upon activation of the IRS or BMP pathways, the translational repression of adipogenic transcription factors (TF), such as peroxisome proliferator-activated receptors (PPARγ) (Altiok et al., 1997), CCAAT- enhancer- binding proteins (C/EBP) or Krüppel-like factors (KLF) (Rosen & MacDougald, 2006) is abolished which allows translocation into the nucleus and induction of expression of adipogenesis genes, such as Glut4, Insr, leptin or aP2 (Lowe et al., 2011; Rosen et al. 2000). Additionally, several micro RNA (miRNA) influence adipogenesis via translational inhibition of adipogenesis promoting or inhibiting factors. For example, miRNA 27 (miR-27) targets PPARγ mRNA for degradation, thus reducing adipogenesis (Lin et al., 2009), whereas miR-103 accelerated adipogenesis by inhibition of anti-adipogenic factor RUNX1 (Xie et al., 2009).

Upon increased transcription and translation of adipogenesis genes, pre-adipocytes change their morphology and start to accumulate lipid droplets in the cytoplasm. Moreover, *de novo* lipogenesis is activated in maturing adipocytes by increased transcription of several key enzymes involved in de novo lipogenesis, such as ATP-citrate lyase (ACLY), acetyl-CoA carboxylases 1 (ACC1), fatty acid synthase (FASN), stearoyl-CoA desaturase-1 (SCD1) (Song et al., 2018). First, citrate produced by the TCA cycle is used to generate acyl-coA via ACLY,

which in turn is converted into malonyl-coA via ACC1. Next, FASN generates palmitate from malonyl-CoA and the palmitate is then used to generate fatty acids via SCD1 (Song et al., 2018). This increase in fatty acid synthesis leads to increased accumulation of lipids in the cytoplasm and to the formation of a single unilocular lipid droplet surrounded by perilipin, which is a hallmark of mature adipocytes.

1.3.4 The role of the WAT in systemic regulation of metabolism

In addition to fat storage, the WAT is also a crucial secretory and endocrine organ (Galic et al., 2010). Via secretion of adipose-tissue derived cytokines, so-called adipokines, the WAT is involved in inter-tissue cross-talk with other metabolically active organs such as the liver, the pancreas as well as the skeletal and cardiac muscle (Romacho et al, 2014). Adipokines, such as different miRNA (Thomou et al., 2017), fatty acids (Zhai et al., 2010), inflammatory cytokines as well as hormones (Mancuso & Bouchard, 2019) are secreted by the WAT in extracellular vesicles, which are taken up by peripheral organs to regulate energy homeostasis and metabolism (Stern et al., 2016). As described previously, the WAT plays a major function in lipid metabolism by the generation or breakdown of fatty acids of various lengths. Adipose-tissue derived free FFA are signalling molecules generated via lipolysis of triacylglycerol (TAG) (Lass et al., 2011). Secreted FFA bind and activate G-protein coupled receptors (GPCR) (Miyamoto et al., 2016) and induce different cellular functions, such as reduction of inflammation (Glass & Olefsky, 2012), neuronal growth and differentiation (Kamata et al., 2007; Katakura et al., 2009) as well as insulin secretion from pancreas (Itoh et al., 2003). Moreover, in low glucose states, secreted FFA from the adipose tissue serve as fuel source for other tissue (Rosen & Spiegelman, 2006). However, excessive lipolysis and FFA secretion can have cytotoxic effects and can cause insulin resistance in distant tissues, such as the liver or the pancreas (Divella et al., 2019; Glass & Olefsky, 2012).

Via secretion of adipose-tissue derived hormones such as leptin, adiponectin and resistin, the WAT directly influences insulin and glucose homeostasis of the entire organism (Harwood, 2012). Interestingly, leptin as well as adiponectin have been reported to have opposing functions compared to resistin. Leptin and adiponectin are involved in the maintenance of insulin sensitivity and glucose homeostasis by reducing gluconeogenesis in the liver, enhancing glucose and FFA uptake and oxidation in liver and skeletal muscle (D'souza et al., 2017; Kershaw & Flier, 2004; Yamauchi et al., 2002). In addition, leptin regulates appetite and subsequently food intake in the melanocortin system of the hypothalamus (Schwartz et al., 2000; Sinha et al., 1996). Moreover, adiponectin has anti-inflammatory properties and can inhibit innate immunity by inhibition of toll like receptor signalling (Yamaguchi et al., 2005). In

contrast, resistin has been reported to induce insulin resistance in the WAT and peripheral tissue (Steppan et al., 2001), however contrasting results in mice and humans are currently challenging these results (Jamaluddin et al., 2012). Nonetheless, higher resistin levels have been linked with CVD (Muse et al., 2015), indicating a direct functional link between adipose tissue endocrine function and disease. Moreover, the WAT is one of the major insulin-sensitive organs next to the skeletal muscle, liver, heart and brain. Upon insulin secretion, insulin binds to the InsR, which activates an intracellular signalling cascade resulting in the translocation of the glucose transporter isoform 4 (GLUT4) onto the cell membrane and increased glucose uptake from the blood (Chadt & Al-Hasani, 2020). Once blood glucose levels are lowered to basal levels, GLUT4 receptors are compartmentalized into storage vesicles and stored in the cytoplasm until renewed insulin stimulation. Consequently genetic ablation of GLUT4 in the WAT induces systemic insulin resistance and increases the risk of diabetes in transgenic mice (Abel et al., 2001). Similarly, insulin resistant WAT cannot sequester GLUT4 to the plasma membrane, which leads to hyperglycemia due to lack of glucose clearance from the blood stream and development of diabetes. Thus, the WAT is a crucial player in maintaining systemic insulin sensitivity, glucose metabolism and energy homeostasis via the secretion of adipokines and the regulation of blood glucose levels.

1.3.5 Ageing and the WAT

The WAT shows distinct changes on the systemic, cellular and the transcriptional level during ageing, and excessive fat is stored in intra-abdominal depots instead of SCAT depots (Schwartz et al., 1990). However, the aged WAT cannot take up the entire excessive fat, which is then deposited in other organs, such as the liver (Nguyen et al., 2018) or the bone marrow (Ambrosi et al., 2017) and subsequently decreases tissue function in the elderly. Moreover, ageing itself in the absence of obesity can lead to adipose tissue dysfunction and increased WAT inflammation, which abrogates the fine-tuned adipose tissue regulatory network and induces insulin resistance in the WAT and peripheral organs (Mancuso & Bouchard, 2019). Correspondingly, Schaum et al. have recently shown that the WAT as well as the SCAT are the first murine tissues to exhibit age-related transcriptomic changes, which are associated with higher intrinsic inflammation and immune response (Schaum et al., 2020). In accordance with a higher inflammatory gene expression, immune cells, such as T cells and macrophages are attracted by pro-inflammatory factors and migrate into the tissue in aged mice, thus increasing the inflammatory environment (Brigger et al., 2020; Lumeng et al., 2011). Moreover, systemic secretion of pro-inflammatory adipokines by the aged WAT can induce insulin resistance and inflammation in other peripheral tissues, thus spreading inflammation from the

WAT to other organs (Mancuso & Bouchard, 2019). Increased inflammatory gene expression can also be partially explained by increased numbers of senescent cells in the aged WAT (Tchkonia et al., 2010).

Senescent cells are post-mitotic cells that are irreversibly arrested in the G0 phase due to cellular stress, such as critically short telomeres, epigenetic de-repression or irreparable DNA damage and are thus unable to replicate anymore. During ageing senescent cells accumulate in various tissues and are considered a hallmark of ageing (López-Otín et al. 2013). Moreover, senescent cells release pro-inflammatory factors, such as IL-1 and IL-6 and matrix metalloproteinases, which can remodel the extracellular matrix and thus attracting immune cells and altering tissue morphology (Basisty et al., 2020; Lau et al., 2019). In addition, neighbouring cells, which take up secreted cytokines and proteins from senescent cells can also become senescent and thereby contribute to increased inflammation and tissue ageing (Nelson et al., 2012). Tchkonia et al. demonstrated that increased secretion of pro-inflammatory cytokines from senescent cells in the WAT negatively affects the AT progenitor population (Tchkonia et al., 2010). The increased inflammatory environment during ageing can cause functional decline in AT progenitors, such as increased lipotoxicity (Guo et al., 2007), reduced proliferation (Kirkland et al., 1990) and decreased differentiation due to reduced expression of differentiation factors (Karagiannides et al., 2001). Importantly, clearance of senescent cells by genetic ablation of $p16^{Ink4a}$ positive cells in various tissues including the WAT can delay ageing and improve tissue function in mice (Baker et al., 2011).

While the expression level of pro-inflammatory cytokines, such as leptin, IL-1 or IL-6, increases, expression of anti-inflammatory cytokines, such as adiponectin or vaspin decreases with age (Mancuso & Bouchard, 2019). Aside from its role in adipogenesis, adiponectin reduces inflammation by inhibition of the pro-inflammatory NFκB and toll like receptor signalling pathways (Ajuwon & Spurlock, 2005; Yamaguchi et al., 2005). Therefore, age-associated reduction of adiponectin contributes to a higher inflammatory state in the WAT and the periphery. Interestingly, the WAT of long-lived women secretes higher amounts of adiponectin (Arai et al., 2006), which is thought to play a protective systemic effect and anti-inflammatory effect on adipose tissue residing macrophages, thus contributing to healthy ageing in centenarians (Ohashi et al., 2010). Additionally, lifespan extending interventions, such as DR, significantly reduces the body fat content, maintain a healthy WAT metabolism as well as insulin sensitivity and reduced WAT inflammation (Corrales et al., 2019; Miller et al., 2017; Rojas et al., 2016). Therefore, improving WAT tissue function during ageing by reducing inflammation might alleviate systemic ageing and thereby contribute to longevity and improved health at old age.

1.4 Obesity

1.4.1 The global prevalence of obesity and obesity risk factors.

Obesity is defined by the WHO as severe overweight with a body mass index (BMI) of over 30kg/m^2 with corresponding increased fat mass in relation to body weight of over 32% for women and over 25% for men (Ezeh et al., 2014). Over the last decades, the worldwide prevalence of obesity steadily increased and it is estimated that approx. 39% of male or female adults and 18% of children aged five to 19 years of age are classified as obese (Global Health Observatory (GHO) data. Overweight and obesity (2017) Website https://www.who.int/gho/ncd/risk_factors/overweight/en/ (last accessed November 15th, 2020)). Especially childhood obesity between 5 and 19 years of age has drastically increased to 5,6% of all girls and to 7,8% of all boys (Bentham et al., 2017) and the prevalence of both childhood and adult obesity is predicted to rise even further (Finkelstein et al., 2012). Obesity has various genetic, dietary and behavioural as well as environmental risk factors that contribute to the disease onset. Recent GWAS studies have found SNP in regulatory elements, such as enhancer or promoter regions or miRNA bindings sites, which are associated with an increased genetic predisposition to develop obesity (Cheng et al., 2018; Herbert et al., 2006; Pan et al., 2018; Voisin et al., 2015). Risk factors for obesity include over nutrition with a diet high in fat and calorie content (Davis, Hodges, & Gillham, 2006; Duvigneaud et al., 2007; Howarth et al., 2005; Ledikwe et al., 2006) in combination with a sedentary lifestyle and lack of exercise (Delvaux et al., 1999; Drewnowski & Darmon, 2005; Martínez-González et al., 1999). Moreover, exposure to various chemicals, which are acting as endocrine factors and disrupt signalling pathways can lead to adult or childhood onset obesity (Gauthier et al., 2014; Rundle et al., 2012).

1.4.2 The effect of obesity on the WAT and WAT inflammation

Obesity is caused by excess energy, which cannot be taken up by other organs and is therefore stored as fatty acids in the adipose tissue depots. Increased food intake and reduced physical activity can lead to this energy surplus and can be causative to the development of obesity. During obesity, adipose tissue depots and lipid droplets in adipocytes largely increase in size (Tchoukalova et al., 2010), which induces cellular stress within adipocytes (Giordano et al., 2013; Özcan et al., 2004). Hypertrophic adipocytes secrete pro-inflammatory cytokines, such as IL-6, IL-1b or TNFα (Coppack, 2001; Hotamisligil et al., 1993; Wueest & Konrad, 2018), which act as chemo attractants to recruit circulating macrophages into the WAT.

Correspondingly, the secretion of anti-inflammatory adipokines, such as TGFβ or adiponectin are significantly reduced in obese compared to lean individuals (Makki et al., 2013). Increased immune cell infiltration in the WAT causes local inflammation but also increased cytokine production and insulin resistance (Shimobayashi et al., 2018; Weisberg et al., 2003). Moreover, residing or infiltrating macrophages change their polarization into an activated, pro-inflammatory state, increase proliferation and secrete pro-inflammatory cytokines, which further drives WAT inflammatory processes (Lumeng et al., 2007; Zheng et al., 2016). Ultimately, hypertrophic adipocytes can commit inflammation-induced programed cell death, a process called pyroptosis, which further increases the levels of cytokines in the WAT (Giordano et al., 2013).

Aside from immune cells, other adipocytes take up the released pro-inflammatory adipokines, which induces intrinsic cellular stress responses and leads to the release of FFA in the circulation, thus aggravating WAT inflammation by activating the innate immune response (Nguyen et al., 2011; Shi et al., 2006). Furthermore, the elevated circulating levels of FFA in the blood stream are sensed by the liver, which increases lipid uptake and storage in the cytoplasm of hepatocytes. Hepatic FFA storage induces steatosis, inflammation, hepatic insulin resistance and ultimately decreased liver function (Divella et al., 2019). Moreover, increased uptake and intracellular storage of FFA in pancreatic β cells leads to reduced insulin secretion, β cells loss and the development of type II diabetes (Oh et al., 2018). However, while obesity is one of the major risk factors for diabetes and insulin resistance, not every obese person develops type II diabetes.

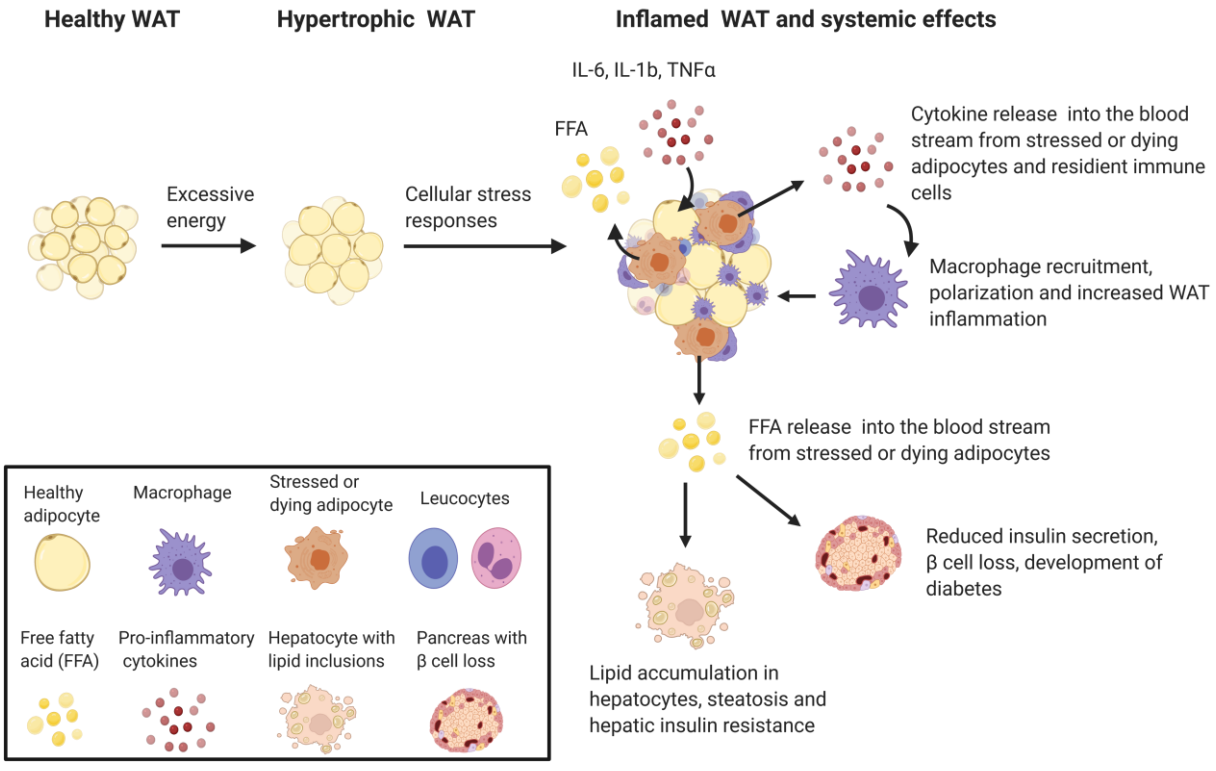

Figure 1.4. 1: The transition from healthy WAT to hypertrophic and inflamed WAT during obesity

Upon excessive energy storage in the WAT, intercellular stress signals in the adipocytes induce secretion of FFA and pro-inflammatory cytokines, which recruit immune cells from the periphery and exacerbate the inflammatory state in the WAT. WAT apoptosis mediates further release of FFA and cytokines into the blood stream, which causes detrimental systemic effects in peripheral tissue. The schematic was created using BioRender.com.

1.4.3 Systemic effects of obesity

Aside from insulin resistance and ectopic accumulation of fat, obesity also has other negative long-term effects in different organ systems, such as the cardiovascular, the pulmonary, the reproductive and the central nervous system (Haslam & James, 2005). Abnormal fat accumulation in the liver and the pancreas induce local inflammation, β cell dysfunction and can cause steatosis, liver cirrhosis, pancreatitis and ultimately diabetes (Ji et al., 2019; Schiavo et al., 2018). Additionally, obesity is associated with many cardiovascular problems, such as arteriosclerosis or hypertension and heart failure (Lakka et al., 2002; Sandfort et al., 2016). Moreover, arteriosclerosis accompanied by poor circulation can obstruct systemic blood flow and in turn cause embolisms or strokes in the brain. In addition, obese individuals have a higher risk to develop certain types of cancer, for example breast, liver or colorectal cancer (Berger, 2014; Haslam & James, 2005), as well as nerve damage in the extremities and the retina as a complication of diabetes and even dementia (O'Brien et al., 2017). Increased body weight can in turn affect the musculoskeletal system and can lead to arthritis, joint pain as well as fat accumulation in the muscle (Hitt et al., 2007; Uezumi et al., 2010). Furthermore, obese individuals have a reduced pulmonary function and an increased risk for asthma, sleep apnoea and respiratory problems (Zammit et al., 2010) compared to lean individuals and severe obesity thus drastically reduces the quality of life of affected individuals. Lastly, obesity can increase male and female infertility by altering the hormonal balance with increased circulating oestrogen levels in females (Green et al., 1988; Grodstein et al., 1994) or reduced circulating testosterone levels (Di Nisio et al., 2020) and increased erectile dysfunction in males (Esposito et al., 2008). In addition, ageing itself is a major risk factor for obesity and metabolic diseases due to more sedentary lifestyle and a lower basal metabolic rate in the elderly (Siervo et al., 2016). Thus, reducing body weight and fat mass can have beneficial systemic effects on the metabolism as well as on tissue-specific phenotypes in humans.

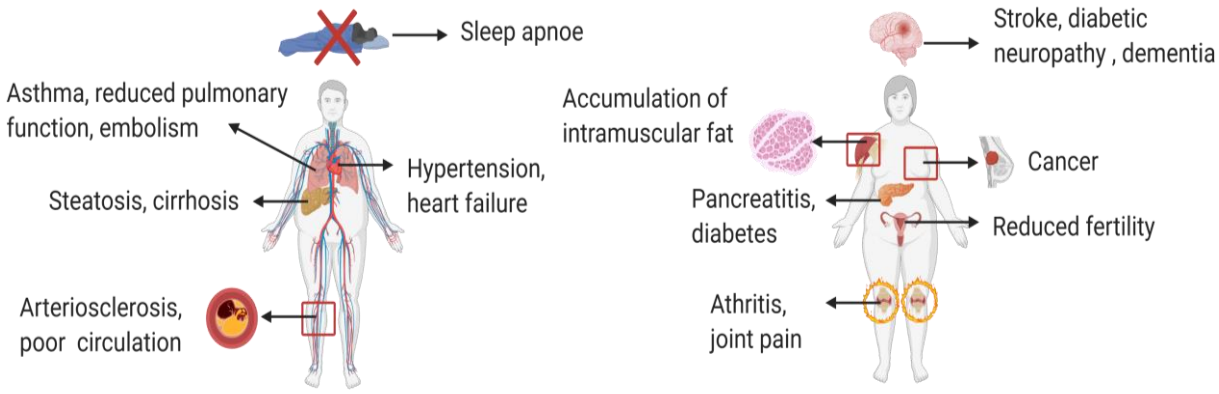

Figure 1.4. 2: Systemic health complications caused by obesity

Obesity causes adverse effects on almost all organ systems, including the gastrointestinal tract, the pulmonary and cardiovascular system, the brain and the endocrine system. The schematic was created using BioRender.com.

1.5 The small intestine

1.5.1 Reasons to study the small intestine

After food intake, the small intestine is the first tissue which comes in contact with the digested food as well as the contained nutrients. Moreover, the small intestine is directly affected by inappropriate dietary habits, such as a western diet rich in carbohydrates and dietary fat but low in dietary fibres, which reduces the gut barrier function (Guerville et al., 2017). Moreover, obesity causes intestinal inflammation and microbiota dysbiosis (Cani et al., 2008), whereas dietary interventions such as DR show beneficial effects on the microbiome (Zhang et al., 2013) and the intestinal barrier function (Ott et al., 2017). Thus, dietary changes impact directly on the small intestine itself but have additional systemic functions through the systemic distribution of up-taken nutrients via the blood and lymph system.

1.5.2 Overview on the gastrointestinal tract in mice and humans

The small intestine is part of the gastrointestinal tract whose main function is the digestion and absorption of nutrients from ingested food. The gastrointestinal tract can be subdivided into different parts, which conduct different functions, namely the mouth and oesophagus, the stomach, small intestine, cecum, large intestine and the rectum. Ingested food is chewed into

smaller pieces in the mouth and travels via the oesophagus into the stomach, in which it is digested using hydrochloric acid (HCL) and pepsin. From the stomach, the pre-digested food travels further into the small intestine, in which digestive enzymes, proteases, lipases and bile acid further break down the pre-digested food. The small intestine can be further subdivided into different sections, which will be elucidated in more detail in the following section. Moreover, the small intestine hosts different bacteria species, which compose the human or murine microbiome and which are involved in the digestion of dietary fibres and in the production of vitamins K and B (Rowland et al., 2018). In addition, the small intestine absorbs digested nutrients, such as carbohydrates, lipids, trace elements, vitamins and amino acids via specialized transporters localized in the cell membrane of the villi on the cell surface and releases them into the blood stream (Kiela & Ghishan, 2016).

From the small intestine, digested food passes to the cecum with the attached appendix, which is a major immunological checkpoint and is then transported into the large intestine. The large intestine, also called colon, removes water, salt and remaining nutrients from the food residues to form faeces. Similar to the small intestine, the colon also contains microbiota species which aid in the final digestion of pre-digested food (Flint et al., 2012) and is divided into different segments. Lastly, the rectum serves as final part of the gastrointestinal tract to excrete indigestible food residues via the anus. The intestine is a plastic organ and can change the percentage of cell types, the villi length as well as the intestinal length itself in response to different stimuli such as pregnancy, exercise, fasting or nutrition (Nilaweera & Speakman, 2018; Park & Im, 2020; Ross & Mayhew, 1985; Sabet Sarvestani et al., 2015).

Despite a high degree of evolutionary conservation, there are notable structural differences in the composition of the gastrointestinal tract between mice and men. Mice possess an additional forestomach containing different *Lactobacillus* species in the stomach structure, which serves as food storage and which is absent in humans (Frese et al., 2011). Moreover, while lacking an appendix mice have a bigger cecum, in which vitamin K and B are produced and plant fibres are digested by bacterial fermentation (Nguyen et al., 2015). Furthermore, the ratio of the small versus the large intestine, as well as the absorptive surface in the small intestine are larger in humans compared to mice, demonstrating that there are functional differences in digestion and absorption between species (Nguyen et al., 2015). In this thesis, we investigated changes in the small intestine upon DR. Therefore, I will focus on the cellular composition, main functions and changes during ageing in more detail in the following sections.

1.5.3 The three segments of the small intestine and their function in digestion and nutrient absorption

As described before, the small intestine can be subdivided into different regions, namely the duodenum, the jejunum and the ileum. All three segments are involved in the digestion and absorption of nutrients, nevertheless all segments possess unique morphological structures as well as functions.

The duodenum is the first segment of the small intestine and starts directly after the sphincter of the stomach. One unique feature of the duodenum, which discriminates this section from the jejunum and ileum, is the presence of several pancreatic and bile ducts, which connect the pancreas and the liver to the small intestine, as well as the presence of Brunner's glands in the submucosa. Brunner's glands are mucous glands that secrete an alkaline, bicarbonate containing mucous to decreases the acidity of the pre-digested food from the stomach. Moreover, via the secretion of epidermal growth factor, Brunner's glands inhibit the secretion of stomach acid to protect the small intestine from increased acidity (Kirkegaard et al., 1984). Upon food intake, bile acid, which is generated in the liver and stored in the gall bladder, is secreted into the duodenum via several bile ducts. Bile acid aids in the transport and absorption of different nutrients, such as lipids, lipophilic vitamins and steroid hormones into the enterocytes by forming an emulsion around the nutrients which facilitates cellular uptake (Chiang, 2009; Qi et al., 2015). Furthermore, several pancreatic ducts are located in the proximal part of the duodenum, which release pancreatic enzymes, such as lipase, amylase and trypsin. These pancreatic enzymes are involved in the enzymatic breakdown of complex lipids, sugars and proteins into fatty acids, carbohydrates, small peptides and amino acids from pre-digested food (Goodman, 2010). Aside from the presence of ducts and Brunner's cells, the duodenum is also the shortest region in the small intestine, measuring on average 4.1cm in female mice and approximately 20cm in humans (Ogiolda et al., 1998).

In contrast to the pre-digestive function of the duodenum, the main digestion and absorption takes place in the jejunum. In the jejunum, various lipids (Wang et al., 2013), trace elements (Kiela & Ghishan, 2016), amino acids and peptides (Curtis et al., 1978; Mitchell & Levin, 1981) and carbohydrates (Ferraris et al., 1993) are absorbed from the lumen into enterocytes. The absorption of nutrients takes place via active or passive transport over the cell membrane in the enterocyte microvilli using specific transporters. From the enterocyte cytoplasm, all nutrients except lipids are transported into the interstitial space, taken up by capillaries, transported via the portal vein into the liver and distributed throughout the body. In contrast, absorbed lipids are systemically distributed via the lymphatic system. The jejunum is the longest intestinal section in mice, whereas in humans, the ileum region is longer (Casteleyn et

al., 2010). Moreover, the ilium as well as the distal part of the jejunum harbour distinct lymphatic follicles, so-called Peyer's patches, which are involved in intestinal immune surveillance (Kobayashi et al., 2019). Aside from the surveillance function, the ileum reabsorbs bile acid (Chiang, 2009), vitamin B12 (Drapanas et al., 1963) as well as other leftover nutrients.

Despite many physiological and morphological similarities between the small intestine of mice and humans, there are notable differences in their structure. The first difference is the length of the small intestine, which is approximately 42.5cm on average in male B6 mice compared to approximately 7m in humans (Gu et al., 2013; Hugenholtz & de Vos, 2018). Second, the length of intestinal villi is greater in mice compared to humans, which points towards increased nutrient uptake (Casteleyn et al., 2010). Third, humans possess a distinct mucosal surface structure, the so-called *plicae circularis* in the jejunum, which increases the villi surface and provides a niche for specific microbiota species and which is not present in mice (Hugenholtz & de Vos, 2018). Even though mice and humans share approximately 89-90% of bacterial genus and taxa, there are still notable differences in the microbiome composition, such as the presence of *Deferribacteres* phyla in mice but not humans (Krych et al., 2013). Interestingly, the microbiome can also adapt to outside stimuli such as dietary changes or increased exercise similar to the small intestine itself (Park & Im, 2020). Thus, the three regions of the small intestine show functional and morphological differences and plasticity across species.

1.5.4 The cell type composition of the small intestine

Here, I will focus on the jejunum section of the small intestine and on its cell type composition. Morphologically, the jejunum has distinct crypt and villi structures to increase the surface area and is lined by a single layer of cells, the intestinal epithelium. The jejunum epithelium is composed of different cell types, which conduct distinct functions in the digestion and absorption of nutrients and the maintenance of the intestinal structure. The major cell types are enterocytes, goblet cells, enteroendocrine cells, Paneth cells, intestinal stem cells (ISC), microfold (M) cells and tuft cells. These cell types show a distinct pattern of distribution, in which differentiated cells are located on the villi, and the stem cell compartment is located in the crypts. The intestinal epithelium renews itself approximately every three to five days and newly formed cells require up to three days to migrate from the crypts to the top of the villi (Krndija et al., 2019), from where old or damaged cells are shed into the lumen. Interestingly, the cellular turnover rate in the intestine changes in disease states and favours goblet cell instead of enterocyte differentiation, to increase intestinal motility and to boost intestinal defensive mechanisms (Cortés et al., 2015; Lee et al., 2014).

All newly formed cells in the small intestine are generated by asymmetric differentiation of ISC, which reside in the Lieberkühn crypts and are the driving force of intestinal renewal and regeneration. Interestingly, ISC can be further sub classified based on gene expression profiles into actively dividing Lgr5 positive ISC, which maintain intestinal homeostasis, and quiescent Bmi1 positive ISC, which are involved in tissue regeneration after damage (Yan et al., 2012). A common feature of both ISC populations is the dependence on stem cell signalling pathways, such as Wnt, Notch or hedgehog pathways for division, to maintain crypt structure and to preserve stemness (Kuhnert et al., 2004; Vanuytsel et al., 2013). Secretion or presentation of Wnt or Notch signalling molecules by Paneth cells and the stroma are crucial to maintain ISC function and lineage commitment (Beumer & Clevers, 2016; Kabiri et al., 2014; Sato et al., 2011). Paneth cells are secretory cells and located next to ISC in the intestinal crypts. In addition to their role in ISC maintenance and differentiation, Paneth cells are also involved in intestinal immunity, by the secretion of anti-microbial peptides, such as lysozyme or α-defensin (Ayabe et al., 2000; Bevins & Salzman, 2011). Upon activation of toll-like receptor signalling cascades, Paneth cells release anti-microbial peptides, which are stored in morphologically distinct secretory granules, into the intestinal lumen (Vaishnava et al., 2008).

After asymmetric division of ISC, newly formed cells terminally differentiate during the migration along the villi. Increased Notch signalling in newly formed progenitor cells mediates differentiation into enterocytes (Korzelius et al., 2019), whereas inhibition of Notch signalling via Atoh1 induces differentiation into the secretory lineage (Kim et al., 2014). Enterocytes are the most abundant cell type in the small intestine and make up approximately 80% of the entire intestinal epithelium (De Santa Barbara et al., 2003). The primary function of enterocytes is the absorption of nutrients from the intestinal lumen via specific transporters and the intracellular transport and exocytosis into the capillary or lymphatic system and subsequently systemic distribution. Tight junctions between enterocytes mediate a tight segregation between the intestinal content in the lumen and the intestinal epithelium and ensure a functional barrier (Chelakkot et al., 2018). Additionally, microvilli structures on the apical side of the enterocytes, which reach into the intestinal lumen, increase the cellular surface area and absorptive capacities. Moreover, enterocytes secrete leptin, which represses hunger signalling in the hypothalamus and subsequently decreases food intake (Morton et al., 1998) and anti-microbial peptides to repel pathogens (Birchenough et al., 2015; O'Neil et al., 1999).

Goblet cells are secretory cells, which secrete Muc2 polymers and other mucins into the lumen, which forms the mucus and protects the surrounding intestinal epithelium (Birchenough et al., 2015). Furthermore, the mucus network serves as anchor for several secreted anti-microbial proteins and to concentrate these proteins next to the intestinal barrier (Muniz et al., 2012). Moreover, goblet cells are actively involved in the immune response against parasite infections via increased mucin secretion (Fujino et al., 1996). Enteroendocrine cells are endocrine cells

in the intestinal mucosa that account for approximately 1% of the cells in the intestine and that act as chemoreceptors to sense nutrient state or toxic substances in the lumen. Different types of enteroendocrine cells exist throughout the gastrointestinal tract. By secreting different hormones, such as the satiety hormones polypeptide YY, ghrelin or glucagon-like peptide-1, enteroendocrine cells can directly induce or reduce food intake, as well as intestinal motility (Psichas et al., 2015). Moreover, enteroendocrine cells are involved in ISC maintenance and division (Amcheslavsky et al., 2014; Van Es et al., 2019) and can even transdifferentiate into stem cell like cells upon ISC ablation (Tetteh et al., 2016).

Given that food and nutrients first encounter the gastrointestinal tract and are absorbed into the blood stream via the intestinal mucosa, it is important to have an intestinal immune surveillance system, which distinguishes pathogenic from commensal bacteria. M cells are part of this immune surveillance in the intestine by taking up antigens from the lumen and presenting them to other antigen presenting cells, such as dendritic cells or macrophages in the Peyer's patches (Kobayashi et al., 2019). In contrast to other intestinal cell types, M cells do not possess apical microvilli to increase phagocytosis (Mabbott et al., 2013). In contrast, Tuft cells are mainly sensory cell types, and are involved in the detection of pathogens. However, parasitic infection increases the number of tuft cells in the intestine, which is associated with increased IL-25 secretion (Leslie, 2019). Therefore, disruption of the intestinal epithelium during ageing or disease states has major systemic impacts.

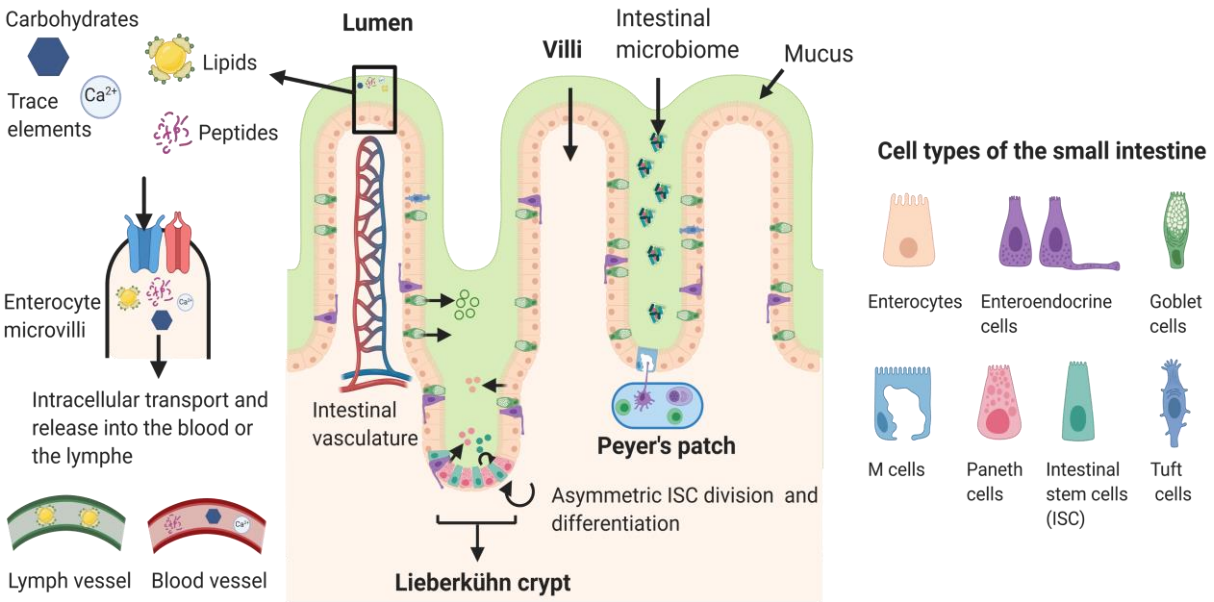

Figure 1.5. 1: The structure of the intestinal epithelium including associated cell types and their cellular localization in the jejunum

The intestinal epithelium in the jejunum displays seven main cell types, namely enterocytes, enteroendocrine cells, goblet cells, Paneth cells, intestinal stem cells (ISC) and tuft cells. Mucus

produced by goblet cells (light green dots) protects the intestinal epithelium and contains the microbiome by providing an anchor point for antimicrobial peptides secreted by Paneth cells (pink dots) or enterocytes (orange dots). Furthermore, Paneth cells secrete growth factors (turquoise dots) to support the ISC. Asymmetric division of ISC gives rise to new intestinal cells. Nutrients are taken up by enterocytes and are systemically distributed through blood or lymph vessels. M cells and tuft cells are part of the intestinal immune surveillance. The schematic was created using BioRender.com.

1.5.5 Changes in the small intestine during the ageing process

Similar to other organs, such as the WAT, the small intestine also exhibits age-associated structural and transcriptional changes. However, in contrast to the WAT, the small intestine exhibits age-associated transcriptional decline only very late in life between 24-27M of age (Schaum et al., 2020). A common transcriptional profile, which is shared between both tissues, is increased inflammatory gene expression, indicating a higher inflammatory state in the aged small intestine (Schaum et al., 2020). Furthermore, increased immune system and immune modulatory protein levels in aged intestinal crypts contribute to intestinal inflammation, which causes several detrimental effects on intestinal function (Gebert et al., 2020).

Nutrient absorption in the intestine declines during ageing, due to microbiome dysfunction, infrequent meals or decreased motility, which can cause malnutrition in the elderly (Holt, 2007). Moreover, old people often suffer from indigestion or drug-induced diarrhoea, which aggravates the deficiency of essential amino acids and vitamins (Drozdowski & Thomson, 2006). Finally, nutrient deficiency originating from the small intestine can cause additional detrimental effects on other organ systems and can further exacerbate age-associated symptoms, such as osteoporosis or frailty (Roberts et al., 2019).

ISC function, number and regeneration is reduced during ageing (Gebert et al., 2020) and ISC differentiation is skewed towards increased secretory lineage differentiation, thus contributing to reduced intestinal absorption at old age (Nalapareddy et al., 2017). Reconstitution of Wnt signalling in ISC or decreased mTORC1 activity by rapamycin treatment or DR have been shown to improve ISC function, differentiation and intestinal health during ageing

The microbiome also exhibits age-associated changes. During ageing, beneficial bacteria such as *Firmicutes* decrease, whereas commensal bacteria *Proteobacteria* and *Bacteroidetes* significantly increase in number and become pathogenic (Maynard & Weinkove, 2018). Furthermore, overgrowth of pathogenic bacteria in the intestine can reduce the intestinal barrier function and induce bacterial migration into the body with subsequently increased inflammation (Thevaranjan et al., 2017). Strikingly, lifelong DR can reverse microbial dysbiosis and reduce intestinal inflammation in ageing mice (Zhang et al., 2013) and retain ISC function

(Yilmaz et al., 2012). Thus, improving intestinal function during ageing could provide beneficial effects on quality of life and the health status of the elderly.

1.6 Aims of the PhD thesis

1. Assessing lipogenesis and mitochondrial biogenesis in late- onset dietary switches compared to chronic controls

- Can late-onset DR initiated at 24M of age induce similar transcriptomic changes and increase lipogenesis gene expression as chronic DR?
- Does late-onset DR increase mitochondrial biogenesis in the WAT?
- Do we detect increased WAT browning and thermogenesis gene expression in response to chronic or late-onset DR?

2. Identifying of the critical phase in life for lifespan extension by DR in mice

- Is there a gradual decline in DR-mediated lifespan extension depending on the age of DR onset?
- Are differences in tumour load at old age responsible for lifespan differences of mid- or late-life DR animals?
- Can mid- or late-life initiated DR reverse the detrimental effects of prolonged AL-feeding and obesity on the metabolism?
- Are improved fitness and frailty at old age responsible for the lifespan differences of mid- or late-life DR animals?

3. Deciphering the effects of mid-or late-onset DR on selected hallmarks of ageing in the small intestine and the WAT

- Has chronic, mid-or late-onset DR an impact on stem cell function and regenerative capacities in the small intestine?
- Are WAT heterogeneity and the differentiation potential of adipose tissue stem cells altered upon mid-or late-onset DR?

4. Assessing WAT inflammation under early, mid- or late- life onset DR

- Does short-term or long-term DR initiated at early, middle-age or late in life reduce adipocyte size?
- Are inflammatory processes in the WAT rendering mice unable to respond to late-life initiated DR?

2. Materials and methods

2.1 Mouse work

2.1.1 Mouse study approval

This study was planned and approved in accordance with the regulations of the Federation of the European Laboratory Animal Science Association (FELASA) and the Landesamt für Natur, Umwelt und Verbraucherschutz, Nordrhein-Westfalen, Germany (reference number 84-02.04.2015.A437).

2.1.2 Mouse breeding and husbandry

Female F1 hybrids (C3B6F1) were generated in- house by mating male C57BL/6 N mice (strain code 027) with C3H/HeOuJ females (strain code 626, both Charles River Laboratories). Mice were weaned at three weeks and randomized into cages containing five animals per cage and ad libitum (AL) access to chow food (V1554-703, Ssniff Spezialdiäten GmbH, Soest) and sterile-filtrated water. Mice were kept in individually ventilated cages (GM500 IVC Type II long, Tecniplast) at constant temperature of 21°C, 50-60% humidity and a 12h light/dark cycle starting at 6am. Environmental enrichment in form of nestles and chewing sticks were provided to prevent dental overgrowth. In total, four separate cohorts were generated and used for lifespan analysis (n=320 mice), tissue collection (n=320 mice), and metabolic (n=90 mice), and fitness phenotyping (n=72 mice),

2.1.3 Food intake measurements and implementation of dietary restriction (DR)

After weaning, mice were kept on AL feeding and their food intake was measured on a weekly basis using custom made food racks. Food racks were only present in 10 AL cages of the lifespan cohort and the weekly food uptake of these 10 cages was used to calculate the amount of food fed to DR animals. A second set of food racks was included in 10 AL cages of the tissue collection cohort, to measure the food intake in an independent cohort and to ensure comparable food consumption between cohorts. At 23M, the food intake measurements in AL cages using specialized food racks were stopped for both cohorts and the special food racks in these cages were replaced with regular ones. Therefore, the amount of food fed to DR animals was kept constant from 23M of age until the end of the experiments for all four mouse cohorts. For the phenotyping groups we did not measure the weekly AL food intake using custom food racks due to the low number of AL cages in both cohorts. Instead, we utilized the

already generated food intake data from the lifespan cohort. To this end, we averaged the food intake measurements of four consecutive weeks to obtain the average food amount on a monthly basis, which corresponded to the age of the animals in months. This averaged food amount was fed to the DR mice for four weeks, after which the next averaged food amount was utilized. Subsequently, from 23M of age until death, DR groups in the phenotyping cohorts obtained the same fixed amounts of food as the DR groups from the lifespan cohort.

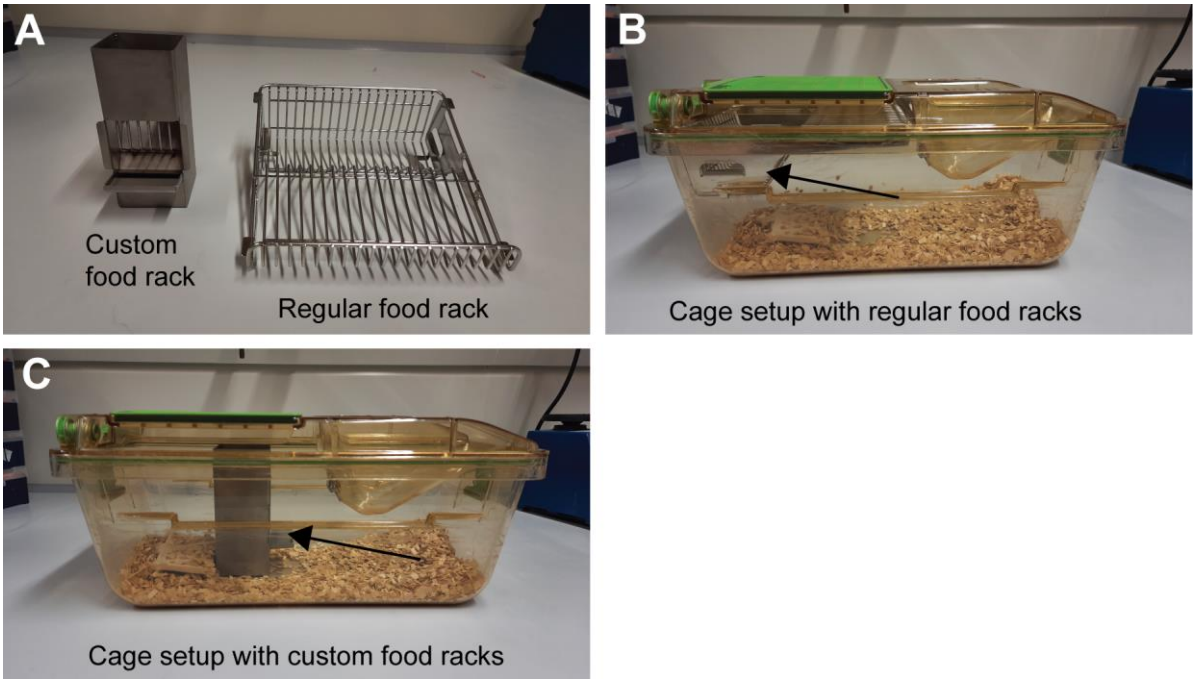

Figure 2. 1: Example pictures of custom and regular food racks in the AL cages.

A) *Example pictures of A custom-made food racks to determine the weekly amount of food intake of AL mice or regular food racks in AL or DR cages.* ***B)*** *The cage setup with regular food racks in the chronic AL, chronic DR and DR switch cages. Animals reach the food in the rack over the entire length of the rack.* ***C)*** *Cage setup with custom food racks to measure the weekly food intake of AL mice. Food was only accessible from the small rectangular area in the front, thus limiting food access. Black arrows indicate the access to the racks in custom or regular food racks.*

Lifelong (chronic) DR treatment was initiated in adult fully-grown 3 months (3M) old animals to exclude developmental effects. DR animals received food once per day in the morning. They were fed with 60% of the food amount consumed by AL animals based on the consumption of AL animals in the previous week. In order to systematically address the effects on health and survival when introduced later in life, DR was introduced at 12M (AL_DR12M), 16M (AL_DR16M), 20M (AL_DR20M) and 24M (AL_DR24M) of age, respectively. Please refer to table 1 for the number of animals, which were used in the respective DR switch in the four different mouse cohorts. In contrast to a previous study in our lab (Hahn et al., 2019), animals

were directly switched to the new diet without an adaptation period. In the lifespan cohort, animals switched at 24M of age corresponded to the animals used for food uptake measurements, i.e., they were housed in cages containing customized food racks until aged 23M, then spent one months in cages with regular food racks before DR was introduced.

Table 1. Number of mice for all cohorts that were switched at the respective time points

	Chronic DR	**AL_DR12M**	**AL_DR16M**	**AL_DR20M**	**AL_DR24M**
Lifespan	50	49	50	45	46
Tissue collection	110	50	33	19	10
Metabolic phenotyping	15	14	15	13	12
Fitness phenotyping	12	12	12	12	8

2.1.4 Post-mortem pathology, necropsy and faecal collection in the lifespan cohort

Animals were checked daily by the care taker to evaluate their health status, to note early signs of tumour growth and to detect deaths. Post-mortem pathology of age-related deaths started when the animals started to die at approximately 19 months of age and pathologies continued until the lifespan was concluded. Necropsy was conducted for each mouse irrespective whether it died a natural death or whether it had to be sacrificed due to bad health. Euthanasia criteria were graded based on the severity of the symptoms and encompassed significant weight loss compared to an appropriate control animal, general physical appearance, such as signs of present infections or tumours, spontaneous activity as well as body temperature, heart and breathing rate. A score between 1-9 points was considered as low strain and the animal was inspected twice daily and the body weight was measured once by the caretakers. Moderate strain was graded with 10-19 points and the mouse was inspected and weighed twice daily by the caretakers and a veterinarian was consulted to consider euthanasia in agreement with the primary investigator. Upon high strain of 20 points and more, the experiment was immediately terminated and the animal was sacrificed using cervical dislocation. Please refer to supplementary table 1 in the supplementary files for the detailed

scoring of the different euthanasia criteria. Tumour load, tumour location as well as additional anomalies were reported for subsequent data analysis. Additionally, faecal samples were collected every two months from all diet groups starting when animals reached 12M of age and were continued in the same two-month rhythm until the last DR animals died. Faecal samples were snap-frozen in liquid nitrogen and stored in -80°C prior to DNA, metabolite and protein extraction, which was conducted in a collaborative project with Carolina Monzó and the research group led by Dr. Dario Valenzano.

2.1.5 Tissue collection and cross-sectional pathology at defined ages

At 5M, 12M, 16M, 20M, 24M and 28M of age, 10 mice per diet group of the tissue collection cohort were sacrificed using cervical dislocation. On the day of dissection, DR animals were not fed with their daily food portion in the morning to avoid acute effects of feeding and nutrient uptake on the harvested tissue. Serum or plasma, liver, skeletal muscle, heart, WAT, BAT, SCAT, lungs, skin, stomach, duodenum, jejunum, ileum, colon, rectum, feces, one kidney, pancreas, femur, thymus, hippocampus, olfactory bulb, striatum, cortex, sensorimotor cortex, hypothalamus, frontal cortex, frontal association cortex and rest brain were dissected and snap-frozen in liquid nitrogen and stored at -80°C for further molecular biological analyses. Skeletal muscle, WAT, liver, BAT, heart, kidney, duodenum, jejunum, ileum, colon, skin, femur samples were excised and fixed in 10% neutral-buffered formalin (HT501320-9.5L, Sigma) for formalin-fixated paraffin embedding (FFPE). During tissue collection, cross-sectional pathology was carried out for each animal. Tumour load and additional anomalies of each dissected animal were recorded, to allow for analyses in a time- and age-controlled manner.

2.1.6 Metabolic phenotyping of late-life DR switch mice

Chronic AL and DR mice were first phenotyped at the age of 5M and subsequent tests were conducted at 9M, 14M, 18M, 22M and 26M of age. DR switch animals were first phenotyped six weeks post-switch and then at the same time points as the chronic control groups (see Figure 3.2.7). To reduce stress, animals were allowed to rest between experiments. Tests were carried out in four consecutive weeks with one test per week. Initially, each diet group encompassed 15 animals. Due to deaths during ageing, animal numbers in the tests varied between 8- 15 mice per diet group. Mice were allowed to acclimatize to the testing room for at least 30min prior to the experiment start. Unless otherwise stated, DR animals were provided with their daily food portion during their regular feeding time in the morning prior to the tests.

2.1.7 Assessing body composition using nuclear magnetic resonance (NMR) tomography

Body weight was determined on a scale (LF50H, Bruker). To assess body composition, lean and fat mass were measured non-invasively via *in vivo* nuclear magnetic resonance (NMR) tomography using a Minispec LF50H (Bruker). Measurements of the fat mass included visceral, subcutaneous, mesenteric and brown fat tissue but did not indicate how the different fat tissues attributed to the total fat mass. Total lean mass was composed of smooth, cardiac and skeletal muscle tissue and free fluid including cerebrospinal fluid and synovial liquid but excluding blood. Together, lean and fat mass, as well as free fluid together accounted for 92-96% of the body weight. To calculate absolute fat or lean weight in gram, fat and lean mass in percent were multiplied with the body weight in g.

2.1.8 Glucose tolerance tests (GTT)

To assess glucose tolerance, animals were fasted for 16h prior to the test. Therefore, food was removed from the AL cages at 5pm on the day before the test. DR animals received an additional 75% of their daily portion at 5pm, to keep the length of the fasting period comparable between the conditions. On the testing day, animals were weighed and syringes containing 20% glucose solution (B.Braun) were prepared individually for each animal according to their body weight with 10µl solution per g weight. Baseline blood glucose levels were measured with a glucose meter (Accu-Check Aviva, Roche) via a small wound on the tip of the tail before intraperitoneal injection of 2g glucose per kg body weight. Blood glucose concentrations were measured 15, 30, 60 and 120min post-injection. After the last measurement, DR animals were provided with their daily food portion and AL animals were allowed free access to food.

2.1.9 Insulin tolerance tests (ITT)

To assess insulin tolerance, DR animals received additional 75% of their daily portion at 8pm on the day before the test, corresponding to the peak food intake of AL animals. On the morning of the testing day, animals were weighed and food was removed from AL cages to avoid feeding during the test. Baseline blood glucose levels were measured before intraperitoneal injection of 0.75 units of insulin (INSUMAN Rapid 100 I.E./ml, Sanofi) in 0.9% isotonic NaCl solution (Deltamedica) Blood glucose levels were measured 15min, 30min and 60min after injection. After completion of the test, DR animals received their daily food portion and AL

animals regained free access to food. If glucose levels fell below a concentration of 40mg/dl during the test, mice were injected with 20% glucose solution to counter hypoglycaemia.

2.1.10 Indirect calorimetry using metabolic cages

To evaluate energy homeostasis under controlled conditions, indirect calorimetry measurements were carried out using metabolic cages (PhenoMaster, TSE systems). Per diet group, eight to twelve mice were randomly selected and single-housed over a period of seven days. First, mice were acclimatised in training cages for three to four days to get accustomed to the specialised food racks and water bottles, which allowed automated measurements of food and water intake. After the acclimatisation period, mice were transferred into the metabolic cages, in which they spent an additional 24h to acclimatise before the actual measurement started. Over the entire measurement period of 48h, mice were exposed to constant temperature and airflow. Measurements of the amount of carbon dioxide production and oxygen consumption, as well as food or water intake were made every 15min and averaged per hour for each individual. Measurement cycles over 24h started at 9:00am and ended at 9:00am the next day with a constant 12h day and night cycle. Lights were on from 6am until 6pm (light phase) and off from 6pm to 6am (dark phase). DR animals in the training or in the metabolic cages were fed between 10 and 10:30am until the experiment was concluded, while AL animals had unrestricted access to food all the time. Uneaten food from the DR cages was removed from the racks in the morning, before new food was provided. The body weight was measured daily in the training cages to validate habituation to the altered food and water supply as well as before the start and after the completion of the metabolic cages to assess weight loss. Mice that exhibited over 10% weight loss during the experiment were excluded from the final analysis. Additionally, lean and fat mass was measured using NMR before and after the measurement in the metabolic cages, to assess CO2 and oxygen consumption and basal energy rates in relation to lean mass. The respiratory exchange ratio (RER) was calculated by dividing exhaled carbon dioxide with inhaled oxygen (vCO2/vO2) in relation to lean mass. Results were averaged per diet group and plotted per hour over the 48h testing period. Spontaneous activity was measured by the number of times the mouse obstructed the laser beam along the X- and Y- axis and the number of beam breaks per hour was recorded. Total activity during 48h was averaged over 24h and beam breaks above 300 breaks per hour were considered as active, whereas less than 300 beam breaks per hour were considered as inactive state. Results were averaged per diet group and plotted per hour over 48h or 24h period or as inactive versus active state.

2.1.11 Fitness phenotyping of late-life DR switch mice

Chronic AL and DR mice were first phenotyped at the age of 5M and subsequent tests were conducted at 9M, 14M, 18M, 22M and 26M of age. Except for electrocardiography (ECG), frailty and body temperature measurements, DR switch animals were phenotyped at all indicated time points to avoid a potential memory bias due to previous phenotypings and to allow direct longitudinal comparisons of pre- and post-DR switch performance. DR switch animals were first tested eight weeks (8W) after the diet switch. To reduce stress, animals were allowed to rest between experiments, which were carried out in five consecutive weeks with one test per week. Mice were weighed on the first day of rotarod, as well as on the first day of the Barnes Maze experiments to monitor body weight during the testing period. Twelve mice per diet group were tested initially. Numbers declined during ageing due to deaths within the groups. All fitness phenotypings were done under blinded conditions. Therefore, cage cards were exchanged with blinding cards by the experimenter assigned with a random number to prevent bias. Cages were tested sequentially according to their respective blinding number starting with the lowest number (1). Mice were allowed to acclimatize to the testing room for at least 30min prior to the experiment start. Unless otherwise stated, DR animals were provided with their daily food portion during their regular feeding time in the morning prior to the tests.

2.1.12 Grip strength assay

Forelimb muscle strength was tested using a non-invasive two-paw grip strength meter (Ugo Basile®). Mice were picked up by the tail, carefully placed on the grip strength meter until forelimbs connected with the triangular pad before the tail was pulled back. The grip strength was recorded as the force the mouse had to utilize to counteract the applied pull on the tail. Each mouse was tested five times with at least 15min in between tests and the individual grip strength was averaged over the five measurements per phenotyping time point.

2.1.13 Rotarod motor coordination assay

RotaRod treadmill is a non-invasive measurement of motor coordination in mice. Motor coordination was tested using RotaRod (TSE Sytems) by measuring the time spent on the rotating wheel. Mice were placed on the rotating rod with an initial speed set at 5rpm. Speed gradually increased from 5rpm to 40rpm within 5min and mice spent maximum 5min on the

rotating wheel. Animals were trained twice daily for three consecutive days until the final measurements on day four. Daily runs were at least 1h apart from each other Runs were regarded as valid if at least 10sec were spent on the wheel and animals had three trials to achieve a valid run. If animas did not reach 10sec, the longest performance out of the three tries was used. Obtained results were averaged per animal and the daily average of each diet group was calculated.

2.1.14 Barnes Maze memory test

Barnes Maze is a novel non-invasive readout adapted to study memory function in mice (Rosenfeld & Ferguson, 2014), which was first described in 1979 (Barnes, 1979). The Barnes Maze utilizes bright illumination as negative stimulus, in contrast to other memory tests, such as the Morris water maze, which is based on water and the mice's' natural dislike of swimming. Therefore, applying this test as a readout for memory significantly reduces the stress levels for the animals. The Barnes Maze (TSE Systems GmbH) is an elevated platform one meter above the ground, with a diameter of one meter and interspersed with 20 holes. An escape box filled with five pieces of bedding material is placed under one hole, whereas the remaining 19 holes are completely covered. To reduce outside stimuli, the platform was surrounded on all four sides by a dark green curtain and in total illuminated with 600 lux white light using four LED flood lights (IP66 30W LED Ustellar). The behaviour of the mice on the platform was recorded using the Videomot2 system (TSE Systems GmbH).

On the first testing day, the mice were individually placed on the platform and covered by an opaque cylinder. After 10sec, the cylinder was lifted up and the animal was gently directed towards the escape box. The animal should enter the box and was allowed to remain there for approximately 15sec, before it was transported back into the home cage. This step was crucial as the animal should associate the escape box with its home cage. After the initial test, animals were allowed to rest for 30min before the second trial began. Mice were again placed on the platform and covered with the opaque cylinder but once the cylinder was lifted, animals had three minutes to enter the escape box and the time until they entered was measured. If animals failed to find or enter the box within three minutes, the test was stopped and the animals were gently directed towards the escape box to refresh their memory. Path, speed and time spent on the platform were tracked per animal using the Videomot2 software (TSE Systems GmbH). The platform was cleaned after each tested cage using Dismozon plus (981187, Hartmann). Animals were trained on three consecutive days with two testing runs per day. The two actual measurements were conducted on the fifth testing day. Animals, who failed to enter the escape box within three minutes were placed back into their home cage immediately and were not

directed towards the escape box. The two recordings of each animal were averaged per day and averaged per diet group.

2.1.15 Body temperature measurement via infrared thermometer or rectal probe

Body temperature was measured non-invasively via the ear using an infrared thermometer (Thermoscan IRT 4020, Braun) or via a rectal probe (RET-3ISO and BAT-12, both Science Products GmbH). As the body temperature correlates significantly with the feeding state of the animals, all mice were measured early in the morning prior to feeding of DR animals and late in the afternoon, in which AL and DR animals exhibited similar feedings states. Mice from the fitness cohort were used to assess body temperature and the measurements were incorporated into the regular phenotyping schedule and took place a week before the motor coordination experiments. The inner-ear body temperature was first measured when mice reached 22M and afterwards repeated every eight weeks until mice were aged 26M. To assess body temperature using an infrared thermometer, mice were restrained and the temperature was measured in the ear. Mice were allowed to rest for at least 2min in- between testings and the temperature was taken three times in the morning and in the afternoon. After the last phenotyping time point at 27M, the core body temperature was measured using a rectal probe. Mice were restrained, the rectal probe was lubricated with Vaseline and carefully inserted approximately 1cm deep into the rectum. Each mouse was measured for 15sec. to assure comparability between individuals. In between mice, the rectal probe was cleaned with Bacillol® AF (973380, Hartman) and dried with a tissue. To compare results with the infrared measurements, the temperature was taken once in the afternoon before the dissection day and once in the morning, before mice were sacrificed using cervical dislocation. DR animals were not provided with food prior to the dissection. For both methods, the average body temperature in relation to feeding state was calculated per animal and averaged per diet group.

2.1.16 Frailty index

To assess frailty and the effect of chronic or mid-life DR on overall health at old age, a modified protocol of the frailty index (Whitehead et al., 2014) was implemented. The frailty index assesses similar parameters used in clinics for humans to score the frailty of an individual and in total, 24 different parameters were tested per animal. Integument was scored via alopecia, loss of fur colour, loss of whiskers, signs of dermatitis and overall coat condition. Scored

musculoskeletal parameters included visible or palpable tumours, distended abdomen, kyphosis, tail stiffening, gait disorders, tremor and palpable sacroiliac region. Vestibular disturbance, hearing loss, eye discharge and swelling, corneal opacity, vision loss and nasal discharge were used to score vestibulocochlear and auditory phenotypes. Digestive and urogenital parameters included malocclusions, signs of diarrhoea and rectal, vaginal or uterine prolapse. To score the respiratory tract and the general condition of an animal, breathing rate and depth, piloerection, body weight and the mouse grimace scale were scored. The scoring of the different frailty parameters was the following: No signs of discomfort or the absences of phenotypes were scored with 0, slight or reduced changes and discomfort was scored with 0.5 and marked abnormalities and obvious signs of pain and discomfort were scored with 1 for each tested parameter. Additionally, the body weight of each individual was measured and the average weight and standard deviation (SD) per control or DR switch group were calculated. Next, the individual body weight was compared to the average body weight of the respective diet group. If the individual exhibited a body weight difference up to 1SD difference from the average of the diet group it belonged to, a score of 0.25 was noted. A score of 0.5 was imposed if the weight difference was up to 2SD in relation to the average and a score of 0.75 was attributed for up to 3SD difference. Finally, a score of 1 was implemented if the individual's body weight exceeded the group average by over 3SD. To calculate the frailty index per animal, the scores of all 26 tested parameters were added up and divided by 26 to calculate the frailty score for each animal. Results were averaged per diet group. The frailty index was conducted at 22M, 24M and 26M of age to assess longitudinal changes in frailty.

2.1.17 Non-invasive electrocardiography (ECG)

Heart rate (HR) as a readout for cardiovascular function and health was analysed using the non-invasive, awake electrocardiogram (ECG) ECGenie system (Mouse Specifics Inc.). Mice were acclimatized on the elevated platform for at least 10min prior to the test. The HR was continuously recorded with 2kHz via an electrode over the four paws and animals were tested for a maximum of 10min. Clean signals, in which single heart beats and single peaks could be discriminated, were saved individually per animal and analysed using e-mouse 16/64 software (Mouse Specifics Inc.). Signals with heart rate variation (HRV) above 35bpm were excluded from the analysis. Obtained heart rates from recorded files were averaged per animal. To ensure data reliability, only mice with more than 100 signals were included in the final diet group specific analysis.

2.2 Molecular biological methods

2.2.1 Paraffin infiltration and tissue sectioning

Paraffin infiltrations of all liver and WAT samples were conducted on the Excelsior™ AS tissue processor (A82300001, ThermoFisher Scientific) in a fully automated manner using the following protocols.

Formalin fixated WAT tissues were gradually dehydrated in 50% EtOH for 120min, 70% EtOH, 80% EtOH and 90% EtOH for 90min each, thrice in 100% EtOH for 5h in total with two refreshings of EtOH after 90min prior to clearing with Xylene for 300min and subsequent infiltration in paraffin for 300min with refreshed solutions after 1h. Formalin fixated tissues were gradually dehydrated in 50%, 70%, 80% and 80% EtOH for 20min each, two steps for 20min and one step for 30min in 100%, followed by clearing with Xylene for 10min, 20min and 30min and infiltration in paraffin twice for 20min and once for 30min. Subsequently, samples were embedded in paraffin on a HistoStar™ embedding station (A81000001, ThermoFisher Scientific) and sectioned into 5µm thin section on an electronic rotary microtome (HM 340 E, ThermoFisher Scientific) equipped with a section transfer system (771200, ThermoFisher Scientific). Sections were dried overnight (OVN) at 37°C and stored at RT until further use.

2.2.2 Generation of tissue microarrays (TMA)

Tissue microarrays (TMA) is method commonly used in molecular pathology, to assess various parameters in a large number of samples on the same slide to reduce the number of slides while maintaining the desired number of samples. Tissue cores are punched from a donor block and inserted into pre-drilled holes on an empty acceptor paraffin block.

Here, TMAs of WAT samples of 5M, 16M, 20M and 24M mice on chronic AL or DR feeding and on tissue samples of AL_DR groups switched at 12M, 16M or 20M of age were generated using a TMA Master II (3D HISTECH). First, the acceptor block was moulded with paraffin in a 24mmx37mm mould, sectioned to create an even surface, and 2mm holes were drilled into the block with 1.1mm distance between the empty cores. Next, 2mm tissue cores were punched from the donor and inserted into the assigned position on the acceptor block. Of each age and diet group, five animals were used. Due to the high sample number, two TMAs containing 35 samples each were created for each tissue type. Animal samples were pre-sectioned and randomly assigned to a position on one of the two TMAs. To ensure antibody performance, old (36M) and young (2M) tissue as well as FFPE irradiated or non-irradiated

HEK cells were incorporated as controls. Furthermore, two FFPE murine lymphoma cell lines L5178Y-S and L5178Y-R were used as internal reference to assess and validate telomere length of the tissue samples. Completely assembled TMAs were baked upside-down on a glass slide for 16h at 42h and cooled for 10min on ice to remove the slide. TMAs were sectioned on a rotary microtome with 5µm thickness as described before.

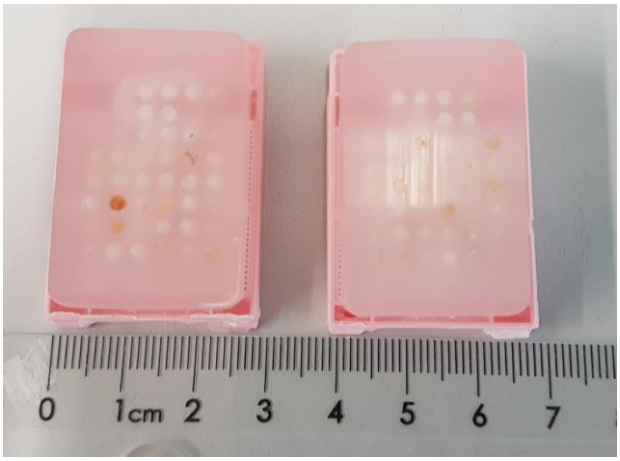

Figure 2. 2: Example TMA of white adipose tissue

2.2.3 Hematoxylin Eosin (HE) staining

Hematoxylin Eosin (HE) stainings were performed on WAT TMA samples on a fully-automated Gemini AS Automated Slide Stainer (A81500002, ThermoFisher Scientific) at RT. Samples were deparaffinised at RT in Xylene for 10min followed by rehydration in 100%, 96% and 70% EtOH for 5min each and brief rehydration in dH_2O. Nuclei were stained with Meyer's Hemalaun (A0884.1000 PanReac AppliChem) for 3min at RT, followed by incubation in luke-warm tap water for 3min and brief rehydration in dH_2O. Cytoplasmic staining with Eosin Y solution 0.5 % in water (X883.2, Roth) was carried out for 1min at RT, followed by two brief washing steps in dH_2O and a gradual dehydration series in 70% EtOH, 96% EtOH and 100% EtOH for 2min each. Slides were incubated twice for 2min in Xylene prior to mounting using a coverslipper (970010-19, ThermoFisher Scientific) and Cytoseal mounting medium (8312-4, ThermoFisher Scientific). Slides were dried OVN at RT before image acquisition on a Nikon Eclipse Ci (Leica) using a 20x objective.

2.2.4 Determination of adipocyte size

To assess how mid- or late-life DR impacted on adipocyte size, HE stained sections of the WAT TMA were analysed following a protocol by Joseph T. Roland using Fiji (Joseph Roland, n.d.). Images including a scale bar of 100µm length was used to calibrate Fiji with 3,24 pixel/µm. First, the coloured HE image was converted into an 8-bit greyscale image, inverted and the background was subtracted using the rolling ball radius with 20 pixel with a sliding paraboloid. The resulting image was segmented using morphological segmentation based on an object image with a gradient radius of three and a watershed segmentation with a tolerance of four pixel using the MorphoLibJ plugin. This step determined the adipocyte cell membrane using morphological segmentation (overlaid dams). The output image was processed using Gaussian blur with a sigma radius of two in order to smoothen the cell membrane. Next, the image was converted into 8-bit greyscale and the threshold was adjusted using mean and black and white as settings with 0 as lower and 14 as upper threshold. The adipocyte area was determined using the measure and label plugin and areas were reported in pixel^2. The adipocyte size in µm^2 was calculated using the following formula for each determined adipocyte:

$$\mu m^2 = \frac{1}{3{,}24^2} * area^2$$

At least three separate HE images were quantified and adipocyte areas were averaged per animal. Data were plotted per time point and diet group in GraphPad Prism and presented as mean with 95% CI. Differences between chronic controls at 5M, 16M, 20M or 24M were calculated using Two-way ANOVA followed by Bonferroni for multiple testing correction. Differences between chronic controls and DR switch groups at individual time points were assessed with One-way ANOVA followed by Bonferroni testing.

2.2.5 Immunohistochemistry (IHC)

Sectioned WAT TMA samples were deparaffinised in Xylene for 10min, gradually rehydrated in a descending EtOH series in 100% EtOH, 96% EtOH and 70% EtOH for 5min each and briefly rehydrated in dH_2O at RT using a StainMate Linear Batch Stainer (ThermoFisher Scientific). Antigen retrieval was carried out using the EMS retriever 2100 (#62706, EMS) with 10mM sodium citrate buffer at pH 6.

10mM sodium citrate buffer pH 6 or pH 6.5

- 2.94g sodium citrate dihydrate Kosher **(W302600, Merck)** was dissolved in 850ml ddH_2O, the pH was adjusted to a final pH of 6 or pH 6.5 using 37% HCl (471020, PanReac AppliChem) and filled up to 1L with ddH_2O.

After antigen retrieval, slides were washed once in 1X PBS (PBS) (18912014, ThermoFisher Scientific) before blocking in 0.3% H_2O_2 in MetOH for 30min at RT to block endogenous peroxidase activity. Slides were washed twice in 1XPBS and endogenous biotin was blocked using the Biotin/Avidin kit according to manufacturer's recommendations (004303, ThermoFisher Scientific). Excessive biotin was removed by two washing steps with 1X PBS and one with 1X PBS-0.5% Triton X 100 (PBS-T; X100, Merck) at room temperature (RT) for 5min each, followed by short rinsing in PBS for 5min to remove excessive Triton. Samples were blocked for 1h at RT in IHC blocking buffer (5% FBS, 2.5% BSA in 1X PBS) prior to primary antibody incubation OVN at 4°C in reaction buffer (0,25% BSA, 5% FBS, 2gr NaCl and 0.1g Triton in 1X PBS). Excessive primary antibody was removed by two subsequent washes with PBS-T and one wash in PBS under rotation at RT for 10min each. Probing with HRP-coupled goat anti rabbit secondary antibody was performed for 1h at RT in the dark. Please refer to table 2 for detailed information on the utilized antibodies for IHC. Samples were washed twice in PBS-T and once in PBS for 10min prior to 3,3′-Diaminobenzidine (DAB, D4168, Merck) visualization. DAB was prepared according to manufacturer's recommendations and diluted 1:5 in 1XPBS. Slides were incubated with DAB working solution for 6min at RT, washed once in dH_2O for 5min before staining with Meyer's Hematoxylin solution for 3min at RT. Nuclei were differentiated for 3min in lukewarm running tap water before dehydration in an ascending EtOH series and xylene. Slides were mounted with cytoseal mounting medium on a cover slipper as described previously and dried OVN prior to image acquisition on a Nikon microscope at 20x magnification

IHC blocking solution:

- 2,5g Fatty Acid-free Bovine Serum Albumin (BSA) (BP9704100, ThermoFisher Scientific)
- 5ml Fetal bovine serum (FBS) (10270-106, Lot: 42G7283K, ThermoFisher Scientific)
- 0.955g PBS buffer (10X Dulbecco's) (A0965, PanReac AppliChem)

Components were dissolved and filled up to 100ml in ddH_2O. Aliquots were stored at -20°C until use.

IHC Reaction buffer:

- 0.25g BSA
- 5ml FBS
- 2gr sodium chloride (NaCl) (A2942, PanReac AppliChem)
- 0.955g PBS
- 0.1g Triton X 100 (X100, Merck)

Buffer components were dissolved and filled up to 100ml in ddH_2O. Aliquots were stored at -20°C until use.

Table 2. List of antibodies used for IHC

Antibody	Source	Cat.#	Concentration	Species
F4/80 (D2S9R) XP®	Cell Signaling Technology	#70076	1:100	Rabbit
Goat anti-Rabbit IgG (H+L) Cross-Adsorbed Secondary Antibody, HRP	ThermoFisher Scientific	G21234	1:500	Goat

2.2.6 Analysis of macrophage infiltration

To assess WAT inflammation, the number of infiltrating macrophages determined by the appearance of crown-like structures (CLS) surrounding adipocytes was determined. The number of CLS was counted on the entire TMA core and two separate stained sections of the respective core were averaged in order to assess CLS in an earlier and later tissue section. Two-way ANOVA followed by Bonferroni post hoc test was used to test for statistically significant differences between chronic AL and DR at 5M, 16M, 20M or 24M. Differences between chronic controls and DR switch groups at individual time points were assessed with One-way ANOVA followed by Bonferroni testing. Data was plotted using mean with 95% CI in Graphpad Prism.

2.2.7 RNA isolation and RTqPCR on WAT of C3B6F1 females

RNA isolation and RTqPCRs were performed on WAT of 20M, 24M or 28M old AL, DR, AL_DR16M or AL_DR20M and on 26M old AL, DR, AL_DR and DR_AL animals (Hahn et al., 2019).

Between 70-120mg snap-frozen WAT samples were homogenized in 1000µl Trizol (15596018 ThermoFisher Scientific) and incubated for 5min at RT followed by centrifugation at full-speed for 10min at 4°C to collect free-floating fat. To avoid carry-over of fat, the Trizol subnatant was carefully transferred to a fresh tube, mixed with 200µl chloroform (366927-100ml, Sigma) and incubated for 10min at RT prior to centrifugation at 12.000g for 15min at 4°C. The aqueous RNA-containing phase was transferred to a fresh tube, mixed with 500µl isopropanol (39559.01 SERVA Electrophoresis), 50µl 3M Sodium acetate and 1.5µl GlycoBlue™ Coprecipitant (AM9515, 15mg/ml, ThermoFisher Scientific) and incubated for 10min at RT followed by centrifugation at 12.000g for 10min at 4°C. The supernatant was removed and the pellet was washed twice with 500µl ice-cold 70% ethanol (A3678 0250, absolute EtOH PanReac AppliChem) and centrifuged at 7.500g for 5min at 4°C. RNA pellets were air-dried for 15min at RT and re-suspended in 50µl DEPC-treated, autoclaved ddH_2O (BD2484-100, Fisher Scientific) followed by DNase treatment to remove genomic DNA contaminations using the DNA-free™ DNA Removal Kit (AM1906, Invitrogen) according to manufacturer's protocol.

RNA concentrations were measured by Qubit™ RNA BR Assay Kit (Q10210, ThermoFisher Scientific) according to manufacturer's protocol and equal concentrations of RNA (1500ng) were used for first-strand cDNA synthesis using SuperScript VILO Master Mix (11755-500, ThermoFisher Scientific) with 120min incubation at 42°C to increase cDNA yield.

Preparation of Taqman Gene Expression Master mix (4369106 Applied Biosciences) and Taqman Gene Expression Assays (see table 3 for further information on utilized probes) was conducted according to manufacturer's protocol and pipetted using a Janus Automated Workstation (PerkinElmer, Waltham, Massachusetts, USA). RTqPCR was carried out on a QuantStudio 6 Flex Real-Time PCR System (ThermoFisher Scientific) and gene expressions were calculated using the $2^{-\Delta\Delta CT}$ method with Pol2ri expression as internal control and normalized to the respective gene expression level of the AL control group.

Table 3. List of Taqman probes used for RTqPCR on WAT

Gene	Taqman probe	Source	Species
Srebpf1	Mm01138344_m1	ThermoFisher Scientific	*Mus musculus*

Fasn	Mm00662319_m1	ThermoFisher Scientific	*Mus musculus*
Elovl6	Mm00851223_s1	ThermoFisher Scientific	*Mus musculus*
Acaca	Mm01304257_m1	ThermoFisher Scientific	*Mus musculus*
Pol2ri	Mm01176661_g1	ThermoFisher Scientific	*Mus musculus*

2.2.8 DNA isolation and mtDNA qPCR on WAT

Total DNA including mitochondrial DNA (mtDNA) of snap-frozen WAT samples was isolated using the DNA Blood and Tissue kit (69506, Qiagen) following the manufacturer's protocol with an additional centrifugation step at 200g for 5min after lysis in ATL buffer and transfer of the supernatant to a fresh tube. DNA concentrations were quantified using the Qubit dsDNA BR Assay kit and manufacturer's recommendations (Q32853, ThermoFisher Scientific).

Total DNA samples were diluted to a final concentration of 2.5ng/µl in nuclease-free water. In order to generate a standard curve for the Q-RT-PCR, DNA samples were pooled and a five-point standard curve was prepared using undiluted pooled DNA and a 2-step serial dilution series ranging from a 1:2 to a 1:16 dilution in nuclease-free water was generated. This five-point standard curve encompassed the dilution factors of the individual samples and ensured that the highest and the lowest dilution factor of the samples were covered in the range of the standard curve. This step was crucial, as the amount of isolated DNA varied between mice.

Per reaction, 4,8µl Taqman gene expression master mix, 0,5µl of the respective Taqman probe and 3,7µl ddH_2O were prepared and stored on ice in the dark prior to pipetting with four technical replicates per WAT sample and taqman probe (see Table 4 for detailed information on the utilized probes). 9µl of the Taqman master mix was mixed with 2µl total DNA (5ng) by pipetting into 384-well plates using a Janus Automated Workstation. After the pipetting steps were completed, the plate was closed with a plastic cover, briefly vortexed to mix the components and spun down to collect the contents at the bottom. DNA was amplified on a QuantStudio 6 Flex Real-Time PCR System using standard curve settings. MtDNA content was calculated by the ratio of mtDNA probes relative to genomic DNA (mtDNA/18S) and normalized to the relative mtDNA content of the AL control group.

Table 4. List of Taqman probes used for mtDNA quantification

Gene	Taqman probe	Source	Species
ATP6	Mm03649417_g1	ThermoFisher Scientific	*Mus musculus*
Rnr2	Mm04260181_s1	ThermoFisher Scientific	*Mus musculus*

Cox1	Mm04225243_g1	ThermoFisher Scientific	*Mus musculus*
18S	Hs99999901_s1	ThermoFisher Scientific	*Human*

2.2.9 Protein preparation and quantification of C3B6F1 WAT samples

Snap-frozen white adipose tissue (WAT) samples were homogenized in Pierce™ RIPA Lysis and Extraction Buffer buffer (ThermoFisher Scientific, 89900) supplemented with phosphatase and protease inhibitor cocktails (Roche), incubated for 10min on ice and sonicated for 5min. After centrifugation for 15min at full-speed at 4°C in a tabletop centrifuge, protein extracts were transferred to fresh tubes and protein concentrations were quantified by Pierce™ BCA assay (ThermoFisher Scientific, 23225). Equal concentrations of protein extracts (25µg) in 1x Laemmli sample buffer were separated on 12% acrylamide gels (Criterion™ TGX Stain-Free™ Protein Gel #5678044, Biorad) and blotted on PVDF membranes (Amersham™ Hybond® P GE10600023 or Immobilon-FL IPFL00010, both Merck) for 1h at 100V on ice.

2.2.10 Western Blot (WB) analysis using HRP-coupled immunoblotting

Membranes were blocked for 1h at RT in 5% non-fat dry milk powder (A0830,1000 PanReac AppliChem) in TBS 0.1% Tween 20 (A4974.500, PanReac AppliChem)(TBS-T) followed by three washing steps for 10min with TBS-T and overnight incubation in primary antibody (for details see Table 5) diluted in sterile filtered 5% fatty-acid free bovine serum albumin (BSA) (BP9704-100, Fisher Scientific) in TBS-T. Blots were washed 3x in TBS 0.2% Tween for 10min, incubated with HRP- coupled secondary antibodies diluted in 5% milk in TBS-T for 1h at RT followed by three washing steps with TBS 0.2% Tween for 10min at RT. Immunoblots were incubated for 5min at RT in Pierce™ ECL Plus Western Blotting Substrate (32132, ThermoFisher Scientific) followed by image acquisition on a ChemiDoc™ XRS+ system (Biorad). Western Blot signals were quantified using Fiji with alpha tubulin as internal control and normalized against AL controls.

2.2.11 WB analysis using the fluorescence- based Odyssey system

Membranes were blocked for 1h at RT in Odyssey® Blocking Buffer (TBS) (927-50000 LI-COR Biosciences) followed by overnight incubation in primary antibody (for details see Table 5)

diluted in Odyssey® Blocking Buffer. Blots were washed four times in TBS 0.2% Tween (TBS-T) for 5min each, incubated with fluorescently labelled secondary antibodies diluted in Odyssey® Blocking Buffer for 1h at RT followed by four washing steps for 5min with TBS-T at RT and image acquisition using the Odyssey Infrared Imaging System (LI-COR Biosciences). Images were converted into greyscale images and signals of the respective proteins were quantified using Fiji with alpha tubulin as internal control and normalized against AL controls.

2.2.12 Stripping of Western Blot membranes and re-probing with different primary antibodies

After image acquisition of p-Akt Thr308 and p-Akt Ser473 or total Akt using the ChemiDoc system, membranes were briefly washed in TBS-T to remove residual ECL solution before incubation with 0.5M NaOH for 15min at RT on a shaker. The membranes were washed twice with TBS-T for 5min each, once with TBS and incubated with ECL solution and subjected to image acquisition to assess residual antibody signal. If residual signal was detected after 10min exposure, the membranes were briefly washed in TBS-T, incubated for additional 15min in 0.5M NaOH, and washed before image acquisition. If no residual signal was detected, the membranes were washed briefly in TBS-T before blocking in 5% milk in TBS-T and OVN incubation with primary antibody as described before.

After image acquisition of phospho or total p70 S6 kinase, the immobilon membrane was imaged on the Odyssey system on the highest intensity to bleach the fluorescent signal. Next, the membrane was washed twice in ddH_2O for 4min each before incubation with 0.2M NaOH for 10min at RT. Residual NaOH was removed by two washing steps in ddH_2O and three washing steps in TBS-T for 4min each. Afterwards, the stripped membrane was imaged with the highest intensity to gauge the intensity of residual signal. Blocking and incubation with primary antibody proceeded according to protocol if no residual signal was detected or the striping process was repeated as described before.

Table 5. List of antibodies used for Western Blot analysis

Antibody	Source	Cat.#	Concentration	Species
UCP1	Cell Signaling Technology	14670	1:1000	Rabbit
α-Tubulin (11H10)	Cell Signaling Technology	2125	1:1000	Rabbit

mtCO1 [1D6E1A8]	Abcam	Ab14705	1:1000	Mouse
NDUFA9	Abcam	Ab14713	1:1000	Mouse
Phospho-p70 S6 Kinase (Thr389)	Cell Signaling Technology	9205	1:1000	Rabbit
p70 S6 Kinase	Cell Signaling Technology	9202	1:1000	Rabbit
Phospho-Akt (Ser473)	Cell Signaling Technology	9271	1:1000	Rabbit
Phospho-Akt (Thr308)	Cell Signaling Technology	9275	1:1000	Rabbit
Akt	Cell Signaling Technology	9272	1:1000	Rabbit
IRDye 680RD Goat anti-Rabbit IgG (H + L), 0.5 mg	LI-COR Biosciences	926-68071	1:15.000	Goat
IRDye® 800CW Goat anti-Mouse IgG (H + L), 0.5 mg	LI-COR Biosciences	926-32210	1:15.000	Goat
Goat anti-Rabbit IgG (H+L) Cross-Adsorbed Secondary Antibody, HRP	ThermoFisher Scientific	G21234	1:10.000	Goat

2.3 Fluorescence-activated cell (FACS) sorting

2.3.1 Isolation and staining of the stromal vascular fraction (SVF) from the WAT for FACS analyses

The protocol for isolation and staining of SVF and mature adipocytes was adapted and modified from Majka and colleagues (Majka et al., 2014) and Church and colleagues (Church, et al., 2014). All isolation and staining steps were performed in a cell culture hood. Unless otherwise stated, all centrifugation steps were carried out at 150g for 5min. Cell isolation and subsequent FACS sorting were performed on 27M old C3B6F1 hybrids on chronic AL feeding,

chronic DR or on DR switches (AL_DR12M, AL_DR16M and AL_DR20M) to investigate WAT heterogeneity.

Animals were sacrificed using cervical dislocation and epididymal fat pads were dissected and placed in 1x PBS. Fat pads were washed once with sterile DPBS in 10cm cell culture dishes and dissected into small tissue pieces using a razor. Tissue fragments were transferred into a 50ml falcon tube and 5ml digestion buffer was added per initial fat pad and incubated for 1h in a shaking water bath at 1000rpm and 37°C.

Krebs-Ringer-HEPES buffer

- 120mM NaCl (A2942, PanReac AppliChem)
- 4,7mM potassium chloride (KCl) (60130, Sigma-Aldrich)
- 2,2mM calcium chloride ($CaCl_2$) (HNO4-2, Roth)
- 10mM 4-(2-hydroxyethyl)-1-piperazineethanesulfonic acid (HEPES) (H3375, Sigma-Aldrich)
- 1,2mM Potassium phosphate monobasic (KH_2PO_4) (P9791, Sigma-Aldrich)
- 1,2mM Magnesium sulfate ($MgSO_4$) (M7506, Sigma-Aldrich)

Stock solutions of 5M NaCl, 500mM KCl, 500mM $CaCl_2$, 100mM KH_2PO_4 and 100mM $MgSO_4$ were prepared in ddH_2O and autoclaved before use. 1M HEPES stock solution was prepared in ddH_2O, the pH was adjusted to pH 7.4 and the solution was sterile filtrated. Buffer components were mixed and dissolved in 200ml ddH2O. The pH was adjusted to pH 7.4 with NaOH, the volume was adjusted to 250ml and the solution was sterile filtrated using ….

Digestion buffer per fat pad

- 1mg/ml Collagenase Type 2 (LS004177, Worthington Biochemical Cooperation)
- 200µm Adenosine (A9251, Merck)
- 2.5mM D(+)-Glucose (HNO6.1, Roth)
- 2% FBS
- 5ml Krebs-Ringer's-HEPES buffer

Stock solutions of 100mM D(+)-Glucose and 10mM adenosine were prepared with ddH2O and sterile filtrated. D(+)-Glucose, FBS, collagenase II and adenosine were added freshly prior to use to 5ml Krebs-Ringer-HEPES buffer and mixed.

After 30min incubation, the tubes were vigorously mixed to ensure complete tissue dissociation. Next, the cell suspension was filtered first through a 400µm filter (43-50400-01,

pluriSelect) and subsequently through a 200µm filter (43-50200-01, pluriSelect). An equal volume of wash buffer was added and the suspension was centrifuged at 150g for 8min to separate the cell types into three layers.

Wash buffer

- Hanks balanced salt solution (HBSS) (14175-053, ThermoFisher Scientific)
- 200µm Adenosine (A9251, Merck)
- 2% FBS

Wash buffer was prepared freshly prior to use by mixing stock solutions from buffer components.

After centrifugation, three layers were obtained. The upper layer contained free floating fat and mature adipocytes, the second layer contained mostly tissue fragments and cells from the stromal vascular fraction (SVF) were located in the pellet. The adipocyte fraction was carefully transferred to a fresh 15ml falcon tube and the intermediate phase was removed to obtain the pellet for SVF isolation.

The SVF cell pellet was washed with wash buffer and centrifuged at 150g for 8min. The supernatant was carefully removed and the cell pellet was washed in wash buffer and centrifuged at 150g. The pellet was transferred to a clean 15ml falcon tube and washed twice in wash buffer. The supernatant was completely removed and Erythrocytes were lysed using Erythrocyte lysis buffer (79217, Qiagen) for 5min at RT. The falcon tube was filled up with wash buffer to stop lysis and cells were centrifuged at 200g for 5min. Cells were resuspended in wash buffer and filtered through a 30µm filter (130-041-407, Miltenyi) into a fresh 15ml falcon tube. Antibodies against CD45, F4/80, CD34, CD29, CD31, CD24 and Sca1 were added at their respective concentration to 100µl wash buffer, mixed and incubated at 37°C 5% CO2 for 30min with a mixing step after 15min (for details see Table 6).

FACS buffer

- Hanks balanced salt solution (HBSS) (14175-053, ThermoFisher Scientific)
- 200µm Adenosine (A9251, Merck)
- 5% FBS

FACS buffer was prepared freshly prior to use by mixing stock solutions from buffer components.

Table 6. Primary antibodies with corresponding fluorophore used for SVF FACS sorting and analyses

Antibody	Clone	Concentration	Source	Fluorophore	Antigen
Alexa Fluor® 700 anti-mouse CD45 Antibody	30-F11	1,5µg	Cat. No. 103128 Biolegend	Alexa Fluor 700	CD45
PE/Cy5 anti-mouse CD34 Antibody	MEC 14.7	2µg	Cat. No. 119312 Biolegend	PE-Cy5	CD34
APC anti-mouse/rat CD29 Antibody	HMβ 1-1	1µg	Cat. No. 102216 Biolegend	APC	CD29
PE-Cy™7 Rat Anti-Mouse Ly-6A/E Sca1	D7	0,15µg	561021 BD Pharmingen ™	PE-Cy7	Ly6A/E Sca1
PE anti-mouse CD31 Antibody	MEC13 .3	1µg	Cat. No. 102508 Biolegend	PE	CD31
FITC anti-mouse CD24 Antibody	M1/69	2,5µg	Cat. No. 101805 BioLegend	FITC	CD24
APC/Cyanine7 anti-mouse F4/80 Antibody	BM8	2µg	Cat. No. 123118 BioLegend	APC/Cy-7	F4/80

The SVF was centrifuged at 200g for 5min and washed thrice with wash buffer to remove excessive antibodies. After the last washing step, the supernatant was completely removed, cells were resuspended in 200µl FACS buffer and filtered through a 30µm filter (352235, Falcon) prior to sorting and 1µg/µl DAPI was added to label dead cells. SVF cells were sorted on a BD FACSAria™ IIIu cell sorter (BD Biosciences) and a 100µm nozzle and 20psi shear pressure in the FACS and imaging facility of the Max-Planck-Institute for Biology of Ageing.

2.3.2 Gating strategy of SVF cells

SVF cells were first gated based on their SSC and forward scattering (FSC) profile, to discriminate between cells and debris. Next, single cells were identified based on FSC and SSC and live cells were gated from DAPI positive dead cells. To assess different cell populations, cells were gated based on the two lineage factors CD45 and CD31. CD45 is a marker of differentiated hematopoietic cells, such as immune cells, and is present on their cell surfaces. The immune cell population was further gated into macrophages based on positive F4/80 staining (CD45+, F4/80+) and all other immune cells with negative F4/80 staining (CD45+, F4/80-). CD31 is an endothelial surface marker and is therefore present on blood vessel endothelium, which were not further sub-classified. Adipocyte progenitor and stem cell populations displayed negative staining for both lineage factor markers (lin-) but stained positive for both mesenchymal stem cell (MSC) markers CD29 and CD34 (lin-, CD29 and CD34 double +). Based on the third MSC markerLy-6A/E (Sca1), adipocyte progenitors were classified as progenitors with Sca1 high ($Sca1^h$) and committed progenitors with Sca1 low ($Sca1^l$). Finally, stem cells were classified as $Sca1^h$ and CD24 positive (refer to table 7 for details). Only alive cells classified as stem cells, progenitors, committed progenitors, immune cells or macrophages were bulk sorted based on cell type into Eppendorf tubes containing Trizol or 1XPBS with 1000 cells per tube. Sorted cells were kept at -80°C for subsequent analyses.

Table 7. Cell type definition based on the gating strategy of different SVF cells

Cell type	Panel
Macrophages	CD45 positive F4/80 positive CD31 negative
Immune cells	CD45 positive F4/80 negative CD31 negative
Endothelial cells	CD31 positive CD45 negative
Committed adipocyte progenitors	CD45 negative CD31 negative CD29 positive

	CD34 positive Sca1 low
Adipocyte progenitors	CD45 negative CD31 negative CD29 positive CD34 positive Sca1 highly positive
Adipose tissue stem cells	CD45 negative CD31 negative CD29 positive CD34 positive Sca1 positive CD24 positive

2.3.3 Antibody staining of AbC antibody capture beads:

To account for laser intensities and bleeding over of fluorophore emission spectra into different channels, AbC™ Total Antibody Compensation beads (A10497, ThermoFisher) were used. Beads were included in all experiments to maintain similar sorting conditions for all sorting dates and animals. Beads were resuspended by vortexing for 10sec and one drop of beads was added per Eppendorf tube. In total, eight tubes were prepared, corresponding to the eight different antibodies used in the SVF panel. The respective dilution of each antibody was added to the beads, mixed well and incubated for 15min in the dark (see Table 8 for details). Beads were washed twice with 1X PBS and centrifuged in between at 200g for 5min to remove excessive unbound antibodies. After the second washing step, beads were resuspended in 500µl FACS buffer and one drop of negative beads was added to each tube and kept in the dark until sorting. For sorting, beads were transferred to FACS tubes and control beads were gated for single fluorophores on forward (FSC) and side scatter (SSC) for compensation.

Table 8. Antibody amounts incubated with capture beads to set up the gating strategy

Antibody	CD45 only	CD34 only	CD29 only	Sca1 only	CD31 only	CD24 only	F4/80 only
Alexa Fluor® 700 anti-mouse CD45 Antibody	0.6µl	No	No	No	No	No	No
PE/Cy5 anti-mouse CD34 Antibody	No	5µl	No	No	No	No	No
APC anti-mouse/rat CD29 Antibody	No	No	2µl	No	No	No	No
PE-Cy™7 Rat Anti-Mouse Ly-6A/E Sca1	No	No	No	1µl undiluted and the rest of the 1:10 dilution	No	No	No
PE anti-mouse CD31 Antibody	No	No	No	No	2µl	No	No
FITC anti-mouse CD24 Antibody	No	No	No	No	No	3µl	No
APC/Cyanine7 anti-mouse F4/80 Antibody	No	No	No	No	No	No	3µl

2.3.4 FACS analysis using FloJo

FACS sorting data was analysed using the FloJo V10 software from BD Biosciences. Files were imported into FloJo, the gating strategy of the different cell types was recreated, and the same gating strategy was applied to all sortings to allow comparisons between diet groups. Sortings from the same animal were concatenated and analysed as batch per sorting day. Cell type frequencies were calculated as percent of alive cells to obtain information on cell type distribution within the viable cell fraction of each animal. Cell type percentages were averaged per diet group and statistically analysed using Graphpad Prism.

2.4 Primary cell and organoid culture

2.4.1 Isolation of the stromal vascular fraction from WAT of 27M old AL, DR and DR switch mice

Animals were sacrificed using cervical dislocation and the WAT depots were dissected out and placed in 1x PBS. The PBS was removed and the WAT was dissected into small pieces using razors and transfer to a 50ml falcon tube. Per mouse, 1mg/ml Collagenase Type 2 (LS004177, Worthington Biochemical Cooperation), 3,4% BSA (10% stock solution prepared in 1x FBS, BP9704100, ThermoFisher Scientific) and 0.75mg DNase I (10104159001, Merck) was dissolved in DMEM/Ham's F12 medium (FG 4815, Merck) with a final volume of 10ml. WAT fragments were incubated in the enzyme solution for 1h at 37°C at 120rpm in a shaking water bath. After 30min of incubation, the samples were vigorously mixed to ensure complete dissociation before a second 30min incubation. The fat-enzyme- suspension was filtered over a 100µm mesh (3523620, Falcon) to retain debris and washed with 15ml SVF growth medium (DMEM high glucose (41966-029, ThermoFisher Scientific) supplemented with 1% Penicillin-Streptomycin (5,000 U/mL) (15070063, ThermoFisher Scientific) and 10% heat-inactivated Fetal Bovine Serum (FBS) (10270-106, Lot: 42G7283K, ThermoFisher Scientific). To pelletize the stromal vascular fraction (SVF), the suspension was centrifuged at 200g for 5min. Next, floating fat and the intermediate layer was removed and the pellet was washed twice with 10ml SVF growth medium and followed by centrifugation and discarding the supernatant. After the last washing step, the resuspended pellet was transferred to a fresh 15ml falcon tube, centrifuged before incubation in 1ml pre-warmed erythrocyte lysis buffer (79217, Qiagen) for 5min at RT to remove erythrocytes. The reaction was stopped by addition of SVF growth medium and the cells were centrifuged at 200g for 5min. The supernatant was discarded and the cells were resuspended in 400µl SVF growth medium before filtering over a pre-wet 30µm mesh (130-041-402, Miltenyi Biotec) into a fresh falcon tube. To assess total cell numbers, 10µl cell suspension was mixed 1:1 with Trypan Blue 0.4% (15250-061) and live cells were counted with Neubauer counting chamber (0640030, Marienfeld Superior). The required amount for 10.000 cells per well was calculated and cells were seeded in a Cellstar 96-well plate (655 180, Greiner Bio One) supplemented with 200µl SVF growth medium and incubated at 37°C with 5% CO_2. Depending on the cell concentrations, either the entire cell suspension was used or a maximum of 10 wells were seeded per diet group. The medium was replaced every second day and SVF cells were grown to confluence before induction.

2.4.2 Induction and differentiation of primary SVF cells and cell fixation

After reaching full confluence, the SVF growth medium was removed and half of the seeded wells per animal were induced for 48h with SVF induction medium. The other half of the wells was kept as undifferentiated controls and received regular SVF growth medium. After 48h, the induction medium was removed and cells were differentiated with SVF differentiation medium for eight days with consecutive medium changes every second day. Following the same pattern, the medium of undifferentiated control cells was replaced with fresh SVF growth medium every two days. Cells were kept at 37°C, 5% CO_2 throughout the entire differentiation process. After eight days of differentiation, the medium was removed and cells were washed once in 1x DPBS to remove residual medium. Cells were fixed with 4% paraformaldehyde (stock concentration 16&, 28908, ThermoFisher Scientific) for 30min at RT, washed twice with 1x DPBS and stored at 4°C until Oil Red O staining. Seeded chronic DR SVF cells, which did not reach full confluence, were treated as non- differentiated controls only.

SVF induction medium

- 1.7µg/ml insulin (I9278, Merck)
- 1nM triiodothyronine (T3) (T2877, Merck), stock concentration 1mM, dissolved in 1M NaOH
- 50µg/ml ascorbic acid (95209, Merck), stock concentration 50mg/ml dissolved in ddH2O
- 17mM D-pantothenic acid (DPA) (P5155, Merck), stock concentration 850mM, dissolved in ddH2O
- 1µM Biotin (B4639, Merck), stock concentration 1mM, dissolved in 0.1M NaOH
- 0.25µM Dexamethasone (D1756, Merck), stock concentration 250µM, dissolved in 100% EtOH
- 0.5mM 3-isobutyl-1-methylxanthine (IBMX) (I5879-5G, Sigma-Aldrich), stock concentration 500mM dissolved in DMSO
- 1µM Rosiglitazone (R2408-10MG, Merck), stock concentration 1mM, dissolved in DMSO

Stock solutions of all components were prepared separately and respective amounts were mixed in accordance with their final concentration with SVF growth medium.

SVF differentiation medium

- 1.7µg/ml insulin (I9278, Merck)
- 1nM triiodothyronine (T3) (T2877, Merck), stock concentration 1mM, dissolved in 1M NaOH
- 50µg/ml ascorbic acid (95209, Merck), stock concentration 50mg/ml dissolved in ddH2O
- 17mM D-pantothenic acid (DPA) (P5155, Merck), stock concentration 850mM, dissolved in ddH2O
- 1µM Biotin (B4639, Merck), stock concentration 1mM, dissolved in 0.1M NaOH

Stock solutions of all components were prepared separately and respective amounts were mixed in accordance with their final concentration with SVF growth medium.

2.4.3 Oil Red O staining, imaging and quantification of primary SVF cells

To assess lipid droplet amounts in differentiated or undifferentiated primary SVF cells, Oil Red O (ORO) staining followed by imaging and dye extraction was performed. ORO working solution was prepared by mixing three parts 0.5% Oil Red O solution in isopropanol (O1391, Merck) with two parts dH_2O. The ORO working solution was incubated for 20min in the dark followed by filtration through a 0.22µm filter (SLGP033RS, Merck Millipore). The storage DPBS was removed and cells were stained with 50µl ORO per well and incubated for 30min at RT on a shaker at 90rpm. Next, cells were washed five times with ddH_2O, stored in ddH_2O before imaging on an EVOS® FL Auto Imaging System (AMF7000, ThermoFisher Scientific). Representative images of differentiated or undifferentiated SVF cells were acquired at 40x magnification using transmitted light in conjunction with the Cy5 LED light cube or at 10x magnification using transmitted light. After image acquisition, the incorporated ORO stain was extracted using 100µl Isopropanol (39559.01, Serva) per well after incubation for 10min at RT on a shaker. The extracted isopropanol was transferred to a fresh 96-well plate and the ORO absorption at 500nm was determined on an Infinite M200 plate reader (Tecan). To correlate the ORO concentrations in the samples, a standard curve of ORO standards with 500µg/ml, 250 µg/ml, 100 µg/ml, 50 µg/ml, 25 µg/ml and 0 µg/ml was prepared and read out alongside the samples. For each sample, the ORO concentration was calculated in relation to the standard curve and technical replicates per animal were averaged. Results were plotted in Graphpad Prism, presented as mean with 95% CI and analysed using Two-Way ANOVA followed by Bonferroni correction for multiple testing.

2.4.4 Isolation of intestinal crypts for primary organoid culture

Intestinal epithelial organoid cultures were generated from 26M old chronic AL, DR control mice or DR switches at 12M, 16M or 20M. Five mice of each diet group were used to establish organoid cultures and the protocol was carried out according to manufacturer's recommendations.

Mice were sacrificed using cervical dislocation and the jejunum part of the small intestine was dissected. Residual mesenteric fat and external membrane was removed and intestinal segments were stored in cold DPBS. The jejunum segment was flushed with cold DPBS, cut open longitudinally and flushed again with DPBS to remove residual food content and mucus. Next, intestinal segments were sectioned into 2mm long sections and washed extensively with DPBS until the supernatant was clear. Leftover DPBS was removed and intestinal sections were digested in 15ml Gentle Cell Dissociation Reagent (07174, Stemcell technologies) for 15min at RT under rotation at 20rpm. In the meantime, 24-well plates were equilibrated to 37°C in a cell culture incubator. The tissue pieces were allowed to settle on ice and the supernatant was discarded. Next, tissue fragments were resuspended in 10ml cold DPBS containing 0.1% BSA and the supernatant was filtered over a sterile 70µm cell strainer (431751, Corning). The procedure was repeated twice and the filtrate was centrifuged at 290g for 5min at 4°C. The supernatant was removed and the pellet was resuspended in 10ml cold DMEM/F12 medium containing HEPES (11330032, ThermoFisher Scientific). Of each sample, a 10µl aliquot was taken and the number of crypts was counted under a light microscope. The resulting crypt numbers were multiplied by 100 to obtain the approximate number per ml. The volume of suspension corresponding to 1000 crypts was centrifuged at 290g for 5min at 4°C. The medium was removed and crypts were resuspended in a 1:1 ratio of Intesticult IntestiCult™ Organoid Growth Medium (06005, Stemcell technologies) and Matrigel® GFR and Phenol Red-Free Basement Membrane Matrix (356231, Corning®). Per animal, three technical replicates were seeded on a 24-well plate, allowed to adhere for 10min at 37°C and carefully submerged in 400µl medium.

Fresh medium was supplied three times per week and organoid outgrowth was assessed on Day 5, 7 and 10 post-seeding. First, the total number of organoids was counted in each well. To obtain reliable results on organoid outgrowth, all buds on at least 20 representative organoids were counted per well. If less than 20 organoids were growing in one well, the outgrowth on all viable organoids was assessed. Results on total organoid number and outgrowth per organoid were averaged between technical replicates and to obtain the average number of buds per organoid the following equation was used:

$$Buds\ per\ organoid = \frac{Sum\ of\ all\ counted\ buds}{Number\ of\ \ counted, representataive\ organoids}$$

Additionally, three representative organoid images were acquired for each well at 20x magnification on a bright field microscope (DM IL LED serial number 369497, Leica).

2.4.5 Passaging of intestinal organoids

Organoids were passaged to assess the influence of early, mid or late-life DR onset on the restoration capacity of intestinal organoid. Therefore, growth medium was completely removed and matrigel domes were broken up in 1ml gentle cell dissociation medium by pipetting up and down for 20 times. Triplicate wells of each mouse were pooled into one replicate using 1ml dissociation reagent. The organoid suspension was transferred to a 15ml falcon tube, additional 250µl dissociation reagent was added and incubated for 10min at RT under rotation at 20rpm. The organoid suspension was pipetted up and down to ensure complete dissociation into crypts. The required amount for approximately 75 crypts per well was calculated, the corresponding volume was transferred into a fresh tube and pelleted at 290g for 5min at 4°C. The supernatant was discarded and crypts were resuspended in an equal amount of 25µl growth medium and 25µl matrigel. Crypts were seeded on a 24-well plate and adhered at 37°C for 10min for matrigel solidification. Per well, 400µl growth medium was added and crypts were cultured at 37°C with 5% CO_2 with medium exchange three times per week.

Organoid outgrowth was counted on Day 3, 5, 7 and 10 post-seeding and five representative images were taken per well on each day of organoid assessment and analysed as described previously.

2.4.6 Seeding of intestinal organoids for staining analyses

Organoids were dissociated in 1X DPBS by pipetting up and down for 20 times and the resulting intestinal crypt suspension was transferred to 2ml Eppendorf tubes. Per mouse, 250µl suspension was transferred in one Eppendorf tube and crypt suspensions from all mice belonging to the same diet group were pooled. Crypts were pelleted for 1min at 2000g on a MiniStar Silverline table top centrifuge (521-2844, VWR), the supernatant was removed and crypts were resuspended in an equal volume of growth medium and matrigel and plated on a LabTek II 8-well chamber slide (154534, ThermoFisher Scientific). Each diet group was seeded in one well on two separate chamber slides. Chamber slides were adhered for 10min at 37°C and crypts were submerged in 300µl growth medium and incubated for 5d with one

medium change after 3d. Leftover organoid suspension was centrifuged for 1min at 2000g, DPBS was removed completely and organoids were frozen at -20°C for further analyses. After 5d of culture, organoids were washed once in 1X PBS, fixed in 4% formaldehyde for 10min at RT, washed once in 1X PBS and blocked for 30min at RT in blocking solution containing 2% skim milk (A0830,1000 PanReac AppliChem) in 1XPBS supplied with 0.1% Triton X 100 (PBS-T). Next, the plastic wells were removed from the chamber slide and primary antibodies raised against Ki67 or Lysozyme in blocking solution were added to the slide, covered with parafilm and incubated in a wet chamber at 4°C OVN. Slides were washed 3x in PBS-T for 5min and incubated with AF488 coupled anti rabbit secondary antibody and 0.5µg/ml DAPI in blocking solution for 1h at RT. Respective amounts of primary and secondary antibodies are listed in Table 9. Slides were washed thrice in PBS-T prior to incubation with Rhodamine Phalloidin (R415, ThermoFisher Scientific) diluted 1:500 in 1XPBS for 5min at RT in the dark. Slides were washed three times in PBS-T prior to mounting in Vectashield mounting medium for fluorescence (H1000; Vector Laboratories).

Table 9. List of antibodies used for organoid stainings

Antibody	Source	Cat. #	Concentration	Species
Lysozyme Polyclonal Antibody	ThermoFisher Scientific	PA5-16668	1:100	Rabbit
Ki-67 Monoclonal Antibody (SP6)	ThermoFisher Scientific	MA5-14520	1:250	Rabbit
Goat anti-Rabbit IgG (H+L) Highly Cross-Adsorbed Secondary Antibody, Alexa Fluor 488	ThermoFisher Scientific	A-11034	1:1000	Goat

2.4.7 Image acquisition and analysis of Ki67 or lysozyme- stained organoids

At least 20 organoids were counted per condition for the lysozyme staining and at least 10 organoids per condition were counted for the Ki67 staining. Lysozyme positive stained cells and Ki67 bright cells were counted per eye and averaged over the total number of counted organoids per well. Data was analyzed in Graphpad Prism using One-way ANOVA followed by Tukey’s test to correct for multiple comparisons.

Representative Z stacks were acquired with 1.5µm step size, with 4096x4096 pixel per image and 400 hertz speed on a Leica SP8 confocal microscope. Between images, the laser power (LP) conditions were kept constant for all diet groups to ensure comparability. To generate representative images, merged colour images were split to acquire separate blue DAPI, red phalloidin and green lysozyme or Ki67 channels. The maximal intensity Z projection of each single channel was created and all three channels were subsequently merged again to obtain a single image using Fiji *(Schindelin et al., 2012).*

2.5 Electron microscopy (EM)

2.5.1 Transmission electron microscopy on jejunum and ileum sections from 20M or 27M old AL, DR and AL_DR switch groups

Electron microscopy (EM) samples of the jejunum section of the small intestine were prepared from 20M or 27M old AL, DR and DR switch groups. At 27M, additional EM samples were generated for the intestinal ileum sections for chronic AL, DR and DR onset at 12M, 16M and 20M of age. Sample preparation, embedding, sectioning and image acquisition were carried out by Janine Klask from the CECAD Imaging facility.

Mice were sacrificed using cervical dislocation, the gastrointestinal tract was dissected into jejunum and ileum sections. Of each intestinal section, two cross-sectional and one longitudinal pieces were cut measuring two millimetre in length. The intestinal tissue sections were fixed for 48h at 4°C in 2% paraformaldehyde (stock concentration 16%, E15711 EM grade, Science Services) and 2% glutaraldehyde (stock concentration 25%, 1.04239.0250, Merck) in 0.1M cacodylate buffer pH 7.3 (A2140,0250 Cacodylic acid sodium salt trihydrate, Biochemica). After fixation for 48h, jejunum or ileum samples were washed four times with 0,1M cacodylate buffer pH 7,2- 7,3 at 4°C for 15min each to remove excessive fixative. Next, samples were post-fixed with 2% Osmium tetroxide (OsO_4) (Science Services) in 0,1 M cacodylate buffer for 2h at 4°C in the dark. After incubation with OsO_4, samples were washed four times with 0,1M cacodylate buffer pH 7,2- 7,3 at 4°C for 15min each to remove excessive staining solution and dehydrated using an ascending EtOH series at 4°C with 50%, 70% EtOH, 90% EtOH and three consecutive dehydration steps in 100% EtOH (AppliChem) for 15min each. To remove residual EtOH, samples were incubated first with a 1:1 ratio of propylen oxide (Merck) and EtOH followed by two incubation steps with pure propylen oxide for 15min at 4°C each. Samples were embedded first in a 1:1 ratio of epoxy resin (Sigma-Aldrich) and propylen

oxide, transferred in 3:1 ratio of epoxy resin and propylen oxide both for 2h at 4°C before an OVN incubation in epoxy resin at 4°C. Samples were immersed in fresh epoxy resin for 2h at RT followed by a final incubation step in epoxy resin for 72h at 62°C. Next, ultra-thin 70nm sections were generated on an ultramicrotome (EM-UC6, Leica) and transferred onto 100µm copper grids (Science Services). Samples were contrasted using 1,5% uranyl acetate (Plano) for 15min at 37°C, then washed for five times in HPLC H_2O before a second contrasting step in lead citrate (Sigma-Aldrich) and NaOH for 4min. Samples were washed five times with 0.02M NaOH followed by five washing steps in HPLC H_2O before image acquisition at RT on a transmission electron microscope (JEM-2100 Plus, JEOL) equipped with a OneView 4K camera (GATAN) using the DigitalMicrograph software. Tight junctions between enterocytes were imaged at 20.00x magnification and paneth cells granules with 2500x magnification with at least 10 images per region of interest. Scale bars were included at 500nM or 5µm, respectively.

2.5.2 Grading of tight junction integrity and paneth cell health in 20M or 27M old intestinal sections

Tight junctions between enterocytes were scored based on electron density (Juricic et al., n.d.; Parikh et al., 2019; Zhao et al., 2018). Grade I tight junctions were defined as narrow, electron dense junctions with two visibly discriminated cell membranes. Grade II tight junctions exhibited two visible cell membranes but with diffuse electron density. Grade III tight junctions were classified with no discriminable cell membranes, low electron density and an overall blurred appearance. The percentage of grade I, II or III tight junctions was calculated and plotted.

Paneth cell pathology was determined based on the appearance of paneth cell granules in the intestinal crypts. Hypodense paneth cell granules were defined as granules with a black core and a white surrounding halo. Crinophagic paneth cell granules were classified as fused granules with autophagosomes or lysosomes for degradation. The percentage of hypodense or crinophagic granules in relation to the total number of granules inside the individual paneth cells was calculated and averaged per animal.

2.6 Cell culture

2.6.1 Culture and maintenance of human or murine cell lines

Unless otherwise stated, all centrifugation steps were performed at 300g for 3min on a Heraeus Multifuge X3R centrifuge (ThermoFisher Scientific) and cells were grown to approximately 90% confluency before splitting or before experiments.

To initiate culture, adherent or suspension cells were thawed at 37°C in a water bath, transferred into a falcon tube containing 5ml pre-warmed corresponding complete medium and centrifuged. The Dimethylsulfoxid (DMSO)-containing supernatant was removed and the cell pellet was carefully re-suspended in complete medium and seeded onto 10cm culture dishes or T75 flasks (658980, Greiner Bio-One). Cells were cultured at 37°C 5% CO_2 and passaged every 2-3 days. For cryopreservation, cells were centrifuged and the cell pellet was re-suspended in complete medium containing 10% DMSO (A994.2, Carl Roth) in cryogenic tubes (122280, Greiner Bio-One). Cells were gradually frozen at -80°C in freezing containers (5100-0001, ThermoFisher Scientific) and stored at -80°C until further use.

2.6.2 Culture of 3T3 L1 cells

Murine 3T3 L1 cells were used as positive controls to validate the performance of the differentiation protocol of primary SVF cells and to ensure that the differentiation process was functioning. 3T3 L1 cells were cultured in SVF growth medium at 37°C and 5% CO_2 until they reached confluence. Cells were washed once with DPBS and detached from the plate using 0.25% trypsin (25050014, ThermoFisher Scientific). Trypsination was stopped by addition of SVF growth medium and cells were either passaged to maintain the culture or counted on a Neubauer counting chamber to assess cell numbers. To control the differentiation process of primary SVF cells, 10.000 or 15.000 cells per well were seeded out on a 96-well plate and cultured to confluence. 3T3 L1 cells were induced and differentiated alongside primary SVF cells using the same media, fixed after eight days of differentiation, stained with ORO, imaged and quantified.

2.6.3 Culture of human embryonic kidney (HEK) cells

UV irradiated or non-irradiated HEK cells were used as positive or negative controls to validate the γ-H2AX antibody performance for DNA damage stainings on the TMAs. HEK cell culture was initiated and maintained as described before. To detach cells from the culture vessel, the DMEM complete medium was removed and cells were washed once with DPBS. Cells were treated with 0.25% trypsin (25050014, ThermoFisher Scientific) for approx. 3min at 37°C, detached from the surface with medium and centrifuged. The cell pellet was re-suspended in growth medium and cells were split into fresh culture vessels or frozen down. For UV irradiation, cells were cultured on 10cm dishes and grown to 90% confluency. Cells were irradiated at 40mJ/cm^2 on a UV cross-linker (UVC 500 cross-linker, Amersham Biosciences) and allowed to recover for 5min at RT before detachment and FFPE treatment. Non-irradiated HEK cells from the same passage served as negative controls.

DMEM complete medium

- DMEM (Dulbecco's Modified Eagle Medium) (61965026, ThermoFisher Scientific)
- Heat-inactivated 10% Fetal Bovine Serum (FBS) (10270-106, Lot: 42G7283K, ThermoFisher Scientific)
- 1% Penicillin-Streptomycin (5,000 U/mL) (15070063, ThermoFisher Scientific)

All media components were mixed and DMEM complete medium was stored at -4°C and pre-warmed to 37°C prior to use.

2.6.4 Mouse lymphoma culture and maintenance

Radio-resistant L5178Y-R cells were derived from a chemically induced lymphoma of a DBA/2 mouse, whereas the thereof derived L5178Y-S cell line is sensitive towards X-ray radiation (Beer, Budzicka, Niepokojczycka, Rosiek, & Szumiel, 1983). Both cell lines are widely used as internal telomere length reference in Q-FISH, as they possess published telomere lengths of 79,7kb or 10,2kb respectively (Canela, Vera, Klatt, & Blasco, 2007). L5178Y-S (93050408-1VL) and L5178Y-R (90062802-1VL) cells were both purchased from Merck.

L5178Y-S cells were cultured as described before and kept at a cell density between 300,000 to 900,000 cells/ml, whereas L5178Y-R cells were cultured between 30,000 to 700,000 cells/ml. For passaging, cells were pipetted up and down in the culture flask to create a single cell suspension. A subset of cell suspension was transferred into new flask and provided with

fresh culture medium. For regular cell culture maintenance, cells were kept in T75 flask. For FFPE treatment, cultures were expanded to CELLSTAR® T175 flasks (661175, Greiner Bio-One) and cultured as described before.

Fisher's complete medium

- Fisher's medium (21475025 ThermoFisher Scientific)
- 2mM glutamine (GlutaMAX™ Supplement, 250300024, ThermoFisher Scientific)
- 10% Horse serum (16050-122 LOT: 1517704 ThermoFisher Scientific)
- 1% Penicillin-Streptomycin (5,000 U/mL) (15070063, ThermoFisher Scientific)

All media components were mixed and Fisher's complete medium was stored at -4°C and pre-warmed to 37°C prior to use.

2.6.5 Fixation and paraffin infiltration of cultured cells

Adherent cells were detached from the culture dish by trypsin treatment and suspension cells were washed off the culture flask as described before. Cells were washed twice with 1X PBS with centrifugation steps in between the washes and fixed with 4% PFA in 1X PBS (Pierce™ 16% Formaldehyde (w/v), Methanol-free, 28908, ThermoFisher Scientific) for 30min at RT. The falcon tube was inverted multiple times during incubation to ensure complete fixation. In the meantime, the HistoGel (Richard-Allan Scientific™ HistoGel™, HG-4000-012, ThermoFisher Scientific) was heated to 65°C to liquefy. After 30min, cells were centrifuged and PFA was removed from the cell pellet. Cells were washed twice in 1X PBS with centrifugation steps in between washes. After the second centrifugation step, cells were transferred into a 2ml Eppendorf tube, washed once again with 1X PBS and centrifuged on a tabletop centrifuge (Eppendorf). All PBS was removed from the cell pellet and an equal amount of liquefied HistoGel was added to the pellet, mixed and allowed to solidify at RT. The solid cell/HistoGel mixture was placed into biopsy cassettes (ThermoFisher Scientific) and infiltrated on the tissue processor using the short infiltration program, as described previously.

2.7 Statistical analyses

Carolina Monzó performed statistical analyses and generated plots for the lifespan, RTqPCR, body composition and the longitudinal phenotyping data using custom Python scripts (v3.7.3, https://www.python.org/) and libraries scipy (Virtanen et al., 2020), pandas (Mckinney, 2010), seaborn, statsmodels (Seabold & Perktold, 2010) and lifelines (Davidson-Pilon et al., 2020) (v0.25.5). Longitudinal analysis of data was performed using custom R scripts (v4.0.2.) and the package lme4 (Bates, Mächler, Bolker, & Walker, 2015) (version 1.1-23). Cox proportional hazard regression analyses were conducted using the package survival (Therneau, 2020) (v3.2-2) in R. Data were plotted in Python and were displayed as mean +/- 95% confidence interval (CI). EM data of 27M old jejunum samples were analysed using linear mixed effect models with covariate correction for cohort, followed by Bonferroni multiple testing correction to calculate statistical differences between diet groups.

For the lifespan and cox proportional hazard regression analyses, animals who died prior to their respective DR switch were excluded from the analyses and in total 249 mice were studied. Pairwise log-rank tests and Bonferroni correction for multiple testing were performed to test lifespan differences between DR switch groups and chronic controls. Cox proportional hazard regression followed by Bonferroni correction was performed to determine whether the dietary regimen could explain the lifespan differences between diet groups. Schoenfeld residuals were analysed to assess if the Cox regression model was appropriate for our dataset. Fisher's test at the 80th percentile of chronic AL deaths with Bonferroni multiple correction testing was used to address statistical differences in maximum lifespan. For pathology assessments, prior deaths in the DR switch groups, except deaths in AL_DR24M, were assigned to chronic AL. Lisa Franziska Drews tested differences in abundance of tumour types and the tumour amount at specific time points using Fisher's tests with the help of Carolina Monzó.

Differences in body composition, body temperature or peak RER activity between chronic controls and DR switch groups at 5M, 10M 14M, 18M, 22M or 26M were calculated using One-way ANOVA with Bonferroni multiple testing correction. For the fitness phenotyping data, animals from all four DR switch groups were regarded as chronic AL animals prior to their respective DR switch. Prior to statistical analyses, the area under the curve (AUC) was calculated for normalized GTT, rotarod and barnes maza data. In contrast, the incremental AUC (iAUC) was determined for the normalized ITT experiments. Next statistical differences between chronic AL and DR animals at 5M, 10M 14M, 18M, 22M or 26M for the different fitness or metabolic phenotypes were calculated using unpaired t tests. To assess differences between DR switch groups in regards to chronic controls, One-way ANOVA followed Bonferroni post-hoc tests for multiple testing correction were carried out using each individual DR switch and comparing it against chronic AL and DR for all phenotyping tests. Generalized

linear mixed effects models (GLME) were used to study longitudinal differences between diet groups or within the same diet group during ageing and across time points for all phenotypings.

I performed the in-time-point statistical analyses and generated plots for most phenotyping experiments, the organoid culture, the WAT morphology assessment, the inflammation stainings, the EM data of 20M old jejunum samples and the primary adipocyte culture using Graphpad Prism 8. Pearson correlation was implemented to assess the correlation between the AUC of the rotarod performance and body weight in the respective phenotyping cohorts at each indicated time point. Data were analysed using unpaired t-tests to assess differences adipocyte size, CLS number or between the phenotyping data of chornic AL and DR animals at each time point. One-way ANOVA followed by Bonferroni post-hoc test were implemented to assess differences between chronic controls and one DR switch at a time for all phenotyping analyses. Two-way ANOVA and Bonferroni correction for multiple testing correction were used to investigate differences CLS, adipocyte size, organoid culture, EM and primary adipocyte culture between controls and switches. Data are displayed as mean +/- 95% CI or standard error of the mean (SEM). Schematics were created with BioRender.com.

3. Results

3.1 Late-life dietary switches to DR or AL fail to induce DR-specific transcriptional reprogramming and mitochondrial expansion in the WAT

Parts of the presented data in section 3.1, except the Western Blots on total OXPHOS complexes as well as AKT and S6K1 pathway activity, were published in Nature Metabolism in 2019 as Hahn et al., 2019. The detailed contributions can be found under section 8 page 224 and the full research article is included in section 12 page 285 in this thesis.

3.1.1 The WAT of late life dietary switches fails to adapt to DR regimen and to increase lipogenesis gene expression to chronic DR levels

We recently concluded a late-life DR onset experiment, in which mice were kept on lifelong (chronic) AL feeding or on lifelong DR initiated at 3M of age. At 24M of age, half of each cohort was switched from AL to DR (AL_DR) or from DR to AL feeding (DR_AL). While animals on early-onset, chronic DR showed reduced mortality rates compared to chronic AL, late-onset DR did not acutely decrease mortality rates after the switch, and had only mild effects on the longer term. Moreover, mice, which were switched from lifelong DR back to AL feeding at 24M exhibited significantly increased mortality and a shortened lifespan, indicating that DR has no long-term protective effect when the treatment is ceased (Hahn et al., 2019).

To assess underlying molecular differences between diet groups that promote DR switch response, we collected tissue two months after the dietary switch at 26M of age and conducted mRNA sequencing of the WAT. We detected increased expression of genes involved in lipogenesis or phospholipid synthesis, such as Sterol Regulatory Element Binding Transcription Factor 1 (Srebf1), Acetyl-CoA Carboxylase Alpha (Acaca), Fatty acid synthase (Fasn) and ELOVL Fatty Acid Elongase 6 (Elovl6) upon DR but not upon late-life diet switches compared to AL feeding (Hahn et al., 2019). We therefore conducted real-time quantitative PCR (RTqPCR) experiments in the WAT of independent mice from the same cohort, to confirm our RNA sequencing findings.

In line with our sequencing data, we observed significantly increased expression levels of all four evaluated lipogenesis genes in chronic DR compared to AL (Fig. 3.1.1A-D). Moreover, DR_AL mice exhibited similar expression of Srebf1, Acaca, Elovl6 and Fasn compared to

chronic AL within two months after the switch back to AL feeding. In line, lipogenesis expression of Acaca, Elovl6 and Fasn did not significantly increase after initiation of DR and only Srebf1 exhibited similar expression levels compared to chronic DR (Fig. 3.1.1.A-D).

Thus, the memory of a previous AL feeding or late-life initiation of AL regimen abrogated the reprogramming of the WAT towards increased lipogenesis gene expression and blocked DR switch response.

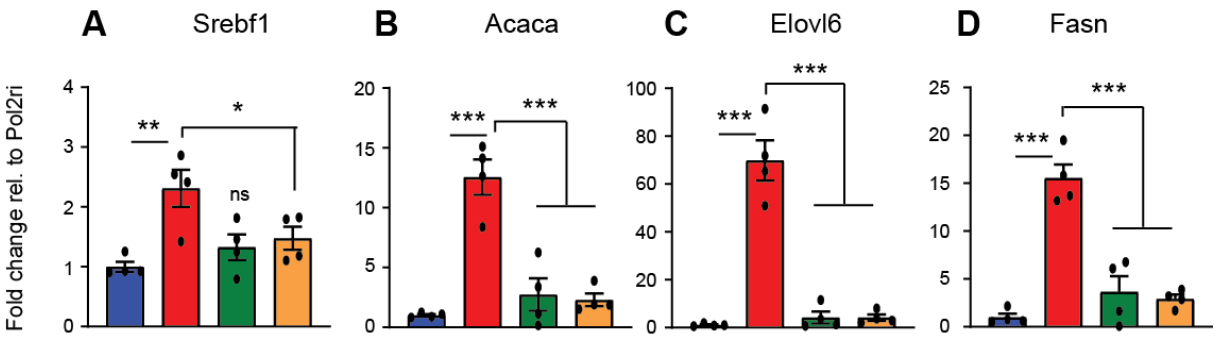

Figure 3.1. 1: Late life DR does not induce expression of lipogenesis genes in the WAT to the same extent as chronic DR.

*Q-RT-PCR analysis of expression of lipogenesis genes in the WAT of 27 months old AL, DR, AL_DR and DR_AL mice (all n=4). Relative expression of **A** Srebf1, **B** Acaca, **C** Elovl6 and **D** Fasn normalized to Pol2ri and AL. One-way ANOVA followed by Tukey's post hoc test with multiple testing correction were implemented to test for statistical differences in gene expression. Data are plotted as mean with SEM and with p values * p<0.05, ** p<0.01 and *** p<0.001 in relation to chronic DR.*

3.1.2 Chronic or late-life DR does not significantly reduce AKT and S6K1 activity in the WAT

Protein kinase B, also commonly referred to as AKT kinase (AKT) is a central effector serine-threonine kinase in several growth hormone receptor pathways, activated by growth hormones such as VEGF (Abid et al., 2004) or insulin (Huang et al., 2018). AKT requires phosphorylation first on the threonine 308 residue (Thr.308) by PDK1 (Alessi et al., 1998) followed by phosphorylation on serine 473 (Ser. 473) by the rictor-mTOR complex (Sarbassov et al., 2005) to reach full activity. Upon activation, AKT phosphorylates it's downstream targets, such as FOXO (Greer & Brunet, 2005), BAD (Datta et al., 1997) or GLUT4 translocation via AS160 (Sano et al., 2003) to regulate cell growth, inhibition of apoptosis and glucose uptake (Huang et al., 2018). P70 S6 kinase 1 (S6K1) regulates cellular growth and survival or translation by target-specific phosphorylation of downstream effector proteins, such as the pro-apoptotic

protein BAD (Harada et al., 2001) or the translation initiation factor eIF4B (Holz et al., 2005). S6K1 is activated via phosphorylation of threonine 389 (Thr.389) and threonine 229 (Alessi et al., 1998) in response to nutrient availability and IIS or mTOR pathway activity (Magnuson et al., 2012; Um et al., 2006). Given that ablation of insulin signalling in the adipose tissue can extend murine lifespan (Bluher et al., 2003) and that nutrient signalling is reduced under DR (Santos et al., 2016), we asked whether DR impacts on AKT and S6K activity in the WAT. To this end, we performed Western Blot analyses on WAT protein extracts to evaluate the ratio of AKT phosphorylation on threonine 308 and serine 473 in relation to total AKT levels, as well as phosphorylation on threonine 389 in relation to total S6K1 levels. Although we did not observe any significant difference in the ratio of phosphorylated versus total AKT or S6K1 in the WAT of DR treated animals (Fig. 3.1.2A-C), we observed a trend towards reduced AKT phosphorylation on both Thr.308 and Ser.473 in chronic DR and AL_DR mice. In contrast, DR_AL WAT exhibited a trend towards increased AKT phosphorylation on both amino acid residues similar to chronic AL, implying that previous DR regimen has no impact on AKT activity after the treatment was ceased (Fig. 3.1.2A and B). Interestingly, while chronic DR and AL_DR mice displayed reduced ratios of phosphorylated versus total S6K1 in the WAT, the same trend was observed for DR_AL, suggesting that S6K1 activity might be influenced by newly imposed or previous DR regimen after AL was re-initiated (Fig. 3.1.2C).

Thus, early or late-life DR or switching mice from DR to AL at 24M did not significantly reduce AKT and S6K1 activity in the WAT compared to chronic AL feeding. However, we identified a trend towards a potential memory of AKT and S6K1 activity in response to previous or newly established DR. Repeating the Western Blot analyses with more replicates would answer the question whether reduced AKT and S6K1 activity in the WAT was linked with DR.

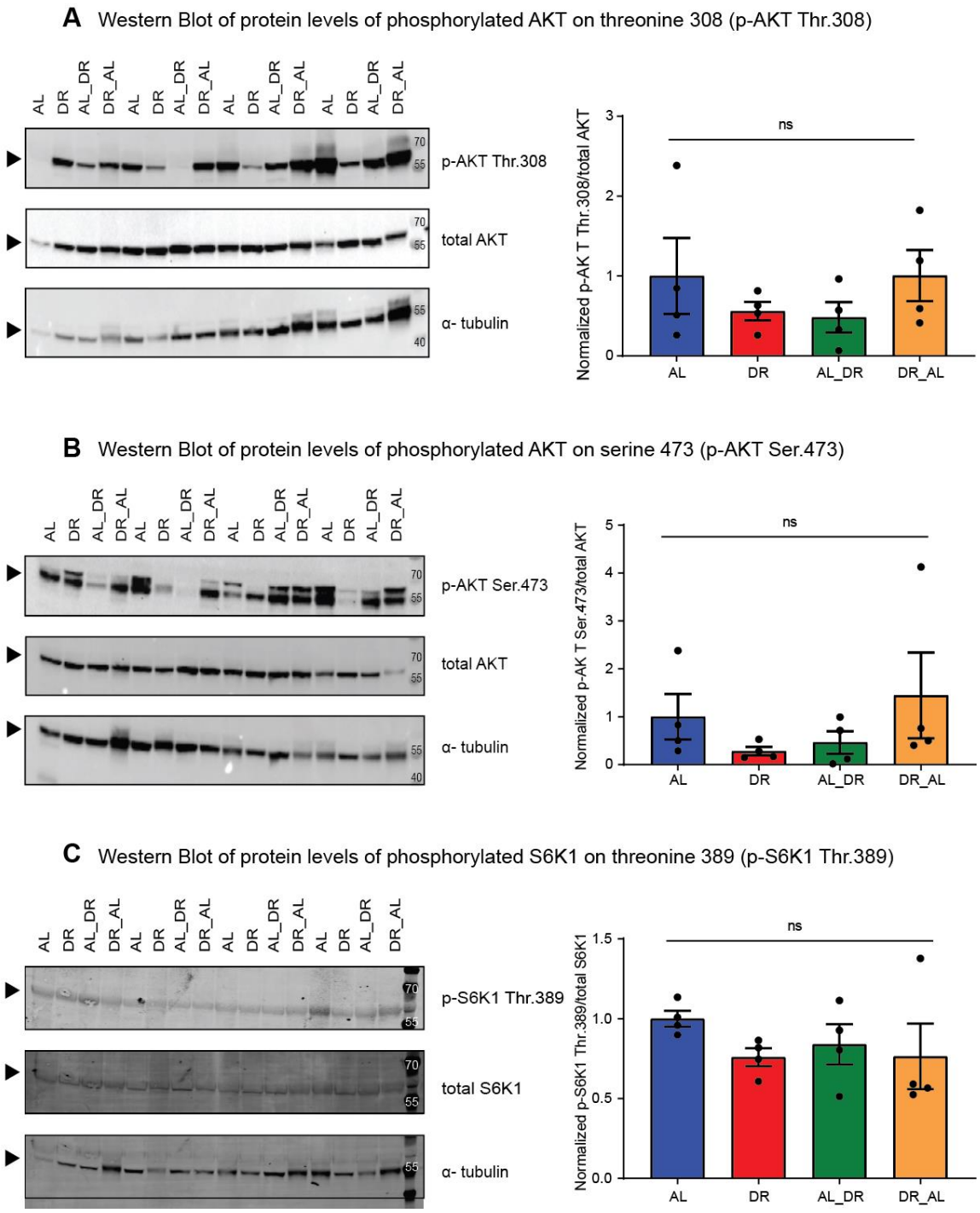

Figure 3.1. 2: Chronic or late-life DR does not significantly reduce AKT and S6K1 activity in the WAT

*Relative protein levels of phosphorylated AKT on **A** threonine 308 or **B** serine 473 in relation to total AKT. **C** relative protein levels of phosphorylated S6 kinase 1 (S6K1) on threonine 389 in relation to total S6K levels. Protein levels of phosphorylated AKT or S6K1 were set relative to total AKT or S6K1 respectively, quantified against alpha tubulin and normalized against AL protein levels. One-way ANOVA followed by Tukey's multiple testing correction were implemented to assess differences in protein levels. Data are plotted as mean with SEM and with p values * p<0.05, ** p<0.01 and *** p<0.001 in relation to chronic DR.*

3.1.3 Increased mitochondrial copy number and complex I and IV protein levels in the WAT might contribute to the lifespan extension upon chronic DR

Mitochondria are organelles in the cytoplasm, often referred to as the powerhouse of the cell, due to their role in supplying the cell with energy in the form of adenosine triphosphate (ATP) via oxidative phosphorylation (Spinelli & Haigis, 2018). Mitochondria possess their own small circular genome (mtDNA), which encodes for the subunits of the five oxidative phosphorylation (OXPHOS) proteins in the respiratory chain responsible for ATP synthesis (Anderson et al., 1981). In addition to their function in ATP production, mitochondria are also involved in several other cellular functions or metabolic pathways, such as lipid metabolism via β oxidation, lipid storage or thermogenesis in the BAT (Benador et al., 2019). Therefore, functional mitochondria are required for proper cell and subsequently systemic tissue function. DR and every-other-day fasting have demonstrated to maintain mitochondrial function during ageing in rats or mice, suggesting that improving mitochondria function by dietary interventions can positively impact on ageing (Castello et al., 2011; Lanza et al., 2012).

Interestingly, RNA sequencing of the WAT identified induction of genes associated with mitochondria under chronic DR but not upon late-life DR (Hahn et al., 2019), suggesting that in contrast to chronic DR a DR switch late in life is not sufficient to induce mitochondrial biogenesis. In order to test this hypothesis, we investigated mitochondrial copy number, as well as OXPHOS protein levels in the WAT of chronic and late-onset DR mice. We first conducted quantitative PCR on the three mitochondrial genes Atp6, encoding the ATP synthase Fo subunit 6, Cox1, encoding cytochrome c oxidase I as well as Rnr2, encoding the mitochondrial 16S ribosomal RNA, to assess mtDNA copy numbers in the WAT. All three mitochondrial genes displayed significantly higher copy numbers in chronic DR, suggesting the WAT of chronic DR mice have more mitochondria compared to chronic AL (Fig. 3.1.3A). Interestingly, late-life initiation of DR at 24M did not increase mtDNA copy numbers within two months after the switch, as AL_DR mice did not show elevated Atp6, Cox1 or Rnr2 levels. However, switching mice from DR back to AL feeding at 24M significantly reduced mtDNA content to chronic AL levels within two months after the switch (Fig. 3.1.3A). To further verify that the late-life DR switch doesn´t induce mitochondrial biogenesis in the WAT, we extracted protein and conducted a Western Blot (WB) analysis using an antibody cocktail targeting the five OXPHOS respiratory chain proteins. As expected, we detected significantly higher protein levels of complex I (CI) and complex IV (CIV) in the WAT of chronic DR compared to chronic AL animals (Fig. 3.1.3B). In line with the hypothesis, protein levels of both CI and CIV were significantly lower in the WAT of AL_DR and DR_AL mice similar to the levels of chronic AL animals (Fig. 3.1.3B). As the immunoblot staining for both CI and CIV were relatively weak, we

repeated the experiment using specific antibodies for complex I (mtCO1) and complex IV (NDUFA9) on two separate membranes in order to confirm the previous WB results. Indeed, we could confirm that both mtCO1 and NDUFA9 protein levels were significantly elevated in chronic DR WAT compared to chronic AL as well as AL_DR and DR_AL mice (Fig.3.1.3C). In contrast, neither mtCO1 nor NDUFA9 exhibited increased protein levels compared to AL in the WAT of AL_DR or DR_AL animals. Thus, in summary these results suggest that chronic DR but not late-life DR induces mitochondrial biogenesis in the WAT and that two months of refeeding were sufficient to reverse this effect in the DR_AL animals.

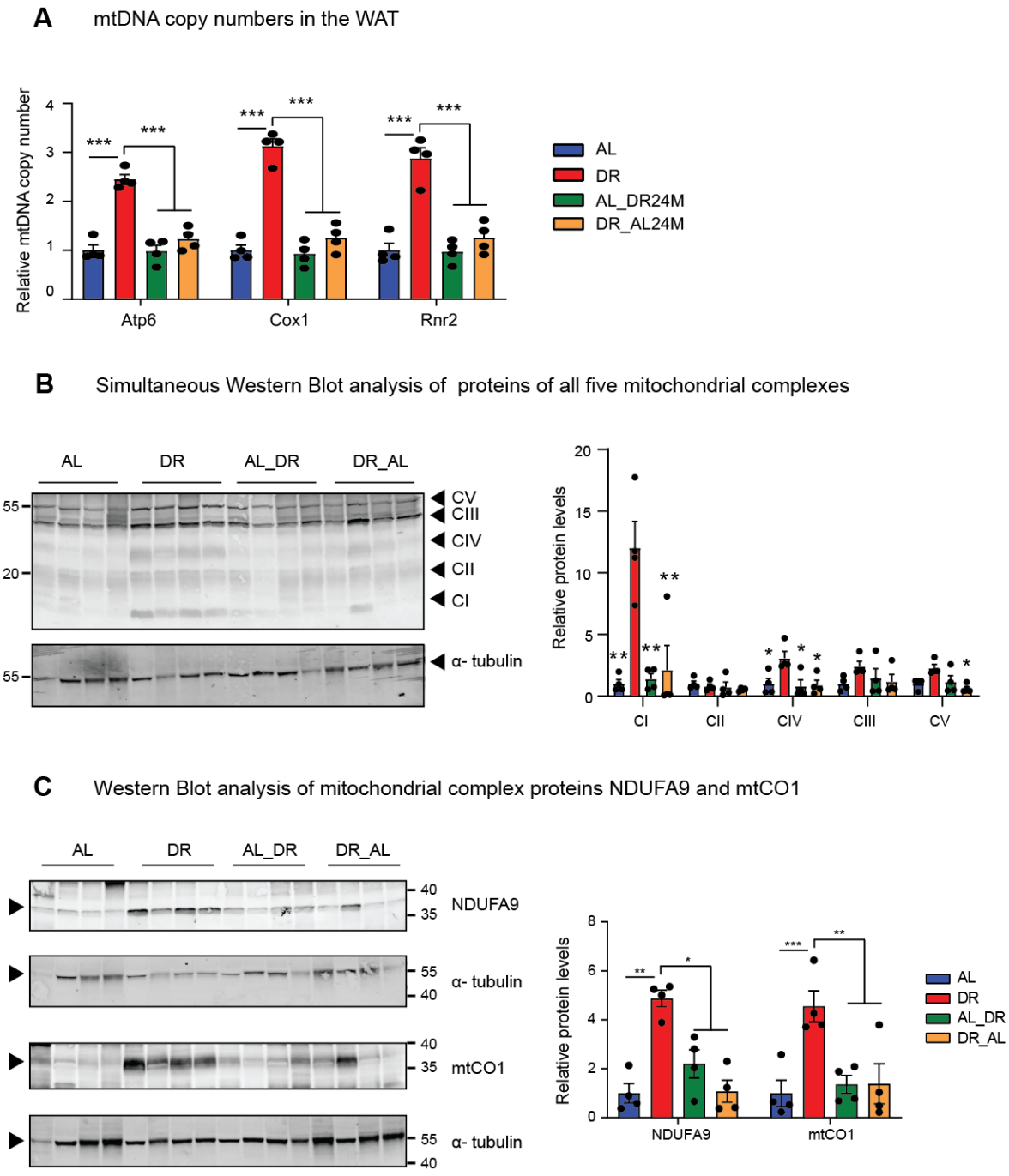

Figure 3.1. 3: Chronic but not late-life DR increased copy number of mitochondrial DNA and complex I and IV protein levels in the WAT

A *QRT-PCR analysis of mitochondrial DNA (mtDNA) copy numbers,* ***B*** *Western blot analysis using an OXPHOS antibody cocktail against all five mitochondrial complexes or* ***C*** *mitochondrial complex I NDUFA9 and complex IV mtCO1 protein levels in the WAT of AL, DR, AL_DR and DR_AL mice (all n=4). mtDNA copy numbers of Atp6, Cox1 and Rnr2 were normalized against the nuclear 18S ribosomal RNA gene and normalized against the respective AL copy number control. Protein levels of complex I (CI), complex II (CII), complex III (CIII), complex IV (CIV), complex V (CV) or NDUFA9 and mtCO1 were first normalized against alpha tubulin and then against AL protein levels. One-way ANOVA followed by Tukey's multiple testing correction were used to test for statistical significance. Data are plotted as mean with SEM. p values * p<0.05, ** p<0.01 and *** p<0.001 in relation to chronic DR.*

3.1.4 No evidence for increased thermogenesis and browning of the WAT upon chronic or late-life DR

Browning of the WAT is associated with increased expression of thermogenic marker genes, increased protein levels of the uncoupling protein 1 (Ucp1), increased numbers of mitochondria in white adipocytes and higher WAT thermogenesis (Abdullahi & Jeschke, 2016). Moreover, recent studies in mice have linked WAT browning and improved WAT metabolism to DR and ageing (Corrales et al., 2019; Fabbiano et al., 2016). Given that chronic DR mice exhibit increased mitochondrial numbers in the WAT (Fig. 3.1.3), we therefore asked if thermogenesis is elevated upon chronic DR. To this end, we first investigated the gene expression levels of the thermogenic marker genes Ppargc1a and Ucp1 in the WAT in relation to chronic AL or DR feeding as well as in late-life AL_DR or DR_AL switches. Q-RT-PCR analysis revealed that expression levels of both Ppargc1a and Ucp1 were not significantly increased on the mRNA level in chronic DR or in any of the late-life switch compared to chronic AL feeding (Fig. 3.1.4A). We next assessed protein abundance of UCP1 in WAT by Western Blot. To confirm the specificity of the UCP1 antibody, we included BAT of 26M AL mice as a positive control. In accordance with the Q-RT-PCR results, UCP1 protein levels in the WAT did not significantly differ between diet groups and remained low for all dietary interventions (Fig. 3.1.4). In contrast, BAT of age-matched AL mice exhibited a band at the expected protein size, indicating that the antibody staining worked (Fig. 3.1.4). Interestingly, one DR_AL mouse exhibited a defined WB band correlating with UCP1, indicating that WAT browning can be induced by DR in our mouse strain but is probably a rare phenotype and likely does not contribute to the increased survival of the DR animals.

In conclusion, we show that chronic DR induces expression of lipogenesis genes and increases mitochondria independently of thermogenesis in the WAT. Late-onset DR treatment did not induce corresponding expression changes, while late onset AL feeding reversed the effect of the previous DR feeding on mitochondrial and lipogenesis gene expression. Thus, our results suggest a memory of previous AL but not DR feeding encoded in the WAT.

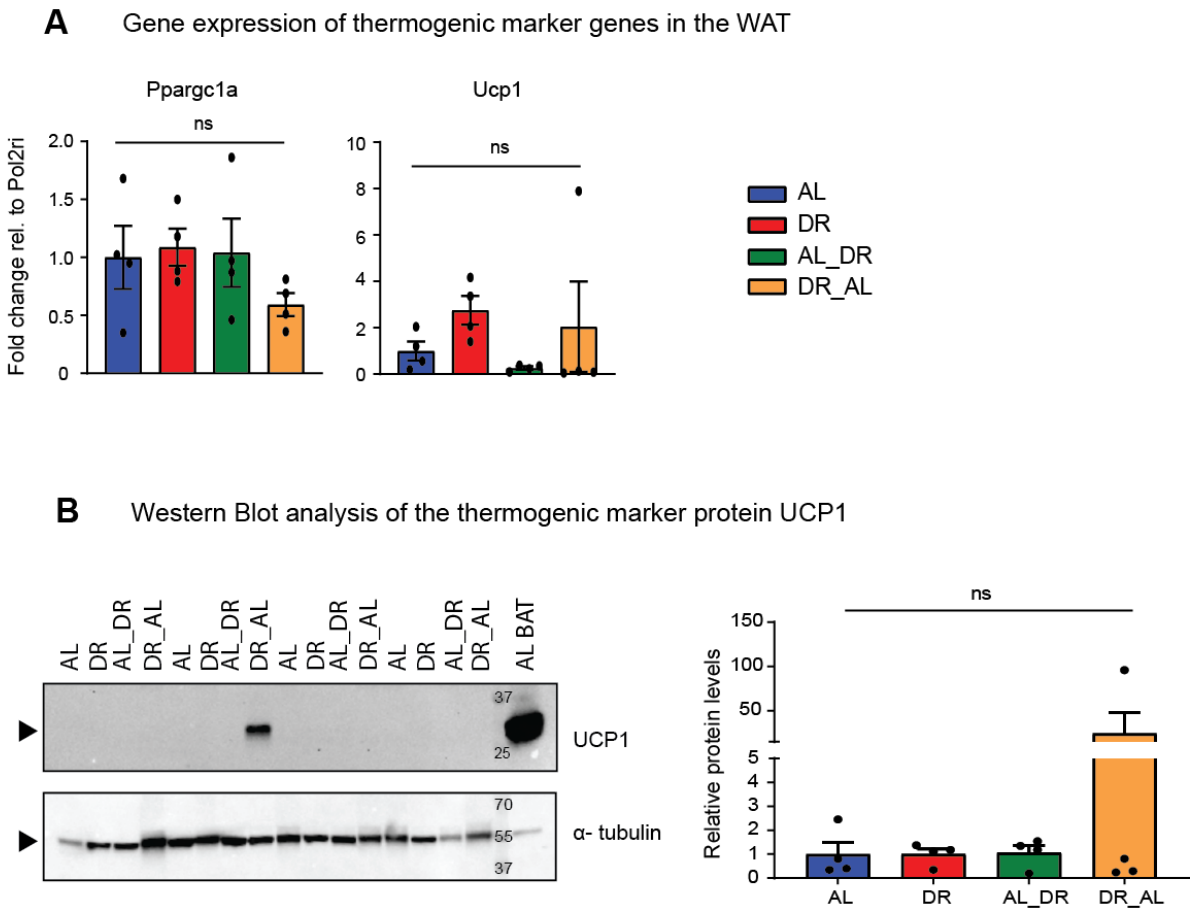

Figure 3.1. 4: Lifelong DR feeding or late-life dietary switches do not induce WAT thermogenesis and browning

A *Q-RT-PCR analysis of mRNA expression of thermogenic marker genes Ppargc1a and Ucp1 relative to Pol2ri and* ***B*** *Western Blot analysis of UCP1 protein levels relative to α-tubulin in the WAT of AL, DR, AL_DR and DR_AL mice (all n=4). One-way ANOVA followed by Tukey's multiple testing correction were implemented to assess gene expression differences. Data are plotted as mean with SEM and with p values * p<0.05, ** p<0.01 and *** p<0.001 in relation to chronic DR or ns as not significant.*

3.2. Early or mid-life but not late-life onset dietary restriction (DR) extends lifespan and health span in mice

3.2.1 Defining the phenocritical period of late-life dietary restriction in mice

Dietary restriction leads to a robust extension of lifespan if the treatment is started early in life and is then maintained lifelong (Fontana & Partridge, 2015). Importantly, we have recently demonstrated that initiation of DR late in life at the age of 24 months only caused a minor beneficial effect on survival in female mice (Hahn et al., 2019). It is currently not known why the old animals lose their responsiveness towards DR and at which age of onset DR still causes beneficial effects. Furthermore, in the previous study only longevity was assessed but it is currently not clear whether DR might still be able to improve health when applied late in life. In order to address these questions, we designed a new mouse study comprising in total 1112 mice to systematically test at which age treatment with DR has still beneficial effects on health and survival (Fig.3.2.1A). As in the previous study we used females of the long-lived C3B6F1 hybrid mouse strain for the new study and DR was implemented as a 40% reduction in food uptake compared to an age-matched AL control group. DR was initiated at 3M of age for the chronic DR group, and at 12M (AL_DR12M), 16M (AL_DR16M), 20M (AL_DR20M) and 24M (AL_DR24M) for the DR switch groups (Fig.3.2.1A). We generated four separate mouse cohorts for the survival analysis (320 animals), tissue collection (320 animals) and two phenotyping cohorts to assess the effect of DR on the metabolism (90 animals) and on fitness (72 animals) during ageing (Fig.3.2.1A).

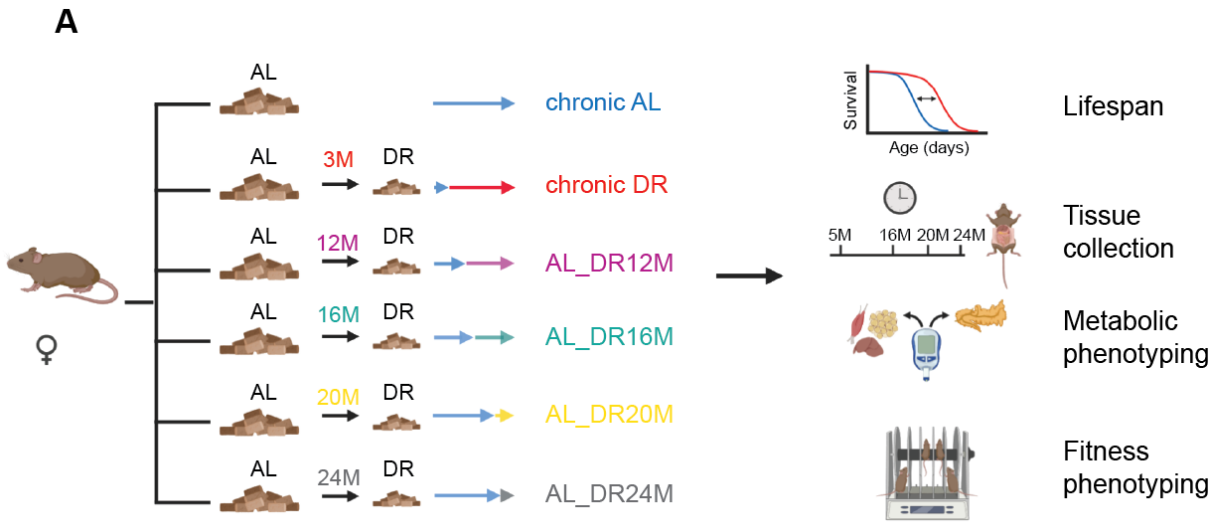

Figure 3.2. 1: Defining the phenocritical period of late-life DR in mice

A *Schematic representation of DR switch groups and mouse cohorts used in this study. Mice were transferred from AL feeding to DR implemented as a 40% reduction in food intake at 3M, 12M, 16M, 20M and 24M and maintained until death. Four separate cohorts for survival analyses (n=320), tissue collection (n=320), metabolic (n=90) and fitness phenotyping (n=72) were generated to address lifespan, health span and molecular parameters in response to the DR switches. The schematic was created with Biorender.com.*

3.2.2 Customized food racks reduce the food intake of chronic AL mice

To adjust the food amount for the DR regimen and to assess the effect of ageing on food intake, we measured the weekly food consumption of AL animals from the lifespan cohort over a course of 23 months using customized food racks (Fig. 3.2.2A). As expected, we observed a steady increase in food intake of AL animals starting at approximately 3.5g at young age until approximately 4.7g were consumed per animal at 23 months (Fig. 3.2.2A). Correspondingly, the food intake of chronic DR animals also increased during ageing but with a 40% reduction compared to AL (Fig. 3.2.2A).

We next evaluated the body weight changes of chronic DR animals over time starting from 3M of age to assess the baseline body weight before DR was initiated. Additional measurements at two weeks, six weeks or nine months post-switch to DR were used to assess body weight changes after short- or long-term treatment (Fig. 3.2.2B). To verify, that the presence of custom food racks did not affect food intake in AL animals, we conducted body weight measurements in a subset of AL mice with regular food racks (AL) or AL mice with custom food racks (AL food

rack) (Fig. 3.2.2B). Interestingly, DR animals were significantly heavier that AL and AL food rack animals at 3M of age at baseline shortly before DR was initiated (Fig. 3.2.2B). Upon short-term DR for two weeks or six weeks, the body weight of chronic DR animals was not significantly different from AL animals, whereas AL food rack mice were significantly lighter compared to DR mice after six weeks of DR (Fig. 3.2.2B). At 12M, chronic DR animals showed significantly reduced body weight compared to both AL and AL food rack animals, confirming that long-term DR regimen leads to a stable weight reduction compared to AL feeding (Fig. 3.1.1C). Unexpectantly, AL mice with custom food racks were significantly lighter compared to AL mice with regular food racks at all four evaluated time points (Fig. 3.2.2B), demonstrating that custom food racks interfered with feeding and significantly affected the food intake. At 12M, AL food rack animals weighed on average 42,09g ± 4,93g and were almost 19% lighter compared to AL mice weighing 51,96g ± 3,79g, suggesting that that AL food rack animals were chronically subjected to a mild form of DR (Fig. 3.2.2B). Therefore, the presence of custom food racks in AL cages itself could already positively affect survival compared to AL mice with regular food racks. Furthermore, we removed the custom food racks from the food intake cages at 23M and former AL food rack animals were switched to 40% DR at 24M of age (AL_DR24M). Therefore, the mild reduction in food intake by the custom food racks prior to the DR switch at 24M could bias the results of the AL_DR24M lifespan.

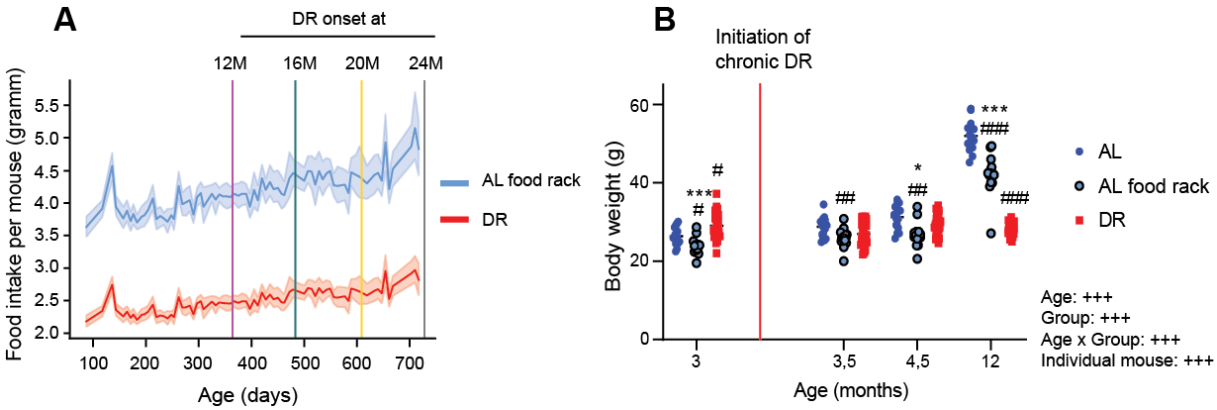

Figure 3.2. 2: Customized food racks reduce the food intake of chronic AL mice

A *Food intake per animal of chronic AL and DR animals over time. Weekly food intake of AL animals was measured using custom food racks in 10 separate cages and averaged to obtain the mean food intake per AL mouse. Food amounts were adjusted weekly to 60% for DR animals, corresponding to a 40% reduction in food intake. Solid lines indicating the switch from AL to DR at 12M (purple), 16M (teal), 20M (yellow) or 24M (grey) of age. After removing the food racks at 23M, mice from the former food rack cages were switched to DR at 24M of age (AL_DR24M). For the other DR switch groups, "naïve", untreated AL mice were utilized. Weekly food measurements were stopped when animals reached aged 23M and the last measured food intake amounts were used until the end of the experiments.* ***C*** *Body weight in AL (n=15), DR (n=30) and AL food rack (n=15) groups over time. AL food rack animals were*

*significantly lighter compared to untreated AL animals at 3M (adj. p=0.012), 3,5M (adj. p=0.0093), 4,5M (adj. p=0.0014) and 12M of age (adj. p<0.0001). Chronic DR animals significantly differed from food rack animals at 3M (adj. p<0.0001), 4,5M (adj. p=0.0451) and 12M of age (adj. p<0.0001). Chronic AL mice were lighter than DR mice at 3M (adj. p=0.0111) and heavier at 12M of age (adj. p<0.0001). Two-way ANOVA followed by Bonferroni multiple testing correction were implemented to assess body weight differences between diet combinations. Data are presented as mean with 95% CI and with p-values * p<0.05 and *** p<0.001 in relation to chronic DR and with p-values # p<0.05, ## p<0.01, ### p<0.001 in relation to chronic AL. Differences, which did not reach statistical significance p> 0.05 were not labelled. Carolina Monzó generated the longitudinal food intake plot.*

3.2.3 DR initiated in mid-life but not in late-life extends median and maximum lifespan compared to chronic AL feeding

We first assessed the survival of the DR switch groups in relation to chronic AL and DR feeding. In accordance with previously published DR studies in the C3B6F1 background (Hahn et al., 2019, 2017), chronic DR significantly increased median survival by 34,5% (782 days chronic AL, 1052 days chronic DR) and maximum survival by 49% (987,7 days chronic AL, 1471,3 days chronic DR) compared to chronic AL feeding (Figure 3.2.3A-D).

Strikingly, both mid-life switches to DR at 12M (AL_DR12M, Fig.3.2.3A) and at 16M (AL_DR16M, Fig. 3.2.3B), significantly extended life compared to chronic AL feeding and to a similar extend as chronic DR treatment. Moreover, AL_DR12M animals had a significantly increased median survival by 29,2% (770 days chronic AL, 995 days AL_DR12M) and maximum survival by 28,59% (962 days chronic AL, 1237,6 days AL_DR12M, $p= 3.96 \times 10^{-7}$) compared to chronic AL feeding (Supplementary table 2). Similarly, AL_DR16M significantly extended median lifespan by 28,19% (775 days chronic AL, 993,5 days AL_DR16M) and maximum survival by 26,88% (962,4 days chronic AL, 1213,4 days AL_DR16M, $p= 1.6 \times 10^{-7}$) compared to chronic AL (Supplementary table 3). In contrast, chronic DR displayed an increase in median lifespan by 6,2% and in maximum lifespan by 12,64% compared to AL_DR12M (Supplementary table 2) and by 6,54% and 14,88% compared to AL_DR16M (Supplementary table 3), indicating that AL feeding for 12M or 16M of age already had some detrimental effects on murine lifespan. Strikingly, when implementing Fisher's test, the differences in maximum lifespan between chronic DR and AL_DR12M (p=0.513) or AL_DR16M (p=0,82) were not significant, demonstrating that AL feeding for 12M or 16M already had some detrimental effects on median but not on maximum lifespan. In contrast, switching animals to DR at 20M (AL_DR20M, Fig. 3.2.3C) did not increase lifespan compared to AL feeding. Correspondingly, AL_DR20M increased median survival by 11,39% (781 days

chronic AL, 870 days AL_DR20M) but the difference in maximum survival compared to AL was not significant (10,08%, 967,15 days chronic AL, 1064,66 days AL_DR20M, p= 0.0515, supplementary table 4). Moreover, median and maximum lifespan were significantly reduced by 21,66% or 30,9% respectively in AL_DR20M compared to DR (0.00095, supplementary table 4), indicating that prolonged AL feeding blunted the response towards newly imposed DR. In contrast, 24M onset of DR (AL_DR24M, Fig. 3.2.3D) had limited effects in prolonging life compared to AL and were shorter-lived than chronic DR. Similarly, AL_DR24M had a higher median survival of 8,04% (821 days chronic AL, 887 days AL_DR24M) but maximum survival was not significantly extended compared to AL feeding (993,55 days chronic AL, 1148 days AL_DR24M, p= 0.1589, supplementary table 5). Therefore, the presence of food racks in the cages lead to a chronic restriction of food intake in AL_DR24M (Fig. 3.2.2B), which was enough to increase lifespan compared to untreated AL mice (Fig. 3.2.3D). When compared to chronic DR animals, median and maximum survival of AL_DR24M was significantly decreased by 20,07% and 21,4% (p=0.000197, supplementary table 5), indicating that a lifelong, less severe reduction in food intake was not as efficient in prolonging life as chronic DR with a 40% reduction. Overall, our results suggest that mice lose their responsiveness towards newly imposed DR between 16M and 20M mice, potentially due to detrimental effects of prolonged AL feeding.

To evaluate whether chronic, less severe food restriction already provided a survival advantage before DR onset at 24M, we compared the number of deaths in each DR group to the corresponding number of deaths in the AL cohort prior to the respective DR switch. During ageing, we detected few; spontaneous deaths in the AL_DR12M, AL_DR20M and chronic AL group prior to DR onset at 12M, 16M or 20M of age (Fig. 3.2.3E); however, no significant difference in the number of deaths were found. In contrast, significantly more chronic AL animals (n=25) died before 24M of age, as opposed to only four deaths in the later AL_DR24M group (Fig. 3.2.3E), demonstrating that the presence of custom food racks in the cages delayed death and thus provided a survival advantage compared to untreated AL animals. We asked next, whether the proportion of euthanized or naturally deceased animals differed between diet groups. Approximately 50% of animals were euthanized and approximately 50% of animals in chronic DR and DR switch groups were naturally deceased Fig. 3.2.3F). Consequently, no difference in the proportion of naturally deceased versus euthanized mice when comparing chronic DR, AL_DR12M, AL_DR16M, AL_DR20M or AL_DR24M (Fig. 3.2.3F). Strikingly, a significantly higher proportion of chronic AL animals were naturally deceased compared to all other DR groups (Fig. 3.2.3F), suggesting that AL animals exhibited fewer tumours or other age-associated comorbidities, which were euthanasia criteria.

To conclude, these results show that initiation of DR mid-life at 12M or 16M extends murine lifespan almost to the same extent as chronic DR feeding, suggesting animals remain

responsive towards newly imposed DR as late as 16M of age. Moreover, a lifelong less severe DR regimen by itself extended lifespan compared to untreated, chronic AL animals.

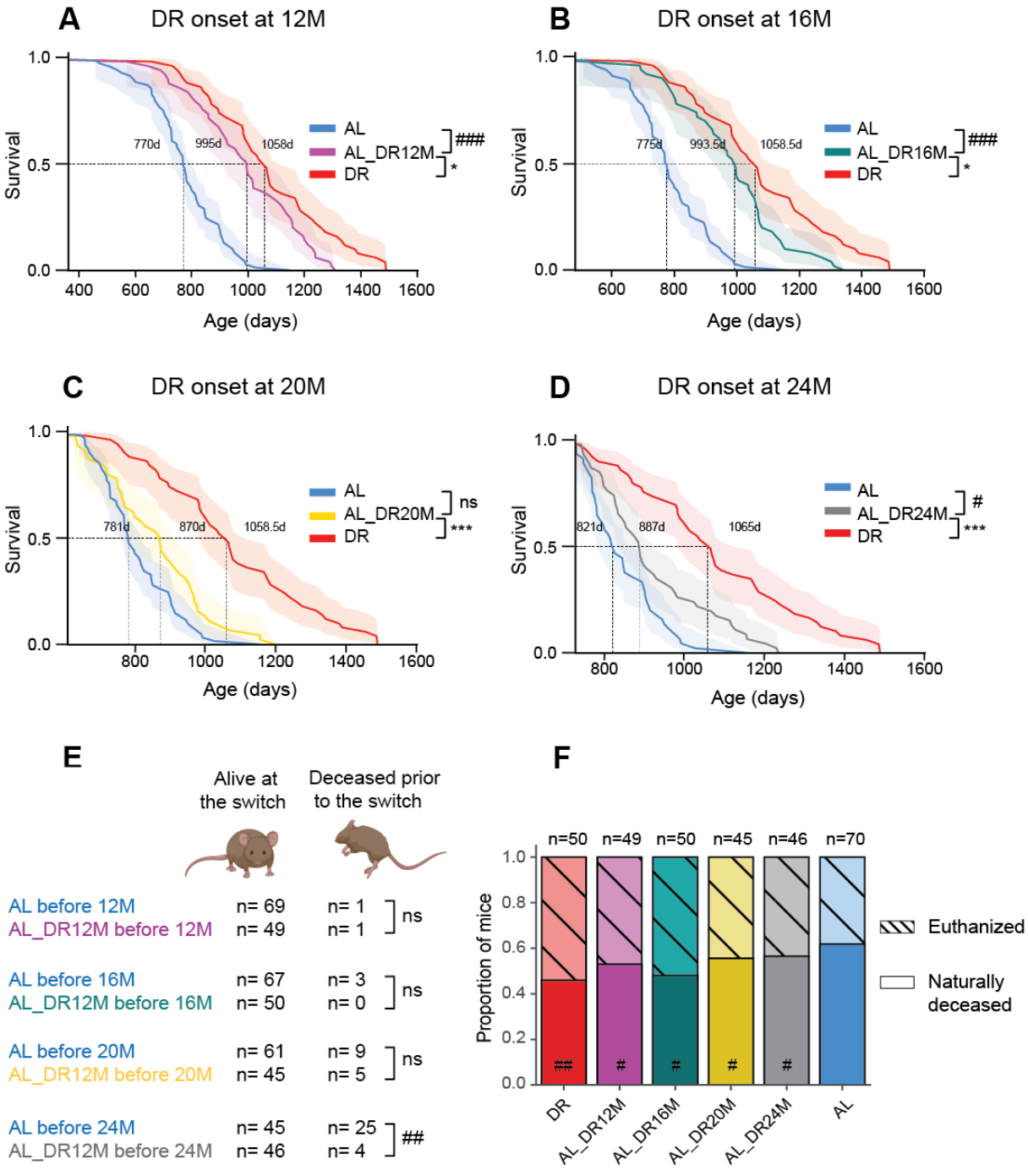

Figure 3.2. 3: DR initiated in mid-life but not in late-life extends median and maximum lifespan compared to chronic AL feeding

*Post-switch Kaplan-Meier survival curves of chronic controls or animals switched at **A** 12 months (AL_DR12M n=49) **B** 16 months (AL_DR16M n= 50) **C** 20 months (AL_DR20M n=46) or **D** 24 months of age (AL_DR24M n=45). Solid lines represent the Kaplan-Meier fit, shaded areas indicate the 95% confidence interval (CI) for the respective diet group and dashed lines mark the median lifespan*

*extension for each treatment. Animals of all diet groups, which died before the respective DR switch, were excluded from the analysis. The animal numbers were the following: comparison to AL_DR12M: chronic AL n=69, DR n=50, AL_DR12M n=49. Comparison to AL_DR16M chronic AL n=67, DR n=50, AL_DR16M n=49. Comparison to AL_DR20M: chronic AL n=61, DR n=50, AL_DR20M n=45. Comparison to AL_DR24M: chronic AL n=45, DR n=49, AL_DR24M n=46. Pairwise log-rank tests were implemented to assess differences between diet combinations. Mice switched at 12M to DR (**A**) significantly differed from chronic DR (adj. p=0.044) and from AL (adj. p=*1.21×10^{-10}). *AL_DR16M (**B**) significantly differed from both DR (adj. p= 0.017) and AL (adj. p=*1.8×10^{-10}*), whereas AL_DR20M (**C**) significantly differed from DR (adj. p=*5.5×10^{-8}*) but not from AL (adj. p=0.054). Animals switched at 24M to DR significantly differed from both chronic DR (adj. p=*3.9×10^{-5}*) and AL (adj. p =* 0.0164*). Median lifespan in days in relation to chronic AL were displayed for each diet group with dotted lines. The lifespan data of chronic AL and DR animals was recently published in a collaborative paper* (Kaeser et al., 2021)*. **E** Number of deaths in the AL cohort compared to the number of deaths in the DR switch cohorts before each diet switch. Significantly less deaths occurred in the AL_DR24M group before the switch at 24M compared to chronic AL (p= 0.0081). Similar amounts of deaths occurred in AL_DR12M (p=0.999), AL_DR16M (p=0.2702) or AL_DR20M (p=0.7786) compared to AL before the respective switch. Fisher's tests were conducted to compare death in the AL cohort and deaths in DR switch cohorts before each diet switch. **F** Proportion of naturally deceased or euthanized animals in chronic AL (n=70), DR (n=50), AL_DR12M (n=49), AL_DR16M (n=50), AL_DR20M (n=45) or AL_DR24M (n=46). Significantly more chronic AL mice died of natural causes compared to chronic DR and DR switch groups. Fisher's tests were conducted to calculate statistical differences between euthanized and naturally deceased animals between diet groups. Data are presented with p-values * p<0.05, ** p<0.01, *** p<0.001 in relation to chronic DR and with p-values # p<0.05, ## p<0.01, ### p<0.001 and ns not significant (p>0.05) in relation to chronic AL. Statistical analyses were conducted and plots were generated by Carolina Monzó and schematics were created with BioRender.com.*

3.2.4 DR, irrespective of the age of onset, improved survival in relation to chronic AL feeding but increased mortality in relation to chronic DR treatment

We next implemented Cox proportional hazard (CPH) analyses to evaluate whether prolonged AL feeding increased mortality and mid- or late-onset DR would improve survival. As expected, when compared to chronic AL feeding, chronic DR had a positive effect on survival and was associated with decreased mortality (Fig. 3.2.4A and B). Most strikingly, DR, irrespective at the age of onset had a similar protective effect on survival compared to AL feeding, indicating that initiation of DR at 20M or 24M still had a positive effect on survival even after long-term AL feeding (Fig. 3.2.4A). However, we detected a clear separation between chronic DR, AL_DR12M or AL_DR16M and AL_DR20M or AL_DR24M, suggesting that initiating DR at

20M or 24M decreased survival compared to earlier DR onset (Fig. 3.2.4A). Potentially, this survival difference could be due to lack of adaptation to the DR regimen or detrimental effects of previous AL feeding. Moreover, the CPH results were largely consistent with our lifespan data, as chronic DR, AL_DR12M, AL_DR16M and AL_DR24M mice displayed significant lifespan extension or increased maximum survival compared to chronic AL (Fig. 3.2.3A-D). Intriguingly, AL_DR20M had a significantly different CPH ratio, despite no significant difference in overall or maximum lifespan (Fig. 3.2.3C and supplementary table 4), indicating that DR onset at 20M could still induce some beneficial effects on survival compared to AL even if AL_DR20M mice were not significantly longer-lived (Fig. 3.2.4A).

When compared to chronic DR, AL_DR12M, AL_DR16M, AL_DR20M and AL_DR24M had significantly different hazard ratios, indicating that even short-term AL feeding for 12M or 16M already increased the mortality risk, compared to lifelong DR treatment (Fig. 3.2.4B). Moreover, these results correspond to the log rank tests of our lifespan (Fig. 3.2.3A- D, Fig. 3.2.4B), as the overall survival of DR switch groups was significantly shorter compared to chronic DR. Furthermore, a shorter duration of AL feeding prior to initiation of DR was less detrimental to survival compared to longer AL duration (Fig. 3.2.4B), as AL_DR12M and AL_DR16M were closer to chronic DR in the CPH analyses than AL_DR20M and AL_DR24M. Interestingly, when compared to chronic AL or DR, AL_DR24M exhibited a better prognosis on mortality or survival contrasting to AL_DR20M, indicating adaptation differences between the two DR switches (Fig. 3.2. 43A). This observation was consistent with our lifespan data (Fig. 3.2.3C and DR) and was likely due to long-term, mild food restriction in AL_DR24M animals prior to DR onset at 24M due to the detrimental effect of customized food racks in the cages (Fig. 3.2.2B). In contrast, untreated, “naïve” AL animals were switched to DR at 20M of age, which did not have the food restriction and survival advantage of AL_DR24M mice.

Thus, chronic, mid- or late-life onset of DR is protective and associated with decreased risk of mortality compared to chronic AL feeding. However, already a short-term duration of previous AL feeding reduced the survival outcome compared to chronic DR animals, which was consistent with the lifespan results.

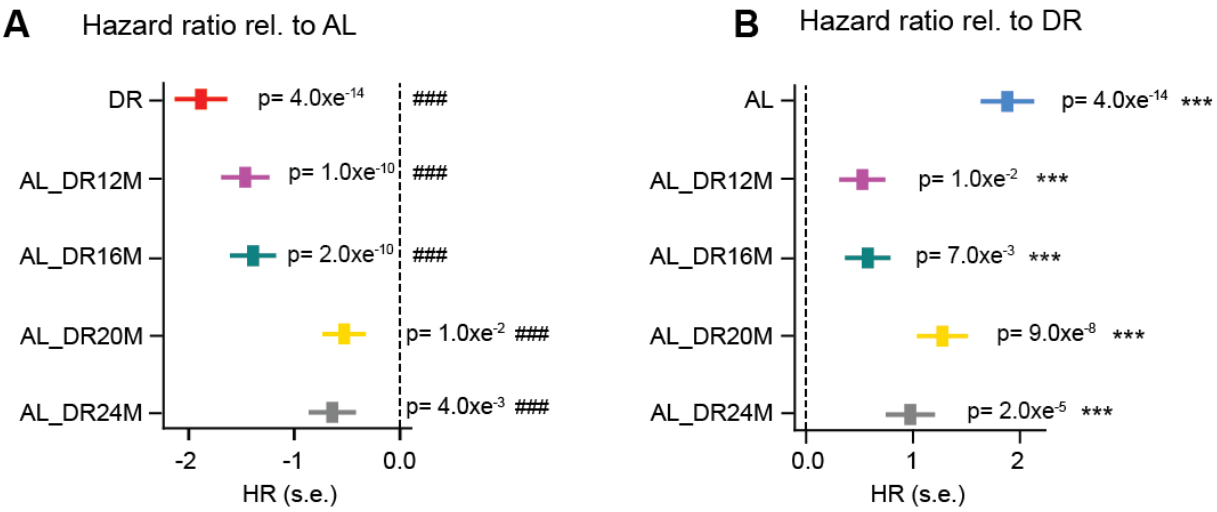

Figure 3.2. 4: DR, irrespective of the age of onset, improved survival in relation to chronic AL feeding but increased mortality in relation to chronic DR treatment

*Cox proportional hazard ratios of DR switch groups relative to **A)** AL-fed animals or **B)** to chronic DR controls to assess lifespan trajectories. Centres represent the coefficient and bars the 95% CI. **A** Early DR onset at 3M (coefficient = -1.8831, p= 4.0xe^{-14}, n=50), mid-life onset at 12M (coefficient= -1.4642, p= 1.0xe^{-10}, n=49) or 16M (coefficient = -1.3906, p= 2.0xe^{-10}, n=50) as well as late-life initiated DR at 20M (coefficient= -0.5289, p= 1.0xe^{-2}, n=45) and 24M (coefficient= -0.6405, p= 4.0xe^{-3}, n=46) exhibit significantly improved survival compared to chronic AL. The number of AL animals differed between cox proportional hazard regressions due to deaths in the AL cohort prior to the respective DR switch. Chronic DR and AL_DR12M were compared against 69 AL animals. AL_DR16M were compared to 67 AL animals, AL_DR20M were compared to 61 AL animals and AL_DR24M were compared to 45 AL animals. **B** Chronic AL (coefficient =1.8831, p=4.0xe^{-14}, n=69) as well as previous AL feeding for 12M (coefficient= 0.5259, p= 1.0xe^{-2}, n=49), 16M (coefficient = 0.5763, p= 7.0xe^{-3}, n=50), 20M (coefficient= 1.2752, p= 1.0xe^{-8}, n=45) or 24M (coefficient= 0.9756, p= 2.0xe^{-5}, n=46) prior to initiation of DR significantly increased the mortality risk compared to chronic DR treatment. Chronic AL, AL_DR12M and AL_DR16M were compared against 50 DR animals. AL_DR20M and AL_DR24M were compared to 49 DR animals due to deaths occurring prior to the 20M and 24M DR switch. Data are presented with p-values *** p<0.001 in relation to chronic DR and with p-values ### p<0.001 in relation to chronic AL. Statistical analyses were conducted and plots were generated by Carolina Monzó.*

3.2.5 AL_DR20M animals have on average less tumours at death than chronic AL animals

DR can not only reduce induced tumour growth in glioblastoma (Mukherjee et al., 2002) or breast cancer mouse models (de Lorenzo et al., 2011) but can also reduce spontaneous tumour growth in ageing mice (Hart & Turturro, 1997). Moreover, several clinical studies in humans currently aim to evaluate the potential of combined radiation or chemotherapy with

DR or DR mimetics, such as metformin, to reduce cancer growth and increase patient survival (Meynet & Ricci, 2014). We therefore asked how the age of DR onset would affect tumour load at death in our DR switch groups and whether there was a correlation of tumour load with survival. To this end, post-mortem pathology was conducted on euthanized or deceased animals in the lifespan cohort, to assess the number and the location of macroscopic tumours at the time of death starting at 20M of age when AL animals began to die. We first evaluated differences in the average tumour load at death of all diet groups in the lifespan cohort, irrespective of the age at which animals died. Interestingly, we detected a trend towards reduced tumour load in chronic or mid-life DR switches but only AL_DR20M mice displayed significantly fewer tumours in relation to chronic AL (Fig. 3.2.5A).

Therefore, we asked next whether the reduction in tumour load in AL_DR20M mice was due to an increased proportion of animals, which died with no or only few detected tumours at death. To this end, we calculated the proportion of animals affected by none (0), one (1), two (2), three (3) or over three (>3) detected lesions, which was previously implemented by Xie and colleagues (Xie et al., 2017). Strikingly, we detected a trend towards an increased proportion of chronic DR, which were tumour free at death (Fig. 3.2.5B). Moreover, similar proportions of AL_DR12M and AL_DR20M mice had no detected lesions compared to chronic AL mice. In contrast, fewer AL_DR16M and AL_DR24M mice died without any tumour (Fig. 3.2.5B). Furthermore, there was a trend towards increased prevalence of primary tumours in all DR switch groups compared to chronic AL or DR controls (Fig. 3.2.5B). Except in AL_DR20M, two tumours were similarly present in all diet groups and three tumours affected fewer AL_DR12M mice at death (Fig. 3.2.5B). Most notably, chronic AL animals exhibited the highest prevalence for multiple tumours at death, whereas more than three tumours were less common in AL_DR20M mice (Fig. 3.2.5B), which could explain the difference in average tumour number at death between the two groups (Fig. 3.2.5A). In contrast, the proportion of chronic DR, AL_DR12M, AL_DR16M or AL_DR24M with multiple lesions at death was comparable, implying that the formation of multiple lesions was not affected by earlier or later onset of DR (Fig. 3.2.5B). Intriguingly despite an eight-month later onset of DR, the overall percentage of AL_DR24M animals affected by no, one or more tumours closely resembled the tumour prevalence of AL_DR16M animals (Fig. 3.2.5B), indicating that a chronic, less severe DR regimen could affect tumour formation similarly to DR onset at 16M. However, when probed for statistical differences in tumour prevalence between diet groups, none of the comparisons reached statistical significance. Therefore, the significant reduction in average tumour load at death in AL_DR20M mice could stem from the reduced prevalence of two or more lesions at death compared to AL mice.

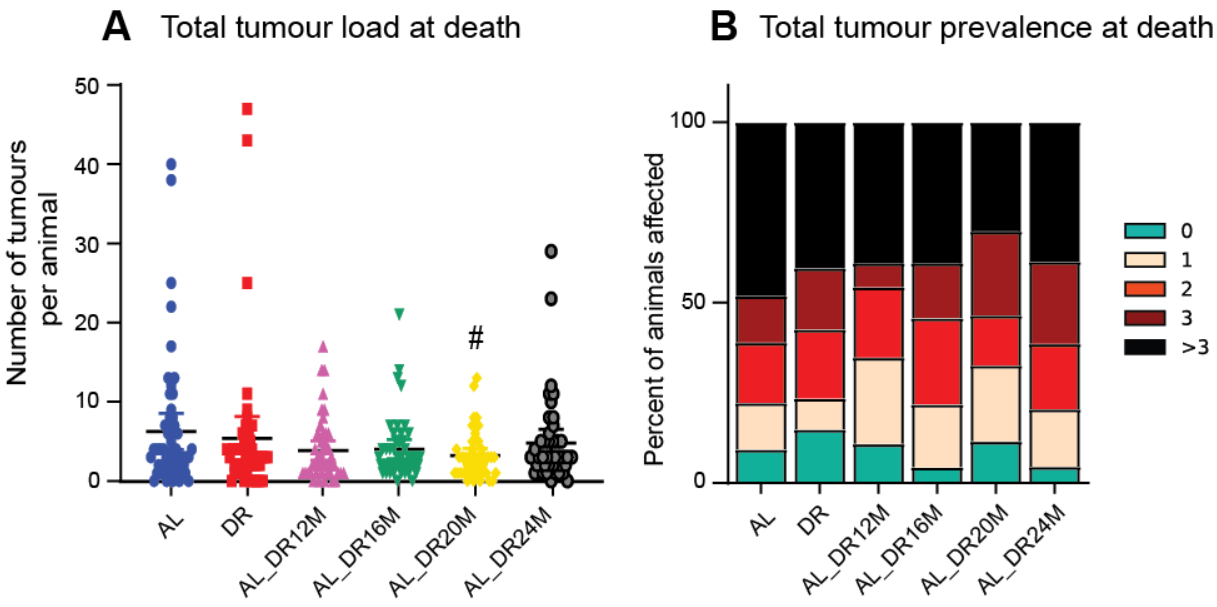

Figure 3.2. 5: AL_DR20M animals have on average less tumours at death than chronic AL animals

A *Total tumour burden at death of naturally deceased or euthanized chronic AL (n= 54), chronic DR (n= 47), AL_DR12M (n= 46), AL_DR16M (n= 46), AL_DR20M (n= 43) or AL_DR24M (n= 44) animals in the entire lifespan cohort. Total number of tumours per animal irrespective of the location or the affected organ were taken into account and animals, which died prior to the respective DR switch, were excluded from the analysis. AL_DR20M had on average fewer tumours (p= 0.0261) than chronic AL animals. No differences in tumour load were observed between chronic AL and early or late-onset DR groups or between DR groups (p> 0.05).* ***B*** *Demographics of the total tumour burden of chronic AL, chronic DR, AL_DR12M, AL_DR16M, AL_DR20M and AL_DR24M. All tumours irrespective of the location or the affected organ were taken into account to calculate the percentage of animals affected by no, one, two, three or more than three tumours and animals, which died prior to the respective DR switch, were excluded from the analysis No significant differences in tumour demographics between diet groups were detected. Student t tests were carried out to assess differences in the average number of tumours and Fisher's test were implemented to compare the prevalence of mice affected or not affected by none, one or more tumours at the time of death between chronic controls and DR switch groups. Data are presented as mean with 95% CI and with p-values # p<0.05 in relation to chronic AL. Differences, which did not reach statistical significance p> 0.05 were not labelled.*

3.2.6 Chronic DR delays early tumour growth but does not decrease tumour burden at old age

In contrast to previous studies (as reviewed by Brandhorst & Longo, 2016 and Longo & Fontana, 2010), we did not detect any statistically significant differences in the average tumour number or prevalence in chronic AL compared to chronic DR mice. However, it is known that the tumour burden increases in an age-dependent manner in humans (DeSantis et al., 2019)

as well as in AL –fed and in restricted mice (Bronson & Lipman, 1991). Therefore, we wondered whether a higher tumour load in exceptionally long-lived DR animals could have masked statistical differences in relation to, on average, shorter-lived chronic AL or late-onset DR mice. To this end, we first plotted the density distribution of deaths occurring in each cohort, which enabled us to investigate the number and prevalence of tumours in prematurely deceased, average aged as well as longest-lived individuals in each diet group (Fig. 3 2.6A). Moreover, this systematic screen ensured, that comparable number of mice were represented in each parts of the density distribution. The centres of the Gaussian distribution were 773,7 days for AL, 1033 days for DR, 968,9 days for AL_DR12M, 1020 days for AL_DR16M, 903 days for AL_DR20M and 847,8 days for AL_DR24M, which closely resembled the median lifespan of the diet groups as previously determined (Fig. 3.2.3A-D). Interestingly, the pattern of the distribution of deaths in AL_DR12M closely resembled distribution of chronic DR mice, which was broader compared to chronic AL mice (Fig. 3.2.6A). In contrast, the distribution of AL_DR16M, AL_DR20M and AL_DR24M displayed a similarly narrow peak distribution as chronic AL, which indicated that the more animals died within a shorter time frame compared to DR and AL_DR12M (Fig. 3.2.6A). Based on the Gaussian density distribution, we determined the number of prematurely deceased, average aged and longest-lived animals in each diet group (Fig. 3.2.6B-D).

We first evaluated the tumour load and prevalence in prematurely deceased chronic controls and DR switch groups (Fig. 3.2.6B). The average age of prematurely deceased animals were 678,1 days for AL, 847,6 for DR, 820,6 AL_DR12M, 849,9 AL_DR16M, 727,4 AL_DR20M and 779,1 AL_DR24M. Strikingly, prematurely deceased chronic DR animals had significantly fewer tumours compared to chronic AL and 16M, 20M and 24M DR switch mice (Fig. 3.2.6B). Moreover, a significantly higher proportion of chronic DR animals were tumour-free at death compared to AL_DR16M and AL_DR24M (Fig. 3.2.6B). Additionally, less chronic DR animals were affected with multiple lesions at death compared to chronic AL (Fig. 3.2.6B), indicating that chronic DR significantly reduced early tumour formation. Intriguingly, the tumour prevalence of prematurely deceased AL_DR24M closely resembled the prevalence of AL_DR16M mice (Fig. 3.2.6B), suggesting that a 60% reduction in food intake following a lifelong less severe DR regimen improved tumour load similarly to 16M onset DR.

Next, we compared the number and prevalence of tumours in average aged animals from each diet group (Fig. 3.2.6C). Interestingly, we detected a trend towards reduced average tumour load in AL_DR20M mice compared to chronic AL or DR in animals that reached the average lifespan of their respective cohort (Fig. 3.2.6C). In contrast, chronic AL, DR, AL_DR12M, AL_DR16M and AL_DR24M displayed on average similar tumour numbers at death (Fig. 3.2.6C), indicating that early or late-onset of DR could not fully inhibit cancerous growth. When assessing tumour prevalence, AL, DR and 12M DR onset exhibited the highest proportion of

tumour-free mice at death, whereas fewer AL_DR16M, AL_DR20M and AL_DR24M mice died without any detected lesion (Fig. 3.2.6C). Interestingly, AL_DR20M mice displayed the highest proportion of mice with only one tumour at death (Fig. 3.2.6C), indicating the reduction in average tumour load was likely attributed to more AL_DR20M mice with fewer lesions compared to the other diet groups. However, when probed for statistical differences between diet groups, none of the comparisons did not reach statistical significance.

Lastly, we assessed the tumour load and prevalence in the longest-lived survivors of each diet group (Fig. 3.2.6D). The average age in days of the longest-lived animals were 916,3 for AL, 1307,8 for DR, 1199,6 for AL_DR12M, 1160,2 for AL_DR16M, 1025,5 for AL_DR20M and 1052 for AL_DR24M. Interestingly, we detected a trend towards reduced average tumour load in DR switch groups compared to chronic AL or DR (Fig. 3.2.6D). Moreover, chronic DR mice exhibited the highest average number of tumours, which could be attributed to the presence of longest-lived animals from the entire lifespan cohort. Correspondingly, all DR animals exhibited at least two lesions and more than 60% of all DR mice harboured more than three tumours at death (Fig. 3.2.6D). In contrast, the prevalence of over three tumours was reduced in chronic AL, AL_DR12M, AL_DR16M, AL_DR20M and AL_DR24M mice (Fig. 3.2.6D), suggesting that lifelong DR cannot fully inhibit but only slow down tumour growth. Strikingly, a small proportion of the longest-lived chronic AL, AL_DR16M and AL_DR20M died without any tumour (Fig. 3.2.6D), demonstrating that these animals died from other causes than cancer.

In summary, chronic DR significantly reduced the onset of spontaneous tumour growth in prematurely deceased animals but could not inhibit tumour formation as animals aged. Intriguingly, AL_DR20M displayed fewer lesions at the median distribution, suggesting that these animals died from other causes than cancer. Moreover, these data indicate that tumour growth could not be a major cause for the lack in late life DR longevity, as the tumour load of AL_DR20M was lower among the median and the longest-lived survivors of this diet group.

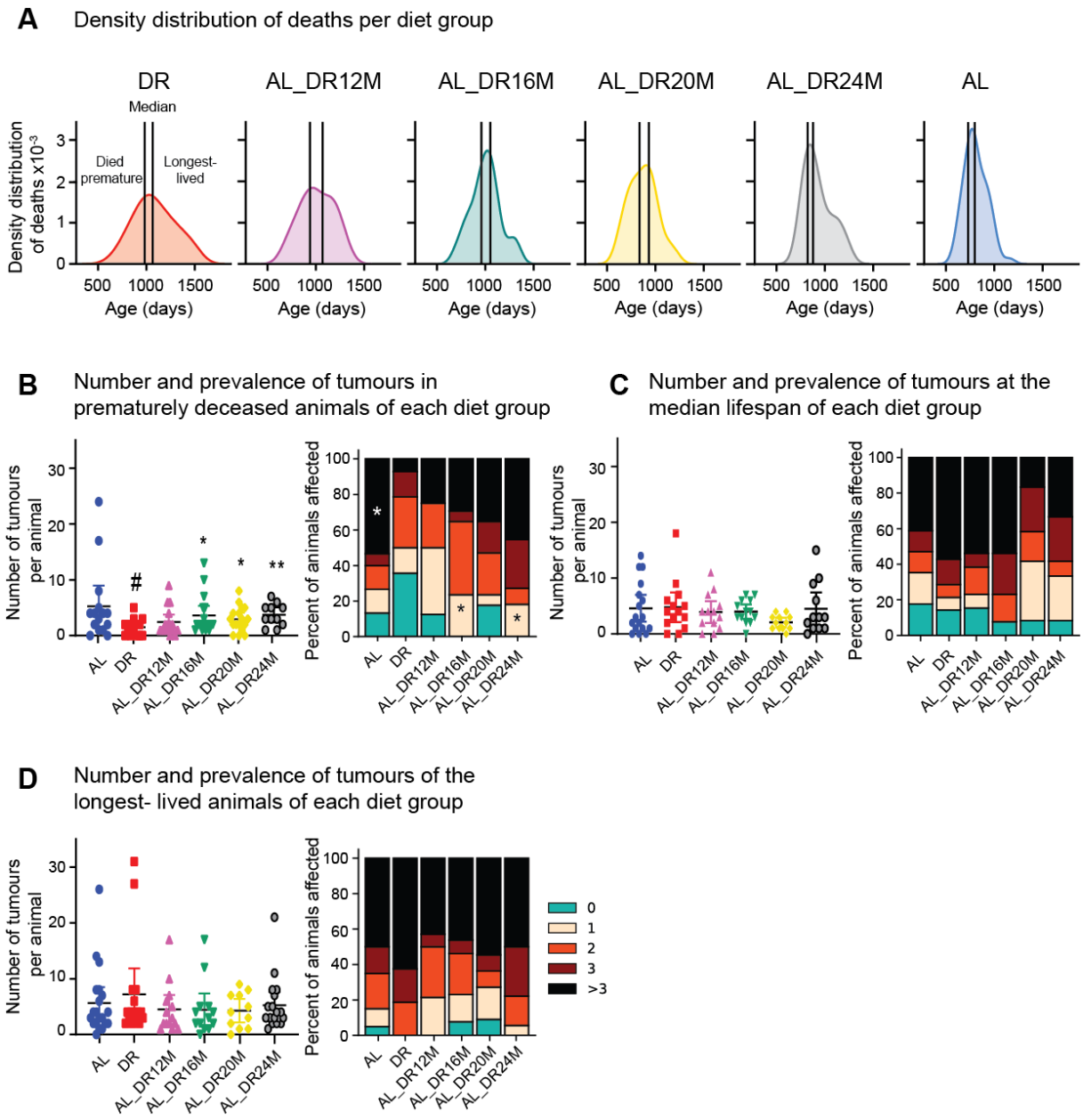

Figure 3.2. 6: Chronic DR delays tumour growth but does not decrease tumour burden at old age

A *Gaussian density distribution of deaths occurring in chronic AL (n= 60), chronic DR (n= 50), AL_DR12M (n= 49), AL_DR16M (n= 50), AL_DR20M (n= 45) or AL_DR24M (n= 46) animals in the entire lifespan cohort. Animals that died before the respective DR switch were excluded from the analyses. First, the Gaussian centre of the distribution was calculated. The centres of the Gaussian distribution were 773,7 days for AL, 1033 days for DR, 968.9 days for AL_DR12M, 1020 days for AL_DR16M, 903 days for AL_DR20M and 847,8 days for AL_DR24M, which closely resembled the median lifespan of each diet group. Next, the number of animals that died prematurely before the centre of the density distribution was determined and animals were represented parts left from the centre (left). Animals that were the longer lived than the median were represented by the right fraction of the density distribution. Total number of tumours per animal irrespective of the location or the affected organ were taken into account and the percentage of animals affected by no, one, two, three or more than three tumours were calculated at the left, centred and right part of the density distribution.* ***B*** *Number and*

tumour prevalence of prematurely deceased animals in the chronic AL (n= 15), chronic DR (n= 14), AL_DR12M (n= 16), AL_DR16M (n= 17), AL_DR20M (n= 17) or AL_DR24M (n= 11) groups in the left density distribution. Prematurely deceased chronic DR animals had significantly fewer tumours at death than chronic AL and AL_DR16M, AL_DR20M and AL_DR24M. ***C*** *Number and tumour prevalence at the median lifespan of chronic AL (n= 17), chronic DR (n= 14), AL_DR12M (n= 13), AL_DR16M (n= 13), AL_DR20M (n= 12) or AL_DR24M (n= 12) in the centred part of the density distribution. The average tumour load or tumour prevalence was not significantly different between diet groups at the median lifespan.* ***D*** *Number and tumour prevalence of the longest-lived chronic AL (n= 20), chronic DR (n= 16), AL_DR12M (n= 14), AL_DR16M (n= 13), AL_DR20M (n= 11) or AL_DR24M (n= 18) in the right part of the density distribution. The average tumour load or tumour prevalence did not significantly differ in the longest-lived individuals of each diet group. Student t tests were carried out to assess differences in the number of tumours in the left, centred or right density distribution between chronic controls and DR switch groups. Fisher's tests were implemented to compare the prevalence of mice affected or not affected by none or at least one tumour at the time of death. Data are presented as mean with 95% CI, as density distribution or in percent and with p-values * p<0.05 and ** p<0.01 in relation to chronic DR and with p-values # p<0.05 in relation to chronic AL. Differences, which did not reach statistical significance p> 0.05 were not labelled. Carolina Monzó calculated and provided the plots of the density distribution at death.*

3.2.7 DR onset at 3M, 12M and 16M protects animals from liver carcinogenesis

We next asked whether DR had any impact on the incidence of different tumour types. To this end, we evaluated which tissues were affected by tumour growth, first irrespective of the age at which the animal died. Interestingly, the dominating tumour types in the lifespan cohort were connective tissue tumours affecting the adipose tissue depots, liver tumours as well as lymph node tumours at different locations in the body (Fig. 3.2.7A). Interestingly, connective tissue tumours showed the highest prevalence in chronic AL mice and the prevalence decreased with earlier DR onset, suggesting a correlation of body fat content and the formation of these tumours (Fig. 3.2.7A). However, no significant differences were observed between diet groups. In contrast, AL_DR24M animals had significantly more lymph node tumours at death compared to chronic AL (Fig. 3.2.7A). With the exception of AL_DR24M animals, the occurrence of lymph node tumour displayed an inverse correlation with the age of DR onset (Fig. 3.2.7A). These data suggest that lymph node tumour occurrence could be linked to longer-lived animals, as lymph node tumours affected more chronic DR animals than chronic AL or AL_DR20M. Strikingly, the incidence of liver tumours was significantly reduced in chronic DR, AL_DR12M and AL_DR16M and the other diet groups (Fig. 3.2.7A and B), indicating that DR initiated at 3M, 12M or 16M of age can protect C3B6F1 females from liver carcinogenesis. Intriguingly,

AL_DR16M displayed an in-between phenotype with lower liver tumour prevalence compared to chronic AL but increased liver tumour prevalence in relation to chronic DR (Fig. 3.2.7A and B).

Next, we sought to investigate if the occurrence of the different tumour types differed between diet groups and whether some tumour types could be observed earlier than other tumour types. To this end, we assessed the prevalence of animals affected or not affected by different tumour types in prematurely deceased, average aged or longest-lived animals, corresponding to the density distribution from Fig. 3.2.6. Similar to the tumour demography in the entire cohort, the most prevalent tumour types in prematurely deceased animals were connective tissue tumours, liver and lymph node tumours as well (Fig. 3.2.7C). Interestingly, we detected a significant increase in connective tissue and liver tumours in AL_DR24M compared to chronic DR (Fig. 3.2.7C). Moreover, compared to chronic AL, liver tumours did not affect prematurely deceased AL_DR12M animals (Fig. 3.2.7C). While there was a trend towards increased liver tumour prevalence in 16M, 20M and 24M onset DR in relation to DR (Fig. 3.2.7C), the comparisons did not reach statistical significance. Next, we evaluated the prevalence of different tumour types in animals, which reached the median lifespan of their respective diet group. Interestingly, the overall prevalence of different tumour types was comparable between diet groups at the median lifespan (Fig. 3.2.7D). Notably, lymph node tumour formation was significantly increased in AL_DR16M mice compared to chronic AL (Fig. 3.2.7D). Moreover, we detected a trend towards increased lymph node tumour prevalence in chronic, 12M and 24M onset DR compared to AL (Fig. 3.2.7D). Interestingly, eye tumours seemed to occur earlier in murine eyes, as only prematurely deceased animals were affected by this tumour type (Fig. 3.2.7C-E=. Taken together, these data suggest that animals were affected by similar lesions irrespective of the age of DR onset or the duration of previous AL feeding at the median age of death of their respective diet group. Lastly, we evaluated the prevalence of different tumour types in the longest-lived animals of each diet group (Fig. 3.2.7E). Interestingly, we detected a trend towards overall higher prevalence for colorectal, liver or uterine tumours in all diet groups (Fig. 3.2.7E), suggesting that ageing affected the occurrence of many different tumour types irrespective of DR or previous AL feeding. Moreover, lymph node tumours affected more than 50% of all long-lived animals, irrespective of the age of DR onset (Fig. 3.2.7.E), suggesting that this tumour type could be linked with old age. Strikingly, we detected an increase in liver carcinogenesis depending on the age of DR onset and chronic DR and AL_DR12M animals displayed significantly lower liver tumour prevalence compared to chronic AL (Fig. 3.2.7E). Moreover, AL_DR24M mice had significantly more liver tumours than chronic DR animals (Fig. 3.2.7E). Intriguingly, liver tumours similarly affected AL_DR16M animals compared to AL_DR20M or AL_DR24M (Fig. 3.2.7E), suggesting that mid-life onset of DR cannot protect the longest-lived animals from liver carcinogenesis at old age. Moreover, the

higher liver tumour prevalence of AL_DR16M in the entire diet group (Fig. 3.6.A), was due to increased liver tumour prevalence in the longest- lived AL_DR16M mice (Fig. 3.2.7E). These data suggest that DR onset at 16M could prevent liver tumour formation in animals, which died prematurely or at the median lifespan but was not able to inhibit liver carcinogenesis in very old AL_DR16M mice.

To conclude, the age of DR onset, as well as the age at which animals died affected the occurrence of different tumour types. Moreover, DR onset at 3M or 12M protected animals from liver carcinogenesis, whereas DR onset at 20M or 24M as well was not able to reduce cancerous growth in the liver. Most strikingly, AL_DR16M mice display an in-between phenotype with a full lifespan extension similar to AL_DR12M but significantly increased liver tumour load in the entire diet group or in the longest-lived mice, suggesting that lifespan and health at old age might not be connected. Intriguingly, a chronic but less severe DR regimen did not significantly affect the formation of different tumour types and liver or connective tissue tumours similarly affected AL_DR24M as chronic AL animals.

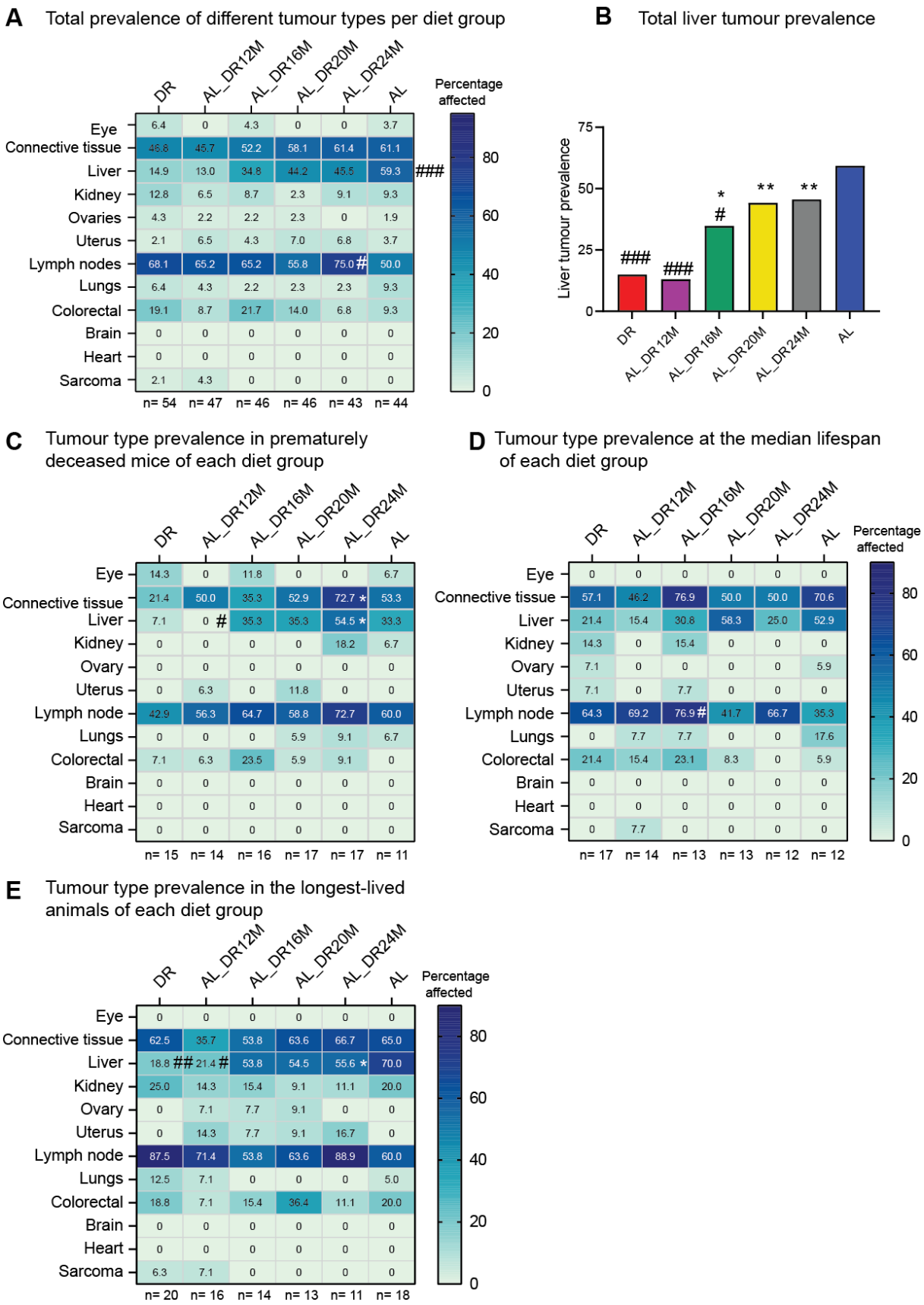

Figure 3.2. 7: DR onset at 3M, 12M and 16M protects animals from liver carcinogenesis

A *Heat map of the total prevalence of different tumour types and* ***B****) proportion of liver tumours in each diet group irrespective of the age of death in the lifespan cohort of chronic AL (n=54), chronic DR (n=47),*

AL_DR12M (n=46), AL_DR16M (n=46), AL_DR20M (n=43) or AL_DR24M (n=44). AL_DR24M animals that died before their corresponding diet switch were excluded from the analysis. Chronic 3M and 12M onset DR grouped together (p=1) and the incidence of liver tumours was significantly lower compared to chronic AL (p=0.001) and DR onset at 20M (p=0.0026) or 24M (p=0.0025) compared to chronic DR. No significant differences were found between chronic AL and AL_DR20M (p=0.1568) or AL_DR24M (p=0.2229). AL_DR16M displayed an intermediate phenotype with increased liver tumour prevalence compared to DR (p=0.032) and reduced liver tumour prevalence compared to AL (p=0.017). AL_DR24M mice had more lymph node tumour than chronic AL (p=0.0133). ***C****) Heat map of different tumour types of prematurely died chronic AL (n= 15), chronic DR (n= 14), AL_DR12M (n= 16), AL_DR16M (n= 17), AL_DR20M (n= 17) or AL_DR24M (n= 11) in the left distribution.* ***D****) Heat map of different tumour types at the median lifespan of chronic AL (n= 17), chronic DR (n= 14), AL_DR12M (n= 13), AL_DR16M (n= 13), AL_DR20M (n= 12) or AL_DR24M (n= 12) in the centred distribution.* ***E****) Heat map of different tumour types of long-lived chronic AL (n= 20), chronic DR (n= 16), AL_DR12M (n= 14), AL_DR16M (n= 13), AL_DR20M (n= 11) or AL_DR24M (n= 18) in the right distribution. Connective tissue tumours, liver tumours and lymph node tumours are the most prevalent tumour types at the three different distributions. The occurrence of tumours varies depending on the diet group and the lifespan distribution. Animal numbers are indicated below the heat map. Fisher's test was implemented to compare the proportion of mice affected or not affected by at least one or multiple liver tumours at the time of death. Data are presented with p-values *** p<0.001 and ns as not significant.*

3.2.8 Cross-sectional pathology at defined ages largely correlates with the tumour load of the lifespan cohort

As the post-mortem pathology of the lifespan animals was not conducted on animals of the same age, differences in tumour load could be attributed to big age differences between animals in the assessed four-month intervals. We therefore performed cross-sectional pathology on animals of the tissue collection cohort, which allowed unbiased analyses of tumour load and type of age-matched chronic control and DR switch groups at 5M, 12M, 16M, 20M, 24M and 28M of age. While no tumours were detected at 5M or 12M in chronic AL or DR (Fig. 3.2.8A and B), first tumours arose in the AL group at 16M of age (Fig. 3.2.8C). Moreover, the average number of tumours in the chronic AL cohort increased in an age-dependent manner with a peak at 28M of age (Fig. 3.2.8D-F). These results indicate that tumour growth occurred earlier and more often in AL animals. In contrast, chronic DR cohort exhibited the first tumours at 24M of age (Fig. 3.2.8E), indicating that chronic DR delayed but did not completely inhibit malignant growth as tumour numbers increased in an age-associated manner albeit to a much slower extent than their chronic AL counterparts (Fig. 3.2.8E and F). Correspondingly, the average number of tumours was significantly higher in chronic AL animals compared to chronic DR at 28M (Fig. 3.2.8F).

Switching animals to DR at 12M resulted in a similar delayed onset of tumour formation as chronic DR (Fig. 3.2.8C-E), however, one tumour was found in an AL_DR12M animal already at 16M of age (Fig. 3.2.8C). Moreover, we detected a trend towards increased tumour load in chronic AL compared to chronic DR or AL_DR12M at 20M, 24M and 28M (Fig. 3.2.8C-F), which did not reach statistical significance. AL_DR16M animals initially displayed an even higher tumour load than chronic AL animals at 20M (Fig. 3.2.8D), whereas significantly fewer tumours were detected at 24M (Fig. 3.2.8E) before tumour load increased again at 28M and closely resembled chronic DR mice (Fig. 3.2.8F). Interestingly, significantly fewer AL_DR16M animals were tumour-free and three tumours significantly affected more animals compared to chronic DR (Fig. 3.2.8D). AL_DR20M animals displayed a higher tumour number at 24M when first cross-sectional pathology was conducted (Fig. 3.2.8E) though tumour load was significantly decreased at 28M of age compared to chronic DR (Fig. 3.2.8F), which was attributed to more tumour-free animals in AL_DR20M. However, at both evaluated time points only six AL_DR20M animals were still alive, indicating that the surviving animals were healthier than the ones, which died prior to the dissection. Furthermore, AL_DR24M exhibited similar tumour load compared to chronic AL at 28M of age (Fig. 3.2.8F), indicating that DR onset at 24M of age in cannot improve tumour load due to prolonged detrimental AL feeding. When evaluating the tumour prevalence at 28M, significantly more AL_DR12M and AL_DR20M were tumour-free at death and chronic AL animals were significantly more affected by over three tumour compared to either DR group (Fig. 3.2.8F).

All in all our cross-sectional pathology results largely correlated with the results obtained from the post-mortem pathology of our lifespan cohort (Fig. 3.2.5A-B and Fig. 3.2.6B-D) and we confirmed reduced tumour prevalence and load in chronic DR compared to AL feeding.

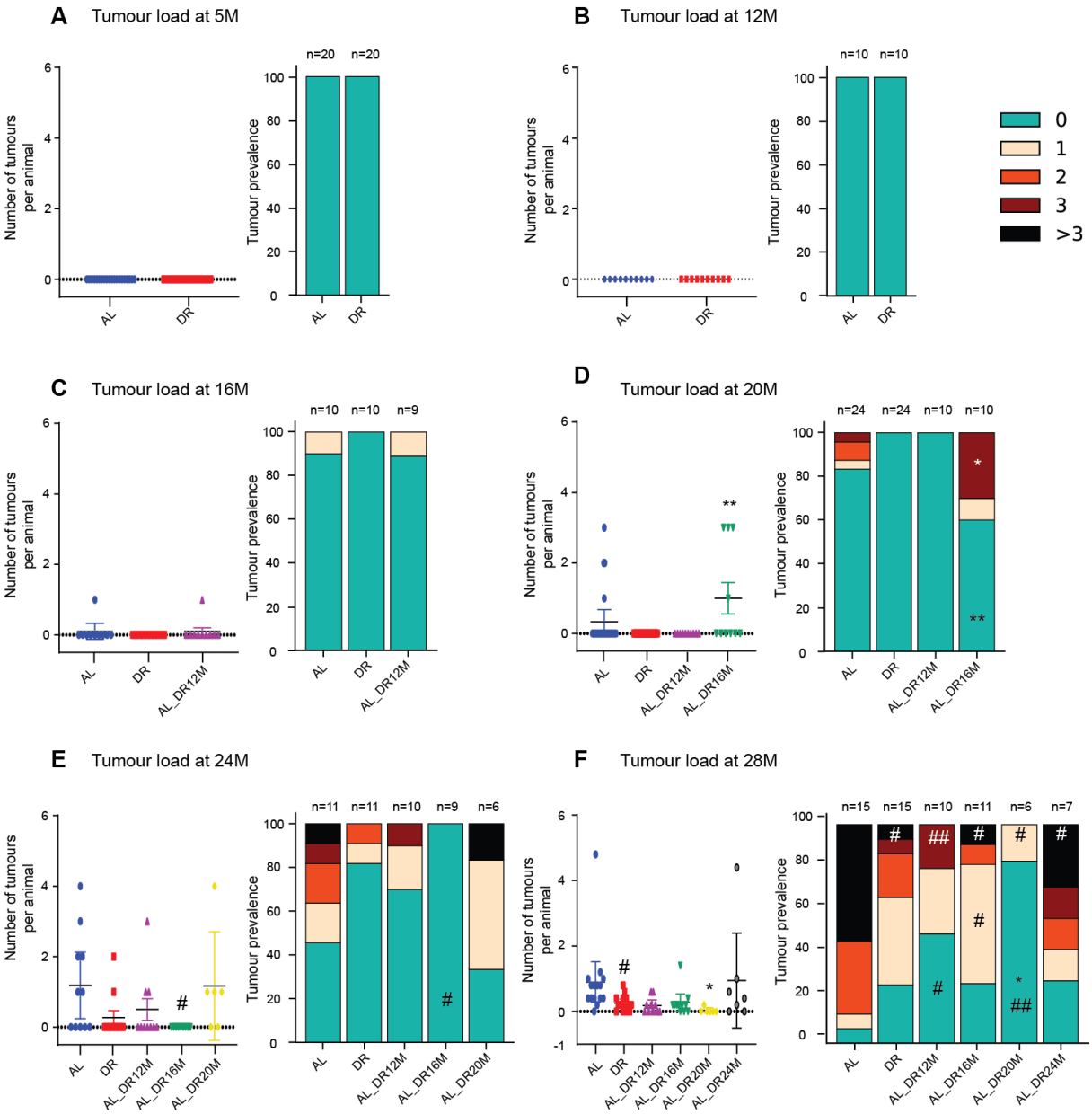

Figure 3.2. 8: Cross-sectional pathology at defined ages largely correlates with the tumour load of the lifespan cohort

*Tumour number and tumour prevalence of chronic AL, DR or DR switch animals **A)** at 5M (AL n=20, DR n=20), **B)** at 12M (AL n=10, DR n=10), **C)** 16M (AL n= 10, DR n= 10, AL_DR12M n= 9), **D)** 20M (AL n= 24, DR n= 24, AL_DR12M n= 10, AL_DR16M n=10), **E)** 24M (AL n= 11, DR n= 11, AL_DR12M n= 10, AL_DR16M n=9, AL_DR20M n=6) or **F)** 28M of age (AL n= 15, DR n= 15, AL_DR12M n= 10, AL_DR16M n=11, AL_DR20M n=6, AL_DR24M n=7). Total number of tumours per animal irrespective of the location or the affected organ were taken into account and the percentage of animals affected by no, one, two, three or more than three tumours were calculated. Animal numbers at the different dissections are indicated above the bars. Naïve, untreated AL animals were switched to DR at 24M of age. Unpaired t tests were carried out to compare the number of tumours per animals between diet groups. Fisher's test were implemented to compare the prevalence of mice affected or not affected by none or at least one*

tumour at the time of death. The number of tumours are presented as mean with 95% CI. Carolina Monzó generated the tumour prevalence plots.

3.2.9 Liver tumour prevalence is reduced at 28M of age upon 3M, 12M or 20M onset DR

We next asked whether we could confirm the reduced incidence of liver tumours in chronic DR, AL_DR12M and AL_DR16M in our tissue collection cohort. To this end, we assessed the prevalence of different tumour types in cross-sectional pathology at specific ages in age-matched animals. Since no tumours were detected at 5M and 12M of age, we focussed our analyses on the 16M, 20M, 24M and 28M time points. In accordance with our lifespan data, the most prevalent tumours at all ages were connective tissue and liver tumours, whereas lymph node tumours were less prevalent and colorectal tumours were more prevalent in the tissue collection cohort (Fig. 3.2.9A-E).

At 16M of age, the majority of animals in each diet group were tumour-free at death (Fig. 3.2.9A and Fig. 3.2.8C). We detected one eye tumour in an AL_DR12M animal one chronic AL mouse displayed a connective tissue tumour. Interestingly, similar to prematurely deceased animals of the lifespan cohort (Fig. 3.2.7B) eye tumours also exclusively occurred at 16M of age in the tissue collection cohort, suggesting that this tumour type indeed only developed early in life. Interestingly, we observed a higher tumour prevalence and more tumour types in animals dissected at 20M of age (Fig. 3.2.9B). Strikingly, AL_DR16M mice displayed the highest tumour prevalence and had significantly more connective tissue tumours compared to both chronic controls and increased liver tumours compared to chronic DR mice (Fig. 3.2.9B). Moreover, we detected lesions in the lungs of AL_DR16M and in the gastrointestinal tract of AL_DR16M and chronic AL (Fig. 3.2.9B). In contrast, chronic DR and AL_DR12M animals had no detected lesion at death, indicating that earlier onset of DR at 3M or 12M could delay tumour growth. However, differences in lung or colorectal tumours did not reach statistical significance in relation to chronic DR.

As expected, we detected a higher tumour prevalence at 24M of age. Strikingly, chronic DR animals first displayed tumours at 24M of age (Fig. 3.2.9C), suggesting that lifelong, early onset of DR could inhibit tumour formation. Interestingly, we observed a significant reduction in connective tissue tumours in AL_DR16M in relation to AL (Fig. 3.2.9C). Moreover, there was a trend towards reduced incidence of connective tissue tumours in chronic DR and AL_DR12M compared to AL (Fig. 3.2.9C), however, the comparisons did not reach statistical significance. Additionally, AL_DR20M and chronic AL animals had a higher prevalence for liver tumours,

which was not significantly different from chronic DR (Fig. 3.2.9C). Moreover, we detected spontaneous cases of lung tumours in AL_DR20M, colorectal tumours in AL_DR12M and chronic AL as well as a brain tumour in a chronic AL mouse (Fig. 3.2.9C).

Compared to previous dissections (Fig. 3.2.9A-C), the tumour prevalence was increased in all diet groups except in AL_DR20M at 28M of age (Fig. 3.2.9D). Interestingly, we detected significantly reduced prevalence for connective tissue tumours in 3M, 12M, 16M and 20M onset of DR compared to chronic AL feeding (Fig.3.2.9D and E). Moreover, chronic, 12M and 20M onset of DR significantly reduced liver carcinogenesis compared to chronic AL (Fig. 3.2.9D and E). Similar to previous findings (Fig. 3.2.7A and D), AL_DR16M displayed an in-between phenotype with increased liver tumour prevalence compared to chronic DR and reduced prevalence in relation to chronic AL (Fig. 3.2.9E). These data confirmed that 16M onset of DR could not fully inhibit liver carcinogenesis at old age in age-matched animals. However, in contrast to previous findings, the comparisons on liver tumour prevalence in AL_DR16M compared to the chronic controls was not statistically significant. Interestingly, chronic AL and DR had significantly more colorectal tumours compared to AL_DR20M, which did not display any colorectal tumours (Fig. 3.2.9D and E). In general, AL_DR20M mice were exceptionally healthy at 28M of age and, except for connective tissue tumours, did not display any other tumour types. However, four AL_DR20M animals already died before dissections and therefore, the surviving AL_DR20M animals were already the longest-lived animals from the diet group (Fig. 3.2.9D). Therefore, it is possible, that these surviving animals were exceptionally healthy compared to the other diet groups, in which fewer animals had already died. In summary, our results on the tumour prevalence in age-matched animals dissected at specific time points largely correlated with our results from the lifespan cohort. At 28M of age, AL_DR16M displayed a similar in-between phenotype of increased liver tumour prevalence and chronic DR and AL_DR12M animals were almost not affected by liver carcinogenesis, as observed before. Unexpectantly, AL_DR20M mice were healthier at 24M and 28M and had reduced tumour prevalence, which could be explained by low animals numbers due to previous deaths at both time points.

To conclude, our data suggests that delayed onset of tumour formation in early DR is one responsible factor for DR-mediated lifespan extension and is associated with increased health at old age. However, DR cannot completely protect from age-associated increase in tumour load, as both early and mid-life DR animals displayed a marked increase of multiple tumours in an age-depending manner. Overall, we observed that the age of DR onset seems to affect tumour formation, as we observed differences in detected tumour types between diet groups. It is possible, that DR is able to suppress or slow down the formation or progression of liver and connective tissue tumours when animals are young but fails to stop malignant tumour growth when animals are old, thus leading to the observed phenotypes.

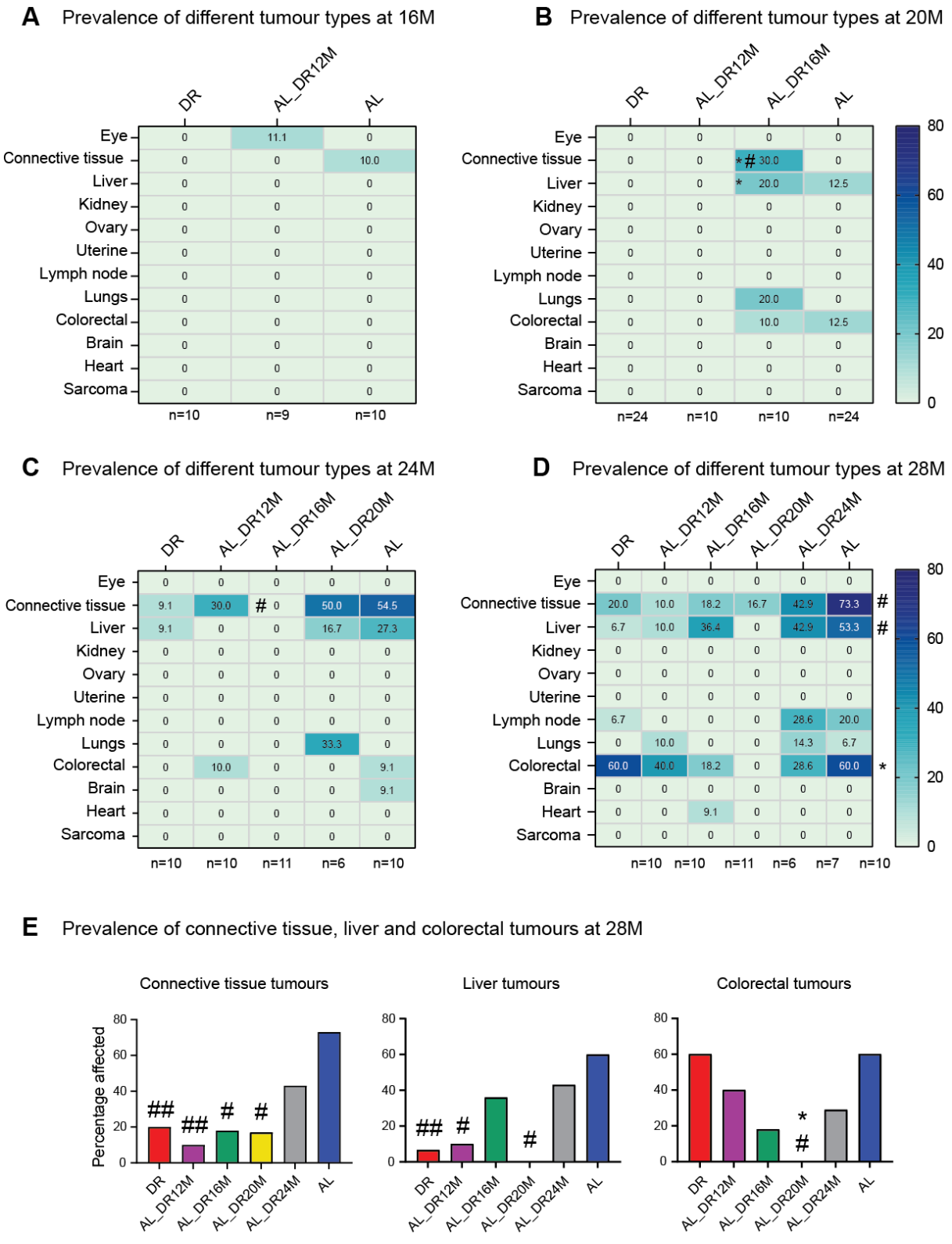

Figure 3.2. 9: Liver tumour prevalence is reduced at 28M of age upon 3M, 12M or 20M onset DR

*Heat map of the different tumour types in the cross-sectional pathology at **A)** 16M (AL n= 10, DR n= 10, AL_DR12M n= 9), **B)** 20M (AL n= 24, DR n= 24, AL_DR12M n= 10, AL_DR16M n=10), **C)** 24M (AL n= 11, DR n= 11, AL_DR12M n= 10, AL_DR16M n=9, AL_DR20M n=6) or **D)** 28M of age (AL n= 15, DR n= 15, AL_DR12M n= 10, AL_DR16M n=11, AL_DR20M n=6, AL_DR24M n=7). Animals that died before their corresponding diet switches were excluded from the analysis. The prevalence of different*

tumour types varied depending on the age of DR onset and the age at dissection. Except at 16M of age, connective tissue and liver tumours were most prevalent at all dissection time points. The age of DR onset influenced the occurrence of different tumour types. ***E)*** *Proportion of connective tissue, liver and colorectal tumours at 28M (AL n= 15, DR n= 15, AL_DR12M n= 10, AL_DR16M n=11, AL_DR20M n=6, AL_DR24M n=7). Except AL_DR24M mice, all other DR groups had fewer connective tissue tumours at death than chronic AL. Liver tumour prevalence was reduced in chronic DR, AL_DR12M and AL_DR20M animals in relation to chronic AL. AL_DR20M mice had fewer colorectal tumours compared to both chronic controls. Fisher's test was implemented to compare the proportion of mice affected or not affected by at least one or multiple liver tumours at the time of death. Animal numbers are indicated below the heat map. Data are presented with p-values *** p<0.001 and ns as not significant. Carolina Monzó conducted the statistical analyses.*

3.2.10 Evaluating the effect of mid-or late-onset DR on metabolic health

Old age and obesity often coincide and are major risk factors for developing chronic metabolic diseases, such as diabetes (Mancuso & Bouchard, 2019; Siervo et al., 2016). Thus, we assessed the metabolic health of animals treated with mid- and late-life DR and compared them to the chronic AL and DR controls. Chronic AL and DR animals were first assessed at 5M and 10M to determine metabolic health at young age and phenotypings were subsequently continued every four months until 26M of age. Metabolic health of DR switch animals was first measured six weeks post-switch and afterwards continued in the same phenotyping interval as chronic controls (Fig. 3.2.10A). At each phenotyping time point, nuclear magnetic resonance (NMR) spectroscopy, glucose (GTT) and insulin tolerance tests (ITT), as well as energy expenditure profiles using metabolic cages were conducted (Fig. 3.2.10A).

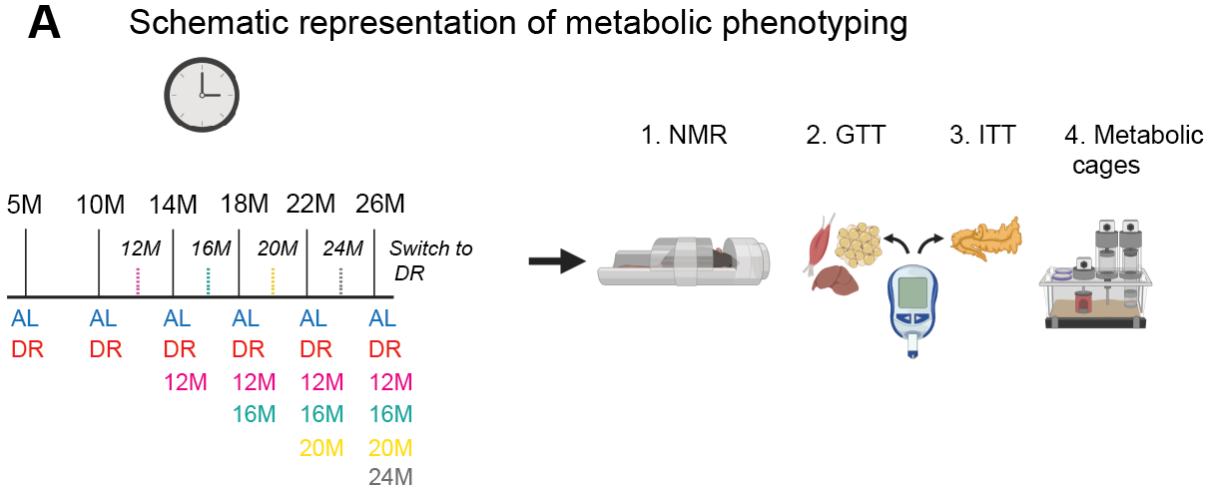

Figure 3.2. 10: Evaluating the effect of mid-or late-onset DR on metabolic health

A *Schematic representation of the metabolic phenotyping cohort. Chronic controls were first assessed at 5M and 10M and continued at 14M, 18M, 22M and 26M of age. DR switch groups were first tested six weeks post-switch to DR and followed the same phenotyping pattern. Animal numbers of chronic controls and DR switch varied between 8-15 animals per diet group depending on the phenotyping time point. Naïve, untreated AL animals were switched to DR at 24M of age. The schematic was created using Biorender.*

3.2.11 DR reverses the effect of early life obesity and restores body weight and fat mass at old age independent of the age of onset

We first measured the body weight by weighing the animals at the indicated time points (Fig. 3.2.10A). As expected, chronic DR animals maintained their body weight throughout life and displayed only minor weight gain with age (Fig. 3.2.11A). In contrast, chronic AL animals gained weight until 22M of age and only displayed reduced body weight at the oldest age of 26M (Fig. 3.2.11A). Switching mice from AL to DR led to a significant reduction in body weight irrespective of the age of DR onset and mice reached the same body weight as chronic DR animals within less than six months post-switch (Fig. 3.2.11A). AL_DR24M animals were not measured after 26M, thus there is no longer term follow up available for this group (Fig. 3.2.10A). Interestingly, our longitudinal body weight data indicated, that the body weight loss of late-onset DR switch animals was greater compared to earlier DR onset (Fig. 3.2.11A). To test this hypothesis, we compared to the body weight of DR switch after six weeks or six months of DR (Fig. 3.2.11B). Intriguingly, AL_DR24M animals were significantly lighter compared to earlier DR switches (Fig. 3.2.11B), whereas no differences were observed between AL_DR12M, AL_DR16M or AL_DR20M animals after six weeks of DR. At six months of DR, AL_DR16M mice were heavier compared to AL_DR12M, which could be due to a higher pre-switch body weight on AL feeding and a higher mean weight after six weeks of DR (Fig. 3.2.11B). As no prior body weight data were available for AL_DR24M animals, it is possible that AL_DR24M similarly lost body weight during ageing, as observed for chronic AL animals (Fig. 3.2.11A). Moreover, given the advanced age, it is possible that AL_DR24M mice were less healthy prior to the switch and animals rapidly lost body weight after the initiation of DR, potentially due to sustained tumour growth or other comorbidities.

We next asked whether the DR-mediated weight loss was attributed due to loss of fat or lean mass by performing NMR spectroscopy. The observed age-related weight gain in AL mice was attributed to increased fat mass and a subsequently decreased lean-to fat mass ratio, which rendered these mice obese (Fig.3.2.11C). Moreover, by the age of 10M, chronic AL mice exhibited a body fat mass above 30% in stark contrast to chronic DR animals, which

maintained their lower fat-to lean mass ratio during ageing (Fig. 3.2.11C). Upon initiation of DR, mice of all DR switch groups significantly lost fat mass. Similar to the body weight within six months post-switch, DR switch mice reached the same fat mass as chronic DR animals (Fig. 3.2.11C). Furthermore, when comparing fat mass six weeks after DR was initiated, the fat mass reduction of AL_DR12M, AL_DR16M and AL_DR20M was similar despite the differences in the age of onset (Fig. 3.2.11D). Interestingly, fat mass reduction of AL_DR24M mice was significantly greater compared to the earlier DR switches (Fig. 3.2.11D) and correlated with differences in body weight (Fig. 3.2.11B), which might be attributed to old age and tumour formation.

Taken together, our data show that chronic DR animals have a reduced body weight and improved fat-to-lean mass ratio, which is maintained during ageing. Upon initiation of DR, independent of age, animals rapidly lose fat mass and increased lean mass. Thus, even at very old age, DR can reverse the excessive fat accumulation caused by early-life obesity.

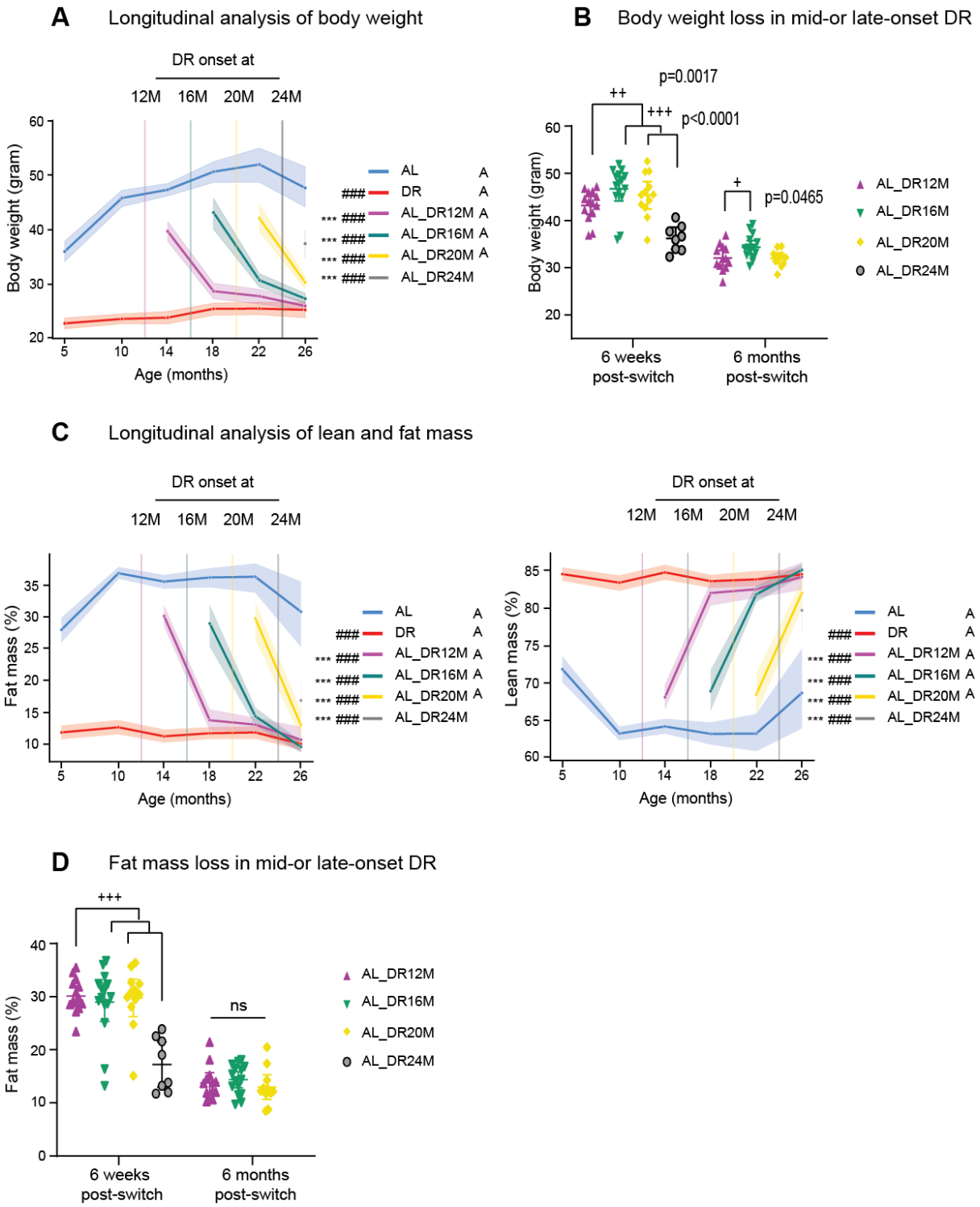

Figure 3.2. 11: DR leads to weight loss and reduces body fat independent of the age of DR onset

A *Body weight at 5M, 10M, 14M, 18M, 22M and 26M of age of chronic AL, DR and DR switch groups using nuclear magnetic resonance (NMR) spectroscopy. DR irrespective of the age of onset significantly reduced body weight after six weeks of DR and animals caught up to chronic DR animals within six months after DR was initiated.* ***B*** *Evaluation of the weight loss after six weeks or six months of DR in AL_DR12M, AL_DR16M, AL_DR20M and AL_DR24M. AL_DR24M animals had a significantly lower body weight six weeks after DR was initiated compared to earlier DR switches. AL_DR16M mice were*

significantly heavier than AL_DR12M after six months of DR. ***C*** *Longitudinal analysis of the relative fat and lean mass of chronic controls and DR switch groups. Correspondingly to loss of body weight, DR switch animals lost fat mas and increased the lean-to-fat mass ratio already after six weeks on DR.* ***D*** *Evaluation of fat mass loss after six weeks or six months of DR in AL_DR12M, AL_DR16M, AL_DR20M and AL_DR24M. AL_DR24M animals had significantly less fat mass six weeks after DR was initiated compared to earlier DR switches. No differences in fat mass were observed between 12M, 16M or 20M onset DR animals after six months of DR. Animal numbers were the following: at 5M AL n= 15, DR n= 15. At 10M AL n= 15, DR n= 15. At 14M AL n= 15, DR n= 15, AL_DR12M n= 14. At 18M AL n= 15, DR n= 15, AL_DR12M n= 13, AL_DR16M n= 15). At 22M AL n= 14, DR n= 15, AL_DR12M n= 13, AL_DR16M n= 15, AL_DR20M n= 12). At 26M of age (AL n= 8, DR n= 14, AL_DR12M n= 9, AL_DR16M n= 11, AL_DR20M n= 11, AL_DR24M n=8). Generalized linear mixed effects models (GLME) were used to evaluate the effect of newly imposed or longer duration of DR on body weight and body composition. Unpaired t tests were conducted to calculate differences in the body weight or fat mass after six weeks or six months of DR between AL_DR12M, AL_DR16M, AL_DR20M and AL_DR24M. Data are presented as mean with the 95% CI as shaded area or error bars. Statistical differences compared to chronic DR are indicated with p-values * p<0.05, and *** p<0.001. Statistical differences in relation to AL are presented as following # p<0.05, ## p< 0.01 and ### p<0.001. Statistical differences between DR switch groups were presented with p value + p<0.05, ++ p< 0.01 and +++ p<0.001. Differences between DR switch groups are indicated with +++ p<0.001. Carolina Monzó conducted GLME analyses and plotted the longitudinal data of the body weight, lean and fat mass.*

3.2.12 DR improves glucose tolerance as early as six weeks post-switch independent of the age of DR onset and maintains it during ageing

Increased circulating blood glucose levels and reduced glucose tolerance are commonly associated with obesity and type II diabetes. Moreover, DR has been associated with improved glucose homeostasis in mice (Matyi et al., 2018) and humans (Fontana et al., 2010). Thus, we performed glucose tolerance tests, to investigate the clearance of blood glucose levels after intraperitoneal glucose injection in chronic controls and DR switch groups. We first tested chronic controls at 5M and 10M of age, to evaluate glucose clearance at young age and after short-term, chronic DR.

As expected, animals on chronic DR displayed increased glucose tolerance compared to chronic AL animals after eight weeks (Fig. 3.2.12A) or seven months of DR (Fig. 3.2.12B), demonstrating that DR increased glucose sensitivity even after short-term treatment. Moreover, chronic DR maintained the significantly improved glucose tolerance even at 26M compared to chronic AL (Fig. 3.2.12F), demonstrating DR even improved glucose metabolism

during ageing. Thus, we next asked whether mid-or late-life initiated DR improved glucose tolerance after short-term or long-term intervention in our DR switch groups. Most strikingly, within six weeks post-switch to DR, restricted animals cleared out injected glucose faster compared to chronic AL animals and irrespective of age of DR onset (Fig. 3.2.12C-F). Moreover, long-term follow-up of AL_DR12M, AL_DR16M and AL_DR20M for up to fourteen, ten or eight months, respectively, after DR was initiated revealed that improved glucose tolerance was maintained during ageing for all DR switch groups (Fig. 3.2.12D-F). Remarkably, in the long -term glucose tolerance was even further improved in AL_DR12M and AL_DR16M compared to chronic DR feeding (Fig. 3.2.12E and F). Interestingly, baseline fasting glucose levels were not significantly different irrespective of age or diet (Fig. 3.2.12A-F).

We next assessed longitudinal changes in glucose tolerance using AUC and GLME analysis. Interestingly, glucose tolerance of chronic AL seemed to improve at old age, which correlated with the body weight loss at 26M and could be due to increased tumour numbers, which took up injected glucose (Fig. 3.2.12G). As expected, glucose tolerance was significantly improved in chronic DR over all six evaluated time points and did not exhibit age-related changes (Fig. 3.2.12G). In contrast, AL_DR12M, AL_DR16M and AL_DR20M exhibited increased glucose tolerance correlating with longer duration of DR (Fig. 3.2.12G). However, upon longer DR duration, glucose tolerance improves and clearance occurs even faster compared to chronic DR in mid-life switches once the adaptation period is completed (Fig. 3.2.12G). These results indicate that the adipose tissue, muscle, liver and brain of DR switches took up the injected glucose faster than chronic DR. However, we are currently still trying to understand what mediates this increased glucose uptake in DR switch groups. As AL_DR24M mice were only tested once, no longitudinal analysis could be conducted.

To conclude, glucose metabolism acutely responds to newly imposed DR and reacts with improved glucose sensitivity as early as six weeks post-switch irrespective of the age of initiation of DR. Additionally, DR can fully reverse the detrimental effects of long-term AL feeding and obesity on glucose metabolism and even maintain the beneficial effects of DR during ageing.

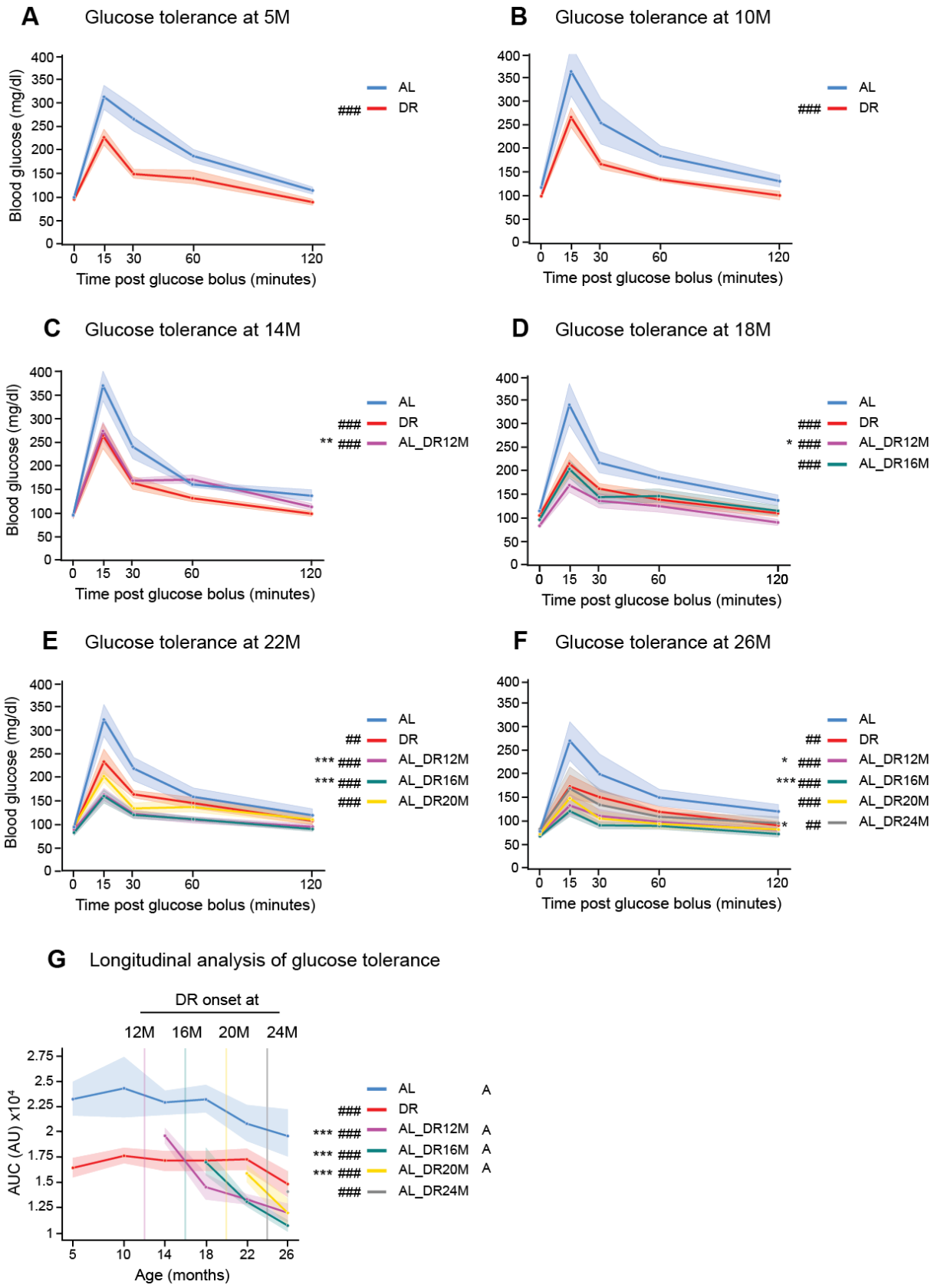

Figure 3.2. 12: DR improves glucose tolerance as early as six weeks post-switch independent of the age of DR onset and maintains it during ageing

Glucose tolerance tests after 16h fasting and injection of 2g glucose per kg body weight in chronic AL and DR at ***A)*** *5M (AL n= 15, DR n= 15) or* ***B)*** *10M (AL n= 15, DR n= 15) of age. Chronic DR increased*

*glucose tolerance compared to chronic AL. Assessment of glucose tolerance of chronic controls and DR switch groups at **C)** 14M (AL n= 15, DR n= 15, AL_DR12M n= 14), **D)** 18M (AL n= 15, DR n= 15, AL_DR12M n= 13, AL_DR16M n= 15), **E)** 22M (AL n= 13, DR n= 15, AL_DR12M n= 13, AL_DR16M n= 15, AL_DR20M n= 12) or **F)** 26M of age (AL n= 9, DR n= 13, AL_DR12M n= 11, AL_DR16M n= 13, AL_DR20M n= 11, AL_DR24M n=10). DR irrespective of the DR onset improved glucose tolerance within six weeks after the respective DR switch. Area under the curve (AUC) analyses and One-way ANOVA followed by Bonferroni correction were used for three-way comparisons between chronic controls and one DR switch at a time at each time point. Differences in AUC between chronic AL or DR were calculated using unpaired t tests at each time point. **G** Longitudinal analysis of glucose tolerance over the six phenotyping time points. GLME followed by Bonferroni corrections were implemented to assess glucose tolerance longitudinally. All data are presented as points with the mean and the 95% CI as shaded areas. Coloured lines in **G** indicate the DR switch time points. Statistical differences compared to chronic DR are indicated with p-values * p<0.05 and *** p<0.001. Statistical differences in relation to AL are presented as following # p<0.05, ## p< 0.01 and ### p<0.001. The letter A behind the diet switch indicates significant differences in GLME between time points. Carolina Monzó conducted the GLME analyses and generated the plots.*

3.2.13 Early- or mid-life onset DR improves short-term insulin sensitivity but only initiation of DR at 3M or 12M of age retains insulin sensitivity during ageing

Many obese individuals exhibit decreased insulin sensitivity and are at an increased risk to develop type II diabetes (Kahn et al., 2006). As all DR switch mice were obese prior the DR treatment, we conducted insulin tolerance tests to evaluate the organismal response towards intraperitoneal insulin injection in chronic controls and DR switch groups. We first tested chronic controls at 5M and 10M of age, to evaluate insulin sensitivity at young age and after short-term, chronic DR. Unexpectedly, chronic DR mice seemed completely insulin insensitive at 5M of age, as insulin injection did not lead to a significant decrease of blood glucose levels in contrast to chronic AL feeding (Fig. 3.2.13A). However, DR animals were provided with 50% of their daily portion directly prior to the test to avoid insulin injection into overnight- starved mice. Thus, the observed insulin insensitivity might be a feeding artefact. Due to the different feeding patterns of AL and DR mice, we adjusted the feeding time and provided DR mice with an additional 50% of their daily portion at 8pm, corresponding to the peak food intake of chronic AL (Fig. 3.2.14A-F), to adjust the metabolic states of the diet groups for all subsequent tests.

At 10 months of age, insulin injection did not decrease blood glucose levels of AL fed mice, suggesting that these mice were already insulin insensitive at this young age (Fig. 3.2.13B). In line with this observation, AL mice were also insulin insensitive at later ages (Fig. 3.2.13C-F).

In contrast, chronic DR animals displayed a gradual reduction of glucose levels after insulin injection, demonstrating that chronic DR treatment keeps animals in an insulin sensitive state during ageing (Fig. 3.2.13B-F). We next asked if DR can also improve insulin sensitivity upon mid-life or late-life treatment. Initiating DR at 12M did not show improved insulin tolerance at 14M, six weeks post-switch to DR compared to chronic AL or DR (Fig. 3.2.13C). Interestingly both AL_DR12M and AL_DR16M mice exhibited a significantly improved insulin sensitivity at 18M compared to AL mice (Fig. 3.2.13D), suggesting that DR required time to reverse diet-induced insulin insensitivity. However, both mid-life DR switches were still less insulin sensitive compared to chronic DR at 18M, indicating that the detrimental effects of long-term AL feeding could not be completely abolished (Fig. 3.2.13D). Indeed, AL_DR20M (Fig. 3.2.13E and F) and AL_DR24M (Fig.3.2.13F) responded towards injected insulin with a drop in blood glucose levels but insulin sensitivity was not significantly improved compared to chronic AL. Remarkably, while AL_DR12M and AL_DR16M regained insulin sensitivity at 18M, both DR switches lost their ability to respond to the insulin bolus during ageing (Fig. 3.2.13E and F), suggesting that mid-life DR only has a short-term beneficial effect on insulin response or our analyses were not powerful enough to detect moderate effects on insulin sensitivity. Strikingly, chronic DR and AL_DR12M animals were more insulin sensitive compared to chronic AL (Fig. 3.2.13F), demonstrating that 3M and 12M onset of DR retained insulin sensitivity during ageing. Interestingly, no differences in insulin sensitivity were observed between chronic DR and the DR switch groups at 26M (Fig. 3.2.13F), which suggests that even chronic DR cannot stop the decline of insulin sensitivity at old age. Lastly, we assessed longitudinal changes in insulin tolerance using AUC and GLME analysis. As we changed the feeding regimen after the 5M time point, we assessed differences in insulin sensitivity between 10M and 26M of age. Chronic AL were already completely insulin insensitive at 10 months of age and this phenotype did not change with advanced age (Fig. 3.2.13G). In contrast, chronic DR retained insulin sensitivity during ageing and even DR onset at 12M of age exhibited a long-term significant improvement, compared to chronic AL (Fig. 3.2.13G). Interestingly, DR onset at 16M, 20M and 24M did not improve insulin sensitivity compared to chronic AL feeding on the long term but we identified a non-significant trend towards improved insulin sensitivity post-switch to DR (Fig. 3.2.13G). These results suggest that even late-onset DR can still mediate beneficial effects on insulin sensitivity in an otherwise insulin insensitive strain. However, the insulin sensitivity of mid- or late-life DR switches did not catch up to chronic DR animals throughout the study (Fig. 3.2.13G), indicating that AL feeding for 12M already had a detrimental effect on insulin sensitivity, which could be improved but not be completely reversed by DR. As AL_DR24M mice were only measured at one time point, no longitudinal assessment could be performed.

To conclude, in contrast to glucose sensitivity, which was restored after six weeks of DR, insulin sensitivity only showed a short-term improvement in AL_DR16M and long-term

improvement only in chronic DR or AL_DR12M. Moreover, insulin sensitivity was never restored back to chronic DR levels (Fig. 3.2.13G), suggesting that DR can only implement some beneficial effects but not fully reverse already occurred insulin insensitivity of previous AL feeding. Additionally, insulin sensitivity does not seem to be a requirement for lifespan extension, as AL_DR16M remained insulin insensitive at old age but animals were similarly long-lived as insulin sensitive AL_DR12M animals. However, it is possible that the short-term improvement in insulin sensitivity in AL_DR16M mice was already enough to mediate beneficial effects on lifespan. In contrast, AL_DR20M and AL_DR24M did not display a short-term improvement compared to AL feeding, which might explain the lack of lifespan extension under late-onset DR.

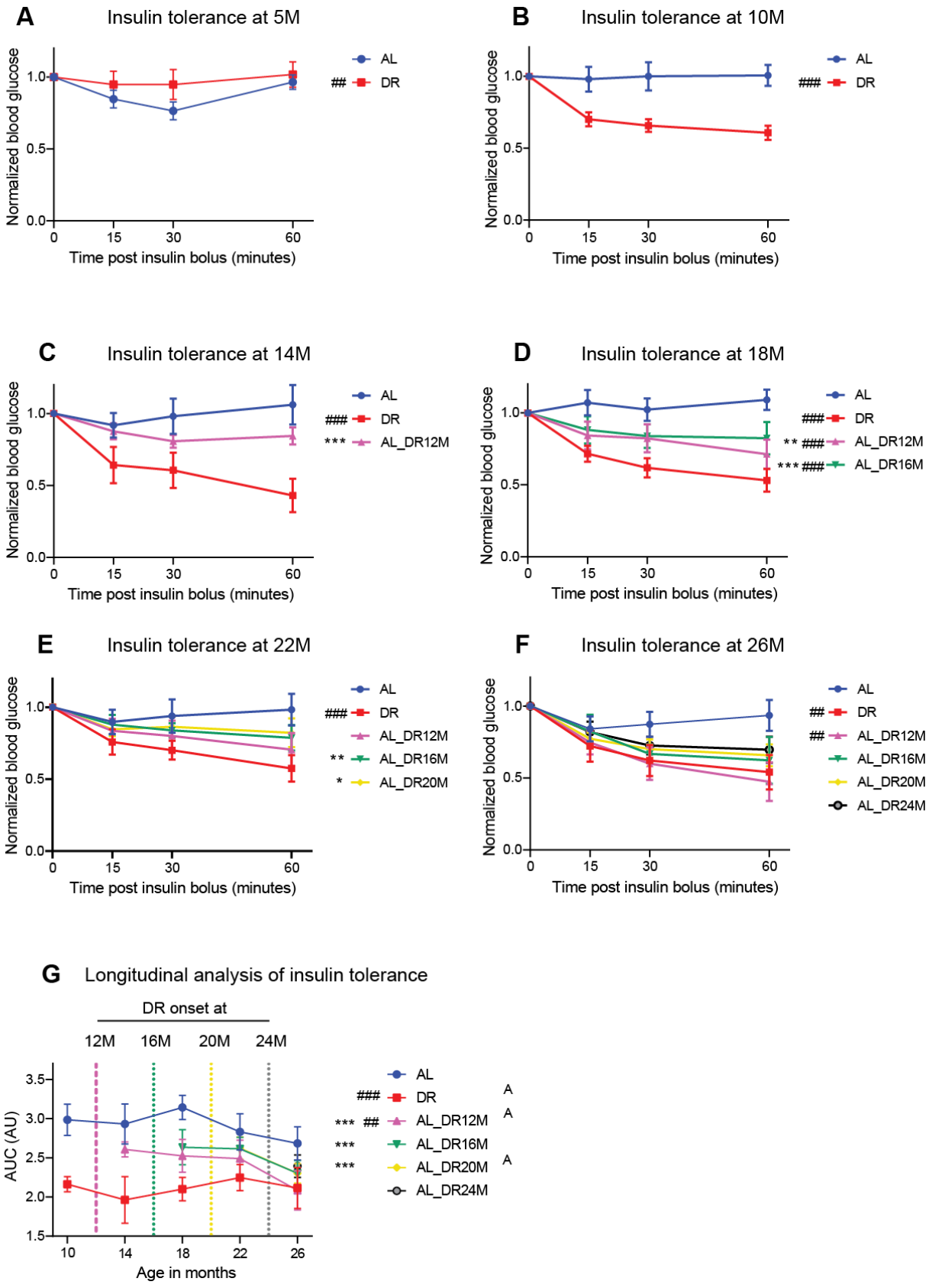

Figure 3.2. 13: Chronic or 12M onset DR retains insulin sensitivity during ageing and reverses the effects of early-life obesity

*Assessing insulin sensitivity after injection of 0.75 Units insulin per kg body weight in chronic AL and DR at **A)** 5M (AL n= 15, DR n= 15) or **B)** 10M (AL n= 15, DR n= 15) of age. Chronic DR increased insulin tolerance compared to chronic AL at 10M. Insulin tolerance of chronic controls and DR switch groups at **C)** 14M (AL n= 15, DR n= 15, AL_DR12M n= 14), **D)** 18M (AL n= 15, DR n= 15, AL_DR12M n= 13, AL_DR16M n= 15), **E)** 22M (AL n= 13, DR n= 15, AL_DR12M n= 13, AL_DR16M n= 15, AL_DR20M n= 12) or **F)** 26M of age (AL n= 8, DR n= 14, AL_DR12M n= 11, AL_DR16M n= 13, AL_DR20M n= 11, AL_DR24M n=10). DR onset at 12M or 16M increased insulin tolerance after six weeks or six months post-switch to DR but but the beneficial effect is lost during ageing. Area under the curve (AUC) analyses and One-way ANOVA followed by Bonferroni correction were used for three-way comparisons between chronic controls and one DR switch at a time at each time point. Differences in AUC between chronic AL or DR were calculated using unpaired t tests at each time point. **G)** Longitudinal analyses of insulin sensitivity of AL, DR and DR switch groups across from 10M of age until 26M of age. The 5M time point was excluded from the analyses due to changes in the DR regimen. GLME followed by Bonferroni correction were used to assess the longitudinal effect of DR on the incremental AUC of insulin sensitivity respectively. Chronic DR and AL_DR12M retain insulin sensitivity during ageing, whereas DR onset at 16M, 20M and 24M did not improve insulin sensitivity compared to chronic AL feeding. Throughout the study, chronic DR animals were more insulin sensitive than the mid- or late-life DR switches. Data are presented as points with the mean and the 95% CI as error bars. Coloured lines in **G** represent the respective switch to DR. Statistical differences compared to chronic DR are indicated with p-values * p<0.05, *** and p<0.001. Statistical differences in relation to AL are presented as following # p<0.05, ## p< 0.01 and ### p<0.001. The letter A indicates significant differences within the same diet group over time. Carolina Monzó conducted the GLME analyses.*

3.2.14 DR alters the timing of the food intake irrespective of the age of DR onset

It has been previously established that chronic DR can change the circadian rhythm from a nocturnal to a diurnal patter, which is associated with the time when the daily food portions are provided (Challet, 2010; Hambly et al., 2007). However, it is currently unknown how mid- or late-onset of DR affects the food or water intake. To this end, we first investigated the timing of the food and water intake in single-housed C3B6F1 females on chronic AL, DR or mid- and late-onset DR.

Chronic AL animals consumed significantly more food compared to chronic, mid- or late-onset DR animals, whereas the food intake was similar between DR groups (Fig. 3.2.14A-F). In accordance with previous DR studies (Hambly et al., 2007), chronic DR animals exhibited a peak in the daily food intake, which correlated with the time when the food was provided in the morning (Fig. 3.2.14A). Moreover, DR animals immediately devoured the entire food portion, followed by an almost 22h long fasting period, which lasted until the next day when the daily

portion was provided. Interestingly, this feeding pattern was established already after two months on DR at 5M (Fig. 3.2.14A) and was maintained after longer DR duration at 10M (Fig. 3.2.14B). In contrast, AL animals fed almost exclusively during the night, which was expected from nocturnal animals (Fig. 3.2.14A). Furthermore, the food intake of chronic AL mice was spread out throughout the entire night and only displayed a small peak around approx. 9pm, which was in stark contrast to the distinct peak of chronic DR animals (Fig. 3.2.14 A and B). Strikingly, AL_DR12M, AL_DR16M and AL_DR20M mice immediately adapt to this feeding pattern within six weeks post-switch to DR (Fig. 3.2.14C-E). In contrast, AL_DR24M mice also adapted to the feeding time in the morning but they started eating later compared to earlier DR switch groups once the food was provided (Fig. 3.2.14F). Additionally, the peak food intake was not as high compare to the other switches and the food intake was more spread out in AL_DR24M (Fig. 3.2.14F). In contrast to the other diet groups, AL_DR24M were tested for the first time at 26M of age. Therefore, animals from the other diet groups had been exposed to the phenomaster system at least once before. It is possible that AL_DR24M either did not adapt as fast to the new food provision system or that the spread- out feeding pattern was a remnant from previous AL –feeding. When evaluating the changes in the average daily food intake over the six phenotypings, chronic AL mice consumed more food at 26M of age compared to earlier time points (Fig. 3.2.14G). In contrast, the food intake of chronic DR and DR switch only slightly increased over time (Fig. 3.2.14G).

In summary, upon food provision, chronic DR and DR switch groups immediately devoured their daily food portion, followed by an almost 22h fasting period. This feeding pattern was established as early as six months post-switch to DR and was even present after long-term DR. Therefore, the distinct combination of food restriction and self-imposed time restricted feeding or intermittent fasting could be mediating some beneficial effects of DR on lifespan and health span.

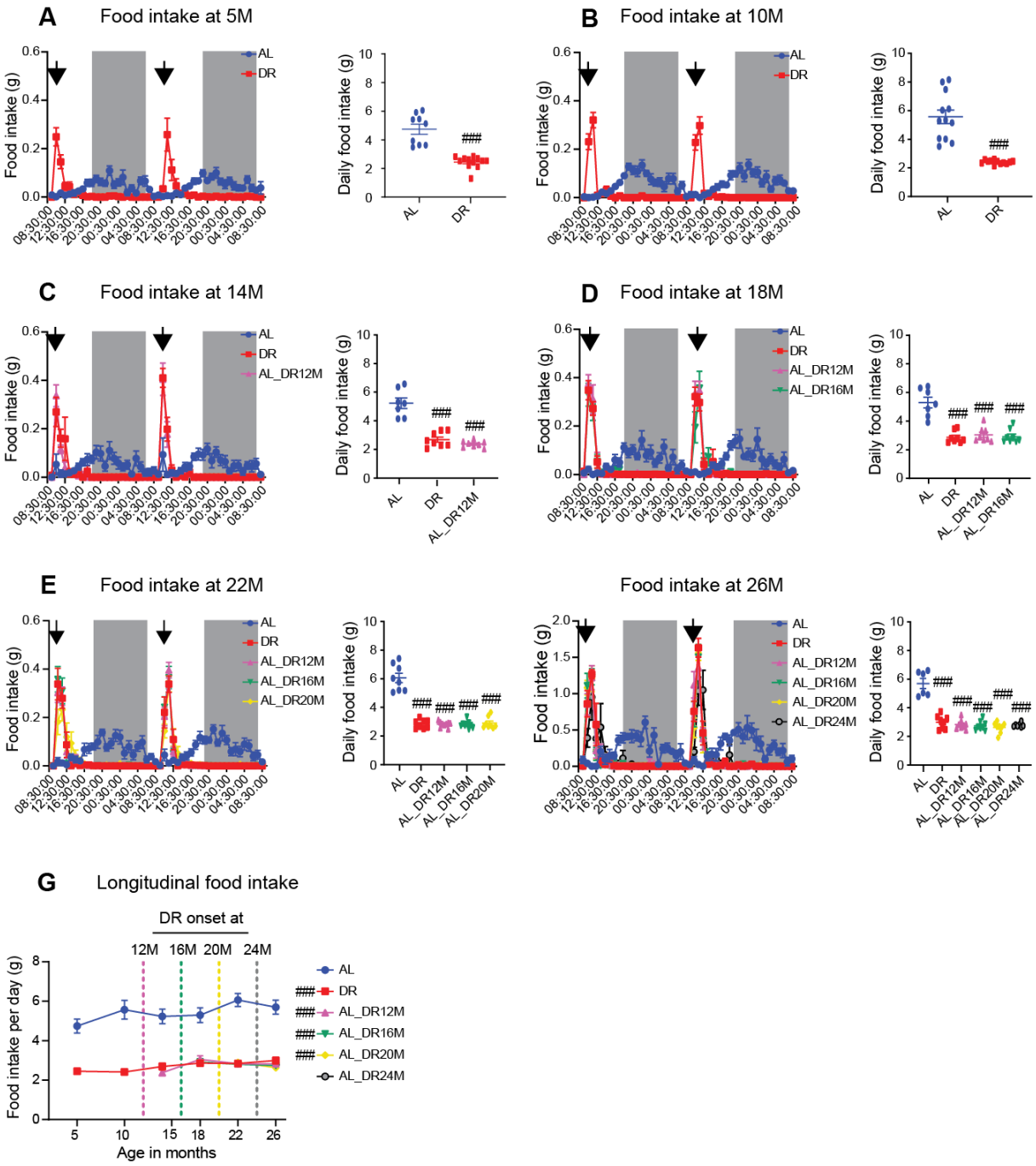

Figure 3.2. 14: DR alters the timing of food intake irrespective of the age of DR onset

*Food intake of single-housed chronic AL or DR animals in metabolic cages over 48h at **A)** 5M (AL n= 9, DR n= 11) or **B)** 10M (AL n= 11, DR n= 12) of age. Chronic DR increased altered the timing of food intake in response to the daily feeding in the morning. Food intake of chronic controls and DR switch groups in the metabolic cages at **C)** 14M (AL n= 7, DR n= 8, AL_DR12M n= 8), **D)** 18M (AL n= 7, DR n= 8, AL_DR12M n= 8, AL_DR16M n= 8), **E)** 22M (AL n= 8, DR n= 9, AL_DR12M n= 9, AL_DR16M n= 9, AL_DR20M n= 8) or **F)** 26M of age (AL n= 6, DR n= 8, AL_DR12M n= 8, AL_DR16M n= 8, AL_DR20M n=8, AL_DR24M n=7). DR irrespective of the age of onset altered the timing of food intake and linked it to the timing of the daily food provision. AL animals almost exclusively fed during the night. Unpaired t tests were implemented to evaluate statistical differences between chronic controls at all evaluated time*

points. One-way ANOVA followed by Bonferroni correction was performed to assess statistical differences in daily food intake between AL, DR and one DR switch group at a time at each time point. ***G*** *Longitudinal analyses of the daily food intake of AL and DR animals across all six evaluated time points was assessed using GLME and Bonferroni post-hoc tests. Animal numbers at the different time points varied between 12 or six animals per diet group. Grey rectangular areas indicate the 12h-long night phase starting at 6pm until 6am and black arrows the feeding time of DR animals between 10am and 10:30am. Data are presented as mean with the SEM and with p-values # p<0.05, ## p>0.01 and ### p<0.001 for comparisons to chronic AL. Carolina Monzó conducted the statistical analyses on the longitudinal food intake.*

3.2.15 The timing of the water intake corresponds to the food intake and is altered by DR irrespective of the age of DR onset

We next aimed to determine whether the water intake of chronic DR and DR switch animals would also exhibit a temporal shift compared to AL animals as the food intake. Intriguingly, the water intake of chronic or mid- and late-onset DR animals largely correlated with the food intake (Fig. 3.2.14A-F) and adapted within six weeks post-switch to DR (Fig. 3.2.15A-F). Upon food provision and during feeding, chronic DR and DR switch groups consumed more water and after the feeding was over, almost no water was consumed (Fig. 3.2.15A-F). Moreover, no significant difference in the water intake were detected between chronic DR and mid- or late-onset DR switches at all evaluated time points (Fig. 3.2.15A-F). Interestingly, the water intake of AL_DR24M mice also displayed the temporal shift but the water intake directly after the feeding was lower and more spread out compared to earlier DR switches (Fig. 3.2.15F) and the overall pattern closely resembled the food intake (Fig. 3.2.14F). Similar to the nocturnal food intake pattern (Fig. 3.2.14A-F), chronic AL animals almost exclusively drank during the night, which was retained during ageing (Fig. 3.2.15A-F). Strikingly, chronic AL consumed significantly more water compared to chronic DR at 5M of age (Fig. 3.2.15A), which could be correlated a smaller portion of food consumed by DR animals. Furthermore, AL mice drank significantly more water compared to all DR groups at 22M of age (Fig. 3.2.15E). However, as four out of eight AL mice had a higher water intake compared to the remaining AL animals (Fig. 3.2.15E), the difference in water intake at 22M of age could be attributed to inter-cage differences (Nicolaus et al., 2016). Longitudinal analyses revealed that the water intake of chronic AL and DR animals was not significantly different during ageing (Fig. 3.2.15G). Interestingly, AL_DR16M animals decreased their water consumption during ageing, whereas AL_DR20M animals increased their water intake across time points, at which they differed from AL or DR animals (Fig. 3.2.15G).

In summary, the water intake of single-housed chronic DR animals displayed a similar temporal shift as the food intake and DR switch animals adapted towards the new pattern shortly after DR was initiated.

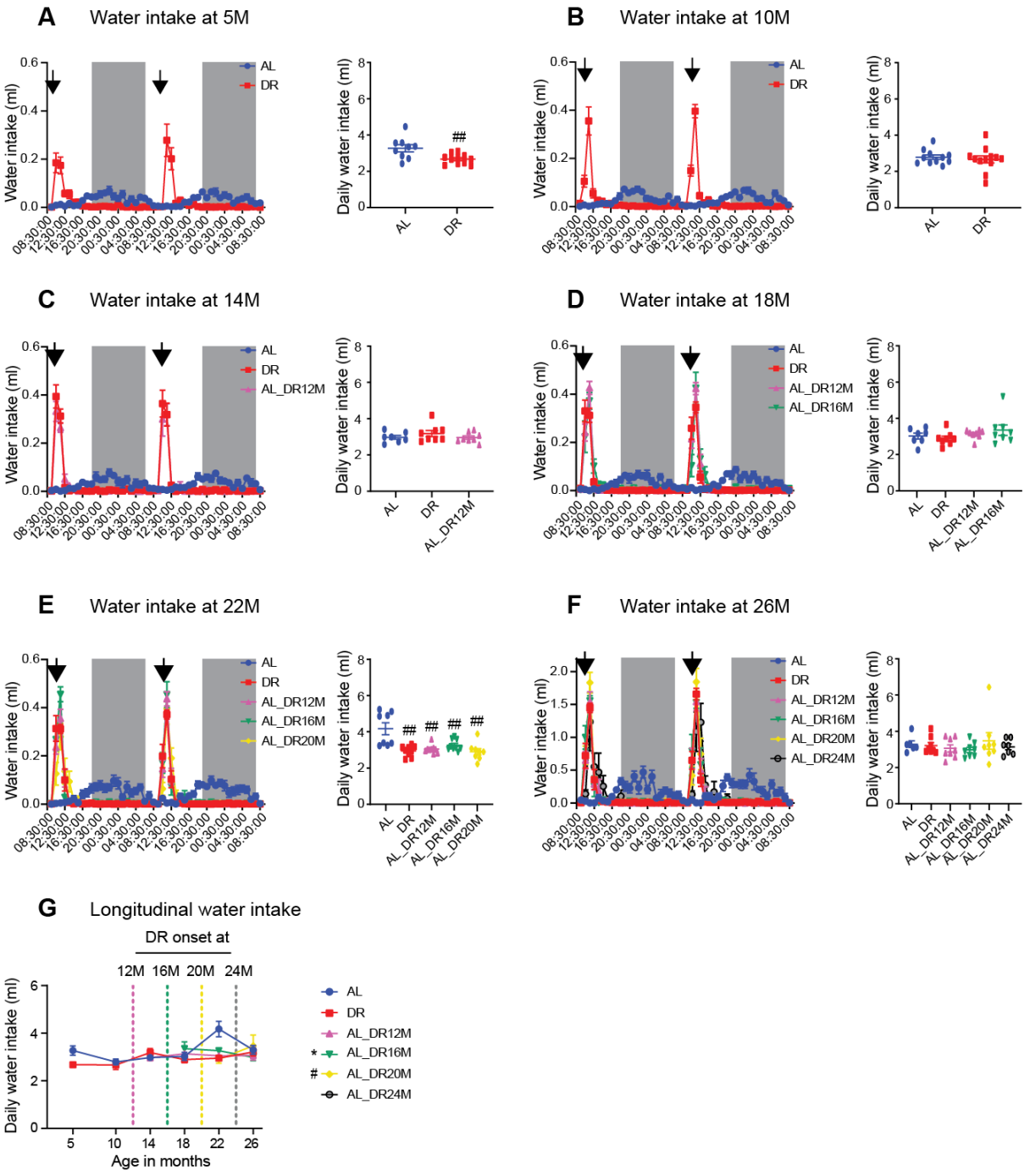

Figure 3.2. 15: The timing of the water intake corresponds to the food intake and is altered by DR irrespective of the age of DR onset

*Water intake of single-housed chronic AL or DR animals in metabolic cages over 48h at **A)** 5M (AL n= 9, DR n= 12) or **B)** 10M (AL n= 11, DR n= 12) of age. The water intake of DR animals was limited to the feeding time and occurred almost exclusively in the morning. Water intake of chronic controls and DR*

*switch groups in the metabolic cages at **C)** 14M (AL n= 7, DR n= 8, AL_DR12M n= 8), **D)** 18M (AL n= 7, DR n= 8, AL_DR12M n= 8, AL_DR16M n= 8), **E)** 22M (AL n= 8, DR n= 9, AL_DR12M n= 9, AL_DR16M n= 9, AL_DR20M n= 8) or **F)** 26M of age (AL n= 6, DR n= 8, AL_DR12M n= 8, AL_DR16M n= 8, AL_DR20M n=8, AL_DR24M n=7). DR irrespective of the age of onset altered the timing of water intake and linked it to the feeding time. The water intake of AL animals occurred almost exclusively during the night. Unpaired t tests were implemented to evaluate statistical differences between chronic controls at all evaluated time points. One-way ANOVA followed by Bonferroni correction was performed to assess statistical differences in daily water intake between AL, DR and one DR switch group at a time at each time point. **G** Longitudinal analyses of the daily water intake of AL and DR animals across all six evaluated time points was assessed using GLME and Bonferroni post-hoc tests. Animal numbers at the different time points varied between 12 or six animals per diet group. Grey rectangular areas indicate the 12h-long night phase starting at 6pm until 6am and black arrows the feeding time of DR animals between 10am and 10:30am. Data are presented as mean with the SEM and with p-values # p<0.05, ## p>0.01 and ### p<0.001 indicating significant differences in relation to chronic AL. Carolina Monzó conducted the statistical analyses on the longitudinal water intake.*

3.2.16 DR alters the timing and macronutrient usage as fuel source of the metabolism irrespective of the age of DR onset

We previously showed that the expression of key lipogenesis genes is increased in the WAT of chronic DR but not in the WAT of late-life onset DR and chronic AL mice (Fig. 3.1.1). Moreover, we found that the timing of the food (Fig. 3.2.14A-F) and water intake (Fig. 3.2.15A-F) shifted in response to early or late-onset DR and correlated with the feeding time of DR animals. To this end, we asked whether the metabolism would also exhibit a temporal shift between chronic AL and DR switch groups. Therefore, we investigated the energy expenditure profiles of chronic controls and DR switch groups in more detail, using the respiratory exchange ratio (RER) as a proxy to determine the effect of DR on utilization of different macronutrients, based on oxygen intake and carbon dioxide exhalation (Schmidt-Nielsen, 1997). A RER of 1.0 indicates carbohydrates are used as main energy source, whereas fatty acid oxidation is the main energy source at an RER of 0.7 (Bruss et al., 2010). Values in between 0.7 and 1 point to a mixture of macromolecules as fuel source.

As expected, we observed a temporal shift in the RER between AL and restricted animals (Fig. 3.2.16A-F), which correlated with the time of food and water intake of DR and AL animals (Fig.3.2.14A-F, Fig. 15A-F), indicating that DR changed the circadian rhythm from a nocturnal to diurnal pattern. Moreover, DR switches also exhibited this change in circadian rhythm in accordance in food intake irrespective of the onset of DR. Interestingly, we observed significant differences in the RER amplitude between chronic AL and DR mice already at young age when

DR was initiated for eight weeks (Fig. 3.2.16A) or seven months (Fig. 3.2.16B). Chronic AL animals almost exclusively fed during the night (Fig. 3.2.14A-F), during which they utilized carbohydrates as energy source and shifted to fatty acids and proteins during the day (Fig.3.2.16A and B). In contrast, chronic DR animals utilized carbohydrates during the day and relied on a mixed fuel source consisting of fatty acids and proteins during the night. However most strikingly, the RER amplitude of chronic DR animals exceeded 1.0, which suggests immediate carbohydrate oxidation to synthesize fatty acids upon feeding (Fig. 3.2.16A and B). Furthermore, this distinct macronutrient utilization of the metabolism of chronic DR mice was maintained during ageing and did not exhibit any age-related changes (Fig. 3.2.16A-F). Thus, we next aimed to test whether the RER of DR switch groups could adapt to the chronic DR RER phenotype. Six weeks after DR was initiated at 14M, 18M, 22M or 26M respectively, AL_DR12M (Fig. 3.2.16C), AL_DR16M (Fig. 3.2.16D), AL_DR20M (Fig. 3.2.16E) or AL_DR24M (Fig. 3.2.16F) exhibited the temporal change in RER timing but the amplitude was significantly lower compared to the chronic DR. However, within the next phenotyping time point, both mid-life DR onset and AL_DR20M showed a similarly high RER amplitude compared to chronic DR (Fig. 3.2.16D-F). We therefore asked if the RER amplitude required a longer time to adjust to the DR regimen. To this end, we implemented GLME analysis on the peak maximum RER activity and followed the DR switch groups over time. Indeed, for the 12M, 16M and 20M DR switches we observed similarly lower RER amplitudes as AL_DR24M six weeks post-switch to DR, however all switch groups caught up to chronic DR levels within six months after DR was initiated (Fig. 3.2.16G). Therefore, we might have observed a similar complete adaptation the RER of AL_DR24M, if we had tested the animals a second time after a longer DR duration.

To conclude, we showed for the first time, that even late-life initiation of DR at 24M can induce a systemic shift in macronutrient utilization towards glycolysis combined with fatty acid synthesis within six weeks post-switch to DR. However, the metabolism requires time to fully adapt to the DR regimen and reached chronic DR levels within six months after DR was initiated.

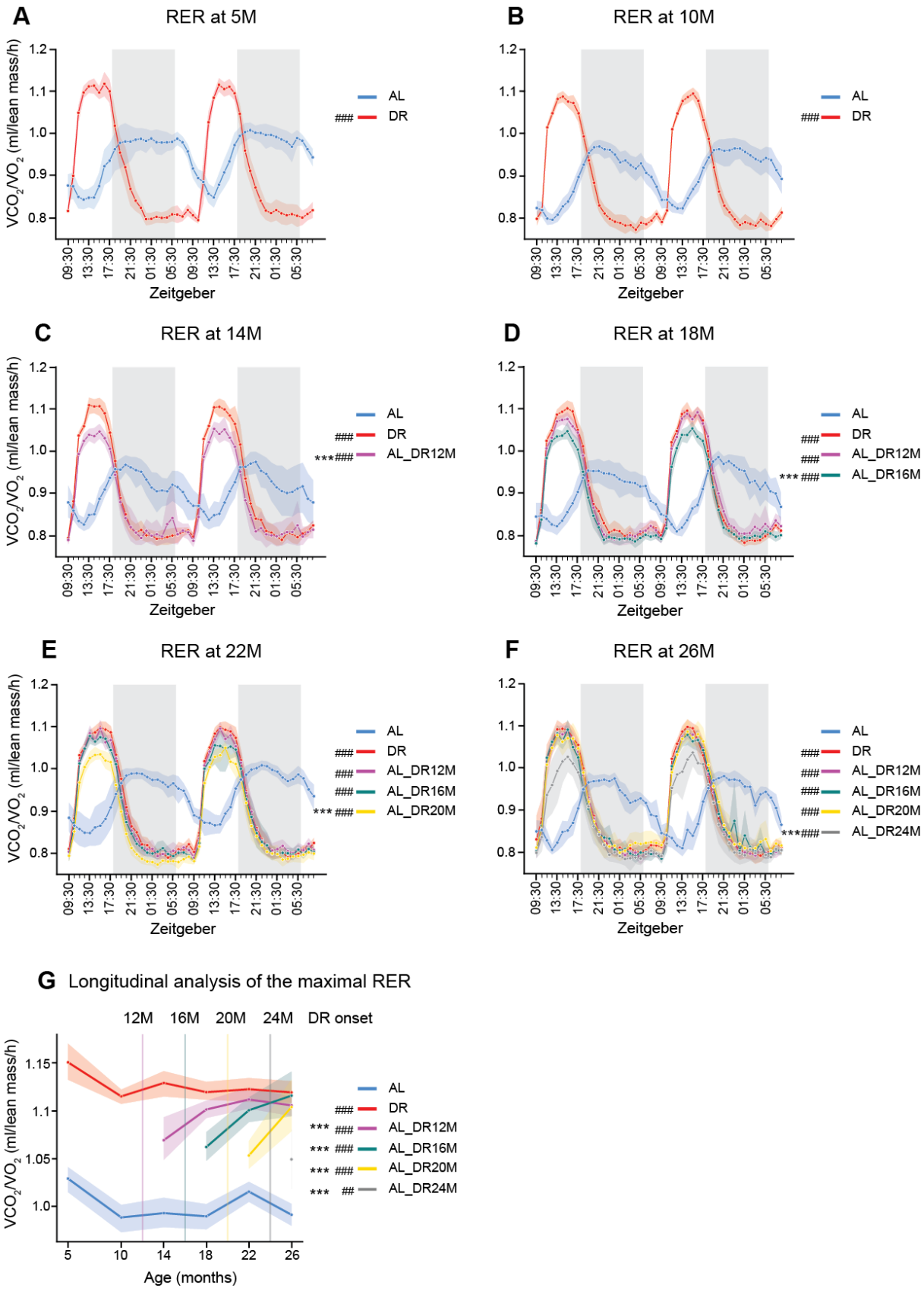

Figure 3.2. 16: DR alters the timing and macronutrient usage irrespective of the age of DR onset

The respiratory exchange ratio (RER) activity of single-housed chronic AL or DR animals in metabolic cages over 48h at ***A)*** *5M (AL n= 9, DR n= 11) or* ***B)*** *10M (AL n= 11, DR n= 12) of age. Chronic DR*

*altered the timing and utilization of macronutrients. RER of chronic controls and DR switch groups in metabolic cages at **C)** 14M (AL n= 7, DR n= 8, AL_DR12M n= 8), **D)** 18M (AL n= 7, DR n= 8, AL_DR12M n= 8, AL_DR16M n= 8), **E)** 22M (AL n= 8, DR n= 9, AL_DR12M n= 9, AL_DR16M n= 9, AL_DR20M n= 8) or **F)** 26M of age (AL n= 6, DR n= 8, AL_DR12M n= 8, AL_DR16M n= 8, AL_DR20M n=8, AL_DR24M n=7). DR irrespective of the age of DR onset significantly altered the timing and utilization of macronutrients. One-way ANOVA were performed to assess statistical differences in peak RER activity between chronic controls and DR switch groups. **G** Longitudinal analyses of the maximum RER peak of AL and DR animals across all six evaluated time points was assessed using GLME and Bonferroni post-hoc tests. Animal numbers at the different time points varied between 12 or six animals per diet group. **H** Effect of AL or DR feeding regimen on the respiratory exchange ratio (RER) in a randomly selected subset of 26M old chronic AL (n=6), DR (n=8), AL_DR12M (n=8), AL_DR16M (n=8), AL_DR20M (n=8) or AL_DR24M (n=7) animals over 48h. Grey rectangular areas indicate the 12h-long night phase starting at 6pm until 6am and black arrows the feeding time of DR animals between 10am and 10:30am. Data are presented as mean ± 95% CI and with p-values * p<0.05, ** p<0.01 and *** p<0.001 for comparisons to chronic DR. P-values # p<0.05, ## p>0.01 and ### p<0.001 indicate significant differences in relation to chronic AL. Statistical analyses were conducted and plots were generated by Carolina Monzó.*

3.2.17 Early and mid-onset DR increases spontaneous home cage activity in single-housed mice

As mentioned before, daytime feeding and DR alter the sleep-wake cycle and animals shift their circadian rhythm from a nocturnal to a diurnal pattern (Challet, 2010). Moreover, it was previously suggested that DR increased spontaneous home cage activity (Abe et al.,1989; Mendoza et al., 2008). Therefore, we investigated the daily activity pattern of single-housed chronic controls and DR switch animals during ageing focussing on the overall activity pattern or analysing the active and inactive phase. In order to group the activity into the active or inactive phase, we selected a cut-off of 300 beam breaks per hour, when AL and DR animals showed reduced activity. Activity over 300 beam breaks per hour was considered as active, whereas fewer activities than 300 beam breaks per hour were considered inactive.

In accordance with previous studies (Mendoza et al., 2008), DR animals displayed increased activity during the day and reduced activity during the night, correlating with a change in the circadian rhythm from a nocturnal to a diurnal pattern (Fig. 3.2.17A-F). However, chronic DR animals only acquired this pattern after longer DR duration. At 5M (Fig. 3.2.17A) or 10M of age (Fig. 3.2.17B), chronic DR animals only displayed increased activity in the morning when the food was provided and the activity peaked again shortly after the lights went out after 6pm when. In contrast, chronic AL animals displayed an almost exclusive activity pattern during the night and rested during the day (Fig. 3.2.17A and B). When comparing the active and the

inactive phase, we did not detect any differences between chronic AL and DR animals at 5M (Fig. 3.2.17A) or 10M of age (Fig. 3.2.17B), which correlated with the overall activity pattern at both time points. Strikingly, DR switch groups immediately adapted to the DR-specific activity pattern within six weeks post-switch to DR, which peaked around the time the daily food potion was provided between 10am and 10:30 am and shortly before and after the lights turned off at 6pm (Fig. 3.2.17C-F). However, the peak activity at the time of feeding seemed lower six weeks post-switch to DR (Fig. 3.2.17C-F) and only caught up to chronic DR upon longer DR treatment (Fig. 3.2.17D-F). Interestingly, we detected differences in the activity phases in the DR switch groups. At 14M, chronic DR animals were significantly more active in the active phase and AL_DR12M displayed a trend towards higher activity compared to AL mice (Fig. 3.2.17C). Similarly, AL_DR16M mice were significantly less active than chronic DR animals six weeks post-switch to DR (Fig. 3.2.17D). In contrast, AL_DR20M and AL_DR24M activity in the active phase was significantly lower compared to chronic DR animals within six weeks (Fig. 3.2.17E and F) or six months (Fig. 3.2.17F) post-switch to DR, suggesting that late-onset DR could not recover spontaneous activity after long-term AL feeding. Intriguingly, the activity in the inactive phase was lower in chronic DR, AL_DR12M and AL_DR16M at 14M (Fig. 3.2.17C) and 18M (Fig. 3.2.17D) as well as in AL_DR16M at 22M (Fig. 3.2.17E) and chronic DR, AL_DR16M and AL_DR20M at 26M of age (Fig. 3.2.17F). Longitudinal analyses revealed significantly increased activity in the active phase of DR, AL_DR12M and AL_DR16M compared to chronic AL (Fig. 3.2.17G). In contrast, AL_DR20M animals were not significantly more active at 22M and 26M compared to AL and significantly less active than DR animals (Fig. 3.2.17G), suggesting that early and mid-life but not late-onset DR prevents age-related decline in locomotor activity. Intriguingly, the longitudinal activity in the inactive phase was significantly lower in DR, AL_DR12M, AL_DR16M and AL_DR20M compared to AL mice (Fig. 3.2.17H), indicating that DR could potentially improve the resting phase and increase sleep quality during ageing. Intriguingly, AL_DR16M animals were even more active in the active phase (Fig. 3.2.17G) and less active in the inactive phase (Fig. 3.2.17H) compared to DR animals.

Taken together, we demonstrated that DR onset as late as 24M of age decreased body weight and fat mass and improved glucose tolerance within six weeks after DR was initiated. In contrast, only chronic DR or AL_DR12M stably improved insulin sensitivity during ageing and reversed the detrimental effects of early life obesity on the insulin metabolism. Furthermore, providing the daily food portions in the morning correlated with food and water consumption in restricted animals and mediated a change in the circadian rhythm. Additionally, DR altered teh activity patterns and the usage of different macronutrients to fuel the metabolism depending on the time of day. Strikingly, insulin sensitivity was only mildly improved upon 16M, 20M and 24M DR onset, suggesting that prolonged AL feeding has detrimental effects on the metabolism that DR cannot improve in the long-term.

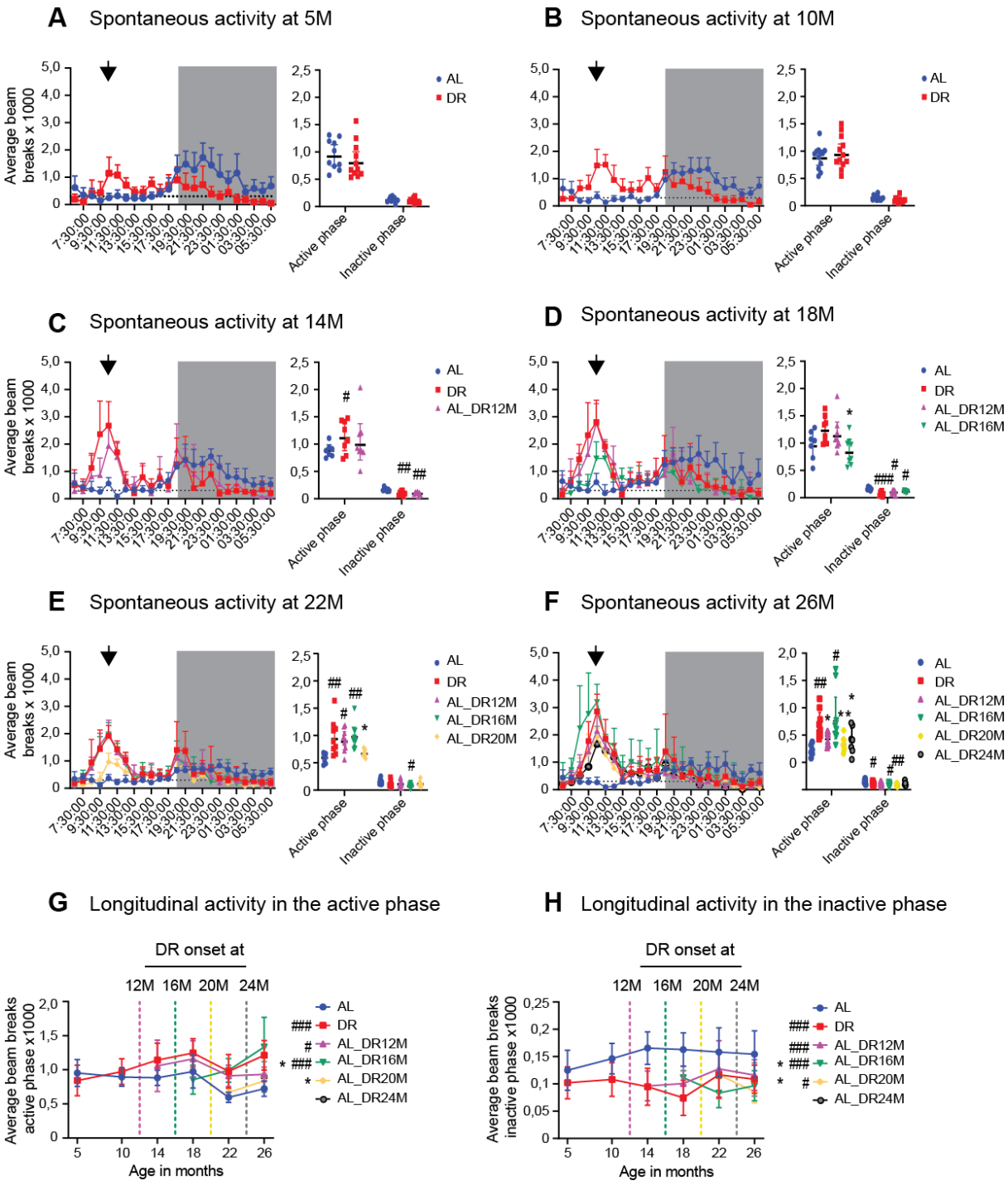

Figure 3.2. 17: Early and mid-onset DR increases spontaneous home cage activity in single-housed mice

*Spontaneous home cage activity of single-housed chronic AL or DR animals in metabolic cages over 24h at **A)** 5M (AL n= 9, DR n= 12) or **B)** 10M (AL n= 11, DR n= 12) of age. DR did not increase in-cage activity at young age. Spontaneous home cage activity of chronic controls and DR switch groups at **C)** 14M (AL n= 7, DR n= 8, AL_DR12M n= 8), **D)** 18M (AL n= 7, DR n= 8, AL_DR12M n= 8, AL_DR16M n= 8), **E)** 22M (AL n= 8, DR n= 9, AL_DR12M n= 9, AL_DR16M n= 9, AL_DR20M n= 8) or **F)** 26M of age (AL n= 6, DR n= 8, AL_DR12M n= 8, AL_DR16M n= 8, AL_DR20M n=8, AL_DR24M n=7). Chronic DR, AL_DR12M and AL_DR16M mice displayed increased spontaneous activity during ageing*

compared to chronic AL. Spontaneous activity did not increase following DR onset at 20M or 24M of age. Unpaired t tests were implemented to evaluate statistical differences between chronic controls at all time points. One-way ANOVA followed by Bonferroni correction was performed to assess statistical differences in daily food intake between AL, DR and one DR switch group at a time at each time point. Longitudinal analyses of the spontaneous activity in ***G)*** *the active phase of* ***H)*** *the inactive phase of AL and DR animals across all six evaluated time points was assessed using GLME followed by Bonferroni correction for multiple testing. Chronic DR, AL_DR12M and AL_DR16M were significantly more active in the active and significantly less active than AL animals in the active and inactive phase respectively. Grey rectangular areas indicate the 12h-long night phase starting at 6pm until 6am and black arrows the feeding time of DR animals between 10am and 10:30am. Dotted lines represent the cut-off at 300 beam breaks per hour. Data are presented as mean + 95% CI and with p-values * p<0.05, ** p<0.01 and *** p<0.001 for comparisons to chronic DR. P-values # p<0.05, ## p>0.01 and ### p<0.001 indicate significant differences in relation to chronic AL.*

3.2.18: Evaluating overall fitness and frailty in response to early, mid- or late-onset DR

Cardiovascular diseases are one of the main causes of death among the elderly (Roth et al., 2017) and many obese people have an increased risk to develop cardiovascular complications (Lavie et al., 2018), such as heart failure (Kenchaiah et al., 2002). Moreover, sarcopenia, as well as declined fitness, skeletal muscle function and memory are tightly associated with the ageing process (Correa-De-Araujo & Hadley, 2014; Yokota et al., 2000). Furthermore, increased fitness has been recently associated with increased cognitive performance (Segaert et al., 2018), thus demonstrating the importance of maintaining physical activity to increase health span at old age. Obesity can be caused by a sedentary lifestyle (Martínez-González et al., 1999) and especially mid-life obesity increases the risk of neurological diseases, such as dementia (Chuang et al., 2016). We therefore asked if DR applied mid or later in life would exhibit beneficial effects and improve overall fitness and memory function in mice and reverse putative negative impacts of obesity on health at old age. To this end, we used a second phenotyping cohort of mice, which were subjected to grip strength, motor coordination and memory tests (Fig. 3.2.18A). As experience, acquired by previous testings, could confound the results, all diet groups including future DR switches were tested at all time points starting from 5M of age (Fig. 3.2.18A). This procedure allowed comparisons of pre-to post-switch performance after mid-or late-life onset DR.

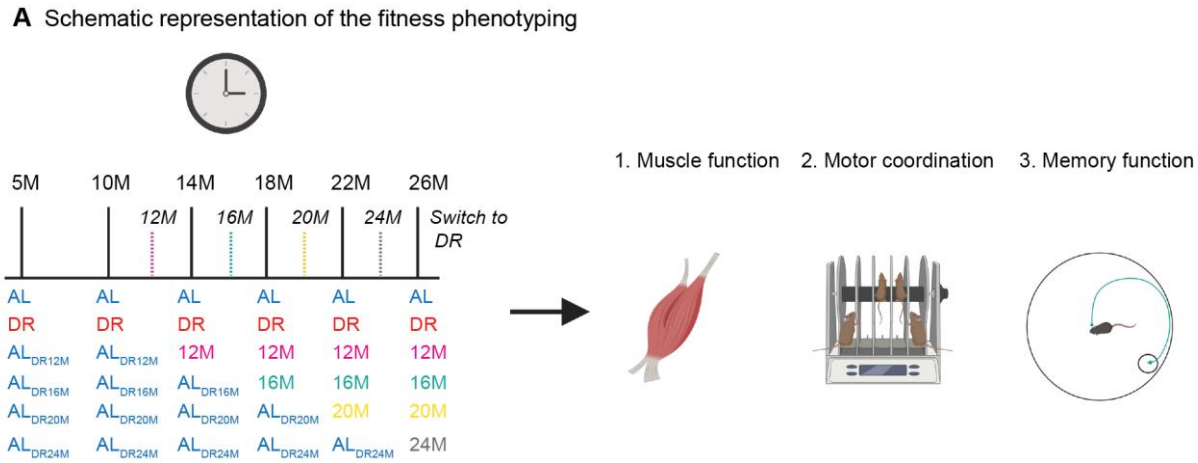

Figure 3.2. 18: Schematic representation of fitness phenotypings

A *Schematic representation of phenotyping for grip strength, motor coordination and memory function. DR switch animals are tested at all phenotyping time points to allow analysis of pre-versus post-switch performance. DR switch groups were first assessed eight weeks post-switch to DR.* AL_{12M}, AL_{16M}, AL_{20M} *or* AL_{24M} *describes mice belonging to the respective switch group, which were tested as AL animals prior to the initiation of DR. Dashed coloured lines mark the switch from AL to DR at the respective ages. The schematic was created using Biorender.com.*

3.2.19: Muscle strength is affected by ageing but not by DR

Two studies on moderate DR in humans showed reduced muscle strength in response to short-term or long-term DR for one or two years (Racette, 2015; Weiss et al., 2007). Thus, we first sought to determine if muscle strength was negatively impacted by short or long-term DR starting at young, middle old or old age by using a front paw grip strength meter. However, no significant difference was observed between chronic DR or AL at 5M (Fig. 3.2.19A) or 10M (Fig. 3.2.19B). Moreover, grip strength did not differ between chronic controls and DR switch groups at 14M (Fig. 3.2.19C), 18M (Fig. 3.2.19D), 22M (Fig. 3.2.19E) or 26M (Fig. 3.2.19F) of age, suggesting full-feeding or DR initiated chronically or late in life did not affect muscle strength. Furthermore, longitudinal analyses did not reveal any significant differences between diet groups (Fig. 3.2.19G). Interestingly, we observed reduced muscle strength during ageing for all diet groups (Fig. 3.2.11G), suggesting that ageing but not diet influenced muscle function. We therefore compared overall grip strength between two consecutive time points, to identify at which age muscle strength first showed age-related decline irrespective of the diet group. Interestingly, we detected first differences in muscle function between 10M and 14M of age, and muscle function decreased further during ageing (Fig.3.2.11H).

Lastly, we wanted to confirm the weight loss under DR in the new mouse cohort and measured body weight on the first day of each phenotyping time point. We could confirm that chronic AL

mice had significantly higher body weight compared to chronic DR and all DR switches in the new cohort (Fig.3.2.11D), reproducing our previous results. Interestingly, all DR switch groups required more time to reach the chronic DR state and AL_DR20M switches did not completely catch up to chronic DR even at 26M (Fig. 3.2.11D), probably as the animals had a higher body weight on AL feeding.

Thus, ageing but not DR or weight loss lead to muscle function decline starting between 10M and 14M of age. Additionally, prolonged DR did not further enhance or slow down this age-related functional decline in contrast to human DR studies, which reported that DR negatively affected muscle strength (Racette et al., 2017).

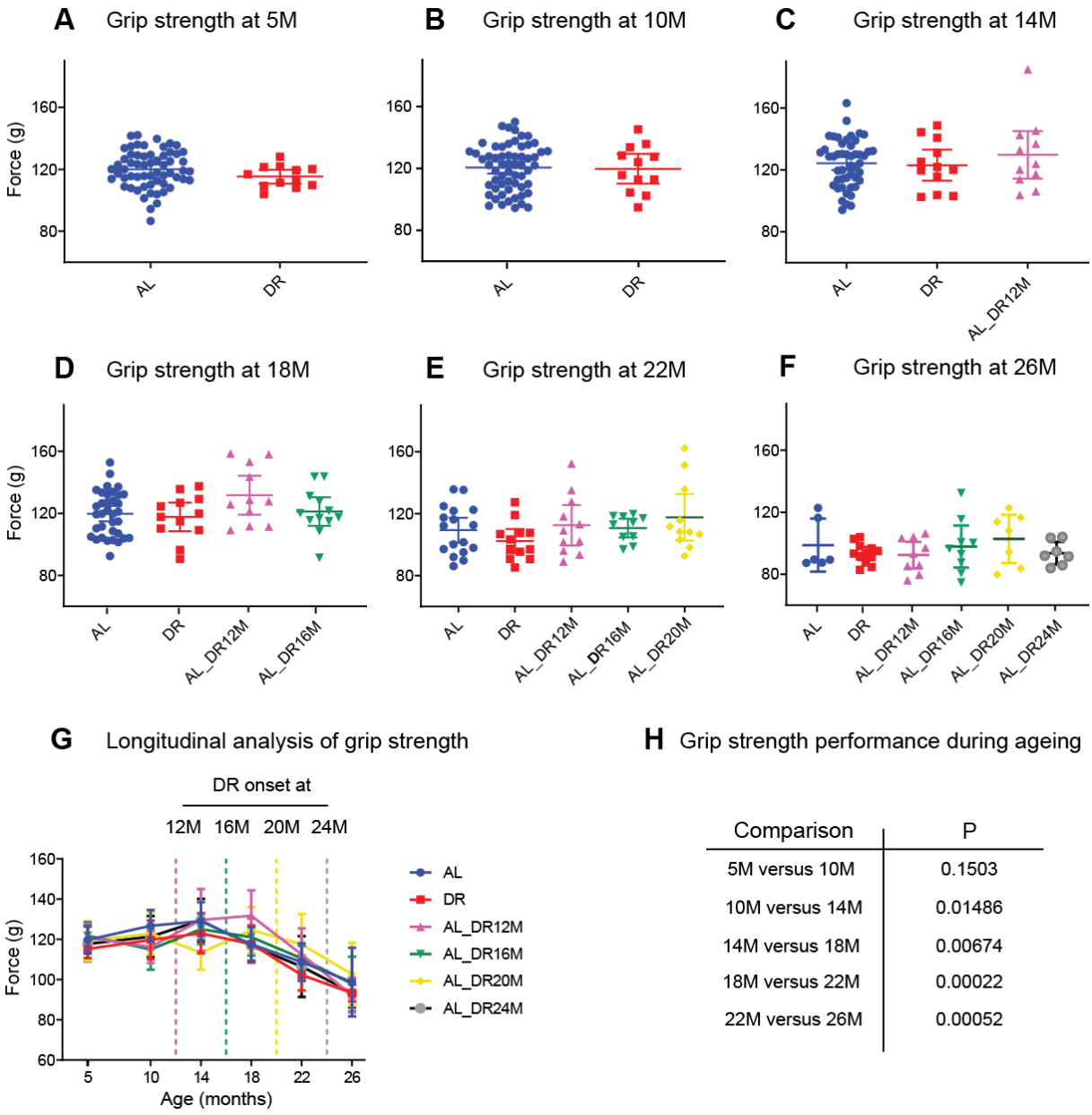

Figure 3.2. 19: Muscle strength is affected by ageing but not by DR in an independent phenotyping cohort

*Analysis of forelimb grip strength in chronic controls AL or DR at **A)** 5M (AL n= 60, DR n= 12) or **B)** 10M (AL n= 60, DR n= 12) of age. AL feeding or chronic DR did not affect muscle strength in young C3B6F1 females. Grip strength of chronic controls and DR switch groups at **C)** 14M (AL n= 48, DR n= 12, AL_DR12M n= 11), **D)** 18M (AL n= 35, DR n= 12, AL_DR12M n= 11, AL_DR16M n= 12), **E)** 22M (AL n= 17, DR n= 12, AL_DR12M n= 11, AL_DR16M n= 10, AL_DR20M n= 11) or **F)** 26M of age (AL n= 6, DR n= 12, AL_DR12M n= 9, AL_DR16M n= 9, AL_DR20M n= 7, AL_DR24M n=7). Chronic, mid- or late-onset DR did not significantly affect muscle strength at all six evaluated time points. Unpaired t tests were implemented to evaluate statistical differences between chronic controls at all time points. One-way ANOVA followed by Bonferroni correction was performed to assess statistical differences in grip strength performance between AL, DR and one DR switch group at a time at each time point. **G** Longitudinal evaluation of grip strength over all six phenotyping time points in all six diet groups. GLME followed by Bonferroni post-hoc tests were implemented to assess differences between diet groups over time but no significant differences were found (p = 0.65). GLME analyses were implemented to evaluate longitudinal intra- and inter-group differences in grip strength across all six time points. **H** One-way ANOVA tests between two consecutive time points revealed age-related decline in grip strength irrespective of diet group and age of DR onset. Data are presented as mean with 95% CI. Data were analysed using GLME or One-way ANOVA with p-values *** p<0.001 in relation to chronic DR, ### p<0.001 in relation to chronic AL. Not significant differences between either chronic AL or DR were not marked. Carolina Monzó conducted the longitudinal GLME analyses, age-related differences in grip strength and the body weight plot.*

3.2.20 Chronic and 12M onset DR but not later DR initiation leads to long-term, stable improvement in motor coordination within eight weeks post-switch to DR

Motor coordination is a complex process, which requires spatial orientation, control of limbs and muscles as well as balance for a flawless execution of the intended movement. Interestingly, a previous study demonstrated that chronic but not DR onset at approx. 15M improved motor coordination in mice, suggesting that DR cannot reverse already occurred damage to the vestibular system if applied to late (Kuhla et al., 2013). However, a systematic analysis at what age DR is still able to improve motor coordination is still missing. To this end, we tested motor coordination using the rotarod by measuring the time spent on the rotating rod. Similar to the grip strength tests, all mice, including future DR switch groups, which were still on AL feeding, were regarded as chronic AL animals before the respective DR switch.

Motor coordination was significantly improved by short-term, chronic DR compared to AL feeding at 5M of age (Fig. 3.2.20A). Moreover, chronic DR displayed significantly improved rotarod performance at 10M of age and already outperformed AL mice at the first testing day (Fig. 3.2.20B). Therefore, we next asked whether mid-life onset DR could improve rotarod

performance. Indeed, AL_DR12M mice significantly improved rotarod performance compared to chronic AL but not to the same extent as chronic DR animals within eight weeks post-switch to DR (Fig. 3.2.20C). In contrast, AL_DR16M mice did not significantly improve motor coordination compared to chronic AL (Fig. 3.2.20D), suggesting that the age of DR onset might influence rotarod performance after the switch. Strikingly, there was no significant performance difference between chronic DR and AL_DR12M and both DR groups had significantly improved motor coordination compared to chronic AL animals (Fig. 3.2.20D). Similar to AL_DR16M at 18M, AL_DR20M mice tested at 22M did not significantly improve motor coordination compared to chronic AL and performed significantly worse in relation to chronic DR (Fig. 3.2.20E). While AL_DR16M animals exhibited improved motor coordination over the course of four days at 22M, the AUC was still significantly differed compared to chronic DR and did not differ from chronic AL mice (Fig. 3.2.20E). Consistently with previous findings, chronic DR animals displayed significantly improved motor coordination at 26M (Fig. 3.2.20F), indicating that chronic DR retained motor coordination performance. Strikingly, even after 10M or 6M post-switch to DR, AL_DR16M and AL_DR20M performed significantly worse in the rotarod test compared to chronic DR (Fig. 3.2.20F). In contrast, we did not detect any significant differences in rotarod performance in AL_DR12M and AL_DR24M compared to chronic controls (Fig. 3.2.20F).

To test differences between diet groups in rotarod performance, as well as to investigate the influence of ageing on motor coordination, we implemented GLME analysis over the AUC of all six time points. Indeed, longitudinal analysis revealed that chronic AL mice showed a significant age-related decrease in motor coordination (Fig. 3.2.20G). In contrast, the performance of DR animals increased between 5M and 10M and the overall performance was significantly better compared to chronic AL animals. Interestingly, we did not detect any statistical evidence for age-related decline of motor coordination in chronic DR (Fig. 3.2.20G), demonstrating that chronic DR retained motor coordination at old age. Interestingly, all DR switch groups displayed decreased performance while on AL feeding (Fig. 3.2.20G). Moreover, only AL_DR12M and AL_DR24M exhibited a significant increase in motor coordination, whereas later onset of DR did not display a big improvement in rotarod performance post-switch to DR (Fig. 3.2.20G). All in all, these results indicate, that the duration of AL feeding had a detrimental effect on motor coordination, which could not be reversed if DR was applied too late.

To sum up, chronic DR or AL_DR12M showed improved rotarod performance during ageing, indicating that DR if applied chronically or at 12M of age can maintain motor coordination even at old age. Moreover, switching mice to DR at 16M had only limited beneficial effect on motor coordination as rotarod performance was independent from body weight. In contrast, DR onset

at 20M or 24M could not improve motor coordination potentially due to already occurred age-related damage in the vestibular system.

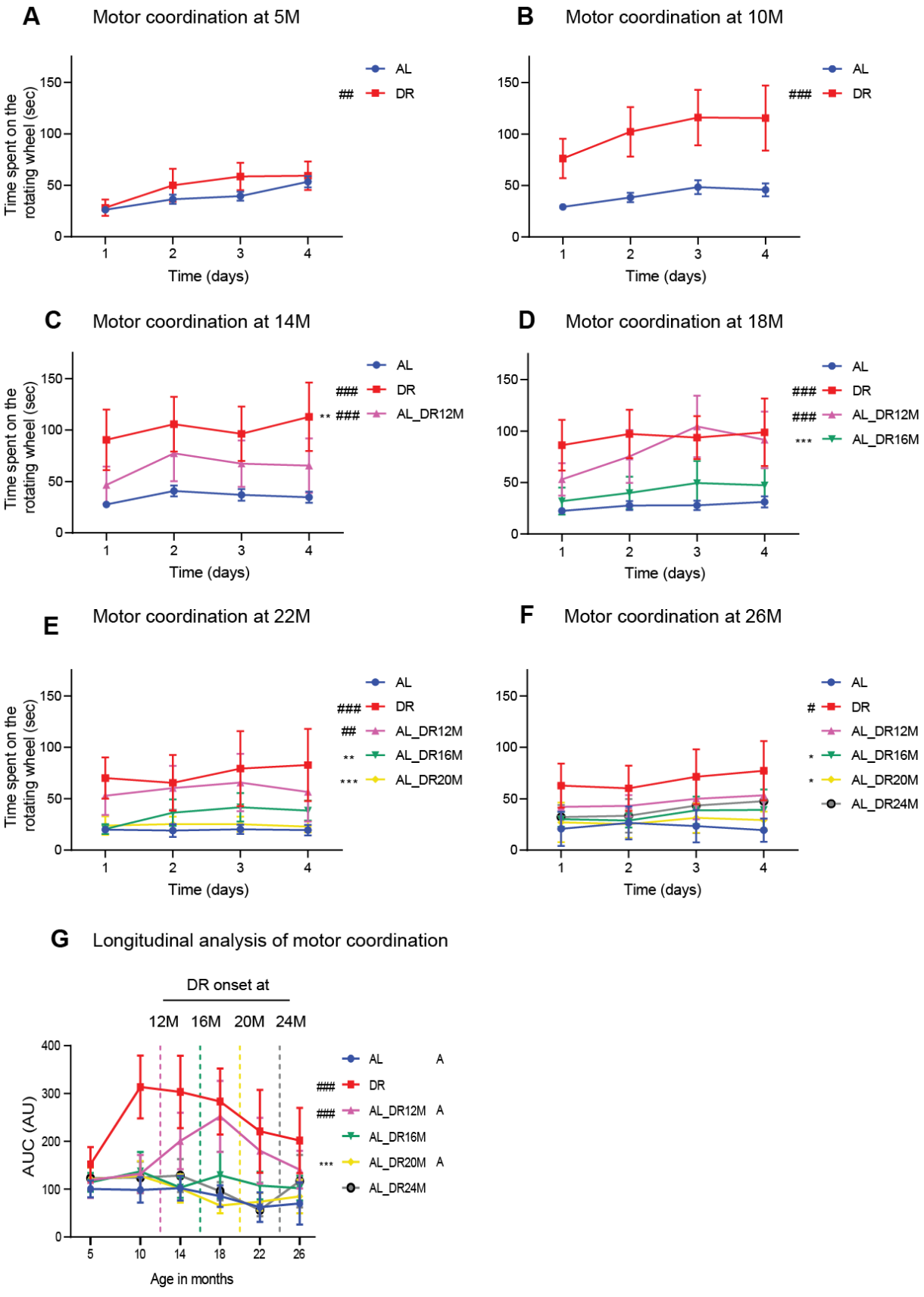

Figure 3.2. 20: Chronic and 12M onset DR but not later DR initiation leads to long-term, stable improvement in motor coordination within eight weeks post-switch to DR

*Motor coordination of chronic AL and DR at **A)** 5M (AL n= 60, DR n= 12) or **B)** 10M (AL n= 60, DR n= 12) of age. Chronic DR increased motor coordination compared to AL feeding. Motor coordination of chronic controls and DR switch groups at **C)** 14M (AL n= 48, DR n= 12, AL_DR12M n= 11), **D)** 18M (AL n= 35, DR n= 12, AL_DR12M n= 11, AL_DR16M n= 12), **E)** 22M (AL n= 17, DR n= 12, AL_DR12M n= 11, AL_DR16M n= 10, AL_DR20M n= 11) or **F)** 26M of age (AL n= 6, DR n= 12, AL_DR12M n= 9, AL_DR16M n= 9, AL_DR20M n= 6, AL_DR24M n=8). Eight weeks post switch, animals improved motor coordination when switched to DR at 3M, 12M or 16M ($p<0.05$) but not at 20M or 24M ($p>0.05$). **G** Chronic or 12M onset DR but not later initiation of DR significantly improved motor coordination compared to AL. To evaluate motor coordination between diet groups, the AUC of all days combined was determined on for each animal. Next, unpaired t tests were implemented to evaluate statistical differences between the AUC of chronic controls at all evaluated time points. One-way ANOVA followed by Bonferroni correction was performed to assess statistical differences in the AUC of rotarod performance between AL, DR and one DR switch group at a time at each time point. GLME analyses were implemented to calculate intra- and inter-group differences in the AUC across all six time points. Data are displayed as mean and 95% CI. Statistical differences in the AUC of rotarod performance on day 1 until day 4 compared to chronic DR are indicated with p-values * $p<0.05$, ** $p<0.01$ and *** $p<0.001$. Statistical differences in relation to AL are presented as following # $p<0.05$, ## $p< 0.01$ and ### $p<0.001$. The letter A indicates significant differences in rotarod performance within the same diet group over time. Carolina Monzó calculated the GLME.*

3.2.21 Lack of rotarod performance is not attributed to body weight differences in DR switch groups

Since rotarod performance might be negatively influenced by weight (Mao et al., 2015), we asked whether the performance difference between chronic AL and DR animals could be explained by their body difference. Moreover, we sought to investigate whether the improvement of the DR switch groups but also the difference towards the chronic DR animals could be explained by the body weight.

We detected a significant correlation between body weight and rotarod performance in chronic AL animals at 5M (Fig. 3.2.21A) and 10M (Fig. 3.2.21B). Interestingly, no significant correlations were observed at later time point at 14M (Fig. 3.2.21C), 18M (Fig. 3.2.21D), 22M (Fig. 3.2.21E) or 26M (Fig. 3.2.21F). These results demonstrate that the rotarod performance of chronic AL animals at young but not at older age was negatively affected by body weight. Strikingly, we did not detect any correlation between body weight and rotarod performance in DR switch groups eight weeks post-switch (Fig. 3.2.21C-F). Interestingly, only AL_DR16M

animals displayed a significant correlation between body weight and rotarod performance at old age (Fig. 3.2.21F), demonstrating that low weight and low performance correlated. Therefore, these results suggest that the lack of improvement in motor coordination post-switch in AL_DR16M, AL_DR20M and AL_DR24M was not due to the body weight differences. To confirm that the weight loss under newly imposed DR in our fitness phenotyping cohort was similar to the metabolic phenotyping cohort, we measured the body weight on the first day of each phenotyping time point. We confirmed that chronic AL mice had significantly higher body weight compared to chronic DR and all DR switches in the new cohort (Fig.3.2.21G), reproducing our previous results. Interestingly, all DR switch groups required more time to reach the chronic DR state and AL_DR20M switches did not completely catch up to chronic DR even at 26M (Fig. 3.2.21G), probably as the animals had a higher body weight on AL feeding.

All in all, differences in motor coordination of DR switches could not be explained by DR-associated weight loss. Thus, DR cannot rescue rotarod performance after prolonged AL feeding and only chronic DR and AL_DR12M mice maintain motor coordination during ageing.

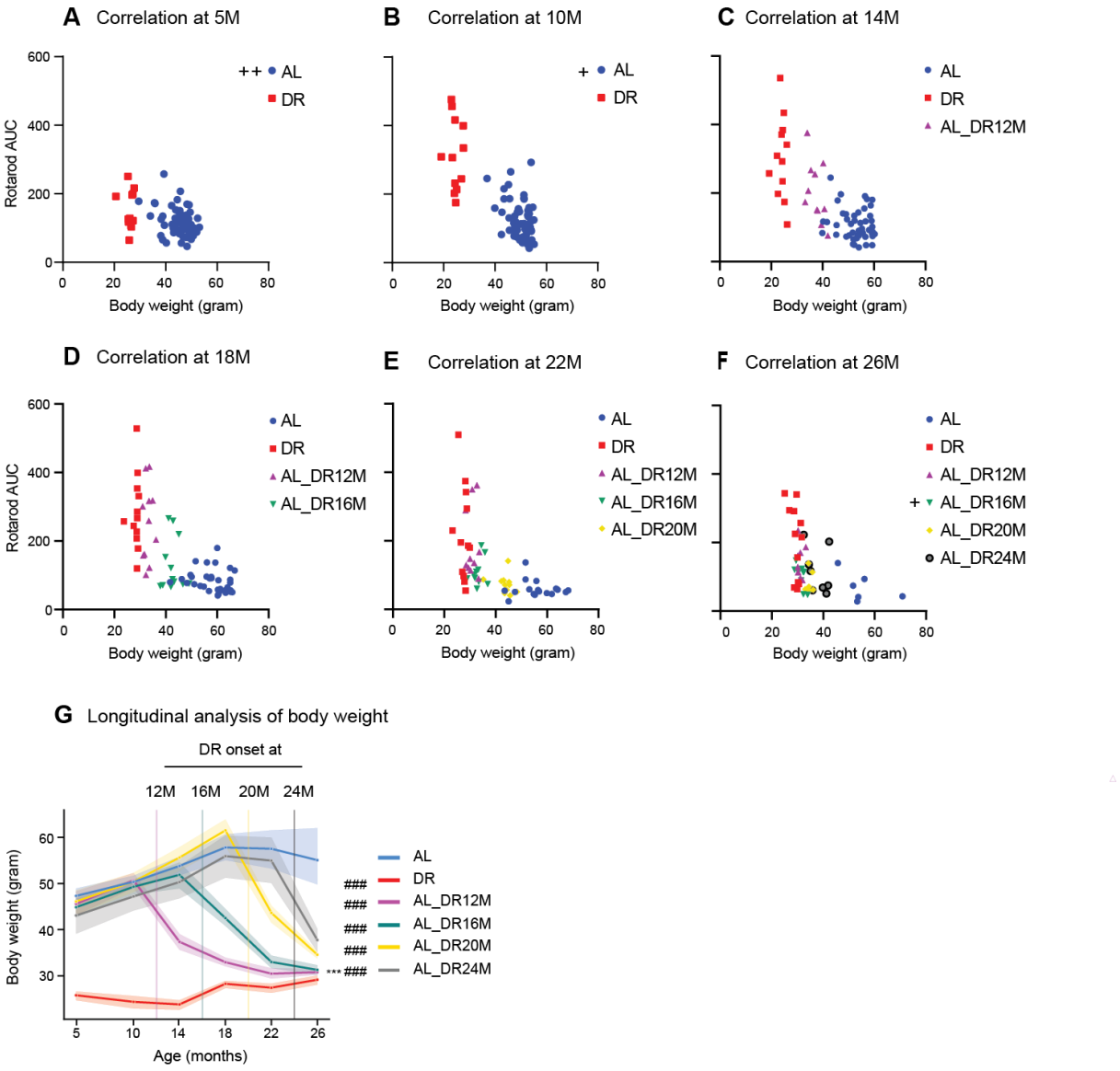

Figure 3.2. 21: Lack of rotarod performance is not attributed to body weight differences in DR switch groups

Pearson correlation of body weight and the AUC of the rotarod performance of chronic AL and DR at ***A)*** *5M (AL n= 60, DR n= 12) or* ***B)*** *10M (AL n= 60, DR n= 12) of age. The rotarod performance correlated with the body weight of chronic AL animals at young age. Pearson correlation of body weight and the AUC of the rotarod performance chronic controls and DR switch groups at* ***C)*** *14M (AL n= 48, DR n= 12, AL_DR12M n= 11),* ***D)*** *18M (AL n= 35, DR n= 12, AL_DR12M n= 11, AL_DR16M n= 12),* ***E)*** *22M (AL n= 17, DR n= 12, AL_DR12M n= 11, AL_DR16M n= 10, AL_DR20M n= 11) or* ***F)*** *26M of age (AL n= 6, DR n= 12, AL_DR12M n= 9, AL_DR16M n= 9, AL_DR20M n= 6, AL_DR24M n=8). The lack of rotarod performance in AL_DR16M, AL_DR20M and AL_DR24M cannot be attributed to differences in body weight.* ***G)*** *Longitudinal measurement of body weight of all diet groups on the first day of the phenotyping regimen for all diet groups and phenotyping time points. GLME were used to calculate body weight differences between diet groups over time. Body weight of DR groups was significantly lower in relation to chronic AL (adj. p<0.001) and not different from chronic DR (adj. p>0.05). Each dot corresponds to the individual body weight in gram and the AUC of the rotarod performance of each*

*tested animal at the indicated time point. Significant correlations between body weight and rotarod performance are indicated with p-values + p<0.05 and ++ p<0.01. Correlations that did not reach statistical significance are not marked. Body weight data are presented with the mean and the 95% CI as shaded area. Statistically significant differences in relation to AL are presented as following # p<0.05, ## p< 0.01 and ### p<0.001. Statistically significant differences in relation to DR are presented as following * p<0.05, ** p< 0.01 and *** p<0.001. Body weight differences that did not reach statistical significance were not marked. Carolina Monzó conducted the GLME analyses of the body weight.*

3.2.22 DR improves memory function irrespective of the age of DR onset

Advanced age is one of the major risk factors to develop several neurological disorders, including dementia (Niccoli & Partridge, 2012). Interestingly, previous studies implementing short- or long-term CR demonstrated that reduction of food intake improved memory and increased neurogenesis in C57BL/6 mice (Bondolfi et al., 2004; Ma et al., 2018). Since no previous studies have investigated memory of the C3B6F1 strain, we aimed to test both age-associated changes and the impact of DR on memory function. To this end, we implemented the dry- land elevated Barnes maze as a readout for memory function at six different time points in murine life.

As expected, we did not detect any difference in time, travelled path and speed on the platform in young chronic AL or DR animals aged 5M (Fig. 3.2.22A) or 10M (Fig. 3.2.22B). Furthermore, no significant differences were observed at 14M between chronic AL, DR and AL_DR12M animals in latency, travelled path or speed (Fig. 3.2.22C). However, we observed a trend towards decreased latency to find the escape box in chronic DR or AL_DR12M animals compared to chronic AL animals (Fig. 3.2.31A-C). Strikingly, AL_DR16M mice found the escape box significantly faster than compared to chronic AL animals at 18M of age (Fig. 3.2.22D). Additionally, we observed a significant improvement in memory function in chronic DR, AL_DR12M and AL_DR20M at 22M (Fig. 3.2.22E) and in chronic DR, AL_DR12M, AL_DR16M and AL_DR24M at 26M (Fig. 3.2.22F) compared to chronic AL feeding. These results indicated that DR feeding, irrespective of the age of DR onset significantly improved memory function at old age. To test differences between diet groups in Barnes maze performance, as well as to investigate the influence of ageing memory function, we implemented GLME analysis over the AUC of all six time points. Strikingly, DR irrespective of the age of DR onset significantly affected the time, animals spent on the platform compared to chronic AL feeding (Fig. 3.2.22G), suggesting that DR improved memory function during ageing in C3B6F1 females. Strikingly, the AUC measurements of chronic AL animals first

decreased until 18M of age and afterwards increased again, indicating that the memory function of chronic AL animals worsened during ageing (Fig. 3.2.22G). Interestingly, the time spent on the platform differed significantly between chronic DR and AL_DR16M animals (Fig. 3.2.22G), which was likely attributed to better performance of chronic DR animals at 5M of age. In contrast, the longitudinal travelled path or speed on the platform were not significantly different between diet groups (Fig. 3.2.22H and I). These results suggest, that the observed differences in the time spent on the platform were not due to faster speed or smaller distances travelled. Intriguingly, all diet groups displayed differences within time points (Fig. 3.2.22G-I), indicating that Barnes maze performance changed during ageing.

To conclude, DR improved memory function irrespective of the age of DR onset in the C3B6F1 strain. However, late-onset DR only leads to a short-term improvement, whereas chronic or mid-life DR onset stably improved memory function during ageing.

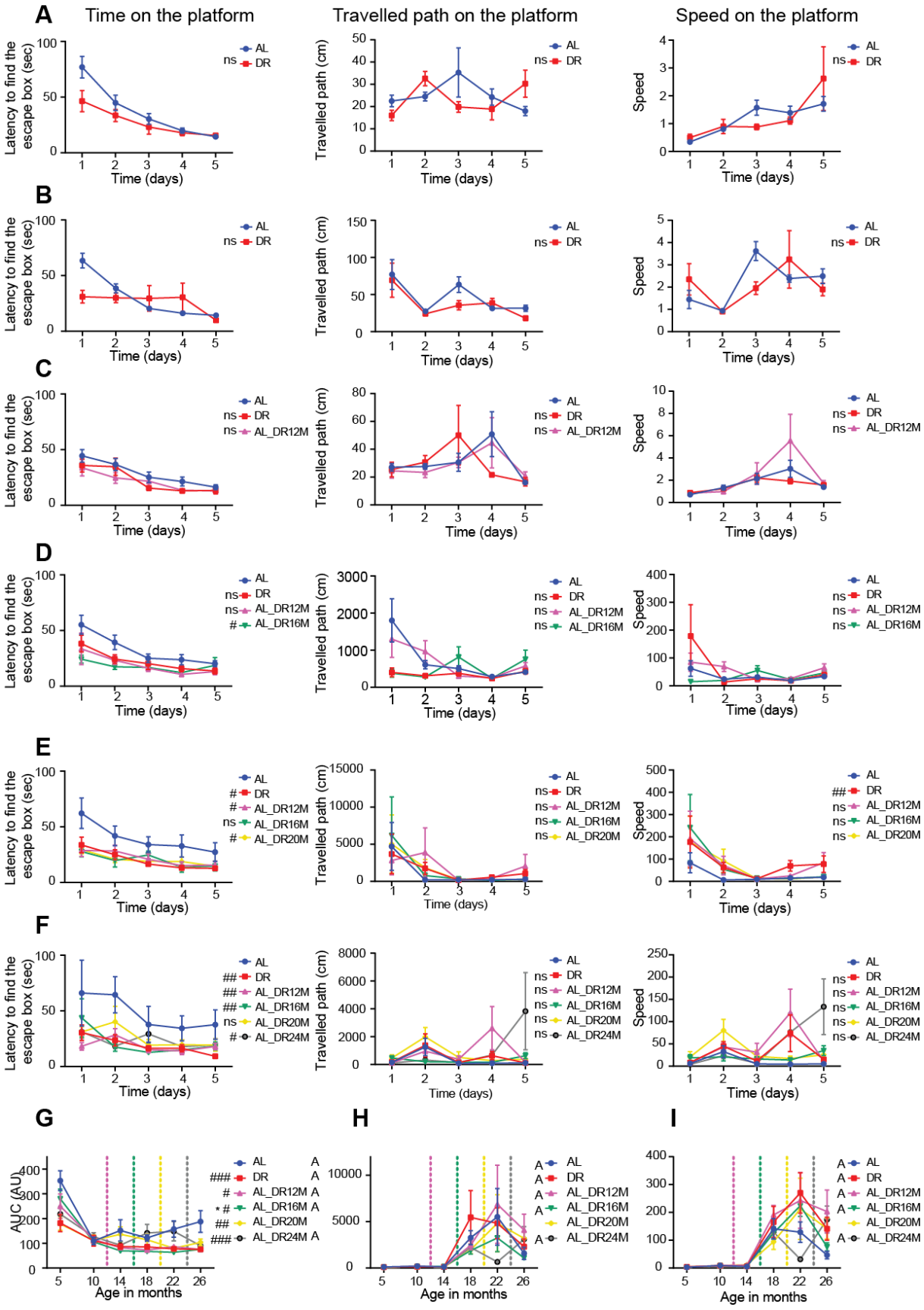

Figure 3.2. 22: DR improves memory function irrespective of the age of DR onset

Estimation of memory function using the dry- land elevated Barnes maze. Over the course of five testing days the time spent on the platform until animals moved into the escape box, the distance they covered until the escape box was found and the speed with which animals moved on the platform was recorded. Cohorts were split into two groups and trained weekly equal number of mice from each diet group each week at all phenotyping time except at 26M of age. Memory function of chronic AL and DR at ***A)*** *5M (AL n= 30, DR n= 6) or* ***B)*** *10M (AL n= 60, DR n= 12) of age. Chronic DR did not improve memory function at young age. We detected a batch effect between chronic AL and DR animals at 5M of age between week 1 and week 2. Only week 2 data were utilized for the analyses. Memory function of chronic controls and DR switch groups at* ***C)*** *14M (AL n= 47, DR n= 12, AL_DR12M n= 11),* ***D)*** *18M (AL n= 35, DR n= 12, AL_DR12M n= 11, AL_DR16M n= 6),* ***E)*** *22M (AL n= 17, DR n= 12, AL_DR12M n= 11, AL_DR16M n= 10, AL_DR20M n= 11) or* ***F)*** *26M of age (AL n= 6, DR n= 12, AL_DR12M n= 9, AL_DR16M n= 9, AL_DR20M n= 6, AL_DR24M n=7). AL_DR16M animals tested in week 1 compared to week two at 18M. Therefore, only data from week 1 were utilized in the 18M time point analyses. Chronic DR, AL_DR12M, AL_DR16M and AL_DR24M displayed improved memory function compared to chronic AL.* ***G)*** *Longitudinal analyses of the AUC of time over all six phenotyping time points.* ***H)*** *Longitudinal analyses of the AUC of the travelled path over all six phenotyping time points.* ***I)*** *Longitudinal analyses of the AUC of the speed over all six phenotyping time points. Unpaired t tests were implemented to evaluate statistical differences in the AUC between chronic controls at all evaluated time points. One-way ANOVA followed by Bonferroni correction was performed to assess statistical differences in the AUC of time, distance travelled or speed (day 1-5) between AL, DR and one DR switch group at a time at each time point. GLME analyses followed by Bonferroni post-hoc tests for multiple testing correction were implemented to calculate intra- and inter-group differences across all six time points. Data are presented as mean ± SEM. Carolina Monzó conducted the GLME analyses.*

3.2.23 Early or mid-life onset DR at 12M or 16M reduces overall frailty during ageing

Recent studies established a frailty index in mice, which scores similar frailty parameters as human frailty tests in the clinics (Kane et al., 2016; Whitehead et al., 2014), thus making it a powerful tool to assess systemic effects of ageing in mice. To assess the influence of late-life DR on frailty, we measured frailty in the mice of all diet groups every eight weeks between 22 and 26 months of age (Fig. 3.2.23A).

Overall, we did not observe much difference in the frailty score between diet groups at 22M of age but there was a trend towards higher frailty in AL, AL_DR16M and AL_DR20M (Fig. 3.2.23B). Interestingly, AL_DR12M mice were significantly less frail than chronic AL mice at 22M, indicating that DR could have a beneficial effect on frailty at later time points. Indeed, when tested at 24M, chronic DR as well AL_DR12M and AL_DR16M mice were less frail than chronic AL, indicating that chronic or mid-life DR reduced age-associated health decline.

Moreover, this phenotype was conserved at 26M of age, as chronic AL mice displayed the overall highest frailty score of all diet groups and both chronic and mid-life DR consistently decreased frailty, demonstrating improved health at old age. Interestingly, we observed a trend towards increased frailty depending on the duration of previous AL feeding, as AL_DR20M and AL_DR24M were frailer compared to chronic DR. Indeed, AL_DR24M mice, which were tested on AL feeding at 22M and 24M, and AL_DR20M mice did not display improved frailty upon newly imposed or longer DR and were significantly frailer compared to chronic DR, indicating that DR cannot slow down gradual health decline during ageing if initiated too late. Parameters, which displayed the greatest change between 22M and 26M of age were loss of fur colour, tail stiffening, palpable or visible tumours, vestibular disturbance, vision loss and changes in the sacroiliac region (data not shown). As expected, longitudinal analysis of the frailty score revealed increased frailty in all diet groups including chronic DR thus demonstrating that health deteriorates during ageing irrespective of diet but chronic and mid-life treatment can slow down health decline (Fig.3.2.23B). However, throughout ageing, chronic DR, AL_DR12M and AL_DR16M retained a better health compared to chronic AL, whereas AL_DR20M and AL_DR24M animals were frailer as chronic DR (Fig. 3.2.23B).

Thus, our data show that introducing DR during mid-life reduces late-life frailty to a similar extent as early-life onset DR. Furthermore, introducing DR later in life did not have an obvious effect on frailty consistent with the lack of lifespan extension in these late diet switches.

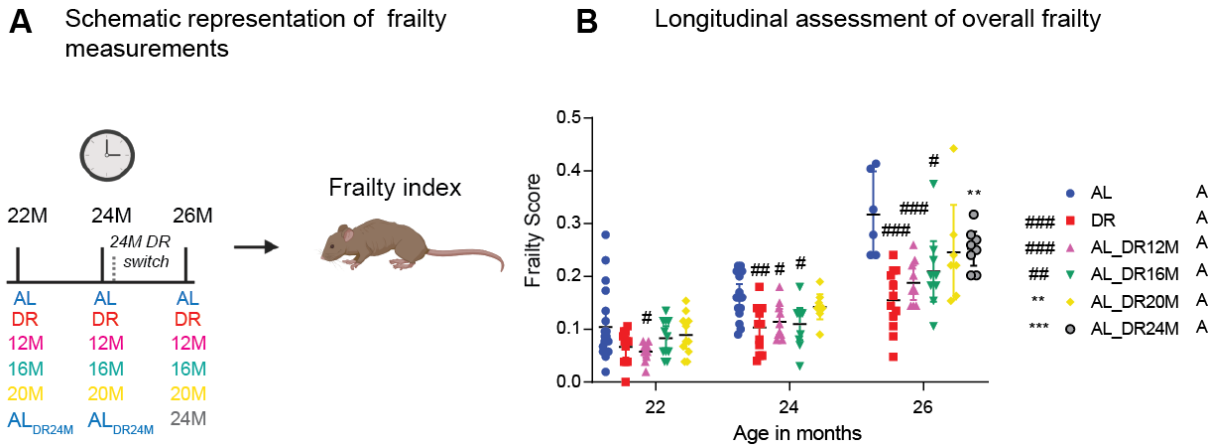

Figure 3.2. 23: Early or mid-life onset DR at 12M or 16M reduces overall frailty during ageing

A *schematic representation of frailty measurements at 22M, 24M or 26M of age. The frailty index was implemented at three different ages of murine life. AL_DR24M switches were evaluated as chronic AL animals at 22M and 24M prior to the DR switch and on newly imposed DR at 26M of age.* ***B*** *Longitudinal assessment of overall frailty of chronic controls and DR switch groups. The animal numbers were the following: at 22M (AL n= 20, DR n= 12, AL_DR12M n= 11, AL_DR16M n= 11, AL_DR20M n= 11), B). At 24M (AL n= 15, DR n= 12, AL_DR12M n= 11, AL_DR16M n= 10, AL_DR20M n= 8). At 26M of age*

*(AL n= 6, DR n= 12, AL_DR12M n= 9, AL_DR16M n= 9, AL_DR20M n= 7, AL_DR24M n=8). Chronic, 12M and 16M onset of DR significantly reduced overall frailty during ageing. AL_DR24M were significantly frailer at 26M than chronic DR. Data between chronic AL and DR were analysed using unpaired t tests at 22M, 24M and 26M. Differences between chronic controls and one DR switch groups at a time were assessed using One-way ANOVA followed by Bonferroni post-hoc tests at 22M, 24M and 26M. Longitudinal changes in overall frailty were analysed using GLME followed by Bonferroni multiple testing correction. Data are displayed as mean and 95% CI. Statistically significant differences compared to chronic DR are indicated with p-values * p<0.05 and *** p<0.001. Statistically significant differences in relation to AL are presented as following # p<0.05, ## p< 0.01 and ### p<0.001. The letter A indicates significant differences within the same diet group over time as determined by GLME analysis. GLME analyses were conducted by Carolina Monzó and schematics were created with BioRender.com.*

3.2.24 Body temperature does not decrease in response to early, mid-life or late-onset DR

Previous studies reported decreased body temperature upon prolonged DR feeding regimen as one of the detrimental effects of DR in single-housed male 129S2/SvPasCrl mice (Corrales et al., 2019) as well as in humans (Soare et al., 2011). However, we did not find evidence for WAT browning or a change in thermogenesis in our previous study using group-housed C3B6F1 female mice (Fig. 3.1.4). Thus, in order to address whether late-life DR would affect body temperature in these animals, we measured body temperature at four different time points (Fig. 3.2.24A). As in mice body temperature depends on the feeding state of the animals, measurements were taken in the morning prior to the feeding of DR animals and in the afternoon to ensure that observed changes were not simply due to different feeding states of AL and DR animals.

We assessed body temperature using an infrared non-invasive thermometer via the ear when animals were 22M, 24M and 26M. In addition, as measurements based on infrared thermometers do not address core body temperature, we also used a rectal probe to have a more precise measurement at the age of 28M (Fig. 3.2.24A). Remarkably, we did not detect any significant differences in body temperature irrespective of diet group in the morning or in the afternoon at all three evaluated time points (Fig. 3.2.24B-C). While infrared thermometry reliably reports the body temperature of humans, body measurements in mice are more variable depending on the site of measurement and the method chosen (C. W. Meyer, Ootsuka, & Romanovsky, 2017). Moreover, it has been recently reported that infrared measurements are less sensitive and readings are approximately two degrees Celsius lower compared to rectal measurements (Kawakami et al., 2018). Therefore, we included an additional measurement time point at 28M, during which we measured the core temperature

using an invasive rectal probe. Strikingly, we detected a significant difference in body temperature across diet groups depending on the feeding state (Fig. 3.2.24E). However, no differences in temperature were detected between diet (Fig. 3.2.24E), suggesting that DR did not impact on body temperature in the C3B6F1 background irrespective of the age of onset or the duration of DR. In contrast to the report by Kawakami and colleagues (Kawakami et al., 2018), we did not observe a big temperature difference in rectal versus infrared measurements (Fig. 3.2.24B-D), suggesting that both methods were equally robust to detect body temperature in C3B6F1 females. To conclude, we demonstrated that chronic or late-life DR does not affect body temperature in female C3B6F1 mice consistent with our previous results on WAT thermogenic gene expression.

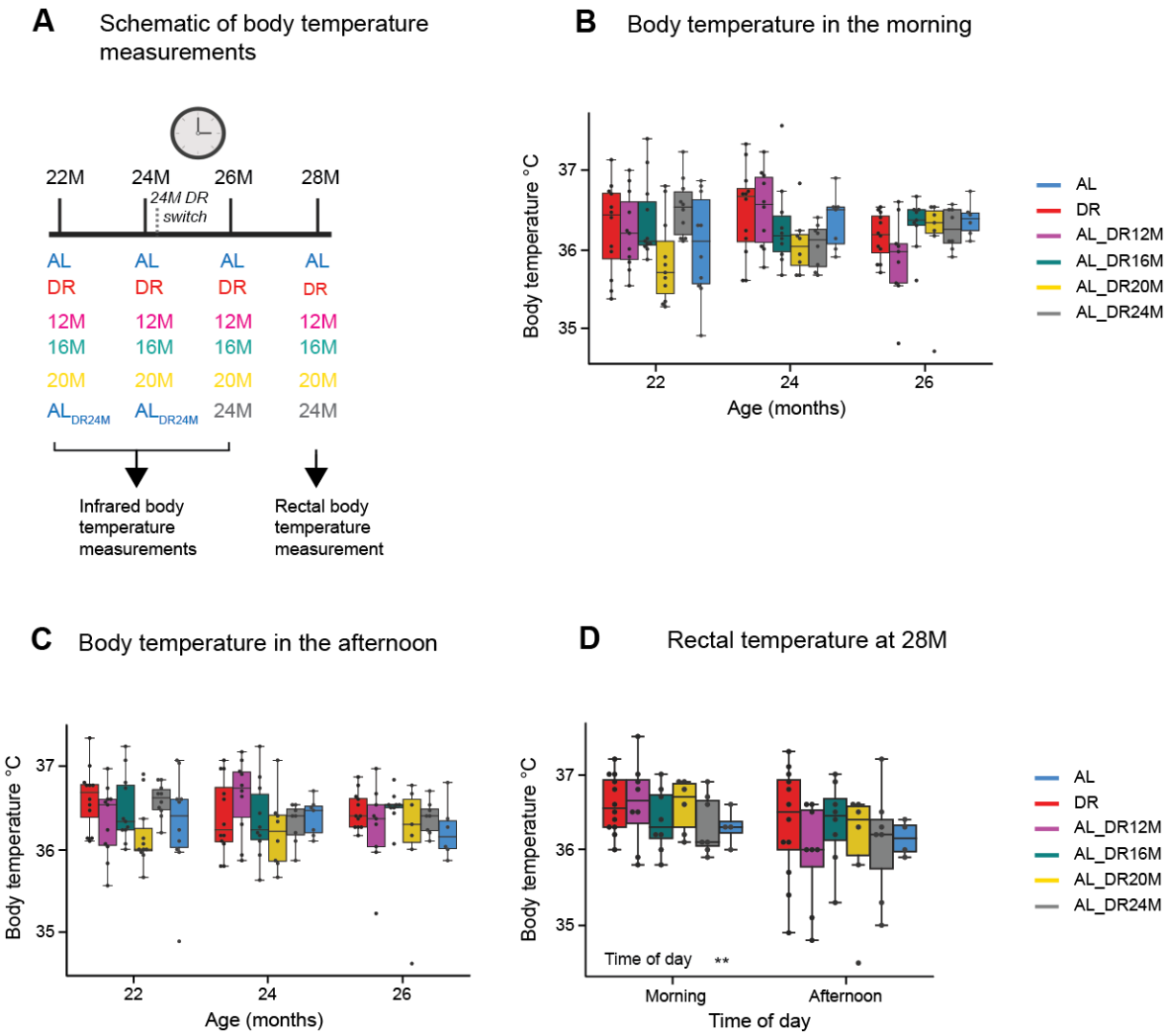

Figure 3.2. 24: Body temperature does not decrease in response to early, mid-life or late-onset DR

A *Schematic representation of the body temperature measurements during ageing. Animals were first assessed at 22M and measurements continued every two months until 26M of age using a non-invasive*

infrared thermometer. Rectal temperature measurements were conducted at 28M. Temperature measurements irrespective of the method were carried out in the morning prior to the feeding and in the afternoon. AL_DR24M mice were counted as AL animals at 22M and 24M before the diet switch and as AL_DR24M after the DR switch at 26M and 28M of age. Longitudinal assessment of body temperature using infrared thermometer ***B*** *in the morning or* ***C*** *in the afternoon. Body temperature differences between morning and afternoon measurements in °C at 22M, 24M or 26M of age. Animal numbers were the following: at 22M (AL n= 20, DR n= 12, AL_DR12M n= 11, AL_DR16M n= 11, AL_DR20M n= 11), at 24M (AL n= 15, DR n= 12, AL_DR12M n= 11, AL_DR16M n= 10, AL_DR20M n= 8) and at 26M of age (AL n= 6, DR n= 12, AL_DR12M n= 9, AL_DR16M n= 9, AL_DR20M n= 7, AL_DR24M n=8). AL_DR24M animals were tested as chronic AL animals at 22M and 24M of age.* ***D)*** *Rectal body temperature measurements in chronic controls and DR switch groups at 28M of age in the morning or afternoon in chronic AL (n= 4), DR (n= 12), AL_DR12M (n= 8), AL_DR16M (n= 8), AL_DR20M (n= 6) and AL_DR24M (n=7). Feeding state (adj. p= 0.0080) but not DR impacts on rectal body temperature at 28M. Data were analysed using One-way ANOVA followed by Bonferroni testing for multiple correction and longitudinal infrared measurements were analysed using GLME with Bonferroni post-hoc tests. Data are displayed as mean and 95% CI. Statistically significant differences in relation to AL are presented as following # p<0.05, ## p< 0.01 and ### p<0.001. Differences in feeding state at 28M were analysed using One-way ANOVA followed by Bonferroni correction with ** p< 0.01. Carolina Monzó conducted the GLME analyses and schematics were created with BioRender.com.*

3.2.25 Chronic, 12M and 20M onset of DR leads to a long-term decrease in heart rate

Cardiovascular diseases are one of the main causes of death among the elderly (Roth et al., 2017) and previous studies reported a beneficial effect of DR on heart function in rats (Shinmura et al., 2011). Moreover, many human studies have linked DR to improved cardiac health (Fontana et al., 2007; Hammer et al., 2008) but no studies are available, which show a beneficial effect of late-life onset DR on cardiovascular function. Therefore, we utilized heart rate as a proxy for heart function using non-invasive electrocardiography (ECG) measurements. We first assessed chronic controls at 5M and 10M and included DR switch groups eight weeks post-switch for the first time in the test (Fig. Fig.3.2.25A).

Strikingly, we detected significantly lower heart rates in chronic DR mice aged 5M (Fig. 3.2.14A) and 10M 5M (Fig. 3.2.14B) compared to chronic AL feeding, suggesting that even short-term chronic DR treatment affected heart function. We therefore hypothesized that switching mice to DR lead to a similar heart rate decrease. Indeed, AL_DR12M also reduced heart rate to a similar extent as chronic DR and compared to AL at 14M (Fig. 3.2.25D). Strikingly, we detected significantly lower heart rates in chronic DR, AL_DR12M and AL_DR16M animals compared to chronic AL feeding (Fig. 3.2.25E). Moreover, no significant

difference were observed between chronic DR and DR switches at 18M, indicating that a short-term, mid-life onset DR regimen could similarly affect heart function as chronic DR treatment.

In contrast, we did not observe any significant difference in the heart rate between diet groups at 22M (Fig. 3.2.25F). Interestingly, AL_DR20M and AL_DR24M exhibited significantly lower heart rates compared to chronic AL or DR but no differences between chronic controls and AL_DR12M or AL_DR16M animals were detected (Fig. 3.2.25G). We therefore plotted the data longitudinally to investigate the heart rate differences between the diet groups over time. Strikingly, longitudinal analysis revealed that the heart rate of AL animals increased between 5M and 10M of age and eventually decreased in an age-related decline, which seemed to accelerate after 18 months of age (Fig. 3.2.25H). In contrast, the heart rate of chronic DR animals increased between 5M and 14M but remained stable after 14M of age without evidence for an age-related decline compared to chronic AL (Fig. 3.2.25H). Indeed, GLME analyses revealed that the longitudinal heart rate of chronic DR animals differed significantly from AL animals (Fig. 3.2.25H), indicating a potential cardioprotective effect by DR. As AL animals started to die after 18M of age, it could be possible that there is an inverse relationship between increased heart rate and mortality, i.e. that AL animals with a higher heart rate at young age could die earlier. Correspondingly, longer-lived AL animals may have lower heart rate, comparable with chronic DR animals. Therefore, the accelerated decline in heart rate after 18M (Fig. 3.2.25H) of age could be explained by the deaths of the short-lived AL animals and could point towards a bias in our analyses towards long-lived AL mice.

Strikingly, switching mice to DR at 12M or 20M but not at 16M even further decreased heart rate within eight weeks or six months post-switch to DR compared to chronic DR (Fig. 3.2.25H). These results raise the question why the later switches at 12M or 20M would lower the heart rate even further than that of the DR cohort and why we did not detect a similar significant drop in AL_DR16M mice (Fig. 3.2.25H). AL_DR12M mice displayed increased lifespan and health span at old, whereas AL_DR16M animals exhibited an intermediate phenotype with a full lifespan but not health span extension and therefore, AL_DR16M animals could display a similar in-between phenotype for the heart rate. Strikingly, AL_DR20M animals also showed significantly lower heart rates (Fig. 3.2.25H) but in contrast to earlier DR switches, AL_DR20M are not long-lived (Fig. 3.2.3C) As some deaths occurred prior to the first phenotyping time point at 22M, it is possible, that similarly to AL animals, we selected for the longest-lived AL_DR20M mice, which displayed the lowest heart rate. The autonomous nervous system, namely the sympathetic and parasympathetic branches, controls the heart rate (Silvani et al., 2016), which can be modulated by dietary interventions (Young & Landsberg, 1982). Strikingly, 6M of DR reduced sympathetic and increased parasympathetic nervous system output as well as decreased heart rate in overweight humans, (De Jonge et al., 2010). It is tempting to speculate, that a similar reduction in parasympathetic nervous system activity could take place

in mice on chronic or even late-onset DR. Therefore, more analyses are necessary to dissect the relationship between reduced heart rate and mid- and late-onset DR.

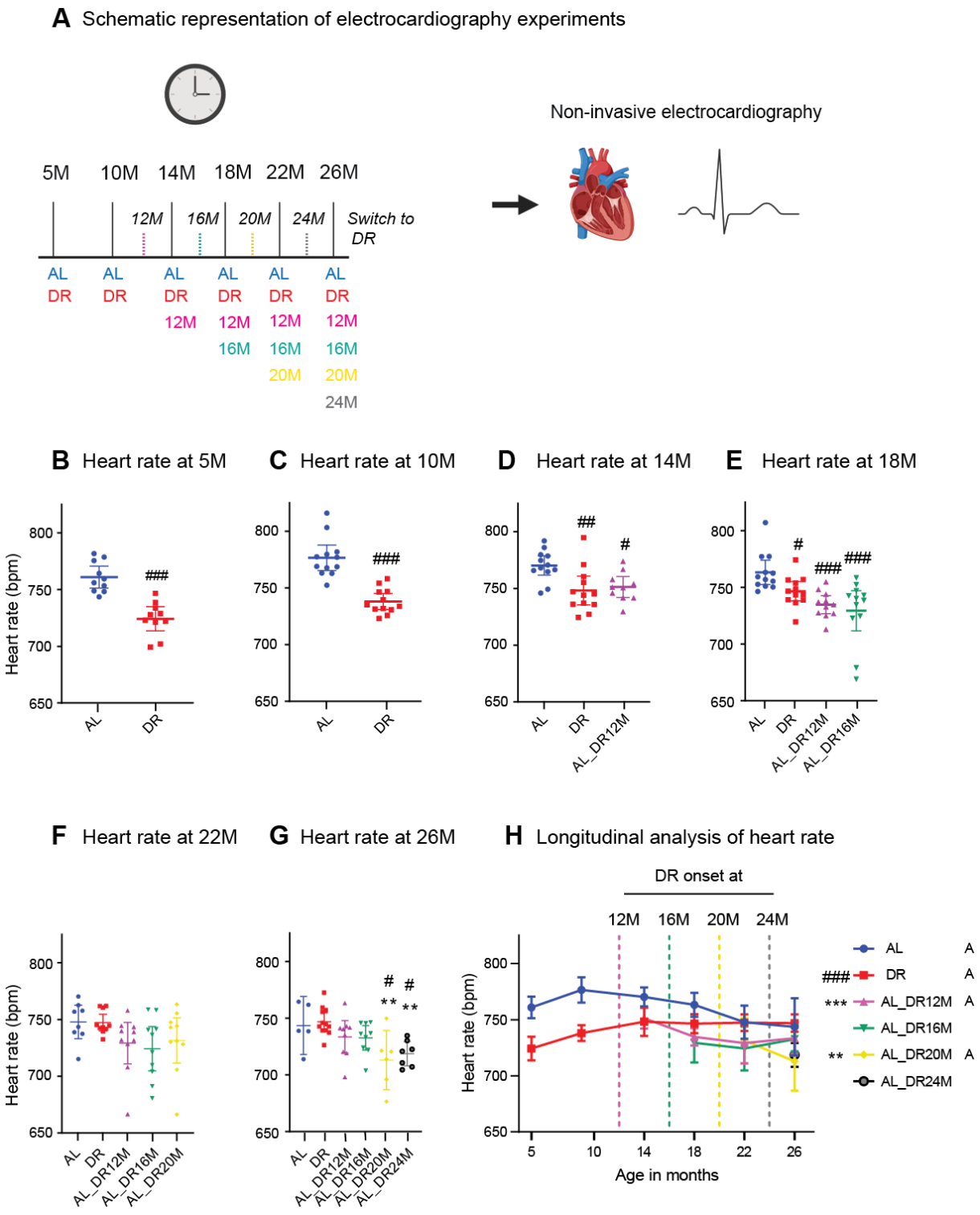

Figure 3.2. 25: Chronic, 12M and 20M onset of DR leads to a long-term decrease in heart rate

A *Schematic representation of electrocardiography experiments. Chronic AL and DR mice were tested at 5M and 10M to assess heart rate in beats per minute (bpm) at young age. To assess the effect of later DR onset on heart rate, DR switch groups were first assessed eight weeks post-switch to DR and*

continuously tested in the same four-month interval as chronic controls. Animal with less than 100 recorded signals were excluded from the analyses. Heart rate of chronic AL and DR at ***B)*** *5M (AL n= 10, DR n= 10) or* ***C)*** *10M (AL n= 12, DR n= 12),* ***D)*** *of age. Chronic DR reduced heart rate compared to AL feeding. Heart rate of chronic controls and DR switch groups at 14M (AL n= 12, DR n= 12, AL_DR12M n= 10),* ***E)*** *18M (AL n= 12, DR n= 12, AL_DR12M n= 11, AL_DR16M n= 12),* ***F)*** *22M (AL n= 8, DR n= 10, AL_DR12M n= 10, AL_DR16M n= 10, AL_DR20M n= 10)or* ***G)*** *26M of age (AL n= 5, DR n= 12, AL_DR12M n= 9, AL_DR16M n= 9, AL_DR20M n= 6, AL_DR24M n=7). Initiation of DR as late as 24M of age reduced heart rate. Unpaired t tests were implemented to test statistical differences between chronic controls at all evaluated time points. One-way ANOVA followed by Bonferroni correction was performed to assess statistical differences in heart rate between AL, DR and one DR switch group at a time at each time point.* ***H)*** *longitudinal analysis of heart rate across all six phenotyping time points. Chronic DR stably reduced heart rate throughout life compared to AL feeding. AL_DR12M and AL_DR20M had lower heart rates than chronic DR. Heart rate changed throughout life for AL, DR, AL_DR12M and AL_DR20M mice. GLME analyses followed by Bonferroni post-hoc tests were implemented to calculate intra- and inter-group differences in the heart rate across all six time points. Data are plotted as mean with 95% CI. Statistically significant differences in relation to AL are presented as following # p<0.05, ## p< 0.01 and ### p<0.001. Statistically significant differences in relation to DR are presented as following * p<0.05, ** p< 0.01 and *** p<0.001. Differences that did not reach statistical significance were not marked. Carolina Monzó conducted the GLME analyses and schematics were created with BioRender.com.*

3.2.26: DR reduces the duration of the RR interval and the ventricular de- and repolarization

ECG is commonly used in clinics as non-invasive means to score cardiac health and function as well as adding prognostic value to diagnose certain cardiac diseases, such as coronary heart disease (Auer et al., 2012), ischemia (De Bacquer et al., 1998) or genetically inherited arrhythmia (Gollob et al., 2001). Heartbeats are subdivided into different segments, intervals and complexes depending on the polarization or repolarizations events occurring in the left and right atria as well as the left and right ventricles. These polarization events mediate the contraction of the heart and subsequently the generation of the heartbeat, followed by the repolarization in the refractory period between two heartbeats. In total, a single heart beat is composed of five waves or groves as well as six intervals or segments and based on differences in the duration of the ECG segments, heart problems can be detected (Becker, 2006). Within the scope of this ECG analysis, the following intervals and segments were tested namely the RR, PQ, PR, QT and corrected QT interval (QTc) as well as the ST segment, QRS complex and normal and corrected QT dispersion (QTc).

We first assessed the RR interval as proxy for the time between heart rates. Interestingly, the RR interval was significantly prolonged in chronic DR compared to chronic AL at 5M, 10M, 14M and 18M and which corresponded to the heart rate data presented before, thus suggesting that the increase in the RR intervals observed upon DR is caused by slower heart rate. Similarly, the RR interval of AL_DR12M and AL_DR16M was longer compared to AL animals at 14M and 18M, while no differences in RR interval duration were detected between diet groups at 22M of age (Fig. 3.2.26B), again coinciding with our heart rate data (Fig. 3.2.25C-F). Similarly, we detected a significant elongation of the RR interval in AL_DR20M and AL_DR24M at 26M of age compared to both chronic controls (Fig. 3.2.26B). Interestingly, the longitudinal RR interval of chronic DR and AL_DR20M mice significantly differed from AL and the RR interval of AL_DR12M or AL_DR20M differed from chronic DR, thus providing a link between reduced heart rate and prolonged RR interval duration. Next, we evaluated the effect of DR on atrial and intraventricular depolarization using the PQ (Fig. 3.2.26C) and PR (Fig. 3.2.26D) intervals as proxy. Interestingly, the PQ interval duration was shorter in chronic DR compared to AL animals at 5M and 10M of age and was prolonged in AL_DR12M compared to chronic DR at 14M (Fig. 3.2.26C). Moreover, we detected a significant elongation of the PR interval in AL_DR20M mice compared to chronic AL or DR at 26M of age (Fig. 3.2.26D). These results indicate that the time between atrial and intraventricular depolarization was altered by chronic or 12M onset DR early in life and in AL_DR20M mice late in life. However, no significant differences in the longitudinal PQ (Fig. 3.2.26C) or PR (Fig. 3.2.26D) interval duration were observed between and within diet groups, suggesting that DR had no long-term effects on atrial and intraventricular depolarization. We detected a significant increase in the QRS complex duration in chronic DR compared to AL mice at 10M of age, however no significant differences in the longitudinal QRS complex duration were observed (Fig. 3.2.26E), suggesting that DR did not affect the depolarization between the right and left ventricle. Next, we focussed on the ST segment duration in response to DR (Fig. 3.2.26F). Interestingly, the ST segment duration was increased in chronic DR compared to AL at 5M but did not significantly differ between chronic controls at later ages (Fig. 3.2.26F). In contrast, we detected a significant increase in the ST segment duration between AL_DR12M and chronic DR at 18M and 26M and between AL_DR20M and chronic DR at 22M and 26M (Fig. 3.2.26F). Moreover, longitudinal analyses revealed that the ST segment duration significantly differed between chronic AL or AL_DR12M and chronic DR (Fig. 3.2.26F), suggesting that early or 12M onset of DR could affect the end of ventricular de- and the beginning of the repolarization events in the heart.

We next assessed the QT interval to evaluate the duration between ventricular de- and repolarization (Locati et al., 2017) in response to chronic or late-onset DR. Interestingly, we detected a significant extension in the QT interval duration between chronic AL and DR at 5M

and 10M of age (Fig. 3.2.26G). Moreover, the QT interval of AL_DR12M, AL_DR16M, AL_DR20M and AL_DR24M was significantly longer compared to chronic DR animals at 18M, 22M and 26M of age (Fig. 3.2.26G). Interestingly, all DR switch groups exhibit differences in the QT interval within four months after the dietary switch, suggesting that mid-or-late-life DR could impact on ventricular and atrial repolarization. When evaluating the longitudinal effect of chronic, mid- or late-onset DR on QT interval duration, the only significant differences were found between chronic DR and AL and between AL_DR12M and chronic DR, indicating that early but not late-onset DR has a longer impact on cardiac health. It is known that the heart rate affects the QT interval, which shortens at faster and lengthens in slower heart rates and thus, the heart rate corrected QT interval (corrected QT interval) is commonly used as readout in ECG measurements (Funck-Brentano & Jaillon, 1993). Therefore, we evaluated the differences in the corrected QT interval between diet groups and across ageing (Fig. 3.2.26H). We detected a significant increase in the corrected QT interval in chronic DR compared to AL at 5M and 14M of age (Fig. 3.2.26H). Moreover, the corrected QT interval was extended in AL_DR16M at 18M and between AL_DR12M and DR at 18M and 26M of age. Moreover, AL_DR20M animals displayed prolonged corrected QT intervals compared to both chronic controls at 22M and 26M (Fig. 3.2.26H). Similar to the uncorrected QT interval, longitudinal analyses revealed that the corrected QT interval significantly differed between chronic AL and DR and between AL_DR12M and chronic DR (Fig. 3.2.26H). These results confirmed that 3M or 12M onset of DR had a long-term effect in ventricular de- and repolarization events, which was independent from the heart rate.

Lastly, we investigated the QT dispersion, which is corrected for the longest and shortest QT intervals in response to chronic or late-onset DR. We detected a significantly longer QT dispersion in chronic AL animals at 5M of age compared to AL and a significantly shorter QT dispersion in AL_DR12M compared to DR at 14M (Fig. 3.2.26I). Interestingly, longitudinal analyses revealed a significant difference in the QT dispersion over multiple time point in chronic DR and AL_DR20M mice (Fig. 3.2.26I). When corrected for the heart rate (corrected QT dispersion), we did not observe any significant differences between diet groups within individual time points but the longitudinal corrected QT dispersion was different between chronic controls and between AL_DR20M and chronic DR (Fig. 3.2.26J). These results suggest that correcting the QT interval for the heart rate or QT variation influences the statistical analyses (Fig. 3.2.26G-J). Moreover, AL_DR12M animals seemed to have a higher QT interval variance irrespective of the heart rate, as no statistical difference between chronic and AL_DR12M were observed when correcting for the highest and lowest QT intervals (Fig. 3.2.26I and J).

Taken together, DR initiated at young, middle-aged or old age reduces the heart rate compared to chronic AL feeding. Moreover, in accordance with a reduction in heart rate, the RR interval

duration and ventricular de- and repolarization correspondingly increased. In contrast, atrial, intraventricular or ventricular depolarization were not significantly affected by DR. All in all, our results point towards a potential cardioprotective effect of DR, which was still implemented even after long-term AL feeding. However, more studies are required to fully explain the effect of chronic, mid- or late-onset DR on cardiac health and to evaluate whether DR reduced sympathetic and increased parasympathetic nervous system output and whether these differences could correlate with lifespan.

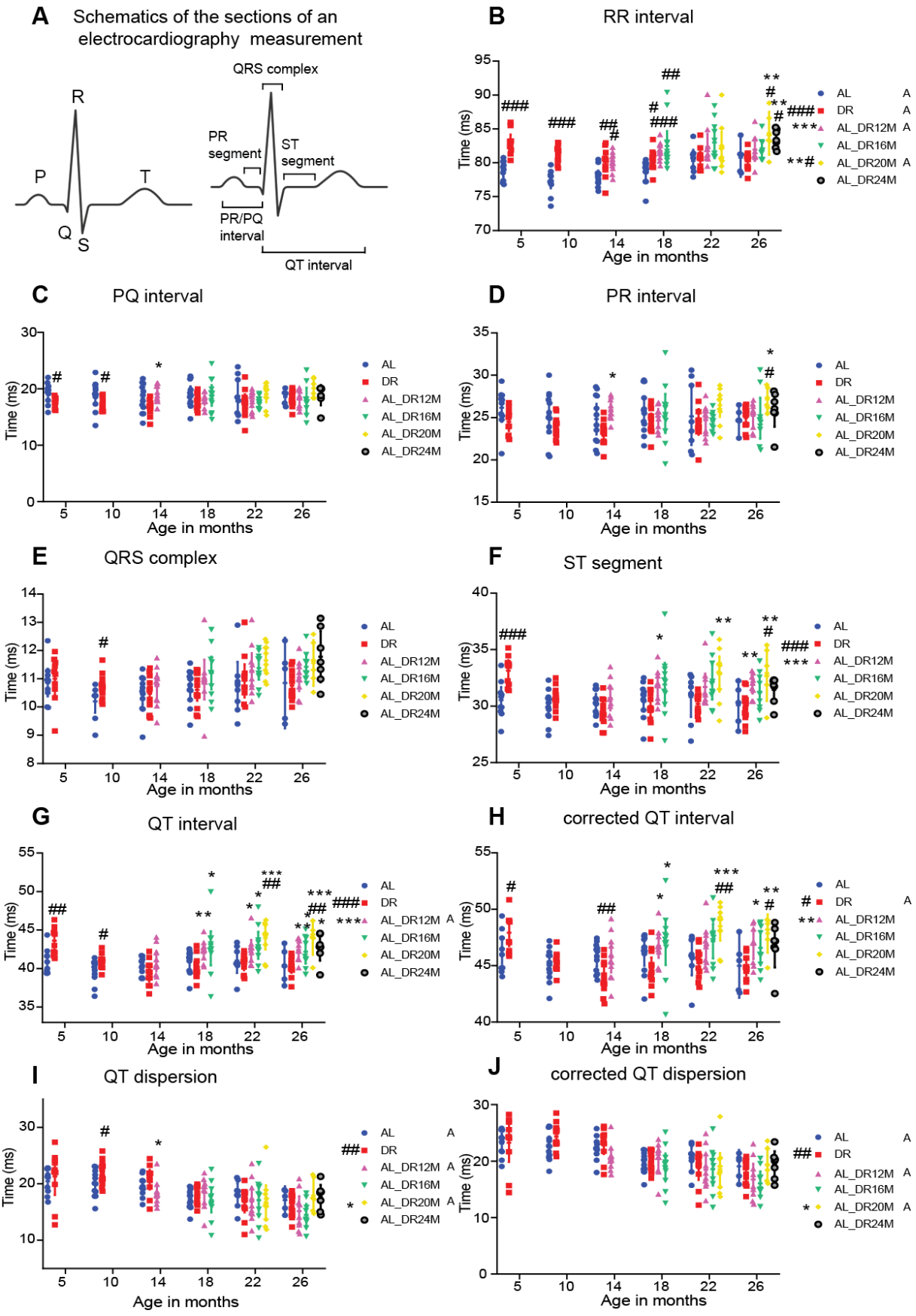

Figure 3.2. 26**: **DR reduces the duration of the RR interval and the ventricular de- and repolarization

A *Schematic representation of the sections of a heartbeat. Depicted are two typical heartbeats recorded via electrography with labelled waves and intervals during a heartbeat. P depicts the P wave during atrial depolarization, whereas Q depicts the Q grove following the depolarization of the intraventricular septum. R corresponds to depolarization of the apex and the lateral walls of the ventricles and S to the depolarization of the ventricle base. T indicates the T wave and ventricular repolarization as the last event during a single heartbeat before a new cycle starts. In addition, the ECG is subdivided into seven different segments. The RR interval describes the time between two ECG peaks and corresponds to the duration between two heartbeats. The PQ or PR interval indicate how fast the action potential is transmitted from the atria to the ventricles, indicating the required time between atrial and intraventricular depolarization, which determines the pace of the heart rate (Toman et al., 2020). The QRS complex indicates the conduction time and depolarization of the right and left ventricles. The ST segment defines the end of ventricular de- and the beginning of the repolarization (Atar & Birnbaum, 2005). The QT interval corresponds to the entire time between ventricular de- and repolarization (Locati et al., 2017), while the QTc interval is the QT interval corrected for the heart rate. The QT dispersion is the uncorrected difference between the longest and shortest QT intervals in a 12-lead ECG (Algra et al., 1985), while the QTc dispersion is corrected for the heart rate (Sahu et al., 2000).* ***B)*** *Longitudinal assessment of the RR interval.* ***C)*** *Longitudinal assessment of the PQ interval.* ***D)*** *Longitudinal assessment of the PR interval.* ***E)*** *Longitudinal assessment of the QRS complex duration.* ***F)*** *Longitudinal assessment of the ST segment.* ***G)*** *Longitudinal assessment of the QT interval.* ***H)*** *Longitudinal assessment of the corrected QT interval* ***I)*** *Longitudinal assessment of the QT dispersion.* ***J)*** *Longitudinal assessment of the corrected QT dispersion. The animal numbers for the complex, segment, dispersion or interval duration of chronic AL and DR were the following for all evaluated ECG parameters: 5M AL n= 10, DR n= 10 and at 10M AL n= 12, DR n= 12. The animals numbers for all evaluated ECG parameters were the following: at 14M: AL n= 12, DR n= 12, AL_DR12M n= 10. At 18M: AL n= 12, DR n= 12, AL_DR12M n= 11, AL_DR16M n= 12. At 22M: AL n= 8, DR n= 10, AL_DR12M n= 10, AL_DR16M n= 10, AL_DR20M n= 10. At 26M: AL n= 5, DR n= 12, AL_DR12M n= 9, AL_DR16M n= 9, AL_DR20M n= 6, AL_DR24M n=7. Unpaired t tests were implemented to evaluate statistical differences between chronic controls at all tested time points. One-way ANOVA followed by Bonferroni correction was performed to assess statistical differences in the ECG intervals between AL, DR and one DR switch group at a time at each time point. GLME analyses followed by Bonferroni post-hoc tests were implemented to calculate intra- and inter-group differences in ECG parameters across all six time points. Animal with less than 100 recorded signals were excluded from the analyses. Data are plotted as mean with 95% CI. Statistically significant differences in relation to AL are presented as following # p<0.05, ## p< 0.01 and ### p<0.001. Statistically significant differences in relation to DR are presented as following * p<0.05, ** p< 0.01 and *** p<0.001. Differences that did not reach statistical significance were not marked. Carolina Monzó conducted the GLME analyses and schematics were created with BioRender.com.*

3.3 DR has no impact on *in vitro* stem cell function and regenerative capacities of the WAT and the small intestine at old age

3.3.1 The WAT of aged chronic DR mice contains more adipose tissue stem cells

The WAT is a heterogeneous tissue, which is composed of different cell types including mature adipocytes, adipose tissue stem cells (ATSC) and different immune cells. Since obesity changes WAT composition and is associated with increased inflammation (Fuster et al., 2016), we aimed to investigate whether onset of DR later in life can reverse changes in WAT cell type composition caused by previous AL feeding.

To this end, we isolated stromal vascular fraction cells (SVF) from the WAT of 27M old AL, DR, AL_DR12M, AL_DR16M and AL_DR20M mice by collagenase digestion and FACS sorted the cells based on different antibody combinations Fig. 3.3.1A) proposed by Church and colleagues (Church et al., 2014). To lower sample size, we excluded AL_DR24M mice from this and future experiments as their WAT does not adapt to DR anymore and the lifespan of AL_DR24M is similar to AL_DR20M. First, we assessed the percentage of live and dead cells from the isolated SVF, to check if the diet group influenced the proportion of live cells during the isolation, however no significant differences were found (Fig. 3.3.1B). Next, we investigated the percentages of lineage-committed cells in the alive population. We identified a trend towards reduced immune cells and increased lineage factor negative cells in the WAT of chronic DR animals but no significant differences in CD31 positive, CD45 positive or lineage factor negative cell were detected (Fig. 3.3.1C). Interestingly, we observed the opposite trend of increased immune cell and reduced lineage factor negative cell populations in AL_DR20M animals (Fig. 3.3.1C). Therefore, to further investigate the immune cell population, we included F4/80 in our antibody panel to evaluate the percentage of macrophages in the WAT. Unexpectantly, AL_DR16M and AL_DR20M exhibited the lowest macrophage percentage in the WAT, in contrast to AL, chronic DR and AL_DR12M, which displayed more macrophages in similar percentages (Fig. 3.3.1D). Moreover, the percentage of macrophage numbers were significantly increased in chronic DR compared to AL_DR16M (Fig. 3.3.1D). Lastly, we investigated the percentage of committed progenitors, progenitor cell as well as ATSC in the WAT. While no significant differences were observed in the percentage of committed progenitors between all five diet groups, we observed a trend towards an increased progenitor

cell population in chronic DR compared to AL (Fig.3.3.1E). Interestingly, the progenitor cell population showed a trend towards decreased numbers depending on the age of DR onset and was significantly reduced in AL_DR20M compared to chronic DR (Fig. 3.3.1E). Furthermore, the percentage of ATSCs was significantly increased in chronic DR compared to chronic AL, AL_DR16M and AL_DR20M and there seems to be a trend towards increased ATSC numbers in AL_DR12M animals (Fig. 3.3.1E). However, none of the DR switch groups exhibited significantly different cell percentage compared to AL feeding for all tested cell populations (Fig. 3.3.1C-E). Thus, our data suggest that lifelong DR alters the cell type composition of the SVF in the WAT in C3B6F1 females and increased ATSC numbers compared to chronic AL. In addition, mid-or late-life onset DR cannot reverse the detrimental effects of previous AL feeding on ATSC numbers.

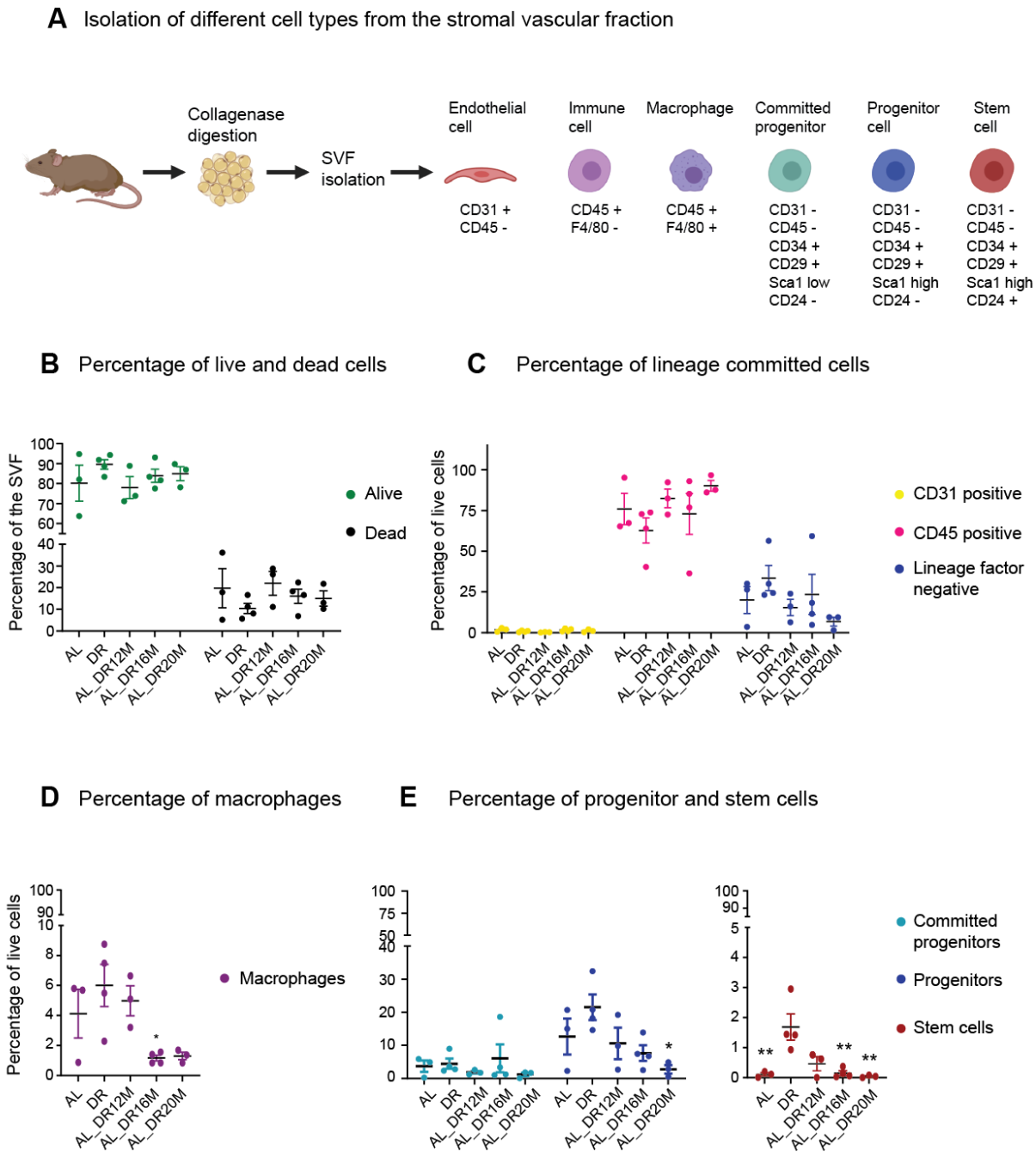

Figure 3.3. 1*: *The WAT of aged chronic DR exhibits a similar cell type composition compared to chronic AL and DR switch groups but has more adipose tissue stem cells

*__A__ schematic representation of the isolation of stromal vascular fraction (SVF) from WAT and cell type classification based on antibody combinations for cell sorting. __A__ Percentage of alive and dead cells in the isolated SVF of 27M old chronic controls and DR switch groups. Percentage of __B__ lineage committed and lineage factor negative cells, of __D__ macrophages or of __E__ progenitor and stem cell populations. Both WAT depots of three AL, AL_DR12M and AL_DR20M and four chronic DR and AL_DR16M mice were utilized. One-way ANOVA followed by Bonferroni multiple correction testing were conducted to evaluate differences in cell type composition between diet groups with * p< 0.05, ** p<0.01 and *** p<0.001 in relation to DR and # p< 0.05, ## p<0.01 and ### p<0.001 in relation to AL. Data are plotted as mean ± SEM.*

3.3.2 Early or late-life DR does not affect the differentiation potential of cultured primary adipocyte progenitor cells

Given that we identified more ATSCs and a trend towards reduced immune cell infiltration in the WAT of chronic DR animals, we next asked if the stem and progenitor population of chronic DR mice exhibit increased differentiation potential into mature adipocytes compared to chronic AL or the DR switch groups. To this end, we isolated and cultured the stromal vascular fraction (SVF) containing adipocyte stem cells and progenitor populations from the WAT of AL, DR, AL_DR12M, AL_DR16M or AL_DR20M mice aged 27M. To assess the differentiation potential of the stem and progenitor cells, we induced differentiation into adipocytes with differentiation medium or kept cells on maintenance medium to investigate spontaneous differentiation. Then, we fixed cells and conducted an Oil Red O staining (ORO) to determine the amount of lipophilic dye incorporated into newly formed lipid droplets as a readout for differentiation (Fig. 3.3.2A). We observed an increased incorporation of ORO in cells treated with differentiation medium compared to control cells irrespective of the diet group the cells were isolated from (Fig. 3.3.2B). In order to quantify the differences, we extracted the incorporated dye using isopropanol and measured the amount of extracted ORO using a standard curve. While we saw significantly more ORO incorporation in the induced cells compared to un-induced cells, no differences between diet groups were observed (Fig. 3.3.2C). Thus, DR irrespective of the age of onset does not improve the differentiation potential of *in vitro* cultured SVF cells compared to lifelong AL feeding.

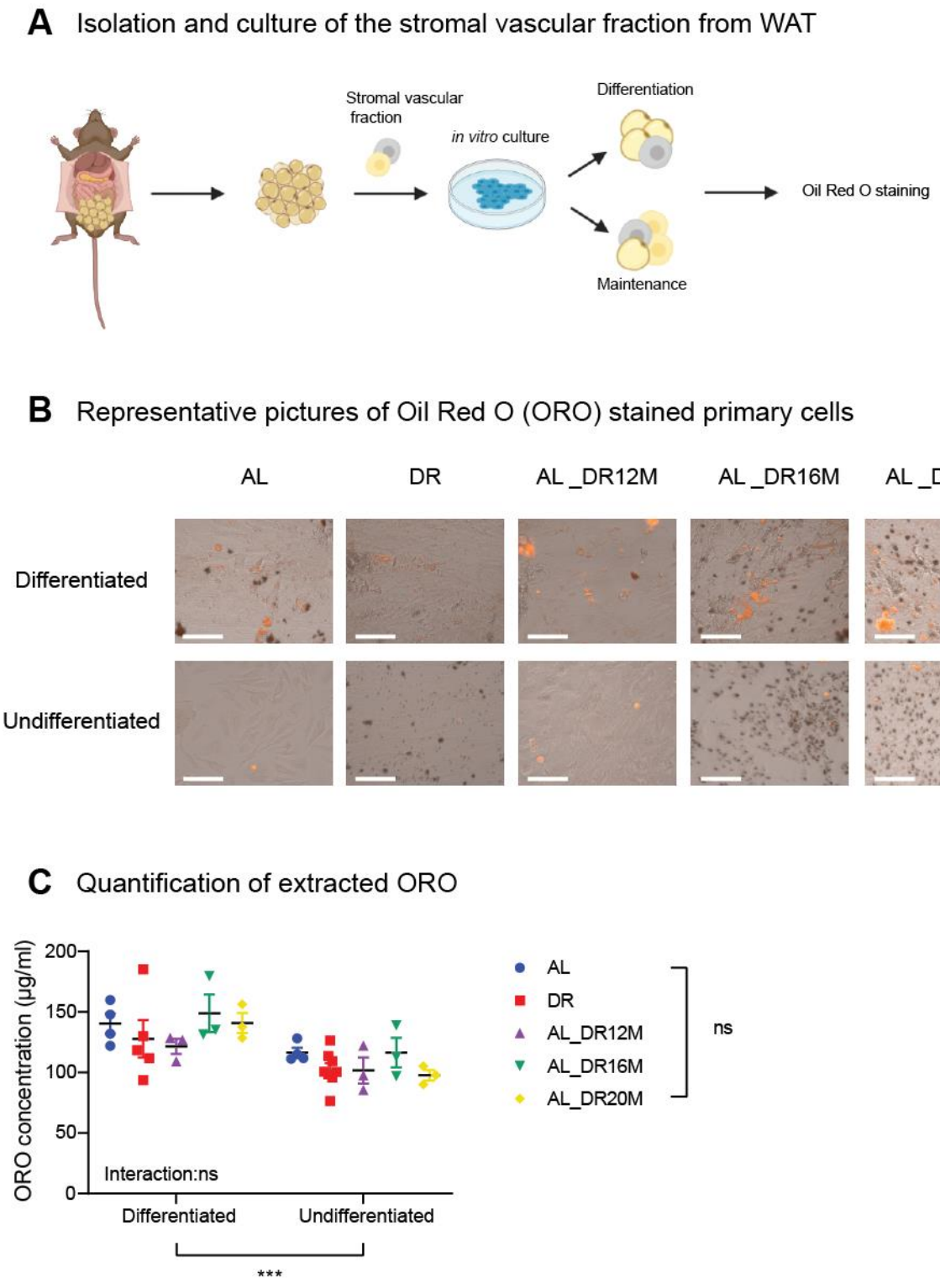

Figure 3.3. 2: Early or late-life DR does not affect the differentiation potential of cultured primary adipocyte progenitor cells

A *Schematic overview on the isolation and culture of stromal vascular fraction (SVF) cells from WAT of chronic AL (n=4), DR (n=8) or DR onset at 12M (n=3), 16M (n=3) or 20M (n=3) aged 27M. SVF cells were differentiated or kept on maintenance medium for 12 days followed by fixation and Oil Red O (ORO) staining.* ***B*** *Representative images of differentiated or undifferentiated primary SVF cells acquired at 40x magnification. Red dots represent incorporated ORO stain in lipid droplets of differentiated*

primary adipocytes. Differentiated and non-differentiated conditions were obtained for all replicates AL and DR switch groups. For chronic DR cultures, only five replicates could be utilized for both differentiation and non-differentiation and three cultures served as non-differentiated controls only. ***C*** *Quantification of extracted ORO stain from primary cells. Differentiated cells incorporated more lipophilic ORO stain than undifferentiated control cells irrespective of the diet group from which they were isolated. Scale bars correspond to 75µm. Data are plotted as mean with SEM and were analysed using Two-way ANOVA followed by Bonferroni multiple testing correction with *** p<0.001 in relation to medium treatment. The schematic created using BioRender.com.*

3.3.3 DR might affect Paneth cell health but not tight junction integrity in 20M old jejunum

Studies have demonstrated that intestinal length steadily increases from infancy until adulthood (Weaver et al., 1991). However, the intestine is a plastic organ and can change the percentage of cell types, the villi length as well as the intestinal length itself in response to different stimuli such as pregnancy or nutrition (Nilaweera & Speakman, 2018; Sarvestani et al., 2015). Furthermore, abundant nutrient availability and overfeeding as seen in obesity have also been shown to influence intestinal plasticity and lead to an increased intestinal length associated with an expansion of enterocytes and a decrease in enteroendocrine cells (Al Mushref & Srinivasan, 2013; Dailey, 2014). In contrast, short-term DR was previously reported to reduce mTORC1 signalling in Paneth cells, thus leading to improved stem cell function under DR (Yilmaz et al., 2012). Paneth cells harbour secretory granules, which contain antimicrobial peptides, such as α-defensin (Bevins & Salzman, 2011). Dysfunctional Paneth cells exhibit abnormal secretory granules, such as hypodense or crinophagic granules, which are commonly observed in patients with Crohn's disease (Cadwell et al., 2008; Thachil et al., 2012). Furthermore, intestinal stem cell (ISC) numbers are increased upon DR (Igarashi & Guarente, 2016) and additionally, DR improved intestinal integrity in a human study of short-term DR in obese women (Ott et al., 2017), demonstrating that a short dietary intervention has beneficial effects on gut barrier function as well as ICS and Paneth cells across species. However, much less is known about the effect of long-term DR on intestinal health and integrity. Therefore, we investigated gut barrier function and Paneth cell health by electron microscopy (EM) in 20M old intestine of chronic AL and DR animals and in mice that were treated for eight (AL_DR12M) or four months (AL_DR16M) with DR, respectively. We selected the second intestinal region (jejunum) for our EM analysis, as it is the main digestion or absorption site for various trace elements (Kiela & Ghishan, 2016), amino acids (Curtis et al., 1978; Mitchell & Levin, 1981) and carbohydrates (Ferraris et al., 1993).

EM on tight junctions between the enterocytes in the intestinal villi showed no significant difference in electron dense (grade I or II) and electron light (grade III) tight junctions between AL, DR or AL_DR12M and AL_DR16M (Fig.3.3.3A), which suggests that long-or short-term DR had no impact on intestinal tight junction integrity. We next evaluated Paneth cell morphology as a readout for intestinal. Therefore, we scored hypodense granules based on the presence of an empty halo-like structure around the black granules. Additionally, we assessed the number of crinophagic secretory granules, which were fused with autophagosomes or lysosomes and thus targeted for degradation. Strikingly, chronic DR and AL_DR12M but not AL_DR16M exhibited significantly fewer hypodense Paneth cell granules compared to chronic AL (Fig. 3.3.3B). Correspondingly, we also detected a non-significant trend towards reduced crinophagic granules in chronic DR and AL_DR12M (Fig. 3.3.3C), indicating that 3M or 12M onset of DR could have a protective effect on Paneth cells, whereas AL_DR16M displayed an in-between phenotype. To investigate whether chronic or mid-life onset short-term DR affected intestinal length in response to reduced food intake, we measured the colon and rectum length as a proxy for intestinal plasticity. Interestingly, chronic DR mice exhibited a significantly shorter colon length compared to chronic AL (Fig. 3.3.3C). In contrast, neither AL_DR12M nor AL_DR16M exhibited colon shortening after eight or four months of DR respectively (Fig.3.3.3C), suggesting that the colon required longer time to adapt to the new dietary regimen.

These results indicate that long-or short-term DR initiated chronically or at middle age could have a beneficial effect on Paneth cell health but only chronic DR affects colon plasticity.

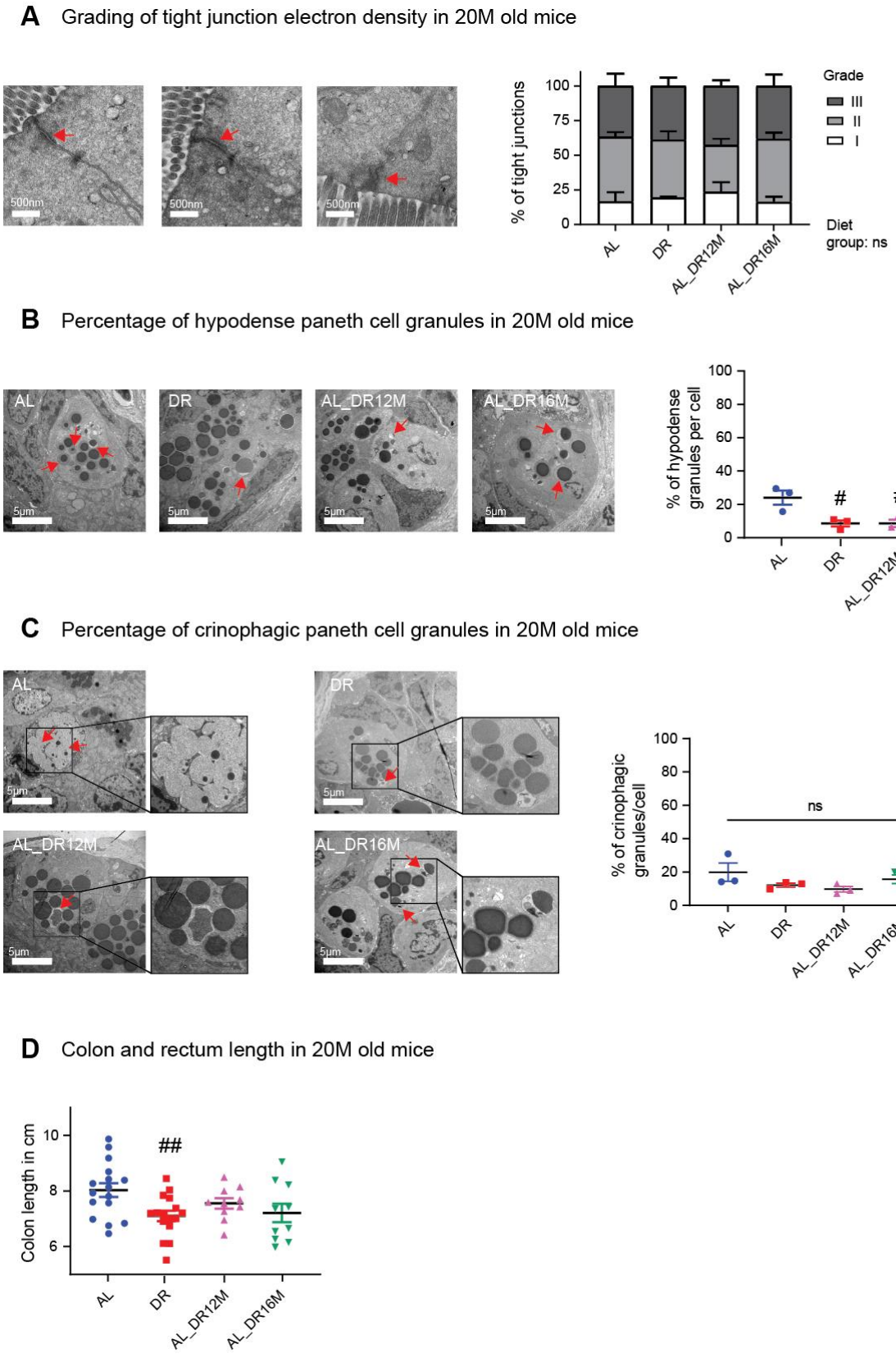

Figure 3.3. 3: DR might affect Paneth cell health but not tight junction integrity in 20M old jejunum

*Electron microscopy (EM) of **A** tight junction integrity, **B** hypodense or **C** autophagy-activated crinophagic Paneth cell granules in 20M old jejunum of AL, DR, AL_DR12M and AL_DR16M mice (n=3 for all groups). Tight junctions were classified based on electron density as grade I with the highest*

electron density, as grade II with reduced electron density or as grade III with the lowest electron density. ***B*** *Paneth cell granules were graded based on the presence or absence of a white halo around the granules as hypodense or normal respectively. Chronic DR (p=0.0285) and AL_DR12M (p=0.0328) but not AL_DR16M (p=0.7249) had significantly fewer hypodense Paneth cell granules compared to chronic AL. No significant difference were detected between chronic DR and AL_DR12M (p=0.9919) or DR and AL_DR16M (0.2780).* ***C*** *Fusion of Paneth cell granules with autosomes or lysosomes and total loss of structural integrity were graded as crinophagic granules. No significant differences were detected between chronic AL and DR (p=0.2383), AL_DR12M (p=0.1494) or AL_DR16M (p=0.5239). Chronic DR were not significantly different compared to AL_DR12M (p=0.2947) or AL_DR16M (p=0.2874).* ***D*** *colon and rectum length in cm of 20M old chronic controls (both n=16), AL_DR12M (n=10) and AL_DR16M (n=10). Chronic DR mice had significantly shorter large intestines than chronic AL (adj. p= 0.0058), whereas no significant differences were observed between chronic AL and AL_DR12M (adj. p= 0.1859) or AL_DR16M (adj. p=0.0574) as well as chronic DR and AL_DR12M (adj. p=0.1222) or AL_DR16M (adj. p=0.7682). Data are plotted as mean with SEM and were analysed using unpaired Student t tests to calculate statistical differences between diet groups. P value p>0.05 indicated not significant (ns) differences in relation to chronic AL or DR. Significant differences were depicted as #p<0.05 and ##p<0.01 in relation to AL.*

3.3.4 Short-term, late-onset DR at 20M reduces numbers of hypodense Paneth cell granules in the jejunum of 27M old mice compared to chronic AL feeding

Since we did not detect any significant differences in Paneth cell health and tight junction integrity at 20M of age, we asked whether functional decline of the small intestine occurred later in murine life and if we could detect differences between diet groups at a later time point. To this end, we generated additional EM samples of chronic controls and DR switch groups aged 27M to investigate the effect of DR on intestinal health at old age.

We observed a trend towards more grade I tight junctions in chronic as well as 12M and 20M onset DR (Fig. 3.3.4A) however; these differences were not statistically significant, indicating that DR did not improve tight junction integrity at old age, consistent with our previous results at 20M. Chronic and mid-life onset DR exhibited a non-significant trend towards fewer hypodense granules compared to chronic AL feeding (Fig. 3.3.4B). Strikingly, AL_DR20M paneth cells had significantly fewer hypodense granules compared to chronic AL (Fig. 3.3.4B), suggesting that late-onset DR does improve Paneth cell health irrespectively of longer AL feeding prior to the switch. In contrast, the percentage of crinophagic granules was not significantly different between diet groups (Fig. 3.3.4C), which suggests that autophagic removal of damaged Paneth cell granules was not influenced by chronic or late-onset DR.

Next, we evaluated whether longer duration of DR feeding affected intestinal plasticity in the large intestine. Similar to our previous results on 20M old mice, chronic DR animals exhibited significantly shorter large intestines compared to chronic AL (Fig. 3.3.4D), suggesting that this phenotype is stable during ageing. Strikingly, long-term mid-onset and short-term late-onset DR reduced colon- rectum length, indicating that initiation of DR as late as 20M could promote intestinal plasticity. Interestingly,

Thus, DR impacts on Paneth cell health but not on tight junction integrity at 20M and 27M of age compared to AL feeding, indicating improved intestinal health during ageing.

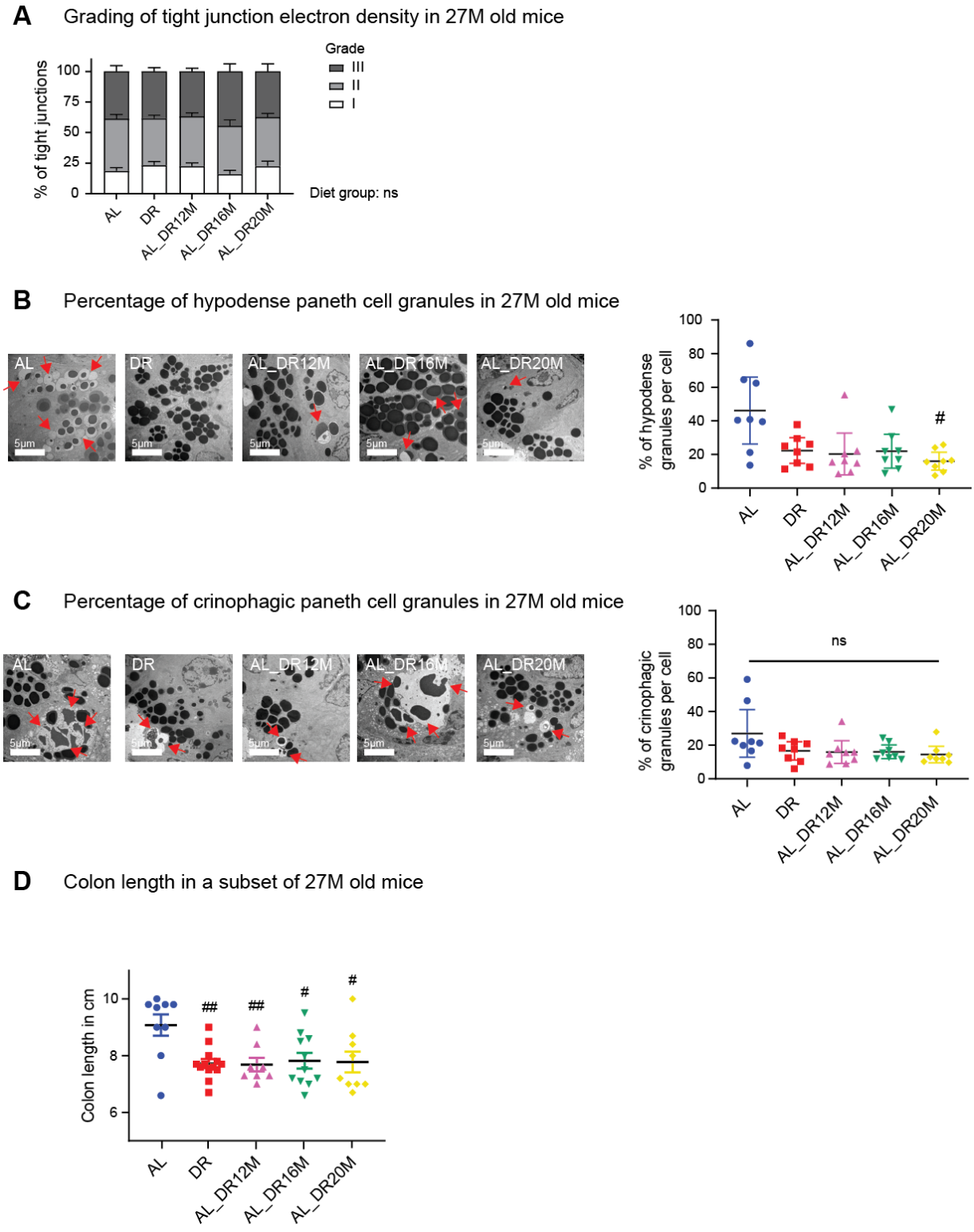

Figure 3.3. 4: Short-term, late-onset DR at 20M reduces numbers of hypodense Paneth cell granules in the jejunum of 27M old mice compared to chronic AL feeding

*Electron microscopy (EM) of **A** tight junction integrity, **B** hypodense or **C** autophagy-activated crinophagic Paneth cell granules in 27M old jejunum samples of AL, DR, AL_DR12M, AL_DR16M and AL_DR20M mice (all n=8, except n=9 for chronic AL). Tight junctions were classified based on electron density as grade I with the highest electron density, as grade II with reduced electron density or as grade III with the lowest electron density. Paneth cell granules were graded based on the presence or absence*

of a white halo around the granules as hypodense or normal respectively. Crinophagic granules were determined as Paneth cell granules which were fused with autophagosomes or lysosomes. Data are plotted as mean with SEM and were analysed using linear mixed models with covariate correction for cohort, followed by Bonferroni multiple testing correction. ***D*** *colon and rectum length in cm in a subset of 27M old chronic AL (n=9), DR (n=13), AL_DR12M (n=8), AL_DR16M (n=11) and AL_DR20M (n=9). Chronic AL mice had significantly longer large intestines compared to chronic DR (p=0.0013), AL_DR12M (p=0.0083), AL_DR16M (p=0.0129) or AL_DR20M (p=0.0242). Large intestines between chronic DR and AL_DR12M (p=0.8980), AL_DR16M (p=0.7593) or AL_DR20M (p=0.8791) were not different. Differences in large intestine length were analysed using unpaired Student t tests between diet groups. Data are plotted as mean with SEM and p value p>0.05 indicated not significant (ns) differences in relation to chronic AL or DR. Significant differences were depicted as #p<0.05 and ##p<0.01 in relation to AL.*

3.3.5 Intestinal organoids of DR switch mice exhibit reduced outgrowth capacity compared to chronic AL or DR

In the recent years, organoids have gained much popularity due to their potential as in *vitro* model organs to study the effect of diseases, mutations or drugs in a miniature setting or for personalized medicine (Grassi et al., 2019; Kim et al., 2020). Organoids are 3D miniature organs, which can be grown from adult tissue and not only recapitulate the structure of the tissue of origin but also exhibit certain basic tissue functions (Yin et al., 2016). Therefore, there is an emerging interest to utilize organoids to study the effects of ageing in a 3D cell-culture based system on various different organs, for example in the liver or the small intestine (Hu et al., 2018). In particular, intestinal organoids established from isolated crypts can be used to assess the outgrowth and regeneration potential as an indirect readout for intestinal stem cell (ISC) activity. Given that the intestinal epithelium is one of the fastest renewing murine tissue (Krndija et al., 2019) and that we detected hints towards improved Paneth cell function upon DR, we asked whether stem cell activity, as measured by organoid outgrowth, would also be affected by the late-life DR switches. Therefore, we isolated crypts from the jejunum section of the small intestine of AL, DR, AL_DR12M, AL_DR16M and AL_DR20M mice aged 27M and cultured them *in vitro*. First, we assessed the potential to form organoids from isolated crypts. Within days after the culture was initiated, isolated crypts of all diet groups formed organoids, thus demonstrating that aged intestinal crypts were able to form organoids independently of the diet group they were isolated from (Fig.3.3.5A). Next, we asked whether we can detect a difference in organoid outgrowth capacity (budding) depending on the diet group. We therefore counted the number of newly formed buds per organoid after five and seven days of culture and compared the average number of buds between diet groups. Interestingly, we observed a

non-significant trend towards increased outgrowth capacity of chronic DR organoids at five and seven days, whereas organoids from the DR switches exhibited a similar outgrowth compared to chronic AL organoids (Fig. 3.3.5C). Next, we asked whether we can detect significant differences in budding after organoids were dissociated and passaged as a readout for the regeneration capacity. We included additional measurements at day three and day ten, to obtain further results on budding after short-term and long-term culture. Similar to the results from the initial crypt culture (Fig.3.3.5A), all diet groups were able to regrow organoids after complete dissociation (Fig.3.3.5B). Moreover, at day 10 post-dissociation, no significant differences were identified between chronic AL and DR organoids. In contrast, we detected a significant decrease in buds per organoid in all DR switch groups compared to chronic DR and a decrease between AL_DR20M and chronic AL (Fig.3.3.5D). Interestingly, this decrease in buds per organoid seemed to correlate with the age of DR onset as AL_DR12M displayed on average more outgrowth potential than AL_DR20M.

Thus, organoid cultures can be established both from freshly isolated crypts as well as from passed organoids of 27M old AL, DR as well as 12M, 16M or 20M onset DR jejunum. However, the regeneration capacity after passaging is decreased in mid-and late-life DR switches compared to chronic controls, suggesting that organoids of DR groups have no memory of prior DR feeding when brought into culture.

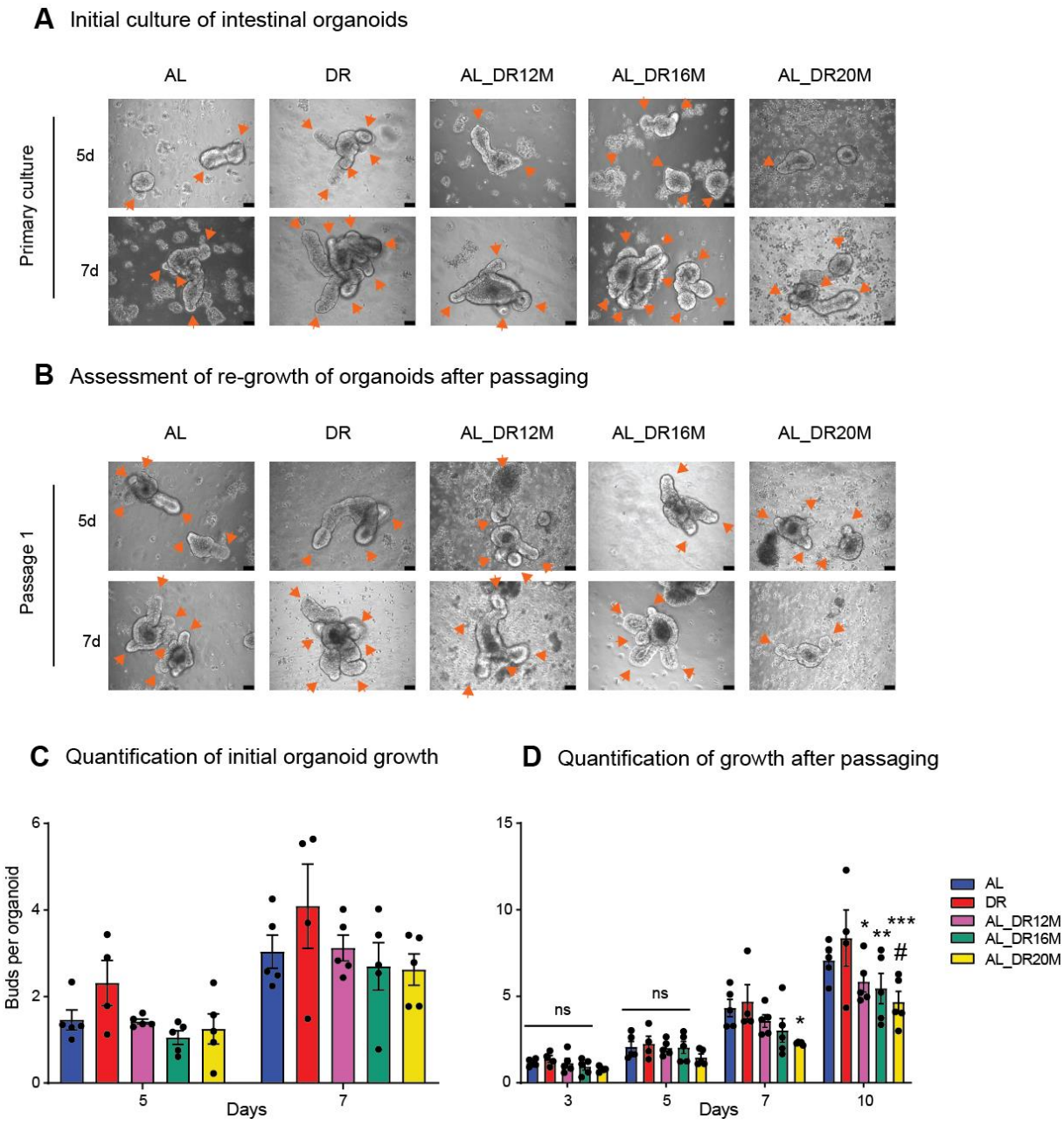

Figure 3.3. 5: Intestinal organoids of DR switch mice exhibit reduced outgrowth capacity compared to chronic AL or DR

*Representative images of **A** the primary culture of isolated crypts or **B** passaged organoids from the jejunum region of the small intestine of 27M old AL, DR, AL_DR12M, AL_DR16M or AL_DR20M mice (all n=5, except chronic DR n=4). Images were acquired on day five and day seven. New outgrowths (buds) are labelled with orange arrows. Quantification of newly formed buds from **C** initial organoid culture or **D** from passaged organoids at day five and seven or day three, five, seven and ten respectively. Outgrowths per organoid were counted for at least 15 organoids and averaged buds per organoid were calculated. Data were plotted as mean with SEM. Two-way ANOVA and Bonferroni multiple testing correction were implemented to assess statistical differences with p values depicted as *p<0.05, **p<0.01 and p<0.001 in relation to DR and as # p<0.05 in relation to AL.*

3.3.6 AL organoids display more proliferating but not more Paneth cells compared to DR switch groups

We have previously demonstrated that organoids established from jejunum crypts of chronic AL or DR mice displayed increased outgrowth and regeneration capacity compared to DR switch groups (Fig.3.3.5C and D). To investigate if increased Paneth cell numbers or more proliferating cells were responsible for the growth differences between chronic controls and DR switch groups, we conducted IF staining against lysozyme and Ki67 in cultured organoids and counted the number of brightly stained cells. While we observed a trend towards increased Paneth cell numbers in the organoids established from chronic DR and DR switch groups compared to AL, statistical analyses did not reveal any significant difference (Fig.3.3.5A). In contrast, we observed the opposite trend for Ki67 bright cells (Fig.3.3.5B). Organoids of chronic AL mice showed more cells with bright Ki67 staining compared to AL_DR12M and AL_DR16M, indicating that the observed differences in outgrowth were due to differences in the number of proliferating cells and not Paneth cells between diet groups.

To conclude this section, we have shown that the composition of the aged WAT is markedly different between chronic DR, AL and DR switch groups. In particular, chronic DR WAT exhibits more ATSCs and macrophages, whereas the percentage of immune cells is reduced. However, *in vitro* culture of isolated SVF cells revealed no significant differences in adipocyte differentiation between diet groups. Similarly, we did not detect differences in stem cell function in the small intestine, as isolated crypts of all diet groups were able to form organoids. However, organoid regrowth capacity was increased in chronic controls but not DR switch groups and was associated with more dividing cells in chronic AL organoids but not with supporting Paneth cells contrasting improved Paneth cell health identified by EM. In summary, the results indicate that previous long-term AL feeding has a major impact on both the small intestine and the WAT. The WAT seems to have a memory of previous AL and the WAT cell type composition remains very similar to chronic AL even after up to 15 months of DR, indicating that DR cannot reverse WAT heterogeneity imposed by prolonged AL feeding. Interestingly, while we observed reduced hypodense granules in DR switch groups compared to chronic AL, suggesting increased Paneth cell health upon DR, the regenerative capacity of intestinal organoids was not improved. This could point to a dual effect of DR on Paneth cells with improved secretory but reduced ISC-supportive function and regenerative capacity. Thus, adipose tissue or intestinal stem cell potential and regeneration play only a minor role in the lifespan extension under 12M or 16M onset DR.

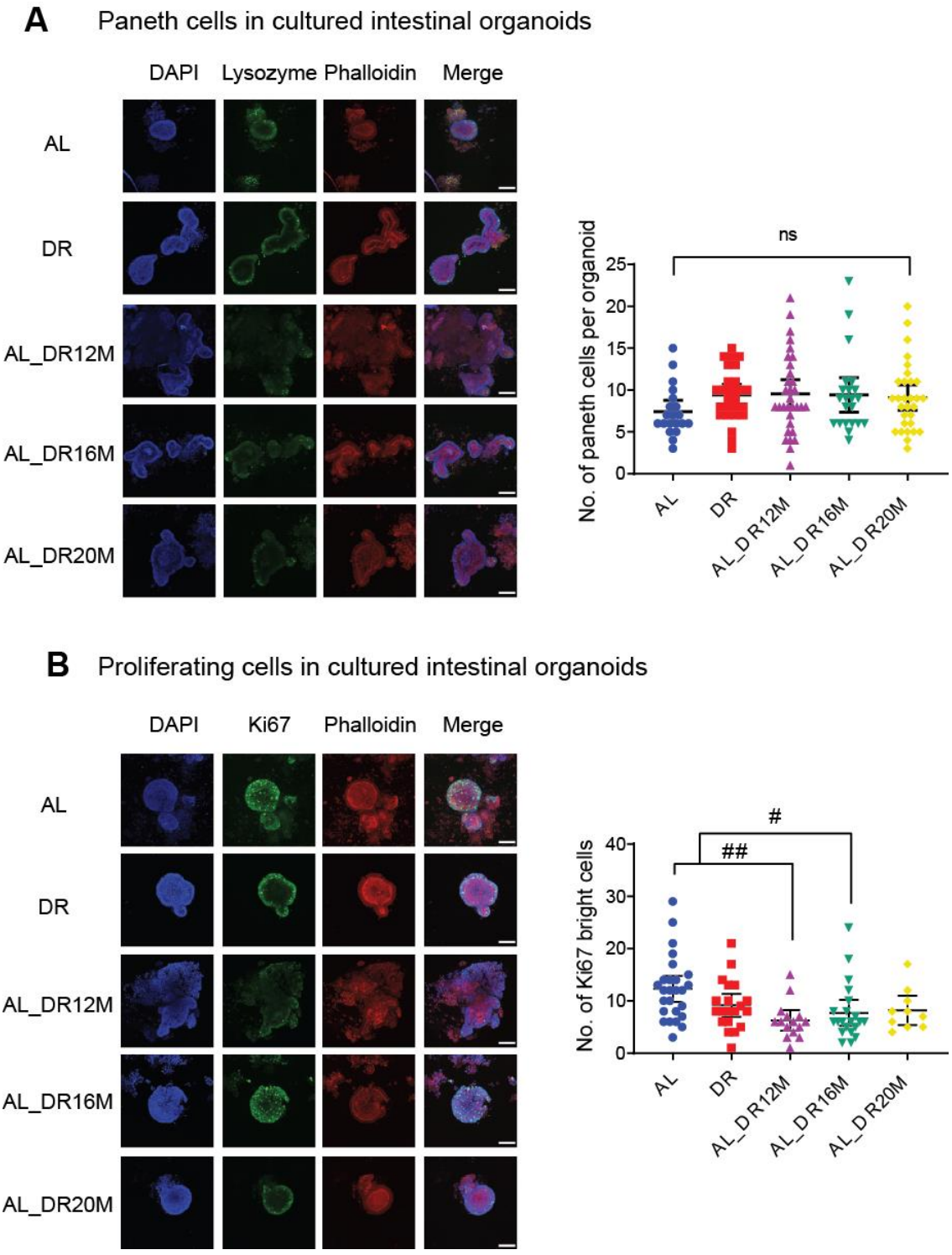

Figure 3.3. 6: AL organoids display more proliferating but not more Paneth cells compared to DR switch groups

*Representative images and quantification of **A** lysozyme or **B** Ki67 stained organoids of AL, DR, AL_DR12M, AL_DR16M and AL_DR20M mice. DAPI (blue) and rhodamine-phalloidin (red) staining were utilized to mark the nuclei as well as the cytoskeleton and to visualize the location of Ki67 or lysozyme positive cells (green). White scale bars correspond to 100µm. Data were plotted as mean with SEM. One-way ANOVA and Bonferroni multiple testing correction were implemented to assess statistical differences with p values depicted as # p<0.05 and ## p<0.01 in relation to AL.*

3.4 DR irrespective of the age of onset affects WAT morphology and integrity

3.4.1 DR switch groups exhibit similar small adipocyte sizes within four months post-switch to DR as chronic DR mice, whereas AL adipocytes decline during ageing

Since chronic AL exhibited significantly higher body weight as well as fat mass and were insulin resistant as early as 10M of age, we first assessed adipose tissue morphology from tissue dissected at young (5M), middle-aged (16M) or old (20M and 24M) age. To this end, we generated WAT-specific tissue microarrays (TMA). TMAs allowed the simultaneous processing of WAT samples from chronic AL, DR as well as 12M, 16M and 20M onset DR mice aged 5M to 24M on the same slides. Samples of 5M old AL and DR animals were used to enable comparisons of WAT morphology during ageing. Tissue samples of DR switch groups were first sampled four months post-switch. Tissue cores of fixated and paraffin embedded WAT were taken from each animal and inserted in empty holes on two acceptor paraffin TMA blocks. WAT cores were randomly allocated on the two TMAs, sectioned and stained using histological stainings or immunohistochemistry (Fig. 3.4.1A).

Given that DR resulted in significantly reduced adipocyte size in the WAT of young, middle-aged or old male mice (Miller et al., 2017), we first conducted histological stainings to assess the general morphology of the WAT of chronic AL or DR controls during ageing. Hematoxylin Eosin (HE) stainings of young, middle-aged and old AL or DR WAT indicated that adipocytes of DR animals were smaller compared to their chronic AL counterparts at all tested time points (Fig. 3.4.1B). Therefore, we implemented image analysis to measure the adipocyte sizes in μm^2 in order to calculate the average fat cell size of AL or DR mice. Image analysis confirmed that even two months after DR was initiated, chronic DR mice exhibited significantly reduced adipocyte size young, middle-aged and old age compared to AL feeding (Fig. 3.4.1C). Interestingly, the adipocyte size of DR mice remained stable throughout life contrasting AL adipocytes, which exhibited a significant age-related decrease in size (Fig. 3.4.1C). This suggested that the WAT of chronic DR mice already adapted to the dietary regimen within two months after DR was initiated and that the distinct DR morphology was retained during ageing. In contrast, the WAT of chronic AL mice was subjected to age-related tissue remodelling and showed a decline in adipocyte size when mice age.

We next assessed WAT morphology of AL_DR12M, AL_DR16M and AL_DR20M animals at 16M, 20M and 24M of age (Fig. 3.4.1A-C) using HE stainings. Within four months post-switch, adipocyte sizes of AL_DR12M, AL_DR16M and AL_DR20M mice were comparable to the size of chronic DR animals (Fig. 3.4.1 B and C). Moreover, the adipocyte size of AL_DR12M or AL_DR16M animals remained constant after the switch (Fig. 3.4.1C). Interestingly, whereas the size of AL_DR20M adipocytes decreased to a similar level as chronic DR, adipocytes were not significantly smaller compared to chronic AL mice at 24M of age (Fig. 3.4.1B). However, it appears, as if this effect was mainly driven by one AL_DR20M animal, which had significantly bigger adipocytes compared to the other three animals of the same diet group (Fig. 3.4.1C). In contrast, adipocytes of AL_DR12M or AL_DR16M were significantly smaller than AL adipocytes, already at four months post-switch to DR and on all evaluated time points. Given that DR switch animals had comparable body weight, fat mass and adipocyte hypertrophy as AL mice, initiating DR at 12M, 16M and 20M of age lead to an adaptation of the adipocyte size in response to the newly imposed dietary regimen. Since only four AL_DR20M animals were used to assess WAT morphology at 24M, more replicates are required to increase statistical power and to verify if 20M onset of DR is less effective in remodelling the WAT compared to earlier DR switches.

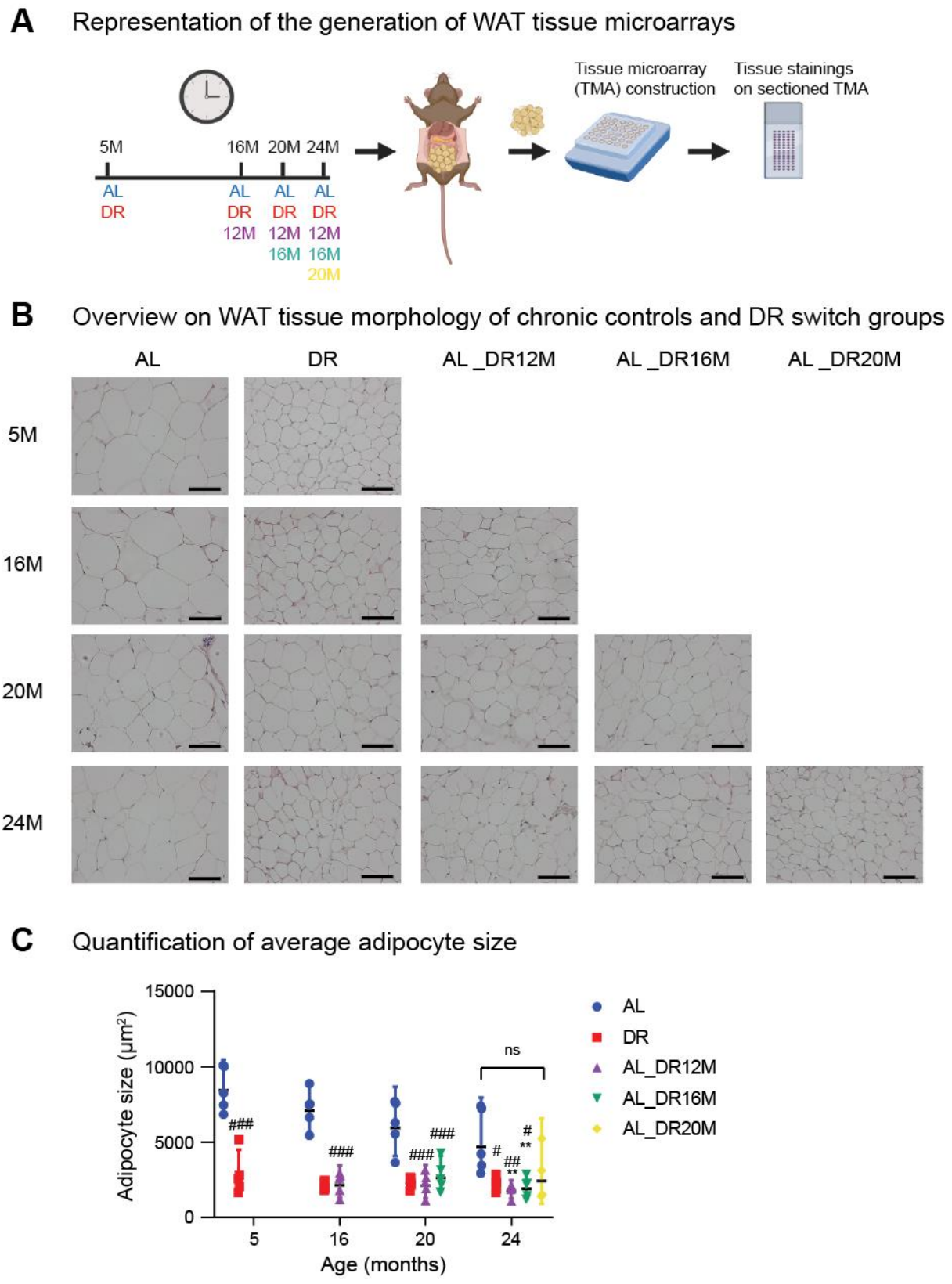

Figure 3.4. 1: DR switch groups exhibit similar small adipocyte sizes within four months post-switch to DR as chronic DR mice, whereas AL adipocytes decline during ageing

A *Generation of white adipose tissue-specific tissue microarrays (TMA) of chronic controls and DR switch groups at 5M, 16M, 20M and 24M of age (n=5 per diet group and time point, except n=4 for*

AL_DR20M at 24M). DR switch groups were first assessed four months post-switch to DR at the respective age. ***B*** *Overview on WAT morphology at 20x magnification of chronic controls and DR switch groups during ageing visualized by HE staining. Scale bars correspond to 100 μm.* ***C*** *Quantification of average adipocyte size in μm^2 of chronic AL, DR during ageing and of DR switch groups at four, eight or twelve months post-switch to DR. Chronic DR regimen maintains smaller adipocyte sizes, whereas AL feeding causes increased adipocyte sizes at all time points. DR switch groups display similarly small adipocyte sizes as chronic DR within four months post-switch to DR and significantly smaller adipocytes compared to chronic AL except AL_DR20M mice at 24M ($p>0.05$). Two-way ANOVA followed by Bonferroni correction for multiple testing were conducted to assess statistical differences between adipocyte sizes of AL or DR animals at 5M, 16M, 20M or 24M. Diet group and age but not the interaction of both factors exhibited statistical significance with a p-value of $p<0.01$ when comparing AL and DR using Two-way ANOVA. One-way ANOVA followed by Bonferroni correction for multiple testing were conducted to assess statistical differences between diet groups at 16M, 20M or 24M. Data are displayed as mean with 95% CI and with p-values ## $p<0.01$ and ### $p< 0.001$ in relation to chronic AL.*

3.4.2 Switching animals to DR increases CLS formation into the WAT four months post-switch, which is reversed upon longer DR duration

Obesity is not only leading to adipocyte hypertrophy but is also associated with increased WAT inflammation and secretion of pro-inflammatory cytokines (Hotamisligil et al, 1993; Weisberg et al., 2003). Moreover, obesity-induced WAT inflammation is characterized by increased infiltration of immune cells, such as macrophages, into the WAT, which surround dying adipocytes and induce local insulin resistance (Makki et al., 2013). Additionally, the recruitment of macrophages into the WAT and the formation of crown-like structures (CLS) around apoptotic adipocytes induces adipocyte clearance and is crucial for tissue remodelling (Odegaard et al., 2007). Recent studies indicate, that short-term DR in male mice reduces WAT inflammation compared to controls (Corrales et al., 2019; Park et al., 2017), however much less is known about the effect of long-term DR on WAT inflammation. As we observed a decreased prevalence of immune cells but increased macrophage abundance in the WAT of aged chronic DR and AL_DR12M but not in AL_DR16M and AL_DR20M (Fig. 3.3.1C and D), we wondered whether chronic or long-term DR treatment could worsen WAT inflammation and increase macrophage infiltration in our model.

To further explore this, we first asked whether we detect differences in WAT inflammation in the WAT of chronic AL or DR during ageing. To this end, we stained WAT of young, middle aged and old mice with a macrophage specific antibody and measured the number of infiltrating macrophages in the WAT, which surround damaged or apoptotic adipocytes and

form so called crown-like structure (CLS) (Cinti et al., 2005). At 5M of age only few, sporadic CLS were observed in AL WAT, whereas CLS levels increased both at 16M and 20M and exhibited the highest occurrence at 24M of age (Fig. 3.4.2A). Strikingly, WAT of chronic DR mice displayed very few CLS at all evaluated time points and there was no age-specific increase in CLS (Fig. 3.4.2A). We next implemented statistical analysis to assess differences in CLS between AL and DR mice. Although we discovered a trend towards higher macrophage infiltration and CLS in AL WAT at 5M, 16M and 20M, statistical significance with a p value below $p<0.05$ was not reached, probably because of the high variability in the AL samples and the low number of replicates analysed (Fig. 3.4.2B). However, we detected significant higher macrophage infiltration and CLS at 24M of age between AL and DR WAT (Fig. 3.4.2B).

We next asked whether onset of DR later in life would also be able to ameliorate WAT inflammation. Surprisingly, we observed an increased incidence of CLS in the WAT of AL_DR12M mice four months post-switch to DR at 16M of age (Fig. 3.4.2A). However, upon longer duration of DR at 20M or 24M of age, the number of CLS in the AL_DR12M WAT decreased and no age-related increase was detected. Moreover, the WAT of AL_DR16M and AL_DR20M mice also exhibited increased macrophage infiltration four months after DR was initiated at 20M or 24M, respectively. Upon longer duration of DR, the number of CLS in AL_DR16M WAT decreased when animals were assessed at 24M of age (Fig. 3.4.2A). We next implemented statistical analyses to compare the number of CLS of DR switch groups at 16M, 20M or 24M to the number of chronic controls of the same age. When compared to the number of CLS of chronic AL or DR at 16M or 20M, the WAT of AL_DR12M and AL_DR16M mice exhibited a trend for increased formation of CLS four months post-switch to DR (Fig. 3.4.2.B). While there was a clear trend for reduced CLS upon longer duration of DR of both AL_DR12M and AL_DR16M, CLS numbers did not differ significantly from either AL or DR at 20M or 24M of age, respectively. Interestingly, after the number of CLS decreased in 12M onset DR, no age-associated increase in WAT inflammation was detected at 24M of age. At 24 months, the number of CLS in AL_DR20M animals was statistically significantly different from chronic DR and even exceeded the average number of AL CLS at 24M of age (Fig. 3.4.2B). Upon initiation of DR, apoptotic or damaged adipocytes seem to recruit macrophages into the WAT to mediate their clearance, suggesting that macrophage infiltration in the context of DR is probably a readout for adipocyte clearance rather than WAT inflammation. As no later time point in the WAT of AL_DR20M mice were studied, it remains unclear whether CLS numbers in this DR switch group would decrease upon longer duration of DR as well. Moreover, normalizing the normalizing the number of CLS per total cells could prove to be a better analysis compared to CLS per core, as chronic DR and DR switch groups have smaller adipocytes than chronic AL. Altogether, these results suggest that upon mid-life or late-life onset DR, the WAT exhibits increased CLS formation, which in case of AL_DR12M and

AL_DR16M decreases upon longer DR duration and could be interpreted as a readout for clearance rather than inflammation.

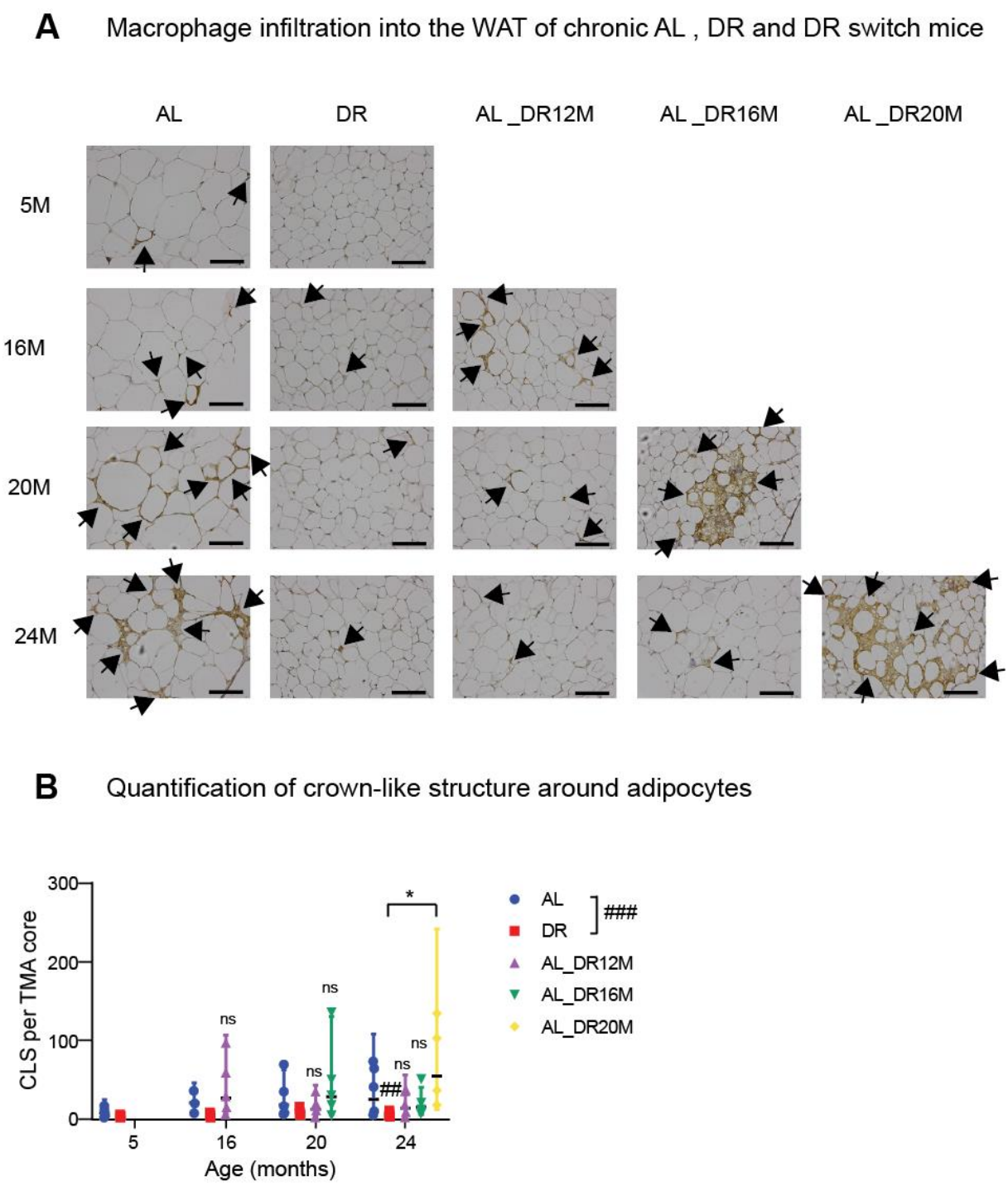

Figure 3.4.2: Chronic AL feeding causes increased macrophage infiltration and WAT inflammation during ageing

A *Representative images of macrophage infiltration into the WAT of chronic controls and DR switch groups visualised by F4/80 staining at 20x magnification (n=5 per diet group and time point, except n=4 for AL_DR20M). Crown-like structures (CLS) are marked with black arrows and scale bars correspond*

to 100μm. ***B*** *quantification of CLS around adipocytes of chronic controls and DR switch groups. Chronic AL mice exhibit increased CLS formation around adipocytes during ageing compared to chronic DR. CLS formation around adipocytes increased four months post-switch to DR but resolves upon longer DR duration. Two-way ANOVA followed by Bonferroni correction for multiple testing were conducted to assess statistical differences between chronic AL and DR at 5M, 16M, 20M or 24M or between chronic controls and DR switch groups at 16M, 20M or 24M. Diet group ($p<0.001$) but not age or the interaction of both factors were significantly different between AL and DR. Data are displayed as mean with 95% CI and with p-values ## $p<0.01$ and ### $p< 0.001$ in relation to chronic AL.*

3.4.3 Expression of fatty acid synthesis genes in the WAT increases in response to late-life DR but never fully recapitulates early onset DR

Chronic DR induced expression of fatty acid synthesis genes in the WAT, however, these changes where not observed when gene expression was measured two months after a late-life (24M) AL to DR switch, suggesting a transcriptional memory of previous AL feeding (Hahn et al., 2019). In order to test, how stable this memory effect is and whether it is also observed in earlier switches, which still have beneficial effects on survival, we measured gene expression of the four switch resistant genes Srebf1, Acaca, Fasn and Elovl6 in WAT of chronic controls and AL_DR16M and AL_DR20M animals at 20M, 24M and 28M corresponding to 4M, 8M or 12M post-switch (Fig. 3.4.3A).

As expected, we observed significantly higher gene expression levels of all four evaluated fatty acid synthesis genes in the WAT of chronic DR animals compared to chronic AL at all three evaluated time points (Fig. 3.4.3 B-D). When comparing the expression of lipogenesis genes in AL_DR16M four months post-switch to DR at 20M, no significantly increased expression compared to AL feeding was detected (Fig. 3.4.3B). Interestingly, Srebf1, Acaca and Fasn also exhibited significantly lower expression levels in AL_DR16M WAT compared to chronic DR (Fig. 3.4.3B). Similarly at 24M, lipogenesis gene expression in AL_DR20M did not differ from chronic AL feeding four months after DR was initiated (Fig. 3.4.3C). In contrast, both Acaca and Fasn expression levels in AL_DR16M WAT showed a significant increase compared to AL but were still at significantly lower levels in relation to DR (Fig. 3.4.3C). Moreover, Srebf1 or Elovl6 expression of neither DR switch exhibited similarly high expression compared to DR at eight or four months post-switch at 24M. We next asked whether lipogenesis gene expression of AL_DR16M or AL_DR20M would catch up to chronic DR levels at after a duration of DR of 12M or 8M respectively.

Most strikingly, we detected significantly increased expression of all four lipogenesis genes in relation to chronic AL feeding in the WAT of AL_DR16M animals at 28M (Fig. 3.4.3D). In contrast, only Acaca and Fasn but not Srebf1 and Elovl6 exhibited higher expression in AL_DR20M WAT in relation to AL (Fig. 3.4.3D). Although, despite a duration of DR for twelve months or eight months, the gene expression levels of both DR switches did not reach the expression levels of chronic DR animals as significantly lower expressions were detected for both DR switches compared to DR at all three evaluated time points (Fig. 3.4.3B-D).

This demonstrated, that the WAT transcriptome showed a response to DR and is able to adapt to the DR regimen, even if DR is initiated as late as at 20M of age. However, animals are largely unable to fully adapt to the chronic DR expression phenotype as AL_DR16M mice still exhibited lower lipogenesis expression levels even twelve months post-switch to DR. Moreover, the adaptation to the DR transcriptome required time as significantly higher expression levels in relation to AL were first detected eight months post-switch to DR in both DR switches at 24M or 28M respectively (Fig. 3.4.3 C and D).

To sum up, DR reduced the adipocyte size independent of the age of DR onset and prevented the age-dependant formation of CLS around macrophages in DR, AL_DR12M and AL_DR16M WAT. In contrast, AL and AL_DR20M WAT exhibited increased macrophage infiltration at 24M of age however; macrophage infiltration in the context of DR is potentially a readout for clearance and not inflammation. Moreover, switching mice from AL to DR at 16M or 20M induced a similarly strong transcriptomic response to DR but the WAT retained a memory of previous AL feeding, thus preventing a full transcriptional reprogramming towards DR even after eight or twelve months on the DR regimen.

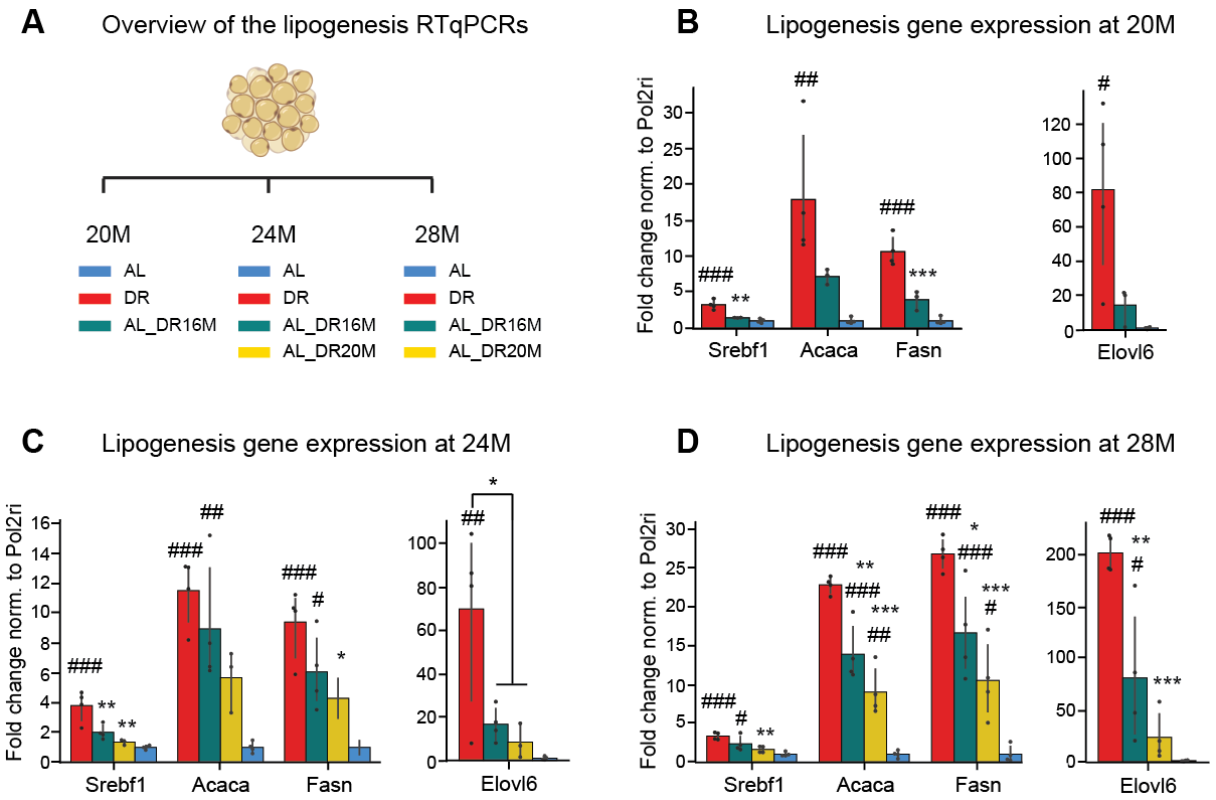

Figure 3.4. 3: Gene expression of fatty acid synthesis enzymes in the WAT slowly increases post-switch to DR but requires time to adapt to the DR regimen

A *schematic representation of Q-RT-PCR analyses of the WAT of chronic AL, DR AL_DR16M or AL_DR20M aged 20M, 24M or 28M. WAT gene expression of Srebf1, Acaca, Fasn and Elovl6 of AL, DR, AL_DR16M or AL_DR20M at* ***B*** *20M (AL and DR n=4, AL_DR16M n=3), at* ***C*** *24M (all n=4 except AL_DR20M with n=3) or* ***D*** *28M of age (n=4). Data are presented as mean with 95% CI. Data were analysed using One-way ANOVA followed by post-hoc Tukey's test with p-values * p<0.05,** p<0.01 and *** p<0.001 in relation to chronic DR. Gene expression differences in relation to AL are presented as following # p<0.05, ## p< 0.01 and ### p<0.001. Plots were generated by Carolina Monzó. The schematic was created using Biorender.com.*

4. Discussion

Ever since the first pioneering study on the effect of reduced food intake and lifespan extension in rodents by McCay and colleagues in 1935 (McCay, Crowell, & Maynard, 1935), numerous studies have tried to unravel the mechanisms underlying DR-mediated lifespan extension. However, the exact mechanisms how DR improves life- and health span are still elusive. Moreover, despite the marked potential of DR for translational application to promote healthy ageing in humans, potential side effects of long-term treatment (Flatt & Partridge, 2018) in addition to compliance difficulties (Meydani et al., 2016; Redman et al., 2018) currently limit the use of DR as geroscientific regimen. Previous studies suggested, that late-onset DR can extend lifespan in mice (Dhahbi et al., 2004), however strain- and sex-specific differences in the response to DR hinder definite conclusions (Mitchell et al., 2016). Therefore, it remains unclear **1)** at what age of onset, DR can still efficiently extend murine lifespan, **2)** if health span is equally extended by late-onset DR and **3)** which underlying molecular and tissue-specific mechanisms could mediate response to DR or lack of thereof. Here, we provide evidence that the critical period of DR-mediated lifespan extension lies between 16M and 20M of age. Additionally, we show that the effects of DR on lifespan and health span can at least partially be uncoupled, and that the beneficial response of DR on overall health is dependent on the age of DR onset. Last, we suggest that cellular, transcriptional and morphological changes in the WAT might contribute to differences in DR responsiveness and lifespan extension.

4.1 Defining the latest age of DR onset for murine lifespan extension

We first assessed the effect of mid-or late-onset of DR on murine lifespan. As expected and in concordance with previously published results in the C3B6F1 strain (Hahn et al., 2017), we confirmed that chronic DR extends life span compared to lifelong AL feeding in C3B6F1 hybrid females (Kaeser et al., 2021). Next, we assessed the effect of mid-life onset at 12M and 16M or late-life onset of DR at 20M or 24M on survival in relation to chronic AL or DR. We show that initiation of DR at 12M and 16M significantly extend murine lifespan compared to chronic AL feeding but not to the same extent as chronic DR, suggesting that earlier AL feeding affects DR responsiveness. Interestingly, while we might have expected a gradual decline in DR responsiveness depending on age of DR onset, there was no significant difference in the mid-life switches in extending lifespan. In contrast, switching animals from AL to DR at 20M or 24M of age had only minor effects on subsequent survival. Thus, we propose that the critical period for DR-mediated lifespan extension lies between 16M, at which animals are still responsive and 20M of age, at which animals loose responsiveness towards newly imposed DR. Notably, our results are in line with most previously published studies on late-life onset DR in mice.

Consistent with the findings of Weindruch and colleagues (Weindruch et al., 1982), AL_DR12M mice were longer lived than chronic AL animals. In addition, we show here that early-onset DR has an even bigger effect on survival than initiation of DR at 12M of age, an observation that Weindruch and colleagues missed as they lacked a chronic DR control group. Moreover, lifespan extension has been observed at 19M onset of DR in mice (Dhahbi et al., 2004; Spindler, 2005) or 18M onset of DR in rats (Ma et al., 2020). In contrast, initiating DR at 17M of age has been shown to decrease lifespan extension compared to chronic DR (Forster et al., 2003). The response of mice towards DR is affected by sex- (Mitchell et al., 2016), level of DR (Mitchell et al., 2015) and the genetic background (Liao et al., 2010). Therefore, initiation of DR before 20M of age is critical for DR-mediated lifespan extension in C3B6F1 females but could be different for other murine strains, such as C57/B6 or DBA2, in which DR initiated at 17M already shortens lifespan (Forster et al., 2003). Noteworthy, lifespan was not negatively affected by DR in C3B6F1 females even when initiated at 24M of age, suggesting that late-life DR is not in general detrimental for mice.

In line with a recently published paper from our lab, we confirmed in an independent mouse cohort that AL_DR24M were not significantly longer-lived compared to chronic AL animals (Hahn et al., 2019). These studies were conducted in two different facilities at the mouse house of the MPI for Molecular Biomedicine in Münster and the MPI for Biology of Ageing in Cologne, respectively, demonstrating that this finding is robust and independent of specific housing conditions. Noteworthy, in our new experiment AL_DR24M mice showed lower mortality compared to AL animals before the initiation of DR at 24 months of age. This is probably the result of reduced food uptake caused by the presence of custom-made food racks in the cages of this cohort, which were used to measure food uptake of the lifespan animals. Initially, we assumed that these racks would not interfere with food uptake, but these mice showed significantly reduced body weight of approximately 19% compared to AL animals from cages without food racks, suggesting that AL_DR24M mice were chronically subjected to a mild form of DR from an early age onwards. This probably explains the improved pre-switch survival compared to AL animals. Indeed, it was previously shown that lifelong reduction of food intake by 10% is sufficient to extend lifespan in rats (Duffy et al., 2001; Richardson et al., 2016). Interestingly, even though these animals showed improved survival before the switch, their lifespan was not extended by the switch to 40% DR. This might indicate that the lower food restriction was not sufficient to prevent the accumulation of systemic detrimental effects in these animals. Studies on graded levels of DR in rats support this hypothesis, as reduction of food intake by 40% but not 10% reduced the incidence of spontaneous leukemia (Richardson et al., 2016).

4.2 Tumour prevalence in response to the age of onset of DR

Inhibition of malignant growth and reduced tumour load at old age is considered as one of the underlying mechanisms, which mediates the beneficial effects of DR on lifespan in inbred mouse strains (Bronson & Lipman, 1991). Moreover, animals undergoing chronic DR showed fewer radiation (Gross & Dreyfuss, 1984; Shang et al., 2014) or carcinogen- induced tumours (Duan et al., 2017; Ploeger et al., 2017). DR also reduces spontaneous cancer incidence in wild-derived mice without inbred comorbidities (Harper et al., 2006).Thus, we asked whether differences in tumour load and the formation of specific tumour types can explain the differences in the lifespan response to DR.

Interestingly, we detected significantly reduced tumour prevalence in prematurely deceased DR animals in the lifespan cohort and reduced tumour load at 28M in the cross-sectional tissue collection cohort. Moreover, first tumours arose in chronic DR animals at 24M, whereas the first tumours in AL animals occurred as early as 16M of age. However, chronic DR delayed tumour formation but could not completely inhibit tumour growth, as the overall tumour load at death irrespective of the age at which animals died did not differ between AL and DR animals in the lifespan cohort. Therefore, we wondered whether mid-life onset DR could be longer-lived due to reduced tumour incidence compared to late-onset DR. However, AL_DR20M mice in the lifespan cohort and in the cross-sectional tissue collection cohort at 28M of age had significantly lower tumour load compared to chronic AL or DR. In contrast, AL_DR12M, AL_DR16M and AL_DR24M animals formed more tumours, indicating that differences in tumour load cannot explain the differences in the lifespan response to mid- or late-onset DR. Moreover, overall tumour prevalence at death or during cross-sectional pathology was not significantly different between chronic DR and AL_DR12M even though we detected a decrease in median lifespan in AL_DR12M. All in all differences in tumour load or tumour type are likely not causal for differences in lifespan extension depending on the age of DR onset and other factors are contributing to the lifespan response to DR. Interestingly, our results of significantly reduced tumour incidence in prematurely deceased animals and delayed tumour growth before 24M of age is in accordance with previous studies (Blackwell et al., 1995; Harbison et al., 2016; Mitchell et al., 2019). Moreover, it was previously suggested that late-onset DR onset can slow down tumour progression but cannot inhibit already occurred tumour formation (Spindler, 2005). Similarly, AL_DR16M, AL_DR20M and AL_DR24M animals, which died before the median age of death of their respective cohort, exhibited on average more tumours than chronic DR animals, indicating that tumour growth occurred earlier in mid- and late-onset DR animals. In contrast to previously published results (Weindruch et al., 1982), the

average tumour load at death of AL_DR12M animals was not significantly different compared to either chronic control. However, we detected a non-significant trend towards reduced total tumour load in AL_DR12M compared to chronic AL animals, indicating that earlier DR onset could reduce tumour growth. As a previous study used BlOC3FI and C57/B6 males and only investigated AL_DR12M without a chronic DR control (Weindruch et al., 1982), it is unclear if 12M of AL feeding would negatively affect tumour formation in their utilized strains. Furthermore, our results on reduced tumour incidence before 24M of age in the cross-sectional pathology and in prematurely deceased lifespan animals are in accordance with previous studies (Blackwell et al., 1995; Harbison et al., 2016; Mitchell et al., 2019).

As total tumour load likely did not correlate with our lifespan data, we wondered if the formation of different tumour types would fit with the lifespan results. Remarkably, chronic or 12M onset of DR significantly reduced the incidence of liver tumours compared to chronic AL feeding. Moreover, we observed significantly increased liver tumour incidence in 20M or 24M DR onset compared to chronic DR animals in both in the post mortem analysis of lifespan animals and the cross sectional analysis in the tissue collection cohort. Strikingly, AL_DR16M animals displayed an in-between phenotype with significantly increased liver tumour prevalence compared to DR but significantly reduced prevalence compared to AL animals. Cross-sectional pathology at specific ages revealed that the liver tumours started to occur in chronic AL and AL_DR16M animals at 20M of age. This would suggest that liver tumours are formed between 12 and 16 months in our animals, and that DR can prevent tumour formation but does not protect against tumour growth once the tumour has formed. However, while there is a clear difference in liver tumour prevalence between AL_DR12 and AL_DR16M, there is no difference in the lifespan of these animals. On the other hand, liver tumour formation is similar between AL_DR16M and 20M, but the lifespan response to DR differs depending on the age of DR onset, suggesting that liver tumours are probably not a causal factor for DR mediated lifespan extension. Intriguingly, our results on liver tumour prevalence are in line with previous studies, which reported a reduction in spontaneous (Blackwell et al., 1995; Mitchell et al., 2019) or carcinogen- induced hepatocellular carcinomas (Duan et al., 2017; Ploeger et al., 2017). In contrast, Dhahbi and colleagues showed that DR onset at 19M reduced tumour load and liver tumour formation already after 2M of DR (Dhahbi et al., 2004). Differences in the utilized mouse strain, the DR regimen and the sex of the animals could account for these differences (Dhahbi et al., 2004). Lymphoma are one of the main tumour types that laboratory mice exhibit at death (Snyder et al., 2016) and chronic DR has been shown to reduce lymphoma incidence upon chronic treatment or when DR was initiated at 12M of age in male mice (Blackwell et al., 1995) Weindruch et al., 1982). However, we observed an opposite trend. Chronic and mid-life onset DR animals exhibited more lymphoma than chronic AL or AL_DR20M mice in our lifespan cohort. Tumours develop in a sex-dependant manner and female mice have a higher

prevalence to develop lymphoma than males (Haines et al., 2001), which could explain the observed differences. As tumour types and malignancies were not characterised histologically, we cannot discriminate whether animals suffered from malignant or benign tumours nor classify the tissue from which the tumour originated. In summary, we show that the age of DR onset affects the formation of different tumour types in a tissue and an age-of onset dependant manner but the tumour load at death does not correlate with lifespan extension under DR.

Still, the question remains why chronic and 12M onset but not later initiation of DR can protect against liver carcinogenesis in particular. One explanation is an increased mutational load in individual cells and reduced efficiency of DNA damage repair proteins during ageing (Da Silva & Schumacher, 2019). It is possible, that AL mice accumulate more mutations in their hepatocytes and although DR is known to have beneficial effects on DNA damage repair (Cabelof et al., 2003) and reduce mutational load (Garcia et al., 2008), late-onset DR cannot repair already occurred damage. However, as mutations arise in all tissues, why is the liver particularly affected? One explanation could be obesity associated with prior AL-feeding. As mentioned before, DR switch animals are obese prior to the initiation of DR and it is likely that they display fatty livers due to the accumulation of excessive lipids in individual hepatocytes. Hepatic FFA storage creates a pro-inflammatory environment (Divella et al., 2019), which attracts immune cells and thus creates further damage in an already damaged cells. If DR is initiated at 3M of age, steatosis does not take place because animals are not yet obese. Moreover, liver tumour formation has not yet occurred at 12M of age, which is why AL_DR12M animals had reduced liver tumour prevalence. In contrast, malignant or pre-malignant growth already occurred in the livers of AL_DR16M, AL_DR20M and AL_DR24M mice and the initiation of DR could not reverse the already occurred damage to the cells but instead only slow down cancerous growth. Therefore, HE as well as IHC stainings for infiltrating immune cells or actively dividing cells could verify if prolonged AL feeding beyond 12M of age leads to irreversible liver damage in AL_DR16M and AL_DR20M mice, which even long-term DR cannot resolve.

4.3 Metabolic health in chronic, mid- or late-onset DR

While it is important to assess the effect of mid-and late-life DR on overall survival, it is equally necessary to examine metabolic health and fitness to gain better understanding of the impact of DR on health at old age. Therefore, we conducted a large-scale longitudinal phenotyping analyses over six consecutive time points on in total six diet groups to dissect the effect of different ages of DR onset and the duration of DR on metabolic health.

4.3.1 Body weight and fat mass

We confirmed that chronic AL animals are obese as early as 10M of age and that chronic DR animals displayed significantly lower body weight in the C3B6F1 background, as reported previously (Hahn et al., 2019, 2017). Moreover, chronic DR animals exhibited significantly reduced fat mass in favour of a higher lean-to fat mass ratio compared to chronic AL feeding during ageing in accordance with current knowledge (Aydin et al., 2015; Cameron et al., 2012; Forster et al., 2003). DR reduced body weight and fat mass irrespective of the age of DR onset and newly switched animals exhibited similar body weight and fat mass as chronic DR animals within six months after DR was initiated. Moreover, we could confirm that AL_DR24M mice were significantly lighter than chronic AL mice and had reduced fat mass as described previously (Hahn et al., 2019). Strikingly, AL_DR12M, AL_DR16M and AL_DR20M mice displayed similar rates of body weight and fat mass loss, whereas AL_DR24M mice were significantly lighter and had less body fat compared to earlier DR switches when assessed after six weeks of DR. Upon DR, mice preferentially reduce the depot sizes of the gonadal WAT (Mitchell et al., 2015) and it has been suggested that preservation of fat mass correlates with lifespan extension under chronic (Liao et al., 2011; Weindruch et al., 1986) or late-onset DR in mice (Hahn et al., 2019) and chronic DR in rats (Bertrand et al., 1980). However, the hypothesis that fat and body weight maintenance determines the lifespan outcome in DR switch animals can only be partially confirmed in our study. We confirmed that AL_DR24M mice are short-lived after late-onset DR (Hahn et al., 2019) and exhibit reduced fat mass and body weight after six weeks of DR compared to AL_DR12M, AL_DR16M and AL_DR20M. Therefore, the lower body weight and fat mass, which could be attributed to more neoplastic lesions, which formed when animals were on AL feeding and which continued to grow after DR was started. The increased loss of body resources could stem from increased energy demands to maintain body functions and to sustain tumour growth. Indeed, Blackwell and colleagues reported that 95% of female C57/B6 mice on chronic AL feeding exhibited tumours by 24 months of age (Blackwell et al., 1995). These findings fits with our hypothesis that AL_DR24M already displayed neoplastic lesions prior to the DR switch compared to 12M, 16M or 20M DR onset, which lead to increased loss of fat and body weight. In contrast, AL_DR20M animals do not support the hypothesis that sustaining fat mass determines lifespan extension under DR. AL_DR20M animals are similarly short-lived as AL_DR24M. Similar to the long-lived AL_DR12M and AL_DR16M mice, AL_DR20M animals retain their body weight and fat mass after the switch. It is possible, that AL_DR20M also exhibited tumours at the time of the DR switch but tumour growth was slowed down and thus, animals did not exhibit similar weight and fat mass reductions as AL_DR24M. However, differences in study design (Liao et al., 2011; Rikke et al., 2006) and strain- specific differences in response to DR (Liao et al. 2010)

could influence the correlation of lifespan extension and fat mass preservation. Liao and colleagues conducted NMR experiments on restricted and control animals at 15-17M of age in different mouse strains but only followed their body weight but not fat mass in weekly measurements until death (Liao et al., 2011; Rikke et al., 2006). Therefore, it remains unclear how the fat mass changed after longer DR duration at old age (Liao et al., 2011).

4.3.2 Restoration of glucose and insulin tolerance by chronic or late-onset DR

AL animals displayed reduced glucose tolerance and insulin insensitivity as early as 10M of age. In contrast, chronic DR animals remained insulin sensitive and glucose tolerant even at old age consistent with previous findings (Dunn et al., 1997; Yu et al., 2019). Onset of DR in mid- or late-life was able to restore glucose tolerance in all DR switch groups in accordance with previous studies on 12M (Selman & Hempenstall, 2012) or 19M (Sheng et al., 2020). Even very late in life, DR still had positive effects on glucose tolerance, as demonstrated by the increased glucose tolerance of AL_DR24M compared to chronic AL mice, suggesting that the aged glucose metabolism can still fully adapt to DR irrespective of the duration of previous AL feeding and the age of DR onset. Similarly to metabolic reprogramming in the RER (Bruss et al., 2010), mid-or late-onset of DR improved glucose tolerance within six weeks post-switch to DR. This timing is consistent with a previous study, which reported that the metabolic adaptation from previous AL feeding occurred already after 10 days of DR (Matyi et al., 2018). Additionally, the effect of DR on glucose tolerance is evolutionary conserved as humans on short-term DR (Heilbronn et al., 2006) or intermittent fasting (Sutton et al., 2018) also display improved glucose sensitivity. Though it is important to note, that the feeding regimen needs to remain constant after metabolic shift from AL to DR as it was previously reported, that short-term DR and refeeding did not have any beneficial long-term effects in female mice in a sex-specific manner (Cameron et al., 2012).

In contrast to glucose tolerance, only AL_DR12M mice displayed long-term improved insulin sensitivity at old age. Moreover, insulin metabolism of old animals required more time to adapt towards DR and AL_DR20M mice became insulin sensitive after 6M of DR. Interestingly, DR onset at 12M in male C57/B6 mice similarly improved insulin sensitivity after longer duration of DR (Selman & Hempenstall, 2012), indicating that insulin sensitivity required time to adapt towards newly imposed DR. Similarly, AL_DR16M, AL_DR20M and AL_DR24M reacted towards injected insulin, suggesting that even late-onset DR improved insulin tolerance but to the same extent as earlier onset of DR. Moreover, fully retained insulin sensitivity is no prerequisite for lifespan extension in C3B6F1 females, as AL_DR16M mice displayed a smaller

improvement in insulin sensitivity but are similarly long-lived as AL_DR12M, suggesting that lifespan extension and metabolic health span might be uncoupled. In summary, DR is able to improve insulin tolerance even at old age, but the beneficial effect of late-onset DR never reaches the effect size of chronic DR treatment. Moreover, the age of DR onset affects insulin sensitivity as earlier DR switches, such as AL_DR12M, displayed significantly improved insulin sensitivity in the long-term, potentially due to shorter duration of previous AL feeding.

However, the question remains why early and mid-life DR has a more beneficial effect on insulin tolerance that onset of DR late in life. Ageing and obesity are known to have detrimental effects on the pancreas where pancreatic β cells are synthesizing and secreting insulin. Pancreatic islet hypertrophy and reduced β cell function was reported in obesity (Figueroa & Taberner, 1994) as well as during normal ageing (Kehm et al., 2018). Moreover, it was demonstrated that insulin resistance accelerated β cell senescence (Aguayo-Mazzucato et al., 2019) and that targeted removal of senescent cells could prevent diabetes (Thompson et al., 2019) and improve glucose homeostasis (Aguayo-Mazzucato et al., 2019). Strikingly, chronic DR can reduce pancreatic islet hypertrophy (Mitchell et al., 2016) and maintained β cell function in rodents (Kanda et al., 2015) and humans (Sathananthan et al., 2015). Intriguingly, Kehm and colleagues observed pancreatic island hypertrophy in 10M old animals (Kehm et al., 2018), which corresponds to the age, at which chronic AL mice become insulin insensitive in our model. Between 10M and 15M, the size of the pancreatic islands remained similar but increased again between 15M and 21M of age, which was associated with increased β cell senescence (Kehm et al., 2018). It is tempting to speculate, that mid-life but not late-life DR onset could still reverse detrimental effects of previous AL feeding on pancreatic islet size and β cell senescence and thus improve insulin sensitivity. However, DR onset at 18M of age has been shown to induce insulin secretion after glucose stimulation but the secreted insulin was unable to mediate glucose uptake in peripheral tissues (Park et al., 2006). Therefore, it is possible that late-onset DR still improves pancreatic β cell health and insulin secretion at old age but does not reverse insulin sensitivity in peripheral tissues. As DR switch animals were obese and had increased WAT depots prior to the initiation of DR, it is tempting to speculate that the WAT could play a role in the modulation of systemic insulin resistance and that a metabolic memory of previous AL feeding could prevent beneficial effects of DR on the WAT and systemic insulin function. However, more experiments in the pancreas and the WAT are necessary to evaluate whether DR can improve pancreas function and the secretory adipokine profile and whether changes in these parameters would correlate with lifespan and insulin sensitivity.

4.3.3 Macronutrient utilization under chronic or late-onset DR

We investigated the RER to evaluate the effect of mid- or late-onset DR on macronutrient utilization. In line with previously published data (Bruss et al., 2010; Corrales et al., 2019), chronic DR altered the timing and the amplitude, in which animals shift between carbohydrate or fatty acid and protein utilization. This temporal shift in the RER correlated with food intake and DR animals used carbohydrate oxidation to synthesize fatty acids, which lead to an RER over 1 (Bruss et al., 2010). An RER close to 0.7 indicates that newly synthesized fatty acids were utilized as energy source for fatty acid oxidation during the night (Bruss et al., 2010; Corrales et al., 2019). Although AL animals utilize carbohydrates as fuel, they do not synthesize fatty acids simultaneously and therefore do not show an RER over 1. All DR switch groups including AL_DR24M animals displayed the same distribution and timing of macronutrient usage as chronic DR animals and the pattern change occurred as early as six weeks post-switch to DR. These results suggest, that metabolism was able to adapt to newly imposed DR even if the diet switch was initiated at old age. Moreover, our results correlate with a previously published study, which demonstrated that two days of DR were enough to induce the metabolic shift of the RER in young male mice (Bruss et al., 2010). However, despite the capacity of the aged metabolism to fully adapt to DR, it required more time to do so. Longitudinal phenotyping of the mid-life onset DR switches confirmed this hypothesis, as all switch cohorts still exhibited significantly higher fat mass compared to chronic DR after six weeks of newly DR treatment but the RER amplitude caught up to chronic DR levels upon longer DR duration. These results suggest, that excessive fat mass was utilized to feed into the metabolism, thus decreasing fat mass over time until the metabolism completely adapted to DR. After the adaptation period was complete, DR switch animals fully relied on the carbohydrate- fuelled fatty acid synthesis and exhibited an RER over 1. Consistently, gene expression levels of key lipogenesis genes in the WAT required time to become significantly upregulated compared to AL upon DR in AL_DR16M or AL_DR20M. However, lipogenesis gene expression levels never reached chronic DR levels even after long-term DR, while the RER fully adapts, indicating that AL feeding retained some detrimental effects on gene expression in the WAT but not on the macronutrient timing and utilization. In the future, it will be interesting to evaluate how DR affects the metabolism in different tissues. To this end, we recently generated a metabolomics dataset of liver samples from chronic controls and DR switch groups aged 5M to 28M. Results from this dataset will provide further insight into the mechanism of DR on liver metabolism in C3B6F1 mice.

4.3.4 DR onset affects the spontaneous home cage activity in single-house mice

Daytime feeding and DR alter the sleep-wake cycle and animals shift their daily rhythm from a nocturnal to a diurnal pattern (Challet, 2010). By assessing spontaneous activity of single-housed mice in the phenomaster, we confirmed that DR induced an almost exclusive daytime activity pattern at all six time points and shifted the resting phase into the dark phase (Mendoza et al., 2008). Similar to our findings on food intake and RER pattern, mid- or late-life onset of DR shifted the spontaneous cage activity to the daytime and animals rested during the night within eight weeks post-switch to DR. Moreover, DR switch animals maintained this activity pattern during ageing. Previous studies suggest that increased activity in restricted animals can be interpreted as foraging for food due to hunger (Abe et al., 1989). Indeed, when comparing the activity profiles of restricted animals with the food intake, daily activity of restricted animals exhibited a distinct peak first when the daily food portion was provided and again with the onset of the dark phase. In contrast, AL animals did not display a peak during the dark phase but activity correlated with food and water intake as previously reported (Zucker, 1971).

When evaluating overall activity during the active phase, we detected no significant differences between chronic AL and DR when animals were young. However, chronic DR animals were more active than AL animals from middle age until old age. These results suggest that there is no hunger-driven food searching behaviour in DR animals and that the difference in activity observed later in life is due to increased fitness. Indeed, spontaneous activity has been shown to decrease during ageing in AL-fed rats (Holloszy et al., 1985) or mice (Logan et al., 2018). The reduction in physical activity in AL animals could be attributed to obesity, which can lead to reduced physical activity both in rodent models of obesity (Bjursell et al., 2008; Stern & Johnson, 1977), and in obese humans (Duvigneaud et al., 2007; Martínez-González et al., 1999). In contrast, chronic DR animals were significantly more active than their AL counterparts even until old age (Holloszy et al., 1985; McCarter et al., 1997). Moreover, high physical activity has been associated with longevity (Holloszy et al., 1985). Strikingly, chronic DR, AL_DR12M and AL_DR16M had higher activity profiles and an extended lifespan compared to chronic AL animals, indicating that chronic or mid-life onset of DR prevents age-related decline in locomotor activity. In contrast, AL_DR20M and AL_DR24M were less active and showed smaller lifespan increase upon late-onset DR. It is tempting to speculate that prolonged AL feeding and obesity reduced fitness and willingness to move in AL_DR20M and AL_DR24M. Moreover, it is possible that late-onset DR cannot rescue physical activity, which could negatively affect overall health and survival.

Interestingly, middle-aged and old AL mice were more active during resting phase compared to age-matched restricted animals, which could indicate increased sleep fragmentation due to prolonged AL feeding. These results contradict with previously published data that reported increased activity during resting phase in DR animals (Acosta-Rodríguez et al., 2017). However, differences in the experimental design using an automated feeder system and voluntary wheel running as well as the use of young male C57/B6J mice aged approx. 3M (Acosta-Rodríguez et al., 2017) could explain the different results. Interestingly, sleep fragmentation increases during ageing (Soltani et al., 2019) as well as in obesity (Fleury Curado et al., 2018) and humans undergoing a short-term DR regimen reported improved sleep quality (Martin et al., 2016). However, it has to be stated, that utilizing laser beam obstruction cannot reliably predict sleep and to confidently investigate sleep under controlled laboratory conditions, epidural electroencephalogram and electromyography measurements would be required (Bastianini et al., 2017).

4.3.5 The influence of feeding time and prolonged fasting on lifespan extension under DR

Rodents, such as rats or mice are nocturnal animals, which rest during the day and are active during the night, during which the majority of food and water is consumed (Zucker, 1971). In our DR study, we provided the daily food portions for DR animals in the morning and subsequently we changed the daily rhythm of our DR animals from a nocturnal to a diurnal pattern, as seen by the shift in the RER profile and as previously described in literature (Challet, 2010; Koubi et al., 1991). Moreover, this diurnal switch occurs even if DR was initiated as late as 24M of age, indicating that animals were still able to adapt to the feeding pattern at old age. Upon food supplementation, DR animals immediately gobble up their daily food portion and then fast until the next morning. Interestingly, this feeding pattern is retained even after animals are on chronic or long-term DR treatment (Hambly et al., 2007).

Therefore, the effects of DR on lifespan are probably a combination of reduced food intake and self-imposed intermittent fasting or time restricted feeding. Our results are consistent with a previous finding (Acosta-Rodríguez et al., 2017), which demonstrated that DR animals consume their daily food portion within two hours after the food was provided and conduct self-imposed time restricted feeding. While this study did not include a survival analysis, time restricted feeding for 12h or DR improved several metabolic parameters, such as glucose tolerance compared to animals on AL food access (Acosta-Rodríguez et al., 2017). Moreover, this DR-specific feeding pattern was confirmed in a second study on intermittent fasting, in which DR animals only had three hours access to restricted food and also shortly consumed

the food after it was provided (Mitchell et al., 2019). Restricting food availability to 13h daily without restricting the food amount can extend murine lifespan and health span, although not to the same extend as CR in combination with an extended fasting period (Mitchell et al., 2019), indicating that fasting without food restriction cannot fully recapitulate the effect of DR on lifespan. Strikingly, we could demonstrate that the combination of food restriction and self-imposed fasting or time restricted feeding effectively extended murine lifespan if DR was initiated chronically or starting at 12M or 16M of age. It is intriguing to speculate that our DR animals would be even longer lived if their circadian rhythm was not altered and if food would have been provided during the night phase. However, more studies are required to evaluate if mid- or late-onset DR without altering the circadian rhythm can extend lifespan, e.g. by supplementing the daily food portions at the beginning of dark phase instead of in the light phase or by utilizing an automated feeder system.

4.4. Fitness and frailty under DR

Aside from various age-associated diseases, aged humans display increased frailty and usually suffer from additional comorbidities at old age (Hanlon et al., 2018). However, aged adults who maintained higher physical exercise throughout life have beneficial effects on lifespan (Mok et al., 2019). However, there is currently only very limited knowledge available if and how late-onset DR affects fitness and frailty. To this end, we investigated fitness and frailty in response to mid-or late-onset DR.

4.4.1 DR does not negatively affect muscle strength

Grip strength measurements were performed to rule out that weight loss and prolonged DR feeding had detrimental effects on muscle strength. Grip strength significantly decreased with age irrespective of the diet group or the age of DR onset. Consistent with our data, age-associated decline in muscle was previously shown for wild type, AL-fed C57/B6 females (Fischer et al., 2016). Early or late-onset DR did not improve or worsen muscle function in C3B6F1 females at all evaluated time points, suggesting that prolonged DR did not negatively affect muscle function. In contrast, studies reported that DR improved muscle function in a strain- and sex- specific manner during ageing (Boldrin et al., 2017) or in a cancer cachexia model (Levolger et al., 2018) and increased satellite cell numbers even after short-term treatment (Cerletti et al., 2013). As previous studies utilized molecular analyses (Boldrin et al., 2017; Cerletti et al., 2013) or injury recovery (Boldrin et al., 2017) as readouts for muscle function, the discrepancy in results between their studies and our can be explained by different

methods, as well as strain and age differences. Moreover, it is possible that forelimb grip strength measurements are not sensitive enough to pick up small changes in muscle function between diet groups during normal ageing. In contrast, the beneficial effects of DR on grip strength in the cancer cachexia model could be attributed to greater muscle decline mediated by the tumour induction, which was further enhanced by AL feeding (Levolger et al., 2018). As DR increased myogenin levels (Levolger et al., 2018), a transcription factor which is expressed in adult satellite cells (Meadows et al., 2008) and is required for skeletal muscle regeneration (Füchtbauer & Westphal, 1992), as well as satellite cells (Boldrin et al., 2017) it is possible that DR improved skeletal muscle histopathology but not grip strength in our mouse model. Therefore, it could be interesting to determine experimentally, whether the skeletal muscles of chronic or DR switch mice display any signs of sarcopenia or improved skeletal muscle histopathology at old age.

4.4.2 Rotarod performance depends on the age of DR onset

Chronic DR increased motor coordination during ageing in our C3B6 F1 hybrid mice, consistent with previous studies in wild type mice (Kuhla et al., 2013), or in a neurological model of trinucleotide expansion disease (Cunha-Santos et al., 2016). Interestingly, the effect of DR on motor coordination seems to be evolutionarily conserved, as aged flies on DR perform better in climbing assays compared to their AL- fed counterparts (Wilson et al., 2020). We observed an improvement of rotarod performance depending on the age of DR-onset. While AL_DR12M animals exhibited increased motor coordination as early as eight weeks post-switch and maintained improved rotarod performance during ageing, onset of DR later than 12 months only had only minor (AL_DR16M) or no beneficial effects on motor coordination. These results suggest that prolonged AL feeding has detrimental effects on motor coordination in mice. However, which factors are regulating or influencing motor coordination?

As chronic AL animals are significantly heavier than chronic DR animals, performance differences could be caused by differences in body weight, as previously suggested (Mao et al., 2015). However, upon initiation of DR, all DR switch animals lost body weight to the same extent, but AL_DR16M, AL_DR20M and AL_DR24M did not significantly improve rotarod performance eight weeks post-switch or upon longer DR duration. Furthermore, we did not find any correlation between rotarod performance and body weight suggesting that body weight is not a causal factor for the observed differences in motor coordination.

Motor coordination is a complex process, which requires spatial orientation, control of limbs and muscles as well as balance for a flawless execution of the intended movement. Balance

and spatial orientation are controlled by the vestibular system, which is located in the inner ear and which is involved in the coordination of complex movements aside from hearing. Studies in humans have shown that the age-associated decline of the vestibular system starts at 40 years and that the highest decline is observed between 75 and 80 years of age (Zalewski, 2015). Vestibular disturbance can lead to a frequent loss of balance and an increased risk for falls and sustaining serious injuries (Herdman et al., 2000; Schlick et al., 2016), thus decreasing quality of life and activity in the elderly. Moreover, the vestibular system of mice exhibits similar age-related synaptic dysfunction, which occurs after 18M of age (Wan et al., 2019), leading to a similar functional decline compared to humans. Strikingly, we detected hardly any improvement in rotarod performance for chronic AL mice at 18M of age, which is consistent with the findings of Wan and colleagues on age-related vestibular synaptic dysfunction in the FVB/N strain (Wan et al., 2019). As muscle strength declined to a similar extent in all diet groups during ageing, differences in motor coordination could point towards increased synaptic dysfunction in the vestibular system of chronic AL animals. Therefore, our data may suggests that chronic or 12M onset of DR can prevent vestibular system decline as animals maintained their motor coordination at old age. Indeed, chronic but not DR onset at approx. 15M improved motor coordination in mice, indicating that DR cannot reverse already occurred damage to the vestibular system if applied to late (Kuhla et al., 2013). These results (Kuhla et al., 2013) are consistent with our findings, as initiating DR at 16M of age or later did only cause minor or no improvement in rotarod performance. Improved motor coordination does not seem to correlate with longevity, as AL_DR16M animals performed worse in the rotarod tests compared to AL_DR12M switches, yet both DR switch groups are equally long-lived. These results show that AL_DR16M animals display an intermediate phenotype, with full lifespan extension but reduced health span at least for some health parameters, such as motor coordination, liver tumour prevalence or insulin metabolism.

4.4.3 Memory function in mid- or late-onset DR

Previous studies implementing short- or long-term DR demonstrated that chronic reduction of food intake improved memory (Khabour et al., 2010; Ma et al., 2018) and increased neurogenesis in C57BL/6 mice (Bondolfi et al., 2004). However, only few studies investigated the effect of mid- or late-onset DR on memory function in mice. In accordance with previously published data, chronic DR improved memory function at old age compared to chronic AL mice (Khabour et al., 2010; Ma et al., 2018). Intriguingly, AL_DR12M, lead to a long-term improvement, whereas AL_DR16M, AL_DR20M or AL_DR24M displayed only short-term improvement in barnes maze performance at 22M or 26M of age, demonstrating that even

late-onset DR can still positively influence memory in C3B6F1 females. Our results are consistent with results from Means and colleagues, who reported that DR onset at 14M of age reversed age-associated decline in memory function compared to age-matched controls (Means et al.,1993). Furthermore, mid-life (Todorovic et al., 2018) or late- onset (Singh et al., 2012) DR in rats similarly improved memory function, similar to our barnes maze data. Still, the question remains how DR improves memory function in mice.

Our recent collaboration with the research group of Prof. Dr. Jucker, whose findings were recently published in Nature Aging (Kaeser et al., 2021), could provide a hypothesis for this question. Kaeser and colleagues identified that circulating protein levels of Neurofilament light chain (Nfl) increased during ageing and can be used to accurately predict mortality in centenarian and non-centenarian humans. Plasma samples from our tissue collection cohort demonstrated that chronic DR reduced circulating Nfl levels which is correlated with a reduction in mortality in chronic DR compared to chronic AL animals. As Nfl is also a protein biomarker implicated in neurodegenerative diseases (Khalil et al., 2018), the findings by Kaeser and colleagues indicate that chronic DR animals could have a better memory function and reduced neurological deterioration during ageing (Kaeser et al., 2021), which is consistent with the improved memory function we observed in the Barnes Maze experiments. As AL_DR12M and AL_DR16M displayed similarly improved memory function, it is tempting to speculate that Nfl levels might also be reduced in AL_DR12M and AL_DR16M. In contrast, DR onset at 20M or 24M did not improve memory function, which could be associated with increased Nfl plasma levels and increased neurological damage occurring during ageing. Additionally, we are collaborating with Dr. Oliver Hahn from the lab of Tony Wyss-Coray. Oliver conducted nuclei sequencing from hippocampus samples of our young AL as well as old AL, DR and AL_DR20M animals to evaluate the effect of ageing and chronic or late-onset DR on the neuronal transcriptome. The hippocampus consists of different neuronal populations including astrocytes, interneurons and subclasses thereof (Zeisel et al., 2015) and is important for spatial memory (Broadbent et al., 2004; Wang & Morris, 2010). Interestingly, DR can stabilize synaptic protein levels in the hippocampus and thus counteract cognitive decline during ageing (Adams et al., 2008). Therefore, it will be very interesting to correlate memory performance, circulating Nfl levels and the hippocampal transcriptome in our DR switch groups to further investigate the effect of mid- or late-onset DR on memory function and brain ageing.

4.4.4 Cardiac function under chronic or late-onset DR

As CVD is one of the major causes of death in humans (Niccoli & Partridge, 2012), it is of particular interest to gauge the effect of DR on heart function. Several studies in rats have

demonstrated that chronic CR reduces heart rate (Mager et al., 2006) and blood pressure (Shinmura et al., 2011), but there are currently no longitudinal studies on the effect of chronic or late-onset DR on cardiovascular function in murine models. Our data provide evidence that chronic DR treatment reduces heart rate compared to chronic AL feeding, in line with previous results in rats (Thomas et al., 1993), mice (Taffet et al., 1997) and humans (Meyer et al., 2006). Interestingly, while AL animals showed an age-related decline in heart rate after 10 months of age, heart rate of DR animals increased up to 14 months of age, and then remained stable during ageing. As we only phenotype animals up to the age of 26 months, it is currently unclear whether DR animals would show an age-related decline later in life. At 20 and 24 months of age, there was no significant difference in heart rate between AL and chronic DR animals. This finding might be influenced by the fact, that the heart rate declines during ageing (Xing et al., 2009) and that chronic AL mice died before 22M or 26M of age and therefore, we were phenotyping the longest surviving AL mice at both time points. Another potential cofounding factor was the observation that at 22M and 26M, chronic DR animals were more active during the recordings and moved more on the platform which might increase their heart rate, whereas chronic AL animals were less active and rested more. Thus, differences in activity between AL and DR animals might have influenced the heart rate measurement at 22M and 26M of age.

Reduced heart rate has previously been associated with increased longevity in mice and humans. Chronic reduction in heart rate using pharmacological interventions extends median lifespan compared to placebo treated mice (Gent et al., 2015) and slower heart is correlated with longevity in humans (Stessman et al., 2013). As heart rate controls the metabolic requirements of the entire body and cardiomyocytes have an immense energy demand (Ferrari et al., 2003). Therefore, a reduction in heart rate would reduce the metabolic demands and could positively influence overall health. However, differences in heart rates are unlikely to underlie the differences in lifespan between the DR switch groups, as animals of all DR switch groups displayed significantly reduced heart rates in relation to chronic AL animals within eight weeks post-switch. This results also indicates that DR has acute effects on cardiac functions even if initiated late in life. Interestingly, DR onset at 12M or 20M further decreased heart rate compared to chronic DR animals, indicating that a short-term DR intervention could be more beneficial than chronic DR for cardiac health, which was reported before in male mice (Li et al., 2016). However, as discussed above the increased activity of chronic DR mice at later time points might have affected these results.

Aside from heart rate, we assessed additional parameters of cardiac health in chronic controls and DR switch groups. We detected a significantly prolonged RR interval between chronic AL and DR animals throughout life. The RR interval describes the time between two ECG peaks, which is inversely correlated with the pace of the heartbeat (Goldberger et al., 2014). Therefore, a longer RR interval corresponds to lower heartrates, whereas a shorter interval

corresponds to faster heartrates. In this light, the lower heart rates of chronic DR animals correlated with prolonged RR intervals as their heart was beating slower. Similarly, AL_DR12M and AL_DR20M animals displayed significantly prolonged RR intervals compared to chronic DR or AL, which also correlated with a reduced heart rate. Intriguingly, RR interval irregularity are often detected prior to myocardial infarction associated with ST fibrillation (Lemmert et al., 2010). The ST segment defines the duration between ventricular de- and repolarization and abnormal patterns of the ST segment have been observed in ischemia (Atar & Birnbaum, 2005). We detected significantly increased ST segment between chronic AL and DR as well as between chronic DR and AL_DR12M, which indicated that chronic DR or AL_DR12M mice could be affected by myocardial ischemia. While ST segment elevation is associated with myocardial ischemia, recent evidence suggests that a reduction in S amplitude and not ST elevation is a more reliable biomarker for ischemia (Boukens et al., 2014). As long-term DR is associated with improved cardiac health in mice with ischemia-induced heart failure (De Lucia et al., 2018), a deeper analysis is necessary to evaluate the diagnostic means of DR-mediated ST segment elongation in our DR study.

The PQ or PR interval indicates how fast the action potential is transmitted from the atria to the ventricles and indicates the required time between atrial and intraventricular depolarization, which determines the pace of the heart rate (Toman et al., 2020). Prolonged PQ or PR intervals can point towards problems in conduction system and can cause an atrial ventricular (AV) block, whereas shortened PQ intervals are commonly found in genetically inherited pre-excitation syndromes, such as Wolff- Parkinson- White syndrome (Cheng et al., 2009; Wolff, Parkinson, & White, 1930). Interestingly, we detected no significant differences in the PQ interval time between diet groups and across ages, suggesting that long-term DR or prolonged AL feeding did not affect atrial and intraventricular depolarization. AL_DR12M mice exhibited significantly prolonged PR intervals compared to chronic DR at 14M of age, which could point towards short-term cardiac conduction anomalies eight weeks post-switch to DR, which resolved upon longer DR duration. Interestingly, AL_DR20M mice displayed significantly increased PR intervals compared to chronic AL and DR mice at 26M, indicating that AL_DR20M mice could have an AV block at old age. Ageing has been suggested to affect the duration of the PR interval and old mice were shown to have an interval prolongation compared to young mice (Jansen et al., 2017), which we did not detect in our study potentially due to differences in study design.

The QRS complex marks the actual contraction of the ventricles and the pumping of the blood. Abnormal duration of the QRS complex itself or the amplitude of the R wave are associated with a delay in conduction time and left or right bundle blocks (Das, 1990). Interestingly, we did not detect any significant differences in the duration of the QRS complex between diet groups, indicating that neither long-term DR nor prolonged AL feeding or ageing delayed

ventricular contraction. We detected an QRS intervals of approximately 11ms, which is slightly higher than results of a large-scale ECG study using 28 different inbred strains (Xing et al., 2009). In this study, QRS duration of CH3/HeJ females was 10,3ms using the same non-invasive ECG method (Xing et al., 2009). As we utilized C3B6F1 hybrid females for our experiments, a higher QRS duration could be due to the crossbreeding of two inbred strains for our study compared to the pure inbred parental strain.

The QT interval marks the time between atrial repolarization and ventricular repolarization and is correlated with the pace of the heart rate. Moreover, prolonged QT intervals indicate that cardiac cells fail to repolarize before a new circle starts, which ultimately causes atrial fibrillation (Pai & Rawles, 1989) or ischemia (Kerr et al., 1987). Lastly, the uncorrected (QT dispersion) or heart rate corrected (QTc) QT dispersion are calculated from the minimal and maximal QT intervals in an ECG and differences in the QT interval can point to myocardial infarctions and sudden cardiac death in humans (Algra et al., 1991; Mirvis, 1985). In male C57/B6 mice, the average QT interval is approximately 40-45ms and the average QTc interval lasts approximately 50ms (Roussel et al., 2016), which is consistent with the obtained QT intervals in our study. Longitudinal analyses revealed that chronic AL animals exhibited significantly different QT and QTc intervals as well as different QT and QTc dispersions compared to chronic DR animals. Interestingly, chronic DR mice displayed significantly longer QT and QTc intervals or dispersions at 5M and 10M and at later phenotyping time points, the interval duration was similar to the duration at 10M of age, whereas the QT dispersion exhibited further age-associated decrease. In contrast, the QT interval of chronic AL mice increased during ageing and the QT dispersion declined until 14M of age and plateaued from 18M of age until 26M of age. Interestingly, both the heart rate corrected and uncorrected QT interval and QT dispersion displayed the same trend indicating that the effect of diet on cardiac repolarization is independent from the heart rate. According to literature, a prolonged QT or QTc interval can point towards reduced repolarization capacity of myocardiocytes (Jeyaraj et al., 2012). Additionally, it was demonstrated that a longer QTc interval could be utilized as predictor for mortality in type I diabetes patients (Rossing et al., 2001). Current literature suggests that weight loss induces changes in cardiac repolarization in humans (Vedel-Larsen et al., 2016) and that chronic DR reduced QTc interval time in rats (Lopez Trinidad et al., 2021), which was associated with improved systemic glucose metabolism. While it is tempting to speculate that prolonged AL feeding and obesity could negatively affect cardiac repolarization in the long-term, it has been reported that the circadian oscillator Klf5 controls QT interval (Jeyaraj et al., 2012). Therefore, the difference in circadian phases might have influenced QT interval duration and QT dispersion between chronic controls. Interestingly, all DR switch animals displayed prolonged QT and QTc intervals compared to chronic DR, suggesting that AL feeding for 12M already had a negative long-term effect on repolarization capacity. While

we gained many interesting insights in the effect of short-term or long-term DR on different heart parameters, more studies are necessary to gain a definitive answer if prolonged AL feeding negatively affects cardiac health and if DR can reverse already occurred cardiac damage. Interestingly, it has been suggested that DR might ameliorate cardiac function at old age by reducing senescent and apoptotic cardiomyocytes (Shinmura et al., 2011), fat accumulation (Hammer et al., 2008), collagen deposition (Dhahbi et al., 2006) and oxidative damage (Dolinsky & Dyck, 2011). In future, we aim to correlate heart rate and cardiac parameters with the age at which animals died, to investigate if the shortest living survivors display the differences in cardiac pace or interval duration vice versa. Moreover, it could be worth to evaluate the amount of senescent cardiomyocytes or collagen deposition to evaluate if DR has a reported cardioprotective effect in C3B6F1 hybrids.

4.4.5 Frailty and lifespan extension under DR

Previous studies reported that long-lived mouse models display reduced frailty compared to their wild type or AL-fed controls, demonstrating that the frailty index is a powerful tool to assess frailty in laboratory animals (Kane et al., 2016; Whitehead et al., 2014). However, much less information is available, on how late-onset DR affects frailty in mice. To this end, we employed the frailty index at three different time points during murine ageing, to assess the effect of mid-life or late-onset DR on overall frailty. As expected, we detected reduced frailty scores for chronic DR compared to AL animals at old age, which correlated with previously published data on frailty in response to DR in C57/B6J mice (Kane et al., 2016). Importantly, AL_DR12M and AL_DR16M mice displayed reduced frailty, which correlates with their increased lifespan extension. Notably, AL_DR24M animals showed increased frailty compared to chronic DR animals, consistent with the lack in lifespan extension in the late-onset DR switch (Hahn et al., 2019). Our data is in part consistent with previously published work by Todorovic and colleagues, who reported that DR onset in male rats between 12M and 18M or between 15M and 21M only lead to a short-term reduction in frailty at 18M compared to age-matched AL animals (Todorovic et al., 2018). In contrast to our findings, DR onset between 12M and 18M had similar frailty scores as AL-fed rats at 24M of age, whereas initiating DR between 15M and 21M increased frailty compared to chronic AL animals (Todorovic et al., 2018). However, Todorovic and colleagues utilized a different frailty protocol, which is mostly based on activity as well as activity-based parameters, such as running time, speed or general activity (Gomez-Cabrera et al., 2017). These differences in the frailty protocol as well as sex- and strain differences likely account or differences in results. Similarly to Whitehead and colleagues

findings (Whitehead et al., 2014), all diet groups exhibited increased frailty indices during ageing, indicating that DR can slow down but not stop frailty at old age.

Interestingly, frailty is an even better determent of biological age compared to DNA methylation clocks, which are commonly used to determine biological age in humans (Kim et al., 2017). Moreover, machine learning algorithms on the frailty index demonstrated that changes in frailty during ageing can precisely predict biological age as well as mortality (Schultz et al., 2020). Consequently, frailty indices are a powerful tool to receive more transferable data on anti-ageing interventions in model organisms and to gauge their putative success in humans. As we have the pathology data of the phenotyping animals, which underwent the frailty index, at our disposal, it will be interesting to evaluate if we can correlate the frailty indices with tumour load at death. In the future, we aim to utilize our entire collected phenotyping and molecular datasets as predictor variables to create a machine-learning model of DR. Based on this model; we can hopefully predict lifespan and health span phenotypes upon DR as well as DR switch response with high confidence.

4.4.6 Lifespan and health span are uncoupled upon mid-life DR treatment

Over the last decade, more and more evidence suggests that lifespan and health span are not necessarily coupled. Studies in *C. elegans* demonstrated that although lifespan was extended by the IIS mutant *daf-2* or the genetic equivalent to DR, *eat-2,* the health span of these long-lived worms was not equally prolonged (Bansal et al., 2015). Similarly, female mice (Kane et al., 2019) or humans (Gordon et al., 2017) are frailer but still longer-lived than males providing evidence in higher organisms that a longer life and good health are not exclusively concomitant. Intriguingly, a recent study evaluated different health parameters in young, old and geriatric mice of both sexes and could show that animals, which performed worse in different health tests had no increased probability of premature death (Fischer et al., 2016). Moreover, the outcome of one health parameter was not correlated with others (Fischer et al., 2016), indicating the complexity of health span and the contribution of individual parameters to overall health. Furthermore, aged mice lacking the adipose tissue lipid binding protein Fabp4/5 displayed improved metabolic health but were not long-lived, suggesting that metabolic health and lifespan can also be uncoupled (Charles et al., 2017).

We observed uncoupling of lifespan and health span in AL_DR16M switch mice. Similar to chronic DR and AL_DR12M mice, DR onset at 16M improved memory function, glucose tolerance and reduced frailty at old age. In contrast, insulin tolerance, motor coordination and

total and liver tumour prevalence were not improved in these mice. The lack of improvement of these phenotypes was not crucial for DR-mediated lifespan extension as AL_DR16M mice were similarly long-lived as AL_DR12M. Thus, while DR is still able to extend lifespan at this age it doesn´t have a positive effect on certain health parameters, potentially because morbidities have already began to form. Consistently, a previously published study in rats demonstrated that late-onset of DR was not able to extend health at old age (Todorovic et al., 2018). Therefore, the decision at which age DR is still effective and when it should be implemented in humans, is a question of perspective. If the overall aim is to extend lifespan and initiate DR as late as possible, initiation at mid-life is the obvious choice as it equally extends lifespan and is able to reverse many detrimental effects of earlier obesity. However, the primary aim of gerontology research is to maintain health until death and to reduce comorbidities and age-associated diseases rather than prolonging human lifespan (Jay Olshansky & Carnes, 2017). Therefore, DR interventions should be started as early as possible to prevent the formation of morbidities during ageing (Kalache et al., 2019). In this perspective, DR should be initiated before the human equivalent of 16M of age at approximately 50 years (Flurkey, Currer, & Harrison, 2007), to maximize the health span extending effect of DR. Ultimately, the decision if and when to initiate DR is up to the individual. Nevertheless, our study has provided first evidence that mid-life onset DR has differential effects on the lifespan and health span outcomes in mice, which should be considered for future mouse studies utilizing DR-mimetics or other dietary or pharmacological interventions.

4.4.7 Are we biasing our results in fitness and metabolic phenotyping towards DR?

The circadian rhythm is regulated by core circadian regulator transcription factors CLOCK, NPAS2 or ARNTL1, which induce the expression of the oscillating genes *period* (*PER*) and *cryptochrome* (*CRY*) (Reinke & Asher, 2019). Per and Cry act as negative repressors on their own gene locus, thus creating a negative feedback loop and inducing a new circadian cycle (Reinke & Asher, 2019). As circadian clock genes are active in every cell type, the circadian rhythm has a major effect on all bodily functions including the sleep-wake cycle (Borbély et al., 2016) or metabolism (Lamia et al., 2008). Moreover, it was demonstrated that diurnal and nocturnal animals exhibit opposite secretion of hormones, such as serotonin (Cuesta et al., 2009) or leptin (Kalsbeek et al., 2001) as well as differential timing of glucose and lipid metabolism (Kumar et al., 2015). Likewise, food intake affects circadian regulation of gene expression in peripheral tissues, such as the liver (Stokkan et al., 2001). It was demonstrated that providing the daily food portions in the morning induces an adaptation of the circadian

rhythm from a nocturnal to a diurnal pattern in response to DR in mice and thus influences both the timing of the metabolism as well as the activity state of the animals (García-Gaytán et al., 2020). Moreover, even without daytime feeding, a restricted dietary regimen itself is potent enough to alter the circadian rhythm of laboratory animals (Mendoza et al., 2008) and leads to metabolic reprogramming (Makwana et al., 2019) as early as two days after DR was initiated (Bruss et al., 2010). Therefore, our AL animals were in a different metabolic state than their DR counterparts for the glucose and insulin tolerance tests, which might have negatively influenced the results. Moreover, previous studies demonstrated, that the timing of exercise has a profound effect on the skeletal muscle transcriptome and metabolome (Sato et al., 2019) as well as on cognitive function (Roedel et al., 2006). Exercise in the early resting phase induced differential transcriptomic and metabolomic changes in the muscle associated with increased glucose and reduced glycerol metabolism and a higher systemic energy expenditure, compared to treadmill exercise conducted in the early active phase (Sato et al., 2019). In contrast, exercise in the early active phase induced lipid, glycerol and amino acid breakdown to fuel the metabolism and activated the HIF1α pathway (Sato et al., 2019). Therefore, DR animals were in their active and AL animals were primarily in their resting phase when the fitness phenotypings were conducted. As the activity of AL mice peaks in the first hour of the dark phase (Brooks & Dunnett, 2009), it is possible that performance differences between chronic AL and DR animals were influenced by differences in the circadian rhythm between chronic controls. Therefore, a potential limitation of this study is the comparability of our results to chronic AL animals, as they might be in a different metabolic and activity state than chronic DR or DR switch animals. However, we undertook steps to improve comparability of the results, for instance by altering the feeding scheme of the DR animals in the ITT and GTT measurements to synchronise the metabolic state. Additionally, if the difference in the metabolic and activity state would have a major influence on the phenotyping experiments, we would except that all late life DR switches should be equally effective in improving fitness and health parameters, as they all change the circadian rhythm to a similar extent after DR was initiated. However, we detected a clear difference in health span and lifespan parameters depending on the age of DR onset even though the animals adapted to the DR regimen. Moreover, as DR switch animals synchronized their circadian as well as activity rhythm to chronic DR after DR was initiated, we can compare the effect of prolonged AL feeding prior to the diet switch to chronic DR. Overall, while we are aware of the potential limitations of our study, the difference in the metabolic and activity state are not a big concern for our results of DR switches and the interpretation of our data. The utilization of an automated feeder system (Acosta-Rodríguez et al., 2017), providing the daily food portions for DR animals in the early evening or changing the light phase of the animal room to last from 6pm to 6am could ensure that all animals are entrained the same way.

4.5 Changes in the WAT upon DR

Animals and humans rapidly lose body weight and fat mass upon initiation of DR. As fat is mainly stored in the WAT, this tissue exhibits major morphological and gene expression changes upon DR. In addition, the WAT is a major secretory tissue, which secretes different metabolic or immune-modulating adipokines, and can thus influence insulin metabolism in the WAT itself or other peripheral tissues. Thus, we measured the effects of late-onset DR on WAT tissue morphology and gene expression.

4.5.1 The transcriptional reprogramming of the WAT depends on the continuity and the duration of the DR regimen

In order to assess the impact of DR on gene expression, we first assessed the transcriptional response of the WAT towards late-life dietary switches from AL to DR and vice versa compared to chronic AL or DR regimen. In accordance with previously published data (Fujii et al., 2017), lifelong DR induced a distinct gene expression profile in the WAT, associated with increased expression of several key lipogenesis genes compared to chronic AL feeding. Moreover, it has been shown that not only gene expression but also lipogenesis protein levels increased upon DR (Valle et al., 2010). However, few studies so far have investigated the effects of late-onset DR on gene expression in the ageing WAT. We show, that gene expression in the WAT remained mostly unresponsive towards newly imposed DR at 24M of age. Moreover, switching mice from DR back to AL feeding for two months almost completely reverted the DR-mediated transcriptome changes in the WAT back to AL levels. These results demonstrate, that in order to benefit from DR at old age, the dietary regimen has to be initiated in early adulthood and more importantly, it has to be maintained until death as there is no long-term protective effect on lifespan or the WAT transcriptome. Additionally, short-term DR at old age is not enough to reverse the memory of previous AL feeding on WAT gene expression. Since we obtained the body and WAT weight at death, but had no information on the body composition upon mid-life or late-life onset DR, we included regular phenotyping time points in our follow-up DR study, which was designed based on the results presented in (Hahn et al., 2019). We identified, that already as early as six weeks post-switch to DR and irrespective of the age of DR onset, mice significantly lost body weight, which was mainly attributed to loss of fat mass. However, mice exhibited a similar body weight as chronic DR mice after approximately six months post-switch to DR.

As AL_DR24M mice were still in the weight loss phase two months post-switch to DR in our previous study, we collected tissue four months after the respective switch to DR in our follow-

up study to investigate the transcriptional profile after longer DR duration. Additionally, we included more time points to collect tissue, to investigate the effects of long-term, late-onset DR on different tissues. Our new Q-RT-PCR data show that lipogenesis gene expression in the WAT is not completely refractory to mid- and late-life DR switch, as lipogenesis genes started to change in response to DR upon longer treatment time. However, strikingly, WAT expression of key lipogenesis genes did not reach the levels of chronic DR even after twelve months of DR treatment, suggesting a long-term memory of gene expression in the WAT far exceeding the two months previously reported.

4.5.2 Increased mitochondrial expansion in the WAT in chronic DR correlates with lifespan extension

In addition to differences in lipogenesis gene expression, RNA sequencing and Q-RT-PCR analyses in the WAT revealed differences in the expression of several mitochondrial biogenesis-promoting genes, such as *Srebf1*. The *Srebf1* gene encodes the Sterol regulatory element-binding protein 1 (SREBP1), which is not only a key lipogenesis factor but is also involved in mitochondrial biogenesis (Fujii et al., 2017). Strikingly, lifelong but not late-onset DR increased mtDNA copy numbers as well as OXOPHOS protein complexes in the WAT at 26M of age. These results indicate, that the WAT of chronic DR mice harbours more mitochondria compared to chronic AL as well as AL_DR24M and DR_AL switch groups. Strikingly, our findings in line with previously published data which demonstrate that chronic DR retained mitochondrial function in aged tissues (Lanza et al., 2012; Valle et al., 2008) and increased mitochondrial biogenesis (Nisoli et al., 2005). As mitochondrial dysfunction is one of the hallmarks of ageing (López-Otín et al., 2013), increasing WAT mitochondrial biogenesis could be one of the mechanisms of lifespan extension upon chronic DR. Lack of mitochondrial biogenesis in AL_DR24M or loss of mitochondria in DR_AL mice could therefore contribute to the shortened lifespans of these diet switches compared to chronic DR. Notably, Fuentealba and colleagues recently conducted a transcriptomic comparison between long-lived, short-lived and progeria mouse models to evaluate transcriptomic changes during ageing (Fuentealba et al., 2021). Strikingly, the transcriptomic profile of short- lived mutants significantly differed from long-lived mice, which exhibited significantly higher expression of mitochondrial biogenesis genes, suggesting that increased mitochondrial numbers could be a determinant to predict longevity (Fuentealba et al., 2021). Therefore, it is tempting to speculate, that reduced mitochondria in the WAT of AL_DR20M but not of AL_DR12M or AL_DR16M mice could add to the lifespan differences of these DR switch groups. To prove this hypothesis,

we aim to assess mtDNA levels in the WAT of chronic controls and AL_DR12M, AL_DR16M and AL_DR20M in the future.

4.5.3 DR does not reduce body temperature in old C3B6F1 females

Decreased body temperature is often associated with DR treatment both in humans and in mice (Cameron et al., 2011; Corrales et al., 2019; Fabbiano et al., 2016; Rikke et al., 2003). Surprisingly, we did not observe difference in body temperature between AL and DR mice or between DR switch mice, neither by using an infrared thermometer on the ear, or by using a rectal probe when measuring female mice after the age of 22 months. Under laboratory conditions, mice are generally housed at a constant temperature of 22°C, which is less than their optimal temperature of 30°C, at which mice reach thermoneutrality (Gaskill et al., 2013). As a result, group-house mice actively seek social contact to nest together in order to reduce thermal stress (Van Loo et al., 2004). Both Corrales, as well as Rikke and colleagues used single-housed animals which may have contributed to the reduced body temperature in response to DR, as animals were not able to reduce thermal stress using social interactions (Corrales et al., 2019; Rikke et al., 2003). Since our mice were housed in groups of five animals, they may have compensated DR-induced thermal stress by social behaviour. Additionally, Cameron, Corrales, Fabbiano and Rikke et al. used different wild type or hybrid mouse strains in their publications. Rikke and colleagues utilized six inbred and 22 hybrid mouse strains and reported strain-dependant differential responses towards DR on body temperature (Rikke et al., 2003). Thus, the finding that DR did not reduce body temperature in our C3B6F1 strain, might be caused by difference in the genetic background. Furthermore, while Rikke and colleagues utilized female mice for their DR experiments, most published studies on the effect of DR utilized male mice, which could point towards a sex-specific difference in body temperature and DR (Cameron et al., 2011; Corrales et al., 2019; Fabbiano et al., 2016). Differences in the age at which animals were measured could also contribute to the different results between our study and published results. While we started body temperature experiments at 22M and conduct the last measurement at 28M to investigate the effect of lifelong DR on body temperature, many studies utilize young (Fabbiano et al., 2016; Rikke et al., 2003) or middle-aged mice (Cameron et al., 2011; Corrales et al., 2019) to assess this phenotype. It has been reported, that aged C57B6 mice have a reduced thermogenic potential even when housed at thermoneutrality compared to young mice (Talan et al., 1996). DR animals are longer lived and there might have been more DR mice in the cages than AL mice at the time we measured body temperature, and thus more social interaction. Potentially, our AL mice were unable to conduct thermoregulation at old age, which is why no significant

differences in body temperature were observed between DR and AL feeding. Measurements in younger AL and DR mice might resolve this issue. In summary, we did not observe reduced body temperature in our DR mice, which might suggest that reduced body temperature and longevity are uncoupled in this strain.

4.5.4 DR does not induce WAT browning in C3B6F1 females

WAT browning is characterized by the formation of so-called brite adipocytes, which are smaller and contain multilocular lipid droplets, increased mitochondrial numbers and are expressing the thermogenesis gene *Ucp1* (Bertholet et al., 2017). Recently, increased browning of the WAT has been linked with short-term or chronic DR and has been suggested to mediate parts of the beneficial response of DR (Corrales et al., 2019; Fabbiano et al., 2016; Sheng et al., 2020). Our histopathology data confirmed reduced adipocyte size even upon late-life onset DR at 20M of age but we observed no evidence for multilocular lipid droplets or WAT browning in either DR group. Furthermore, Western Blot analyses on 26M old WAT of chronic controls, AL_DR24M and DR_AL mice failed to detect *Ucp1* expression in the WAT of these animals, suggesting that DR does not cause WAT browning in our C3B6F1 hybrid mouse strain. Consistent with our data, DR failed to induce SCAT browning in obese humans (Barquissau et al., 2018). The ability of the adipose tissue to form brite adipocytes is known to be both strain (Guerra et al., 1998; Li et al., 2014) and adipose tissue dependant and associated with increased browning in the SCAT compared to other WAT depots (Ferrannini et al., 2016). Li and investigated the browning propensity in primary adipocyte precursor isolated from WAT of two commonly used mouse strains (Li et al., 2014). Strikingly, they demonstrated that adipocyte precursor cells from C57/B6 mice showed low browning propensity in culture compared to cells from the 129/S6 strain (Li et al., 2014), which was likely attributed to transcriptional regulatory networks involving transcription factors, such as Mxd1 and Fh11 (Li et al., 2019). Strikingly, C57/B6-129/S6 hybrid mice, had intermediate browning ability compared to their parental strains due to transcriptional favouring of 129S6 alleles, such as for *Ucp1* or *Klf4,* which are required for browning (Li et al., 2019). Given that we utilize C57/B6 males to generate our C3B6F1 hybrids, it is possible that reduced browning propensity in our model is due to favouring of non-browning C57/B6 alleles even under DR conditions. Moreover, Corrales and colleagues utilize a sub-strain of the 129 line for their studies, which could have a similarly high browning capability as 129/S6, which could in turn explain why they observe higher browning in their SCAT and WAT tissue (Corrales et al., 2019). Moreover, increasing age also diminishes the browning ability of the WAT after cold exposure, which declines as early as 6M of age and further deteriorates during ageing (Berry et al., 2017;

Rogers et al., 2012). Fabbiano and colleagues recently demonstrated a link between DR and WAT browning through type II immune signalling (Fabbiano et al., 2016). However, this study initiated DR in 8W old mice directly with a 40% reduction in food intake and thus, it is questionable if increased browning upon short-term DR was mediated by DR itself or by developmental bias caused by DR (Fabbiano et al., 2016). The latter might be the case, as 3 months of DR treatment initiated at 19M of age did not increase WAT browning in another study (Sheng et al., 2020), suggesting that aged adipocyte precursor cells cannot induce brite adipocyte differentiation, which might explain why we did not detect evidence for WAT browning in our adult onset DR paradigm. In summary, browning of the WAT is unlikely to contribute to DR mediated lifespan and health span extension, as our mice were long-lived and healthier at old age, but showed no signs of WAT browning.

4.5.5 ATSC numbers in chronic or late-onset DR

The WAT is a highly heterogeneous tissue, which exhibits plasticity in response towards different dietary regimens, such as obesity (Weisberg et al., 2003) or DR (Miller et al., 2017). We therefore investigated WAT cell type composition in 27M old animals upon chronic or late-onset DR compared to chronic AL feeding. In this section, I will discuss the results on ATSC and adipogenic differentiation, whereas the next section will focus on the immune cell abundance and macrophage infiltration into the WAT.

As reduced stem cell function is one of the hallmarks of ageing, it is hypothesized that parts of the beneficial effects of DR is mediated by improving SC function during ageing. Indeed, DR positively affects SC function in various murine tissues, such as the skin (Forni et al., 2017), the small intestine (Bruens et al., 2020) or the skeletal muscle (Cerletti et al., 2013) and could thus improve tissue function and homeostasis for healthy ageing. However, it is known that DR can harbour multifaceted and contrasting effects on SCs by either reducing or increasing SC proliferation depending on the tissue type and only few studies have investigated ATSC proliferation and differentiation upon DR (Murphy & Thuret, 2015). We could show that early or 12M onset of DR rescues ATSC depletion at old age, whereas DR onset at 16M or 20M did not increase ATSC numbers. This phenotype could stem from ATSC exhaustion due to increased cell proliferation upon longer AL feeding in chronic AL, AL_DR16M and AL_DR20M, which was still reversible in chronic DR or AL_DR12M and thus resulted in a higher ATSC pool in the WAT of these early onset DR animals. Our results are in line with a published study on ATSC proliferation, which reported that ATSC proliferation decreases during ageing in AL-fed mice (Kirkland et al., 1990). However, why is there such a strong difference in ATSC numbers depending on the age of DR onset? It is possible that the WAT microenvironment changes

during ageing, and this might negatively affect ATSC function. Indeed, two recently published sequencing studies on different murine tissues demonstrated, that increased inflammatory signatures are a feature of murine ageing and occur in the WAT (The Tabula Muris Consortium, 2020; Schaum et al., 2020). Moreover, the WAT is the first tissue to exhibit age-associated changes in gene expression, which takes place as early as 15M of age (Schaum et al., 2020) and is associated with increased pro-inflammatory gene expression in WAT progenitor cells (The Tabula Muris Consortium, 2020). Correspondingly, it has been demonstrated that mid-life onset of DR at 15M in mice reduced inflammatory gene expression, DNA damage and senescence in the WAT (Ishaq et al., 2018), indicating that initiation of DR before 16M of age in mice can positively remodel the WAT. Therefore, 3M and 12M onset of DR could mediate a rejuvenating and protective effect on ATSC, by reducing the inflammatory environment in the WAT during ageing and by promoting division thus increasing the ATSC pool. In contrast, initiation of DR after 15M cannot improve WAT heterogeneity and remodel the WAT microenvironment as the cells including WAT progenitors have already undergone age-associated and potentially irreversible transcriptional reprogramming.

4.5.6 Adipogenic differentiation upon chronic or late-onset DR

As ageing reduces the differentiation potential of adipocyte precursor cells through reduced expression of adipocyte differentiation factors (Karagiannides et al., 2001) we aimed to investigate if isolated ATSC of chronic DR and AL_DR12M mice showed increased *in vitro* differentiation. Surprisingly, when culturing isolated SVF from aged chronic controls and DR switch groups, we did not observe any difference in *in vitro* differentiation between the diet groups, suggesting that while more ATSC are present in the WAT of chronic DR and AL_DR12M mice, their differentiation potential was not improved in the *in vitro* setting. Although unexpected, there are several reasons why we do not see changes in between AL and DR in ATSC *in vitro* differentiation including the advanced age of the animals, culture conditions and the choice of adipose tissue. Most in *vitro* differentiation experiments are conducted in young mice, aged 6-12 weeks due to their higher differentiation potential (Kilroy et al., 2018). Moreover, the different adipose tissue depots show differences in their differentiation potential and SVF from SCAT have a higher differentiation potential compared to SVF from the WAT (Meissburger et al., 2016). Strikingly, a recent large-scale study on isolated human SVF cells reported, that the adipogenic potential is highly dependent on the age of the individual it was isolated from and significantly declines at 60 years of age (Kawagishi-Hotta et al., 2017). As we utilized the WAT of 27M old mice for our experiments, we might not have seen an effect because we by utilized the least differentiating WAT depot

and too old mice. Additionally, culture conditions prior to inducing differentiation might also play a role, due to the absence of immune cells, systemic cytokines and a high abundance of growth factors in the culture medium. These factors also could have promoted the differentiation of chronic AL and 16M and 20M onset DR SVF or hindered the differentiation of the SVF chronic DR and AL_DR12M. *In vivo* BrdU pulse-chase experiments and subsequent FACS sorting for BrdU positive mature adipocytes would be a better approach to verify, whether chronic or 12M onset DR positively affect adipogenic differentiation in the WAT.

4.5.7 WAT morphology in chronic or late-onset DR

Upon initiation of DR, mice lose body weight in, which is mostly due to a reduction in body fat mass. As we observed increased macrophage numbers in chronic DR compared to 16M and 20M onset DR but a trend towards reduced immune cells in chronic DR in the FACS experiments, we asked whether DR negatively affected WAT morphology and increased WAT inflammation. In accordance with previously published data, chronic DR significantly decreased adipocyte size (Miller et al., 2017) compared to chronic AL feeding and aged AL-fed mice exhibited a reduction in adipocyte size during ageing (Ziegler et al., 2019). Upon initiation of DR at 12M, 16M or 20M, adipocyte size was reduced within 4M post-switch to DR. Interestingly, a similar reduction in adipocyte size following mid-life onset DR study was recently shown in rats , (Ma et al., 2020), thus supporting our results.

4.5.8 Discrepancy in macrophage numbers in chronic DR in IHC and FACS

CLS formation, as a read out for macrophage infiltration, was significantly reduced in 24M old DR mice compared to AL animals. In contrast, we observed significantly more macrophages by FACS analysis in 27M old DR mice compared to AL animals or AL_DR16M and AL_DR20M animals. Thus, there seems to be a discrepancy between the results obtained by immunohistochemistry and the FACs analysis. As tissues were not perfused for the FASCS analysis it is possible, that the increase in sorted macrophages in chronic DR mice could stem from circulating macrophages from blood vessels but not from CLS around adipocytes. It has been shown that DR improves endothelial function (García-Prieto & Fernández-Alfonso, 2016) and induces blood vessel formation, thus resulting in a higher vasculature network in the dermis (Forni et al., 2017). It is tempting to speculate, that the WAT of chronic DR animals is also highly vascularized and could harbour more circulating macrophages, which were

subsequently sorted. In contrast, only CLS around adipocytes were counted in the IHC experiments and other tissue residing macrophages were disregarded. Additionally, F4/80 is a general macrophage marker, which labels both classically activated M1 and alternatively activated M2 macrophages (Chinetti-Gbaguidi & Staels, 2011). According to the M1/M2 paradigm, M1 macrophages are implicated in innate immune defence and have been associated with pro-inflammatory properties (Orecchioni et al., 2019). In contrast, M2 macrophages are activated anti-inflammatory cytokines and are frequently described to possess anti-inflammatory functions (Chinetti-Gbaguidi & Staels, 2011; Martinez & Gordon, 2014). Additionally, M2 macrophages are thought to resemble tissue-resident macrophages, which are involved in the clearance of cell debris, pathogens and in the regulation of WAT lipolysis (Davies et al., 2013). Moreover, M2 macrophages are implicated in the clearance of apoptotic adipocytes from the WAT, thus enabling tissue remodelling and homeostasis (Odegaard et al., 2007). Furthermore, obesity has been associated with a phenotypic switch from anti-inflammatory M2 towards pro-inflammatory M1 macrophages, thus increasing the inflammatory environment in the WAT (Lumeng et al., 2007). Short-term DR has been shown to reduce both M1 and M2 type macrophages in the WAT (Narita et al., 2018), to reduce the expression of pro-inflammatory cytokines (Park et al., 2017) and the occurrence of CLS in the WAT (Corrales et al., 2019). Thus, these studies suggest that the WAT of DR mice is less inflamed than the WAT of AL mice, consistent with our IHC data. In accordance with current knowledge (Lumeng et al., 2011), AL WAT exhibited an age-associated increase in CLS pointing towards increased inflammatory processes during ageing. Therefore, the increased macrophage numbers in chronic DR mice we observed at 27M could be due to age-associated increase, which becomes apparent only at very advanced ages. As F4/80 does not discriminate between M1 and M2 macrophages, we speculate that chronic DR animals possess more M2 type macrophages in the WAT, thus preventing the onset of inflammation. Q-RT-PCR on sorted macrophages from 27M old animals could verify if more anti- than pro-inflammatory macrophages are residing in the WAT of chronic DR mice.

4.5.9 CLS in the WAT as putative clearance and not inflammation readout upon chronic or late-onset DR

Unexpectantly, short-term DR for four months initiated at 12M, 16M or 20M resulted in higher CLS numbers, which then decreased upon longer DR treatment. These results point towards a DR induced short-term increase in macrophage infiltration into the WAT. As macrophages are known to clear out apoptotic adipocytes from WAT this might indicate a clearance mechanisms and not inflammation. Several points support this hypothesis. AL mice are obese,

potentially via increased proliferation and differentiation of adipocyte precursor cells (Rigamonti et al., 2011). Obesity has been shown to alter the WAT proteome and increases the abundance of proteins involved in apoptosis, which indicates that adipocyte death is frequently occurring in the hypertrophic WAT (Plubell et al., 2017). Upon initiation of DR, adipocytes shrink to utilize stored fat to meet energy demands and reprogram metabolism towards a DR profile, while maintaining adipocyte number (Porter et al., 2004). However, it is possible that upon mid- and late-life DR, adipocytes fail to adapt to the transcriptional reprogramming, secrete cytokines to attract macrophages and are ultimately cleared out by macrophages. Instead, adipocyte precursor cells could be actively proliferating to replace the cleared adipocytes and to prevent cell number loss. By conducting gene expression experiments, we showed that the adaptation of the WAT towards newly imposed DR requires approx. eight months to increase lipogenesis gene expression compared to AL-feeding. It is tempting to speculate, that a similar amount of time is required for the clearance of non-adapted, apoptotic adipocytes. Indeed, in a recently published study on DR in humans, three months of DR did not reduce cytokine levels and the immune cell composition in the SCAT of obese women despite loss of body weight (Sbierski-Kind et al., 2020). Studies in mice have reported, that a short-term restricted dietary intervention on HFD, low-fat diet or on standard chow did not reduce inflammation (Jung et al., 2013; Rodrigues et al., 2020; Schmitz et al., 2016) but instead increased or maintained macrophage density in the WAT (Lijnen et al., 2012; Schmitz et al., 2016). Even though only Schmitz and colleagues evaluated CLS in the WAT and the other studies utilized gene expression or cytokine levels as readouts for their analyses, weight loss after short-term DR for three months was not sufficient to reduce inflammatory signatures in the WAT (Sbierski-Kind et al., 2020; Schmitz et al., 2016). Although these results were generated using different feeding regimens, they correlate with our findings that in the initial weight loss phase four months post-switch to DR, the WAT shows increased CLS in the WAT. Moreover, following weight loss, macrophage infiltration in the WAT remains high for up to six months post-weight loss start before decreasing (Zamarron et al., 2017), which is in line with the reduced CLS number we observed after eight months of DR. Still, the question remains why more macrophages infiltrate into the WAT after DR was initiated. After lipolysis or weight loss upon DR, tissue residing macrophages take up FFA and cholesterol released from adipocytes, to regulate the lipid flux in the WAT (Kosteli et al., 2010). Cholesterol is taken up by the ATP- binding cassette sub-family G member 1 (ABCG1) transporter (Kennedy et al., 2005), which has been implicated to mediate the phenotypic switch from M1 to M2 type macrophages in DR (Wei et al., 2015). Remarkably, the expression and translation of ABCG1 was significantly increased upon weight loss after obesity, indicating that anti-inflammatory macrophages are required for WAT remodelling and the reduction and clearance of lipids (Wei et al., 2015). Strikingly, our previous WAT RNA sequencing dataset confirms our hypothesis

as AL_DR24M animals display significantly upregulated *ABCG1* mRNA levels after two months of DR (Hahn et al., 2019). Therefore, the need for increased lipid efflux during the weight loss phase, coupled with increased adipocyte turnover could explain why we observe higher CLS numbers at four months post-switch to DR.

We therefore propose, that upon mid-or late-onset DR, mice lose fat mass, which induces lipolysis and increases adipocyte death in the WAT. In turn, more macrophages are attracted into the WAT to clear our maladaptive adipocytes and to increase the lipid efflux from the WAT, potentially via ABCG1, which in turns induces a phenotypic switch from M1 to M2 macrophages. Upon the completion of this clearing process, which ends when mice stabilized their body weight and fat mass at approximately six months post-switch to DR, M2 macrophages emigrate from the WAT into the blood stream. It is tempting to speculate, that parts of the reason why 20M onset DR does not extend lifespan is because the adaptation process in AL_DR20M mice is incomplete or inefficient. As the WAT and the body weight require approx. six months to fully adapt to DR, AL_DR20M mice are already of an advanced age when the DR is initiated and many mice died within the initial adaptation period before the process can be completed and before DR could have beneficial effects. This could also explain, why AL_DR20M mice exhibited the lowest macrophage numbers compared to earlier DR switches in the FACS experiments as these animals represented the longest survivors of their diet group. Therefore, their WAT could have successfully adapted to DR, which resulted in emigration and consequently lower WAT macrophage numbers at 27M. In contrast, switching mice at 12M or 16M is still early enough that animals could complete the DR adaptation process in the WAT, which could have contributed to the lifespan extension upon mid-life DR. A recent study on the transcriptomic profile of mid-life onset DR in rats in parts support this hypothesis (Ma et al., 2020). Ma and colleagues initiated DR at 18M in rats and collected tissue of DR as well as of old and young AL animals aged 27M to conduct single nuclei sequencing analyses in different tissues (Ma et al., 2020). Strikingly, DR onset at 18M efficiently induced transcriptional reprogramming in various tissues including the WAT and mediated a shift from pro- to anti-inflammatory gene expression and M2 macrophage polarization after 9M of DR (Ma et al., 2020). Moreover, rats undergoing DR from 18M onwards were significantly longer lived compared to chronic AL animals, providing a link between WAT adaptation, M2 macrophage polarization and lifespan extension (Ma et al., 2020).

In summary, it is likely that in the context of mid- or late-onset DR, macrophages are a readout for clearance and the adaptation process in the WAT and are subsequently not a good read-out to assess WAT inflammation. Therefore, other circulating and infiltrating immune cells could prove to be better predictors for inflammatory processes in the context of DR. It was recently shown that eosinophils play a major role in WAT inflammation and systemic inflammatory processes (Brigger et al., 2020) and that chronic (Fabbiano et al., 2016) or late-

onset of DR at 18M (Ma et al., 2020) can reduce granulocyte infiltration in the WAT. Moreover, other immune cells from the innate or adaptive immune system also play a crucial role in this process to promote or reduce WAT inflammation (Liu & Nikolajczyk, 2019). As macrophage infiltration is but one aspect of WAT inflammation and by limiting our analysis to macrophages, we potentially missed other cell types, which play a role in adipose tissue inflammatory processes and which could be significantly different between the DR switch groups.

Thus, by including an additional time point at 28M, we can test whether CLS numbers in AL_DR20M WAT decrease or remain stable upon longer DR treatment and thus confirm whether macrophage infiltration in the context of DR is truly an inflammation or a clearance phenotype. Furthermore, with an additional time point at 28M, which is closer to the 27M old mice used for the FACS experiments, we can determine whether ageing also increased macrophage numbers and CLS in chronic DR, thus confirming our FACS data. Additionally, we plan to measure the expression and protein levels of pro- inflammatory cytokines IL-6 and IL-10, as well as the anti-inflammatory, M2-associated cytokines IL-10 and IL-4 in the WAT, to gain a second readout on WAT inflammation. Last, by implementing further stainings with T cell or eosinophil-specific antibodies, we could test if other immune cells are a better predictor of WAT inflammation in the context of DR.

4.5.10 Future experiments and ongoing projects to assess the role of the WAT in DR switch response

In the future, it would be interesting to check if other immune cells, such as eosinophils or T cells, play a role in WAT inflammation and are better predictors of inflammatory processes than macrophage infiltration in the context of DR. Moreover, we aim to assess the WAT adipokine regulatory axis in more detail. First, we intent to compare pro-inflammatory IL-6 and IL-1 as well as anti-inflammatory IL-10 mRNA expression levels the WAT and interleukin serum levels to confirm WAT-specific and systemic inflammation between diet groups. Secondly, we plan to focus more on the circulating and WAT-specific miRNA profile.

miRNA are of particular interest to us**,** due to their role in the systemic regulation of many different cellular processes, such as the metabolism (Ji & Guo, 2019), differentiation and stemness (Sarshad et al., 2018), cell cycle progression (Bueno & Malumbres, 2011) and various signalling pathways (Inui et al., 2010). miRNA are single-stranded, non-coding RNA molecules of on average 22 nucleotides in length, which are co-transcribed as miRNA precursors from the intronic or exonic regions of their host genes (Chiang et al., 2010). After several processing steps involving key miRNA modification enzymes, such as Drosha or Dicer,

newly generated mature miRNA molecules are incorporated into the RNA-induced silencing (RISC) complex in the cytoplasm and regulate target mRNAs via mRNA degradation or inhibition of translation (Wu & Belasco, 2008). Additionally, miRNAs are systemically distributed in the blood stream via exosomes and can thus regulate target mRNA in peripheral tissues. For instance, adipose-tissue specific miRNA, which are secreted by mature adipocytes, act systemically in different tissues such as the liver, skeletal muscle or pancreas to modify the metabolism (Ji & Guo, 2019; Thomou et al., 2017). Moreover, patients suffering from obesity exhibit distinct miRNA profiles and the use of serum miRNA to predict or diagnose diabetes and obesity-related disorders are currently investigated in the clinics (Pescador et al., 2013). Interestingly, not only age-associated diseases, such as CVD, cancer or Parkinson's disease but also ageing itself changes the circulating miRNA profile due to reduced Dicer expression and protein levels, which subsequently reduces miRNA biogenesis and dysregulates the fine-tuned regulatory network (Mori et al., 2012; Reis et al., 2016). Thus, differential miRNA profiles are currently evaluated for their use to predict the susceptibility for certain diseases based on serum miRNA abundance (Fehlmann et al., 2020). However, only few studies have investigated the systemic role of miRNAs during ageing or in different longevity models such as DR. Short-term early onset DR in mice induced miRNA expression involved in mitochondrial proteostasis (Zhang et al., 2019) and lifelong DR in DR in rhesus monkeys reduced miRNAs involved in IIS signalling (Schneider et al., 2017). Moreover, fat specific knockout of Dicer abrogated the beneficial effects of DR on insulin and glucose metabolism, indicating that miRNA processing in the WAT is required for the beneficial effects of DR (Reis et al., 2016). In the future, we plan to assess the circulatory miRNA profile in the serum of young and old chronic AL and DR animals to distinguish differences in miRNA abundance under chronic DR and ageing. Additionally, we will identify the circulating miRNA profile of AL_DR12M, AL_DR16M and AL_DR20M mice, to investigate if DR onset at 20M can still induce the expression of a DR-specific circulatory miRNA profile. In a broader sense, specific DR responsive miRNAs could be used as serum biomarkers to predict DR switch response and lifespan extension in mid- but not late-onset DR. As many miRNAs exhibit a high degree of evolutionary conservation between species, we aim to test our identified miRNA candidates in serum samples from humans on short-term or long-term DR to evaluate the predictive potential in a human setting.

4.6 Permeability, stem cell function and Paneth cell health in the small intestine under DR

4.6.1 The effect of DR on intestinal permeability and plasticity

An intact barrier function of the intestinal epithelium is crucial to prevent digested food and the microbiome bacteria from entering in the paracellular space and to induce local as well as systemic inflammatory processes (Chelakkot et al., 2018). Intestinal permeability is attributed to reduced mucus secretion of goblet cells (Birchenough et al., 2015), a more pathogenic microbiome damaging the epithelium or a loss of tight junctions between cells (Lee et al., 2018). Moreover, ageing has been shown to increase intestinal permeability due to a reduction of tight junction proteins and is associated with higher intrinsic intestinal inflammation (Sovran et al., 2019) and shorter intestinal length of both small and large intestine (Moorefield et al., 2017). Therefore, we addressed if early, mid-life or late-onset DR could have beneficial effects on intestinal permeability and health using EM and we measured the length of the large intestine as a readout for intestinal plasticity. Interestingly, we did not observe any significant differences in tight junction integrity between chronic AL and chronic, 12M, 16M or 20M onset DR at 20M or 27M of age, indicating that intestinal integrity is not negatively affected by prolonged AL feeding. This observation correlates with previously published data, which reported no difference in colonic epithelial integrity between chronic AL or DR in old rats aged 28M (Ma et al., 1992). However, as we utilized 27M old animals for our EM analysis, we could have biased our results towards the longest and healthiest surviving AL mice. Similarly, animals aged 20M could have been too young to observe any significant differences in tight junction integrity, as the small intestine exhibits the first transcriptional decline at approx. 24M of age (Schaum et al., 2020).

Interestingly, we detected significantly shorter colon and rectum lengths between chronic controls at 20M, and between chronic AL and chronic or mid- or late-onset DR at 27M, suggesting that even short-term, late-onset DR shortens the large intestine irrespective of the age of DR onset. However, in the case of AL_DR12M, mice required a longer time to shorten their large intestine, as no significant difference was observed between AL_DR12M and chronic AL after 8M on DR. Furthermore, the large intestine length of chronic AL mice appears to increase instead of decrease during ageing, which is contrary to previously published data (Moorefield et al., 2017). Additionally, a recently published study reported improved intestinal barrier function and restored intestinal length after 3M of DR, initiated at 12M of age (Di et al., 2020). However, as Di and colleagues only investigated middle-aged mice, it is possible that

any age-related changes would occur at a later stage and that the utilized animals were simply too young and had not yet adapted to DR. Additionally, the utilization of different techniques to measure intestinal integrity could also explain the differences between our study and Di and colleagues. We performed EM on the jejunum section to directly assess and grade tight junction morphology in our animals, whereas Di and colleagues measured the thickness of the intestinal mucus (Di et al., 2020). It is possible, that implementing a different method, such as measuring the thickness of the intestinal mucus or conducting plasma lipopolysaccharide binding protein (LBP) measurements could show differences in intestinal integrity in our diet groups. LBP is an acute phase response protein, secreted by hepatocytes in response to bacterial lipopolysaccharide levels in the blood stream (Schumann et al., 1996). Increased LBP levels in the serum have been associated with obesity-induced insulin resistance and increased intestinal inflammation (Rojo et al., 2007). In contrast, short-term DR reduced circulating LBP levels in obese women (Ott et al., 2017) or in metformin-treated mice (Moreno-Navarrete et al., 2012), suggesting that DR could have beneficial effects on intestinal barrier function. Therefore, measuring plasma LBP levels in young 5M chronic AL and DR as well as in corresponding 20M and 27M old controls, AL_DR12M, AL_DR16M and AL_DR20M mice could help to verify whether the intestinal integrity of mid-or late-life DR switches is compromised by prolonged AL-feeding. Furthermore, we plan to investigate tight junction integrity using ileum samples collected from the same 27M old chronic controls and DR switch mice, to determine if different intestinal regions show differences in tight junction decline at old age.

4.6.2 The effect of chronic or late-onset DR on Paneth cell health

Ageing can affect the differentiation potential of stem cells in a tissue-specific manner (Kim, Kim et al., 2008). Within the gut aged ISC are expressing higher levels of Atoh1 than young ISC, which subsequently reduces Notch signalling and leads to increased differentiation into secretory cells, such as goblet cells and Paneth cells and reduces enterocyte differentiation (Korzelius et al., 2019; Nalapareddy et al., 2017). Moreover, Paneth cell numbers are increased during ageing (Moorefield et al., 2017) and are supporting or inhibiting ISC function and differentiation (Pentinmikko et al., 2019). As DR was shown to decrease mTORC1 activity and increased Bst1 levels in Paneth cells, which improved ISC function during ageing (Yilmaz et al., 2012), we asked whether Paneth cell health is similarly improved by mid- or late-onset as chronic DR treatment. We utilized EM in the jejunum region and graded secretory granules as hypodense Paneth cell granules as readout for abnormal maturation and crinophagic granules for the fusion of secretory granules with autophagosomes (Adolph et al., 2013).

Hypodense granules decreased in chronic DR and AL_DR12M but not in AL_DR16M mice compared to AL mice aged 20M. When evaluating a second time point at 27M of age, there was a trend for significantly reduced hypodense granules in all DR groups compared to chronic AL but only the comparison with AL_DR20M reached statistical significance. Moreover, ageing increased the percentage of damaged granules irrespective of the diet group but to a lesser extend for animals on DR. Interestingly, no differences were observed for the number of crinophagic granules between diet groups at 20M or 27M of age. Hypodense or crinophagic Paneth cell granules are also observed in the small intestine of Crohn's disease patients (Cadwell et al., 2008; Thachil et al., 2012), suggesting that the Paneth cells of AL mice are more damaged compared to DR animals. Mechanistically, it was demonstrated that the Zinc transporter ZnT2 is crucial for the import of Zinc ions into secretory granules and that lack of ZnT2 impairs both the formation and the secretory function of Paneth cell granules (Podany et al., 2015). It is tempting to speculate, that ZnT2 protein levels could be reduced in the Paneth cells of AL mice, which could lead to Paneth cell dysfunction upon prolonged AL feeding. In contrast, chronic or late-onset DR could maintain or increase ZnT2 protein levels after the DR switch, which could improve Paneth cell health throughout ageing. Interestingly, ZnT2 loss also induces microbial stress in the small intestine due to the lack of secretion of antimicrobial peptides (Podany et al., 2016), thus directly linking the secretory function of Paneth cell granules and the microbiome. As mentioned before, ageing alters the microbiome and leads to the overgrowth of commensal bacterial species, which become pathogenic (Maynard & Weinkove, 2018), whereas chronic DR prevents this age-associated pathogenic microbiome remodelling (Zhang et al., 2013). It is tempting to speculate, that even upon late-onset DR, the microbiome of AL_DR20M mice adapts to DR. This adaptation would require increased secretion of antimicrobial peptides, such as lysozyme or α-defensin, to reduce bacterial overgrowth. Indeed, the secretion of antimicrobial peptides from Paneth cell granules is induced by pro-inflammatory cytokines, such as IFN-γ (Farin et al., 2014) or IL-13 (Stockinger et al., 2014). Therefore, to counteract bacterial overgrowth by long-term AL feeding, Paneth cells could increase ZnT2 levels, which leads to remodelling and the functional restoration of Paneth cell granules in response to DR. A recent study by Gebert and colleagues partially support this hypothesis (Gebert et al., 2020). Gebert and colleagues observed, that short-term DR treatment initiated at 18M of age induced proteome changes in the intestine, which were associated with increased innate immune response proteins, such as Defa20 or Defa22 (Gebert et al., 2020). However, more experiments are required to check if ZnT2 levels change during ageing in C3B6F1 females and if DR would rescue microbiome composition and ZnT2 levels to improve Paneth cell health. Nevertheless, these results point towards increased Paneth cell health under chronic, mid- or late-onset DR following detrimental AL feeding. To evaluate whether Paneth cell health is differentially affected by ageing in a different intestinal

region, we plan to investigate hypodense and crinophagic granules in ileum samples collected from the same 27M old chronic controls and DR switch mice.

4.6.3 The effect of chronic or late-onset DR on organoid formation capacity, *in vitro* differentiation and ISC division

Organoid cultures allow to assess stem cell activity or differentiation in an *in vitro* setting on a fully functionally 3D viable miniature organ (Sato et al., 2011). In our study, we investigated the formation and regrowth potential of intestinal organoids isolated from 27M old chronic controls and DR switch animals. Strikingly, chronic DR seemingly increased the outgrowth capacity of organoids established from freshly isolated intestinal crypts compared to chronic AL or later DR onset. Unexpectantly, upon complete dissociation and re-plating, no significant differences in regrowth were detected between chronic AL and DR organoids. These results are consistent with a recently published study, which reported no differences in organoid formation upon short-term DR compared to AL-fed B6 mice (Di et al., 2020). Moreover, it was demonstrated that organoids established from old AL animals show reduced *in vitro* growth compared to young animals (Cui et al., 2019; Uchida et al., 2019) but this difference was only observed after multiple passages (Nalapareddy et al., 2017). Therefore, it is possible that upon prolonged culture, we would have seen a significant difference in organoid formation between chronic AL and DR. Strikingly, organoids from 12M, 16M or 20M DR onset formed significantly fewer new buds compared to chronic controls, suggesting that the regrowth capacity was impaired in animals switched to DR later than 3M of age. Interestingly, there seems to be a graded decline in regrowth capacity depending on the age of DR onset and AL_DR12M One possible explanation for the lack of regrowth capacity is the inability of DR switch organoids to quickly adapt to changes of nutrient availability. Throughout life, DR switch animals either remained on AL-feeding for 12M, 16M or 20M or on DR for an extended period of time before crypts were isolated and introduced into culture with “full -feeding” nutrient availability again. Interestingly, the ability to quickly react to internal or external environmental changes declines during ageing, a process called declined adaptive homeostasis (Pomatto & Davies, 2017). It is possible, that organoids from chronic DR are able to respond but DR switches can only partially adapt to the changed culturing conditions. Supporting this hypothesis in an in vivo setting, short-term DR followed by AL refeeding in young or old mice showed, that aged mice were unable to fully revert the crypt proteome, whereas young mice rapidly adapted back to AL conditions (Gebert et al., 2020). Similar to our results, after a period of DR applied at 18M of age, intestinal crypts were not fully able to react towards increased nutrient availability of AL feeding.

As ageing does not only reduce ISC numbers, but also lowers ISC division and skews ISC differentiation in favour of secretory cells (Nalapareddy et al., 2017), we next assessed if DR could rescue the differentiation and number of cycling cells within intestinal organoids. Interestingly, we did not observe a shift towards increased secretory lineage differentiation in organoids derived from chronic AL animals, as lysozyme positive Paneth cell numbers were similar between diet groups. However, previous studies utilized fixated section of the small intestine (Moorefield et al., 2017; Nalapareddy et al., 2017) to assess the number of goblet or Paneth cells during ageing and not organoids, which could account for the differences in the obtained results. Interestingly, the number of Ki67 bright cells were not significantly different in organoids established from chronic AL or DR animals, which would suggest that lifelong overfeeding had no detrimental effect on ISC. However, as the longest-lived survivors of the AL group were utilized to establish the organoid culture, it is possible that the ISC of these animals were particularly healthy. However, it is also possible, that due to the advanced age of the animals and prolonged AL-feeding, the ISC contracted mutations, which were beneficial for *in vitro* organoid growth and division. Interestingly, such a mechanism has been shown for prolonged HFD-feeding (Beyaz et al., 2016). HFD also induced intestinal organoid formation and re-growth after passaging and animals were more prone to develop spontaneous intestinal adenomas, indicating increased accumulation of mutations and tumorigenicity of ISC (Beyaz et al., 2016). If chronic AL-feeding has a similar effect on ISC as HFD-feeding, the results on organoid growth and Ki67 positive cells could have been confounded by increased tumorigenic potential of AL-derived ISC. Since chronic DR can reduce spontaneous mutations (Garcia et al., 2008) and rescue stem cell function (Mihaylova et al., 2018), it is possible that chronic DR improved regrowth capacity and ISC division in our hands as well. However, due to accumulation of mutations and malignant growth of ISC in AL organoids, the beneficial effect of chronic DR was not apparent. The fact that AL_DR12M, AL_DR16M or AL_DR20M did not show increased Ki67 bright cells suggests, that mid-life or late-life onset of DR cannot rescue reduced ISC division in *in vitro* settings. Morphology assessments as well as IHC with Ki67 on fixated small intestine samples could verify if mid-or late-onset DR cannot reverse the detrimental effects of earlier AL-feeding and reverse the reduced enterocyte differentiation and ISC division capacity.

5. Supplementary tables

Supplementary table 1. Criteria for euthanasia in the mouse cohorts

Beobachtungen	**Punkte**
I. Körpergewicht (im Vergleich mit Tieren gleichen Geschlechts, Alters und Diät). Das Gewicht wird an zwei aufeinanderfolgenden Tagen bestimmt, da die normalen Gewichtsschwankungen bei Mäusen z.T. erheblich sind.	
- Normal	0
- ≤ 90 % einer geeigneten Kontrolle	5
- ≤ 80 % einer geeigneten Kontrolle	20
II. Allgemeines körperliches Erscheinungsbild (z.B. Anzeichen für vorliegende Infektionen oder Tumore)	
- Normal für das entsprechende Alter des Tieres	0
- Infektion	6
- Tumor ≤ 1,44 cm^2	9
- Tumor ≥ 1,44 cm^2 unter Erhalt des Körpergewichts	12
- Tumor interferiert mit der Nahrungsaufnahme, kontinuierlicher oder schneller Gewichtsverlust, Ulzeration des Tumors, Metastasenbildung, usw.	20
- sichtbarer Aszites	20
- Dyspnoe	20
III. Spontanverhalten	
- normales Verhalten	0
- geringe Abweichungen vom Normalverhalten	3
- eingeschränkte Motorik oder Hyperkinetik	5
- Selbstisolation, Lethargie, ausgeprägte Hyperkinetik bzw. Verhaltensstereotypie, Koordinationsstörungen, Parese die nicht mit der Futteraufnahme interferiert	15
- Schmerzlaute beim Ergreifen, Automutilation, Agonie, Paralyse und Parese die mit der Futteraufnahme interferieren	20
IV. Klinischer Befund	
- Temperatur, Puls und Atmung normal	0
- geringe Abweichungen von der Normalsituation	5
- deutlich erhöhte Atemfrequenz	15

Bewertung	**Punkte**
Keine Belastung (kein Handlungsbedarf)	0
Geringe Belastung (Weitere Beobachtung, engmaschige Überprüfung des Gesundheitszustandes durch zweimal tägliche Kontrolle und einmal tägliches Wiegen der betroffenen Tiere)	1-9
Mittelgradige Belastung (sehr genaue Beobachtung durch zweimal tägliche Kontrolle und Wiegen der betroffenen Tiere, tierärztliche Betreuung, Analgesie, in Abstimmung mit dem Versuchsleiter wird eine Tötung des Tieres abgewogen)	10-19
Hochgradige Belastung (Versuchsabbruch, sofortige Tötung des Tieres durch zervikale Dislokation)	≥ 20

Supplementary table 2. Median and maximum lifespan of chronic controls and AL_DR12M

	Chronic AL	**Chronic DR**	**AL_DR12M**
Median lifespan (days)	770	1058	995
% increase in median lifespan in relation to chronic AL		37,47 %	29,2%
% increase in median lifespan in relation to chronic DR			6,4%
Maximum lifespan (days)	962	1394	1237,6
% increase in maximum lifespan in relation to chronic AL	%	44,84%	28,59%
% increase in maximum lifespan in relation to chronic DR			12,64
Fisher's test maximum lifespan in relation to chronic AL		p-value = $6,85 \times 10^{-9}$	p-value = $3,96 \times 10^{-7}$
Fisher's test maximum lifespan in relation to chronic DR			p-value = 0,513 s

Supplementary table 3. Median and maximum lifespan of chronic controls and AL_DR16M

	Chronic AL	**Chronic DR**	**AL_DR16M**
Median lifespan (days)	775	1058,5	993,5
% increase in median lifespan in relation to chronic AL		36,58%	28,19%
% increase in median lifespan in relation to chronic DR			6,54%
Maximum lifespan (days)	962,4	1394	1213,4
% increase in maximum lifespan in relation to chronic AL		44,84%	26,88%
% increase in maximum lifespan in relation to chronic DR			14,88
Fisher's test maximum lifespan in relation to chronic AL		p-value = $9,07 \times 10^{-9}$	p-value = $1,6 \times 10^{-7}$
Fisher's test maximum lifespan in relation to chronic DR			p-value = 0,82

Supplementary table 4 Median and maximum lifespan of chronic controls and AL_DR20M

	Chronic AL	**Chronic DR**	**AL_DR20M**
Median lifespan (days)	781	1058,5	870
% increase in median lifespan in relation to chronic AL		35,5%	11,39%
% increase in median lifespan in relation to chronic DR			21,66%
Maximum lifespan (days)	967,15	1394	1064,66
% increase in maximum lifespan in relation to chronic AL		44,13%	10,08%
% increase in maximum lifespan in relation to chronic DR			30,9%
Fisher's test maximum lifespan in relation to chronic AL		p-value = $3{,}76 \times 10^{-8}$	p-value = 0,0515
Fisher's test maximum lifespan in relation to chronic DR			p-value = 0,00095

Supplementary table 5. Median and maximum lifespan of chronic controls and AL_DR24M

	Chronic AL	**Chronic DR**	**AL_DR24M**
Median lifespan (days)	821	1065	887
% increase in median lifespan in relation to chronic AL		29,72%	8,04%
% increase in median lifespan in relation to chronic DR			20,07%
Maximum lifespan (days)	993,55	1394	1148
% increase in maximum lifespan in relation to chronic AL		40,3 %	15,54 %
% increase in maximum lifespan in relation to chronic DR			21,4 %
Fisher's test maximum lifespan in relation to chronic AL		p-value = $1{,}88 \times 10^{-7}$	p-value = 0,1589
Fisher's test maximum lifespan in relation to chronic DR			p-value = 0,000197

6. List of figures

7. List of tables

8. Contributions

Dr. Sebastian Grönke and Prof. Dr. Linda Partridge designed the DR study including the lifespan, phenotyping and tissue collection cohorts and supervised my PhD research. I conducted the post-mortem pathologies, the phenotypings as well as all the molecular work and statistical analyses presented in this thesis.

Carolina Monzó conducted the statistical analyses and generated the plots of the lifespan, cox-proportional hazard regression analyses, the longitudinal phenotyping and the EM data as indicated in the figure legends. Nathalie Jauré helped me with the FACS sortings of the WAT, which were carried out with the help and support of the FACS and Imaging facility staff Lena Schumacher and Kat Folz-Donahue. Intestinal organoid cultures were set up with the help of Sina Azami, who also provided invaluable insight and advice on the confocal imaging of Ki67 or lysozyme stained organoids. Electron microscopy data was generated at the CECAD imaging facility under the leadership of Dr. Astrid Schauss, while Janine Klask and Beatrix Martiny prepared and imaged the EM samples. Andrea Mesaros and Martin Purrio aided me with the glucose and insulin tolerance tests and performed the phenomaster experiments. Oliver Hendrich, Ramona Jansen, Sandra Buschbaum, Andre Pahl and Ramona Hoppe helped with the dissections as well as the weighing of the daily food portions for the DR mice. The comparative biology core facility and in particular Kristina Mussmann, Doreen Briel and Jerome Henn were responsible for the daily feeding of my animals as well as the breeding of my phenotyping cohorts.

9. References

Abdullahi, A., & Jeschke, M. G. (2016). White Adipose Tissue Browning: A Double-edged Sword. *Trends in Endocrinology and Metabolism*, *27*(8), 542–552. https://doi.org/10.1016/j.tem.2016.06.006

Abe, H., Kida, M., Tsuji, K., & Mano, T. (1989). Feeding cycles entrain circadian rhythms of locomotor activity in CS mice but not in C57BL/6J mice. *Physiology and Behavior*, *45*(2), 397–401. https://doi.org/10.1016/0031-9384(89)90146-7

Abel, E. D., Peroni, O., Kim, J. K., Kim, Y. B., Boss, O., Hadro, E., … Kahn, B. B. (2001). Adipose-selective targeting of the GLUT4 gene impairs insulin action in muscle and liver. *Nature*. https://doi.org/10.1038/35055575

Abid, M. R., Guo, S., Minami, T., Spokes, K. C., Ueki, K., Skurk, C., … Aird, W. C. (2004). Vascular Endothelial Growth Factor Activates PI3K/Akt/Forkhead Signaling in Endothelial Cells. *Arteriosclerosis, Thrombosis, and Vascular Biology*, *24*(2), 294–300. https://doi.org/10.1161/01.ATV.0000110502.10593.06

Acosta-Rodríguez, V. A., de Groot, M. H. M., Rijo-Ferreira, F., Green, C. B., & Takahashi, J. S. (2017). Mice under Caloric Restriction Self-Impose a Temporal Restriction of Food Intake as Revealed by an Automated Feeder System. *Cell Metabolism*, *26*(1), 267-277.e2. https://doi.org/10.1016/j.cmet.2017.06.007

Adams, M. M., Shi, L., Linville, M. C., Forbes, M. E., Long, A. B., Bennett, C., … Brunso-Bechtold, J. K. (2008). Caloric restriction and age affect synaptic proteins in hippocampal CA3 and spatial learning ability. *Experimental Neurology*. https://doi.org/10.1016/j.expneurol.2008.01.016

Adolph, T. E., Tomczak, M. F., Niederreiter, L., Ko, H. J., Böck, J., Martinez-Naves, E., … Blumberg, R. S. (2013). Paneth cells as a site of origin for intestinal inflammation. *Nature*. https://doi.org/10.1038/nature12599

Aguayo-Mazzucato, C., Andle, J., Lee, T. B., Midha, A., Talemal, L., Chipashvili, V., … Bonner-Weir, S. (2019). Acceleration of β Cell Aging Determines Diabetes and Senolysis Improves Disease Outcomes. *Cell Metabolism*. https://doi.org/10.1016/j.cmet.2019.05.006

Ajuwon, K. M., & Spurlock, M. E. (2005). Adiponectin inhibits LPS-induced NF-κB activation and IL-6 production and increases PPARγ2 expression in adipocytes. *American Journal of Physiology - Regulatory Integrative and Comparative Physiology*. https://doi.org/10.1152/ajpregu.00397.2004

Al Mushref, M., & Srinivasan, S. (2013). Effect of high fat-diet and obesity on gastrointestinal motility. *Annals of Translational Medicine*, *1*(2), 1–11. https://doi.org/10.3978/j.issn.2305-5839.2012.11.01

Alessi, D., Kozlowski, M. T., Weng, Q. P., Morrice, N., & Avruch, J. (1998). 3-phosphoinositide-dependent protein kinase 1 (PDK1) phosphorylates and activates the p70 S6 kinase in vivo and in vitro. *Current Biology*, *8*(2), 69–81. https://doi.org/10.1016/S0960-9822(98)70037-5

Algra, A., Tijssen, J. G. P., Roelandt, J. R. T. C., Pool, J., & Lubsen, J. (1991). QTc prolongation measured by standard 12-lead electrocardiography is an independent risk factor for sudden death due to cardiac arrest. *Circulation*, *83*(6), 1888–1894. https://doi.org/10.1161/01.CIR.83.6.1888

Allan, C. A., Strauss, B. J. G., Burger, H. G., Forbes, E. A., & McLachlan, R. I. (2008). Testosterone therapy prevents gain in visceral adipose tissue and loss of skeletal muscle in nonobese aging men. *Journal of Clinical Endocrinology and Metabolism*. https://doi.org/10.1210/jc.2007-1291

Altiok, S., Xu, M., & Spiegelman, B. M. (1997). PPARγ induces cell cycle withdrawal: Inhibition of E2f/DP DNA-binding activity via down-regulation of PP2A. *Genes and Development*, *11*(15), 1987–1998. https://doi.org/10.1101/gad.11.15.1987

Ambrosi, T. H., Scialdone, A., Graja, A., Gohlke, S., Jank, A. M., Bocian, C., … Schulz, T. J. (2017). Adipocyte Accumulation in the Bone Marrow during Obesity and Aging Impairs Stem Cell-Based Hematopoietic and Bone Regeneration. *Cell Stem Cell*. https://doi.org/10.1016/j.stem.2017.02.009

Amcheslavsky, A., Song, W., Li, Q., Nie, Y., Bragatto, I., Ferrandon, D., … Ip, Y. T. (2014). Enteroendocrine cells support intestinal stem-cell-mediated homeostasis in Drosophila. *Cell Reports*. https://doi.org/10.1016/j.celrep.2014.08.052

Arai, Y., Nakazawa, S., Kojima, T., Takayama, M., Ebihara, Y., Shimizu, K., … Hirose, N. (2006). High adiponectin concentration and its role for longevity in female centenarians. *Geriatrics and Gerontology International*. https://doi.org/10.1111/j.1447-0594.2006.00304.x

Atar, S., & Birnbaum, Y. (2005). Ischemia-induced ST-segment elevation: Classification, prognosis, and therapy. *Journal of Electrocardiology*, *38*(4 SUPPL.), 1–7. https://doi.org/10.1016/j.jelectrocard.2005.06.098

Auer, R., Bauer, D. C., Marques-Vidal, P., Butler, J., Min, L. J., Cornuz, J., … for the Health ABC study. (2012). Association of Major and Minor ECG Abnormalities With Coronary Heart Disease Events. *JAMA*, *307*(14), 1497–1505.

https://doi.org/10.1001/jama.2012.434

Austad, S. N., & Fischer, K. E. (2016). Sex Differences in Lifespan. *Cell Metabolism*. https://doi.org/10.1016/j.cmet.2016.05.019

Ayabe, T., Satchell, D. P., Wilson, C. L., Parks, W. C., Selsted, M. E., & Ouellette, A. J. (2000). Secretion of microbicidal α-defensins by intestinal Paneth cells in response to bacteria. *Nature Immunology*. https://doi.org/10.1038/77783

Aydin, C., Jarema, K. A., Phillips, P. M., & Gordon, C. J. (2015). Caloric restriction in lean and obese strains of laboratory rat: Effects on body composition, metabolism, growth and overall health. *Experimental Physiology*, *100*(11), 1280–1297. https://doi.org/10.1113/EP085469

Baker, D. J., Wijshake, T., Tchkonia, T., Lebrasseur, N. K., Childs, B. G., Van De Sluis, B., … Van Deursen, J. M. (2011). Clearance of p16 Ink4a-positive senescent cells delays ageing-associated disorders. *Nature*. https://doi.org/10.1038/nature10600

Bansal, A., Zhu, L. J., Yen, K., & Tissenbaum, H. A. (2015). Uncoupling lifespan and healthspan in caenorhabditis elegans longevity mutants. *Proceedings of the National Academy of Sciences of the United States of America*. https://doi.org/10.1073/pnas.1412192112

Barazzoni, R., Gortan Cappellari, G., Zanetti, M., Klaus, K. A., Semolic, A., Johnson, M. L., & Nair, K. S. (2020). Higher unacylated ghrelin and insulin sensitivity following dietary restriction and weight loss in obese humans. *Clinical Nutrition*. https://doi.org/https://doi.org/10.1016/j.clnu.2020.06.014

Barnes, C. A. (1979). Memory deficits associated with senescence: A neurophysiological and behavioral study in the rat. *Journal of Comparative and Physiological Psychology*, *93*(1), 74–104. https://doi.org/10.1037/h0077579

Barquissau, V., Léger, B., Beuzelin, D., Martins, F., Amri, E. Z., Pisani, D. F., … Langin, D. (2018). Caloric Restriction and Diet-Induced Weight Loss Do Not Induce Browning of Human Subcutaneous White Adipose Tissue in Women and Men with Obesity. *Cell Reports*. https://doi.org/10.1016/j.celrep.2017.12.102

Bartke, A., & Brown-Borg, H. (2004). Life Extension in the Dwarf Mouse. *Current Topics in Developmental Biology*, *63*, 403–414. https://doi.org/10.1016/B978-012369391-4/50035-7

Bartke, A., Masternak, M. M., Al-regaiey, K. A., & Bonkowski, M. S. (2007). Effects of Dietary Restriction on the Expression of Insulin-Signaling-Related Genes in Long-Lived Mutant Mice, *35*, 69–82.

Basisty, N., Kale, A., Jeon, O. H., Kuehnemann, C., Payne, T., Rao, C., … Schilling, B. (2020).

A proteomic atlas of senescence-associated secretomes for aging biomarker development. *PLoS Biology*. https://doi.org/10.1371/journal.pbio.3000599

Bastianini, S., Alvente, S., Berteotti, C., Lo Martire, V., Silvani, A., Swoap, S. J., … Cohen, G. (2017). Accurate discrimination of the wake-sleep states of mice using non-invasive whole-body plethysmography. *Scientific Reports*. https://doi.org/10.1038/srep41698

Bates, D., Mächler, M., Bolker, B. M., & Walker, S. C. (2015). Fitting Linear Mixed-Effects Models Using lme4, *67*(1). https://doi.org/10.18637/jss.v067.i01

Becker, D. E. (2006). Fundamentals of Electrocardiography Interpretation. *Anesth Prog.*, *53*(2), 53–64. https://doi.org/10.2344/0003-3006(2006)53[53:FOEI]2.0.CO;2

Beekman, M., Schutte, B. A. M., Akker, E. B. va. den, Noordam, R., Dibbets-Schneider, P., de Geus-Oei, L. F., … Slagboom, P. E. (2020). Lifestyle-Intervention-Induced Reduction of Abdominal Fat Is Reflected by a Decreased Circulating Glycerol Level and an Increased HDL Diameter. *Molecular Nutrition and Food Research*. https://doi.org/10.1002/mnfr.201900818

Beer, J. Z., Budzicka, E., Niepokojczycka, E., Rosiek, O., & Szumiel, I. (1983). Loss of Tumorigenicity with Simultaneous Changes in Radiosensitivity and Photosensitivity during in Vitro Growth of L5178Y Murine Lymphoma Cells1, (October), 4736–4742.

Benador, I. Y., Veliova, M., Liesa, M., & Shirihai, O. S. (2019). Mitochondria Bound to Lipid Droplets: Where Mitochondrial Dynamics Regulate Lipid Storage and Utilization. *Cell Metabolism*, *29*(4), 827–835. https://doi.org/10.1016/j.cmet.2019.02.011

Benito, A. I., Furlong, T., Martin, P. J., Anasetti, C., Appelbaum, F. R., Doney, K., … Deeg, H. J. (2001). Sirolimus (rapamycin) for the treatment of steroid-refractory acute graft-versus-host disease. *Transplantation*. https://doi.org/10.1097/00007890-200112270-00010

Bentham, J., Di Cesare, M., Bilano, V., Bixby, H., Zhou, B., Stevens, G. A., … Cisneros, J. Z. (2017). Worldwide trends in body-mass index, underweight, overweight, and obesity from 1975 to 2016: a pooled analysis of 2416 population-based measurement studies in 128·9 million children, adolescents, and adults. *The Lancet*, *390*(10113), 2627–2642. https://doi.org/10.1016/S0140-6736(17)32129-3

Benvenuto, C., Coscia, I., Chopelet, J., Sala-Bozano, M., & Mariani, S. (2017). Ecological and evolutionary consequences of alternative sex-change pathways in fish. *Scientific Reports*. https://doi.org/10.1038/s41598-017-09298-8

Berger, N. A. (2014). Obesity and cancer pathogenesis. *Annals of the New York Academy of Sciences*. https://doi.org/10.1111/nyas.12416

Bernier-Latmani, J., Cisarovsky, C., Demir, C. S., Bruand, M., Jaquet, M., Davanture, S., … Petrova, T. V. (2015). DLL4 promotes continuous adult intestinal lacteal regeneration and

dietary fat transport. *Journal of Clinical Investigation*. https://doi.org/10.1172/JCI82045

Berry, D. C., Jiang, Y., Arpke, R. W., Close, E. L., Uchida, A., Reading, D., … Graff, J. M. (2017). Cellular Aging Contributes to Failure of Cold-Induced Beige Adipocyte Formation in Old Mice and Humans. *Cell Metabolism*, *25*(1), 166–181. https://doi.org/10.1016/j.cmet.2016.10.023

Bertholet, A. M., Kazak, L., Chouchani, E. T., Bogaczyńska, M. G., Paranjpe, I., Wainwright, G. L., … Kirichok, Y. (2017). Mitochondrial Patch Clamp of Beige Adipocytes Reveals UCP1-Positive and UCP1-Negative Cells Both Exhibiting Futile Creatine Cycling. *Cell Metabolism*. https://doi.org/10.1016/j.cmet.2017.03.002

Bertrand, H. A., Lynd, F. T., Masoro, E. J., & Yu, B. P. (1980). Changes in adipose mass and cellularity through the adult life of rats fed ad libitum or a life-prolonging restricted diet. *Journals of Gerontology*. https://doi.org/10.1093/geronj/35.6.827

Betz, M. J., & Enerbäck, S. (2018). Targeting thermogenesis in brown fat and muscle to treat obesity and metabolic disease. *Nature Reviews Endocrinology*. https://doi.org/10.1038/nrendo.2017.132

Beumer, J., & Clevers, H. (2016). Regulation and plasticity of intestinal stem cells during homeostasis and regeneration. *Development (Cambridge)*. https://doi.org/10.1242/dev.133132

Bevins, C. L., & Salzman, N. H. (2011). Paneth cells, antimicrobial peptides and maintenance of intestinal homeostasis. *Nature Reviews Microbiology*, *9*(5), 356–368. https://doi.org/10.1038/nrmicro2546

Beyaz, S., Mana, M. D., Roper, J., Kedrin, D., Saadatpour, A., Hong, S. J., … Yilmaz, Ö. H. (2016). High-fat diet enhances stemness and tumorigenicity of intestinal progenitors. *Nature*. https://doi.org/10.1038/nature17173

Birchenough, G. M. H., Johansson, M. E. V., Gustafsson, J. K., Bergström, J. H., & Hansson, G. C. (2015). New developments in goblet cell mucus secretion and function. *Mucosal Immunology*. https://doi.org/10.1038/mi.2015.32

Bjursell, M., Gerdin, A. K., Lelliott, C. J., Egecioglu, E., Elmgren, A., Törnell, J., … Bohlooly-Y, M. (2008). Acutely reduced locomotor activity is a major contributor to Western diet-induced obesity in mice. *American Journal of Physiology - Endocrinology and Metabolism*. https://doi.org/10.1152/ajpendo.00401.2007

Blackwell, B. N., Bucci, T. J., Hart, R. W., & Turturro, A. (1995). Longevity, body weight, and neoplasia in ad libitum-fed and diet- restricted C57BL6 mice fed NIH-31 open formula diet. *Toxicologic Pathology*. https://doi.org/10.1177/019262339502300503

Bluher, M., Kahn, B. B., & Kahn, R. C. (2003). Extended Longevity in Mice Lacking the Insulin

Receptor in Adipose Tissue. *Science*, *299*(5606), 572–574. https://doi.org/10.1126/science.1078223

Bókony, V., Milne, G., Pipoly, I., Székely, T., & Liker, A. (2019). Sex ratios and bimaturism differ between temperature-dependent and genetic sex-determination systems in reptiles. *BMC Evolutionary Biology*. https://doi.org/10.1186/s12862-019-1386-3

Boldrin, L., Ross, J. A., Whitmore, C., Doreste, B., Beaver, C., Eddaoudi, A., … Morgan, J. E. (2017). The effect of calorie restriction on mouse skeletal muscle is sex, strain and time-dependent. *Scientific Reports*, *7*(1), 1–16. https://doi.org/10.1038/s41598-017-04896-y

Bonaccio, M., Di Castelnuovo, A., Costanzo, S., Gialluisi, A., Persichillo, M., Cerletti, C., … Iacoviello, L. (2018). Mediterranean diet and mortality in the elderly: A prospective cohort study and a meta-analysis. *British Journal of Nutrition*, *120*(8), 841–854. https://doi.org/10.1017/S0007114518002179

Bondolfi, L., Ermini, F., Long, J. M., Ingram, D. K., & Jucker, M. (2004). Impact of age and caloric restriction on neurogenesis in the dentate gyrus of C57BL/6 mice. *Neurobiology of Aging*, *25*(3), 333–340. https://doi.org/10.1016/S0197-4580(03)00083-6

Bonkowski, M. S., Rocha, J. S., Masternak, M. M., Al Regaiey, K. A., & Bartke, A. (2006). Targeted disruption of growth hormone receptor interferes with the beneficial actions of calorie restriction. *Proceedings of the National Academy of Sciences of the United States of America*. https://doi.org/10.1073/pnas.0600161103

Borbély, A. A., Daan, S., Wirz-Justice, A., & Deboer, T. (2016). The two-process model of sleep regulation: A reappraisal. *Journal of Sleep Research*. https://doi.org/10.1111/jsr.12371

Boukens, B. J., Rivaud, M. R., Rentschler, S., & Coronel, R. (2014). Misinterpretation of the mouse ECG: 'Musing the waves of Mus musculus'. *Journal of Physiology*. https://doi.org/10.1113/jphysiol.2014.279380

Bozcuk, A. N. (1972). DNA synthesis in the absence of somatic cell division associated with ageing in Drosophila subobscura. *Experimental Gerontology*. https://doi.org/10.1016/0531-5565(72)90022-8

Brandhorst, S., & Longo, V. D. (2016). Fasting and caloric restriction in cancer prevention and treatment. In *Recent Results in Cancer Research*. https://doi.org/10.1007/978-3-319-42118-6_12

Brigger, D., Riether, C., van Brummelen, R., Mosher, K. I., Shiu, A., Ding, Z., … Eggel, A. (2020). Eosinophils regulate adipose tissue inflammation and sustain physical and immunological fitness in old age. *Nature Metabolism*. https://doi.org/10.1038/s42255-020-0228-3

Broadbent, N. J., Squire, L. R., & Clark, R. E. (2004). Spatial memory, recognition memory, and the hippocampus. *Proceedings of the National Academy of Sciences of the United States of America*. https://doi.org/10.1073/pnas.0406344101

Bronson, R. T., & Lipman, R. D. (1991). Reduction in rate of occurrence of age related lesions in dietary restricted laboratory mice. *Growth, Development and Aging*.

Brooks, S. P., & Dunnett, S. B. (2009). Tests to assess motor phenotype in mice: A user's guide. *Nature Reviews Neuroscience*. https://doi.org/10.1038/nrn2652

Broughton, S., & Partridge, L. (2009). Insulin/IGF-like signalling, the central nervous system and aging. *Biochem. J*, *418*, 1–12. https://doi.org/10.1042/BJ20082102

Bruens, L., Ellenbroek, S. I. J., Suijkerbuijk, S. J. E., Azkanaz, M., Hale, A. J., Toonen, P., … van Rheenen, J. (2020). Calorie Restriction Increases the Number of Competing Stem Cells and Decreases Mutation Retention in the Intestine. *Cell Reports*, *32*(3), 107937. https://doi.org/10.1016/j.celrep.2020.107937

Bruss, M. D., Khambatta, C. F., Ruby, M. A., Aggarwal, I., & Hellerstein, M. K. (2010). Calorie restriction increases fatty acid synthesis and whole body fat oxidation rates. *American Journal of Physiology - Endocrinology and Metabolism*, *298*(1), 108–116. https://doi.org/10.1152/ajpendo.00524.2009

Bueno, M. J., & Malumbres, M. (2011). MicroRNAs and the cell cycle. *Biochimica et Biophysica Acta - Molecular Basis of Disease*. https://doi.org/10.1016/j.bbadis.2011.02.002

Burnett, R., Chen, H., Szyszkowicz, M., Fann, N., Hubbell, B., Pope, C. A., … Spadaro, J. V. (2018). Global estimates of mortality associated with longterm exposure to outdoor fine particulate matter. *Proceedings of the National Academy of Sciences of the United States of America*, *115*(38), 9592–9597. https://doi.org/10.1073/pnas.1803222115

Cabelof, D. C., Yanamadala, S., Raffoul, J. J., Guo, Z. M., Soofi, A., & Heydari, A. R. (2003). Caloric restriction promotes genomic stability by induction of base excision repair and reversal of its age-related decline. *DNA Repair*. https://doi.org/10.1016/S1568-7864(02)00219-7

Cadwell, K., Liu, J. Y., Brown, S. L., Miyoshi, H., Loh, J., Lennerz, J. K., … Virgin IV, H. W. (2008). A key role for autophagy and the autophagy gene Atg16l1 in mouse and human intestinal Paneth cells. *Nature*, *456*(7219), 259–263. https://doi.org/10.1038/nature07416

Cameron, K. M., Golightly, A., Miwa, S., Speakman, J., Boys, R., & von Zglinicki, T. (2011). Gross energy metabolism in mice under late onset, short term caloric restriction. *Mechanisms of Ageing and Development*, *132*(4), 202–209. https://doi.org/10.1016/j.mad.2011.04.004

Cameron, K. M., Miwa, S., Walker, C., & von Zglinicki, T. (2012). Male mice retain a metabolic

memory of improved glucose tolerance induced during adult onset, short-term dietary restriction. *Longevity & Healthspan*, *1*(1), 3. https://doi.org/10.1186/2046-2395-1-3

Canela, A., Vera, E., Klatt, P., & Blasco, M. a. (2007). High-throughput telomere length quantification by FISH and its application to human population studies. *Proceedings of the National Academy of Sciences of the United States of America*, *104*(13), 5300–5305. https://doi.org/10.1073/pnas.0609367104

Cani, P. D., Bibiloni, R., Knauf, C., Neyrinck, A. M., & Delzenne, N. M. (2008). Changes in gut microbiota control metabolic diet–induced obesity and diabetes in mice. *Diabetes*. https://doi.org/10.2337/db07-1403.Additional

Casteleyn, C., Rekecki, A., Van Der Aa, A., Simoens, P., & Van Den Broeck, W. (2010). Surface area assessment of the murine intestinal tract as a prerequisite for oral dose translation from mouse to man. *Laboratory Animals*. https://doi.org/10.1258/la.2009.009112

Castello, L., Maina, M., Testa, G., Cavallini, G., Biasi, F., Donati, A., … Chiarpotto, E. (2011). Alternate-day fasting reverses the age-associated hypertrophy phenotype in rat heart by influencing the ERK and PI3K signaling pathways. *Mechanisms of Ageing and Development*, *132*(6–7), 305–314. https://doi.org/10.1016/j.mad.2011.06.006

Cerletti, M., Jang, Y. C., Finley, L. W. S., Haigis, M. C., & Wagers, A. J. (2013). Short-term calorie restriction enhances skeletal muscle stem cell function, *38*(5), 1148–1161. https://doi.org/10.1016/j.stem.2012.04.002.Short-term

Cesari, M., Leeuwenburgh, C., Lauretani, F., Onder, G., Maraldi, C., Guralnik, J. M., … Ferrucci, L. (2009). Frailty syndrome and skeletal muscle: results from the Invecchiare in Chianti study. *Am J Clin Nutr.*, *83*(5), 1142–1148.

Chadt, A., & Al-Hasani, H. (2020). Glucose transporters in adipose tissue, liver, and skeletal muscle in metabolic health and disease. *Pflugers Archiv European Journal of Physiology*. https://doi.org/10.1007/s00424-020-02417-x

Challet, E. (2010). Interactions between light, mealtime and calorie restriction to control daily timing in mammals. *Journal of Comparative Physiology B: Biochemical, Systemic, and Environmental Physiology*. https://doi.org/10.1007/s00360-010-0451-4

Charles, K. N., Li, M.-D., Engin, F., Arruda, A. P., Inouye, K., Khan, G., … Hotamisligil, S. (2017). Uncoupling of Metabolic Health from Longevity through Genetic Alteration of Adipose Tissue Lipid- Binding Proteins. *Cell Reports*, *21*, 393–402. https://doi.org/10.1016/j.celrep.2017.09.051

Chelakkot, C., Ghim, J., & Ryu, S. H. (2018). Mechanisms regulating intestinal barrier integrity and its pathological implications. *Experimental and Molecular Medicine*, *50*(8).

https://doi.org/10.1038/s12276-018-0126-x

Chen, J., Astle, C. M., & Harrison, D. E. (2003). Hematopoietic senescence is postponed and hematopoietic stem cell function is enhanced by dietary restriction. *Experimental Hematology*. https://doi.org/10.1016/S0301-472X(03)00238-8

Cheng, M., Mei, B., Zhou, Q., Zhang, M., Huang, H., Han, L., & Huang, Q. (2018). Computational analyses of obesity associated loci generated by genome-wide association studies. *PLoS ONE*, *13*(7), 1–13. https://doi.org/10.1371/journal.pone.0199987

Cheng, S., Keyes, M. J., Larson, M. G., McCabe, E. L., Newton-Cheh, C., Levy, D., … Wang, T. J. (2009). Long-term Outcomes in Individuals with a Prolonged PR Interval or First-Degree Atrioventricular Block. *JAMA*, *301*(24), 2571–2577. https://doi.org/10.1001/jama.2009.888

Chiang, H. R., Schoenfeld, L. W., Ruby, J. G., Auyeung, V. C., Spies, N., Baek, D., … Bartel, D. P. (2010). Mammalian microRNAs: Experimental evaluation of novel and previously annotated genes. *Genes and Development*. https://doi.org/10.1101/gad.1884710

Chiang, J. Y. L. (2009). Bile acids: Regulation of synthesis. *Journal of Lipid Research*, *50*(10), 1955–1966. https://doi.org/10.1194/jlr.R900010-JLR200

Chinetti-Gbaguidi, G., & Staels, B. (2011). Macrophage polarization in metabolic disorders: Functions and regulation. *Current Opinion in Lipidology*. https://doi.org/10.1097/MOL.0b013e32834a77b4

Choe, S. S., Huh, J. Y., Hwang, I. J., Kim, J. I., & Kim, J. B. (2016). Adipose tissue remodeling: Its role in energy metabolism and metabolic disorders. *Frontiers in Endocrinology*. https://doi.org/10.3389/fendo.2016.00030

Chuang, Y. F., An, Y., Bilgel, M., Wong, D. F., Troncoso, J. C., O'Brien, R. J., … Thambisetty, M. (2016). Midlife adiposity predicts earlier onset of Alzheimer's dementia, neuropathology and presymptomatic cerebral amyloid accumulation. *Molecular Psychiatry*, *21*(7), 910–915. https://doi.org/10.1038/mp.2015.129

Church, C., Berry, R., & Rodeheffer, M. S. (2014). NIH Public Access, 31–46. https://doi.org/10.1016/B978-0-12-411619-1.00003-3.Isolation

Church, C. D., Berry, R., & Rodeheffer, M. S. (2014). Isolation and study of adipocyte precursors. In *Methods in Enzymology*. https://doi.org/10.1016/B978-0-12-411619-1.00003-3

Cinti, S., Mitchell, G., Barbatelli, G., Murano, I., Ceresi, E., Faloia, E., … Obin, M. S. (2005). Adipocyte death defines macrophage localization and function in adipose tissue of obese mice and humans. *Journal of Lipid Research*. https://doi.org/10.1194/jlr.M500294-

JLR200

Clancy, D. J., Gems, D., Harshman, L. G., Oldham, S., Stocker, H., Hafen, E., … Partridge, L. (2001). Extension of life-span by loss of CHICO, a Drosophila insulin receptor substrate protein. *Science*. https://doi.org/10.1126/science.1057991

Clutton-Brock, T. H., & Isvaran, K. (2007). Sex differences in ageing in natural populations of vertebrates. *Proceedings of the Royal Society B: Biological Sciences*. https://doi.org/10.1098/rspb.2007.1138

Colman, R. J., Anderson, R. M., Johnson, S. C., Kastman, E. K., Kosmatka, K. J., Beasley, M., … Weindruch, R. (2009). Caloric Restriction Delays Disease Onset and Mortality in Rhesus Monkeys. *Science*, *325*(10 July), 201–204. https://doi.org/10.1126/science.1173635

Colman, R. J., Mark Beasley, T., Allison, D. B., & Weindruch, R. (2012). Skeletal effects of long-term caloric restriction in rhesus monkeys. *Age*, *34*(5), 1133–1143. https://doi.org/10.1007/s11357-011-9354-x

Consortium, T. tabula morris, Almanzar, N., Antony, J., Baghel, A. S., Bakerman, I., Bansal, I., … Zou, J. (2020). A single-cell transcriptomic atlas characterizes ageing tissues in the mouse. *Nature*. https://doi.org/10.1038/s41586-020-2496-1

Coolbaugh, C. L., Damon, B. M., Bush, E. C., Welch, E. B., & Towse, T. F. (2019). Cold exposure induces dynamic, heterogeneous alterations in human brown adipose tissue lipid content. *Scientific Reports*. https://doi.org/10.1038/s41598-019-49936-x

Coppack, S. W. (2001). Pro-inflammatory cytokines and adipose tissue. *Proceedings of the Nutrition Society*. https://doi.org/10.1079/pns2001110

Corrales, P., Vivas, Y., Izquierdo-Lahuerta, A., Horrillo, D., Seoane-Collazo, P., Velasco, I., … Medina-Gomez, G. (2019). Long-term caloric restriction ameliorates deleterious effects of aging on white and brown adipose tissue plasticity. *Aging Cell*, *18*(3), 1–16. https://doi.org/10.1111/acel.12948

Correa-De-Araujo, R., & Hadley, E. (2014). Skeletal muscle function deficit: A new terminology to embrace the evolving concepts of sarcopenia and age-related muscle dysfunction. *Journals of Gerontology - Series A Biological Sciences and Medical Sciences*, *69 A*(5), 591–594. https://doi.org/10.1093/gerona/glt208

Cortés, A., Muñoz-Antoli, C., Martín-Grau, C., Esteban, J. G., Grencis, R. K., & Toledo, R. (2015). Differential alterations in the small intestine epithelial cell turnover during acute and chronic infection with Echinostoma caproni (Trematoda). *Parasites and Vectors*. https://doi.org/10.1186/s13071-015-0948-5

Coschigano, K. T., Clemmons, D., Bellush, L. L., & Kopchick, J. J. (2000). Assessment of

growth parameters and life span of GHR/BP gene-disrupted mice. *Endocrinology*, *141*(7), 2608–2613. https://doi.org/10.1210/endo.141.7.7586

Cuesta, M., Clesse, D., Pévet, P., & Challet, E. (2009). From daily behavior to hormonal and neurotransmitters rhythms: Comparison between diurnal and nocturnal rat species. *Hormones and Behavior*. https://doi.org/10.1016/j.yhbeh.2008.10.015

Cui, H., Tang, D., Garside, G. B., Zeng, T., Wang, Y., Tao, Z., … Tao, S. (2019). Wnt Signaling Mediates the Aging-Induced Differentiation Impairment of Intestinal Stem Cells. *Stem Cell Reviews and Reports*, *15*(3), 448–455. https://doi.org/10.1007/s12015-019-09880-9

Cunha-Santos, J., Duarte-Neves, J., Carmona, V., Guarente, L., De Almeida, L. P., & Cavadas, C. (2016). Caloric restriction blocks neuropathology and motor deficits in Machado-Joseph disease mouse models through SIRT1 pathway. *Nature Communications*. https://doi.org/10.1038/ncomms11445

Curtis, K. J., Kim, Y. S., Perdomo, J. M., & Whitehead, J. S. (1978). Protein digestion and absorption in the rat. *J Physiol.*, *274*, 409–419. https://doi.org/10.1113/jphysiol.1978.sp012156

D'souza, A. M., Neumann, U. H., Glavas, M. M., & Kieffer, T. J. (2017). The glucoregulatory actions of leptin. *Molecular Metabolism*. https://doi.org/10.1016/j.molmet.2017.04.011

Da Silva, P. F. L., & Schumacher, B. (2019). DNA damage responses in ageing. *Open Biology*. https://doi.org/10.1098/rsob.190168

Dailey, M. J. (2014). Nutrient-induced intestinal adaption and its effect in obesity. *Physiology and Behavior*, *136*, 74–78. https://doi.org/10.1016/j.physbeh.2014.03.026

Das, G. (1990). QT interval and repolarization time in patients with intraventricular conduction delay. *Journal of Electrocardiology*, *23*(1), 49–52. https://doi.org/10.1016/0022-0736(90)90150-Z

Datta, S. R., Dudek, H., Xu, T., Masters, S., Haian, F., Gotoh, Y., & Greenberg, M. E. (1997). Akt phosphorylation of BAD couples survival signals to the cell- intrinsic death machinery. *Cell*, *91*(2), 231–241. https://doi.org/10.1016/S0092-8674(00)80405-5

Davidson-Pilon, C., Kalderstam, J., Jacobson, N., sean-reed, Kuhn, B., Zivich, P., … jlim13. (2020). CamDavidsonPilon/lifelines: v0.25.5. https://doi.org/10.5281/ZENODO.4050560

Davies, L. C., Jenkins, S. J., Allen, J. E., & Taylor, P. R. (2013). Tissue-resident macrophages. *Nature Immunology*, *14*(10), 986–995. https://doi.org/10.1038/ni.2705

Davis, J. N., Hodges, V. A., & Gillham, M. B. (2006). Normal-Weight Adults Consume More Fiber and Fruit than Their Age- and Height-Matched Overweight/Obese Counterparts. *Journal of the American Dietetic Association*, *106*(6), 833–840.

https://doi.org/10.1016/j.jada.2006.03.013

De Bacquer, D., De Backer, G., Kornitzer, M., & Blackburn, H. (1998). Prognostic value of ECG findings for total, cardiovascular disease, and coronary heart disease death in men and women. *Heart*, *80*(6), 570–577. https://doi.org/10.1136/hrt.80.6.570

De Jonge, L., Moreira, E. A. M., Martin, C. K., & Ravussin, E. (2010). Impact of 6-month caloric restriction on autonomic nervous system activity in healthy, overweight, individuals. *Obesity*. https://doi.org/10.1038/oby.2009.408

de Lorenzo, M. S., Baljinnyam, E., Vatner, D. E., Abarzúa, P., Vatner, S. F., & Rabson, A. B. (2011). Caloric restriction reduces growth of mammary tumors and metastases. *Carcinogenesis*, *32*(9), 1381–1387. https://doi.org/10.1093/carcin/bgr107

De Lucia, C., Gambino, G., Petraglia, L., Elia, A., Komici, K., Femminella, G. D., … Rengo, G. (2018). Long-term caloric restriction improves cardiac function, remodeling, adrenergic responsiveness, and sympathetic innervation in a model of postischemic heart failure. *Circulation: Heart Failure*. https://doi.org/10.1161/CIRCHEARTFAILURE.117.004153

de Sá, P. M., Richard, A. J., Hang, H., & Stephens, J. M. (2017). Transcriptional regulation of adipogenesis. *Comprehensive Physiology*. https://doi.org/10.1002/cphy.c160022

De Santa Barbara, P., Van Den Brink, G. R., & Roberts, D. J. (2003). Development and differentiation of the intestinal epithelium. *Cellular and Molecular Life Sciences*. https://doi.org/10.1007/s00018-003-2289-3

Deelen, J., Beekman, M., Uh, H. W., Broer, L., Ayers, K. L., Tan, Q., … Slagboom, P. E. (2014). Genome-wide association meta-analysis of human longevity identifies a novel locus conferring survival beyond 90 years of age. *Human Molecular Genetics*, *23*(16), 4420–4432. https://doi.org/10.1093/hmg/ddu139

Deelen, J., Evans, D. S., Arking, D. E., Tesi, N., Nygaard, M., Liu, X., … Murabito, J. M. (2019). A meta-analysis of genome-wide association studies identifies multiple longevity genes. *Nature Communications*, *10*(1). https://doi.org/10.1038/s41467-019-11558-2

Deelen, J., Uh, H. W., Monajemi, R., Van Heemst, D., Thijssen, P. E., Böhringer, S., … Beekman, M. (2013). Gene set analysis of GWAS data for human longevity highlights the relevance of the insulin/IGF-1 signaling and telomere maintenance pathways. *Age*, *35*(1), 235–249. https://doi.org/10.1007/s11357-011-9340-3

Delvaux, K., Lysens, R., Philippaerts, R., Thomis, M., Vanreusel, B., Claessens, A. L., … Lefevre, J. (1999). Associations between physical activity, nutritional practices and health-related anthropometry in Flemish males: A 5-year follow-up study. *International Journal of Obesity*. https://doi.org/10.1038/sj.ijo.0801052

DeSantis, C. E., Miller, K. D., Dale, W., Mohile, S. G., Cohen, H. J., Leach, C. R., … Siegel,

R. L. (2019). Cancer statistics for adults aged 85 years and older, 2019. *CA: A Cancer Journal for Clinicians*. https://doi.org/10.3322/caac.21577

Dhahbi, J. M., Kim, H. J., Mote, P. L., Beaver, R. J., & Spindler, S. R. (2004). Temporal linkage between the phenotypic and genomic responses to caloric restriction. *Proceedings of the National Academy of Sciences of the United States of America*, *101*(15), 5524–5529. https://doi.org/10.1073/pnas.0305300101

Dhahbi, J. M., Tsuchiya, T., Kim, H. J., Mote, P. L., & Spindler, S. R. (2006). Gene expression and physiologic responses of the heart to the initiation and withdrawal of caloric restriction. *Journals of Gerontology - Series A Biological Sciences and Medical Sciences*. https://doi.org/10.1093/gerona/61.3.218

Di Nisio, A., Sabovic, I., De Toni, L., Rocca, M. S., Dall'Acqua, S., Azzena, B., … Foresta, C. (2020). Testosterone is sequestered in dysfunctional adipose tissue, modifying androgen-responsive genes. *International Journal of Obesity*. https://doi.org/10.1038/s41366-020-0568-9

Di, W., Lv, Y., Xia, F., Sheng, Y., Liu, J., & Ding, G. (2020). Improvement of intestinal stem cells and barrier function via energy restriction in middle-aged C57BL/6 mice. *Nutrition Research*, *81*, 47–57. https://doi.org/10.1016/j.nutres.2020.06.015

Divella, R., Mazzocca, A., Daniele, A., Sabbà, C., & Paradiso, A. (2019). Obesity, nonalcoholic fatty liver disease and adipocytokines network in promotion of cancer. *International Journal of Biological Sciences*. https://doi.org/10.7150/ijbs.29599

Dolinsky, V. W., & Dyck, J. R. B. (2011). Calorie restriction and resveratrol in cardiovascular health and disease. *Biochimica et Biophysica Acta - Molecular Basis of Disease*. https://doi.org/10.1016/j.bbadis.2011.06.010

Dönertaş, H. M., Fuentealba, M., Partridge, L., & Thornton, J. M. (2019). Identifying Potential Ageing-Modulating Drugs In Silico. *Trends in Endocrinology and Metabolism*. https://doi.org/10.1016/j.tem.2018.11.005

Drake, I., Sonestedt, E., Ericson, U., Wallström, P., & Orho-Melander, M. (2018). A Western dietary pattern is prospectively associated with cardio-metabolic traits and incidence of the metabolic syndrome. *British Journal of Nutrition*, *119*(10), 1168–1176. https://doi.org/10.1017/S000711451800079X

Drapanas, T., Williams, J. S., Mcdonald, J. C., Heyden, W., Bow, T., & Spencer, R. P. (1963). Role of the Ileum in the Absorption of Vitamin B12 and Intrinsic Factor (NF). *JAMA: The Journal of the American Medical Association*. https://doi.org/10.1001/jama.1963.73700180001009

Drewnowski, A., & Darmon, N. (2005). The economics of obesity: dietary energy density and

energy cost. *The American Journal of Clinical Nutrition*. https://doi.org/10.1093/ajcn/82.1.265s

Drozdowski, L., & Thomson, A. B. R. (2006). Aging and the intestine. *World Journal of Gastroenterology*. https://doi.org/10.3748/wjg.v12.i47.7578

Duan, T., Sun, W., Zhang, M., Ge, J., He, Y., Zhang, J., … Yu, P. (2017). Dietary restriction protects against diethylnitrosamine-induced hepatocellular tumorigenesis by restoring the disturbed gene expression profile. *Scientific Reports*, *7*(January), 1–13. https://doi.org/10.1038/srep43745

Duffy, P. H., Seng, J. E., Lewis, S. M., Mayhugh, M. A., Aidoo, A., Hattan, D. G., … Feuers, R. J. (2001). The effects of different levels of dietary restriction on aging and survival in the Sprague-Dawley rat: Implications for chronic studies. *Aging Clinical and Experimental Research*. https://doi.org/10.1007/bf03353422

Dunn, S. E., Kari, F. W., French, J., Leininger, J. R., Travios, G., Wilson, R., & Barrett, and J. C. (1997). Dietary Restriction Reduces Insulin-like Growth Factor I Levels, Which Modulates Apoptosis, Cell Proliferation, and Tumor Progression in p53-deficient Mice. *Cancer*, *57*(21), 4667–4672.

Duvigneaud, N., Wijndaele, K., Matton, L., Philippaerts, R., Lefevre, J., Thomis, M., … Duquet, W. (2007). Dietary factors associated with obesity indicators and level of sports participation in Flemish adults: A cross-sectional study. *Nutrition Journal*. https://doi.org/10.1186/1475-2891-6-26

Edrey, Y. H., Hanes, M., Pinto, M., Mele, J., & Buffenstein, R. (2011). Successful aging and sustained good health in the naked mole rat: A long-lived mammalian model for biogerontology and biomedical research. *ILAR Journal*, *52*(1), 41–53. https://doi.org/10.1093/ilar.52.1.41

Entringer, S., Rasmussen, J., Cooper, D. M., Ikenoue, S., Waffarn, F., Wadhwa, P. D., & Buss, C. (2017). Association between supraclavicular brown adipose tissue composition at birth and adiposity gain from birth to 6 months of age. *Pediatric Research*. https://doi.org/10.1038/pr.2017.159

Esposito, K., Giugliano, F., Ciotola, M., De Sio, M., D'Armiento, M., & Giugliano, D. (2008). Obesity and sexual dysfunction, male and female. *International Journal of Impotence Research*. https://doi.org/10.1038/ijir.2008.9

Ezeh, U., Pall, M., Mathur, R., & Azziz, R. (2014). Association of fat to lean mass ratio with metabolic dysfunction in women with polycystic ovary syndrome. *Human Reproduction*, *29*(7), 1508–1517. https://doi.org/10.1093/humrep/deu096

Fabbiano, S., Suárez-Zamorano, N., Rigo, D., Veyrat-Durebex, C., Stevanovic Dokic, A., Colin,

D. J., & Trajkovski, M. (2016). Caloric Restriction Leads to Browning of White Adipose Tissue through Type 2 Immune Signaling. *Cell Metabolism*, *24*(3), 434–446. https://doi.org/10.1016/j.cmet.2016.07.023

Farin, H. F., Karthaus, W. R., Kujala, P., Rakhshandehroo, M., Schwank, G., Vries, R. G. J., … Clevers, H. (2014). Paneth cell extrusion and release of antimicrobial products is directly controlled by immune cell-derived IFN-γ. *Journal of Experimental Medicine*. https://doi.org/10.1084/jem.20130753

Fehlmann, T., Lehallier, B., Schaum, N., Hahn, O., Kahraman, M., Li, Y., … Keller, A. (2020). Common diseases alter the physiological age-related blood microRNA profile. *Nature Communications*. https://doi.org/10.1038/s41467-020-19665-1

Ferrannini, G., Namwanje, M., Fang, B., Damle, M., Li, D., Liu, Q., … Qiang, L. (2016). Genetic backgrounds determine brown remodeling of white fat in rodents. *Molecular Metabolism*. https://doi.org/10.1016/j.molmet.2016.08.013

Ferrari, R., Censi, S., Mastrorilli, F., & Boraso, A. (2003). Prognostic benefits of heart rate reduction in cardiovascular disease. *European Heart Journal, Supplement*. https://doi.org/10.1016/S1520-765X(03)90002-2

Ferraris, R. P., Casirola, D. M., & Vinnakota, R. R. (1993). Dietary carbohydrate enhances intestinal sugar transport in diabetic mice. *Diabetes*, *42*(11), 1579–1587. https://doi.org/10.2337/diab.42.11.1579

Figueroa, C. D., & Taberner, P. V. (1994). Pancreatic islet hypertrophy in spontaneous maturity onset obese-diabetic CBA/Ca mice. *International Journal of Biochemistry*, *26*(10–11), 1299–1303. https://doi.org/10.1016/0020-711X(94)90099-X

Finkelstein, E. A., Khavjou, O. A., Thompson, H., Trogdon, J. G., Pan, L., Sherry, B., & Dietz, W. (2012). Obesity and severe obesity forecasts through 2030. *American Journal of Preventive Medicine*, *42*(6), 563–570. https://doi.org/10.1016/j.amepre.2011.10.026

Fischer, K. E., Hoffman, J. M., Sloane, L. B., Gelfond, J. A. L., Soto, V. Y., Richardson, A. G., & Austad, S. N. (2016). A cross-sectional study of male and female C57BL/6Nia mice suggests lifespan and healthspan are not necessarily correlated. *Aging*, *8*(10), 2370–2391. https://doi.org/10.18632/aging.101059

Flatt, T., & Partridge, L. (2018). Horizons in the evolution of aging. *BMC Biology*. https://doi.org/10.1186/s12915-018-0562-z

Fleury Curado, T., Pho, H., Berger, S., Caballero-Eraso, C., Shin, M. K., Sennes, L. U., … Polotsky, V. Y. (2018). Sleep-disordered breathing in C57BL/6J mice with diet-induced obesity. *Sleep*, *41*(8), 1–9. https://doi.org/10.1093/sleep/zsy089

Flint, H. J., Scott, K. P., Louis, P., & Duncan, S. H. (2012). The role of the gut microbiota in

nutrition and health. *Nature Reviews Gastroenterology and Hepatology*. https://doi.org/10.1038/nrgastro.2012.156

Flurkey, K., Currer, J., & Harrison, D. (2007). *The Mouse in Aging Research*. (J. Fox, S. Barthold, M. Davisson, C. Newcomer, F. Quimby, & A. Smith, Eds.), *The Mouse in Biomedical Research 2nd Edition* (2nd ed.). Buglington, MA: American College Laboratory Animal Medicine (Elsevier).

Fontana, L., Klein, S., & Holloszy, J. O. (2010). Effects of long-term calorie restriction and endurance exercise on glucose tolerance, insulin action, and adipokine production. *Age*, *32*(1), 97–108. https://doi.org/10.1007/s11357-009-9118-z

Fontana, L., Meyer, T. E., Klein, S., & Holloszy, J. O. (2004). Long-term calorie restriction is highly effective in reducing the risk for atherosclerosis in humans. *Proceedings of the National Academy of Sciences of the United States of America*. https://doi.org/10.1073/pnas.0308291101

Fontana, L., & Partridge, L. (2015). Promoting health and longevity through diet: From model organisms to humans. *Cell*, *161*(1), 106–118. https://doi.org/10.1016/j.cell.2015.02.020

Fontana, L., Partridge, L., & Longo, V. D. (2010). Extending healthy life span-from yeast to humans. *Science*. https://doi.org/10.1126/science.1172539

Fontana, L., Villareal, D. T., Das, S. K., Smith, S. R., Meydani, S. N., Pittas, A. G., … Holloszy, J. O. (2016). Effects of 2-year calorie restriction on circulating levels of IGF-1, IGF-binding proteins and cortisol in nonobese men and women: A randomized clinical trial. *Aging Cell*, *15*(1), 22–27. https://doi.org/10.1111/acel.12400

Fontana, L., Villareal, D. T., Weiss, E. P., Racette, S. B., Steger-May, K., Klein, S., & Holloszy, J. O. (2007). Calorie restriction or exercise: Effects on coronary heart disease risk factors. A randomized, controlled trial. *American Journal of Physiology - Endocrinology and Metabolism*, *293*(1), 197–202. https://doi.org/10.1152/ajpendo.00102.2007

Fontana, L., Weiss, E. P., Villareal, D. T., Klein, S., & Holloszy, O. (2009). Long-term effects of calorie or protein restriction on serum IGF-1 and IGFBP-3 concentration in humans. *Aging Cell*, *7*(5), 681–687. https://doi.org/10.1111/j.1474-9726.2008.00417.x.Long-term

Forni, M. F., Peloggia, J., Braga, T. T., Chinchilla, J. E. O., Shinohara, J., Navas, C. A., … Kowaltowski, A. J. (2017). Caloric Restriction Promotes Structural and Metabolic Changes in the Skin. *Cell Reports*, *20*(11), 2678–2692. https://doi.org/10.1016/j.celrep.2017.08.052

Forster, M. J., Morris, P., & Sohal, R. S. (2003). Genotype and age influence the effect of caloric intake on mortality in mice. *The FASEB Journal : Official Publication of the Federation of American Societies for Experimental Biology*, *17*(6), 690–692.

https://doi.org/10.1096/fj.02-0533fje

Frese, S. A., Benson, A. K., Tannock, G. W., Loach, D. M., Kim, J., Zhang, M., … Walter, J. (2011). The evolution of host specialization in the vertebrate gut symbiont Lactobacillus reuteri. *PLoS Genetics*. https://doi.org/10.1371/journal.pgen.1001314

Fried, S. K., Lee, M. J., & Karastergiou, K. (2015). Shaping fat distribution: New insights into the molecular determinants of depot- and sex-dependent adipose biology. *Obesity*. https://doi.org/10.1002/oby.21133

Füchtbauer, E. -M, & Westphal, H. (1992). MyoD and myogenin are coexpressed in regenerating skeletal muscle of the mouse. *Developmental Dynamics*. https://doi.org/10.1002/aja.1001930106

Fuentealba, M., Fabian, D. K., Dönertaş, H. M., Thornton, J. M., & Partridge, L. (2021). Transcriptomic profiling of long- and short-lived mutant mice implicates mitochondrial metabolism in ageing and shows signatures of normal ageing in progeroid mice. *Mechanisms of Ageing and Development*. https://doi.org/10.1016/j.mad.2021.111437

Fujii, N., Narita, T., Okita, N., Kobayashi, M., Furuta, Y., Chujo, Y., … Higami, Y. (2017). Sterol regulatory element-binding protein-1c orchestrates metabolic remodeling of white adipose tissue by caloric restriction. *Aging Cell*. https://doi.org/10.1111/acel.12576

Fujino, T., Fried, B., Ichikawa, H., & Tada, I. (1996). Rapid expulsion of the intestinal trematodes Echinostoma trivolvis and E. caproni from C3H mice by trapping with increased goblet cell mucins. *International Journal for Parasitology*. https://doi.org/10.1016/0020-7519(95)00125-5

Funck-Brentano, C., & Jaillon, P. (1993). Rate-corrected QT interval: Techniques and limitations. *The American Journal of Cardiology*. https://doi.org/10.1016/0002-9149(93)90035-B

Fuster, J. J., Ouchi, N., Gokce, N., & Walsh, K. (2016). Obesity-induced changes in adipose tissue microenvironment and their impact on cardiovascular disease. *Circulation Research*, *118*(11), 1786–1807. https://doi.org/10.1161/CIRCRESAHA.115.306885

Galic, S., Oakhill, J. S., & Steinberg, G. R. (2010). Adipose tissue as an endocrine organ. *Molecular and Cellular Endocrinology*. https://doi.org/10.1016/j.mce.2009.08.018

García-Gaytán, A. C., Miranda-Anaya, M., Turrubiate, I., López-De Portugal, L., Bocanegra-Botello, G. N., López-Islas, A., … Méndez, I. (2020). Synchronization of the circadian clock by time-restricted feeding with progressive increasing calorie intake. Resemblances and differences regarding a sustained hypocaloric restriction. *Scientific Reports*. https://doi.org/10.1038/s41598-020-66538-0

García-Prieto, C. F., & Fernández-Alfonso, M. S. (2016). Caloric restriction as a strategy to

improve vascular dysfunction in metabolic disorders. *Nutrients*. https://doi.org/10.3390/nu8060370

Garcia, A. M., Busuttil, R. A., Calder, R. B., Doll??, M. E. T., Diaz, V., McMahan, C. A., … Vijg, J. (2008). Effect of Ames dwarfism and caloric restriction on spontaneous DNA mutation frequency in different mouse tissues. *Mechanisms of Ageing and Development*, *129*(9), 528–533. https://doi.org/10.1016/j.mad.2008.04.013

Gaskill, B. N., Gordon, C. J., Pajor, E. A., Lucas, J. R., Davis, J. K., & Garner, J. P. (2013). Impact of nesting material on mouse body temperature and physiology. *Physiology and Behavior*. https://doi.org/10.1016/j.physbeh.2012.12.018

Gauthier, M. S., Rabasa-Lhoret, R., Prud'homme, D., Karelis, A. D., Geng, D., Van Bavel, B., & Ruzzin, J. (2014). The metabolically healthy but obese phenotype is associated with lower plasma levels of persistent organic pollutants as compared to the metabolically abnormal obese phenotype. *Journal of Clinical Endocrinology and Metabolism*, *99*(6), 1061–1066. https://doi.org/10.1210/jc.2013-3935

Gebert, N., Cheng, C. W., Kirkpatrick, J. M., Di Fraia, D., Yun, J., Schädel, P., … Ori, A. (2020). Region-Specific Proteome Changes of the Intestinal Epithelium during Aging and Dietary Restriction. *Cell Reports*, *31*(4). https://doi.org/10.1016/j.celrep.2020.107565

Gems, D., & Partridge, L. (2013). Genetics of Longevity in Model Organisms: Debates and Paradigm Shifts. *Annu. Rev. Physiol*, *75*, 621–644. https://doi.org/10.1146/annurev-physiol-030212-183712

Gent, S., Kleinbongard, P., Dammann, P., Neuhäuser, M., & Heusch, G. (2015). Heart rate reduction and longevity in mice. *Basic Research in Cardiology*. https://doi.org/10.1007/s00395-014-0460-7

Gilsanz, V., Hu, H. H., & Kajimura, S. (2013). Relevance of brown adipose tissue in infancy and adolescence. *Pediatric Research*. https://doi.org/10.1038/pr.2012.141

Giordano, A., Murano, I., Mondini, E., Perugini, J., Smorlesi, A., Severi, I., … Cinti, S. (2013). Obese adipocytes show ultrastructural features of stressed cells and die of pyroptosis. *Journal of Lipid Research*, *54*(9), 2423–2436. https://doi.org/10.1194/jlr.M038638

Glass, C. K., & Olefsky, J. M. (2012). Inflammation and lipid signaling in the etiology of insulin resistance. *Cell Metabolism*. https://doi.org/10.1016/j.cmet.2012.04.001

Goldberger, J. J., Johnson, N. P., Subacius, H., Ng, J., & Greenland, P. (2014). Comparison of the physiologic and prognostic implications of the heart rate versus the RR interval. *Heart Rhythm*. https://doi.org/10.1016/j.hrthm.2014.07.037

Gollob, M. H., Green, M. S., Tang, A. S. L., Gollob, T., Karibe, A., Hassan, A.-S., … Roberts, R. (2001). Identification of a Gene Responsible for Familial Wolff–Parkinson–White

Syndrome. *N Engl J Med*, *344*(24), 1823–1831. https://doi.org/10.1056/NEJM200106143442403

Gomez-Cabrera, M. C., Garcia-Valles, R., Rodriguez-Mañas, L., Garcia-Garcia, F. J., Olaso-Gonzalez, G., Salvador-Pascual, A., … Viña, J. (2017). A New Frailty Score for Experimental Animals Based on the Clinical Phenotype: Inactivity as a Model of Frailty. *Journals of Gerontology - Series A Biological Sciences and Medical Sciences*. https://doi.org/10.1093/gerona/glw337

Goodman, B. E. (2010). Insights into digestion and absorption of major nutrients in humans. *American Journal of Physiology - Advances in Physiology Education*. https://doi.org/10.1152/advan.00094.2009

Grassi, L., Alfonsi, R., Francescangeli, F., Signore, M., De Angelis, M. L., Addario, A., … Bonci, D. (2019). Organoids as a new model for improving regenerative medicine and cancer personalized therapy in renal diseases. *Cell Death and Disease*, *10*(3). https://doi.org/10.1038/s41419-019-1453-0

Greco, E. A., Pietschmann, P., & Migliaccio, S. (2019). Osteoporosis and sarcopenia increase frailty syndrome in the elderly. *Frontiers in Endocrinology*, *10*(APR), 1–10. https://doi.org/10.3389/fendo.2019.00255

Green, B. B., Weiss, N. S., & Daling, J. R. (1988). Risk of ovulatory infertility in relation to body weight. *Fertility and Sterility*. https://doi.org/10.1016/s0015-0282(16)60305-9

Greer, E. L., & Brunet, A. (2005). FOXO transcription factors at the interface between longevity and tumor suppression. *Oncogene*, *24*(50), 7410–7425. https://doi.org/10.1038/sj.onc.1209086

Grodstein, F., Goldman, M. B., & Cramer, D. W. (1994). Body mass index and ovulatory infertility. *Epidemiology*. https://doi.org/10.1097/00001648-199403000-00016

Grönke, S., Clarke, D.-F., Broughton, S., Andrews, T. D., & Partridge, L. (2010). Molecular evolution and functional characterization of Drosophila insulin-like peptides. *PLoS Genetics*, *6*(2), e1000857. https://doi.org/10.1371/journal.pgen.1000857

Gross, L., & Dreyfuss, Y. (1984). Reduction of the incidence of radiation-induced tumors in rats after restriction of food intake. *Proceedings of the National Academy of Sciences of the United States of America*. https://doi.org/10.1073/pnas.81.23.7596

Grotewiel, M. S., Martin, I., Bhandari, P., & Cook-Wiens, E. (2005). Functional senescence in Drosophila melanogaster. *Ageing Research Reviews*. https://doi.org/10.1016/j.arr.2005.04.001

Gu, S., Chen, D., Zhang, J. N., Lv, X., Wang, K., Duan, L. P., … Wu, X. L. (2013). Bacterial Community Mapping of the Mouse Gastrointestinal Tract. *PLoS ONE*.

https://doi.org/10.1371/journal.pone.0074957

Guerra, C., Koza, R. A., Yamashita, H., Walsh, K., & Kozak, L. P. (1998). Emergence of brown adipocytes in white fat in mice is under genetic control effects on body weight and adiposity. *Journal of Clinical Investigation*. https://doi.org/10.1172/JCI3155

Guerville, M., Leroy, A., Sinquin, A., Laugerette, F., Michalski, M. C., & Boudry, G. (2017). Western-diet consumption induces alteration of barrier function mechanisms in the ileum that correlates with metabolic endotoxemia in rats. *American Journal of Physiology - Endocrinology and Metabolism*. https://doi.org/10.1152/ajpendo.00372.2016

Guevara-Aguirre, J., Balasubramanian, P., Guevara-Aguirre, M., Wei, M., Madia, F., Cheng, C.-W., … Longo, V. D. (2011). Growth Hormone Receptor Deficiency Is Associated with a Major Reduction in Pro-Aging Signaling, Cancer, and Diabetes in Humans. *Science Translational Medicine*, *3*(70), 70ra13-70ra13. https://doi.org/10.1126/scitranslmed.3001845

Guo, W., Pirtskhalava, T., Tchkonia, T., Xie, W., Thomou, T., Han, J., … Kirkland, J. L. (2007). Aging results in paradoxical susceptibility of fat cell progenitors to lipotoxicity. *American Journal of Physiology - Endocrinology and Metabolism*. https://doi.org/10.1152/ajpendo.00557.2006

Gutierrez, E., Wiggins, D., Fielding, B., & Gould, A. P. (2007). Specialized hepatocyte-like cells regulate Drosophila lipid metabolism. *Nature*. https://doi.org/10.1038/nature05382

Hahn, O., Drews, L. F., Nguyen, A., Tatsuta, T., Gkioni, L., Hendrich, O., … Partridge, L. (2019). A nutritional memory effect counteracts the benefits of dietary restriction in old mice. *Nature Metabolism*, *1*(November). https://doi.org/10.1038/s42255-019-0121-0

Hahn, O., Grönke, S., Stubbs, T. M., Ficz, G., Hendrich, O., Krueger, F., … Partridge, L. (2017). Dietary restriction protects from age-associated DNA methylation and induces epigenetic reprogramming of lipid metabolism. *Genome Biology*, *18*(1), 56. https://doi.org/10.1186/s13059-017-1187-1

Haines, D. C., Chattopadhyay, S., & Ward, J. M. (2001). Pathology of Aging B6;129 Mice. *Toxicologic Pathology*. https://doi.org/10.1080/019262301753385988

Hambly, C., Mercer, J. G., & Speakman, J. R. (2007). Hunger does not diminish over time in mice under protracted caloric restriction. *Rejuvenation Research*. https://doi.org/10.1089/rej.2007.0555

Hammer, S., Van Der Meer, R. W., Lamb, H. J., Schär, M., De Roos, A., Smit, J. W. A., & Romijn, J. A. (2008). Progressive caloric restriction induces dose-dependent changes in myocardial triglyceride content and diastolic function in healthy men. *Journal of Clinical Endocrinology and Metabolism*, *93*(2), 497–503. https://doi.org/10.1210/jc.2007-2015

Hanlon, P., Nicholl, B. I., Jani, B. D., Lee, D., McQueenie, R., & Mair, F. S. (2018). Frailty and pre-frailty in middle-aged and older adults and its association with multimorbidity and mortality: a prospective analysis of 493 737 UK Biobank participants. *The Lancet Public Health*, *3*(7), e323–e332. https://doi.org/10.1016/S2468-2667(18)30091-4

Harada, H., Andersen, J. S., Mann, M., Terada, N., & Korsmeyer, S. J. (2001). p70S6 kinase signals cell survival as well as growth, inactivating the pro-apoptotic molecule BAD. *Proceedings of the National Academy of Sciences of the United States of America*, *98*(17), 9666–9670. https://doi.org/10.1073/pnas.171301998

Harbison, C. E., Lipman, R. D., & Bronson, R. T. (2016). Strain- and Diet-Related Lesion Variability in Aging DBA/2, C57BL/6, and DBA/2xC57BL/6 F1 Mice. *Veterinary Pathology*. https://doi.org/10.1177/0300985815612152

Harel, I., Benayoun, B. A., Machado, B., Singh, P. P., Hu, C. K., Pech, M. F., … Brunet, A. (2015). A platform for rapid exploration of aging and diseases in a naturally short-lived vertebrate. *Cell*. https://doi.org/10.1016/j.cell.2015.01.038

Harper, J. M., Leathers, C. W., & Austad, S. N. (2006). Does caloric restriction extend life in wild mice? *Aging Cell*. https://doi.org/10.1111/j.1474-9726.2006.00236.x

Harrison, D. E., Strong, R., Sharp, Z. D., Nelson, J. F., Astle, C. M., Flurkey, K., … Miller, R. A. (2010). Rapamycin fed late in life extends lifespan in genetically heterogeneous mice. *Nature*, *460*(7253), 392–395. https://doi.org/10.1016/S1073-5437(10)79498-5

Hart, R. W., & Turturro, A. (1997). Dietary restrictions and cancer. In *Environmental Health Perspectives*. https://doi.org/10.1289/ehp.97105s4989

Harwood, H. J. (2012). The adipocyte as an endocrine organ in the regulation of metabolic homeostasis. *Neuropharmacology*, *63*(1), 57–75. https://doi.org/10.1016/j.neuropharm.2011.12.010

Haslam, D. W., & James, W. P. T. (2005). Obesity. In *Lancet*. https://doi.org/10.1016/S0140-6736(05)67483-1

Haun, C., Alexander, J., Stainier, D. Y., & Okkema, P. G. (1998). Rescue of Caenorhabditis elegans pharyngeal development by a vertebrate heart specification gene. *Proceedings of the National Academy of Sciences of the United States of America*. https://doi.org/10.1073/pnas.95.9.5072

Heilbronn, L. K., De Jonge, L., Frisard, M. I., DeLany, J. P., Larson-Meyer, D. E., Rood, J., … Ravussin, E. (2006). Effect of 6-month calorie restriction on biomarkers of longevity, metabolic adaptation, and oxidative stress in overweight individuals: A randomized controlled trial. *Journal of the American Medical Association*. https://doi.org/10.1001/jama.295.13.1539

Herbert, A., Gerry, N. P., McQueen, M. B., Heid, I. M., Pfeufer, A., Illig, T., … Christman, M. F. (2006). A common genetic variant is associated with adult and childhood obesity. *Science*. https://doi.org/10.1126/science.1124779

Herdman SJ, Blatt P, Schubert MC, T. R. (2000). Falls in patients with vestibular deficits. *Am J Otol.*, *21*(6), 847–851.

Hipp, M. S., Kasturi, P., & Hartl, F. U. (2019). The proteostasis network and its decline in ageing. *Nature Reviews Molecular Cell Biology*. https://doi.org/10.1038/s41580-019-0101-y

Hitt, H. C., McMillen, R. C., Thornton-Neaves, T., Koch, K., & Cosby, A. G. (2007). Comorbidity of Obesity and Pain in a General Population: Results from the Southern Pain Prevalence Study. *Journal of Pain*. https://doi.org/10.1016/j.jpain.2006.12.003

Holloszy, J. O., Smith, E. K., Vining, M., & Adams, S. (1985). Effect of voluntary exercise on longevity of rats. *Journal of Applied Physiology*. https://doi.org/10.1152/jappl.1985.59.3.826

Holt, P. R. (2007). Intestinal malabsorption in the elderly. *Digestive Diseases*. https://doi.org/10.1159/000099479

Holz, M. K., Ballif, B. A., Gygi, S. P., & Blenis, J. (2005). mTOR and S6K1 mediate assembly of the translation preinitiation complex through dynamic protein interchange and ordered phosphorylation events. *Cell*, *123*(4), 569–580. https://doi.org/10.1016/j.cell.2005.10.024

Holzenberger, M., Dupont, J., Ducos, B., Leneuve, P., Géloën, A., Even, P. C., … Le Bouc, Y. (2003). IGF-1 receptor regulates lifespan and resistance to oxidative stress in mice. *Nature*. https://doi.org/10.1038/nature01298

Hotamisligil, G. S., Shargill, N. S., & Spiegelman, B. M. (1993). Adipose expression of tumor necrosis factor-α: Direct role in obesity-linked insulin resistance. *Science*, *259*(5091), 87–91. https://doi.org/10.1126/science.7678183

Hotzi, B., Kosztelnik, M., Hargitai, B., Takács-Vellai, K., Barna, J., Bördén, K., … Vellai, T. (2018). Sex-specific regulation of aging in Caenorhabditis elegans. *Aging Cell*. https://doi.org/10.1111/acel.12724

Howarth, N. C., Huang, T. T. K., Roberts, S. B., & McCrory, M. A. (2005). Dietary fiber and fat are associated with excess weight in young and middle-aged US adults. *Journal of the American Dietetic Association*. https://doi.org/10.1016/j.jada.2005.06.001

Hu, J. L., Todhunter, M. E., LaBarge, M. A., & Gartner, Z. J. (2018). Opportunities for organoids as new models of aging. *Journal of Cell Biology*, *217*(1), 39–50. https://doi.org/10.1083/jcb.201709054

Huang, X., Liu, G., Guo, J., & Su, Z. Q. (2018). The PI3K/AKT pathway in obesity and type 2 diabetes. *International Journal of Biological Sciences*, *14*(11), 1483–1496. https://doi.org/10.7150/ijbs.27173

Hugenholtz, F., & de Vos, W. M. (2018). Mouse models for human intestinal microbiota research: a critical evaluation. *Cellular and Molecular Life Sciences*. https://doi.org/10.1007/s00018-017-2693-8

Huylmans, A. K., MacOn, A., & Vicoso, B. (2017). Global Dosage Compensation Is Ubiquitous in Lepidoptera, but Counteracted by the Masculinization of the Z Chromosome. *Molecular Biology and Evolution*. https://doi.org/10.1093/molbev/msx190

Igarashi, M., & Guarente, L. (2016). mTORC1 and SIRT1 Cooperate to Foster Expansion of Gut Adult Stem Cells during Calorie Restriction. *Cell*, *166*(2), 436–450. https://doi.org/10.1016/j.cell.2016.05.044

Ikeno, Y., Hubbard, G. B., Lee, S., Cortez, L. A., Lew, C. M., Webb, C. R., … Bartke, A. (2009). Reduced incidence and delayed occurrence of fatal neoplastic diseases in growth hormone receptor/binding protein knockout mice. *Journals of Gerontology - Series A Biological Sciences and Medical Sciences*, *64*(5), 522–529. https://doi.org/10.1093/gerona/glp017

Inui, M., Martello, G., & Piccolo, S. (2010). MicroRNA control of signal transduction. *Nature Reviews Molecular Cell Biology*. https://doi.org/10.1038/nrm2868

Ishaq, A., Schröder, J., Edwards, N., von Zglinicki, T., & Saretzki, G. (2018). Dietary Restriction Ameliorates Age-Related Increase in DNA Damage, Senescence and Inflammation in Mouse Adipose Tissuey. *Journal of Nutrition, Health and Aging*. https://doi.org/10.1007/s12603-017-0968-2

Itoh, Y., Kawamata, Y., Harada, M., Kobayashi, M., Fujii, R., Fukusumi, S., … Fujino, M. (2003). Free fatty acids regulate insulin secretion from pancreatic β cells through GPR40. *Nature*. https://doi.org/10.1038/nature01478

Jagger, C., Gillies, C., Moscone, F., Cambois, E., Van Oyen, H., Nusselder, W., & Robine, J. M. (2008). Inequalities in healthy life years in the 25 countries of the European Union in 2005: a cross-national meta-regression analysis. *The Lancet*, *372*(9656), 2124–2131. https://doi.org/10.1016/S0140-6736(08)61594-9

Jamaluddin, M. S., Weakley, S. M., Yao, Q., & Chen, C. (2012). Resistin: Functional roles and therapeutic considerations for cardiovascular disease. *British Journal of Pharmacology*. https://doi.org/10.1111/j.1476-5381.2011.01369.x

Jang, Y. C., Liu, Y., Hayworth, C. R., Bhattacharya, A., Lustgarten, M. S., Muller, F. L., … Van Remmen, H. (2012). Dietary restriction attenuates age-associated muscle atrophy by

lowering oxidative stress in mice even in complete absence of CuZnSOD. *Aging Cell*, *11*(5), 770–782. https://doi.org/10.1111/j.1474-9726.2012.00843.x.

Jansen, H. J., Moghtadaei, M., MacKasey, M., Rafferty, S. A., Bogachev, O., Sapp, J. L., … Rose, R. A. (2017). Atrial structure, function and arrhythmogenesis in aged and frail mice. *Scientific Reports*. https://doi.org/10.1038/srep44336

Jay Olshansky, S., & Carnes, B. A. (2017). Primary prevention with a capital p. *Perspectives in Biology and Medicine*. https://doi.org/10.1353/pbm.2017.0037

Jeyaraj, D., Haldar, S. M., Wan, X., McCauley, M. D., Ripperger, J. A., Hu, K., … Jain, M. K. (2012). Circadian rhythms govern cardiac repolarization and arrhythmogenesis. *Nature*. https://doi.org/10.1038/nature10852

Ji, C., & Guo, X. (2019). The clinical potential of circulating microRNAs in obesity. *Nature Reviews Endocrinology*, *15*(12), 731–743. https://doi.org/10.1038/s41574-019-0260-0

Ji, J., Petropavlovskaia, M., Khatchadourian, A., Patapas, J., Makhlin, J., Rosenberg, L., & Maysinger, D. (2019). Type 2 diabetes is associated with suppression of autophagy and lipid accumulation in β-cells. *Journal of Cellular and Molecular Medicine*. https://doi.org/10.1111/jcmm.14172

Jiang, N., Du, G., Tobias, E., Wood, J. G., Whitaker, R., Neretti, N., & Helfand, S. L. (2013). Dietary and genetic effects on age-related loss of gene silencing reveal epigenetic plasticity of chromatin repression during aging. *Aging*. https://doi.org/10.18632/aging.100614

Jones, O. R., Scheuerlein, A., Salguero-Gómez, R., Camarda, C. G., Schaible, R., Casper, B. B., … Vaupel, J. W. (2014). Diversity of ageing across the tree of life. *Nature*, *505*(7482), 169–173. https://doi.org/10.1038/nature12789

Jung, D. Y., Ko, H. J., Lichtman, E. I., Lee, E., Lawton, E., Ong, H., … Kim, J. K. (2013). Short-term weight loss attenuates local tissue inflammation and improves insulin sensitivity without affecting adipose inflammation in obese mice. *American Journal of Physiology - Endocrinology and Metabolism*. https://doi.org/10.1152/ajpendo.00462.2012

Juricic, P., Lu, Y.-X., Paulitz, J., Lu, J., Nespital, T., Azami, S., … Partridge, L. (n.d.). Full geroprotection from brief rapamycin treatment by persistently increased intestinal autophagy. *Manuscript in Revision*.

Kabiri, Z., Greicius, G., Madan, B., Biechele, S., Zhong, Z., Zaribafzadeh, H., … Virshup, D. M. (2014). Stroma provides an intestinal stem cell niche in the absence of epithelial Wnts. *Development (Cambridge)*. https://doi.org/10.1242/dev.104976

Kaeser, S. A., Lehallier, B., Thinggaard, M., Häsler, L. M., Apel, A., Bergmann, C., … Jucker, M. (2021). A neuronal blood marker is associated with mortality in old age. *Nature Aging*.

https://doi.org/10.1038/s43587-021-00028-4

Kahn, S. E., Hull, R. L., & Utzschneider, K. M. (2006). Mechanisms linking obesity to insulin resistance and type 2 diabetes. *Nature*, *444*(7121), 840–846. https://doi.org/10.1038/nature05482

Kalache, A., de Hoogh, A. I., Howlett, S. E., Kennedy, B., Eggersdorfer, M., Marsman, D. S., … Griffiths, J. C. (2019). Nutrition interventions for healthy ageing across the lifespan: a conference report. *European Journal of Nutrition*. https://doi.org/10.1007/s00394-019-02027-z

Kalsbeek, A., Fliers, E., Romijn, J. A., La Fleur, S. E., Wortel, J., Bakker, O., … Buijs, R. M. (2001). The suprachiasmatic nucleus generates the diurnal changes in plasma leptin levels. *Endocrinology*. https://doi.org/10.1210/endo.142.6.8197

Kamata, Y., Shiraga, H., Tai, A., Kawamoto, Y., & Gohda, E. (2007). Induction of neurite outgrowth in PC12 cells by the medium-chain fatty acid octanoic acid. *Neuroscience*. https://doi.org/10.1016/j.neuroscience.2007.03.001

Kanda, Y., Hashiramoto, M., Shimoda, M., Hamamoto, S., Tawaramoto, K., Kimura, T., … Kaku, K. (2015). Dietary restriction preserves the mass and function of pancreatic β cells via cell kinetic regulation and suppression of oxidative/ER stress in diabetic mice. *Journal of Nutritional Biochemistry*, *26*(3), 219–226. https://doi.org/10.1016/j.jnutbio.2014.10.007

Kane, A. E., Hilmer, S. N., Boyer, D., Gavin, K., Nines, D., Howlett, S. E., … Mitchell, S. J. (2016). Impact of Longevity Interventions on a Validated Mouse Clinical Frailty Index. *Journals of Gerontology - Series A Biological Sciences and Medical Sciences*, *71*(3), 333–339. https://doi.org/10.1093/gerona/glu315

Karagiannides, I., Tchkonia, T., Dobson, D. E., Steppan, C. M., Cummins, P., Chan, G., … Kirkland, J. L. (2001). Altered expression of C/EBP family members results in decreased adipogenesis with aging. *American Journal of Physiology - Regulatory Integrative and Comparative Physiology*, *280*(6 49-6), 1772–1780. https://doi.org/10.1152/ajpregu.2001.280.6.r1772

Karastergiou, K., Smith, S. R., Greenberg, A. S., & Fried, S. K. (2012). Sex differences in human adipose tissues - The biology of pear shape. *Biology of Sex Differences*. https://doi.org/10.1186/2042-6410-3-13

Katakura, M., Hashimoto, M., Shahdat, H. M., Gamoh, S., Okui, T., Matsuzaki, K., & Shido, O. (2009). Docosahexaenoic acid promotes neuronal differentiation by regulating basic helix-loop-helix transcription factors and cell cycle in neural stem cells. *Neuroscience*. https://doi.org/10.1016/j.neuroscience.2009.02.057

Kawagishi-Hotta, M., Hasegawa, S., Igarashi, T., Yamada, T., Takahashi, M., Numata, S., …

Akamatsu, H. (2017). Enhancement of individual differences in proliferation and differentiation potentials of aged human adipose-derived stem cells. *Regenerative Therapy*. https://doi.org/10.1016/j.reth.2016.12.004

Kawakami, Y., Sielski, R., & Kawakami, T. (2018). Mouse body temperature measurement using infrared thermometer during passive systemic anaphylaxis and food allergy evaluation. *Journal of Visualized Experiments*, *2018*(139), 6–11. https://doi.org/10.3791/58391

Kehm, R., König, J., Nowotny, K., Jung, T., Deubel, S., Gohlke, S., … Höhn, A. (2018). Age-related oxidative changes in pancreatic islets are predominantly located in the vascular system. *Redox Biology*. https://doi.org/10.1016/j.redox.2017.12.015

Kenchaiah, S., Evans, J. C., Levy, D., Wilson, P. W. F., Benjamin, E. J., Larson, M. G., … Vasan, R. S. (2002). Obesity and the Risk of Heart Failure. *N Engl J Med*, *346*(5), 305–310.

Kennedy, M. A., Barrera, G. C., Nakamura, K., Baldán, Á., Tarr, P., Fishbein, M. C., … Edwards, P. A. (2005). ABCG1 has a critical role in mediating cholesterol efflux to HDL and preventing cellular lipid accumulation. *Cell Metabolism*. https://doi.org/10.1016/j.cmet.2005.01.002

Kenyon, C., Chang, J., Gensch, E., Rudner, A., & Tabtiang, R. (1993). A C. elegans mutant that lives twice as long as wild type. *Nature*. https://doi.org/10.1038/366461a0

Kerr, C. R., Hacking, A., & Henning, H. (1987). Effects of transient myocardial ischemia on the QT interval in man. *Can J Cardiol*, *3*(8), 383–386.

Kershaw, E. E., & Flier, J. S. (2004). Adipose tissue as an endocrine organ. In *Journal of Clinical Endocrinology and Metabolism*. https://doi.org/10.1210/jc.2004-0395

Khabour, O. F., Alzoubi, K. H., Alomari, M. A., & Alzubi, M. A. (2010). Changes in spatial memory and BDNF expression to concurrent dietary restriction and voluntary exercise. *Hippocampus*. https://doi.org/10.1002/hipo.20657

Khalil, M., Teunissen, C. E., Otto, M., Piehl, F., Sormani, M. P., Gattringer, T., … Kuhle, J. (2018). Neurofilaments as biomarkers in neurological disorders. *Nature Reviews Neurology*. https://doi.org/10.1038/s41582-018-0058-z

Kiela, P. R., & Ghishan, F. K. (2016). Physiology of Intestinal Absorption and Secretion. *Best Pract Res Clin Gastroenterol.*, *30*(2), 145–159. https://doi.org/10.1016/j.bpg.2016.02.007

Kilroy, G., Dietrich, M., Wu, X., Gimble, J. M., & Floyd, Z. E. (2018). Isolation of murine adipose-derived stromal/stem cells for adipogenic differentiation or flow cytometry-based analysis. *Methods in Molecular Biology*, *1773*, 137–146. https://doi.org/10.1007/978-1-4939-7799-4_11

Kim, J., Koo, B. K., & Knoblich, J. A. (2020). Human organoids: model systems for human biology and medicine. *Nature Reviews Molecular Cell Biology*, *21*(10), 571–584. https://doi.org/10.1038/s41580-020-0259-3

Kim, M. J., Kim, M. H., Kim, S. A., & Chang, J. S. (2008). Age-related deterioration of hematopoietic stem cells. *International Journal of Stem Cells*. https://doi.org/10.15283/ijsc.2008.1.1.55

Kim, S., Myers, L., Wyckoff, J., Cherry, K. E., & Jazwinski, S. M. (2017). The frailty index outperforms DNA methylation age and its derivatives as an indicator of biological age. *GeroScience*. https://doi.org/10.1007/s11357-017-9960-3

Kim, T. H., Li, F., Ferreiro-Neira, I., Ho, L. L., Luyten, A., Nalapareddy, K., … Shivdasani, R. A. (2014). Broadly permissive intestinal chromatin underlies lateral inhibition and cell plasticity. *Nature*. https://doi.org/10.1038/nature12903

Kirkegaard, P., Olsen, P. S., Nexo, E., Holst, J. J., & Poulsen, S. S. (1984). Effect of vasoactive intestinal polypeptide and somatostatin on secretion of epidermal growth factor and bicarbonate from Brunner's glands. *Gut*. https://doi.org/10.1136/gut.25.11.1225

Kirkland, J. L., Hollenberg, C. H., & Gillon, W. S. (1990). Age, anatomic site, and the replication and differentiation of adipocyte precursors. *American Journal of Physiology - Cell Physiology*. https://doi.org/10.1152/ajpcell.1990.258.2.c206

Kobayashi, N., Takahashi, D., Takano, S., Kimura, S., & Hase, K. (2019). The Roles of Peyer's Patches and Microfold Cells in the Gut Immune System: Relevance to Autoimmune Diseases. *Frontiers in Immunology*. https://doi.org/10.3389/fimmu.2019.02345

Korzelius, J., Azami, S., Ronnen-Oron, T., Koch, P., Baldauf, M., Meier, E., … Jasper, H. (2019). The WT1-like transcription factor Klumpfuss maintains lineage commitment of enterocyte progenitors in the Drosophila intestine. *Nature Communications*. https://doi.org/10.1038/s41467-019-12003-0

Kosteli, A., Sugaru, E., Haemmerle, G., Martin, J. F., Lei, J., Zechner, R., & Ferrante, A. W. (2010). Weight loss and lipolysis promote a dynamic immune response in murine adipose tissue. *Journal of Clinical Investigation*. https://doi.org/10.1172/JCI42845

Koubi, H. E., Robin, J. P., Dewasmes, G., Le Maho, Y., Frutoso, J., & Minaire, Y. (1991). Fasting-induced rise in locomotor activity in rats coincides with increased protein utilization. *Physiology and Behavior*. https://doi.org/10.1016/0031-9384(91)90075-Y

Krndija, D., Marjou, F. El, Guirao, B., Richon, S., Leroy, O., Bellaiche, Y., … Vignjevic, D. M. (2019). Active cell migration is critical for steady-state epithelial turnover in the gut. *Science*. https://doi.org/10.1126/science.aau3429

Krych, L., Hansen, C. H. F., Hansen, A. K., van den Berg, F. W. J., & Nielsen, D. S. (2013).

Quantitatively Different, yet Qualitatively Alike: A Meta-Analysis of the Mouse Core Gut Microbiome with a View towards the Human Gut Microbiome. *PLoS ONE*. https://doi.org/10.1371/journal.pone.0062578

Kuhla, A., Lange, S., Holzmann, C., Maass, F., Petersen, J., Vollmar, B., & Wree, A. (2013). Lifelong Caloric Restriction Increases Working Memory in Mice. *PLoS ONE*, *8*(7). https://doi.org/10.1371/journal.pone.0068778

Kuhnert, F., Davis, C. R., Wang, H. T., Chu, P., Lee, M., Yuan, J., … Kuo, C. J. (2004). Essential requirement for Wnt signaling in proliferation of adult small intestine and colon revealed by adenoviral expression of Dickkopf-1. *Proceedings of the National Academy of Sciences of the United States of America*. https://doi.org/10.1073/pnas.2536800100

Kuk, J. L., Katzmarzyk, P. T., Nichaman, M. Z., Church, T. S., Blair, S. N., & Ross, R. (2006). Visceral fat is an independent predictor of all-cause mortality in men. *Obesity*. https://doi.org/10.1038/oby.2006.43

Kumar Jha, P., Challet, E., & Kalsbeek, A. (2015). Circadian rhythms in glucose and lipid metabolism in nocturnal and diurnal mammals. *Molecular and Cellular Endocrinology*. https://doi.org/10.1016/j.mce.2015.01.024

Kurtz, P., Jones, A. E., Tiwari, B., Link, N., Wylie, A., Tracy, C., … Abrams, J. M. (2019). Drosophila p53 directs nonapoptotic programs in postmitotic tissue. *Molecular Biology of the Cell*. https://doi.org/10.1091/mbc.E18-12-0791

Lakka, H. M., Lakka, T. A., Tuomilehto, J., & Salonen, J. T. (2002). Abdominal obesity is associated with increased risk of acute coronary events in men. *European Heart Journal*. https://doi.org/10.1053/euhj.2001.2889

Lamia, K. A., Storch, K. F., & Weitz, C. J. (2008). Physiological significance of a peripheral tissue circadian clock. *Proceedings of the National Academy of Sciences of the United States of America*. https://doi.org/10.1073/pnas.0806717105

Lamming, D. W., Ye, L., Katajisto, P., Goncalves, M. D., Saitoh, M., Stevens, D. M., … Baur, J. A. (2012). Rapamycin-induced insulin resistance is mediated by mTORC2 loss and uncoupled from longevity. *Science*. https://doi.org/10.1126/science.1215135

Landrigan, P. J., Fuller, R., Acosta, N. J. R., Adeyi, O., Arnold, R., Basu, N. (Nil), … Zhong, M. (2018). The Lancet Commission on pollution and health. *The Lancet*, *391*(10119), 462–512. https://doi.org/10.1016/S0140-6736(17)32345-0

Lanza, I. R., Zabielski, P., Klaus, K. A., Morse, D. M., Heppelmann, C. J., Bergen, H. R., … Nair, K. S. (2012). Chronic caloric restriction preserves mitochondrial function in senescence without increasing mitochondrial biogenesis. *Cell Metabolism*, *16*(6), 777–788. https://doi.org/10.1016/j.cmet.2012.11.003

Lass, A., Zimmermann, R., Oberer, M., & Zechner, R. (2011). Lipolysis - A highly regulated multi-enzyme complex mediates the catabolism of cellular fat stores. *Progress in Lipid Research*. https://doi.org/10.1016/j.plipres.2010.10.004

Lau, L., Porciuncula, A., Yu, A., Iwakura, Y., & David, G. (2019). Uncoupling the Senescence-Associated Secretory Phenotype from Cell Cycle Exit via Interleukin-1 Inactivation Unveils Its Protumorigenic Role. *Molecular and Cellular Biology*. https://doi.org/10.1128/mcb.00586-18

Lavie, C. J., Arena, R., Alpert, M. A., Milani, R. V., & Ventura, H. O. (2018). Management of cardiovascular diseases in patients with obesity. *Nature Reviews Cardiology*, *15*(1), 45–56. https://doi.org/10.1038/nrcardio.2017.108

Ledikwe, J. H., Blanck, H. M., Khan, L. K., Serdula, M. K., Seymour, J. D., Tohill, B. C., & Rolls, B. J. (2006). Dietary energy density is associated with energy intake and weight status in US adults. *American Journal of Clinical Nutrition*, *83*(6), 1362–1368. https://doi.org/10.1093/ajcn/83.6.1362

Lee, B., Moon, K. M., & Kim, C. Y. (2018). Tight junction in the intestinal epithelium: Its association with diseases and regulation by phytochemicals. *Journal of Immunology Research*. https://doi.org/10.1155/2018/2645465

Lee, M.-J., & Fried, S. K. (2017). Sex-dependent Depot Differences in Adipose Tissue Development and Function; Role of Sex Steroids. *Journal of Obesity & Metabolic Syndrome*. https://doi.org/10.7570/jomes.2017.26.3.172

Lee, S. H., Jung, B. K., Park, J. H., Shin, E. H., & Chai, J. Y. (2014). Increased intestinal epithelial cell turnover and intestinal motility in Gymnophalloides seoi-infected C57BL/6 mice. *Korean Journal of Parasitology*, *52*(3), 273–280. https://doi.org/10.3347/kjp.2014.52.3.273

Leitner, B. P., Huang, S., Brychta, R. J., Duckworth, C. J., Baskin, A. S., McGehee, S., … Chen, K. Y. (2017). Mapping of human brown adipose tissue in lean and obese young men. *Proceedings of the National Academy of Sciences of the United States of America*. https://doi.org/10.1073/pnas.1705287114

Lemaître, J. F., Ronget, V., Tidière, M., Allainé, D., Berger, V., Cohas, A., … Gaillard, J. M. (2020). Sex differences in adult lifespan and aging rates of mortality across wild mammals. *Proceedings of the National Academy of Sciences of the United States of America*, *117*(15), 8546–8553. https://doi.org/10.1073/pnas.1911999117

Lemmert, M. E., Majidi, M., Krucoff, M. W., Bekkers, S. C. A. M., Crijns, H. J. G. M., Wellens, H. J. J., … Gorgels, A. P. M. (2010). RR-interval irregularity precedes ventricular fibrillation in ST elevation acute myocardial infarction. *Heart Rhythm*, *7*(1), 65–71.

https://doi.org/10.1016/j.hrthm.2009.09.024

Leonov, A., Feldman, R., Piano, A., Arlia-Ciommo, A., Lutchman, V., Ahmadi, M., … Titorenko, V. I. (2017). Caloric restriction extends yeast chronological lifespan via a mechanism linking cellular aging to cell cycle regulation, maintenance of a quiescent state, entry into a non-quiescent state and survival in the non-quiescent state. *Oncotarget*. https://doi.org/10.18632/oncotarget.20614

Leslie, M. (2019). Closing in on a century-old mystery, scientists are figuring out what the body's 'tuft cells' do. *Science*. https://doi.org/10.1126/science.aax4947

Levolger, S., van den Engel, S., Ambagtsheer, G., IJzermans, J. N. M., & de Bruin, R. W. F. (2018). Caloric restriction is associated with preservation of muscle strength in experimental cancer cachexia. *Aging*. https://doi.org/10.18632/aging.101724

Li, N., Guenancia, C., Rigal, E., Hachet, O., Chollet, P., Desmoulins, L., … Vergely, C. (2016). Short-term moderate diet restriction in adulthood can reverse oxidative, cardiovascular and metabolic alterations induced by postnatal overfeeding in mice. *Scientific Reports*. https://doi.org/10.1038/srep30817

Li, Y., Bolze, F., Fromme, T., & Klingenspor, M. (2014). Intrinsic differences in BRITE adipogenesis of primary adipocytes from two different mouse strains. *Biochimica et Biophysica Acta - Molecular and Cell Biology of Lipids*. https://doi.org/10.1016/j.bbalip.2014.06.003

Li, Y., Schnabl, K., Gabler, S. M., Willershäuser, M., Reber, J., Karlas, A., … Klingenspor, M. (2018). Secretin-Activated Brown Fat Mediates Prandial Thermogenesis to Induce Satiation. *Cell*. https://doi.org/10.1016/j.cell.2018.10.016

Li, Y., Schwalie, P. C., Bast-Habersbrunner, A., Mocek, S., Russeil, J., Fromme, T., … Klingenspor, M. (2019). Systems-Genetics-Based Inference of a Core Regulatory Network Underlying White Fat Browning. *Cell Reports*. https://doi.org/10.1016/j.celrep.2019.11.053

Liao, C. Y., Rikke, B. A., Johnson, T. E., Diaz, V., & Nelson, J. F. (2010). Genetic variation in the murine lifespan response to dietary restriction: From life extension to life shortening. *Aging Cell*. https://doi.org/10.1111/j.1474-9726.2009.00533.x

Liao, C. Y., Rikke, B. A., Johnson, T. E., Gelfond, J. A. L., Diaz, V., & Nelson, J. F. (2011). Fat maintenance is a predictor of the murine lifespan response to dietary restriction. *Aging Cell*. https://doi.org/10.1111/j.1474-9726.2011.00702.x

Lijnen, H. R., Van Hul, M., & Hemmeryckx, B. (2012). Caloric restriction improves coagulation and inflammation profile in obese mice. *Thrombosis Research*. https://doi.org/10.1016/j.thromres.2011.05.023

Lin, Q., Gao, Z., Alarcon, R. M., Ye, J., & Yun, Z. (2009). A role of miR-27 in the regulation of adipogenesis. *FEBS Journal*. https://doi.org/10.1111/j.1742-4658.2009.06967.x

Liu, R., & Nikolajczyk, B. S. (2019). Tissue immune cells fuel obesity-associated inflammation in adipose tissue and beyond. *Frontiers in Immunology*. https://doi.org/10.3389/fimmu.2019.01587

Locati, E. T., Bagliani, G., & Padeletti, L. (2017). Normal Ventricular Repolarization and QT Interval: Ionic Background, Modifiers, and Measurements. *Cardiac Electrophysiology Clinics*. https://doi.org/10.1016/j.ccep.2017.05.007

Logan, S., Owen, D., Chen, S., Chen, W. J., Ungvari, Z., Farley, J., … Sonntag, W. E. (2018). Simultaneous assessment of cognitive function, circadian rhythm, and spontaneous activity in aging mice. *GeroScience*. https://doi.org/10.1007/s11357-018-0019-x

Longo, V. D., & Fontana, L. (2010). Calorie restriction and cancer prevention: metabolic and molecular mechanisms. *Trends in Pharmacological Sciences*. https://doi.org/10.1016/j.tips.2009.11.004

López-Otín, C., Blasco, M. A., Partridge, L., Serrano, M., & Kroemer, G. (2013). The hallmarks of aging. *Cell*, *153*(6). https://doi.org/10.1016/j.cell.2013.05.039

Lopez Trinidad, L. M., Martinez, R., Kapravelou, G., Galisteo, M., Aranda, P., Porres, J. M., & Lopez-Jurado, M. (2021). Caloric restriction, physical exercise, and CB1 receptor blockade as an efficient combined strategy for bodyweight control and cardiometabolic status improvement in male rats. *Scientific Reports*, *11*(1), 1–16. https://doi.org/10.1038/s41598-021-83709-9

Lowe, C. E., O'Rahilly, S., & Rochford, J. J. (2011). Adipogenesis at a glance. *Journal of Cell Science*. https://doi.org/10.1242/jcs.079699

Lu, J., Temp, U., Müller-Hartmann, A., Esser, J., Grönke, S., & Partridge, L. (2020). Sestrin is a key regulator of stem cell function and lifespan in response to dietary amino acids. *Nature Aging*. https://doi.org/10.1038/s43587-020-00001-7

Lumeng, C. N., Bodzin, J. L., & Saltiel, A. R. (2007). Obesity induces a phenotypic switch in adipose tissue macrophage polarization. *Journal of Clinical Investigation*. https://doi.org/10.1172/JCI29881

Lumeng, C. N., Liu, J., Geletka, L., Delaney, C., Delproposto, J., Desai, A., … Yung, R. L. (2011). Aging Is Associated with an Increase in T Cells and Inflammatory Macrophages in Visceral Adipose Tissue. *The Journal of Immunology*. https://doi.org/10.4049/jimmunol.1102188

Ma, L., Wang, R., Dong, W., & Zhao, Z. (2018). Caloric restriction can improve learning and memory in C57/BL mice probably via regulation of the AMPK signaling pathway.

Experimental Gerontology, *102*(November 2017), 28–35. https://doi.org/10.1016/j.exger.2017.11.013

Ma, S., Sun, S., Geng, L., Song, M., Wang, W., Ye, Y., … Liu, G. H. (2020). Caloric Restriction Reprograms the Single-Cell Transcriptional Landscape of Rattus Norvegicus Aging. *Cell*, *180*(5), 984-1001.e22. https://doi.org/10.1016/j.cell.2020.02.008

Ma, T. Y., Hollander, D., Dadufalza, V., & Krugliak, P. (1992). Effect of aging and caloric restriction on intestinal permeability. *Experimental Gerontology*. https://doi.org/10.1016/0531-5565(92)90059-9

Mabbott, N. A., Donaldson, D. S., Ohno, H., Williams, I. R., & Mahajan, A. (2013). Microfold (M) cells: Important immunosurveillance posts in the intestinal epithelium. *Mucosal Immunology*. https://doi.org/10.1038/mi.2013.30

Macpherson, A. J., & Uhr, T. (2004). Induction of Protective IgA by Intestinal Dendritic Cells Carrying Commensal Bacteria. *Science*. https://doi.org/10.1126/science.1091334

Mager DE, Wan R, Brown M, Cheng A, Wareski P, Abernethy DR, M. M. (2006). Caloric restriction and intermittent fasting alter spectral measures of heart rate and blood pressure variability in rats. *FASEB J.*, (6), 631–637. https://doi.org/10.1096/fj.05-5263com

Magnuson, B., Ekim, B., & Fingar, D. C. (2012). Regulation and function of ribosomal protein S6 kinase (S6K) within mTOR signalling networks. *Biochemical Journal*, *441*(1), 1–21. https://doi.org/10.1042/BJ20110892

Mahé, E., Morelon, E., Lechaton, S., Sang, K. H. L. Q., Mansouri, R., Ducasse, M. F., … Bodemer, C. (2005). Cutaneous adverse events in renal in renal transplant recipients receiving sirolimus-based therapy. *Transplantation*. https://doi.org/10.1097/01.TP.0000151630.25127.3A

Mair, W., Piper, M. D. W., & Partridge, L. (2005). Calories do not explain extension of life span by dietary restriction in Drosophila. *PLoS Biology*. https://doi.org/10.1371/journal.pbio.0030223

Majka, S. M., Miller, H. L., Helm, K. M., Acosta, A. S., Childs, C. R., Kong, R., & Klemm, D. J. (2014). Analysis and isolation of adipocytes by flow cytometry. *Methods in Enzymology*, *537*, 281–296. https://doi.org/10.1016/B978-0-12-411619-1.00015-X

Makki, K., Froguel, P., & Wolowczuk, I. (2013). Adipose Tissue in Obesity-Related Inflammation and Insulin Resistance: Cells, Cytokines, and Chemokines. *ISRN Inflammation*. https://doi.org/10.1155/2013/139239

Makwana, K., Gosai, N., Poe, A., & Kondratov, R. V. (2019). Calorie restriction reprograms diurnal rhythms in protein translation to regulate metabolism. *FASEB Journal*. https://doi.org/10.1096/fj.201802167R

Mancuso, P., & Bouchard, B. (2019). The impact of aging on adipose function and adipokine synthesis. *Frontiers in Endocrinology*. https://doi.org/10.3389/fendo.2019.00137

Mannick, J. B., Del Giudice, G., Lattanzi, M., Valiante, N. M., Praestgaard, J., Huang, B., … Klickstein, L. B. (2014). mTOR inhibition improves immune function in the elderly. *Science Translational Medicine*. https://doi.org/10.1126/scitranslmed.3009892

Mannick, J. B., Morris, M., Hockey, H. U., Roma, G., Beibel, M., Kulmatycki, K., … Klickstein, L. B. (2018). TORC1 inhibition enhances immune function and reduces infections in the elderly. *Science Translational Medicine*. https://doi.org/10.1126/scitranslmed.aaq1564

Mao, J. H., Langley, S. A., Huang, Y., Hang, M., Bouchard, K. E., Celniker, S. E., … Snijders, A. M. (2015). Identification of genetic factors that modify motor performance and body weight using Collaborative Cross mice. *Scientific Reports*, *5*(October), 1–9. https://doi.org/10.1038/srep16247

Martin, C. K., Bhapkar, M., Pittas, A. G., Pieper, C. F., Das, S. K., Williamson, D. A., … Roberts, S. B. (2016). Effect of calorie restriction on mood, quality of life, sleep, and sexual function in healthy nonobese adults the CALERIE 2 randomized clinical trial. *JAMA Internal Medicine*. https://doi.org/10.1001/jamainternmed.2016.1189

Martínez-González, M., Martínez, J. A., Hu, F. B., Gibney, M. J., & Kearney, J. (1999). Physical inactivity, sedentary lifestyle and obesity in the European Union. *Int J Obes Relat Metab Disord.*, *23*(11), 1192–1201. https://doi.org/10.1038/sj.ijo.0801049.

Martínez, D. E. (1998). Mortality patterns suggest lack of senescence in hydra. *Experimental Gerontology*. https://doi.org/10.1016/S0531-5565(97)00113-7

Martinez, F. O., & Gordon, S. (2014). The M1 and M2 paradigm of macrophage activation: Time for reassessment. *F1000Prime Reports*. https://doi.org/10.12703/P6-13

Matai, L., Sarkar, G. C., Chamoli, M., Malik, Y., Kumar, S. S., Rautela, U., … Mukhopadhyay, A. (2019). Dietary restriction improves proteostasis and increases life span through endoplasmic reticulum hormesis. *Proceedings of the National Academy of Sciences of the United States of America*. https://doi.org/10.1073/pnas.1900055116

Mattison, J. A., Colman, R. J., Beasley, T. M., Allison, D. B., Kemnitz, J. W., Roth, G. S., … Anderson, R. M. (2017). Caloric restriction improves health and survival of rhesus monkeys. *Nature Communications*, *8*(May 2016). https://doi.org/10.1038/ncomms14063

Mattison, J. a., Roth, G. S., Beasley, T. M., Tilmont, E. M., Handy, A. M., Herbert, R. L., … de Cabo, R. (2012). Impact of caloric restriction on health and survival in rhesus monkeys from the NIA study. *Nature*, *489*(7415), 318–321. https://doi.org/10.1038/nature11432

Matyi, S., Jackson, J., Garrett, K., Deepa, S. S., & Unnikrishnan, A. (2018). The effect of different levels of dietary restriction on glucose homeostasis and metabolic memory.

GeroScience, *40*(2), 139–149. https://doi.org/10.1007/s11357-018-0011-5

Maynard, C., & Weinkove, D. (2018). The Gut Microbiota and Ageing. In J. R. Harris & V. I. Korolchuk (Eds.), *Biochemistry and Cell Biology of Ageing: Part I Biomedical Science* (pp. 351–371). Singapore: Springer Singapore. https://doi.org/10.1007/978-981-13-2835-0_12

Maynard, L. M., Wisemandle, W., Roche, A. F., Chumlea, W. C., Guo, S. S., & Siervogel, R. M. (2001). Childhood body composition in relation to body mass index. *Pediatrics*. https://doi.org/10.1542/peds.107.2.344

McCarter, R. J. M., Shimokawa, I., Ikeno, Y., Higami, Y., Hubbard, G. B., Yu, B. P., & McMahan, C. A. (1997). Physical activity as a factor in the action of dietary restriction on aging: Effects in Fisher 344 rats. *Aging Clinical and Experimental Research*. https://doi.org/10.1007/bf03340130

McCay, C., Crowell, M., & Maynard, L. (1935). The effect of retarded growth upon the length of life span and upon the ultimate body size. 1935. *The Journal of Nutrition*, *10*(1), 63–79.

Mckinney, W. (2010). Data Structures for Statistical Computing in Python, *1*(Scipy), 56–61.

Meadows, E., Cho, J. H., Flynn, J. M., & Klein, W. H. (2008). Myogenin regulates a distinct genetic program in adult muscle stem cells. *Developmental Biology*. https://doi.org/10.1016/j.ydbio.2008.07.024

Means, L. W., Higgins, J. L., & Fernandez, T. J. (1993). Mid-life onset of dietary restriction extends life and prolongs cognitive functioning. *Physiology and Behavior*. https://doi.org/10.1016/0031-9384(93)90243-9

Meissburger, B., Perdikari, A., Moest, H., Müller, S., Geiger, M., & Wolfrum, C. (2016). Regulation of adipogenesis by paracrine factors from adipose stromal-vascular fraction - a link to fat depot-specific differences. *Biochimica et Biophysica Acta - Molecular and Cell Biology of Lipids*. https://doi.org/10.1016/j.bbalip.2016.06.010

Mendoza, J., Drevet, K., Pévet, P., & Challet, E. (2008). Daily meal timing is not necessary for resetting the main circadian clock by calorie restriction. *Journal of Neuroendocrinology*. https://doi.org/10.1111/j.1365-2826.2007.01636.x

Meydani, S. N., Das, S. K., Pieper, C. F., Lewis, M. R., Klein, S., Dixit, V. D., … Fontana, L. (2016). Long-term moderate calorie restriction inhibits inflammation without impairing cell-mediated immunity: A randomized controlled trial in non-obese humans. *Aging*. https://doi.org/10.18632/aging.100994

Meyer, C. W., Ootsuka, Y., & Romanovsky, A. A. (2017). Body Temperature Measurements for Metabolic Phenotyping in Mice. *Frontiers in Physiology*, *8*(July), 1–13. https://doi.org/10.3389/fphys.2017.00520

Meyer, T. E., Kovács, S. J., Ehsani, A. A., Klein, S., Holloszy, J. O., & Fontana, L. (2006). Long-term caloric restriction ameliorates the decline in diastolic function in humans. *Journal of the American College of Cardiology*. https://doi.org/10.1016/j.jacc.2005.08.069

Meynet, O., & Ricci, J. E. (2014). Caloric restriction and cancer: Molecular mechanisms and clinical implications. *Trends in Molecular Medicine*, *20*(8), 419–427. https://doi.org/10.1016/j.molmed.2014.05.001

Mihaylova, M. M., Cheng, C. W., Cao, A. Q., Tripathi, S., Mana, M. D., Bauer-Rowe, K. E., … Yilmaz, Ö. H. (2018). Fasting Activates Fatty Acid Oxidation to Enhance Intestinal Stem Cell Function during Homeostasis and Aging. *Cell Stem Cell*, *22*(5), 769-778.e4. https://doi.org/10.1016/j.stem.2018.04.001

Miller, G. E., Chen, E., & Parker, K. J. (2011). Psychological Stress in Childhood and Susceptibility to the Chronic Diseases of Aging: Moving Toward a Model of Behavioral and Biological Mechanisms. *Psychological Bulletin*, *137*(6), 959–997. https://doi.org/10.1037/a0024768

Miller, K. N., Burhans, M. S., Clark, J. P., Howell, P. R., Polewski, M. A., DeMuth, T. M., … Anderson, R. M. (2017). Aging and caloric restriction impact adipose tissue, adiponectin, and circulating lipids. *Aging Cell*, *16*(3), 497–507. https://doi.org/10.1111/acel.12575

Miller, R. A., Harrison, D. E., Astle, C. M., Fernandez, E., Flurkey, K., Han, M., … Strong, R. (2014). Rapamycin-mediated lifespan increase in mice is dose and sex dependent and metabolically distinct from dietary restriction. *Aging Cell*. https://doi.org/10.1111/acel.12194

Mirvis, D. M. (1985). Spatial variation of QT intervals in normal persons and patients with acute myocardial infarction. *Journal of the American College of Cardiology*, *5*(3), 625–631. https://doi.org/10.1016/S0735-1097(85)80387-9

Mitchell, M. A., & Levin, R. J. (1981). Amino acid absorption in jejunum and ileum in vivo — a kinetic comparison of function on surface area and regional bases. *Experientia*, *37*, 265–266. https://doi.org/10.1007/BF01991646

Mitchell, S. E., Delville, C., Konstantopedos, P., Hurst, J., Derous, D., Green, C., … Speakman, J. R. (2015). The effects of graded levels of calorie restriction: II. Impact of short term calorie and protein restriction on circulating hormone levels, glucose homeostasis and oxidative stress in male C57BL/6 mice. *Oncotarget*. https://doi.org/10.18632/oncotarget.4003

Mitchell, S. J., Bernier, M., Mattison, J. A., Aon, M. A., Kaiser, T. A., Anson, R. M., … de Cabo, R. (2019). Daily Fasting Improves Health and Survival in Male Mice Independent of Diet Composition and Calories. *Cell Metabolism*, *29*(1), 221-228.e3.

https://doi.org/10.1016/J.CMET.2018.08.011

Mitchell, S. J., Madrigal-Matute, J., Scheibye-Knudsen, M., Fang, E., Aon, M., González-Reyes, J. A., … De Cabo, R. (2016). Effects of Sex, Strain, and Energy Intake on Hallmarks of Aging in Mice. *Cell Metabolism*, *23*(6), 1093–1112. https://doi.org/10.1016/j.cmet.2016.05.027

Miyagi, S., Iwama, N., Kawabata, T., & Hasegawa, K. (2003). Longevity and Diet in Okinawa, Japan: The Past, Present and Future. *Asia-Pacific Journal of Public Health*, *15*(SUPPL.), 3–9. https://doi.org/10.1177/101053950301500s03

Miyamoto, J., Hasegawa, S., Kasubuchi, M., Ichimura, A., Nakajima, A., & Kimura, I. (2016). Nutritional signaling via free fatty acid receptors. *International Journal of Molecular Sciences*. https://doi.org/10.3390/ijms17040450

Mok, A., Khaw, K. T., Luben, R., Wareham, N., & Brage, S. (2019). Physical activity trajectories and mortality: Population based cohort study. *The BMJ*, *365*. https://doi.org/10.1136/bmj.l2323

Monzio Compagnoni, G., Di Fonzo, A., Corti, S., Comi, G. P., Bresolin, N., & Masliah, E. (2020). The Role of Mitochondria in Neurodegenerative Diseases: the Lesson from Alzheimer's Disease and Parkinson's Disease. *Molecular Neurobiology*, *57*(7), 2959–2980. https://doi.org/10.1007/s12035-020-01926-1

Moorefield, E. C., Andres, S. F., Blue, R. E., Van Landeghem, L., Mah, A. T., Santoro, M. A., & Ding, S. (2017). Aging effects on intestinal homeostasis associated with expansion and dysfunction of intestinal epithelial stem cells. *Aging*. https://doi.org/10.18632/aging.101279

Morelon, E., Stern, M., Israel-Biet, D., Correas, J. M., Danel, C., Mamzer-Bruneel, M. F., … Kreis, H. (2001). Characteristics of sirolimus-associated interstitial pneumonitis in renal transplant patients. *Transplantation*. https://doi.org/10.1097/00007890-200109150-00008

Moreno-Navarrete, J. M., Ortega, F., Serino, M., Luche, E., Waget, A., Pardo, G., … Fernández-Real, J. M. (2012). Circulating lipopolysaccharide-binding protein (LBP) as a marker of obesity-related insulin resistance. *International Journal of Obesity*. https://doi.org/10.1038/ijo.2011.256

Mori, M. A., Raghavan, P., Thomou, T., Boucher, J., Robida-Stubbs, S., MacOtela, Y., … Kahn, C. R. (2012). Role of microRNA processing in adipose tissue in stress defense and longevity. *Cell Metabolism*. https://doi.org/10.1016/j.cmet.2012.07.017

Morton, N. M., Emilsson, V., Liu, Y. L., & Cawthorne, M. A. (1998). Leptin action in intestinal cells. *Journal of Biological Chemistry*. https://doi.org/10.1074/jbc.273.40.26194

Mukherjee, P., El-Abbadi, M. M., Kasperzyk, J. L., Ranes, M. K., & Seyfried, T. N. (2002). Dietary restriction reduces angiogenesis and growth in an orthotopic mouse brain tumour model. *British Journal of Cancer*, *86*(10), 1615–1621. https://doi.org/10.1038/sj.bjc.6600298

Muniz, L. R., Knosp, C., & Yeretssian, G. (2012). Intestinal antimicrobial peptides during homeostasis, infection, and disease. *Frontiers in Immunology*. https://doi.org/10.3389/fimmu.2012.00310

Munshi-South, J., & Wilkinson, G. S. (2010). Bats and birds: Exceptional longevity despite high metabolic rates. *Ageing Research Reviews*. https://doi.org/10.1016/j.arr.2009.07.006

Murphy, T., & Thuret, S. (2015). The systemic milieu as a mediator of dietary influence on stem cell function during ageing. *Ageing Research Reviews*, *19*, 53–64. https://doi.org/10.1016/j.arr.2014.11.004

Muse, E. D., Feldman, D. I., Blaha, M. J., Dardari, Z. A., Blumenthal, R. S., Budoff, M. J., … Allison, M. A. (2015). The association of resistin with cardiovascular disease in the Multi-Ethnic Study of Atherosclerosis. *Atherosclerosis*. https://doi.org/10.1016/j.atherosclerosis.2014.12.044

Nalapareddy, K., Nattamai, K. J., Kumar, R. S., Karns, R., Wikenheiser-Brokamp, K. A., Sampson, L. L., … Geiger, H. (2017). Canonical Wnt Signaling Ameliorates Aging of Intestinal Stem Cells. *Cell Reports*, *18*(11), 2608–2621. https://doi.org/10.1016/j.celrep.2017.02.056

Narita, T., Kobayashi, M., Itakura, K., Itagawa, R., Kabaya, R., Sudo, Y., … Higami, Y. (2018). Differential response to caloric restriction of retroperitoneal, epididymal, and subcutaneous adipose tissue depots in rats. *Experimental Gerontology*. https://doi.org/10.1016/j.exger.2018.01.016

Nations, U. (2019). *World Population Ageing 2019*. *Economic and Social Affairs, Population Division*. Retrieved from http://link.springer.com/chapter/10.1007/978-94-007-5204-7_6

Nedergaard, J., Bengtsson, T., & Cannon, B. (2007). Unexpected evidence for active brown adipose tissue in adult humans. *American Journal of Physiology - Endocrinology and Metabolism*. https://doi.org/10.1152/ajpendo.00691.2006

Nelson, G., Wordsworth, J., Wang, C., Jurk, D., Lawless, C., Martin-Ruiz, C., & von Zglinicki, T. (2012). A senescent cell bystander effect: Senescence-induced senescence. *Aging Cell*. https://doi.org/10.1111/j.1474-9726.2012.00795.x

Nguyen, K. D., Qiu, Y., Cui, X., Goh, Y. P. S., Mwangi, J., David, T., … Chawla, A. (2011). Alternatively activated macrophages produce catecholamines to sustain adaptive thermogenesis. *Nature*, *480*(7375), 104–108. https://doi.org/10.1038/nature10653

Nguyen, P., Valanejad, L., Cast, A., Wright, M., Garcia, J. M., El-Serag, H. B., … Timchenko, N. A. (2018). Elimination of Age-Associated Hepatic Steatosis and Correction of Aging Phenotype by Inhibition of cdk4-C/EBPα-p300 Axis. *Cell Reports*, *24*(6), 1597–1609. https://doi.org/10.1016/j.celrep.2018.07.014

Nguyen, T. L. A., Vieira-Silva, S., Liston, A., & Raes, J. (2015). How informative is the mouse for human gut microbiota research? *DMM Disease Models and Mechanisms*. https://doi.org/10.1242/dmm.017400

Niccoli, T., & Partridge, L. (2012). Ageing as a risk factor for disease. *Current Biology*, *22*(17), R741–R752. https://doi.org/10.1016/j.cub.2012.07.024

Nicolaus, M. L., Bergdall, V. K., Davis, I. C., & Hickman-Davis, J. M. (2016). Effect of ventilated caging on water intake and loss in 4 strains of laboratory mice. *Journal of the American Association for Laboratory Animal Science*.

Nilaweera, K. N., & Speakman, J. R. (2018). Regulation of intestinal growth in response to variations in energy supply and demand. *Obesity Reviews*, *19*(December), 61–72. https://doi.org/10.1111/obr.12780

Nisoli, E., Tonello, C., Cardile, A., Cozzi, V., Bracale, R., Tedesco, L., … Carruba, M. O. (2005). Calorie restriction promotes mitochondrial biogenesis by inducing the expression of eNOS. *Science (New York, N.Y.)*, *310*(5746), 314–317. https://doi.org/10.1126/science.1117728

O'Brien, P. D., Hinder, L. M., Callaghan, B. C., & Feldman, E. L. (2017). Neurological consequences of obesity. *The Lancet Neurology*. https://doi.org/10.1016/S1474-4422(17)30084-4

O'Neil, D. A., Porter, E. M., Elewaut, D., Anderson, G. M., Eckmann, L., Ganz, T., & Kagnoff, M. F. (1999). Expression and regulation of the human beta-defensins hBD-1 and hBD-2 in intestinal epithelium. *Journal of Immunology (Baltimore, Md. : 1950)*.

Odegaard, J. I., Ricardo-Gonzalez, R. R., Goforth, M. H., Morel, C. R., Subramanian, V., Mukundan, L., … Chawla, A. (2007). Macrophage-specific PPARγ controls alternative activation and improves insulin resistance. *Nature*, *447*(7148), 1116–1120. https://doi.org/10.1038/nature05894

Ogiolda, L., Wanke, R., Rottmann, O., Hermanns, W., & Wolf, E. (1998). Intestinal dimensions of mice divergently selected for body weight. *Anatomical Record*, *250*(3), 292–299. https://doi.org/10.1002/(SICI)1097-0185(199803)250:3<292::AID-AR4>3.0.CO;2-2

Oh, Y. S., Bae, G. D., Baek, D. J., Park, E. Y., & Jun, H. S. (2018). Fatty acid-induced lipotoxicity in pancreatic beta-cells during development of type 2 diabetes. *Frontiers in Endocrinology*. https://doi.org/10.3389/fendo.2018.00384

Ohashi, K., Parker, J. L., Ouchi, N., Higuchi, A., Vita, J. A., Gokce, N., … Walsh, K. (2010). Adiponectin promotes macrophage polarization toward an anti-inflammatory phenotype. *Journal of Biological Chemistry*. https://doi.org/10.1074/jbc.M109.088708

Olsen, A., Vantipalli, M. C., & Lithgow, G. J. (2006). Checkpoint proteins control survival of the postmitotic cells in Caenorhabditis elegans. *Science*. https://doi.org/10.1126/science.1124981

Omodei, D., & Fontana, L. (2011). Calorie restriction and prevention of age-associated chronic disease. *FEBS Letters*. https://doi.org/10.1016/j.febslet.2011.03.015

Orecchioni, M., Ghosheh, Y., Pramod, A. B., & Ley, K. (2019). Macrophage polarization: Different gene signatures in M1(Lps+) vs. Classically and M2(LPS-) vs. Alternatively activated macrophages. *Frontiers in Immunology*. https://doi.org/10.3389/fimmu.2019.01084

Ott, B., Skurk, T., Hastreiter, L., Lagkouvardos, I., Fischer, S., Büttner, J., … Hauner, H. (2017). Effect of caloric restriction on gut permeability, inflammation markers, and fecal microbiota in obese women. *Scientific Reports*, *7*(1), 1–10. https://doi.org/10.1038/s41598-017-12109-9

Özcan, U., Cao, Q., Yilmaz, E., Lee, A. H., Iwakoshi, N. N., Özdelen, E., … Hotamisligil, G. S. (2004). Endoplasmic reticulum stress links obesity, insulin action, and type 2 diabetes. *Science*. https://doi.org/10.1126/science.1103160

Pai, G. R., & Rawles, J. M. (1989). The QT interval in atrial fibrillation. *Heart*, *61*(6), 510–513. https://doi.org/10.1136/hrt.61.6.510

Pan, D. Z., Garske, K. M., Alvarez, M., Bhagat, Y. V., Boocock, J., Nikkola, E., … Ko, A. (2018). Integration of human adipocyte chromosomal interactions with adipose gene expression prioritizes obesity-related genes from GWAS. *Nature Communications*, *9*(1). https://doi.org/10.1038/s41467-018-03554-9

Parikh, K., Antanaviciute, A., Fawkner-Corbett, D., Jagielowicz, M., Aulicino, A., Lagerholm, C., … Simmons, A. (2019). Colonic epithelial cell diversity in health and inflammatory bowel disease. *Nature*. https://doi.org/10.1038/s41586-019-0992-y

Park, C. Y., Park, S., Kim, M. S., Kim, H. K., & Han, S. N. (2017). Effects of mild calorie restriction on lipid metabolism and inflammation in liver and adipose tissue. *Biochemical and Biophysical Research Communications*, *490*(3), 636–642. https://doi.org/10.1016/j.bbrc.2017.06.090

Park, J. C., & Im, S. H. (2020). Of men in mice: the development and application of a humanized gnotobiotic mouse model for microbiome therapeutics. *Experimental and Molecular Medicine*. https://doi.org/10.1038/s12276-020-0473-2

Park, S., Komatsu, T., Hayashi, H., Yamaza, H., Chiba, T., Higami, Y., … Shimokawa, I. (2006). Calorie restriction initiated at middle age improved glucose tolerance without affecting age-related impairments of insulin signaling in rat skeletal muscle. *Experimental Gerontology*. https://doi.org/10.1016/j.exger.2006.06.055

Partridge, L., Deelen, J., & Slagboom, P. E. (2018). Facing up to the global challenges of ageing. *Nature*, *561*(7721), 45–56. https://doi.org/10.1038/s41586-018-0457-8

Paschos, G. K., Tang, S. Y., Theken, K. N., Li, X., Verginadis, I., Lekkas, D., … FitzGerald, G. A. (2018). Cold-Induced Browning of Inguinal White Adipose Tissue Is Independent of Adipose Tissue Cyclooxygenase-2. *Cell Reports*. https://doi.org/10.1016/j.celrep.2018.06.082

Pentinmikko, N., Iqbal, S., Mana, M., Andersson, S., Cognetta, A. B., Suciu, R. M., … Katajisto, P. (2019). Notum produced by Paneth cells attenuates regeneration of aged intestinal epithelium. *Nature*, *571*(7765), 398–402. https://doi.org/10.1038/s41586-019-1383-0

Peoples, J. N., Saraf, A., Ghazal, N., Pham, T. T., & Kwong, J. Q. (2019). Mitochondrial dysfunction and oxidative stress in heart disease. *Experimental and Molecular Medicine*. https://doi.org/10.1038/s12276-019-0355-7

Pescador, N., Pérez-Barba, M., Ibarra, J. M., Corbatón, A., Martínez-Larrad, M. T., & Serrano-Ríos, M. (2013). Serum Circulating microRNA Profiling for Identification of Potential Type 2 Diabetes and Obesity Biomarkers. *PLoS ONE*. https://doi.org/10.1371/journal.pone.0077251

Pettan-Brewer, C., & M. Treuting, P. M. (2011). Practical pathology of aging mice. *Pathobiology of Aging & Age-Related Diseases*, *1*(00), 1–16. https://doi.org/10.3402/pba.v1i0.7202

Pikala, M., Burzyńska, M., & Maniecka-Bryła, I. (2020). Changes in mortality and years of life lost due to lung cancer in Poland, 2000-2016. *Journal of Translational Medicine*, *18*(1), 1–10. https://doi.org/10.1186/s12967-020-02354-4

Ploeger, J. M., Manivel, J. C., Boatner, L. N., & Mashek, D. G. (2017). Caloric restriction prevents carcinogen-initiated liver tumorigenesis in mice. *Cancer Prevention Research*, *10*(11), 660–670. https://doi.org/10.1158/1940-6207.CAPR-17-0174

Plubell, D. L., Wilmarth, P. A., Zhao, Y., Fenton, A. M., Minnier, J., Reddy, A. P., … Pamir, N. (2017). Extended multiplexing of tandem mass tags (TMT) labeling reveals age and high fat diet specific proteome changes in mouse epididymal adipose tissue. *Molecular and Cellular Proteomics*. https://doi.org/10.1074/mcp.M116.065524

Podany, A. B., Phillips, B. E., Soybel, D. I., & Kelleher, S. L. (2015). Absence of the zinc transporter ZnT2 in the intestinal Paneth cell increases susceptibility of mucosal crypt cells to microbial stress. *Journal of the American College of Surgeons*.

https://doi.org/10.1016/j.jamcollsurg.2015.08.195

Podany, A. B., Wright, J., Lamendella, R., Soybel, D. I., & Kelleher, S. L. (2016). ZnT2-Mediated Zinc Import Into Paneth Cell Granules Is Necessary for Coordinated Secretion and Paneth Cell Function in Mice. *CMGH*. https://doi.org/10.1016/j.jcmgh.2015.12.006

Pomatto, L. C. D., & Davies, K. J. A. (2017). The role of declining adaptive homeostasis in ageing. *Journal of Physiology*. https://doi.org/10.1113/JP275072

Porter, M. H., Fine, J. B., Cutchins, A. G., Bai, Y., & DiGirolamo, M. (2004). Sexual dimorphism in the response of adipose mass and cellularity to graded caloric restriction. *Obesity Research*. https://doi.org/10.1038/oby.2004.18

Psichas, A., Reimann, F., & Gribble, F. M. (2015). Gut chemosensing mechanisms. *Journal of Clinical Investigation*. https://doi.org/10.1172/JCI76309

Pujol, E., Proenza, A. M., Roca, P., & Lladó, I. (2006). Changes in mammary fat pad composition and lipolytic capacity throughout pregnancy. *Cell and Tissue Research*. https://doi.org/10.1007/s00441-005-0085-0

Qi, Y., Jiang, C., Cheng, J., Krausz, K. W., Li, T., Ferrell, J. M., … Chiang, J. Y. L. (2015). Bile acid signaling in lipid metabolism: Metabolomic and lipidomic analysis of lipid and bile acid markers linked to anti-obesity and anti-diabetes in mice. *Biochimica et Biophysica Acta - Molecular and Cell Biology of Lipids*. https://doi.org/10.1016/j.bbalip.2014.04.008

Qiu, X., Brown, K., Hirschey, M. D., Verdin, E., & Chen, D. (2010). Calorie restriction reduces oxidative stress by SIRT3-mediated SOD2 activation. *Cell Metabolism*. https://doi.org/10.1016/j.cmet.2010.11.015

Racette. (2015). One Year of Caloric Restriction in Humans: Feasibility and Effects on Body Composition and Abdominal Adipose Tissue, *61*(9), 943–950.

Racette, S. B., Rochon, J., Uhrich, M. L., Villareal, D. T., Das, S. K., Fontana, L., … Kraus, W. E. (2017). Effects of Two Years of Calorie Restriction on Aerobic Capacity and Muscle Strength. *Medicine and Science in Sports and Exercise*, *49*(11), 2240–2249. https://doi.org/10.1249/MSS.0000000000001353

Racette, S. B., Weiss, E. P., Villareal, D. T., Arif, H., Steger-May, K., Schechtman, K. B., … Holloszy, J. O. (2006). One year of caloric restriction in humans: Feasibility and effects on body composition and abdominal adipose tissue. *Journals of Gerontology - Series A Biological Sciences and Medical Sciences*. https://doi.org/10.1093/gerona/61.9.943

Redman, L. M., Smith, S. R., Burton, J. H., Martin, C. K., Il'yasova, D., & Ravussin, E. (2018). Metabolic Slowing and Reduced Oxidative Damage with Sustained Caloric Restriction Support the Rate of Living and Oxidative Damage Theories of Aging. *Cell Metabolism*. https://doi.org/10.1016/j.cmet.2018.02.019

Reed, M. J., Penn, P. E., Li, Y., Birnbaum, R., Vernon, R. B., Johnson, T. S., … Wolf, N. S. (1996). Enhanced cell proliferation and biosynthesis mediate improved wound repair in refed, caloric-restricted mice. *Mechanisms of Ageing and Development*. https://doi.org/10.1016/0047-6374(96)01737-X

Regan, J. C., Khericha, M., Dobson, A. J., Bolukbasi, E., Rattanavirotkul, N., & Partridge, L. (2016). Sex difference in pathology of the ageing gut mediates the greater response of female lifespan to dietary restriction. *ELife*. https://doi.org/10.7554/eLife.10956

Regan, J. C., & Partridge, L. (2013). Gender and longevity: Why do men die earlier than women? Comparative and experimental evidence. *Best Practice and Research: Clinical Endocrinology and Metabolism*. https://doi.org/10.1016/j.beem.2013.05.016

Reinke, H., & Asher, G. (2019). Crosstalk between metabolism and circadian clocks. *Nature Reviews Molecular Cell Biology*. https://doi.org/10.1038/s41580-018-0096-9

Reis, F. C. G., Branquinho, J. L. O., Brandão, B. B., Guerra, B. A., Silva, I. D., Frontini, A., … Mori, M. A. (2016). Fat-specific Dicer deficiency accelerates aging and mitigates several effects of dietary restriction in mice. *Aging*. https://doi.org/10.18632/aging.100970

Richardson, A., Austad, S. N., Ikeno, Y., Unnikrishnan, A., & Mccarter, R. J. (2016). Significant life extension by ten percent dietary restriction. *Annals of the New York Academy of Sciences*. https://doi.org/10.1111/nyas.12982

Ricquier, D., & Bouillaud, F. (2000). Mitochondrial uncoupling proteins: From mitochondria to the regulation of energy balance. *Journal of Physiology*. https://doi.org/10.1111/j.1469-7793.2000.00003.x

Rigamonti, A., Brennand, K., Lau, F., & Cowan, C. A. (2011). Rapid cellular turnover in adipose tissue. *PLoS ONE*. https://doi.org/10.1371/journal.pone.0017637

Rikke, B. A., Battaglia, M. E., Allison, D. B., & Johnson, T. E. (2006). Murine weight loss exhibits significant genetic variation during dietary restriction. *Physiological Genomics*. https://doi.org/10.1152/physiolgenomics.00068.2006

Rikke, B. A., Yerg, J. E., Battaglia, M. E., Nagy, T. R., Allison, D. B., & Johnson, T. E. (2003). Strain variation in the response of body temperature to dietary restriction. *Mechanisms of Ageing and Development*. https://doi.org/10.1016/S0047-6374(03)00003-4

Roberts, H. C., Lim, S. E. R., Cox, N. J., & Ibrahim, K. (2019). The challenge of managing undernutrition in older people with frailty. *Nutrients*. https://doi.org/10.3390/nu11040808

Rockstroh, D., Landgraf, K., Wagner, I. V., Gesing, J., Tauscher, R., Lakowa, N., … Körner, A. (2014). Direct evidence for brown adipose tissue in different fat depots in children. *Diabetes*.

Rodeheffer, M. S., Birsoy, K., & Friedman, J. M. (2008). Identification of White Adipocyte Progenitor Cells In Vivo. *Cell*. https://doi.org/10.1016/j.cell.2008.09.036

Rodrigues, M. O. M., Evangelista-Silva, P. H., Neves, N. N., Moreno, L. G., Santos, C. S., Rocha, K. L. S., … Esteves, E. A. (2020). Caloric restriction-induced weight loss with a high-fat diet does not fully recover visceral adipose tissue inflammation in previously obese c57bl/6 mice. *Applied Physiology, Nutrition and Metabolism*, *45*(12), 1353–1359. https://doi.org/10.1139/apnm-2020-0220

Roedel, A., Storch, C., Holsboer, F., & Ohl, F. (2006). Effects of light or dark phase testing on behavioural and cognitive performance in DBA mice. *Laboratory Animals*. https://doi.org/10.1258/002367706778476343

Rogers, N. H., Landa, A., Park, S., & Smith, R. G. (2012). Aging Leads to a Programmed Loss of Brown Adipocytes in Murine Subcutaneous White Adipose Tissue Nicole. *Aging Cell*, *11*(6), 1–18. https://doi.org/10.1111/acel.12010.

Rojas, J. X. S., Frutos, M. G. S., Horrillo, D., Lauzurica, N., Oliveros, E., Carrascosa, J. M., … Ros, M. (2016). Differential Development of Inflammation and Insulin Resistance in Different Adipose Tissue Depots Along Aging in Wistar Rats: Effects of Caloric Restriction. *Journals of Gerontology - Series A Biological Sciences and Medical Sciences*. https://doi.org/10.1093/gerona/glv117

Rojo, Ó. P., San Román, A. L., Arbizu, E. A., Martínez, A. D. L. H., Sevillano, E. R., & Martínez, A. A. (2007). Serum lipopolysaccharide-binding protein in endotoxemic patients with inflammatory bowel disease. *Inflammatory Bowel Diseases*. https://doi.org/10.1002/ibd.20019

Roland, J. (n.d.). Adipose Tissue Segmentation in Fiji. *Digital Histology Shared Resource*, 15.

Romacho, T., Elsen, M., Röhrborn, D., & Eckel, J. (2014). Adipose tissue and its role in organ crosstalk. *Acta Physiologica*. https://doi.org/10.1111/apha.12246

Rosen, E. D., & MacDougald, O. A. (2006). Adipocyte differentiation from the inside out. *Nature Reviews Molecular Cell Biology*. https://doi.org/10.1038/nrm2066

Rosen, E. D., & Spiegelman, B. M. (2006). Adipocytes as regulators of energy balance and glucose homeostasis. *Nature*. https://doi.org/10.1038/nature05483

Rosen, E. D., Walkey, C. J., Puigserver, P., & Spiegelman, B. M. (2000). Transcriptional regulation of adipogenesis. *Genes and Development*. https://doi.org/10.1101/gad.14.11.1293

Rosenfeld, C. S., & Ferguson, S. A. (2014). Barnes maze testing strategies with small and large rodent models. *Journal of Visualized Experiments*, (84), 1–15. https://doi.org/10.3791/51194

Ross, G. A., & Mayhew, T. M. (1985). Effects of fasting on mucosal dimensions in the duodenum, jejunum and ileum of the rat. *Journal of Anatomy*, *142*, 191–200.

Rossi, D. J., Bryder, D., Zahn, J. M., Ahlenius, H., Sonu, R., Wagers, A. J., & Weissman, I. L. (2005). Cell intrinsic alterations underlie hematopoietic stem cell aging. *Proceedings of the National Academy of Sciences of the United States of America*. https://doi.org/10.1073/pnas.0503280102

Rossing, P., Breum, L., Major-Pedersen, A., Sato, A., Winding, H., Pietersen, A., … Parving, H. H. (2001). Prolonged QTc interval predicts mortality in patients with Type 1 diabetes mellitus. *Diabetic Medicine*. https://doi.org/10.1046/j.1464-5491.2001.00446.x

Roth, G. A., Johnson, C., Abajobir, A., Abd-Allah, F., Abera, S. F., Abyu, G., … Murray, C. (2017). Global, Regional, and National Burden of Cardiovascular Diseases for 10 Causes, 1990 to 2015. *Journal of the American College of Cardiology*, *70*(1), 1–25. https://doi.org/10.1016/j.jacc.2017.04.052

Rotstein, B., & Paululat, A. (2016). On the Morphology of the Drosophila Heart. *Journal of Cardiovascular Development and Disease*. https://doi.org/10.3390/jcdd3020015

Roussel, J., Champeroux, P., Roy, J., Richard, S., Fauconnier, J., Le Guennec, J. Y., & Thireau, J. (2016). The Complex QT/RR Relationship in Mice. *Scientific Reports*, *6*(May), 1–9. https://doi.org/10.1038/srep25388

Rowland, I., Gibson, G., Heinken, A., Scott, K., Swann, J., Thiele, I., & Tuohy, K. (2018). Gut microbiota functions: metabolism of nutrients and other food components. *European Journal of Nutrition*. https://doi.org/10.1007/s00394-017-1445-8

Ruby, J. G., Smith, M., & Buffenstein, R. (2018). Naked mole-rat mortality rates defy gompertzian laws by not increasing with age. *ELife*. https://doi.org/10.7554/eLife.31157

Rundle, A., Hoepner, L., Hassoun, A., Oberfield, S., Freyer, G., Holmes, D., … Whyatt, R. (2012). Association of childhood obesity with maternal exposure to ambient air polycyclic aromatic hydrocarbons during pregnancy. *American Journal of Epidemiology*, *175*(11), 1163–1172. https://doi.org/10.1093/aje/kwr455

Rutters, F., Pilz, S., Koopman, A. D., Rauh, S. P., Te Velde, S. J., Stehouwer, C. D., … Dekker, J. M. (2014). The association between psychosocial stress and mortality is mediated by lifestyle and chronic diseases: The Hoorn Study. *Social Science and Medicine*, *118*(C), 166–172. https://doi.org/10.1016/j.socscimed.2014.08.009

S. Anderson, A. T. Bankier, B. G. Barrell, M. H. L. de Bruijn, A. R. Coulson, J. Drouin, I. C. Eperon, D. P. Nierlich, B. A. Roe, F. Sanger, P. H. Schreier, A. J. H. Smith, R. S. & I. G. Y. (1981). Sequence and organization of the human mitochondrial genome. *Nature*, *290*(April), 457–465.

Saari, T. J., Raiko, J., U-Din, M., Niemi, T., Taittonen, M., Laine, J., … Virtanen, K. A. (2020). Basal and cold-induced fatty acid uptake of human brown adipose tissue is impaired in obesity. *Scientific Reports*. https://doi.org/10.1038/s41598-020-71197-2

Sabath, N., Itescu, Y., Feldman, A., Meiri, S., Mayrose, I., & Valenzuela, N. (2016). Sex determination, longevity, and the birth and death of reptilian species. *Ecology and Evolution*. https://doi.org/10.1002/ece3.2277

Sabet Sarvestani, F., Rahmanifar, F., & Tamadon, A. (2015). Histomorphometric changes of small intestine in pregnant rat. *Veterinary Research Forum : An International Quarterly Journal*, *6*(1), 69–73.

Sahu, P., Lim, P. O., Rana, B. S., Struthers, A. D., & P.o, L. (2000). QT dispersion in medicine: Electrophysiological Holy Grail or fool's gold? *QJM - Monthly Journal of the Association of Physicians*, *93*(7), 425–431. https://doi.org/10.1093/qjmed/93.7.425

Saltiel, A. R., & Kahn, C. R. (2001). Insulin signalling and the regulation of glucose and lipid metabolism. *Nature*, *414*(6865), 799–806. https://doi.org/10.1038/414799a

Sandfort, V., Lai, S., Ahlman, M. A., Mallek, M., Liu, S., Sibley, C. T., … Bluemke, D. A. (2016). Obesity Is Associated With Progression of Atherosclerosis During Statin Treatment. *Journal of the American Heart Association*. https://doi.org/10.1161/JAHA.116.003621

Sano, H., Kane, S., Sano, E., Mîinea, C. P., Asara, J. M., Lane, W. S., … Lienhard, G. E. (2003). Insulin-stimulated phosphorylation of a Rab GTPase-activating protein regulates GLUT4 translocation. *Journal of Biological Chemistry*, *278*(17), 14599–14602. https://doi.org/10.1074/jbc.C300063200

Santos, J., Leitão-Correia, F., Sousa, M. J., & Leão, C. (2016). Dietary Restriction and Nutrient Balance in Aging. *Oxidative Medicine and Cellular Longevity*, *2016*. https://doi.org/10.1155/2016/4010357

Sarbassov, D. D., Guertin, D. A., Ali, S. M., & Sabatini, D. M. (2005). Phosphorylation and regulation of Akt/PKB by the rictor-mTOR complex. *Science*, *307*(5712), 1098–1101. https://doi.org/10.1126/science.1106148

Sarshad, A. A., Juan, A. H., Muler, A. I. C., Anastasakis, D. G., Wang, X., Genzor, P., … Hafner, M. (2018). Argonaute-miRNA Complexes Silence Target mRNAs in the Nucleus of Mammalian Stem Cells. *Molecular Cell*. https://doi.org/10.1016/j.molcel.2018.07.020

Sathananthan, M., Shah, M., Edens, K. L., Grothe, K. B., Piccinini, F., Farrugia, L. P., … Vella, A. (2015). Six and 12 weeks of caloric restriction increases β cell function and lowers fasting and postprandial glucose concentrations in people with type 2 diabetes. *Journal of Nutrition*. https://doi.org/10.3945/jn.115.210617

Sato, S., Basse, A. L., Schönke, M., Chen, S., Samad, M., Altıntaş, A., … Sassone-Corsi, P.

(2019). Time of Exercise Specifies the Impact on Muscle Metabolic Pathways and Systemic Energy Homeostasis. *Cell Metabolism*. https://doi.org/10.1016/j.cmet.2019.03.013

Sato, T., Van Es, J. H., Snippert, H. J., Stange, D. E., Vries, R. G., Van Den Born, M., … Clevers, H. (2011). Paneth cells constitute the niche for Lgr5 stem cells in intestinal crypts. *Nature*. https://doi.org/10.1038/nature09637

Sbierski-Kind, J., Mai, K., Kath, J., Jurisch, A., Streitz, M., Kuchenbecker, L., … Spranger, J. (2020). Association between Subcutaneous Adipose Tissue Inflammation, Insulin Resistance, and Calorie Restriction in Obese Females. *The Journal of Immunology*, *205*(1), 45–55. https://doi.org/10.4049/jimmunol.2000108

Schaum, N., Lehallier, B., Hahn, O., Pálovics, R., Hosseinzadeh, S., Lee, S. E., … Wyss-Coray, T. (2020). Ageing hallmarks exhibit organ-specific temporal signatures. *Nature*, *583*(July). https://doi.org/10.1038/s41586-020-2499-y

Schiavo, L., Busetto, L., Cesaretti, M., Zelber-Sagi, S., Deutsch, L., & Iannelli, A. (2018). Nutritional issues in patients with obesity and cirrhosis. *World Journal of Gastroenterology*. https://doi.org/10.3748/wjg.v24.i30.3330

Schindelin, J., Arganda-Carreras, I., Frise, E., Kaynig, V., Longair, M., Pietzsch, T., … Cardona, A. (2012). Fiji: An open-source platform for biological-image analysis. *Nature Methods*. https://doi.org/10.1038/nmeth.2019

Schlick, C., Schniepp, R., Loidl, V., Wuehr, M., Hesselbarth, K., & Jahn, K. (2016). Falls and fear of falling in vertigo and balance disorders: A controlled cross-sectional study. *Journal of Vestibular Research: Equilibrium and Orientation*, *25*(5–6), 241–251. https://doi.org/10.3233/VES-150564

Schmidt-Nielsen, K. (1997). *Animal Physiology: Adaptation and Environment*. Cambridge: Cambridge University Press.

Schmitz, J., Evers, N., Awazawa, M., Nicholls, H. T., Brönneke, H. S., Dietrich, A., … Brüning, J. C. (2016). Obesogenic memory can confer long-term increases in adipose tissue but not liver inflammation and insulin resistance after weight loss. *Molecular Metabolism*. https://doi.org/10.1016/j.molmet.2015.12.001

Schneider, A., Dhahbi, J. M., Atamna, H., Clark, J. P., Colman, R. J., & Anderson, R. M. (2017). Caloric restriction impacts plasma microRNAs in rhesus monkeys. *Aging Cell*. https://doi.org/10.1111/acel.12636

Schultz, M. B., Kane, A. E., Mitchell, S. J., MacArthur, M. R., Warner, E., Vogel, D. S., … Sinclair, D. A. (2020). Age and life expectancy clocks based on machine learning analysis of mouse frailty. *Nature Communications*. https://doi.org/10.1038/s41467-020-18446-0

Schumann, R. R., Kirschning, C. J., Unbehaun, A., Aberle, H. P., Knope, H. P., Lamping, N., … Herrmann, F. (1996). The lipopolysaccharide-binding protein is a secretory class 1 acute-phase protein whose gene is transcriptionally activated by APRF/STAT/3 and other cytokine-inducible nuclear proteins. *Molecular and Cellular Biology*. https://doi.org/10.1128/mcb.16.7.3490

Schwartz, M. W., Woods, S. C., Porte, D., Seeley, R. J., & Baskin, D. G. (2000). Central nervous system control of food intake. *Nature*. https://doi.org/10.1038/35007534

Schwartz, R. S., Shuman, W. P., Bradbury, V. L., Cain, K. C., Fellingham, G. W., Beard, J. C., … Abrass, I. B. (1990). Body fat distribution in healthy young and older men. *Journals of Gerontology*. https://doi.org/10.1093/geronj/45.6.M181

Seabold, S., & Perktold, J. (2010). Statsmodels : Econometric and Statistical Modeling with Python, (Scipy), 92–96.

Segaert, K., Lucas, S. J. E., Burley, C. V., Segaert, P., Milner, A. E., Ryan, M., & Wheeldon, L. (2018). Higher physical fitness levels are associated with less language decline in healthy ageing. *Scientific Reports*, *8*(1), 1–10. https://doi.org/10.1038/s41598-018-24972-1

Sehgal, S. N., Baker, H., & Vézina, C. (1975). Rapamycin (Ay-22,989), a New Antifungal Antibiotic. II. Fermentation, Isolation and Characterization. *The Journal of Antibiotics*. https://doi.org/10.7164/antibiotics.28.727

Selman, C., & Hempenstall, S. (2012). Evidence of a metabolic memory to early-life dietary restriction in male C57BL/6 mice. *Longevity & Healthspan*, *1*(1), 1–11. https://doi.org/10.1186/2046-2395-1-2

Selman, C., Lingard, S., Choudhury, A. I., Batterham, R. L., Claret, M., Clements, M., … Withers, D. J. (2008). Evidence for lifespan extension and delayed age-related biomarkers in insulin receptor substrate 1 null mice. *The FASEB Journal : Official Publication of the Federation of American Societies for Experimental Biology*, *22*(3), 807–818. https://doi.org/10.1096/fj.07-9261com

Selman, C., Partridge, L., & Withers, D. J. (2011). Replication of extended lifespan phenotype in mice with deletion of insulin receptor substrate 1. *PLoS ONE*, *6*(1), 3–5. https://doi.org/10.1371/journal.pone.0016144

Selman, C., Tullet, J. M. A., Wieser, D., Irvine, E., Lingard, S. J., Choudhury, A. I., … Withers, D. J. (2009). Ribosomal Protein S6 Kinase 1 Signaling Regulates Mammalian Life Span. *Science*, *461*(October), 140–144.

Seto, B. (2012). Rapamycin and mTOR: a serendipitous discovery and implications for breast cancer. *Clinical and Translational Medicine*. https://doi.org/10.1186/2001-1326-1-29

Shang, Y., Kakinuma, S., Yamauchi, K., Morioka, T., Kokubo, T., Tani, S., … Shimada, Y. (2014). Cancer prevention by adult-onset calorie restriction after infant exposure to ionizing radiation in B6C3F1 male mice. *International Journal of Cancer*. https://doi.org/10.1002/ijc.28751

Sheng, Y., Xia, F., Chen, L., Lv, Y., Lv, S., Yu, J., … Ding, G. (2020). Differential Responses of White Adipose Tissue and Brown Adipose Tissue to Calorie Restriction During Aging. *The Journals of Gerontology: Series A*, *XX*(Xx), 1–7. https://doi.org/10.1093/gerona/glaa070

Shevah, O., & Laron, Z. (2007). Patients with congenital deficiency of IGF-I seem protected from the development of malignancies: A preliminary report. *Growth Hormone and IGF Research*. https://doi.org/10.1016/j.ghir.2006.10.007

Shi, H., Kokoeva, M. V., Inouye, K., Tzameli, I., Yin, H., & Flier, J. S. (2006). TLR4 links innate immunity and fatty acid-induced insulin resistance. *Journal of Clinical Investigation*. https://doi.org/10.1172/JCI28898

Shimobayashi, M., Albert, V., Woelnerhanssen, B., Frei, I. C., Weissenberger, D., Meyer-Gerspach, A. C., … Hall, M. N. (2018). Insulin resistance causes inflammation in adipose tissue. *Journal of Clinical Investigation*. https://doi.org/10.1172/JCI96139

Shinmura, K., Tamaki, K., Sano, M., Murata, M., Yamakawa, H., Ishida, H., & Fukuda, K. (2011). Impact of long-term caloric restriction on cardiac senescence: Caloric restriction ameliorates cardiac diastolic dysfunction associated with aging. *Journal of Molecular and Cellular Cardiology*, *50*(1), 117–127. https://doi.org/10.1016/j.yjmcc.2010.10.018

Siervo, M., Lara, J., Celis-Morales, C., Vacca, M., Oggioni, C., Battezzati, A., … Bertoli, S. (2016). Age-related changes in basal substrate oxidation and visceral adiposity and their association with metabolic syndrome. *European Journal of Nutrition*. https://doi.org/10.1007/s00394-015-0993-z

Silvani, A., Calandra-Buonaura, G., Dampney, R. A. L., & Cortelli, P. (2016). Brain-heart interactions: Physiology and clinical implications. *Philosophical Transactions of the Royal Society A: Mathematical, Physical and Engineering Sciences*. https://doi.org/10.1098/rsta.2015.0181

Singh, R., Lakhanpal, D., Kumar, S., Sharma, S., Kataria, H., Kaur, M., & Kaur, G. (2012). Late-onset intermittent fasting dietary restriction as a potential intervention to retard age-associated brain function impairments in male rats. *Age*. https://doi.org/10.1007/s11357-011-9289-2

Sinha, M. K., Ohannesian, J. P., Heiman, M. L., Kriauciunas, A., Stephens, T. W., Magosin, S., … Caro, J. F. (1996). Nocturnal rise of leptin in lean, obese, and non-insulin-dependent

diabetes mellitus subjects. *Journal of Clinical Investigation*. https://doi.org/10.1172/JCI118551

Snyder, J. M., Ward, J. M., & Treuting, P. M. (2016). Cause-of-Death Analysis in Rodent Aging Studies. *Veterinary Pathology*. https://doi.org/10.1177/0300985815610391

Soare, A., Cangemi, R., Omodei, D., Holloszy, J. O., & Fontana, L. (2011). Long-term calorie restriction, but not endurance exercise, lowers core body temperature in humans. *Aging*, *3*(4), 374–379. https://doi.org/10.18632/aging.100280

Soltani, S., Chauvette, S., Bukhtiyarova, O., Lina, J. M., Dubé, J., Seigneur, J., … Timofeev, I. (2019). Sleep–Wake Cycle in Young and Older Mice. *Frontiers in Systems Neuroscience*. https://doi.org/10.3389/fnsys.2019.00051

Song, Z., Xiaoli, A. M., & Yang, F. (2018). Regulation and metabolic significance of De Novo lipogenesis in adipose tissues. *Nutrients*. https://doi.org/10.3390/nu10101383

Sovran, B., Hugenholtz, F., Elderman, M., Van Beek, A. A., Graversen, K., Huijskes, M., … Wells, J. M. (2019). Age-associated Impairment of the Mucus Barrier Function is Associated with Profound Changes in Microbiota and Immunity. *Scientific Reports*. https://doi.org/10.1038/s41598-018-35228-3

Spalding, K. L., Arner, E., Westermark, P. O., Bernard, S., Buchholz, B. A., Bergmann, O., … Arner, P. (2008). Dynamics of fat cell turnover in humans. *Nature*. https://doi.org/10.1038/nature06902

Spindler, S. R. (2005). Rapid and reversible induction of the longevity, anticancer and genomic effects of caloric restriction. *Mechanisms of Ageing and Development*. https://doi.org/10.1016/j.mad.2005.03.016

Spinelli, J. B., & Haigis, M. C. (2018). The multifaceted contributions of mitochondria to cellular metabolism. *Nature Cell Biology*, *20*(7), 745–754. https://doi.org/10.1038/s41556-018-0124-1

Staiano, A. E., & Katzmarzyk, P. T. (2012). Ethnic and sex differences in body fat and visceral and subcutaneous adiposity in children and adolescents. *International Journal of Obesity*. https://doi.org/10.1038/ijo.2012.95

Steck, S. E., & Murphy, E. A. (2020). Dietary patterns and cancer risk. *Nature Reviews Cancer*, *20*(2), 125–138. https://doi.org/10.1038/s41568-019-0227-4

Steppan, C. M., Bailey, S. T., Bhat, S., Brown, E. J., Banerjee, R. R., Wright, C. M., … Lazar, M. A. (2001). The hormone resistin links obesity to diabetes. *Nature*. https://doi.org/10.1038/35053000

Stern, J. H., Rutkowski, J. M., & Scherer, P. E. (2016). Adiponectin, Leptin, and Fatty Acids in

the Maintenance of Metabolic Homeostasis through Adipose Tissue Crosstalk. *Cell Metabolism*. https://doi.org/10.1016/j.cmet.2016.04.011

Stern, J. S., & Johnson, P. R. (1977). Spontaneous activity and adipose cellularity in the genetically obese Zucker rat (fafa). *Metabolism*. https://doi.org/10.1016/0026-0495(77)90104-4

Stessman, J., Jacobs, J. M., Stessman-Lande, I., Gilon, D., & Leibowitz, D. (2013). Aging, resting pulse rate, and longevity. *Journal of the American Geriatrics Society*. https://doi.org/10.1111/jgs.12060

Stockinger, S., Albers, T., Duerr, C. U., Ménard, S., Pütsep, K., Andersson, M., & Hornef, M. W. (2014). Interleukin-13-mediated paneth cell degranulation and antimicrobial peptide release. *Journal of Innate Immunity*. https://doi.org/10.1159/000357644

Stokkan, K. A., Yamazaki, S., Tei, H., Sakaki, Y., & Menaker, M. (2001). Entrainment of the circadian clock in the liver by feeding. *Science*. https://doi.org/10.1126/science.291.5503.490

Sun, L. Y., Spong, A., Swindell, W. R., Fang, Y., Hill, C., Huber, J. A., … Bartke, A. (2013). Growth hormone-releasing hormone disruption extends lifespan and regulates response to caloric restriction in mice. *ELife*. https://doi.org/10.7554/elife.01098

Sutton, E. F., Beyl, R., Early, K. S., Cefalu, W. T., Ravussin, E., & Peterson, C. M. (2018). Early Time-Restricted Feeding Improves Insulin Sensitivity, Blood Pressure, and Oxidative Stress Even without Weight Loss in Men with Prediabetes. *Cell Metabolism*, *27*(6), 1212-1221.e3. https://doi.org/10.1016/j.cmet.2018.04.010

Swindell, W. R. (2012). Dietary restriction in rats and mice: A meta-analysis and review of the evidence for genotype-dependent effects on lifespan. *Ageing Research Reviews*, *11*(2), 254–270. https://doi.org/10.1016/j.arr.2011.12.006

Taffet, G. E., Pham, T. T., & Hartley, C. J. (1997). The age-associated alterations in late diastolic function in mice are improved by caloric restriction. *Journals of Gerontology - Series A Biological Sciences and Medical Sciences*. https://doi.org/10.1093/gerona/52A.6.B285

Talan, M. I., Kirov, S. A., & Kosheleva, N. A. (1996). Nonshivering thermogenesis in adult and aged C57BL/6J mice housed at 22°C and at 29°C. *Experimental Gerontology*, *31*(6), 687–698. https://doi.org/10.1016/S0531-5565(96)00095-2

Taormina, G., Ferrante, F., Vieni, S., Grassi, N., Russo, A., & Mirisola, M. G. (2019). Longevity: Lesson from model organisms. *Genes*. https://doi.org/10.3390/genes10070518

Tchkonia, T., Morbeck, D. E., Von Zglinicki, T., Van Deursen, J., Lustgarten, J., Scrable, H., … Kirkland, J. L. (2010). Fat tissue, aging, and cellular senescence. *Aging Cell*, *9*(5), 667–

684. https://doi.org/10.1111/j.1474-9726.2010.00608.x

Tchoukalova, Y. D., Votruba, S. B., Tchkonia, T., Giorgadze, N., Kirkland, J. L., & Jensen, M. D. (2010). Regional differences in cellular mechanisms of adipose tissue gain with overfeeding. *Proceedings of the National Academy of Sciences of the United States of America*. https://doi.org/10.1073/pnas.1005259107

Terzibasi, E., Lefrançois, C., Domenici, P., Hartmann, N., Graf, M., & Cellerino, A. (2009). Effects of dietary restriction on mortality and age-related phenotypes in the short-lived fish Nothobranchius furzeri. *Aging Cell*, *8*(2), 88–99. https://doi.org/10.1111/j.1474-9726.2009.00455.x

Tetteh, P. W., Basak, O., Farin, H. F., Wiebrands, K., Kretzschmar, K., Begthel, H., … Clevers, H. (2016). Replacement of Lost Lgr5-Positive Stem Cells through Plasticity of Their Enterocyte-Lineage Daughters. *Cell Stem Cell*. https://doi.org/10.1016/j.stem.2016.01.001

Thachil, L., Hugot, J. P., Arbeille, B., Paris, R., Grodet, A., Peuchmaur, M., … Viala, J. (2012). Abnormal activation of autophagy-induced crinophagy in paneth cells from patients with Crohn's disease. *Gastroenterology*, *142*(5), 1097-1099.e4. https://doi.org/10.1053/j.gastro.2012.01.031

Therneau, T. M. (2020). A Package for Survival Analysis in R.

Thevaranjan, N., Puchta, A., Schulz, C., Naidoo, A., Szamosi, J. C., Verschoor, C. P., … Bowdish, D. M. E. (2017). Age-Associated Microbial Dysbiosis Promotes Intestinal Permeability, Systemic Inflammation, and Macrophage Dysfunction. *Cell Host and Microbe*. https://doi.org/10.1016/j.chom.2017.03.002

Thomas, J., Bertrand, H., Stacy, C., & Herlihy, J. T. (1993). Long-term caloric restriction improves baroreflex sensitivity in aging Fischer 344 rats. *Journals of Gerontology*. https://doi.org/10.1093/geronj/48.4.B151

Thomou, T., Mori, M. A., Dreyfuss, J. M., Konishi, M., Sakaguchi, M., Wolfrum, C., … Kahn, C. R. (2017). Adipose-derived circulating miRNAs regulate gene expression in other tissues. *Nature*, *542*(7642), 450–455. https://doi.org/10.1038/nature21365

Thompson, P. J., Shah, A., Ntranos, V., Van Gool, F., Atkinson, M., & Bhushan, A. (2019). Targeted Elimination of Senescent Beta Cells Prevents Type 1 Diabetes. *Cell Metabolism*. https://doi.org/10.1016/j.cmet.2019.01.021

Todorovic, S. T., Smiljanic, K. R., Ruzdijic, S. D., Mladenovic Djordjevic, A. N., & Kanazir, S. D. (2018). Effects of different dietary protocols on general activity and frailty of Male Wistar rats during aging. *Journals of Gerontology - Series A Biological Sciences and Medical Sciences*. https://doi.org/10.1093/gerona/gly015

Toman, O., Hnatkova, K., Smetana, P., Huster, K. M., Šišáková, M., Barthel, P., … Malik, M. (2020). Physiologic heart rate dependency of the PQ interval and its sex differences. *Scientific Reports*, *10*(1), 1–17. https://doi.org/10.1038/s41598-020-59480-8

Trichopoulou, A., Martínez-González, M. A., Tong, T. Y. N., Forouhi, N. G., Khandelwal, S., Prabhakaran, D., … de Lorgeril, M. (2014). Definitions and potential health benefits of the Mediterranean diet: Views from experts around the world. *BMC Medicine*. https://doi.org/10.1186/1741-7015-12-112

Tulsian, R., Velingkaar, N., & Kondratov, R. (2018). Caloric restriction effects on liver mTOR signaling are time-of-day dependent. *Aging*. https://doi.org/10.18632/aging.101498

Uchida, R., Saito, Y., Nogami, K., Kajiyama, Y., Suzuki, Y., Kawase, Y., … Saito, H. (2019). Epigenetic silencing of Lgr5 induces senescence of intestinal epithelial organoids during the process of aging. *NpAging and Mechanisms of Disease*, *5*(1), 1–5. https://doi.org/10.1038/s41514-018-0031-5

Uezumi, A., Fukada, S. I., Yamamoto, N., Takeda, S., & Tsuchida, K. (2010). Mesenchymal progenitors distinct from satellite cells contribute to ectopic fat cell formation in skeletal muscle. *Nature Cell Biology*. https://doi.org/10.1038/ncb2014

Um, S. H., D'Alessio, D., & Thomas, G. (2006). Nutrient overload, insulin resistance, and ribosomal protein S6 kinase 1, S6K1. *Cell Metabolism*, *3*(6), 393–402. https://doi.org/10.1016/j.cmet.2006.05.003

Vaishnava, S., Behrendt, C. L., Ismail, A. S., Eckmann, L., & Hooper, L. V. (2008). Paneth cells directly sense gut commensals and maintain homeostasis at the intestinal host-microbial interface. *Proceedings of the National Academy of Sciences of the United States of America*. https://doi.org/10.1073/pnas.0808723105

Valle, A., Guevara, R., García-Palmer, F. J., Roca, P., & Oliver, J. (2008). Caloric restriction retards the age-related decline in mitochondrial function of brown adipose tissue. *Rejuvenation Research*, *11*(3), 597–604. https://doi.org/10.1089/rej.2007.0626

Valle, A., Sastre-Serra, J., Roca, P., & Oliver, J. (2010). Modulation of white adipose tissue proteome by aging and calorie restriction. *Aging Cell*, *9*(5), 882–894. https://doi.org/10.1111/j.1474-9726.2010.00613.x

van den Berg, L. J. M., Tollenaar, M. S., Compier-de Block, L. H. C. G., Bakermans-Kranenburg, M. J., & Elzinga, B. M. (2019). An intergenerational family study on the impact of experienced and perpetrated child maltreatment on neural face processing. *Psychoneuroendocrinology*, *103*(January), 266–275. https://doi.org/10.1016/j.psyneuen.2019.01.030

Van Es, J. H., Wiebrands, K., López-Iglesias, C., Van De Wetering, M., Zeinstra, L., Van Den

Born, M., … Clevers, H. (2019). Enteroendocrine and tuft cells support Lgr5 stem cells on Paneth cell depletion. *Proceedings of the National Academy of Sciences of the United States of America*. https://doi.org/10.1073/pnas.1801888117

Van Heemst, D., Beekman, M., Mooijaart, S. P., Heijmans, B. T., Brandt, B. W., Zwaan, B. J., … Westendorp, R. G. J. (2005). Reduced insulin/IGF-1 signalling and human longevity. *Aging Cell*, *4*(2), 79–85. https://doi.org/10.1111/j.1474-9728.2005.00148.x

Van Loo, P. L. P., Van De Weerd, H. A., Van Zutphen, L. F. M., & Baumans, V. (2004). Preference for social contact versus environmental enrichment in male laboratory mice. *Laboratory Animals*. https://doi.org/10.1258/002367704322968867

van Marken Lichtenbelt, W. D., Vanhommerig, J. W., Smulders, N. M., Drossaerts, J. M. A. F. L., Kemerink, G. J., Bouvy, N. D., … Teule, G. J. J. (2009). Cold-Activated Brown Adipose Tissue in Healthy Men. *New England Journal of Medicine*. https://doi.org/10.1056/nejmoa0808718

Vanuytsel, T., Senger, S., Fasano, A., & Shea-Donohue, T. (2013). Major signaling pathways in intestinal stem cells. *Biochimica et Biophysica Acta - General Subjects*. https://doi.org/10.1016/j.bbagen.2012.08.006

Vedel-Larsen, E., Iepsen, E. W., Lundgren, J., Graff, C., Struijk, J. J., Hansen, T., … Kanters, J. K. (2016). Major rapid weight loss induces changes in cardiac repolarization. *Journal of Electrocardiology*. https://doi.org/10.1016/j.jelectrocard.2016.02.005

Vera, E., Bernardes de Jesus, B., Foronda, M., Flores, J. M., & Blasco, M. A. (2013). Telomerase Reverse Transcriptase Synergizes with Calorie Restriction to Increase Health Span and Extend Mouse Longevity. *PLoS ONE*, *8*(1). https://doi.org/10.1371/journal.pone.0053760

Villareal, D. T., Fontana, L., Weiss, E. P., Racette, S. B., Steger-May, K., Schechtman, K. B., … Holloszy, J. O. (2006). Bone mineral density response to caloric restriction-induced weight loss or exercise-induced weight loss: A randomized controlled trial. *Archives of Internal Medicine*. https://doi.org/10.1001/archinte.166.22.2502

Virtanen, P., Gommers, R., Oliphant, T. E., Haberland, M., Reddy, T., Walt, S. J. Van Der, … Millman, K. J. (2020). computing in Python, *17*(March). https://doi.org/10.1038/s41592-019-0686-2

Voisin, S., Almén, M. S., Zheleznyakova, G. Y., Lundberg, L., Zarei, S., Castillo, S., … Schiöth, H. B. (2015). Many obesity-associated SNPs strongly associate with DNA methylation changes at proximal promoters and enhancers. *Genome Medicine*, *7*(1). https://doi.org/10.1186/s13073-015-0225-4

Walford, R. L., Harris, S. B., & Gunion, M. W. (1992). The calorically restricted low-fat nutrient-

dense diet in Biosphere 2 significantly lowers blood glucose, total leukocyte count, cholesterol, and blood pressure in humans. *Proceedings of the National Academy of Sciences of the United States of America*. https://doi.org/10.1073/pnas.89.23.11533

Walford, Roy L., Mock, D., Verdery, R., & MacCallum, T. (2002). Calorie restriction in biosphere 2: Alterations in physiologic, hematologic, hormonal, and biochemical parameters in humans restricted for a 2-year period. *Journals of Gerontology - Series A Biological Sciences and Medical Sciences*. https://doi.org/10.1093/gerona/57.6.B211

Wan, G., Ji, L., Schrepfer, T., Gong, S., Wang, G. P., & Corfas, G. (2019). Synaptopathy as a mechanism for age-related vestibular dysfunction in mice. *Frontiers in Aging Neuroscience*, *11*(JUN), 1–13. https://doi.org/10.3389/fnagi.2019.00156

Wang, C., Maddick, M., Miwa, S., Jurk, D., Czapiewski, R., Saretzki, G., … von Zglinicki, T. (2010). Adult-onset, short-term dietary restriction reduces cell senescence in mice. *Aging*, *2*(9), 555–566. https://doi.org/100196 [pii]

Wang, J., Ho, L., Qin, W., Rocher, A. B., Seror, I., Humala, N., … Pasinetti, G. M. (2005). Caloric restriction attenuates β-amyloid neuropathology in a mouse model of Alzheimer's disease. *The FASEB Journal*. https://doi.org/10.1096/fj.04-3182fje

Wang, S. C., Bednarski, B., Patel, S., Yan, A., Kohoyda-Inglis, C., Kennedy, T., … Arbabi, S. (2003). Increased depth of subcutaneous fat is protective against abdominal injuries in motor vehicle collisions. *Annual Proceedings / Association for the Advancement of Automotive Medicine. Association for the Advancement of Automotive Medicine*.

Wang, S. H., & Morris, R. G. M. (2010). Hippocampal-neocortical interactions in memory formation, consolidation, and reconsolidation. *Annual Review of Psychology*. https://doi.org/10.1146/annurev.psych.093008.100523

Wang, T. Y., Liu, M., Portincasa, P., & Wang, D. Q. H. (2013). New insights into the molecular mechanism of intestinal fatty acid absorption. *European Journal of Clinical Investigation*. https://doi.org/10.1111/eci.12161

Warner, D. A., & Shine, R. (2008). The adaptive significance of temperature-dependent sex determination in a reptile. *Nature*. https://doi.org/10.1038/nature06519

Weadick, C. J., & Sommer, R. J. (2016). Mating system transitions drive life span evolution in Pristionchus nematodes. *American Naturalist*. https://doi.org/10.1086/685283

Weaver, L. T., Austin, S., & Cole, T. J. (1991). Small intestinal length: A factor essential for gut adaptation. *Gut*, *32*(11), 1321–1323. https://doi.org/10.1136/gut.32.11.1321

Wei, H., Tarling, E. J., McMillen, T. S., Tang, C., & LeBoeuf, R. C. (2015). ABCG1 regulates mouse adipose tissue macrophage cholesterol levels and ratio of M1 to M2 cells in obesity and caloric restriction. *Journal of Lipid Research*. https://doi.org/10.1194/jlr.M063354

Weindruch, R., Walford, R. L., Fligiel, S., & Guthrie, D. (1986). The retardation of aging in mice by dietary restriction: Longevity, cancer, immunity and lifetime energy intake. *Journal of Nutrition*, *116*(4), 641–654. https://doi.org/10.1093/jn/116.4.641

Weindruch, Richard, Chia, D., Barnett, E. V., & Walford, R. L. (1982). Dietary restriction in mice beginning at 1 year of age: Effects on serum immune complex levels. *Age*, *5*(4), 111–112. https://doi.org/10.1007/BF02431272

Weisberg, S. P., McCann, D., Desai, M., Rosenbaum, M., Leibel, R. L., & Ferrante, A. W. (2003). Obesity is associated with macrophage accumulation in adipose tissue. *Journal of Clinical Investigation*, *112*(12), 1796–1808. https://doi.org/10.1172/JCI200319246

Weiss, E. P., Racette, S. B., Villareal, D. T., Fontana, L., Steger-May, K., Schechtman, K. B., … Holloszy, J. O. (2007). Lower extremity muscle size and strength and aerobic capacity decrease with caloric restriction but not with exercise-induced weight loss. *Journal of Applied Physiology*, *102*(2), 634–640. https://doi.org/10.1152/japplphysiol.00853.2006

Whitehead, J. C., Hildebrand, B. A., Sun, M., Rockwood, M. R., Rose, R. A., Rockwood, K., & Howlett, S. E. (2014). A clinical frailty index in aging mice: Comparisons with frailty index data in humans. *Journals of Gerontology - Series A Biological Sciences and Medical Sciences*, *69*(6), 621–632. https://doi.org/10.1093/gerona/glt136

Wilkinson, J. E., Burmeister, L., Brooks, S. V., Chan, C. C., Friedline, S., Harrison, D. E., … Miller, R. A. (2012). Rapamycin slows aging in mice. *Aging Cell*. https://doi.org/10.1111/j.1474-9726.2012.00832.x

Willcox, D. C., Willcox, B. J., Todoriki, H., & Suzuki, M. (2009). The okinawan diet: Health implications of a low-calorie, nutrient-dense, antioxidant-rich dietary pattern low in glycemic load. *Journal of the American College of Nutrition*, *28*(November 2013), 500S-516S. https://doi.org/10.1080/07315724.2009.10718117

Wilson, K. A., Beck, J. N., Nelson, C. S., Hilsabeck, T. A., Promislow, D., Brem, R. B., & Kapahi, P. (2020). GWAS for Lifespan and Decline in Climbing Ability in Flies upon Dietary Restriction Reveal decima as a Mediator of Insulin-like Peptide Production. *Current Biology*. https://doi.org/10.1016/j.cub.2020.05.020

Wolff, L., Parkinson, J., & White, P. D. (1930). Bundle-branch block with short P-R interval in healthy young people prone to paroxysmal tachyardia. *Am Heart J.*, *5*, 685–704. https://doi.org/10.1016/S0002-8703(30)90086-5

Worley, K. C., Warren, W. C., Rogers, J., Locke, D., Muzny, D. M., Mardis, E. R., … Wilson, R. K. (2014). The common marmoset genome provides insight into primate biology and evolution. *Nature Genetics*. https://doi.org/10.1038/ng.3042

Wu, L., & Belasco, J. G. (2008). Let Me Count the Ways: Mechanisms of Gene Regulation by

miRNAs and siRNAs. *Molecular Cell*. https://doi.org/10.1016/j.molcel.2007.12.010

Wu, Z., Tan, J., Chi, Y., Zhang, F., U, J., Song, Y., … Liu, Y. (2018). Mesenteric adipose tissue contributes to intestinal barrier integrity and protects against nonalcoholic fatty liver disease in mice. *American Journal of Physiology - Gastrointestinal and Liver Physiology*. https://doi.org/10.1152/ajpgi.00079.2018

Wueest, S., & Konrad, D. (2018). The role of adipocyte-specific IL-6-type cytokine signaling in FFA and leptin release. *Adipocyte*. https://doi.org/10.1080/21623945.2018.1493901

Xie, H., Lim, B., & Lodish, H. F. (2009). MicroRNAs induced during adipogenesis that accelerate fat cell development are downregulated in obesity. *Diabetes*. https://doi.org/10.2337/db08-1299

Xie, K., Neff, F., Markert, A., Rozman, J., Aguilar-Pimentel, J. A., Amarie, O. V., … Ehninger, D. (2017). Every-other-day feeding extends lifespan but fails to delay many symptoms of aging in mice. *Nature Communications*, *8*(1). https://doi.org/10.1038/s41467-017-00178-3

Xing, S., Tsaih, S. W., Yuan, R., Svenson, K. L., Jorgenson, L. M., So, M., … Korstanje, R. (2009). Genetic influence on electrocardiogram time intervals and heart rate in aging mice. *American Journal of Physiology - Heart and Circulatory Physiology*. https://doi.org/10.1152/ajpheart.00681.2008

Yamada, Y., Kemnitz, J. W., Weindruch, R., Anderson, R. M., Schoeller, D. A., & Colman, R. J. (2018). Caloric Restriction and Healthy Life Span: Frail Phenotype of Nonhuman Primates in the Wisconsin National Primate Research Center Caloric Restriction Study. *Journals of Gerontology - Series A Biological Sciences and Medical Sciences*, *73*(3), 273–278. https://doi.org/10.1093/gerona/glx059

Yamaguchi, N., Argueta, J. G. M., Masuhiro, Y., Kagishita, M., Nonaka, K., Saito, T., … Yamashita, Y. (2005). Adiponectin inhibits Toll-like receptor family-induced signaling. *FEBS Letters*. https://doi.org/10.1016/j.febslet.2005.11.019

Yamamoto, R., Palmer, M., Koski, H., Curtis-Joseph, N., & Tatar, M. (2020). Mapping Drosophila insulin receptor structure to the regulation of aging through analysis of amino acid substitutions. *BioRxiv*, 2020.06.30.180505. https://doi.org/10.1101/2020.06.30.180505

Yamauchi, T., Kamon, J., Minokoshi, Y., Ito, Y., Waki, H., Uchida, S., … Kadowaki, T. (2002). Adiponectin stimulates glucose utilization and fatty-acid oxidation by activating AMP-activated protein kinase. *Nature Medicine*. https://doi.org/10.1038/nm788

Yan, K. S., Chia, L. A., Li, X., Ootani, A., Su, J., Lee, J. Y., … Kuo, C. J. (2012). The intestinal stem cell markers Bmi1 and Lgr5 identify two functionally distinct populations.

Proceedings of the National Academy of Sciences of the United States of America. https://doi.org/10.1073/pnas.1118857109

Yan, L., Gao, S., Ho, D., Park, M., Ge, H., Wang, C., … Vatner, S. F. (2013). Calorie restriction can reverse, as well as prevent, aging cardiomyopathy. *Age*. https://doi.org/10.1007/s11357-012-9508-5

Yasuo Kagawa. (1978). Impact of Westernization on the Nutrition of Japanese Changes in Physique, Cancer, Longevity and Centenarians. *Preventive Medicine*.

Yilmaz, Ö. H., Katajisto, P., Lamming, D. W., Gültekin, Y., Bauer-Rowe, K. E., Sengupta, S., … Sabatini, D. M. (2012). MTORC1 in the Paneth cell niche couples intestinal stem-cell function to calorie intake. *Nature*, *486*(7404), 490–495. https://doi.org/10.1038/nature11163

Yin, X., Mead, B. E., Safaee, H., Langer, R., Karp, J. M., & Levy, O. (2016). Engineering Stem Cell Organoids. *Cell Stem Cell*, *18*(1), 25–38. https://doi.org/10.1016/j.stem.2015.12.005

Yokota, M., Miyanaga, K., Yonemura, K., Watanabe, H., Nagashima, K., Naito, K., … Neufeld, R. W. (2000). Declining of memory functions of normal elderly persons. *Psychiatry and Clinical Neurosciences*, *54*(2), 217–225. https://doi.org/10.1046/j.1440-1819.2000.00662.x

Young, J. B., & Landsberg, L. (1982). Diet-induced changes in sympathetic nervous system activity: Possible implications for obesity and hypertension. *Journal of Chronic Diseases*. https://doi.org/10.1016/0021-9681(82)90118-7

Yu, D., Tomasiewicz, J. L., Yang, S. E., Miller, B. R., Wakai, M. H., Sherman, D. S., … Lamming, D. W. (2019). Calorie-Restriction-Induced Insulin Sensitivity Is Mediated by Adipose mTORC2 and Not Required for Lifespan Extension. *Cell Reports*, *29*(1), 236-248.e3. https://doi.org/10.1016/j.celrep.2019.08.084

Zalewski, C. K. (2015). Aging of the Human Vestibular System. *Seminars in Hearing*, *36*(3), 175–196. https://doi.org/10.1055/s-0035-1555120

Zamarron, B. F., Mergian, T. A., Cho, K. W., Martinez-Santibanez, G., Luan, D., Singer, K., … Lumeng, C. N. (2017). Macrophage proliferation sustains adipose tissue inflammation in formerly obese mice. *Diabetes*. https://doi.org/10.2337/db16-0500

Zammit, C., Liddicoat, H., Moonsie, I., & Makker, H. (2010). Obesity and respiratory diseases. *International Journal of General Medicine*. https://doi.org/10.2147/IJGM.S11926

Zeisel, A., M͡oz-Manchado, A. B., Codeluppi, S., Lönnerberg, P., Manno, G. La, Juréus, A., … Linnarsson, S. (2015). Cell types in the mouse cortex and hippocampus revealed by single-cell RNA-seq. *Science*. https://doi.org/10.1126/science.aaa1934

Zhai, W., Xu, C., Ling, Y., Liu, S., Deng, J., Qi, Y., … Xu, G. (2010). Increased lipolysis in adipose tissues is associated with elevation of systemic free fatty acids and insulin resistance in perilipin null mice. *Hormone and Metabolic Research*. https://doi.org/10.1055/s-0029-1243599

Zhang, C., Li, S., Yang, L., Huang, P., Li, W., Wang, S., … Zhao, L. (2013). Structural modulation of gut microbiota in life-long calorie-restricted mice. *Nature Communications*, *4*. https://doi.org/10.1038/ncomms3163

Zhang, R., Wang, X., Qu, J. H., Liu, B., Zhang, P., Zhang, T., … Liu, D. P. (2019). Caloric Restriction Induces MicroRNAs to Improve Mitochondrial Proteostasis. *IScience*. https://doi.org/10.1016/j.isci.2019.06.028

Zhao, M., Xiong, X., Ren, K., Xu, B., Cheng, M., Sahu, C., … Ruan, H. (2018). Deficiency in intestinal epithelial O-GlcNAcylation predisposes to gut inflammation. *EMBO Molecular Medicine*. https://doi.org/10.15252/emmm.201708736

Zheng, C., Yang, Q., Cao, J., Xie, N., Liu, K., Shou, P., … Shi, Y. (2016). Local proliferation initiates macrophage accumulation in adipose tissue during obesity. *Cell Death and Disease*. https://doi.org/10.1038/cddis.2016.54

Ziegler, A. K., Damgaard, A., Mackey, A. L., Schjerling, P., Magnusson, P., Olesen, A. T., … Scheele, C. (2019). An anti-inflammatory phenotype in visceral adipose tissue of old lean mice, augmented by exercise. *Scientific Reports*. https://doi.org/10.1038/s41598-019-48587-2

Zucker, I. (1971). Light-dark rhythms in rat eating and drinking behavior. *Physiology and Behavior*. https://doi.org/10.1016/0031-9384(71)90078-3

10. Eidesstattliche Erklärung

Erklärung zur Dissertation
gemäß der Promotionsordnung vom 12. März 2020

Diese Erklärung muss in der Dissertation enthalten sein.
(This version must be included in the doctoral thesis)

„Hiermit versichere ich an Eides statt, dass ich die vorliegende Dissertation selbstständig und ohne die Benutzung anderer als der angegebenen Hilfsmittel und Literatur angefertigt habe. Alle Stellen, die wörtlich oder sinngemäß aus veröffentlichten und nicht veröffentlichten Werken dem Wortlaut oder dem Sinn nach entnommen wurden, sind als solche kenntlich gemacht. Ich versichere an Eides statt, dass diese Dissertation noch keiner anderen Fakultät oder Universität zur Prüfung vorgelegen hat; dass sie - abgesehen von unten angegebenen Teilpublikationen und eingebundenen Artikeln und Manuskripten - noch nicht veröffentlicht worden ist sowie, dass ich eine Veröffentlichung der Dissertation vor Abschluss der Promotion nicht ohne Genehmigung des Promotionsausschusses vornehmen werde. Die Bestimmungen dieser Ordnung sind mir bekannt. Darüber hinaus erkläre ich hiermit, dass ich die Ordnung zur Sicherung guter wissenschaftlicher Praxis und zum Umgang mit wissenschaftlichem Fehlverhalten der Universität zu Köln gelesen und sie bei der Durchführung der Dissertation zugrundeliegenden Arbeiten und der schriftlich verfassten Dissertation beachtet habe und verpflichte mich hiermit, die dort genannten Vorgaben bei allen wissenschaftlichen Tätigkeiten zu beachten und umzusetzen. Ich versichere, dass die eingereichte elektronische Fassung der eingereichten Druckfassung vollständig entspricht."

Teilpublikationen:

Hahn, O., Drews, L.F., Nguyen, A. et al. A nutritional memory counteracts the benefits of dietary restriction in old mice. Nat Metab 1, 1059–1073 (2019). https://doi.org/10.1038/s42255-019-0121-0

Datum, Name und Unterschrift

Köln, 22.3.2021

Lisa Drews

(Lisa Drews)

11. Curriculum vitae

Lisa Franziska Drews

Geburtsdatum- und Ort:	27. Dezember 1991 in Groß-Umstadt
Adresse:	Redwitzstraße 28, 50937 Köln
Nationalität:	Deutsch
E-Mail:	lisa.drews@gmail.com

AUSBILDUNG

Seit 03/ 2017	**Doktorandin** am *Max- Planck- Institut für Biologie des Alterns bei Prof. Dr. Linda Partridge, Universität zu Köln* Dissertation: „Late-life effects of earlier dietary restriction on lifespan, health span and tissue-specific phenotypes”
08/ 2014 - 01/ 2017	**Master of Medical Science in Molekularmedizin,** *Universität Uppsala, Schweden* Titel der Master thesis: “Combined BET and CDK inhibition as novel therapeutic strategy for glioblastoma”
10/ 2011 - 07/ 2014	**Bachelor of Science in Humanbiologie** *Philipp University Marburg, Germany* Titel der Bachelor thesis: “Characterization of PRMT4 and Mi-2 interplay”
09/ 2002 - 06/ 2011	**Abitur** an der Max-Planck-Schule, Groß-Umstadt

PUBLIKATIONSLISTE

Hahn, O., **Drews, L.F.**, et al. *A nutritional memory effect counteracts the benefits of dietary restriction in old mice*. Nat Metab (2019) https://doi.org/10.1038/s42255-019-0121-0

Datum, Name und Unterschrift

Köln, 22.03.2021 Lisa Drews

(Lisa Drews)

12. Publications

As indicated in section 3.1, part of the results presented in this section were published in 2019 in Nature Metabolism. My contribution to the included publication titled “A nutritional memory effect counteracts the benefits of dietary restriction in old mice”, on which I (Drews, L.F.) am listed as second author, is the following: I performed extracted RNA, DNA and protein from WAT for subsequent Western Blot, gene expression and mitochondrial copy number analyses. Additionally, I extracted RNA from BAT and prepared samples for subsequent sequencing. Moreover, I generated WAT explant cultures from aged AL and DR mice, implemented the *in vitro* lipid transfection and performed the initial sample preparation together with Lisonia Gkioni. The study designed and the manuscript co-written by Sebastian Grönke, Andreas Bayer, Michael J. O. Wakelam, Oliver Hahn and Linda Partridge. Scott Pletcher performed the power analyses for the late-life onset lifespan experiments. The RNA isolation for subsequent sequencing experiments were performed by Oliver Hendrich. Thomas Langer and Takashi Tatsuta designed and conducted the *in vitro* pulse–chase experiments and lipid chromatography on the transfected WAT explant cultures. Qifeng Zhang and Michael J. O. Wakelam conducted the lipidomic profiling, while An Nguyen conceptualized and performed the lipidome network analysis. Finally, Oliver Hahn performed most of the lifespan and bioinformatic analyses. All authors read and approved the final manuscript. The published manuscript has been added to this thesis to facilitate consultation (next page).

Hahn, O., **Drews, L.F**., Nguyen, A. et al. A nutritional memory effect counteracts the benefits of dietary restriction in old mice. Nat Metab 1, 1059–1073 (2019).
https://doi.org/10.1038/s42255-019-0121-0

nature metabolism

ARTICLES

https://doi.org/10.1038/s42255-019-0121-0

A nutritional memory effect counteracts the benefits of dietary restriction in old mice

Oliver Hahn[1,2,3], Lisa F. Drews[1], An Nguyen[4], Takashi Tatsuta[1], Lisonia Gkioni[1], Oliver Hendrich[1], Qifeng Zhang[4], Thomas Langer[1], Scott Pletcher[5], Michael J. O. Wakelam[4*], Andreas Beyer[2,6*], Sebastian Grönke[1*] and Linda Partridge[1,7*]

Dietary restriction (DR) during adulthood can greatly extend lifespan and improve metabolic health in diverse species. However, whether DR in mammals is still effective when applied for the first time at old age remains elusive. Here, we report results of a late-life DR-switch experiment using 800 mice. Female mice aged 24 months were switched from an ad libitum (AL) diet to DR or vice versa. Strikingly, the switch from DR to AL acutely increases mortality, whereas the switch from AL to DR causes only a weak and gradual increase in survival, suggesting the body has a memory of earlier nutrition. RNA sequencing in liver and brown and white adipose tissue (BAT and WAT, respectively) demonstrates a largely refractory transcriptional and metabolic response in fat tissue to DR after an AL diet, particularly in WAT, and a proinflammatory signature in aged preadipocytes, which is prevented by chronic DR feeding. Our results provide evidence for a 'nutritional memory' as a limiting factor for DR-induced longevity and metabolic remodelling of WAT in mammals.

DR, reduced food intake while avoiding malnutrition, profoundly extends lifespan in most model and non-model organisms, including rodents and, potentially, humans[1]. Even when applied in the short term, DR rapidly induces a broad-spectrum improvement of metabolic health[2,3] and acutely enhances survival in disease models of hypertrophy and ischaemia–reperfusion injury[2,4]. Considering the therapeutic potential of DR-related nutritional and pharmacological interventions for treating age-related diseases in humans[5] it is thus pivotal to examine if these pervasive benefits can be effectively induced at any time point in life.

In fruit flies, DR instigated at young or old age acutely lowers age-specific mortality, independent of prior diet, whereas switching long-term DR-fed flies back to AL feeding causes an equally acute and almost complete elevation of mortality[6]. However, late-onset DR experiments in rodents older than 12 months[7,8] have yielded contradictory results[9,10], which may in part be attributable to varying experimental designs. Furthermore, previous studies in mice have quantified the response to DR mainly by focusing on survivorship, which is a cumulative measure, and is thus not suitable to detect acute effects. Age-specific mortality, in contrast, measures the instantaneous hazard of death at a given moment in life, but it requires larger cohort sizes[11,12]. Profiling mortality dynamics in large cohorts of mice could, therefore, resolve whether DR improves health acutely when applied for the first time in old individuals. Similarly, age-specific mortality could identify lasting protective effects of long-term DR after switching back to unrestricted feeding.

The effects of DR are mediated in part by tissue-specific shifts in patterns of gene expression. In mice and primates, transcriptional profiling has suggested changes in energy homeostasis, mitochondrial function and lipid metabolism are key processes by which DR improves health at old age[13–17]. Two integrative meta-analyses of cross-tissue transcriptome datasets commonly identified differential regulation of lipogenic genes as a key signature of DR in mammals[14,18]. Consistently, lipid profiles change during normal ageing, whereas DR and related lifespan-extending interventions remodel lipid composition in *C. elegans*, *Drosophila* and mammals, and some of these changes are causal and essential for increased lifespan[19].

Further evidence for a causal role of lipid metabolism under DR in mammals comes from the correlation of maintenance of fat mass with a stronger lifespan extension under DR in inbred[20] and recombinant inbred mouse strains[21]. However, the precise role of lipid metabolism in mammalian longevity is probably complex and tissue specific. In the liver, DR causes transcriptional repression of the key lipogenic transcription factor sterol regulatory element binding transcription factor 1 (*Srebf1*) and its related target genes, paralleled by reduced triglyceride (TG) content[22], which may protect the tissue from age-related onset of steatosis. In contrast, the white adipose tissue (WAT), classically regarded as responsible for storing fat, responds to DR by strong upregulation of de novo lipogenesis genes and elevated phospholipid (PL) levels[23]. The role of WAT-specific shifts in lipogenesis and phospholipid metabolism in improved health under DR is, however, still unknown.

We have investigated the effect of late-onset AL and DR feeding in a large cohort of mice. While newly imposed AL feeding resulted in a rapid, steep increase in mortality, switching the mice from AL to DR feeding resulted in only a slight decrease in mortality rate, which remained much higher than in chronically DR animals. Individual mice that preserved their fat content after the switch to DR showed a greater drop in mortality. In BAT and WAT, the RNA transcript profiles of previously AL-fed mice remained largely

[1]Max Planck Institute for Biology of Ageing, Cologne, Germany. [2]Cellular Networks and Systems Biology, CECAD, University of Cologne, Cologne, Germany. [3]Department of Neurology and Neurological Sciences, Stanford University School of Medicine, Stanford, CA, USA. [4]Inositide lab, The Babraham Institute, Cambridge, UK. [5]Department of Molecular & Integrative Physiology and the Geriatrics Center, University of Michigan, Ann Arbor, USA. [6]Center for Molecular Medicine Cologne, University of Cologne, Cologne, Germany. [7]Department of Genetics, Evolution and Environment, Institute of Healthy Ageing, University College London, London, UK. *e-mail: Michael.wakelam@babraham.ac.uk; Andreas.beyer@uni-koeln.de; Sebastian.Groenke@age.mpg.de; Partridge@age.mpg.de

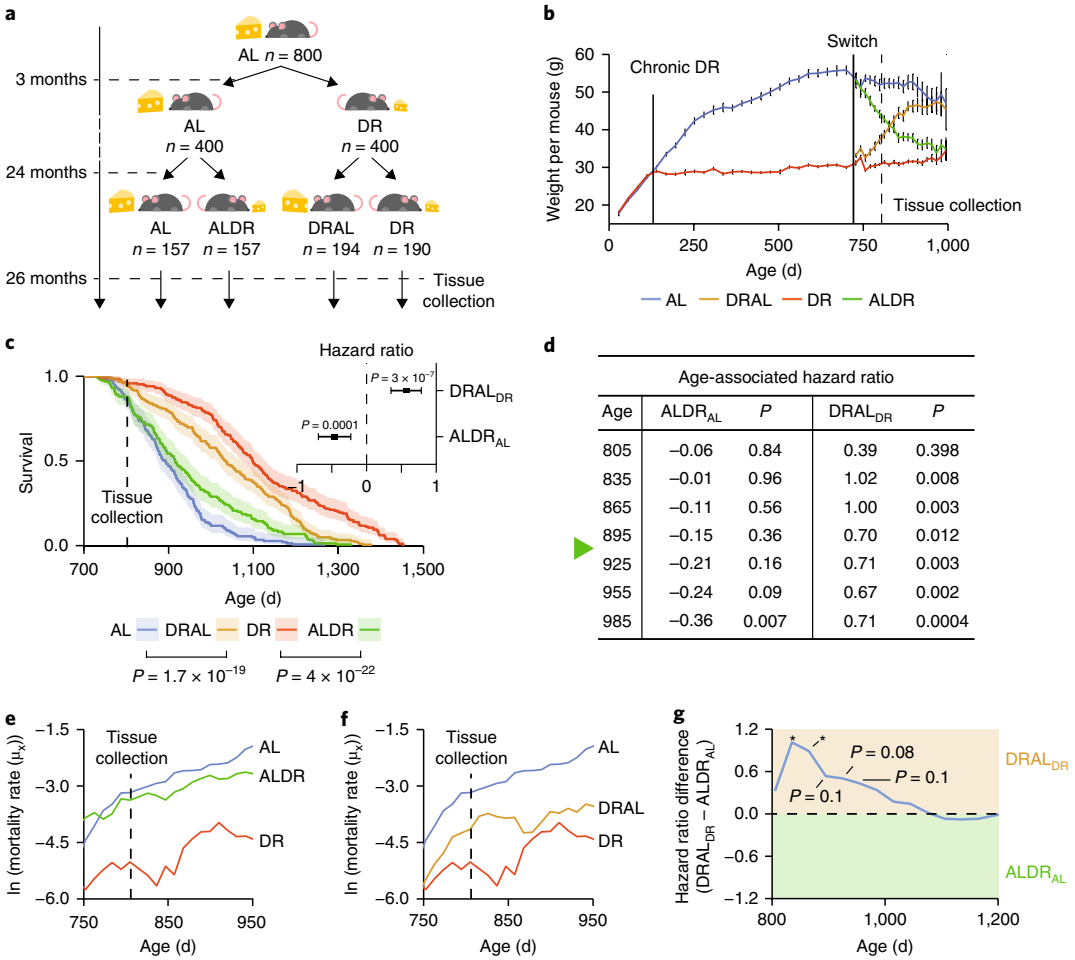

Fig. 1 | Demography of dietary restriction in mice. a, Schematic representation of the switch experiment. Animal numbers per treatment group are indicated. **b**, Body weights for chronic and switch diet cohorts (mean ± 95% confidence intervals). Solid lines indicate when chronic DR and diet switches began. The dashed line indicates the tissue-collection time point. $n = 45$ biologically independent animals per diet. **c**, Post-switch Kaplan–Meier (KM) survival curves for chronic and switch diet cohorts. Data represents $n = 157$ (AL), $n = 157$ (DR), $n = 190$ (DR) and $n = 194$ (DRAL) biologically independent animals. Solid lines represent the KM fit, and the shaded area represents the 95% confidence interval. Cox regression was used to avoid making assumptions about the shape of the trajectories. ALDR mice differed significantly in their hazard ratio from both chronically DR-fed (hazard ratio = 1.16, $P < 0.0001$; Wald test) and AL-fed mice (hazard ratio = −0.46, $P < 0.0001$; see inset; Wald test). DRAL mice differed significantly in their hazard ratios from both chronically AL-fed (hazard ratio = −1.05, $P < 0.0001$) and DR-fed mice (hazard ratio = 0.5, $P < 0.0001$; see inset). $DRAL_{DR}$, hazard ratio of DRAL cohort relative to DR controls; $ALDR_{AL}$, hazard ratio of DRAL cohort relative to AL controls. Centres represent the hazard ratio, and error bars the s.e. **d**, Post-switch hazard ratios of ALDR-fed mice relative to chronic AL-fed animals (middle columns) and DRAL-fed mice relative to chronic DR-fed animals (right columns). To profile age-specific effects, Cox regression analysis was restricted to animals that died before the indicated age. The green mark indicates the median lifespan of the ALDR cohort. **e**,**f**, Age-specific, log-transformed mortality rates of mice in response to ALDR (**e**) and DRAL (**f**) switch diets. Mortality rates were truncated after the AL cohort had reached 20% survival (<30 mice). Data represent $n = 157$ (AL), $n = 157$ (DR), $n = 190$ (DR) and $n = 194$ (DRAL) biologically independent animals. **g**, Hazard ratio difference between both switch diets after normalizing against corresponding pre-switch diet groups (Wald test). Cox regressions were repeated while iteratively extending the analysed time interval by 1 month. The association between the resulting string of hazard ratios (one ratio per repeated analysis) and analysed age span (*x* axis) is denoted. Cox regression analysis was restricted to animals that had died before the indicated age, or was used when the AL cohort had reached 25% survival (40 mice).

refractory to late-life DR, which coincided with major age-related shifts in white adipose progenitor cells. Both switch-resistant genes and lipidomic profiles of WAT pointed to impaired membrane lipogenesis and mitochondrial biogenesis in response to late-life DR. A nutritional memory thus limited both increased survival and metabolic remodelling of WAT in response to DR imposed late in life.

Results

Acute mortality shift in response to late-onset ad libitum, but not late-onset dietary restriction, in mice. We conducted a diet-switch experiment in mice (Fig. 1a) using 800 females of the B6D2F1 hybrid strain, which show a robust lifespan extension under DR feeding[22,24]. This large number of animals enabled profiling of age-specific mortality. Animals were bred in three breeding rounds. DR began when mice were at 12 weeks of age, with stepwise restriction over 4 weeks until DR mice reached 40% of the food intake of AL controls. A subset of the AL and DR animals was subjected to a diet switch after 20% of the AL-fed animals had died, corresponding to 24 months of age at the onset of the diet switch (721–746 d, depending on breeding cohort); we estimated that this subset would have >95% power to detect a reversal in mortality rates over a 6-month period and maximized statistical power to detect changes in mortality rate. Half of the AL cohort was subjected to stepwise DR over 4 weeks (late-onset DR; ALDR), while half of the chronic-DR-fed

mice received a reciprocal food increase back to the level of AL controls (late-onset AL; DRAL). Both diet switches caused weight gain and loss equivalent to what was seen with chronic AL or DR feeding, respectively, reaching the level of the chronic diet groups within 8 months following the switch (Fig. 1b). The rate of weight gain of old DRAL mice was highly similar to that observed in young AL animals (Extended Data Fig. 1a). While absolute food intake was comparable between old AL and DRAL mice (Extended Data Fig. 1b,c) relative to their lower body weight, DRAL animals exhibited a slightly higher food intake (Extended Data Fig. 1d). Thus, 21 months of DR feeding did not permanently lower the endogenous food intake target of these mice.

Animals that switched to DR showed only a delayed and incomplete reduction in mortality rate compared with chronic DR mice (Fig. 1c–e and Extended Data Fig. 1b). For the first 7 months after the switch, during which their median lifespan was passed, ALDR mice showed no significant improvement in mortality (Fig. 1d,e). When analysing survival data for the whole duration of the experiment, two out of three breeding cohorts showed no significant response to the ALDR switch. (Extended Data Fig. 1b,c). Therefore, late-onset DR caused no measurable increase in survival in a large fraction of old animals. In stark contrast, the reciprocal switch from DR to unrestricted feeding caused an acute increase in mortality in all three breeding cohorts (Fig. 1d,f and Extended Data Fig. 2b,c). For the first 4 months post-switch, the shift in mortality relative to the prior diet group was significantly higher for the DRAL switch than for the ALDR switch, before gradually reduced mortality under ALDR reached a similar effect size (Fig. 1g). This further suggests that long-term DR late in life induced partial protection against mortality, consistent with observations in long-term DR flies[6]. Age-specific mortality in the mice was thus dependent on past nutrition, and this dependency was stronger for mice with a history of AL than mice fed a DR.

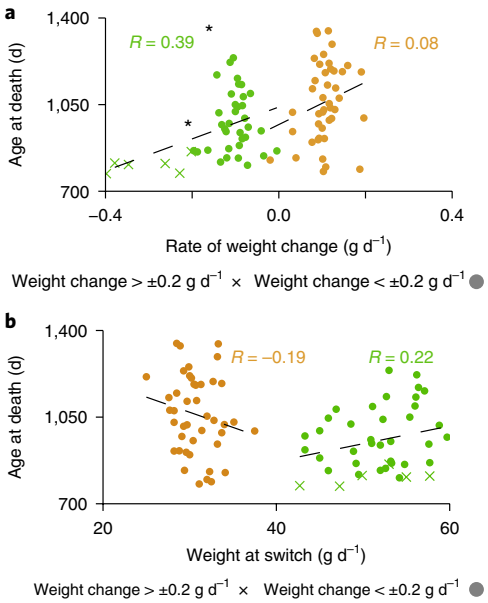

Fig. 2 | Post-switch weight change correlates with survival outcome under late-onset DR. a, Scatterplot representation of mouse-specific rates of weight change versus mouse-specific age at death for both ALDR and DRAL switch cohorts. Linear regression analysis found a significant association for weight change and age at death for the ALDR switch cohort. Animals with a weight loss higher than 0.2 g d^{-1} are marked with an X. **b**, Scatterplot representation of mouse-specific weights at switch date versus mouse-specific age at death for both ALDR (green) and DRAL (orange) switch cohorts. Linear regression found no significant association. Animals with a weight loss higher than 0.2 g d^{-1} are marked with an X. $n = 45$ biologically independent animals per diet.

Preservation of body weight associates with late-onset dietary restriction outcome. The strong effect of a history of AL feeding on subsequent mortality under DR could indicate the presence of a physiological memory that may impede the molecular changes mediating the benefits of DR. Interestingly, there was a significant inverse association between the animal-specific rate of weight change and age at death for the ALDR but not DRAL cohort (Fig. 2a). There was, however, no association between the absolute weight pre-switch and lifespan in either of the switch groups (Fig. 2b). In agreement with previous findings on chronic DR regimens[20,21], preservation of weight and, specifically, fat may thus increase the responsiveness of survival to late-onset DR, implicating a role for lipid metabolism.

Brown and white adipose tissue, but not liver, show a transcriptional memory of ad libitum feeding. In light of a possible memory effect of AL feeding on lipid metabolism, we next investigated the molecular memory of AL feeding in liver, BAT and gonadal WAT, which fulfil key functions in lipid turnover and storage. Tissues were sampled 2 months post-switch, when the effects on mortality were the most disparate between the two switch diets (compare Fig. 1e–g). In contrast, body (Fig. 1b) and adipose weights (Fig. 3b,c) indicated that the two diet switches had already caused comparable changes in fat tissue mass at this time point (Fig. 3a). RNA sequencing (RNA-seq) profiling revealed high transcriptional similarity between DRAL mice and chronic AL controls in all three tissues, indicating that late-onset AL feeding induced a transcriptional profile similar to chronic AL feeding. Similarly, hepatic transcriptional profiles from ALDR mice clustered with the DR controls. In strong contrast, in BAT, and even more in WAT, ALDR profiles clustered with those of the AL diet (Fig. 3c,d), and were thus resistant to the diet switch. Chronic DR caused significant gene expression changes in 3,569 genes in liver, 2,412 in BAT and 3,296 in WAT, when compared with expression in AL controls. Of these, only 62 genes (~2%) in the liver, but 866 genes (~35%) in the BAT and a total of 1,609 genes (~50%) in the WAT, were still differentially expressed between DR and ALDR mice 2 months post-switch (Fig. 3e). These 'switch-resistant' genes in the adipose tissues are candidates for a transcriptional memory of AL feeding. In DRAL switch mice, we detected only 22 (0.8%) switch-resistant genes in the liver, 19 (0.08%) in BAT and 423 (~13%) switch-resistant genes in the WAT (Fig. 3f).

To analyse the transcriptional similarity between chronic and newly DR animals, we focused on genes that were differentially up- or downregulated under chronic DR (Fig. 3g). Plotting for each gene the scaled expression in response to chronic or late-onset DR confirmed an almost complete transcriptional adaptation to the ALDR switch in the liver, while both adipose tissues remained largely refractory (Fig. 3g). Corresponding to the acute rise in mortality, DRAL mice broadly adopted the expression profile of chronic AL fed animals across tissues, as did ALDR mice in the liver. (Fig. 3g). In addition, unsupervised hierarchical clustering revealed that ALDR switch-resistant genes in adipose tissues were not resistant in general, because their expression adopted an AL-like pattern under the reciprocal DRAL switch (Fig. 3h and Extended Data Fig. 3a). Thus, the liver transcriptome remained acutely responsive to either diet change, whilst the adipose tissue was specifically unresponsive to late-onset DR.

The incomplete reprogramming of RNA expression in response to late-onset DR could simply indicate that the adipose tissues respond slowly to DR, which would argue against the presence of a specific memory of AL feeding. To investigate this possibility, we repeated the experiment in young mice by switching AL-fed

animals to DR (young ALDR), starting when mice were aged 12 weeks (Fig. 3i). As in the experiment in old mice, tissues were collected 2 months post-switch for expression profiling. Strikingly, there was a complete transcriptional reprogramming in all three tissues (Fig. 3j and Extended Data Fig. 3c,d). Genes that were resistant to the switch in old ALDR mice showed full sensitivity in young ALDR mice. Thus, the adipose tissue transcriptome was highly responsive to newly DR switches in young mice, but this transcriptional flexibility markedly declined with age, in particular in the WAT.

Taken together, switching mice from DR back to full feeding caused a rapid loss of DR-related RNA expression patterns, implying no or only a weak memory of a prior DR regimen. In contrast, chronic AL feeding caused the formation of an adipose-tissue-specific gene expression memory over time. This reduced transcriptional flexibility of BAT and WAT in response to DR mirrored the resistance of age-specific mortality to late-onset DR.

Chronic ad libitum feeding causes a proinflammatory expression pattern in preadipocytes. Age-related changes have been previously identified to impair the differentiation of WAT preadipocytes into brite adipocytes under cold exposure in aged mice[25–27], and we hypothesized that a similar process could contribute to the reduced transcriptional flexibility of the WAT in old AL mice. To test this hypothesis, we obtained publicly available single-cell (sc) RNA-seq data of the gonadal stromal-vascular-fraction (SVF) from the Tabula muris consortium[28], comprising cells isolated from 3- and 24-month-old AL-fed mice. Indeed, preadipocytes from old mice exhibited profound transcriptional shifts, including decreased expression of growth and differentiation factors and elevated expression of inflammatory response genes and secretable cytokines, such as C–C motif chemokine ligand 2 (CCL2) and (CCL7) (Extended Data Fig. 4a–d). We further found a significant, inverse association between the gene expression changes in aged preadipocytes and those observed under DR with bulk RNA-seq. This association was still significant when limited to ALDR switch-resistant genes, which were functionally enriched for inflammatory response genes and chemokines (Extended Data Fig. 4e,f and Supplementary Table 1). Many of these genes were found to be particularly, or even exclusively, expressed in preadipocytes (Extended Data Fig. 4g,h). Thus, expression patterns in bulk RNA-seq may indeed reflect those found by scRNA-seq. Our analysis thus strongly suggests that preadipocytes lower the expression of growth and differentiation factors associated with WAT plasticity[29,30] while acquiring an inflammatory phenotype during ageing under AL-diet conditions. This phenotype appears to be strongly prevented by DR, but not by late-onset DR. The transcriptional memory of AL diet may thus be, in part, rooted in preadipocytes.

Mitochondrial biogenesis in white adipose tissue is impaired under late-onset dietary restriction. We next investigated the molecular pathways affected by the transcriptional memory of AL feeding because these could point to mechanisms that improve health under chronic DR. Whereas analysis of switch-resistant genes in the liver showed no major gene ontology enrichment (Extended Data Fig. 5a), the corresponding analysis in BAT revealed increased lipid transporter activity and largely downregulated mitochondrial function, including markers of uncoupling-dependent thermogenesis (Fig. 3k, Extended Data Fig. 6a–d and Supplementary Table 2). Switch-resistant genes in WAT showed the strongest functional enrichment for various mitochondria-related pathways, fatty-acid metabolism and phospholipid biosynthesis, all of which were upregulated under chronic and young ALDR but not old ALDR feeding (Fig. 3k and Supplementary Table 3). In addition, we identified a switch-resistant reduction of inflammatory response and interferon-gamma-related genes. The increase in mitochondrial gene expression in WAT contrasts with the downregulation of the same gene set in BAT, indicating that the declining transcriptional flexibility acts in a tissue-specific manner.

To test whether the shifts in gene expression could be correlated with functional consequences, we characterized the predicted switch-resistant upregulation of mitochondrial function in the WAT because this tissue exhibited the most switch-resistant genes and strongest functional enrichment. Indeed, genes associated with mitochondria in WAT (both nuclear and mitochondrially encoded genes) showed globally increased expression under chronic DR compared with that under either switch diet (Fig. 4a). Furthermore, expression of the transcription factor peroxisome proliferator-activated receptor gamma coactivator 1-alpha (PGC-1α, encoded by *Ppargc1a*), a key driver of mitochondrial biogenesis, was significantly increased in chronic DR and in young ALDR mice, but was resistant to the ALDR switch (Fig. 4b). Consistent with this observation, chronic DR increased abundance of mitochondrial DNA (mtDNA), protein levels of mitochondrial complex I and IV subunits (mtCO1; NDUFA9) and key mitochondrial metabolites (propionyl- and succinyl-CoA), all of which were resistant to the ALDR switch (Fig. 4c–e and Extended Data Fig. 6e). Of note, expression levels of various thermogenic processes such as UCP1 (uncoupling[31]), CKMT1 (creatine cycling[32]) and SERCA2b (Ca^{2+} cycling[33]) were unaffected by diet (Fig. 4f,g and Extended Data Fig. 6 f–h). Remarkably, all parameters of mitochondrial activity reverted back to the level of AL controls in the DRAL switch (Fig. 4b–e), in line with only weak messenger RNA expression differences between chronic and late-onset AL and only a small fraction of the DR-related transcriptional program still being active (Fig. 3f–h, Extended Data Fig. 6I and Supplementary Table 4). Long-term AL feeding thus interfered with elevated, uncoupling-independent mitochondrial biogenesis and activity in the WAT in response to late-onset DR.

Fig. 3 | Detection of an age- and tissue-specific transcriptional memory of prior AL feeding. a, Organ weight of gonadal fat pads at dissection time point (805 d). One-way ANOVA followed by two-sided post-hoc Tukey test; $n=10$ biologically independent animals per diet. Means ± s.e.m. **b–d**, Principal component analysis plot of RNA-seq data in liver (**b**), BAT (**c**) and gonadal WAT (**d**). **e**,**f**, Venn diagrams depicting the overlap of differentially expressed genes in liver (left), BAT (middle) and WAT (right) under DR feeding (**e**), relative to the AL or ALDR group; and under AL feeding (**f**), relative to the DR or DRAL groups. Switch-resistant genes are highlighted in red. **g**, Boxplot representation of scaled expression levels of differentially up- and downregulated genes under chronic DR as opposed to chronic AL controls in all three tissues. Boxplots indicate expression levels of ALDR switch-resistant genes. Whiskers represent the 1st and 5th quartiles, box edges represent the 2nd and 4th quartiles and the centre line represents the third quartile/median. **h**, Heatmap of unsupervised clustering of expression changes for ALDR switch-resistant genes in WAT; colour bar represents *z* score range. **i**, Schematic representation of the DR switch experiment in young mice. **j**, Boxplot representation of scaled expression levels of differentially up- and downregulated genes under chronic DR as opposed to levels in chronic AL controls in BAT and WAT of ALDR switch mice at a young age (5 months, 5m). Boxplot components are defined in **g**. **k**, Representative GO enrichment of ALDR switch-resistant genes in BAT (left) and WAT (right). Lengths of bars represent negative ln-transformed *P* using two-sided Fisher's exact test. Colours indicate gene-wise $\log_2$ fold-changes ($\log_2$(FC)) between DR and ALDR mice. Numbers beside bars indicate differentially expressed genes in that GO category. The complete list of enriched GO terms can be found in Supplementary Tables 2 and 3. Biologically independent animals used for RNA-seq: liver: $n=3$ (AL, DR, ALDR, DRAL, ALDR 5m, AL 5m); BAT: $n=3$ (AL, DR, DRAL, AL 5m, ALDR 5m) $n=5$ (ALDR); WAT: $n=3$ (AL, DR, ALDR, AL 5m) $n=5$ (ALDR, DRAL). ***$P<0.0001$.

De novo lipogenesis in white adipose tissue exhibits the strongest memory of prior ad libitum feeding. In order to find putatively causal mediators of the transcriptional memory in the WAT, we plotted for each gene the $\log_2$-fold expression change in response to chronic or late-onset DR relative to chronic AL and ranked each gene's influence on the resulting linear fit. The 50 switch-resistant genes with the highest influence (as determined via Cook's distance; Fig. 5a,b) were enriched primarily for lipid metabolism, including fatty acid (FA) biosynthesis, TG metabolism and phospholipid biosynthesis (Fig. 5c). They included the key lipogenic transcription factor SREBF1 (ref. [34]) and several of its corresponding downstream targets (Fig. 5d,e), *Acly, Acaca* (*Acc*), *Fasn*, *Scd1* and *Elovl6*, which

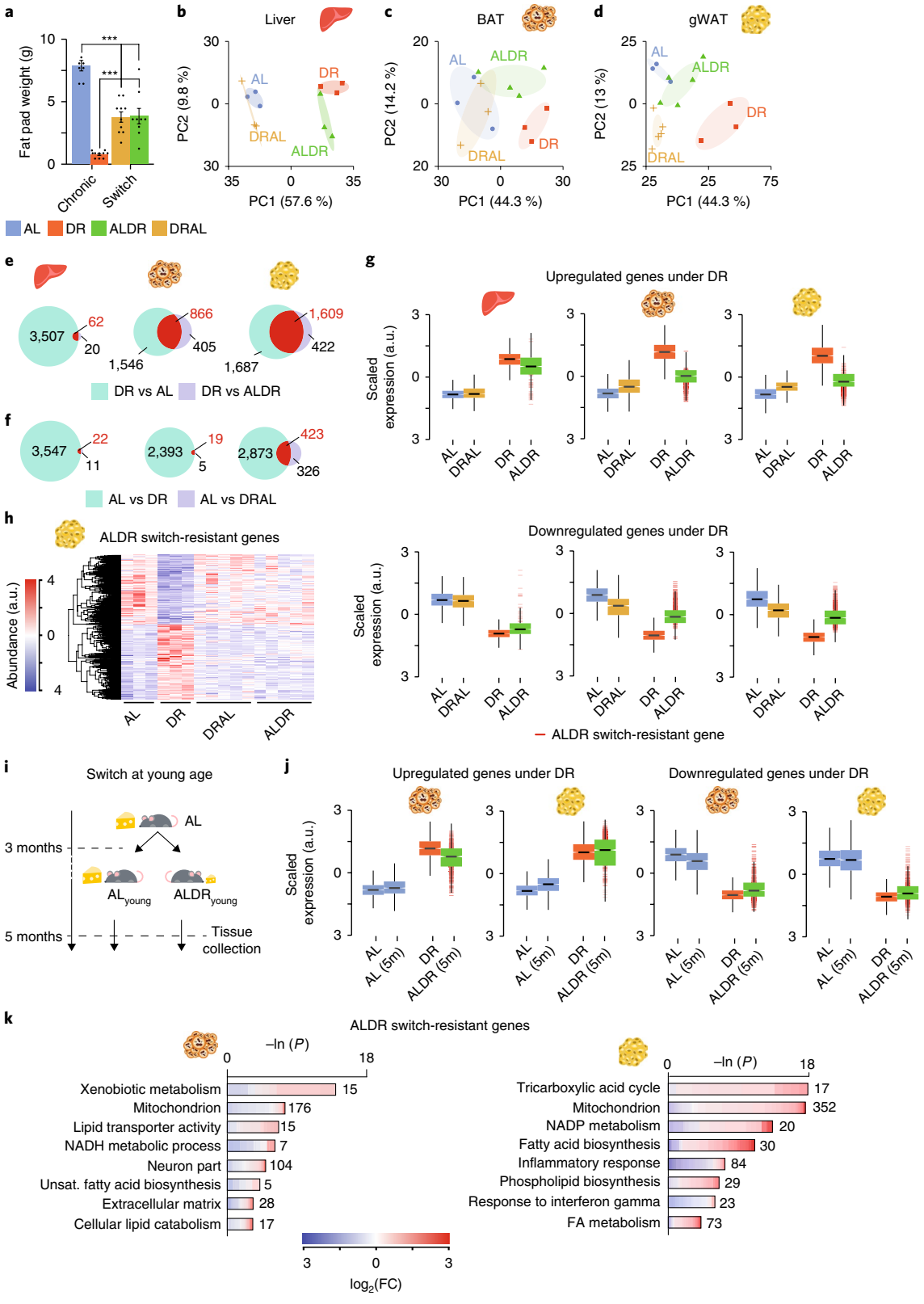

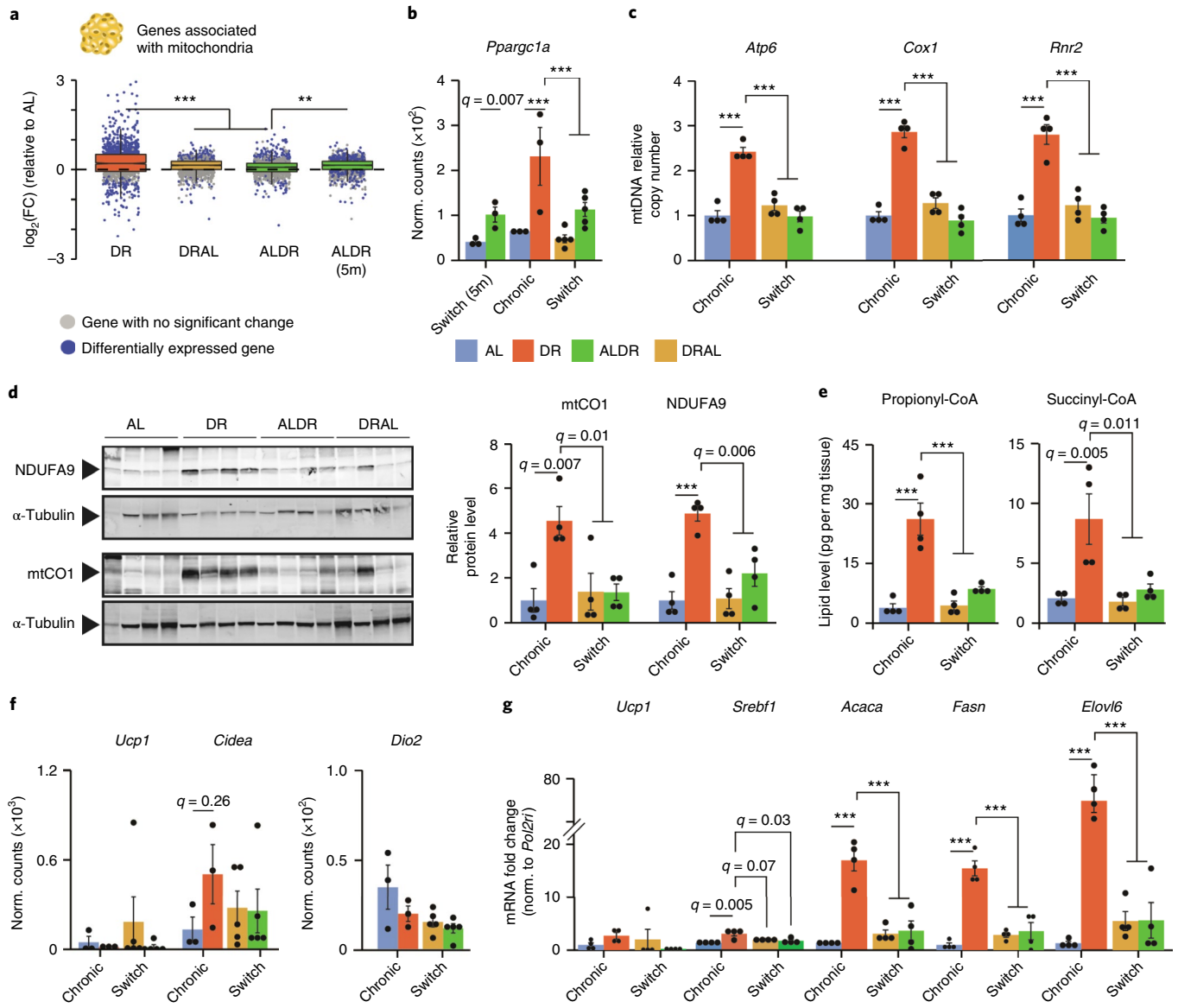

Fig. 4 | WAT-specific impairment of mitochondrial biogenesis under late-onset DR. a, Distribution of gene-wise expression changes in WAT under chronic DR and switch diets relative to chronic AL feeding for genes associated with the GO term 'Mitochondrion' ($n = 1299$ genes). Whiskers represent the first and fifth quartiles, box edges represent the second and fourth quartiles and the centre line represents the third quartile/median. Two-sided Wilcoxon rank-sum test, adjusted for multiple testing. **b**, *Ppargc1a* (encoding PGC1α) mRNA expression (RNA-seq, normalized (norm.) counts) in WAT. Two-sided Wald test, adjusted for multiple testing. **c**, mtDNA copy number in WAT. One-way ANOVA, two-sided Tukey post hoc test. **d**, Western blot analysis of mtCO1 and NDUFA9 in WAT, with α-tubulin used as a loading control. One-way ANOVA, two-sided Tukey post hoc test. **e**, Propionyl- and succinyl-CoA levels in WAT. One-way ANOVA, two-sided Tukey post hoc test. **f**, mRNA expression (RNA-seq) of thermogenic marker genes in WAT. Two-sided Wald test, adjusted for multiple testing. **g**, mRNA expression (qRT-PCR) of *Ucp1*, *Srebf1*, *Acaca*, *Fasn* and *Elovl6* in the WAT relative to *Polr2i*. One-way ANOVA, two-sided Tukey post hoc test. Biologically independent animals used: RNA-seq: $n = 3$ (AL, DR, ALDR, AL 5 m) $n = 5$ (ALDR, DRAL); western blot, qPCR and lipidomics: $n = 4$ per diet. Data are means ± s.e.m., $^{***}q < 0.0001$.

code for key enzymes in FA synthesis, desaturation and elongation[34]. Their expression was strongly upregulated (some more than ten-fold, (Figs. 4g and 5e) in chronic DR and in young ALDR mice, but they remained largely refractory to the ALDR switch at old age.

We next explored the metabolic consequences of these changes in gene expression, by full liquid chromatography–tandem mass spectrometry (LC–MS/MS) profiling of the WAT lipidome. This allowed quantification of 516 lipid species and 32 different classes with a dynamic range of ~5×10^7, including the major neutral lipid, (lyso-)phospholipid and sphingolipid classes[35]. Our dataset thus permitted a global and unbiased analysis of cellular lipid dynamics (Supplementary Table 5). Consistent with transcriptional upregulation of de novo lipogenesis, we detected elevated levels of free FAs in chronic DR and young ALDR mice, including intermediate metabolites of FA synthesis, palmitate and palmitoelate (Fig. 5f–h). In contrast, late-onset DR did not cause a similar increase in FAs, while DRAL mice had FA levels lowered to those of chronic AL controls. These results suggest that imperfect activation of lipogenesis is a direct consequence of the transcriptional memory in the WAT of old ALDR mice.

Chronic dietary restriction causes white adipose tissue autonomous reprogramming of phospholipid synthesis. To better understand the possible functions of newly synthesized FAs in the WAT

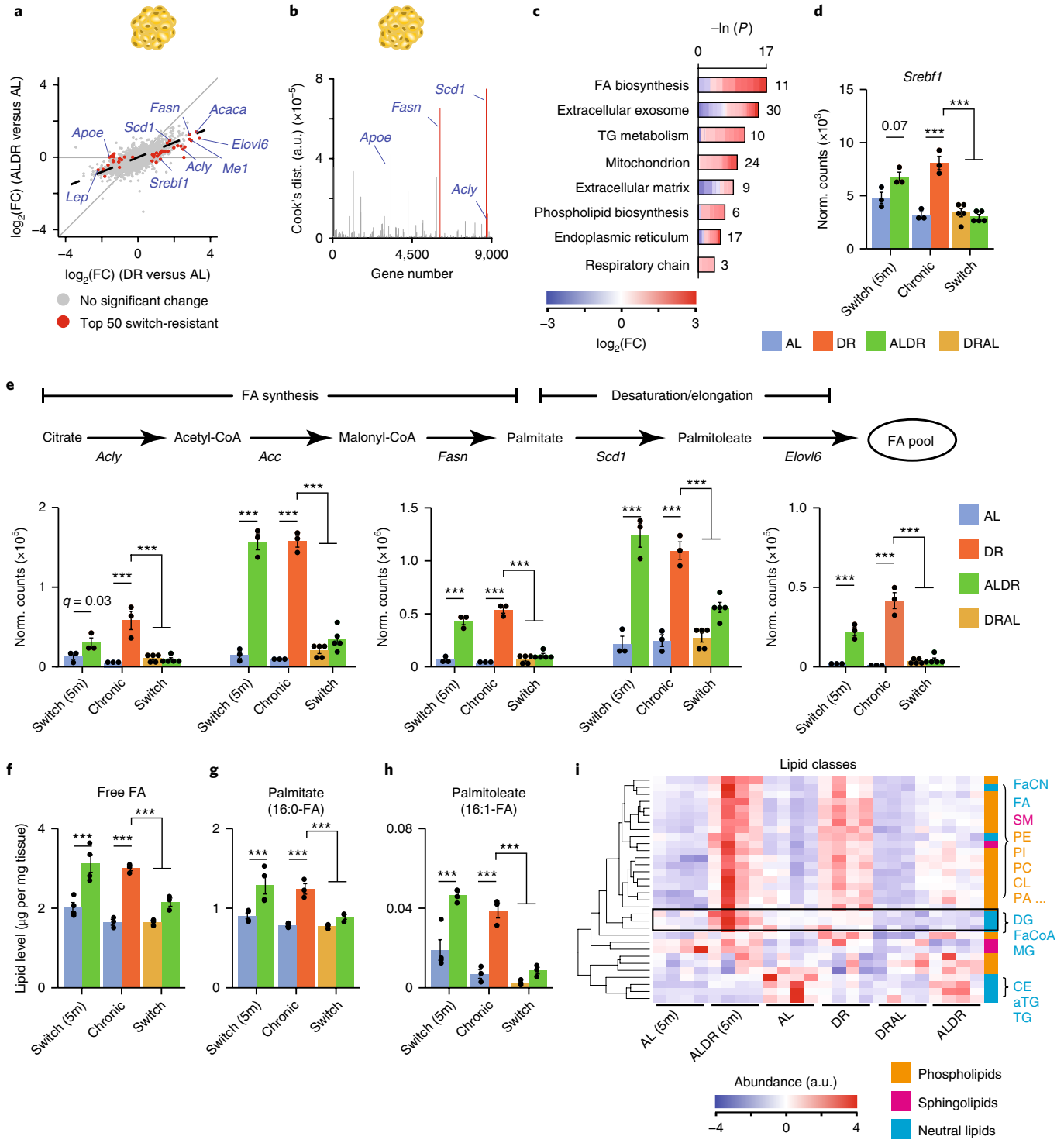

Fig. 5 | WAT-specific transcriptional memory predicts impaired activation of de novo lipogenesis under late-onset DR. a, Scatterplots depicting the expression change for each gene under DR or ALDR feeding (relative to AL) in WAT. The top 50 switch-resistant genes are highlighted in red. **b**, Gene-wise Cook's distances from weighted linear regression analysis of expression changes under DR or ALDR feeding (relative to AL) in WAT. Genes were given an arbitrary number. **c**, GO enrichment of the top 50 ALDR switch-resistant genes. Colours indicate gene-wise $\log_2$ fold-changes ($\log_2$(FC)) between DR and ALDR mice. Lengths of bars represent negative ln-transformed *P* values, determined using two-sided Fisher's exact test. Numbers beside bars indicate numbes of differently expressed genes in that GO category. **d**, *Srebf1* mRNA expression (RNA-seq). **e**, mRNA expression (RNA-seq) of key de novo synthesis genes in WAT. Two-sided Wald test, adjusted for multiple testing. **f**–**h**, Abundance of the total pool of free fatty acids (**f**), palmitate (**g**) and palmitoleate (**h**) in WAT. One-way ANOVA followed by two-sided post-hoc Tukey test. **i**, Heatmap of unsupervised clustering of abundance changes for measured lipid classes in WAT; color bar represents *z* score range. Black box highlights lipids with induction specifically in young ALDR mice. FACN, fatty acyl carnitine; SM, phingomyelin; PI, phosphatidylinositol; MG, monoglyceride; FACoA, fatty acyl coenzyme A; CE, ceramides; aTG, alkyltriglyceride. Biologically independent animals used for RNA-seq: $n = 3$ (AL, DR, ALDR, AL 5m) $n = 5$ (ALDR, DRAL). The RNA-seq experiment was done once. Biologically independent animals used for lipidomics: $n = 4$ per diet. Data are means ± s.e.m., ***$q < 0.0001$.

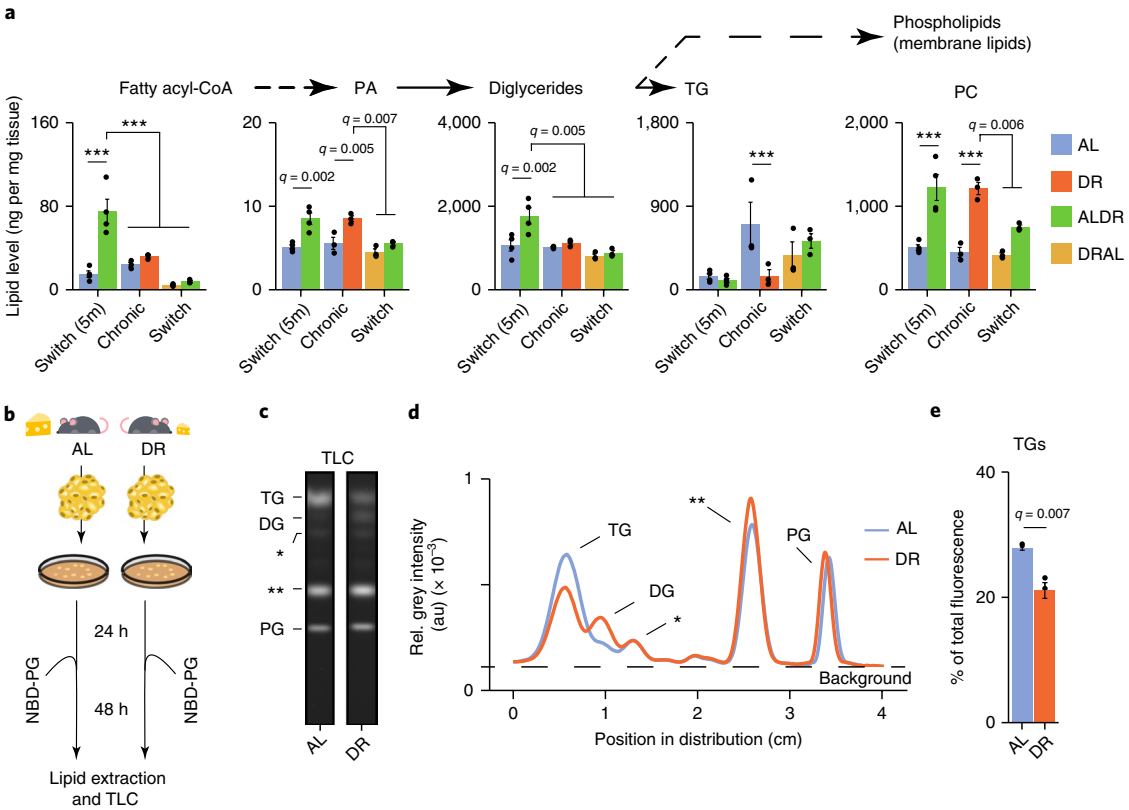

Fig. 6 | DR remodels lipid flux in adipose tissue. a, Abundance of lipid classes involved in synthesis of complex lipid molecules, as measured in WAT; $n = 4$ biologically independent animals per diet. One-way ANOVA followed by two-sided post-hoc Tukey test. TGs were extracted separately, and absolute lipidome values cannot directly be compared to other lipid classes. **b**, Schematic representation of the WAT explant culture experiment. The experiment was done once with $n = 3$ biologically independent, 24-month-old animals per diet. Each isolated WAT depot was equally distributed across three wells and incubated with NBD-PG and transfectant ($n = 2$ technical replicates) or transfectant only ($n = 1$ negative control). **c**, Representative fluorescence profile of TLC-separated lipids extracted from explant-cultured adipocytes after incubation with exogenously supplied NBD-PG. Lipids were separated by TLC and analysed by fluorescence scanning. Lipid species with low polarity run on top. Standard phospholipids allowed the identification of lipid spots representing TG, diglyceride (DG) and PG levels (the asterisks indicate unidentified lipid species). Full TLC scan and analysis details are presented in Extended Data Fig. 8. **d**, Relative fluorescence-intensity profile in explant cultures derived from AL- and DR mice (biological replicates $n = 3$ biologically independent animals; technical replicates $n = 2$; the asterisks indicate unidentified lipid species). **e**, Relative fluorescent signal in the TG band. $n = 3$ biologically independent, 24-month-old animals per diet; technical replicates were averaged prior to analysis. Two-sided Student's t test. Data are means ± s.e.m., ***$q < 0.0001$.

of DR-fed mice, we conducted unsupervised hierarchical clustering of all measured lipid classes. Free FAs clustered closely with several phospholipid classes (Fig. 5i), such as phosphatidic acid (PA), phosphatidylethanolamine (PE) and phosphatidylcholine (PC), which were all elevated in chronic DR fed mice (Figs. 5i and 6a). Levels of neutral TGs, however, were markedly reduced (Figs. 5i and 6a). In addition, fatty acyl-CoA and diglycerides, which mark the transition between FA synthesis and biogenesis of complex lipid structures[36], showed a strong peak in young ALDR mice only (Figs. 5i and 6a). Consistent with the major transcriptional reprogramming, DR thus instigated broad-spectrum changes in the WAT lipidome. In agreement with previous studies[23], DR-fed mice appeared to use newly synthesized FAs to build various types of membrane lipids, and this process remained refractory to the ALDR switch at old age.

Consistent with the shift towards phospholipid synthesis, levels of neutral TGs were markedly reduced (Figs. 5i and 6a). Notwithstanding, we assumed that at least a fraction of newly synthesized FAs would also be incorporated into TGs. Given that rapid de novo synthesis results in generally shorter and less saturated FAs, we thus analysed the relative TG profile for global shifts in elongation and desaturation. Indeed, chronic and short-term DR at young age decreased the chain length of TG-associated FAs, a shift not observed under late-onset DR (Extended Data Fig. 7a,b). Similarly, the relative fraction of saturated and mono-unsaturated TGs was elevated in young ALDR and chronic DR-fed animals, but not in old ALDR mice (Extended Data Fig. 7c,d). The molecular composition of TGs in the WAT thus further supported highly active lipogenesis under chronic but not late-onset DR.

To experimentally verify that the observed phospholipid profiles were a consequence of tissue-specific changes in lipid utilization and not confounded by lipid import from other tissues (such as the liver), we conducted an ex vivo pulse–chase experiment (Fig. 6b). To this end, we employed highly water-soluble phosphatidylglycerol (PG) with fluorophor-labeled fatty acyl groups (NBD-PG), which, in contrast to most lipid classes, is readily taken up and used by mammalian cells in culture[37]. Adipose tissue explants from freshly isolated WAT of chronically DR- or AL-fed 24-month-old mice from an independent cohort were seeded for 24 h, before the tissue cultures were incubated with NBD-PG and a transfection agent for 48 h. Subsequent lipid extraction and thin-layer chromatography (TLC) visualized the distribution of fluorescent fatty acyl groups among several lipid classes, representing new lipid molecules that were synthesized by turnover of NBD-PG (Fig. 6b,c and Extended Data Fig. 8a,b).

Lipid extracts of both DR- and AL-derived adipocytes showed a clear and equally strong fluorescent PG band, indicating potent

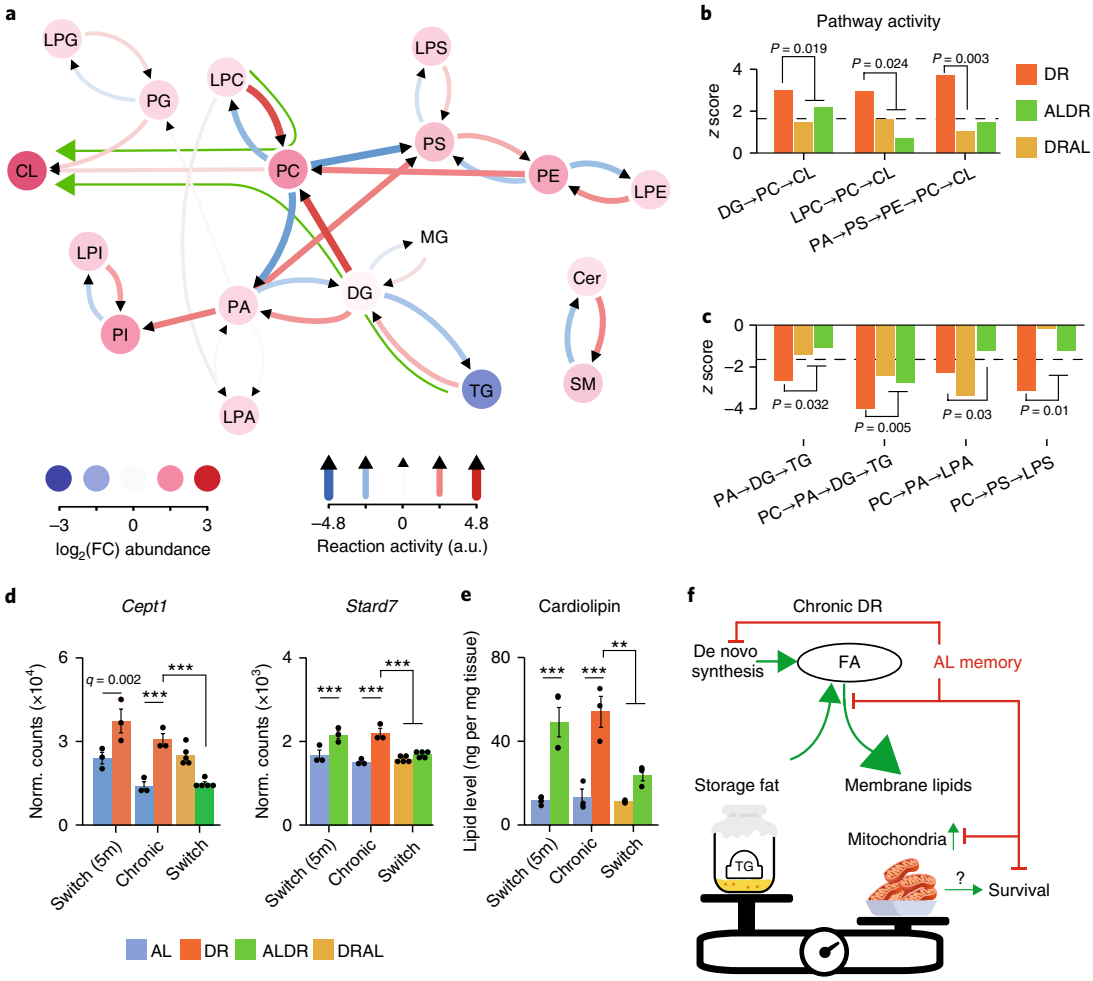

Fig. 7 | Chronic, but not late-onset, DR reprograms lipid synthesis to promote mitochondrial membrane synthesis. a, Analysis of lipid pathway activity in the WAT of DR-fed mice relative to AL controls. Red and blue arrows show reactions with positive and negative activity, respectively. Coloured circles indicate relative $\log_2$-transformed abundance of lipid classes. Green arrows indicate the major predicted lipid flux across the network. PS, phosphatidylserine; LPS, lysophosphatidylserine; LPC, lysophosphatidylcholine; LPA, lysophosphatidic acid; LPE, lysophosphatidylethanolamine; LPI, lysophosphatidylinositol; LPG lysophosphatidylglycerol **b**,**c**, Active (**b**) and inactive (**c**) pathways under DR and switch diets relative to AL control (dashed line indicates significance threshold). One-sided Student's *t* tests (forward or reverse reaction) were used to calculate *P* values before *z* transformation. *P* values above the bar graph indicate significance for the pathway relative to DR. Pathway activity was predicted on the basis of lipidomics data, with $n = 4$ biologically independent animals per diet. **d**, mRNA expression (RNA-seq) of key genes in PC synthesis (*Cept1*) and transport (*Stard7*), which map to differentially active pathways. Two-sided Wald test, adjusted for multiple testing. **e**, Cardiolipin levels in WAT of chronic or switch diet fed mice (lipidomics). One-way ANOVA followed by two-sided post-hoc Tukey test. **f**, Schematic representation of the reprogrammed transcriptome and lipidome in the WAT of chronically DR-fed mice. Processes with impaired activation as a result of prior AL feeding are indicated. Biologically independent animals used: RNA-seq: $n = 3$ (AL, DR, ALDR, AL 5m) $n = 5$ (ALDR, DRAL); Lipidomics: $n = 4$ per diet. Data are means ± s.e.m., $^{***}q < 0.0001$, $^{**}q < 0.01$.

cellular uptake of NBD-PG, and the specificity of the fluorescence was confirmed by tissue cultures incubated without PG (Fig. 6c,d and Extended Data Fig. 8a–c). In agreement with the steady-state lipid levels measured by lipidomics, the fluorescent signal was differentially distributed among the individual lipid classes in a diet-dependent manner, suggesting a global shift in use of lipid mass (Fig. 6d). Indeed, DR-derived adipocytes had a markedly weaker signal in the TG band, indicative of a reduced breakdown of phospholipids to fuel synthesis of neutral storage fats (Fig. 6d,e). Instead, DR-derived samples exhibited significantly increased fluorescence intensity in fractions with higher polarity, especially diglycerides, which run below the TG band (Fig. 6d,e and Extended Data Fig. 3a,b). Unidentified lipid fractions with even higher polarity (which can include FAs and membrane lipids), were also significantly increased under DR. Thus, DR-fed mice rewired the lipid flux in WAT autonomously so that TG synthesis was reduced while diglycerides and membrane lipids were increasingly built up.

Cardiolipin metabolism links lipogenesis with mitochondrial biogenesis under late-onset dietary restriction. Finally, we determined whether specific membrane lipids were affected by the restructuring of the lipidome in WAT of chronic DR mice. We employed a lipid-reaction analysis approach[38] to gauge the activity of whole pathways on the basis of steady-state metabolite levels as measured by lipidomics. Strikingly, chronic DR, but not late-onset DR, caused widespread reprogramming of almost the entire lipidome to promote the synthesis of phospholipids, especially PC and cardiolipin (CL) (Fig. 7a,b and Extended Data Fig. 9a,b). Simultaneously, pathways that degrade membrane lipids or convert them to triglycerides were significantly less active (Fig. 7c). This shift in lipid use from storage fat to phospholipids concurs with results from the ex vivo experiment (compare Fig. 6c,d), which validates our pathway analysis. Switch-resistant expression patterns of key genes involved in TG lipolysis (patatin-like phospholipase domain-containing 2 (*Pnpla2*, also known as *Atgl*), lipase e, hormonse sensitive type (*Lipe*, also

known as *Hsl*)[39,40]), PA and PC synthesis (1-acylglycerol-3-phosphate O-acyltransferase 1 (*Agpat1*)–*Agpat3*, choline phosphotransferase-1 (*Chpt1*)[36,41]) and re-acetylation of lyso-phospholipids (lysophosphatidylcholine acyltransferase 3 (*Lpcat3*)[41]), were in line with the predicted pathway activity (Fig. 7d and Extended Data Fig. 9c). The transcriptional memory of prior AL feeding was thus paralleled by a metabolic memory. In contrast, metabolic consequences of long-term DR were rapidly reversed when DR mice were switched back to AL feeding (Fig. 7b,c and Extended Data Fig. 8b,c).

CL is usually synthesized from PG and is almost exclusively located in the membranes of mitochondria[35]. Interestingly, CL levels showed a four-fold induction in chronic-DR-fed and in young ALDR-fed mice, the strongest increase of all lipid classes (Fig. 7e), although findings from both the ex vivo experiments and network analysis indicated no significant differences between CL synthesis and PG (Fig. 7a,c and Extended Data Fig. 7b). Instead, lipid pathway analysis suggested that CL levels became increasingly dependent on PC under chronic DR feeding. CL levels are proportional to mitochondrial mass, which depends on phospholipid supply to the organelle, including trafficking of PC[42–44]. PC is the most abundant lipid species in mitochondria[35] and must be imported from the endoplasmic reticulum (ER) via its exclusive transport protein STARD7 (refs. [44–46]). The gene encoding this protein was also identified as a switch-resistant gene (Fig. 7d), thus suggesting that PC synthesis and PC transport from the ER to mitochondria was impaired. Our results therefore link DR-related mitochondrial biogenesis in the WAT (Fig. 4) with increased synthesis of membrane lipids, which would be required during the expansion of mitochondrial mass (Fig. 7f). In this model, the strong transcriptional memory of past AL feeding for lipogenesis, membrane lipid remodelling and downstream cardiolipin synthesis would pose a bottleneck for mitochondrial biogenesis (Fig. 7f).

In summary, we have demonstrated a strong dependence of age-specific mortality on past AL feeding, paralleled by strongly age-related changes in preadipocytes and formation of a strong gene-expression and metabolic memory in adipose tissues, which impeded the coordinated reprogramming of lipid metabolism and mitochondrial activity under late-onset DR. Long-term DR-fed mice, however, retained only a weak memory of past nutrition and responded acutely to changes in diet.

Discussion

Potential DR-related therapies applicable for humans would ideally function in the older people, as they experience the greatest burdens of age-related metabolic pathologies, including type 2 diabetes[5]. Furthermore, it is important to understand whether over-nutrition in early adulthood can be completely overcome by subsequent diet. We have therefore performed a systematic assessment of prior diet effects on mortality, tissue-specific gene expression and lipidome dynamics in young and old mice.

Previous studies of late-onset DR have yielded inconclusive results. Onset of DR at 17 or 24 months was first reported to have no or even a worsening effect on survivorship of male, single-housed mice in a 3-month follow-up period[9]. However, this study instigated DR without an adaptation period, monitored survival only over a period of 90 days and did not specify the switch cohort size. A further study of group-housed male mice suggested that there was a strong improvement of survival when DR was initiated at 19 months of age, before mice of the control cohort started to die[10]. However, the absence of a chronic DR control precluded any conclusion about the completeness of the survival effect relative to chronic DR. Neither study employed cohort sizes appropriate for profiling of age-specific mortality, and therefore could not probe for acute effects owing to the cumulative nature of survival data.

We have investigated the consequences of late-life diet changes with large cohorts of control and switch diet groups, and followed all animals until death. We chose the switch time point a priori on the basis of statistical power and the cohorts' mortality. However, even with this large group of mice, conclusions on age-specific mortality are reliable only in the first 6–9 months post-switch, before too few AL mice were left for statistically valid comparisons. We further recognize that, owing to the comparatively small number of weighed animals, the statistically significant association between weight loss and survival in the ALDR cohort is predominantly driven by a few mice. Even though these few low-responders showed no evidence of being sick, exhibited average weights at the beginning of the switch, and were present among all cohorts, a larger and more targeted study will be necessary to assess our initial observation. Nevertheless, the robustness of our findings is supported by consistent results across breeding cohorts, with lifespans of AL and DR mice showing statistically insignificant differences. We saw a significant response of mortality to the ALDR switch only in breeding cohort 2. Such batch-specific variation has also been seen in the changes in mouse lifespans in response to rapamycin[47].

Our study demonstrates that long-term DR can lead to a partial, lasting protective effect when returning to full feeding, as the mortality of late-onset AL mice remained below that of chronic AL-fed mice. A similar, albeit weaker, protective effect was observed for female flies, and the magnitude of the effect increased with the duration of prior DR feeding[6]. This suggests an evolutionarily conserved function of long-term DR, which may have implications for humans too. A chronically maintained, healthy lifestyle may thus confer some benefits even when changing nutritional behaviour late in life. However, our results also demonstrate that many health benefits of DR can be lost upon returning to full feeding. Furthermore, profiling of liver, BAT and WAT implied that the lasting benefits are unrelated to the effects of DR on metabolic health, as these were acutely reversed to the level of chronically AL-fed mice. Our findings thus suggest that other mechanism or tissues mediate the long-term protective effect of DR. For example, DR reduces the occurrence of neoplasia across tissues[48,49], and delayed cancer onset may thus keep mortality lowered after refeeding, as fatal tumours would require time to develop.

There may be multiple, non-mutually-exclusive explanations of the refractoriness to the mortality of old mice to newly imposed DR, including accumulation of damage to DNA and genomic instability, senescent cells and irreversible pathologies. We have identified an adipose-tissue transcriptional and metabolic memory that impedes metabolic reprogramming under DR and that could thus limit the capacity of the mice to reduce their mortality. This phenomenon appears to be independent of genomic context, as we observed switch-resistant genes coding for mitochondrial processes in BAT and WAT yet regulated in opposite directions. In contrast to adipose tissues, and in agreement with previous studies[10], the hepatic transcriptome retained plasticity and was able to respond to dietary changes at late age. Tissue-independent mechanisms could be involved in formation of the metabolic memory. For instance, DR remodels the gut microbiome, which causally contributes to metabolic reprogramming in liver and WAT[50,51]. Loss of DR-essential microbiome species during ageing under AL feeding could thus render mice refractory to late-onset DR.

As another candidate, tissue-specific mechanism, we discovered major transcriptional shifts in WAT preadipocytes of old AL-fed mice, suggesting that stem cell and/or precursor exhaustion contributes to the WAT memory. This is interesting, since tissue-resident stem/progenitor cells show differing transcriptome shifts during ageing, with, for example, neuronal stem cells exhibiting few intrinsic expression shifts compared with hematopoietic stem cells[52,53]. Given that pre-adipocyte differentiation is strongly influenced by immune-derived factors and chemokines[54–56], the increased inflammatory signature and lowered growth factor secretion could indicate a compromised differentiation potential and thus loss of

transcriptional flexibility during ageing. Although we only had access to scRNA-seq profiles of AL-fed mice, the switch-resistant repression of inflammatory genes under DR (such as interferon response genes) could, in this model, represent a way of maintaining plasticity in the adipose tissue through prevention of sterile inflammation. Interestingly, the WAT of AL-fed mice exhibits—prior to any other tissue—major age-related expression shifts, most notably of inflammatory genes, at 15 months of age[57]. It is noteworthy that ex vivo WAT explant cultures from DR-fed mice still retained clear differences in TG and membrane lipogenesis after 72 h incubation in a medium with all nutrients in abundance and without exposure to the systemic DR environment, thus supporting the role of tissue- and/or cell-type-specific effects as mediators of the transcriptional memory.

We found that the impaired transcriptional activation of key mitochondrial and lipid metabolism pathways under late-onset DR accurately predicted compromised mitochondrial biogenesis, de novo lipogenesis and phospholipid dynamics in the WAT. Taking advantage of our extensive lipidomics dataset and published pathway databases, we successfully applied a new reaction-dynamics analysis[38], yielding ex vivo-validated predictions based on measurements of steady-state levels at just a single time point. Considering that lipogenesis is strongly downregulated in the liver of DR-fed mice[22], and that TGs in the WAT contain FAs with shorter chain length and fewer double bonds—an indicator of rapidly de novo synthesized FAs—the switch-resistant lipid dynamics are likely a result of tissue-autonomous changes. Consistent with our findings, DR is known to promote lipogenesis in the WAT[23,58] and to increase mitochondrial biogenesis[3]. Although mitochondrial biogenesis after 4 weeks of DR was shown to promote non-shivering thermogenesis in WAT[3], we found no evidence for UCP1-mediated thermogenic activity in mice treated for 2 or 22 months with DR, suggesting this to be a transient phenotype or one that is dependent on environmental and/or husbandry conditions. We also found no evidence for thermogenic activity through UCP1-indendent mechanisms such as Ca^{2+} or creatine cycling[32,33]. Notably, rodents, monkeys and humans show reduced core body temperature in response to long-term DR[59], suggesting lowered thermogenic activity under DR. Consistently, we observed evidence for 'whitening' of the BAT in the lifelong DR group in our RNA-seq dataset, with downregulation of mitochondrial genes, including that encoding UCP1, suggesting decreased mitochondria-dependent thermogenesis in the BAT of DR-fed mice. DR-induced whitening of BAT has previously been shown in a rat model of type 2 diabetes[60], but was not seen in a recent study of male, single-housed mice[61]. This might reflect gender differences in the response of the BAT to DR[62] or could be caused by different husbandry conditions. In contrast to single-housed animals, group-housed DR mice may be able to reduce energy-demanding thermogenesis in the BAT by behavioural adaptation, for example increased huddling. Notwithstanding, we cannot preclude altered activity of yet unknown thermogenic processes, and thus future studies should assess thermogenic capacity on a functional level by measuring respiration of adipose tissue directly. Our analysis further suggests a role for WAT-specific synthesis of new FAs in order to provide membrane lipids, such as PC and CL, during expansion of mitochondrial biomass. However, we cannot exclude that low lipogenesis in ALDR mice is a reaction to impaired mitochondrial biogenesis to prevent an overflow of lipids due to low beta-oxidation capacity. Also, newly synthesized FAs themselves might have additional roles. The FA palmitoleate, for example, which was strongly induced under chronic and early-life-onset DR but not late-onset DR, is secreted from the WAT and can act as a bioactive lipokine to remodel metabolism in liver and muscle[63].

In agreement with our model, cold-induced browning of WAT, which also increases mitochondrial expansion, reduces TG abundance and leads to elevated levels of free FAs, PC and CL[64]. Moreover, synthesis of CL is essential for mitochondrial biogenesis during cold exposure[65]. Finally, whole-body deletion of the lipogenic transcription factor SREBF1c abrogates lipogenesis and mitochondrial biogenesis in the WAT of DR-fed mice, thus strongly implicating SREBF1-driven lipid synthesis in adipose tissue as a limiting element for mitochondrial dynamics and, potentially, essential for improved survival under DR[58]. In line with this hypothesis, induction of mitochondrial biogenesis by the PGC1α homologue *spargel* in the fat body, an organ functionally analogous to the mammalian liver and WAT, is sufficient to extend lifespan in *Drosophila*[66]. Given the important endocrine role of the adipose tissue[67], DR-related remodelling of the WAT may lead to differential secretion of critical endocrine signals that coordinate the systemic response to DR. It will thus be a key task in the future to assess the dependence of reduced mortality under DR on lipogenesis and or mitochondrial biogenesis in the WAT specifically. This could lead to new strategies to maintain the effectiveness of DR when applied late-onset, or could even partially replicate the physiological benefits of reduced food intake under unrestricted feeding.

Methods

Mouse husbandry and DR protocol. The DR study was performed in accordance with the recommendations and guidelines of the Federation of the European Laboratory Animal Science Association (FELASA), with all protocols approved by the Landesamt für Natur, Umwelt und Verbraucherschutz, Nordrhein-Westfalen, Germany (reference no. 8.87-50.10.37.09.176 and 84-02.04.2015.A437) (Nature Research Reporting Summary). Female F_1 hybrid mice (C3B6F1) were generated in-house by crossing C3H/HeOuJ females with C57BL/6NCrl males (strain codes 626 and 027, respectively, Charles River Laboratories). Experimental animals were generated in 3 breeding batches with 300, 280 and 220 animals in breeding round F_1, F_2 and F_3, respectively (Nature Research Nature Research Reporting Summary). Lifespans of chronic DR and AL mice from the F_1 breeding round were previously published[22]. Litter size was adjusted to a maximum of 8 pups by removing male pups within 3 d of birth. Pups were weaned at 3–4 weeks of age and were randomly assigned to cages upon weaning (Nature Research Reporting Summary). Animals were housed in groups of 5 females in individually ventilated cages under specific-pathogen-free conditions with constant temperature (21 °C), 50–60% humidity and a 12-hour light–dark cycle. For environmental enrichment, mice had constant access to nesting material and chew sticks. All mice received commercially available rodent chow (ssniff R/M-H autoclavable, ssniff Spezialdiäten) and were provided with acidified water ad libitum. Food consumption of the AL group was measured weekly, and DR animals received 60% of the food amount consumed by AL animals. To avoid developmental effects, chronic DR treatment was started at 12 weeks of age. Late-life ALDR and DRAL diet switches were introduced when 20% of AL animals of the respective control cohort had died, corresponding to ~24 months of age. DR was introduced stepwise, by reducing the food delivered by 10% per week over 4 consecutive weeks. DR animals were fed once per day, and all animals were checked daily for their well-being and any deaths. Fifteen animals per cohort (3 cages) were weighed weekly (up to the age of 6 months), then monthly (6–23 months), and then again weekly following the diet switch. Ten mice per diet group of the F3 cohort were euthanized at the ages of 5 and 27 months, corresponding to 2 months (short-term) and 24 months (long-term) DR treatment. All mice were killed within a period of 3 h prior to the regular feeding time of the DR mice. Mice were killed by cervical dislocation, and tissues were rapidly collected and snap-frozen using liquid nitrogen.

Post-switch lifespan and mortality analysis. Animals that had died before the diet switch were eliminated from the mortality analysis. Cox regression of post-switch survival curves was performed using custom RStudio (https://www.rstudio.com/) scripts and the following packages: survival, survminer and flexsurv (Nature Research Reporting Summary). Survival data were modelled with two factors, diet and breeding cohort (~ diet + cohort; diet factor levels: AL, DR, ALDR, DRAL; cohort factor levels: F_1, F_2, F_3). Schoenfeld residuals were analysed to confirm that the data underlying the Cox regression in Fig. 1c met the proportionality assumption. Contrasts were used to compare the hazard ratios between ALDR relative to AL and between DRAL relative to DR ($ALDR_{AL}$ and $DRAL_{DR}$; 'switch versus past diet'). We repeated the analysis with altered contrasts to analyse the hazard ratio difference between ALDR relative to DR and the DRAL relative to AL ($ALDR_{DR}$ and $DRAL_{AL}$; 'switch versus new diet'). In order to directly compare the effects of each diet switch relative to their previous diet, we further introduced a contrast to subtract the hazard ratios of $ALDR_{AL}$ from $DRAL_{DR}$ ('hazard ratio difference'; Fig. 1g).

Analyses were repeated for each cohort separately, for which the 'cohort' factor was omitted. To determine if the results of the cohort-wise Cox regression could be accounted for by the larger cohorts of animals under DR and DRAL feeding, which

could alone have produced more significant differences for comparisons involving those groups, we repeated each analysis 1,000 times while randomly downsampling the DR and DRAL groups to match the number of AL- and ADLR-fed mice. The resulting distributions of *P* values for each analysis were plotted as boxplots (Extended Data Fig. 1c).

To test for acute effects of either switch diet, we performed Cox regression for the first 2 months post-switch, censoring all mice that were still alive at the end of that period. We repeated the Cox regression and iteratively extended the analysed time interval by1 month. *P* values and hazard ratios for $ALDR_{AL}$, $DRAL_{DR}$ and the hazard ratio difference were recorded for each iteration (Fig. 1d,g).

Visualizing age-specific mortality rate. Events of death were summarized in bins of 10 d. Mortality (μ_x) was estimated as $\mu_x = -\ln(p_x)$, where p_x is the probability of an individual alive at age $x-1$ surviving to age x. Data for Fig. 1e,f were smoothed by averaging μ_x over 3 10-d bins. Mortality trajectories were truncated when $n < 40$ AL-fed mice (equivalent to 25% survival).

Calculating rate of weight change. We monitored the weight of 15 mice per diet group and breeding cohort. We used generalized additive modelling to determine the inflection point of the weight gain/loss curve, which we found at day 889 (equivalent to roughly 145 d on new diet). Rate of weight change for each animal was estimated by linear regression over the weight trajectory for this interval. We thereby limited the analysis to the interval before the trajectories plateaued.

In order to compare the weight increase between chronic and late-onset AL mice, we performed linear modelling of the weight change in young chronic-AL-fed mice, starting at the same average body weight as the DRAL cohort. To allow comparability, we analysed only the period until the AL-fed mice reached the same weight as DRAL animals at the inflection point.

Analysis of food-intake quantification. Average food intake of chronic or late-onset AL fed mice was monitored through food consumption per cage. In order to normalize food consumption to body weight, we estimated the average body weight from the weighing group.

RNA sequencing and analysis. We isolated RNA from liver, BAT and epididymal WAT of AL, DR, ALDR and DRAL female mice at old age (27 months), as well as AL and ALDR female mice at young age (5 months). For liver tissue, we profiled the transcriptome of three biological replicates per treatment and age group. For BAT, we profiled three biological replicates per treatment and age group, with two extra replicates for old ALDR mice. In case of WAT, we profiled three biological replicates per treatment and age group, with two extra replicates for old ALDR and DRAL mice from the same cohort (three to five). RNA was isolated using Trizol Reagent (no. 15596018, Thermo Fisher Scientific, Germany) according to the manufacturer's protocol before samples were treated with DNase using the TURBO DNA-free Kit (Thermo Fisher Scientific). RNA quality was measured using the Agilent TapeStation System (Agilent Technologies). RNA-seq library preparation and sequencing were performed by the Max Planck Genome Centre Cologne, Germany (http://mpgc.mpipz.mpg.de/home/). According to the facility's procedure, stranded TruSeq RNA-seq libraries were prepared as described in[68], using 3 µg of rRNA-depleted RNA as input for liver and WAT, and 1 µg polyA-enriched RNA for BAT. Multiplexed libraries were sequenced with 2 × 40 million, 100-bp paired-end reads on an Illumina HiSeq2500 (Illumina) liver and WAT, and 1 × 25 million, 150-bp reads for BAT. Liver RNA-seq data for young ALDR, young AL, old DR and old AL mice were previously published[22] and are publicly available under the Gene Expression Omnibus (GEO) ID GSE92486. Liver RNA-seq data for old ALDR and DRAL-fed mice and RNA-seq data from BAT and WAT are available under GEO ID GSE124772.

Raw sequence reads were trimmed to remove adaptor contamination and poor-quality reads using Trim Galore! (v0.3.7, parameters: --paired --length 25). Trimmed sequences were aligned using Tophat2 (ref. [69]) (v2.0.14, parameters: --no-mixed --library-type=fr-firststrand -g 2 -p 15 -r 500 --mate-std-dev 525). Multi-mapped reads were filtered. Data visualization and analysis were performed using SeqMonk (http://www.bioinformatics.babraham.ac.uk/projects/seqmonk/), custom RStudio (https://www.rstudio.com/) scripts and the following Bioconductor packages: Deseq2 (ref. [70]), topGO[71] and org.Mm.eg.db (Nature Research Reporting Summary). To account for tissue-specific expression, we defined all genes with a fragments per kilobase of transcript per million mapped reads value of >2 in at least half of all samples as 'expressed'. Unless stated otherwise, the set of expressed genes was used as background for all functional enrichment analyses involving expression data. *P* values were adjusted for multiple testing.

To identify global expression changes for genes associated with mitochondria, we retrieved the list of genes associated with the gene ontology term 'mitochondrion' (GO:0005739) and plotted the $\log_2$ fold changes for each diet group as opposed to the chronic, old or AL diet group.

Single-cell RNA-sequencing analysis. Pre-processed and annotated scRNA-seq data (FACS followed by Smart-seq2 protocol) from gonadal adipose tissue (of mice aged 3 and 24 months old) were obtained from the Tabula Muris Senis consortium[28]. Given the lack of data from aged female mice, we focused our analyses on samples derived from male mice. Additionally, cells with fewer than 200 or more than 6,500 genes were excluded. This yielded 1,962 high-quality cell transcriptomes derived from four young and four old biological replicates. Data visualization and analysis were performed using custom Rstudio scripts and the following Bioconductor packages: Seurat (version 3)[72] and topGO (Nature Research Reporting Summary). Data normalization, scaling and identification of variable genes was performed using Seurat's built-in vst method with 2,000 features to select. A shared-nearest-neighbours graph was constructed using the first 10 Principal component (PC) dimensions before clustering cells using Seurat's built-in FindClusters function with a resolution of 0.4 and default parameters. Annotations for preadipocytes were adopted from the Tabula Muris Senis consortium (referred by the consortium as 'mesenchymal stem cell of adipose'). Differentially expressed genes between young and old preadipocytes were identified using Seurat's FindMarkers function (parameters: only.pos = F min.pct = 0.01 thresh.use = 0.01, test = 'MAST'). In order to compare the expression changes observed on the single-cell level with mRNA patterns on the tissue level, functional enrichment analysis was run with the set of WAT bulk RNA-seq expressed genes as background.

To test for a potential association between gene-expression changes measured in aged preadipocytes and in WAT of DR-fed mice, we considered only genes that changed significantly in both datasets. We plotted $\log_2$ fold expression changes during pre-adipocyte ageing versus expression changes on the tissue level under DR, and the distribution of genes among the four resulting quadrants was tested for directionality using Fisher's exact test. ALDR switch-resistant genes that showed a significant inverse association between both datasets were further analysed for functional enrichment using topGO.

Comparing transcriptional shifts between diet groups. To compare the global transcriptional shifts induced by chronic and late-onset DR, we defined significantly up- or downregulated genes between chronic DR and AL as a reference set. For each of these genes, expression values were scaled by the root-mean-square (using R's scale function) across all samples. The resulting distribution for all genes was visualized as boxplots. The expression patterns for ALDR switch-resistant genes in ALDR switch mice were additionally highlighted.

To identify top switch-resisting genes, we performed weighted linear regression by correlating the expression changes across all genes. For each gene, we retrieved and correlated the $\log_2$ fold change values from Deseq2 for the comparisons of chronic DR versus chronic AL and late-onset DR versus chronic AL. In addition, we provided the $\log_{10}$-transformed average expression ('base mean') for each gene as weight for the linear fit, to compensate for weakly expressed genes having larger $\log_2$ fold changes. Genes were ranked according to their Cook's distance, and the top 50 genes that were also classified as 'switch-resistant', were selected. Given that both the *x* and *y* axis represent data normalized to the same reference group (that is are not independent), the resulting correlation may be estimated incorrectly. Expression levels of selected candidates were therefore verified via quantitative real-time PCR (qRT–PCR).

Quantification of RNA Transcripts by quantitative real-time PCR. qRT–PCR was conducted on tissues that were derived from the same tissue collection group (but not identical mice) as the ones used for RNA-seq. In order to isolate total RNA from WAT for qRT–PCR analysis, samples were homogenized in Trizol (ThermoFisher Scientific), incubated 5 min at RT and then centrifuged at full-speed (16,100*g*) for 10 min at 4 °C in a tabletop centrifuge. To avoid carry-over of the resultant fat layer, the Trizol subnatant was carefully transferred to a fresh tube, mixed with 200 µl chloroform (no. 366927-100 ml, Sigma Aldrich) and incubated for 10 min at RT prior to centrifugation at 12,000*g* for 15 min at 4 °C. The aqueous RNA-containing phase was transferred to a fresh tube, mixed with 500 µl isopropanol, 50 µl 3 M sodium acetate and 15 µl GlycoBlue coprecipitant (AM9515, ThermoFisher Scientific) and incubated for 10 min at RT followed by centrifugation at 12,000*g* for 10 min at 4 °C. The supernatant was removed, and the pellet was washed twice with 500 µl ice-cold 70% ethanol and centrifuged at 7,500*g* for 5 min at 4 °C. Pellets were air-dried for 15 min at RT and re-suspended in 50 µl diethyl pyrocarbonate (DEPC)-treated, autoclaved double-distilled water followed by DNase treatment to remove genomic DNA contaminations using the DNA-free DNA Removal Kit (AM1906, Invitrogen). RNA concentrations were measured using the Qubit RNA BR Assay Kit (Q10210, ThermoFisher Scientific). We used 1.5 µg of RNA for first-strand cDNA synthesis using SuperScript VILO Master Mix (no. 11755-500, ThermoFisher Scientific) with 120 min incubation at 42 °C to increase cDNA yield. qRT–PCR analysis was conducted using the Taqman Gene Expression Master mix (no. 4369106, Applied Biosciences) and the following Taqman probes (ThermoFisher Scientific): *Srebf1* (Mm01138344_m1), *Acaca* (Mm01304257_m1), *Elovl6* (Mm00851223_s1), *Fasn* (Mm00662319_m1), *Polr2i* (Mm01176661_g1), *Ucp1* (Mm01244861_m1). Pipetting was carried out using a Janus Automated Workstation (PerkinElmer). qRT-PCR was done on a QuantStudio 6 Flex Real-Time PCR System (ThermoFisher Scientific) and gene expression was calculated using the $-2^{-\Delta\Delta Ct}$ method with *Polr2i* expression as internal control and normalized to the respective gene expression level of the AL control group.

Protein purification and western blotting. Protein purification and western blotting were conducted on tissues that were derived from the same tissue collection group (but not identical mice) as the ones used for RNA-seq. For western blot analysis, WAT samples were homogenized in Pierce RIPA Lysis and Extraction Buffer buffer (no. 89900, ThermoFisher Scientific) supplemented with PhosSTOP phosphatase inhibitor cocktail (no. 4906837001, Roche) and cOmplete, Mini, EDTA-free Protease Inhibitor Cocktail (no. 11836170001, Roche). Homogenates were incubated for 10 min on ice and then sonicated for 5 min. After centrifugation for 15 min at 4 °C full-speed (16,100*g*) in a table top centrifuge, protein extracts were transferred to fresh tubes, and protein concentrations were quantified using the Pierce BCA assay (no. 23225, ThermoFisher Scientific). We separated 25 µg of protein extract per sample on 12% acrylamide gels (no. 5678044, Criterion TGX Stain-Free Protein Gel, Bio-Rad) and blotted these on polyvinylidene difluoride (PVDF) membranes (Immobilon-FL IPFL00010, Merck) for 1 h at 100 V on ice. Membranes were blocked for 1 h at RT in Odyssey Blocking Buffer (TBS) (927-50000 LI-COR Biosciences), followed by overnight incubation in the following primary antibodies diluted in Odyssey Blocking Buffer: NDUFA9 (1:1,000, AB_301431, Abcam), mtCO1 (1:1,000, AB_2084810, Abcam), α-tubulin 11H10 (1:1,000, AB_2619646, Cell Signaling Technology). Blots were washed 4 times with TBS 0.2% Tween (TBS-T), incubated with fluorescently labelled secondary antibodies (1:15,000, IRDye 680RD, (AB_10956166, LI-COR Biosciences), IRDye 800CW (1:15,000, AB_621842, LI-COR Biosciences)) diluted in Odyssey Blocking Buffer for 1 h at RT followed by 4 washing steps with TBS-T at RT. Image acquisition was done using an Odyssey Infrared Imaging System (LI-COR Biosciences). For the western blot analysis of UCP1, samples were blotted on Amersham Hybond PVDF membranes (GE10600023, Merck), blocked for 1 h at RT in 5% non-fat dry milk powder (A0830, 1000 PanReac AppliChem) and washed 3 times in TBS-T. Membranes were incubated OVN with the following primary antibodies diluted in sterile filtered 5% fatty-acid-free bovine serum albumin (BP9704-100, Fisher Scientific) in TBS-T: UCP1 (1:1,000, AB_2687530) or α-tubulin 11H10, (1:1,000, AB_2619646) both obtained from Cell Signaling Technology. Blots were washed three times in TBS-T and incubated with anti-rabbit HRP-coupled secondary antibodies (1:10,000, AB_2536530, ThermoFisher Scientific) diluted in 5% milk in TBS-T for 1 h at RT, which was followed by 3 washing steps in TBS-T before incubation in ECL solution (Pierce ECL Plus Western Blotting Substrate, 32132, ThermoFisher Scientific) and image acquisition on a ChemiDoc XRS + System (Bio-Rad). After UCP1 image acquisition, blots were stripped in 0.5 M sodium hydroxide (S8045-500G, Sigma) for 1 h at RT, washed 3 times in TBS-T before ECL incubation and image acquisition to control for residual UCP1 signal. Blots were washed 3 times in TBS-T before blocking and incubation in primary α-tubulin antibody as described before.

Protein bands were quantified using the Fiji software package[73] with α-tubulin as loading control. Samples were normalized against the respective AL control.

Analysis of mtDNA copy number. mtDNA copy-number quantification was conducted on tissues that were derived from the same tissue collection group (but not identical mice) as the ones used for RNA-seq. To analyse mtDNA copy number, total DNA of WAT samples was isolated using the DNA Blood and Tissue kit (69506, Qiagen) with an additional centrifugation step at 200*g* for 5 min after lysis in ATL buffer. DNA concentrations were quantified using the Qubit dsDNA BR Assay kit (Q32853, ThermoFisher Scientific). qPCR was carried out in a QuantStudio 6 Flex Real-Time PCR System (Applied Biosystems) using the Taqman Universal PCR Master Mix (Applied Biosystems). Reactions were run in quadruplicates on 384-well plates using 5 ng of total DNA per reaction. Specific Taqman probes were used to quantify the nuclear 18S gene, (Hs99999901_s1) and the *Rnr2* (Mm04260181_s1), *Atp6* (Mm03649417_g1) and *Cox1* (Mm04225243_g1) genes for mtDNA (ThermoFisher Scientific). Data were analysed using a standard curve method, and relative mtDNA content was calculated by the ratio of mtDNA probes relative to genomic DNA (mtDNA/18S). Results were normalized to the relative mtDNA content of the AL control group.

Lipidome measurement and analysis. Extraction, measurement and quantification of lipids were performed following the published protocol[74]. Therefore, 50 mg of WAT from the same mice used for RNA-seq measurement were used for lipid extraction (4 replicates per age and diet). Tissue pieces were homogenized before lipids were extracted using the Folch method. The lower phase was recovered and resuspended in 150 µl chloroform, while the upper aqueous phase was isolated, dried and resuspended in 100 µl in chloroform/methanol/water (2:5:1, by volume). Isolated lipids were analysed by LC–MS/MS using an Orbitrap Elite mass spectrometer (Thermo Fisher Scientific) with both positive and negative electrospray ionization[75].

The naturally occurring lipids originating from the WAT samples were identified by reference to 80 µl of a standard mixture of synthetic lipids containing C17-acyl groups rather than the even numbers of carbon atoms. This sample of lipid standard contained 17:0-cholesterol ester, 17:1/17:1/17:1-triacylglycerol, 17:1/17:1/17:1-1-alkyltriacylglcerol, 17:0/18:1-diacylglycerol, 17:0/18:1-alkyldiacylglycerol, 17:0-monoacylglycerol, 17:0-free FA, 17:0-fatty-acyl coenzyme A, 13:0-fatty-acyl coenzyme A, 17:0-fatty-acyl carnitine, 17:0/18:1-phosphatidic acid, 17:0/18:1-phosphatidylcholine, 17:0/18:1-alkylphosphatidylcholine, 17:0/18:1-phosphatidylethanolamine, 17:0/18:1-alkylphosphatidylethanolamine, 17:0/18:1-phosphatidylglycerol, 17:0/20:4-phosphatidylinositol, 17:0/18:1-phosphatidylserine, 14:0/14:0/14:0/14:0-cardiolipin, C17-platelet-activating factor (50 ng), C17-2-lysoplatelet-activating factor, 17:0-2-lysophosphatidic acid, 17:0-2-lysophosphatidylcholine, 17:0-2-alkyllysophosphatidylcholine, 17:1-2-lysophosphatidylethanolamine, 17:1-2-alkyllysophosphatidylethanolamine, 17:12-lysophosphatidylglycerol, 17:1-2-lysophosphatidylinositol, 17:1-2-lysophosphatidylserine, C17-ceramide, C17-sphingosine-1-phosphate, C17-sphingomyelin.

Lipid species were normalized to synthetic standards to quantify their absolute abundance. Lipid species of the same class were summarized to quantify abundance levels of the entire lipid class. Abundance differences in individual lipid species or lipid classes were tested by one-way analysis of variance (ANOVA) followed by a post-hoc Tukey test for pairwise comparisons across all treatment and age groups. For elongation and saturation analysis, TG species with the same number of carbons/double bonds were calculated as a percentage of the entire TG lipidome. We conducted one-way ANOVA with post-hoc Tukey HSD for each chain length/saturation to test for significant differences.

White adipose tissue explant culture and lipid transfection. WAT explant cultures were generated from 24-month-old female AL and DR mice of an independent cohort. Mice were euthanized using cervical dislocation, and epididymal WAT pads were collected and placed in explant culture growth medium (Dulbecco's MEM/Ham's F12 cell culture medium (FG4815, Merck) containing 1% penicillin–streptomycin (5,000 U ml^{-1}) (no. 15070063, ThermoFisher Scientific), 10% fetal bovine serum (no. 10270106, Gibco), 17 µM D-pantothenic acid (Sigma, P5155) and 33 µM biotin (B4639, Sigma). Fat pads were washed once in sterile DPBS (14190-094, ThermoFisher Scientific) and cut into small pieces using a razor blade. Tissue pieces were transferred to a 70 µm MACS SmartStrainer (130-098-462, Miltenyi) and washed with 35 ml DBPS to remove free-floating fat. Excess liquid was removed and tissue explants were transferred to six-well plates (657160, Greiner Bio-One). Explant cultures were allowed to adhere at RT for 10 min, were supplied with pre-warmed 2 ml growth medium and were incubated at 37 °C, 5% CO_2 for 24 h prior to lipid transfection. Lipid transfections with 18:1-12:0 NBD-PG (1-oleoyl-2-12-[(7-nitro-2-1,3-benzoxadiazol-4-yl)amino]dodecanoyl)-*sn*-glycero-3-[phospho-rac-(1-glycerol)] (ammonium salt) (no. 810166C, Avanti Polar Lipids) were conducted according to the manufacturer's recommendations. Per well, 30 nM NBD-PG in chloroform was evaporated and dissolved in 195 µl Opti-MEM I Reduced Serum Medium (31985070, Gibco) and sonicated for 15 min in a chilled sonicator water bath to improve solubility. Lipofectamine 3000 (L3000-001, ThermoFisher Scientific) mixtures with 3.75 µl lipofectamine per well were prepared according to the manufacturer's recommendations in Opti-MEM medium. Lipofectamine and NBD-PG were mixed in a 1:1 ratio and incubated for 15 min at RT in the dark. Lipofectamine control or NBD-PG were added drop-wise to the respective well and mixed. Explant cultures were incubated for 48 h before samples were snap frozen and stored at −20 °C.

Thin-layer chromatography of lipids. Extraction of lipids from adipose tissue was performed according to ref. [76], with modifications. WAT explant cultures were homogenized in 500 µl of 255 mM ammonium carbonate by Precellys 24 beads beater (2 × 20 s, 6,500 r.p.m. with ceramic beads). We mixed 120 µl homogenate with 900 µl of chloroform/methanol (1:2 (vol/vol)). After mixing for 30 min, H_2O (0.12 ml) was added followed by vortexing. After the addition of 0.3 ml chloroform and 0.3 ml H_2O, the sample was mixed again for 10 min, and phase separation was induced by centrifugation (800*g*, 2 min). The lower chloroform phase was carefully transferred to a clean glass vial. The upper water phase was mixed with 10 µl 1 N HCl and 300 µl chloroform, and extraction was repeated. After phase separation, the lower chloroform phase was carefully transferred to the glass vial with the chloroform phase from the first extraction. The solvent was evaporated by a gentle stream of argon at 37 °C. Lipids were dissolved in 100 µl of chloroform/methanol (1:1 (vol/vol)). We spotted 4 µl of the lipid samples on a high-performance thin-layer chromatography plate (Merck Silica gel 60 F_{254}) and developed with chloroform/methanol/water/triethylamine 30:35:7:35 (vol/vol/vol/vol). Analysis of fluorescent signals was performed using the Typhoon Trio laser scanner (λ_{em} = 526 nm, λ_{ex} = 488 nm) and the ImageQuant software (GE Healthcare). Thin-layer chromatography plates were stained with 470 mM $CuSO_4$ in 8.5% *o*-phosphoric acid and subsequently incubated for 10 min at 180 °C.

Thin layer chromatography fluorescent signal analysis. Distribution of fluorescent signal was analysed with Fiji[73]. First, the distribution and width of each fluorescent band was quantified by vertical paths run through the centre of each lane using 'integrated density' as measurement. Since there was no fluorescent signal from cells incubated without NBD-PG, it can be assumed that all the fluorescence in the NBD-transfected cells was originally PG. Thus, the sample-wise relative distribution of fluorescent signal (that is relative conversion rate of PG into other lipid species) can be obtained by normalising against the total sum

of the integrated signal, thereby removing potential differences in cell number or PG uptake. Data from technical replicates were averaged after quantification. Fluorescent and non-fluorescent lipid standards were run in parallel to identify individual lipid classes and to estimate the influence of the fluorescent label on the retention behaviour of the TLC. TG band was identified as the top most running band after $CuSO_4$ staining and scanning.

Next, the fluorescent signal of each band was measured using the 'regions of interest' option in Fiji. For each band (TG, CL, PG, and so on) the selected area was of equal size across all samples. Measured values were normalised against the sample-wise, total fluorescent signal as quantified by a bin spanning all bands together. Data from technical replicates were averaged after quantification.

Lipid reaction network analysis. Reaction network analysis was performed as described previously in ref. [38]. This method calculates statistical z scores for all possible lipid pathways in order to predict whether a particular pathway is active or inactive in DR- as compared with AL-fed mice. Reactions with higher z scores were classified as active. First, we retrieved all publicly annotated reactions and lipid pathways from Reactome[77] to construct a network of reactions. Using the lipidomics dataset, we calculated the molecular concentrations for each lipid species and class, before computing for each reaction the so-called reaction weight (ω) as a ratio of product over substrate. Next, we performed, for each reaction, one-sided Student's t tests using the weights observed under chronic DR or AL feeding, to identify reactions with differential activity. Resulting P values were converted to z scores using the qnorm function (call: qnorm(1 − P)) provided by the R package 'stats'. We chose the significance level (P) to be 0.05, corresponding to a $z_i > 1.645$ for reaction i to be determined as significantly active under DR as opposed to AL. For visualization, we multiplied the z score with −1 for cases where the reaction was significantly more active under AL as opposed to DR.

Finally, we calculated an average z score for each possible combination of reactions (that is pathways) to detect consistent changes in the flux across multiple reaction steps. With A (A_1,A_2,…,A_k) being the pathway of interest, where A_i (i=1,2,…,) are metabolites, we calculate the average z score Z_A of the pathway as follows:

$$Z_A = \frac{1}{\sqrt{k-1}} \sum_{i=1}^{k-1} Z_i \quad (1)$$

Z_i represents the z score for each reaction involved in the pathway. As shown in ref. [38], Z_A follows a normal distribution. To determine if a pathway A was significantly more active in DR- compared with AL-fed mice, we chose the significance level (P) to be 0.05, corresponding to a $Z_A > 1.645$. For visualization, we multiplied the Z_A with −1 for cases where the pathway was significantly more active under AL as opposed to DR. k denotes the total number of reactions.

We repeated the analysis correspondingly for the ALDR and DRAL groups with AL-fed mice used as reference.

Quantification and statistical analysis. *Statistical analysis and sample sizes.* RStudio (https://www.rstudio.com/) and Deseq2 (ref. [70]) were used for statistical analysis. Data are expressed as mean ± s.e.m. P values were calculated using the following tests: Deseq2's Wald test (RNA-seq data), Fisher's exact test (enrichment analysis); Wald and likelihood ratio test (Cox regression); Student's t test with Pearson's product-moment correlation (correlation between weight/weight change and age at death); t test (fluorescent signal intensity), one-sided t test (lipid reaction network activity); one-way ANOVA followed by a post-hoc Tukey test for pairwise comparisons (if not specified). Quantile–quantile plots were analysed to confirm that data met assumptions of the statistical approach when t tests and regression were used. Schoenfeld residuals were analysed to confirm that the data underlying the Cox regression in Fig. 1c met the proportionality assumption.

P values less than 0.05 were considered statistically significant with a type II error of β = 0.2. Where multiple testing was performed, the adjusted P values were used to determine significance. $q < 0.0001$ were marked with ***. When comparing values measured under chronic DR with those observed under DRAL and ALDR, and in both tests the q values were below 0.05, the larger of the two was indicated in the figure (Nature Research Reporting Summary).

Reporting summary. Further information on research design is available in the Nature Research Reporting Summary linked to this article.

Data availability

The data that support the findings of this study are available from the corresponding authors upon request. Raw bulk RNA-sequencing data are available under accession numbers GSE92486 and GSE124772 on the NCBI Gene Expression Omnibus database. Analysed lipidomics data are available under Supplementary Table 5.

Received: 16 April 2019; Accepted: 10 September 2019;
Published online: 21 October 2019

References

1. Fontana, L. & Partridge, L. Promoting health and longevity through diet: from model organisms to humans. *Cell* **161**, 106–118 (2015).
2. Hine, C. et al. Endogenous hydrogen sulfide production is essential for dietary restriction benefits. *Cell* **160**, 132–144 (2015).
3. Fabbiano, S. et al. Caloric restriction leads to browning of white adipose tissue through type 2 immune signaling. *Cell Metab.* **24**, 434–446 (2016).
4. Kobara, M. et al. Short-term caloric restriction suppresses cardiac oxidative stress and hypertrophy caused by chronic pressure overload. *J. Card. Fail.* **21**, 656–666 (2015).
5. Partridge, L., Deelen, J. & Slagboom, P. E. Facing up to the global challenges of ageing. *Nature* **561**, 45–56 (2018).
6. Mair, W., Goymer, P., Pletcher, S. D. & Partridge, L. Demography of dietary restriction and death in Drosophila. *Science* **301**, 1731–1733 (2003).
7. Weindruch, R. The retardation of aging by caloric restriction: studies in rodents and primates. *Toxicol. Pathol.* **24**, 742–745 (1996).
8. Merry, B. J., Kirk, A. J. & Goyns, M. H. Dietary lipoic acid supplementation can mimic or block the effect of dietary restriction on life span. *Mech. Ageing Dev.* **129**, 341–348 (2008).
9. Forster, M. J., Morris, P. & Sohal, R. S. Genotype and age influence the effect of caloric intake on mortality in mice. *FASEB J.* **17**, 690–692 (2003).
10. Dhahbi, J. M., Kim, H.-J., Mote, P. L., Beaver, R. J. & Spindler, S. R. Temporal linkage between the phenotypic and genomic responses to caloric restriction. *Proc. Natl Acad. Sci. USA* **101**, 5524–5529 (2004).
11. Vaupel, J. W. et al. Biodemographic trajectories of longevity. *Science* **280**, 855–860 (1998).
12. Carey, J. R. What demographers can learn from fruit fly actuarial models and biology. *Demography* **34**, 17–30 (1997).
13. Jiang, T., Liebman, S. E., Lucia, M. S., Phillips, C. L. & Levi, M. Calorie restriction modulates renal expression of sterol regulatory element binding proteins, lipid accumulation, and age-related renal disease. *J. Am. Soc. Nephrol.* **16**, 2385–2394 (2005).
14. Swindell, W. R. Genes and gene expression modules associated with caloric restriction and aging in the laboratory mouse. *BMC Genomics* **10**, 585 (2009).
15. Kuhla, A., Blei, T., Jaster, R. & Vollmar, B. Aging Is Associated With a Shift of Fatty Metabolism Toward Lipogenesis. *J. Gerontol. A Biol. Sci. Med. Sci.* **66A**, 1192–1200 (2011).
16. Gillespie, Z. E., Pickering, J. & Eskiw, C. H. Better living through chemistry: Caloric restriction (CR) and CR mimetics alter genome function to promote increased health and lifespan. *Front. Genet.* **7**, 142 (2016).
17. Rhoads, T. W. et al. Caloric restriction engages hepatic RNA processing mechanisms in rhesus monkeys. *Cell Metab.* **27**, 677–688.e5 (2018).
18. Plank, M., Wuttke, D., van Dam, S., Clarke, S. A. & de Magalhães, J. P. A meta-analysis of caloric restriction gene expression profiles to infer common signatures and regulatory mechanisms. *Mol. Biosyst* **8**, 1339–1349 (2012).
19. Papsdorf, K. & Brunet, A. Linking lipid metabolism to chromatin regulation in aging. *Trends Cell Biol.* https://doi.org/10.1016/j.tcb.2018.09.004 (2018).
20. Mitchell, S. J. et al. Effects of sex, strain, and energy intake on hallmarks of aging in mice. *Cell Metab.* **23**, 1093–1112 (2016).
21. Liao, C.-Y. et al. Fat maintenance is a predictor of the murine lifespan response to dietary restriction. *Aging Cell* **10**, 629–639 (2011).
22. Hahn, O. et al. Dietary restriction protects from age-associated DNA methylation and induces epigenetic reprogramming of lipid metabolism. *Genome Biol.* **18**, 56 (2017).
23. Charles, K. N. et al. Uncoupling of metabolic health from longevity through genetic alteration of adipose tissue lipid-binding proteins. *Cell Rep.* **21**, 393–402 (2017).
24. Weindruch, R., Walford, R. L., Fligiel, S. & Guthrie, D. The retardation of aging in mice by dietary restriction: longevity, cancer, immunity and lifetime energy intake. *J. Nutr.* **116**, 641–654 (1986).
25. Rogers, N. H. & Smith, R. G. Brown-to-white transition in subcutaneous fat: linking aging and disease. *Aging (Albany NY)* **4**, 728–729 (2012).
26. Berry, D. C. et al. Cellular aging contributes to failure of cold-induced beige adipocyte formation in old mice and humans. *Cell Metab.* **25**, 166–181 (2017).
27. Wang, W. et al. A PRDM16-driven metabolic signal from adipocytes regulates precursor cell fate. *Cell Metab.* **30**, 174–189.e5 (2019).
28. Pisco, A. O. et al. A Single cell transcriptomic atlas characterizes aging tissues in the mouse. Preprint at https://doi.org/10.1101/661728 (2019).
29. Konishi, M. et al. Role of Fgf10 in cell proliferation in white adipose tissue. *Mol. Cell. Endocrinol.* **249**, 71–77 (2006).
30. Petrus, P. et al. Transforming growth factor-β3 regulates adipocyte number in subcutaneous white adipose tissue. *Cell Rep.* **25**, 551–560.e5 (2018).
31. Townsend, K. L. & Tseng, Y.-H. Brown fat fuel utilization and thermogenesis. *Trends Endocrinol. Metab.* **25**, 168–177 (2014).
32. Kazak, L. et al. A creatine-driven substrate cycle enhances energy expenditure and thermogenesis in beige fat. *Cell* **163**, 643–655 (2015).

33. Ikeda, K. et al. UCP1-independent signaling involving SERCA2b-mediated calcium cycling regulates beige fat thermogenesis and systemic glucose homeostasis. *Nat. Med.* **23**, 1454–1465 (2017).
34. Wang, Y., Viscarra, J., Kim, S.-J. & Sul, H. S. Transcriptional regulation of hepatic lipogenesis. *Nat. Rev. Mol. Cell Biol.* **16**, 678–689 (2015).
35. van Meer, G., Voelker, D. R. & Feigenson, G. W. Membrane lipids: where they are and how they behave. *Nat. Rev. Mol. Cell Biol.* **9**, 112–124 (2008).
36. Shindou, H. & Shimizu, T. Acyl-CoA:Lysophospholipid acyltransferases. *J. Biol. Chem.* **284**, 1–5 (2008).
37. Potting, C. et al. TRIAP1/PRELI complexes prevent apoptosis by mediating intramitochondrial transport of phosphatidic acid. *Cell Metab.* **18**, 287–295 (2013).
38. Nguyen, A., Rudge, S. A., Zhang, Q. & Wakelam, M. J. Using lipidomics analysis to determine signalling and metabolic changes in cells. *Curr. Opin. Biotechnol.* **43**, 96–103 (2017).
39. Zimmermann, R. et al. Fat mobilization in adipose tissue is promoted by adipose triglyceride lipase. *Science* **306**, 1383–1386 (2004).
40. Haemmerle, G. et al. Defective lipolysis and altered energy metabolism in mice lacking adipose triglyceride lipase. *Science* **312**, 734–737 (2006).
41. van der Veen, J. N. et al. The critical role of phosphatidylcholine and phosphatidylethanolamine metabolism in health and disease. *BBA-Biomembranes* **1859**, 1558–1572 (2017).
42. Osman, C., Haag, M., Wieland, F. T., Brügger, B. & Langer, T. A mitochondrial phosphatase required for cardiolipin biosynthesis: the PGP phosphatase Gep4. *EMBO J.* **29**, 1976–1987 (2010).
43. Tamura, Y. et al. Role for two conserved intermembrane space proteins, Ups1p and Ups2p, [corrected] in intra-mitochondrial phospholipid trafficking. *J. Biol. Chem.* **287**, 15205–15218 (2012).
44. Saita, S. et al. PARL partitions the lipid transfer protein STARD7 between the cytosol and mitochondria. *EMBO J.* **37**, e97909 (2018).
45. Horibata, Y. & Sugimoto, H. StarD7 mediates the intracellular trafficking of phosphatidylcholine to mitochondria. *J. Biol. Chem.* **285**, 7358–7365 (2010).
46. Horibata, Y. et al. StarD7 Protein deficiency adversely affects the phosphatidylcholine composition, respiratory activity, and cristae structure of mitochondria. *J. Biol. Chem.* **291**, 24880–24891 (2016).
47. Harrison, D. E. et al. Rapamycin fed late in life extends lifespan in genetically heterogeneous mice. *Nature* **460**, 392–395 (2009).
48. Ikeno, Y. et al. Do Ames dwarf and calorie-restricted mice share common effects on age-related pathology? *Pathobiol. Aging Age Relat. Dis.* **3**, 20833 (2013).
49. Brandhorst, S. & Longo, V. D. Fasting and caloric restriction in cancer prevention and treatment. *Recent Results Cancer Res.* **207**, 241–266 (2016).
50. Zhang, C. et al. Structural modulation of gut microbiota in life-long calorie-restricted mice. *Nat. Commun.* **4**, 2163 (2013).
51. Fabbiano, S. et al. Functional gut microbiota remodeling contributes to the caloric restriction-induced metabolic improvements. *Cell Metab.* **28**, 907–921 (2018).
52. Florian, M. C. et al. A canonical to non-canonical Wnt signalling switch in haematopoietic stem-cell ageing. *Nature* **503**, 392–396 (2013).
53. Kalamakis, G. et al. Quiescence modulates stem cell maintenance and regenerative capacity in the aging brain. *Cell* **176**, 1407–1419.e14 (2019).
54. Lee, M.-W. et al. Activated type 2 innate lymphoid cells regulate beige fat biogenesis. *Cell* **160**, 74–87 (2015).
55. Huang, Z. et al. The FGF21–CCL11 axis mediates beiging of white adipose tissues by coupling sympathetic nervous system to type 2 immunity. *Cell Metab.* **26**, 493–508.e4 (2017).
56. Wang, W. & Seale, P. Control of brown and beige fat development. *Nat. Rev. Mol. Cell Biol.* **17**, 691–702 (2016).
57. Schaum, N. et al. The murine transcriptome reveals global aging nodes with organ-specific phase and amplitude. Preprint at https://doi.org/10.1101/662254 (2019).
58. Fujii, N. et al. Sterol regulatory element-binding protein-1c orchestrates metabolic remodeling of white adipose tissue by caloric restriction. *Aging Cell* **16**, 508–517 (2017).
59. Soare, A., Cangemi, R., Omodei, D., Holloszy, J. O. & Fontana, L. Long-term calorie restriction, but not endurance exercise, lowers core body temperature in humans. *Aging (Albany NY)* **3**, 374–379 (2011).
60. Lapa, C. et al. Whitening and impaired glucose utilization of brown adipose tissue in a rat model of type 2 diabetes mellitus. *Sci. Rep.* **7**, 16795 (2017).
61. Corrales, P. et al. Long-term caloric restriction ameliorates deleterious effects of aging on white and brown adipose tissue plasticity. *Aging Cell* **18**, e12948 (2019).
62. Valle, A., García-Palmer, F. J., Oliver, J. & Roca, P. Sex differences in brown adipose tissue thermogenic features during caloric restriction. *Cell. Physiol. Biochem.* **19**, 195–204 (2007).
63. Cao, H. et al. Identification of a lipokine, a lipid hormone linking adipose tissue to systemic metabolism. *Cell* **134**, 933–944 (2008).
64. Lynes, M. D. et al. Cold-activated lipid dynamics in adipose tissue highlights a role for cardiolipin in thermogenic. *metabolism. Cell Rep.* **24**, 781–790 (2018).
65. Sustarsic, E. G. et al. Cardiolipin synthesis in brown and beige fat mitochondria is essential for systemic energy homeostasis. *Cell Metab.* **28**, 159–174.e11 (2018).
66. Tain, L. S. et al. A proteomic atlas of insulin signalling reveals tissue-specific mechanisms of longevity assurance. *Mol. Syst. Biol.* **13**, 939 (2017).
67. Kajimura, S., Spiegelman, B. M. & Seale, P. Brown and beige fat: physiological roles beyond heat generation. *Cell Metab.* **22**, 546–559 (2015).
68. Sultan, M. et al. A simple strand-specific RNA-Seq library preparation protocol combining the Illumina TruSeq RNA and the dUTP methods. *Biochem. Biophys. Res. Commun.* **422**, 643–646 (2012).
69. Kim, D. et al. TopHat2: accurate alignment of transcriptomes in the presence of insertions, deletions and gene fusions. *Genome Biol.* **14**, R36 (2013).
70. Love, M. I., Huber, W. & Anders, S. Moderated estimation of fold change and dispersion for RNA-seq data with DESeq2. *Genome Biol.* **15**, 550 (2014).
71. Alexa, A. & Rahnenfuhrer, J. *Bioconductor - topGO, R package version* (2010).
72. Stuart, T. et al. Comprehensive integration of single-cell data. *Cell* **177**, 1888–1902.e21 (2019).
73. Schindelin, J. et al. Fiji: an open-source platform for biological-image analysis. *Nat. Meth.* **9**, 676–682 (2012).
74. Peck, B. et al. Inhibition of fatty acid desaturation is detrimental to cancer cell survival in metabolically compromised environments. *Cancer Metab.* **4**, 6 (2016).
75. Clark, J. et al. Quantification of PtdInsP3 molecular species in cells and tissues by mass spectrometry. *Nat. Meth.* **8**, 267–272 (2011).
76. Bligh, E. G. & Dyer, W. J. A rapid method of total lipid extraction and purification. *Can. J. Biochem. Physiol.* **37**, 911–917 (1959).
77. Fabregat, A. et al. The Reactome Pathway Knowledgebase. *Nucleic Acids Res.* **46**, D649–D655 (2018).

Acknowledgements

We thank R. Weindruch, J. Nelson, R. Miller, C. Selman, D. Withers and F. Kiefer for their advice on the mouse dietary restriction protocol and Dietmar Vestweber and the Max Planck Institute for Molecular Biomedicine, Münster, Germany, for kindly allowing us to conduct our studies at their facilities. We further thank I. Gravemeier, U. Hill, J. Matutat, A. Mesaros and B. Neuhaus for assistance with mouse work. We thank T. Wyss-Coray and the Tabula Muris consortium for kindly granting access to their single-cell transcriptome atlas, and for advice and supervision during the corresponding analysis. We acknowledge funding from the Max Planck Society, Bundesministerium für Bildung und Forschung Grant SyBACol 0315893A-B (to AB and LP) and the European Research Council under the European Union's Seventh Framework Programme (FP7/2007-2013)/ERC grant agreement number 268739 to L.P. M.J.O.W., A.N. and Q.Z. thank the BBSRC (BB/P013384/1) and the MRC (MR/M004821/1) for financial support.

Author contributions

S.G., A.B., M.J.O.W. and L.P. designed the experiments and drafted the manuscript together with O. Hahn. S.P. conceptualized and performed power analyses to determine the required number of animals for the switch experiments, and guided the mortality data analysis. O. Hendrich performed the RNA-seq. L.F.D. performed qPCR and western blot experiments. T.T. and T.L. designed and conducted the in vitro pulse–chase experiments with L.F.D. and L.G. Q.Z. and M.J.O.W. conducted the lipidomic profiling. A.N. conceptualized and performed the lipidome network analysis. O. Hahn performed most of the lifespan and bioinformatic analyses. All authors read and approved the final manuscript.

Competing interests

The authors declare no competing interests.

Additional information

Supplementary information is available for this paper at https://doi.org/10.1038/s42255-019-0121-0.

Correspondence and requests for materials should be addressed to M.J.O.W., A.B., S.G. or L.P.

Peer review information Primary Handling Editor: Christoph Schmitt

Reprints and permissions information is available at www.nature.com/reprints.

Publisher's note Springer Nature remains neutral with regard to jurisdictional claims in published maps and institutional affiliations.

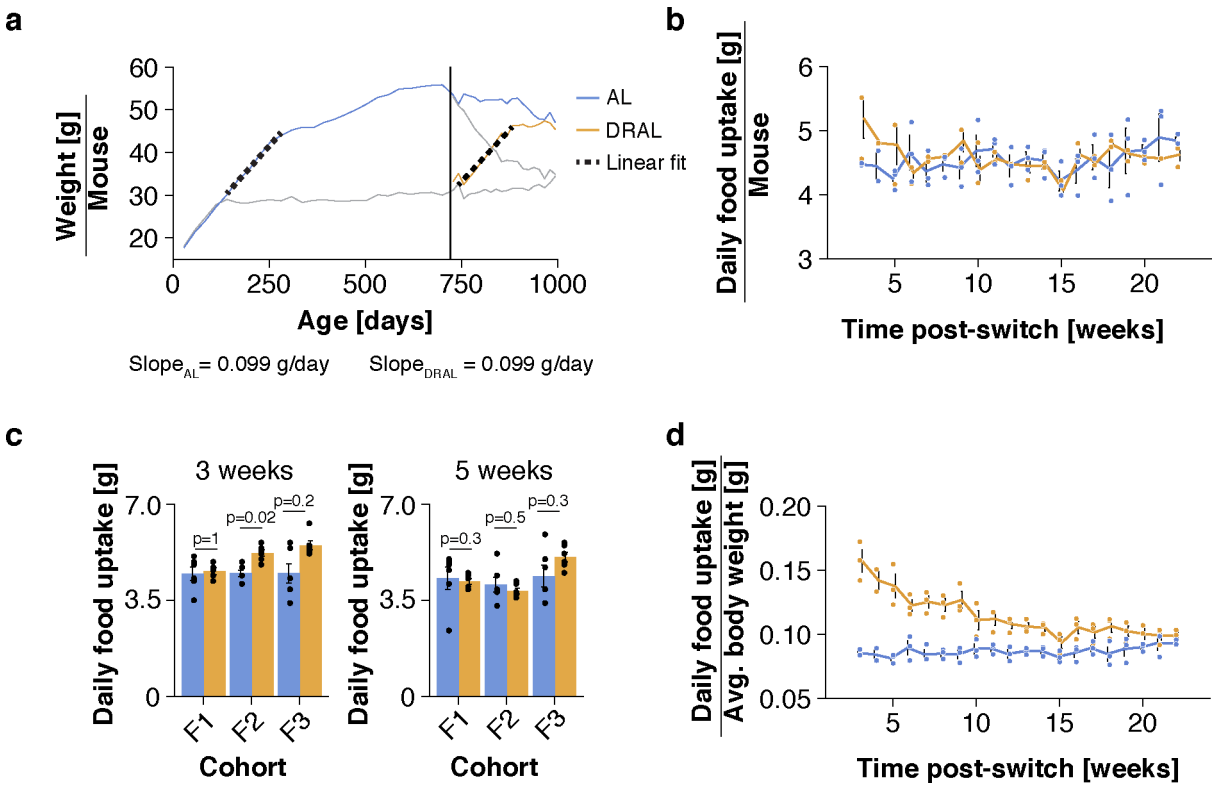

Extended Data Fig. 1 | Food intake of AL and DRAL mice. Body weights for chronic and switch AL cohorts. Solid lines indicate when chronic DR and diet switches were applied. The dashed lines indicates linear fit of weight gain for both cohorts. Slope of linear fits are indicated below. $n = 45$ biologically independent animals per diet. **b**, Averaged daily food intake per mouse. Each point represents the values from one cohort, encompassing 6 cages each. $n = 3$ cohorts per diet. **c**, Average daily food uptake for 3- and 5-weeks post-switch, split by cohorts and individual cage. $n = 6$ biologically independent cages per diet and cohort. Two-sided Wilcoxon rank-sum test, adjusted for multiple testing. **d**, Averaged daily food intake per mouse after normalizing against average body weight. Each point represents the values from one cohort, encompassing six cages. $n = 3$ cohorts per diet. Means ± s.e.m.

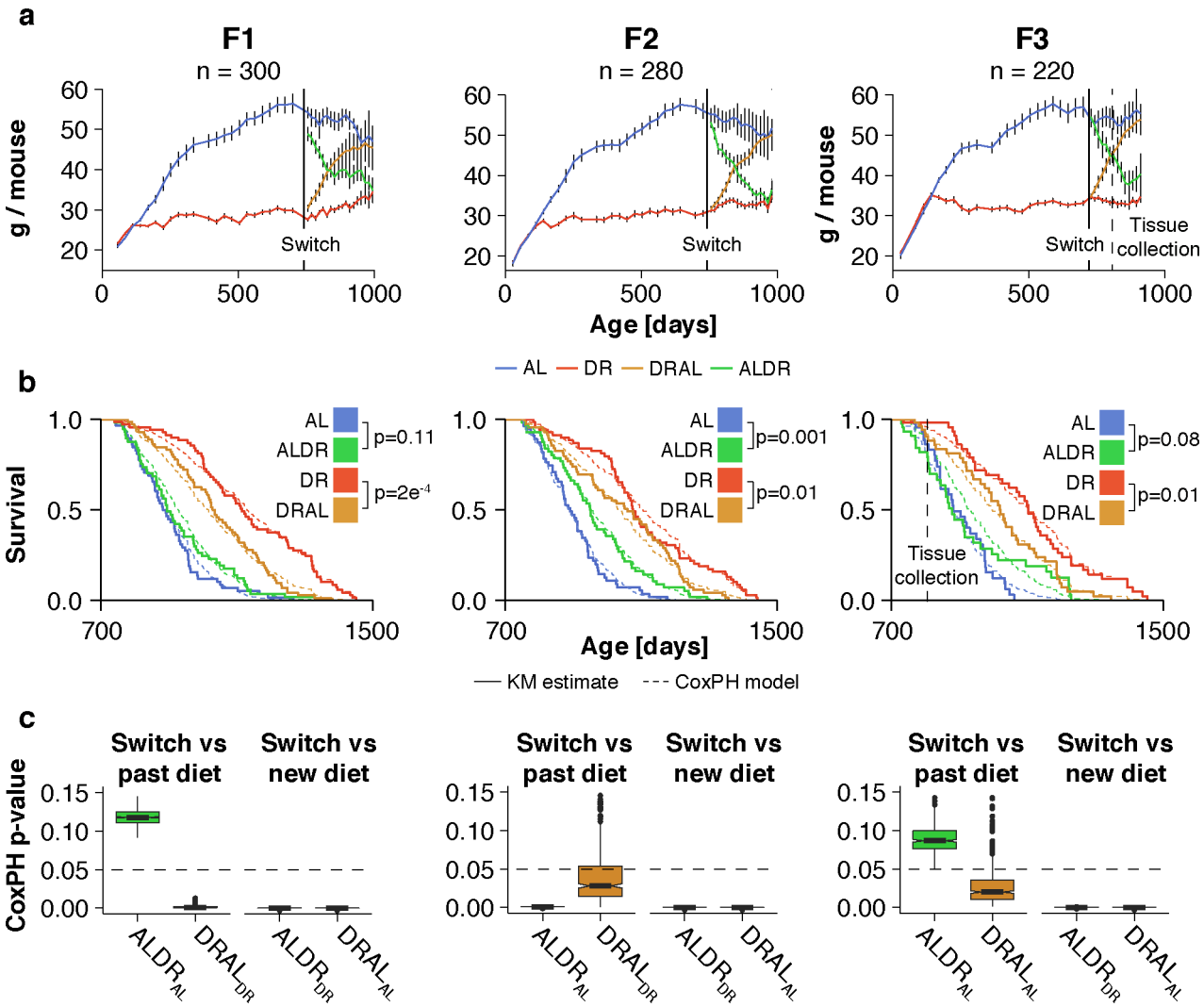

Extended Data Fig. 2 | Demography of dietary restriction for each of the three breeding cohorts. a, Pre- and post-switch weight curves for chronic and switch diet mice from the 3 breeding cohorts (± 95% confidence intervals). Solid and dashed lines indicate the time point for diet switch and tissue collection, respectively. Tissues were collected from the F3 cohort only. The number above the graph indicates total cohort size at birth. $n = 15$ biologically independent animals per diet and cohort. **b**, Cohort-specific post-switch KM survival curves for chronic and switch diet cohorts. Cox regression (dashed line) was used to avoid making assumptions about the shape of the trajectories. **c**, Cohort-specific distribution of P values as computed from $n = 1{,}000$ Cox regression analyses with random down-sampling of DRAL and DR cohorts to match the size of AL/ALDR cohorts. Analyses were run relative to the pre- and post-switch control. The dashed line indicates significance threshold. Whiskers represent 1st and 5th quartiles, box edges represent 2nd and 4th quartiles, and the centre line represents the 3rd quartile/median. Outliers are marked by points. **b**,**c**, Biologically independent animals per cohort at start of switch: F1: $n = 58$ (AL) $n = 69$ (DR), $n = 72$ (DRAL), $n = 57$ (ALDR); F2: $n = 55$ (AL) $n = 69$ (DR), $n = 69$ (DRAL), $n = 56$ (ALDR); F3: $n = 44$ (AL) $n = 52$ (DR), $n = 53$ (DRAL), $n = 44$ (ALDR). Means ± s.e.m.

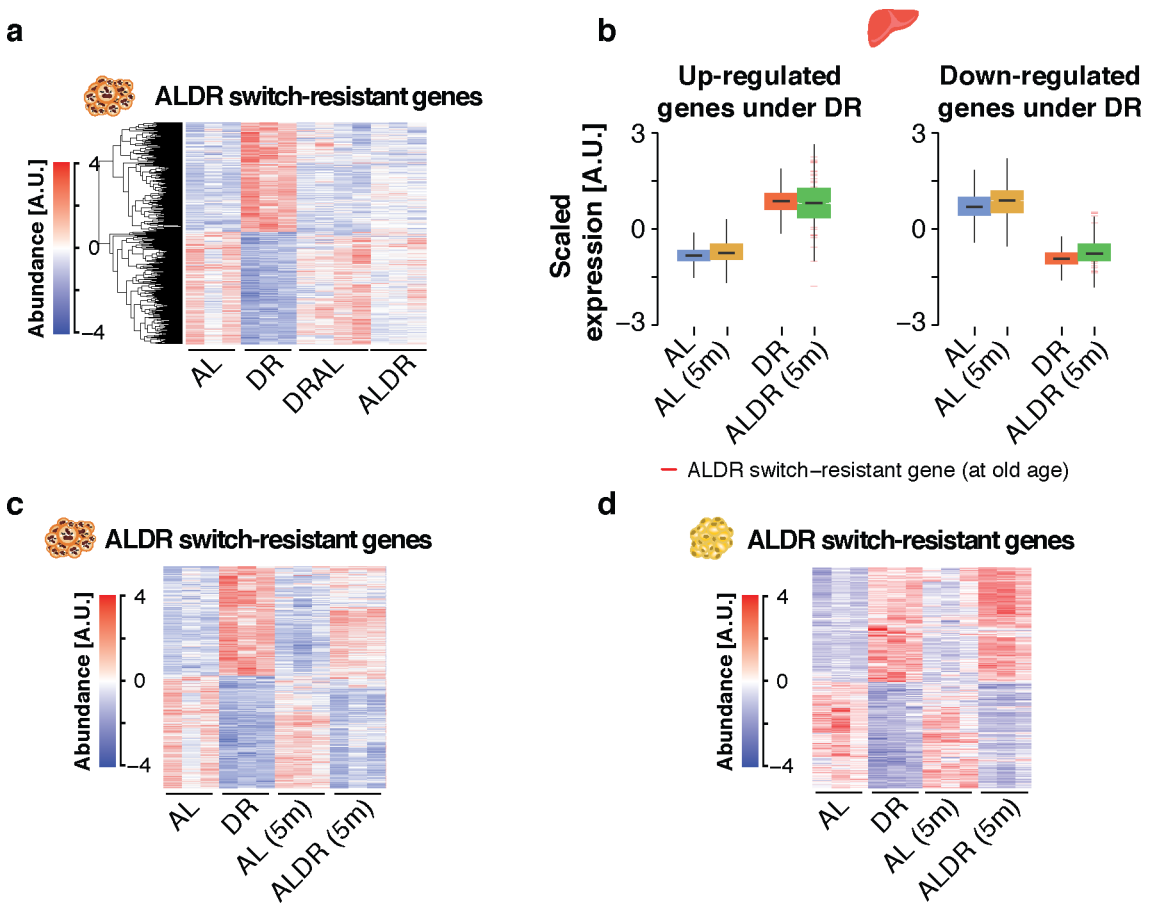

Extended Data Fig. 3 | Transcriptional reprogramming in response to early-onset DR and late-onset AL. a, Heatmap of unsupervised clustering of expression changes for ALDR switch-resistant genes in BAT ($n = 3$–5 per group; colour bar represents z score range). **b**, Boxplot representation of scaled expression levels of differentially up- and downregulated genes under chronic DR as opposed to chronic AL controls in livers of ALDR switch mice at a young age. Whiskers represent 1st and 5th quartiles, box edges represent 2nd and 4th quartiles, and the centre line represents the 3rd quartile/median. **c**,**d**, Heatmap of expression changes for ALDR switch-resistant genes in BAT (**c**) and WAT (**d**) of young ALDR switch mice ($n = 3$ per group; colour bar represents z score range). Biologically independent animals used for RNA-seq: Liver: $n = 3$ (AL, DR, ALDR, DRAL, ALDR 5m, AL 5m); BAT: $n = 3$ (AL, DR, DRAL, AL 5m, ALDR 5m) $n = 5$ (ALDR); WAT: $n = 3$ (AL, DR, ALDR, AL 5m) $n = 5$ (ALDR, DRAL).

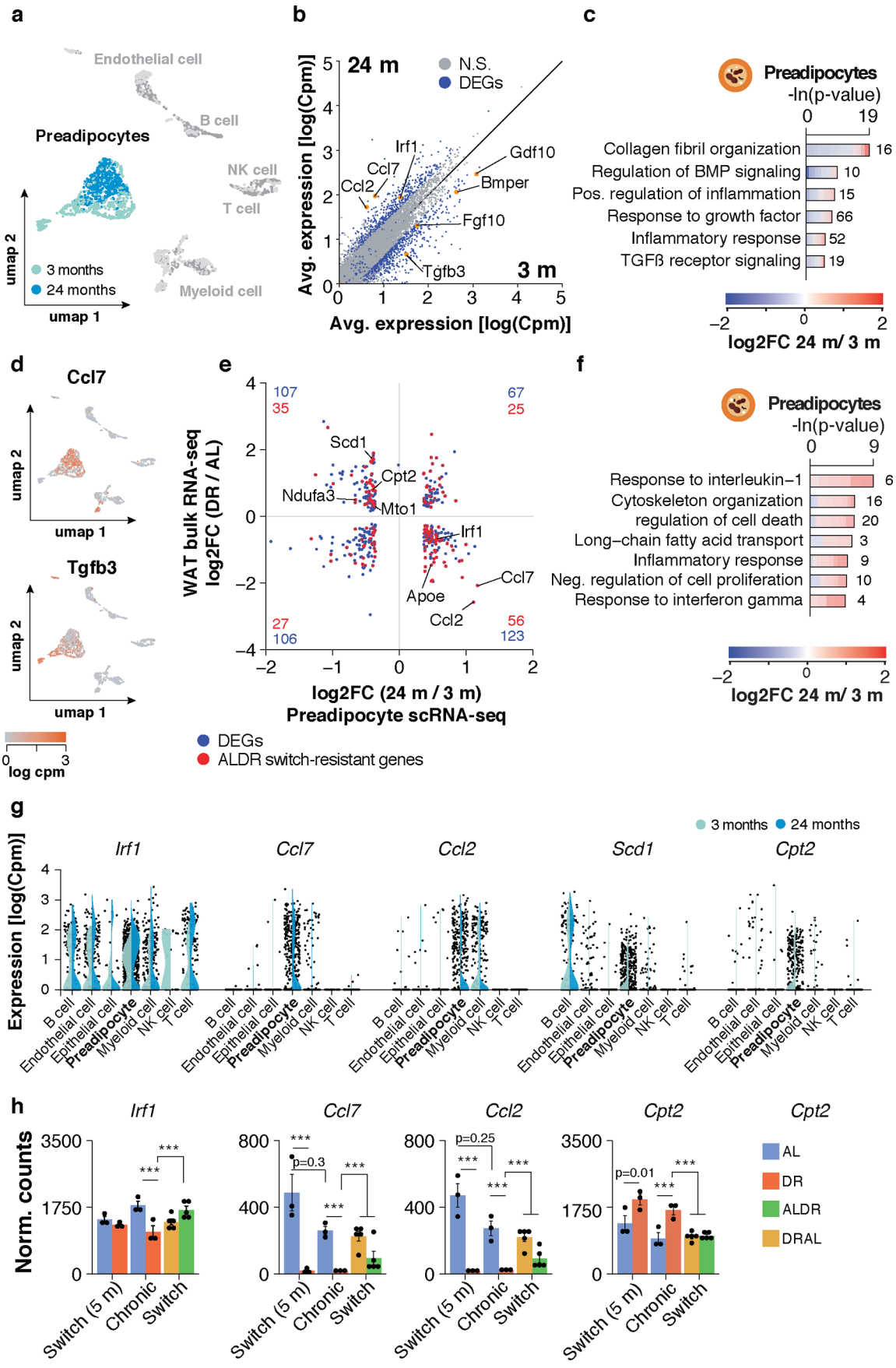

Extended Data Fig. 4 | see figure caption on next page.

Extended Data Fig. 4 | scRNA-seq profiling of the stromal–vascular fraction in young and old WAT. a, t-SNE visualization of scRNA-seq data (FACS Smart-seq2) from the GAT stromal–vascular fraction, split by age. Preadipocytes as annotated by the Tabula Muris Consortium are coloured by age. **b**, Scatterplot representation of average expression levels of genes of young and old preadipocytes. Differentially expressed genes (DEGs) are indicated in blue. **c**, Representative GO enrichment of the top 300 differentially expressed genes between old and young preadipocytes. Lengths of bars represent negative ln-transformed *P* values, calculated using two-sided Fisher's exact test. **d**, t-SNE visualisation of scRNA-seq data coloured by expression of two regulated genes, *Ccl7* and *Tgfb3*. **e**, Scatterplot of expression differences between old and young preadipocytes (by scRNA-seq) versus expression differences between DR and AL (by bulk RNA-seq). The number of common DEGs in each quadrant is indicated in blue, and the number of ALDR switch-resistant genes is indicated in red. There was a significant inverse association as determined by two-sided Fisher's exact test for common DEGs ($P = 0.0026$) and when analysis was limited to ALDR switch-resistant genes ($P = 0.003$). **f**, Representative GO enrichment of 91 switch-resistant genes following the inverse association in **e**. Lengths of bars represent negative ln-transformed *P* values, calculated using two-sided Fisher's exact test. The complete list of enriched GO terms can be found in Supplementary Table 1. **g**, Violin plot representing expression of selected genes across all profiled cell types. Points indicate cell-wise expression levels, and the violin indicates average distribution of expression split by age. **h**, mRNA expression (RNA-seq) of the same genes WAT. *Scd1* expression is shown in Fig. 5. Two-sided Wald test, adjusted for multiple testing. All scRNA-seq data represents cells that were derived and processes from $n = 4$ biologically independent mice per age group, encompassing a total of $n = 1{,}962$ biologically independent cells. Biologically independent animals used for bulk RNA-seq: n=3 (AL, DR, ALDR, AL 5m) n=5 (ALDR, DRAL). Means ± s.e.m., $^{***}P < 0.0001$.

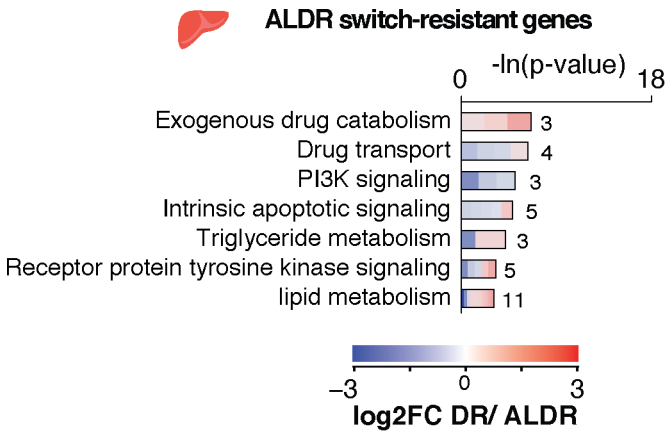

Extended Data Fig. 5 | Extended functional enrichment analysis of liver. Representative GO enrichment of ALDR switch-resistant genes in the liver. Lengths of bars represent negative ln-transformed *P* values, calculated using two-sided Fisher's exact test. Biologically independent animals used for RNA-seq: $n = 3$.

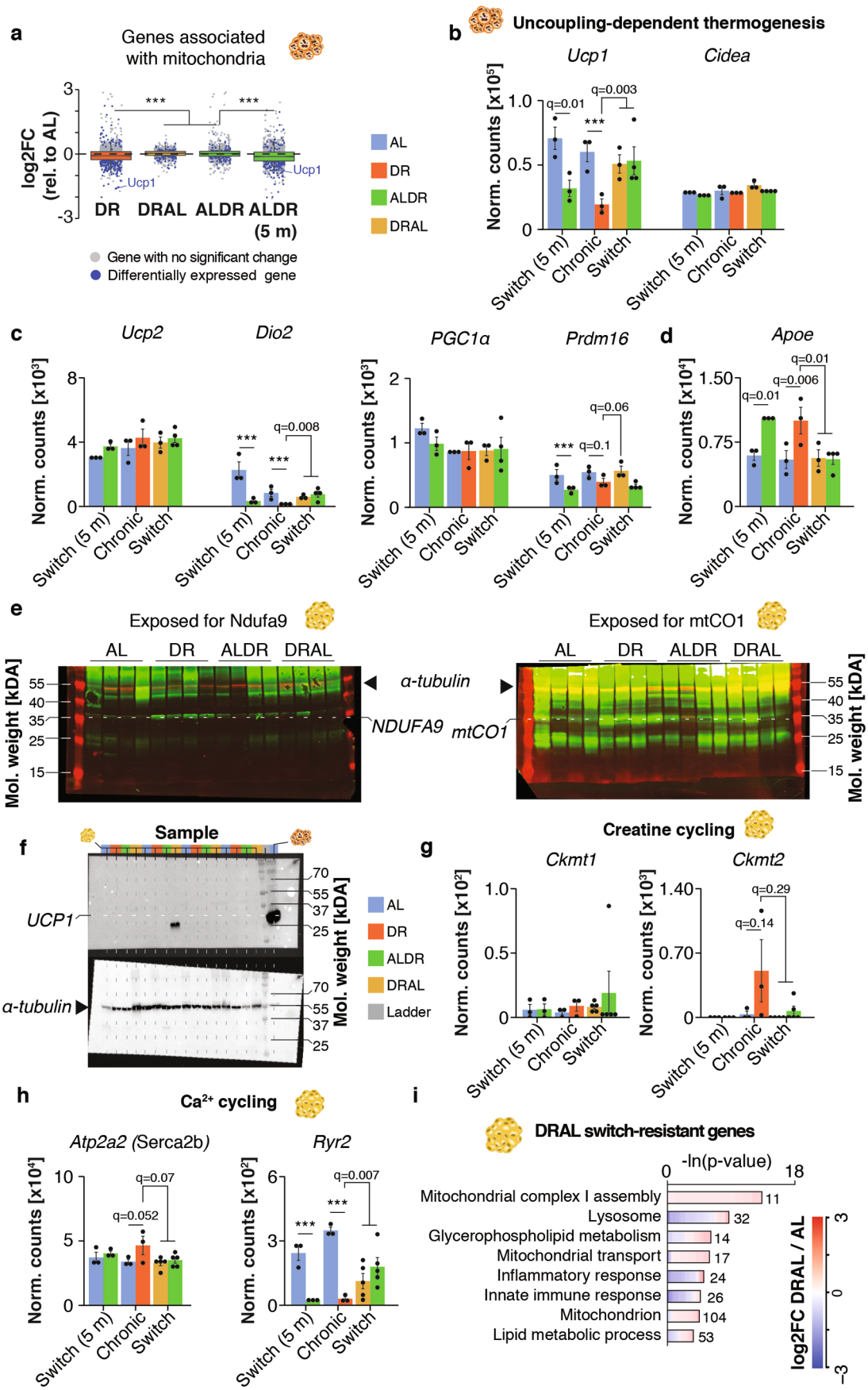

Extended Data Fig. 6 | see figure caption on next page.

Extended Data Fig. 6 | Thermogenic marker expression in WAT and BAT. a, Distribution of gene-wise expression changes in BAT under chronic DR and switch diets relative to chronic AL feeding for genes associated with the GO term 'Mitochondrion' ($n = 1299$ genes). Whiskers represent 1st and 5th quartiles, box edges represent 2nd and 4th quartiles, and the centre line represents the 3rd quartile/median. Two-sided Wilcoxon rank-sum test, adjusted for multiple testing. **b**, mRNA expression (RNA-seq) of thermogenic marker genes in BAT. **c**, mRNA expression (RNA-seq) of marker for thermogenesis and mitochondrial biogenesis in BAT. **d**, *Apoe* mRNA expression (RNA-seq) in BAT. Two-sided Wald test, adjusted for multiple testing. **e**, Whole LICOR western blot image of Fig. 4d. **f**, Western blot analysis of UCP1 in WAT, with α-tubulin as loading control. Tissue extract from one BAT sample (very right lane) was included as positive control for the UCP1 antibody. **g**,**h**, mRNA expression (RNA-seq) of uncoupling-independent, thermogenic marker genes in WAT for creatine cycling (**g**) and Ca^{2+} cycling (**h**). Two-sided Wald test, adjusted for multiple testing. **i**, DRAL switch-resistant genes in WAT. Lengths of bars represent negative ln-transformed *P* values using two-sided Fisher's exact test. The complete list of enriched GO terms can be found in Supplementary Table 4. Biologically independent animals used for RNA-seq: BAT: $n = 3$ (AL, DR, DRAL, AL 5m, ALDR 5m) $n = 5$ (ALDR); WAT: $n = 3$ (AL, DR, ALDR, AL 5m) $n = 5$ (ALDR, DRAL). The Western blot analysis was done once using tissues of $n = 4$ biologically independent animals per diet that were derived from the same cohort but were not identical to the mice used for RNA-seq. Means ± s.e.m., $^{***}q < 0.0001$.

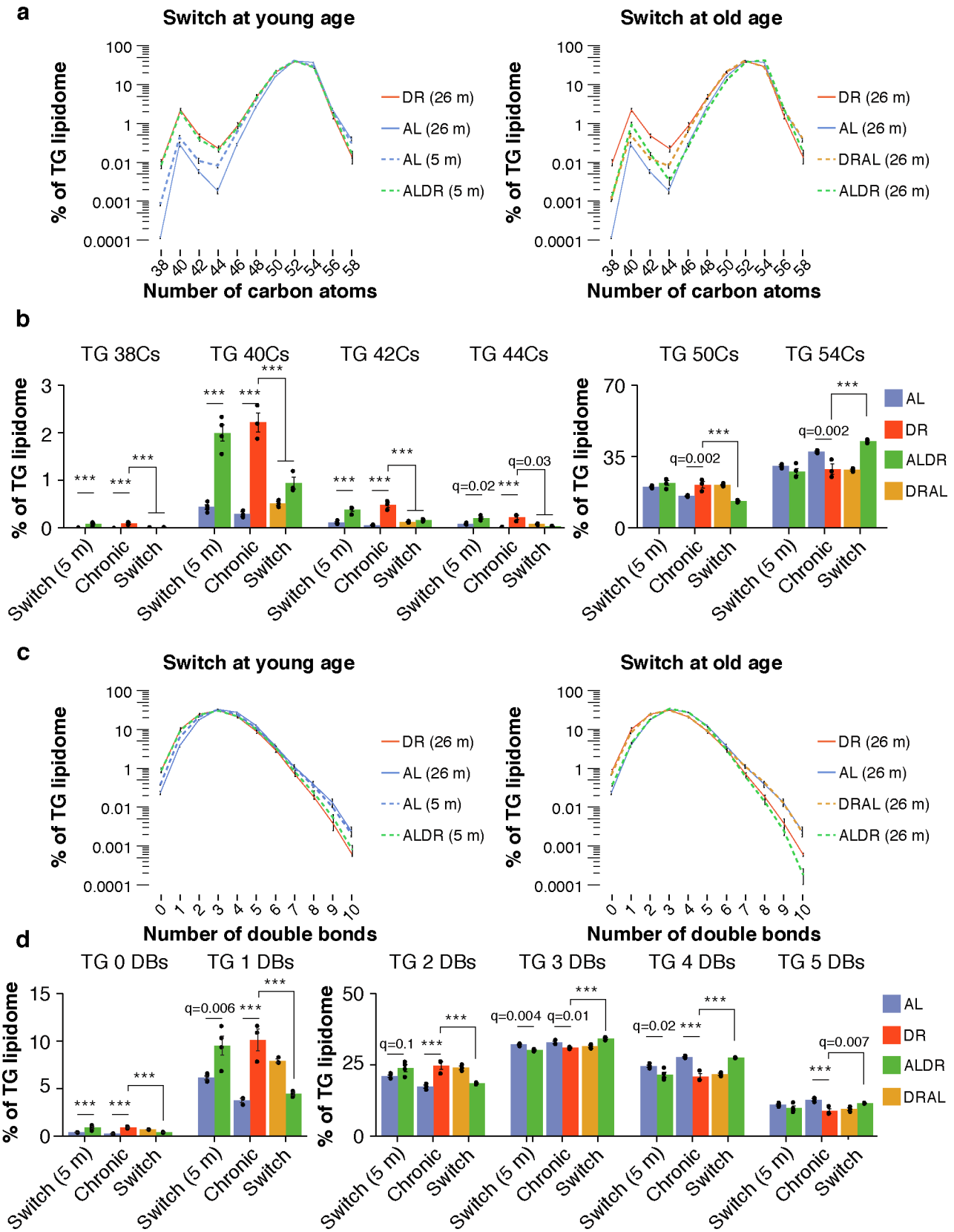

Extended Data Fig. 7 | Triglyceride composition in WAT. a, Distribution of TG species for the switch at young (left) and old (right) age classified according to the number of carbon atoms as proxy for TG-associated chain length. Values represent normalized relative abundances (0–100%) on a logarithmic scale. **b**, Selected TG groups classified according to associated chain length. Values are identical to the ones in **a**. One-way ANOVA followed by two-sided post-hoc Tukey test. **c**, Distribution of TG species for the switch at young (left) and old (right) age, classified according to the number of double bonds in TG-associated chains. Values represent normalized relative abundances (0–100%) on a logarithmic scale. **d**, Selected TG groups classified according to the number of double bonds. Values are identical to the ones in **c**. One-way ANOVA followed by two-sided post-hoc Tukey test. Biologically independent animals used for Lipidomics: $n = 4$ per diet. Means ± s.e.m., $^{***}P < 0.001$.

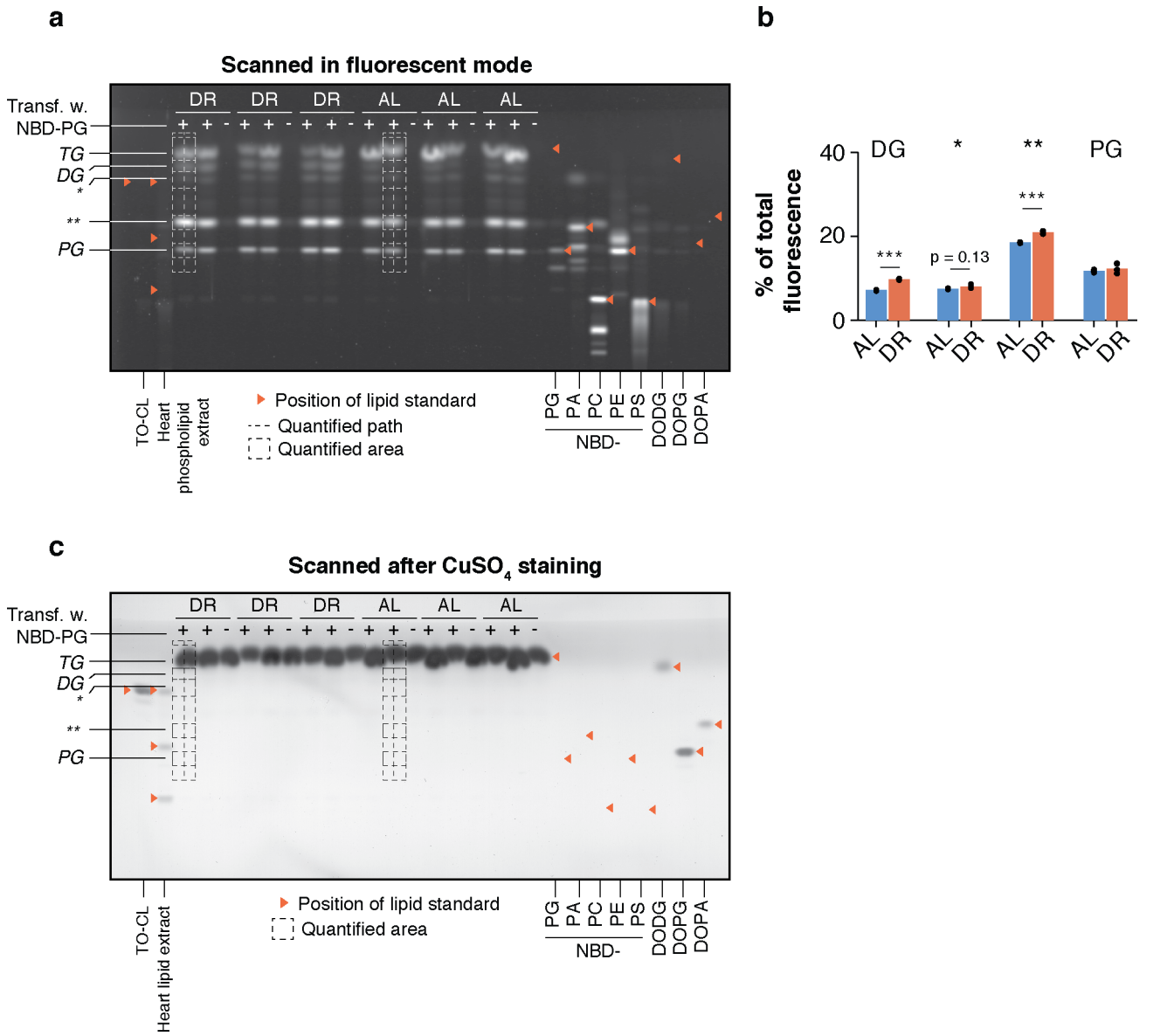

Extended Data Fig. 8 | Fluorescence signal analysis of pulse–chase experiment outcome. a, Cellular uptake profiles of exogenously supplied NBD-PG by explant-cultured adipocytes. Lipids were separated by TLC and analysed by fluorescence scanning. The TLC analysis was done once with lipid extracts from $n = 3$ biologically independent mice per diet (indicated above), with $n = 3$ technical replicates each. For each biological replicate, two technical replicates were co-incubated with NBD and one with just the transfection agent. The dashed line represents the paths used to quantify fluorescent signal distribution in Fig. 6d. Dashed boxes represent the areas used to quantify individual bands. Lipid species with low polarity run on top, with TGs being represented by the top band. Fluorescent lipids run slightly lower than non-fluorescent lipids. Standard phospholipids allowed the identification of lipid spots representing TG, DG and PG levels (the asterisks indicate unidentified lipid species). Applied non-fluorescent standard lipids involve: Tetra-oleoyl CL (TO-CL); CL-rich phospholipid-extract from heart; palmitoyl-oleoyl-DG (PODG), di-oleoyl-PG (DOPG); di-oleoyl-PA (DOPA). Fluorescent NBD-labelled lipids involve: PG, PA, PC, PE, PS. **b**, Relative fluorescent signal in each of the major bands. $n = 3$ biologically independent, 24-month-old animals per diet; technical replicates were averaged prior analysis. Two-sided *t* test. Data for the TG band are shown in Fig. 6e. **c**, Non-fluorescent scans of identical TLC plate after staining with $CuSO_4$. Due to high abundance of TGs (upper band) in adipocytes, no phospholipids can be observed. Standard phospholipids allowed the identification of lipid spots.

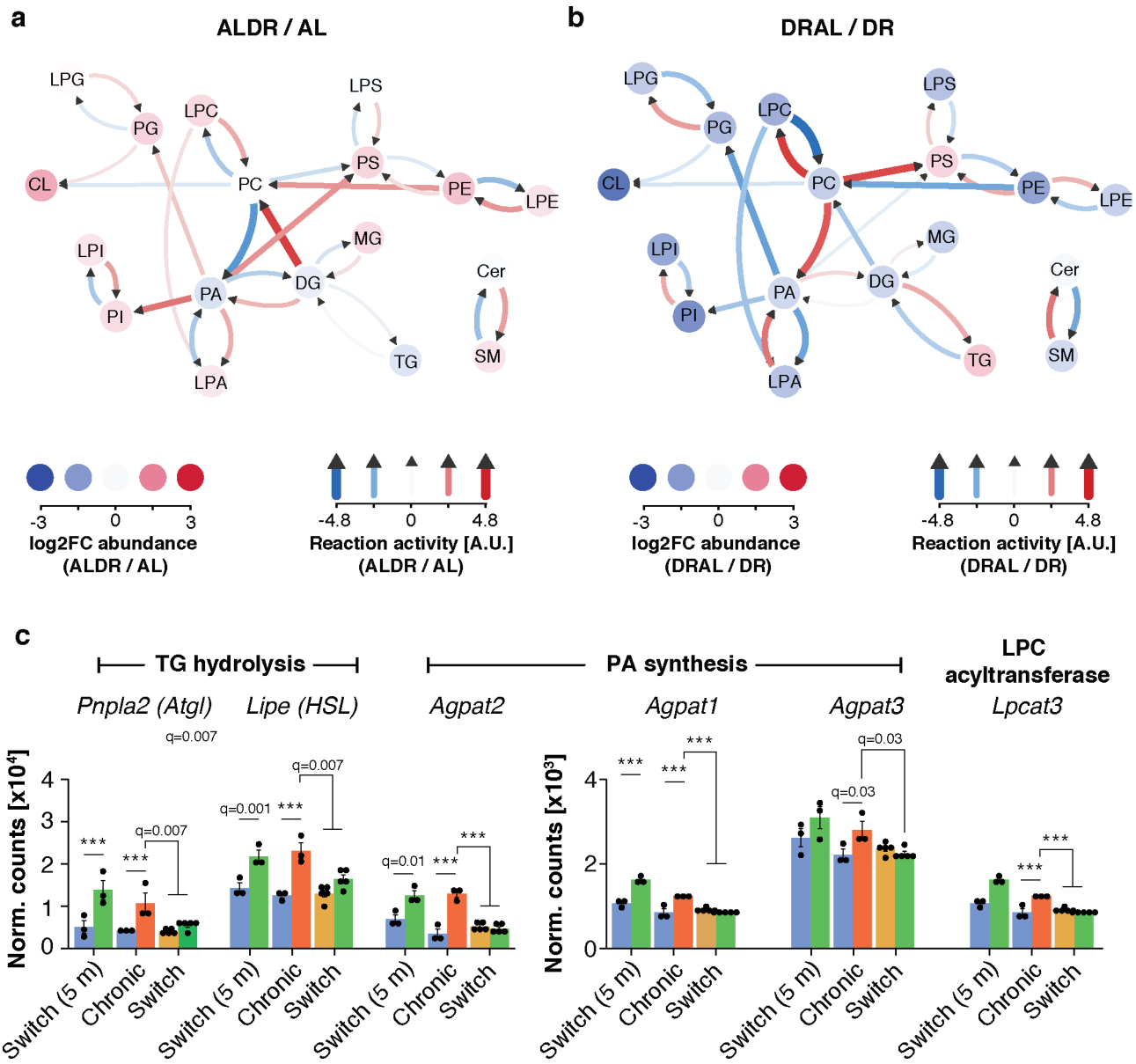

Extended Data Fig. 9 | Lipid reaction analysis in ALDR and DRAL mice. a,**b**, Analysis of lipid pathway activity in WAT of ALDR (**a**) or DRAL (**b**) mice relative to AL control. Red and blue arrows show reactions with positive and negative activity, respectively. Coloured circles indicate relative $\log_2$-transformed abundance of lipid classes involved. **c**, mRNA expression (RNA-seq) of key genes mapping to differentially active pathways in Fig. 7a. Two-sided Wald test, adjusted for multiple testing. Biologically independent animals used: RNA-seq: $n = 3$ (AL, DR, ALDR, AL 5m) $n = 5$ (ALDR, DRAL); Lipidomics: $n = 4$ per diet. Means ± s.e.m., $^{***}q < 0.0001$.

Michael J.O. Wakelam
Andreas Beyer
Sebastian Grönke
Corresponding author(s): Linda Partridge

Last updated by author(s): Sep 2, 2019

Reporting Summary

Nature Research wishes to improve the reproducibility of the work that we publish. This form provides structure for consistency and transparency in reporting. For further information on Nature Research policies, see Authors & Referees and the Editorial Policy Checklist.

Statistics

For all statistical analyses, confirm that the following items are present in the figure legend, table legend, main text, or Methods section.

n/a	Confirmed	
☐	☒	The exact sample size (*n*) for each experimental group/condition, given as a discrete number and unit of measurement
☐	☒	A statement on whether measurements were taken from distinct samples or whether the same sample was measured repeatedly
☐	☒	The statistical test(s) used AND whether they are one- or two-sided *Only common tests should be described solely by name; describe more complex techniques in the Methods section.*
☐	☒	A description of all covariates tested
☐	☒	A description of any assumptions or corrections, such as tests of normality and adjustment for multiple comparisons
☐	☒	A full description of the statistical parameters including central tendency (e.g. means) or other basic estimates (e.g. regression coefficient) AND variation (e.g. standard deviation) or associated estimates of uncertainty (e.g. confidence intervals)
☒	☐	For null hypothesis testing, the test statistic (e.g. *F*, *t*, *r*) with confidence intervals, effect sizes, degrees of freedom and *P* value noted *Give P values as exact values whenever suitable.*
☒	☐	For Bayesian analysis, information on the choice of priors and Markov chain Monte Carlo settings
☒	☐	For hierarchical and complex designs, identification of the appropriate level for tests and full reporting of outcomes
☐	☒	Estimates of effect sizes (e.g. Cohen's *d*, Pearson's *r*), indicating how they were calculated

Our web collection on statistics for biologists contains articles on many of the points above.

Software and code

Policy information about availability of computer code

Data collection	Odyssey Infrared Imaging System. Application software version 3.0.30. LI-COR Biosciences QuantStudio Software V1.3. ThermoFisher Scientific ImageQuant TL 8.2 software. GE Healthcare ChemiDoc™ XRS+ System + Image Lab 5.1 software, Biorad.
Data analysis	Raw sequence reads were trimmed using Trim Galore! (v0.3.7). Trimmed sequences were aligned using Tophat2 (v2.0.14). RStudio was used for statistical analysis. The following, publicly-available R packages were used: Deseq2, survival, survminer, flexsurv, ggplot2, topGO, org.Mm.eg.db, Seurat (version 3). Data visualization and analysis were performed using SeqMonk. The Fiji software package was used to quantify protein bands in western blot and fluorescent intensity in thin layer chromatography.

For manuscripts utilizing custom algorithms or software that are central to the research but not yet described in published literature, software must be made available to editors/reviewers. We strongly encourage code deposition in a community repository (e.g. GitHub). See the Nature Research guidelines for submitting code & software for further information.

Data

Policy information about availability of data

All manuscripts must include a data availability statement. This statement should provide the following information, where applicable:

- Accession codes, unique identifiers, or web links for publicly available datasets
- A list of figures that have associated raw data
- A description of any restrictions on data availability

All the data generated or analysed during this study are include in the published article and its Supplementary Information files, and are available from the

corresponding authors. Raw RNA-sequencing data are available under accession numbers GSE92486 and GSE124772 on the NCBI Gene expression Omnibus database. Analysed lipidomics data are available under Table S3. Correspondence and requests for material should be addressed to S.G. and L.P.

Field-specific reporting

Please select the one below that is the best fit for your research. If you are not sure, read the appropriate sections before making your selection.

☒ Life sciences ☐ Behavioural & social sciences ☐ Ecological, evolutionary & environmental sciences

For a reference copy of the document with all sections, see nature.com/documents/nr-reporting-summary-flat.pdf

Life sciences study design

All studies must disclose on these points even when the disclosure is negative.

Sample size	Sample size for RNA-seq and lipidome profiling were based on accepted guideline papers (e.g. Conesa et al., 2016; Genome Biology) and prior, published studies by our lab investigating the effects of dietary restriction (DR) on hepatic transcriptome and lipidome (Hahn et al., 2017; Genome Biology and Hahn et al., 2018; Plos Genetics). To investigate the sample size needed to obtain robust results as to whether late-onset DR results in an acute reversal of mortality, we used actual data from dietary restriction experiments. To objectively determine the impact of acute DR on mortality dynamics after a dietary switch, we used standard survival analysis techniques (including log-rank and Cox regression) as well as methods of mortality analysis developed by co-author Scott Pletcher (Pletcher et al., 2000). We followed the assumptions that (i) Gompertz mortality dynamics apply (i.e., death rates increase exponentially throughout life); (ii) life-long DR produces a 25% extension of lifespan; and (iii) a substantial time-lag would be required for mortality rates in the switched cohorts to reach levels seen in the life-long DR cohort. Our power analyses identified that, for all conditions that were investigated, at least 100 animals per cohort would be sufficient to detect mortality reversal over 90% of the time (i.e., statistical power > 0.90). Based on our calculations of statistical power, we proposed to age 200 animals per treatment (ad libitium, DR, and switch from ad libitum to DR) and execute the switch to DR following the death of 20% of the ad libitum cohort.
Data exclusions	No data was excluded.
Replication	We validated findings from RNA-seq profiling (switch-resistant mitochondrial biogenesis; switch-resistant lipogenesis) with orthogonal wet lab methods, such as qPCR profiling of mtDNA content, RNA expression levels of selected genes and protein abundance as measured by western blot. Shifts in lipid turnover as predicted by the lipidome analysis were verified using ex-vivo pulse chase experiments.
Randomization	Upon weaning female mice of each breeding cohort were randomly assigned to cages and were fed AL. DR was introduced at the age of 12 weeks in half of the cages of each breeding cohort. Before the late-life diet switch we randomized cages in the rack. This was done to avoid re-allocating old mice to new cages.
Blinding	DR treatment requires daily feeding of mice with a defined amount of food, therefore, blinding of DR animals was not possible. However, scoring of dead animals in the lifespan analysis was done by mouse care takers, who were not aware of the study design, thus preventing bias. Lipidome, ex vivo pulse chase and western blot analysis were done under blinded conditions.

Reporting for specific materials, systems and methods

We require information from authors about some types of materials, experimental systems and methods used in many studies. Here, indicate whether each material, system or method listed is relevant to your study. If you are not sure if a list item applies to your research, read the appropriate section before selecting a response.

Materials & experimental systems

n/a	Involved in the study
☐	☒ Antibodies
☒	☐ Eukaryotic cell lines
☒	☐ Palaeontology
☐	☒ Animals and other organisms
☒	☐ Human research participants
☒	☐ Clinical data

Methods

n/a	Involved in the study
☒	☐ ChIP-seq
☒	☐ Flow cytometry
☒	☐ MRI-based neuroimaging

Antibodies

Antibodies used	NDUFA9, 1:1000, AB_301431, Abcam mtCO1, AB_2084810, Abcam α-Tubulin 11H10, AB_2619646, Cell Signaling Technology IRDye 680RD, AB_10956166, LI-COR Biosciences IRDye 800CW, AB_621842, LI-COR Biosciences UCP1, AB_2687530, Cell Signaling Technology

anti-rabbit HRP, AB_2536530, ThermoFisher Scientific

Validation

NDUFA9, 1:1000, AB_301431, Abcam. Validated by the company and by users (cited 7 times).
mtCO1, AB_2084810, Abcam. Validated by the company and by users (cited 268 times).
α-Tubulin 11H10, AB_2619646, Cell Signaling Technology. Validated by the company and by users (cited 273 times).
IRDye 680RD, AB_10956166, LI-COR Biosciences. Validated by the company and by users (cited 9 times).
IRDye 800CW, AB_621842, LI-COR Biosciences. Validated by the company and by users (cited 65 times).
UCP1, AB_2687530, Cell Signaling Technology. Validated by the company and by users (cited 11 times).
anti-rabbit HRP, AB_2536530, ThermoFisher Scientific. Validated by the company and by users (cited 140 times).

Animals and other organisms

Policy information about studies involving animals; ARRIVE guidelines recommended for reporting animal research

Laboratory animals	Mus musculus. Female F1 hybrid mice (C3B6F1) were generated in-house by crossing C3H/HeOuJ females with C57BL/6 NCrl males (strain codes 626 and 027, respectively, Charles River Laboratories). Experimental animals were generated in three breeding batches with 300, 280 and 220 animals in breeding round F1, F2 and F3, respectively. Animals were monitored from birth to death. Median life spans (F1, F2, F3 in days): AL (858, 866, 843), DR (1097, 1074, 1098), AL_DR (863, 914, 833), DR_AL (1024, 1051, 1013). The oldest animal (DR, F3) died at the age of 1453 days.
Wild animals	Our study did not involve any wild animals.
Field-collected samples	Our study did not involve any field-collected samples.
Ethics oversight	The DR study was performed in accordance with the recommendations and guidelines of the Federation of the European Laboratory Animal Science Association (FELASA), with all protocols approved by the Landesamt für Natur, Umwelt und Verbraucherschutz, Nordrhein-Westfalen, Germany (reference numbers: 8.87-50.10.37.09.176 and 84-02.04.2015.A437).

Note that full information on the approval of the study protocol must also be provided in the manuscript.